Advances in Polymer Science 264

Deepalekshmi Ponnamma
Sabu Thomas *Editors*

Non-Linear Viscoelasticity of Rubber Composites and Nanocomposites

Influence of Filler Geometry and Size in Different Length Scales

Springer

264
Advances in Polymer Science

Aims and Scope

The series Advances in Polymer Science presents critical reviews of the present and future trends in polymer and biopolymer science. It covers all areas of research in polymer and biopolymer science including chemistry, physical chemistry, physics, material science.

The thematic volumes are addressed to scientists, whether at universities or in industry, who wish to keep abreast of the important advances in the covered topics.

Advances in Polymer Science enjoys a longstanding tradition and good reputation in its community. Each volume is dedicated to a current topic, and each review critically surveys one aspect of that topic, to place it within the context of the volume. The volumes typically summarize the significant developments of the last 5 to 10 years and discuss them critically, presenting selected examples, explaining and illustrating the important principles, and bringing together many important references of primary literature. On that basis, future research directions in the area can be discussed. Advances in Polymer Science volumes thus are important references for every polymer scientist, as well as for other scientists interested in polymer science - as an introduction to a neighboring field, or as a compilation of detailed information for the specialist.

Review articles for the individual volumes are invited by the volume editors. Single contributions can be specially commissioned.

Readership: Polymer scientists, or scientists in related fields interested in polymer and biopolymer science, at universities or in industry, graduate students.

Special offer:

For all clients with a standing order we offer the electronic form of Advances in Polymer Science free of charge.

More information about this series at
http://www.springer.com/series/12

Deepalekshmi Ponnamma • Sabu Thomas
Editors

Non-Linear Viscoelasticity of Rubber Composites and Nanocomposites

Influence of Filler Geometry and Size in Different Length Scales

Springer

Editors
Deepalekshmi Ponnamma
Sabu Thomas
School of Chemical Sciences
Mahatma Gandhi University
Kottayam
India

ISSN 0065-3195 ISSN 1436-5030 (electronic)
ISBN 978-3-319-08701-6 ISBN 978-3-319-08702-3 (eBook)
DOI 10.1007/978-3-319-08702-3
Springer Cham Heidelberg New York Dordrecht London

Library of Congress Control Number: 2014953903

Printed on acid-free paper

Springer is part of Springer Science+Business Media (www.springer.com)

Preface

Rubber has since many year had a significant impact on human life. Rubber products mark one of the building blocks of technology and industry. This material is widely used to manufacture erasers to flexible conductors. Various types of particles are also used to fill rubber and to make micro as well as nanocomposites (depending on the nature of filler) having excellent properties. A lot of publications are produced each year about rubber and its composites, and its increasing importance makes its study essential.

The manufacture of both natural and synthetic rubber based products is basically done by following the procedure of melt mixing. Extruders as well as Haake mixing equipments are used for this purpose. Since the properties of the obtained composites depend on the nature of dispersion of the fillers in rubber, the particles have to be uniformly distributed throughout the medium. For this, knowledge of the flow behavior of rubber is very necessary. All elastomers are viscoelastic in nature and the study of their viscoelasticity is known as rheology. Since the terms rubber, polymer, and elastomer are synonyms, throughout this book these terms are used interchangeably. The viscoelastic nature can be linear and nonlinear depending on the response of the materials with respect to time. The viscoelasticity of elastomers is nonlinear in nature and this book deals with a thorough study of the nonlinear behavior of rubber composites and nanocomposites.

Fillers in nanodimensions are classified in to three categories—one, two, and three dimensions, respectively, based on their number of sides in nano. For instance nanofibers come under one dimensional, nanoplates like clay and graphene under 2D and nano-spheres under 3D fillers. The nonlinear viscoelastic behavior of rubbers filled with these three kinds of filler categories are discussed subsequently in Chaps. 2 to 4. In Chap. 2 the readers can see a good introduction about the different types of nanofillers and the authors talk about nanotubes, nanorods, and nanofibers in depth. Different preparation methods of the nanocomposites, mode of dispersion, and its influence on surface morphologies of various elastomers, chemical modifications on the filler, etc. are studied. Rheological properties including cure kinetics, storage and loss moduli, and complex viscosities as functions of

frequency, time, temperature etc. along with the dynamic mechanical properties of the nanocomposites are thoroughly investigated.

For better performance the fillers must have good interfacial interaction with the rubber medium. This is a matter of great importance and Sadasivuni and Grohens have addressed the nonlinear viscoelasticity of rubber reinforced nanoplatelets based on such molecular interactions existing in the system. The filler–filler and filler–rubber interactions are studied with the help of rheology and certain theories. For this the nonlinear stress response of rubbers and its composites to an applied strain is noted and it is found that the 2D filler particles increase the level of viscometric properties. Here in this chapter the readers will get a basic knowledge about an important behavior of rubber nanocomposites which is known as Payne effect.

Chapter 4 investigates the rheological and the dynamic mechanical properties of rubber nanocomposites filled with spherical nanoparticles, like POSS, titanium dioxide, and nanosilica. Here also the crucial parameter of interfacial interaction in nanocomposite systems under dynamic-mechanical conditions is discussed. After discussing about filled mono-matrix medium in the first three chapters, the next chapter gives information about the nonlinear viscoelastic behavior of rubber–rubber blend composites and nanocomposites with fillers of different particle size. Here in Chap. 5 we can observe a wide discussion about the influence of filler geometry, distribution, size, and filler loading on the dynamic viscoelastic behavior. These specific surface area and the surface structural features of the fillers influence the Payne effect as well. The authors explain the addition of spherical or near-spherical filler particles always increase the level of both the linear and the nonlinear viscoelastic properties whereas the addition of high-aspect-ratio, fiber-like fillers increase the elasticity as well as the viscosity.

Effect of hybrid fillers on the nonlinear viscoelasticity of rubber composites and nanocomposite is the subject of dialogue for Chap. 6. In addition to carbon nanoparticles, the mineral fillers, biofillers, fibers, Nanorods, Nanocubes, Nanoflowers, etc. are introduced with their influence on nonlinear viscoelasticity of rubbers. This chapter is a nice survey about the synergy of fillers by Chaki et al. A significant factor in rubber technology is its vulcanization and how it depends on the nonlinear viscoelastic behavior of rubber is dealt with in the following chapter. In the presence of cross-link networks, the viscoelasticity differs and the factors influencing this phenomenon are very complex and obscure. From this chapter the readers will get a new reading experience about the nonlinear viscoelastic behaviors of cured rubbers with simplest mutle-networks—double-network. Song's transient double-network model, double-network formed by twice curing and the specific cross-link network formed in metal salts of unsaturated carboxylic acids reinforced rubbers, is also introduced.

The last two chapters give emphasis to the theoretical side of the nonlinear viscoelasticity of rubber composites. Thus an attempt to cover both experimental and theoretical sides is done in this book and as the editors we feel we have succeeded in it. Chapter 8 by Markovic et al. explains about a constitutive model able to reproduce both static and dynamic material responses based on the behavior

of carbon black-filled rubbers. Several nonlinear viscoelastic models have been examined thoroughly by highlighting the advantages and disadvantages. The dependence of the parameters like temperature, strain rate, shape factor, etc. on the nonlinear viscoelasticity are also dealt with. The quasi-static experimental results allowed the influence of the Mullins effect on the quasi-static response and this induces transverse isotropy in the material. The mechanism of Payne effect includes the breakdown of different networks, namely the filler–filler network, the weak polymer–filler network, the chemical network, and the entanglement network, and Maier and Goritz model is applied to explain the nonlinear behavior. The complex functions of time, strain, strain rate, temperature, and composition on the linear and the nonlinear domains for the rubber and compounds are analyzed in the last chapter. The material functions in their full complexity on the processing behavior and the mechanical properties of rubber systems are provided. The author claims the heterogeneity and interactions between phases add to complexity and so an experimental approach of material functions and their pragmatical connection with processing aspects remain mandatory, as done in the last section.

In short this book will give a new experience to the reader about the viscoelastic behavior of rubber nanocomposites. Almost all areas of nonlinear viscoelasticity are covered by emphasizing both experimental and theoretical sides.

Kottayam, India

Deepalekshmi Ponnamma
Sabu Thomas

Contents

Biography of Volume Editors

Mrs. Deepalekshmi Ponnamma is doing Doctoral Research in Polymer Nanocomposites at School of Chemical Sciences, Mahatma Gandhi University, Kottayam, India. She has about 4 years of research experience in nanomaterials and their polymer nanocomposites. Her study is mainly focussed on the properties of carbon nanotube reinforced elastomer composite systems. She has been a visiting student for many universities abroad. She has published eight papers in international journals and eight book chapters. She has participated in several international conferences and has best poster and oral presentation awards to her credit. She has edited three books as well.

Prof. Sabu Thomas is an outstanding leader with sustained international acclaims for his work in polymer science and engineering, polymer nanocomposites, elastomers, polymer blends, interpenetrating polymer networks, polymer membranes, green composites and nanocomposites, nanomedicine, and green nanotechnology. Dr. Thomas's ground breaking inventions in polymer nanocomposites, polymer blends, and green bionanotechnological sciences have made transformative differences in the development of new materials for automotive, space, housing, and biomedical fields. He has received a number of national and international awards which include: Fellowship of the Royal Society of Chemistry, MRSI award, CRSI award, and Sukumar Maithy award. He holds a position of No. 5 in the list of most productive researchers in India. Prof. Thomas has published over 600 peer reviewed publications, reviews, and book chapters. He has co-edited 30 books and is the inventor of 3 patents. The H index of Prof. Thomas is 65 and he has more than 15,000 citations. He has supervised 64 PhD theses.

Contributors

Jaroslava Budinski-Simendić Faculty of Technology, University of Novi Sad, Novi Sad, Serbia

Tapan Kumar Chaki Rubber Technology Centre, Indian Institute of Technology, Kharagpur, WB, India

Yukun Chen School of Mechanical and Automotive Engineering, South China University of Technology, Guangzhou, China

Neena George Department of Polymer Science and Rubber Technology, Cochin University of Science & Technology, Kochi, India

Yves Grohens LIMATB Laboratory, Université de Bretagne Sud, Lorient, France

Karun Kumar Jana School of Materials Science and Technology, Indian Institute of Technology (BHU), Varanasi, India

Rani Joseph Department of Polymer Science and Rubber Technology, Cochin University of Science & Technology, Kochi, India

Vojislav Jovanović Faculty of Natural Science and Mathematics, University of Priština, Priština, Serbia

Jean L. Leblanc UPMC – Paris Sorbonne Universités, Polymer Rheology and Processing, Vitry-sur-Seine, France

Pralay Maiti School of Materials Science and Technology, Indian Institute of Technology (BHU), Varanasi, India

UPMC – Paris Sorbonne Universités, Polymer Rheology and Processing, Vitry-sur-Seine, France

Milena Marinović-Cincović University of Belgrade, Institute of Nuclear Science Vinča, Belgrade, Serbia

Gordana Marković Tigar, Pirot, Serbia

Ajalesh B. Nair Department of Polymer Science and Rubber Technology, Cochin University of Science & Technology, Kochi, India

Intelligent Polymer Nanomaterials Lab, Polymer-Nano Science and Technology, Chonbuk National University, Duckjin-gu, Jeonju, Republic of Korea

Suryakanta Nayak Rubber Technology Centre, Indian Institute of Technology, Kharagpur, WB, India

Mrinal Patel School of Materials Science and Technology, Indian Institute of Technology (BHU), Varanasi, India

Deepalekshmi Ponnamma School of Chemical Sciences, Mahatma Gandhi University, Kottayam, Kerala, India

Dipak Rana Industrial Membrane Research Institute, Department of Chemical and Biological Engineering, University of Ottawa, Ottawa, ON, Canada

Kishor Kumar Sadasivuni School of Chemical Sciences, Mahatma Gandhi University, Kottayam, Kerala, India

Suzana Samaržija-Jovanović Faculty of Natural Science and Mathematics, University of Priština, Priština, Serbia

Michał Strankowski Chemical Faculty, Polymer Technology Department,, Gdansk University of Technology, Gdansk, Poland

Sabu Thomas School of Chemical Sciences, Mahatma Gandhi University, Kottayam, Kerala, India

Centre for Nanoscience and Nanotechnology, Mahatma Gandhi University, Kottayam, Kerala, India

Chuanhui Xu School of Chemistry and Chemical Engineering, Guangxi University, Nanning, China

School of Materials Science and Engineering, South China University of Technology, Guangzhou, China

Origin of Nonlinear Viscoelasticity in Filled Rubbers: Theory and Practice

Deepalekshmi Ponnamma and Sabu Thomas

Abstract The present chapter is written as an introduction towards this book on nonlinear viscoelasticity of rubber composites and nanocomposites. Rather than introducing the concept of the book to the readers this chapter reveals the basics behind rubber viscoelasticity and explains both linearity and nonlinearity from this behavior. Various filler reinforced rubbers are introduced emphasising the flow behavior of such nanocomposites. Major mathematical models proposed by Kraus, Huber and Vilgis and Maier and Goritz for the 'Payne Effect' are briefly addressed based on the filler matrix interactions existing in the composite systems.

Keywords Elastomer • Rheology • Dynamics • Modeling • Interfacial interactions

1 Introduction

Rubber is one of the most useful raw materials in industry and technology. The word rubber came from its capability to remove marks on paper and is coined with Priestly (1770). This material is available in nature in the form of latex tapped from the Brazilian rubber tree *Havea Brasiliensis*. The solid natural rubber is obtained through coagulating the latex. It is chemically unsaturated hydrocarbon and is produced widely in artificial means as well. Examples of synthetic rubbers include butyl rubber, silicone rubber, nitrile rubber etc. Depending on the usage rubbers are classified as special purpose and general purpose rubbers and a brief survey of this aspect is done by our group recently [1]. The consumer rubber products vary from erasers, raincoats, footwear play balls etc.; to engineering products such as rubber tyres, and multifarious rubber components for all engineering applications

D. Ponnamma
School of Chemical Sciences, Mahatma Gandhi University, Priyadarshini Hills P.O., Kottayam 686 560, Kerala, India

S. Thomas (✉)
School of Chemical Sciences, Mahatma Gandhi University, Priyadarshini Hills P.O., Kottayam 686 560, Kerala, India

Centre for Nanoscience and Nanotechnology, Mahatma Gandhi University, Priyadarshini Hills P.O., Kottayam 686 560, Kerala, India
e-mail: sabupolymer@yahoo.com

D. Ponnamma, S. Thomas (eds.), *Non-Linear Viscoelasticity of Rubber Composites and Nanocomposites*, Advances in Polymer Science 264, DOI 10.1007/978-3-319-08702-3_1

[1]. Rubber had also gotten attention as a reliable and durable material for protecting mild steel and concrete storage tanks, process vessels, pickling lines, mixers, reactors, agitators, pipelines, tank trucks, railroad tank cars, ship tankers, and exhaust gas scrubbers against corrosion. Nowadays acid resistant or anticorrosive rubbers are being used in construction field. Rubber is also used for protection of other materials against fire, heat and wearing. Rubber gives excellent performance as a construction material, in vibration and shock dampening, in elimination of structural noise and is the ultimate material for sealing systems [1–3]. For each application individual functional properties are optimized to meet specific requirements.

1.1 Brief History and Introduction of Rubber

The history of rubber may start with the report of Anghieria in 1525 that the Mexican tribes were using elastic balls for playing. However the first scientific study of rubber was undertaken by Charles de la Condamine along with Fresnau in 1735 and they reported rubber to be a "type of condensed resinous oil". It was Magellan who suggested the use of rubber as an eraser. Priestley popularized rubber in England as India rubber. Following Condamine, Macquer suggested the use of rubber in making flexible tubes. The attempt to use rubber in clothing accessories is also reported by Nadier in 1820. The most important invention in rubber was that made by Goodyear in 1840. This vulcanization/grafting developed more resistant varieties of rubber products and this regulated the technology during industrial revolution. By 1880s researches revealed the chemistry behind polymerization of isoprene and this was the springboard for the massive development of artificial rubbers. Rubber based materials are widely applied in various applications such as gloves, toys, balls, tyres, hoses, engine mountings, dock fenders, seismic bearings etc. Thanks to its multiple applications, particularly in the expanding automobile industry [4].

Rubber products have become more demanding throughout the world especially Brazil, Thailand, Malaysia, Ceylon, Singapore and Colonies in Asia. Based on advantages in terms of available land and labor, Indonesia has maintained a significant share in global output since the 1980s. By 2001, natural rubber consumption accounted for some 40 % of the total amount of rubber consumed worldwide. This promoted the advanced study of rubber and the works of Payne, Graham, Wiesner and Gérard contributed much in this regard. Since the rubber industry prompted the development of modern civilization the need of synthesizing rubber alternatives became stronger throughout the world. Rubber was used to coat wires used in every factory, home, office and military facilities. The drop in natural rubber production in Brazil triggered the need for low-cost products supplies in order to manufacture tyres [5, 6]. Under these circumstances development of rubber like materials became a necessary. All the pressures for rubber alternatives during the second world war triggered the production of synthetic elastomers. The reasons

behind the massive development of the synthetic rubber were, it could be vulcanized easily, its low costs and enhanced performances like gas impermeability. Since styrene butadiene rubber and butadiene rubber are widely used in tyre manufacture they are the most widely consumed type of synthetic rubber. Acrylonitrile rubber is used to make oil resistant materials and the neoprene rubber is known for its resistance to ageing and weathering, ozone attack and flame retardancy. Another synthetic rubber chloroprene has excellent oil resistance, thermal stability, flame resistance, ozone resistance and good mechanical properties [1].

The main characteristics which make rubber of great importance to the technology are its strength, the adhesion and strength of its bonding to metals and other substrates. The elasticity or deformability enables it to be used in extension, compression, shear, torsion or combinations of these. Rubber is easy to mold in to any shape and size due to its resilience, resistance to fatigue and abrasion and resistance to attack by corrosive chemicals. The rubber technologists are however facing challenges in developing materials applicable in high temperature conditions, nuclear radiation, ablation in the rocket industry and mechanical abuse in ore mining industries, oil well industries etc. The usefulness of rubbers in the industries has three main reasons of which the first is its usability in the variety of environments, deformity and durability and possibility of convenient equipment designs. Rubber is a good construction material especially for chemical plants as they resist corrosion against chemicals, acids and alkalies. The third reason is its easiness to convert to usable products readily and rapidly at a relatively lower cost [5–8].

1.2 Towards Rubber Properties

Rubber comes in the category of elastomers and according to Berins [2] an elastomer is capable of rapid elastic recovery after being stretched to at least twice its length at room temperature at any humidity. Due to the ease of deformation [3], softness and hardness, rubbers resist corrosion and erosion and have equal importance as that of steel. Rubbers exhibit excellent properties like low thermal expansivity and the properties become more pronounced during vulcanization or interlinking by sulphur. The structure of rubber is a 3D zigzag with freely rotating bonds that allow the polymer chains to change their length by coiling or uncoiling. During heating the rubber chains rotate freely and thus coil or uncoil without changing the internal energy unlike most solids which expand in volume upon the application of thermal energy. This allows stretching and un-stretching of the rubber without any change in the internal energy. However upon stretching rubber experiences a restoring force, which is entropic in nature (as rubber pulls back to a disordered state at maximum entropy). Stretching align the rubber chains into a more ordered state with lower entropy [6].

In elastomers weak intermolecular forces exist and they undergo immediate, linear and reversible response to high strain to an applied force. This response is

analogous to the movement of a spring according to Hooke's Law. The parallel spring and dashpot model explains viscoelasticity as non-linear, time dependent mechanical response. An ideal elastomer only exhibits an elastic response whereas in the real elastomer case both viscoelastic and elastic responses are seen especially at higher strains. Depending on the mechanical response the chemical structure and molecular architecture of elastomers change considerably. The application of high strain to the elastomers uncoils the random molecular coils and aligns them into more linear conformations. When molecules are in fully extended conformations uncoiling of chain segments occurs and this limits the elastic response. The elastomer macromolecules have flexible chains and so it responds immediately and reversibly. This explanation is valid at ambient conditions of temperature as the elastomer properties vary at temperatures below the glass transition. The viscous flow occurring in elastomers at high extensions and under strain for longer times is called creep. All these behavior of elastomer chains is observed if the polymer is uncrosslinked. But chemical cross-linking prevents the molecular movement and the unstrained shape of an elastomer cannot be altered and the elastomer cannot be reprocessed or recycled once crosslinked. This fact is considered to be a disadvantage for rubber applications [8–15].

1.3 Rubber Nanocomposites

Rubber however has some limitations such as swelling in oils, ageing, ozone attack, and attack by flame, although most of them can be overcome to a great extent by compounding techniques and with the use of specialty synthetic rubbers. Therefore various kinds of fillers such as metal oxides, carbon black, silica particles, graphitic particles and carbon nanotubes are usually employed for their effective reinforcement. Upon the incorporation of stiff fillers into elastomers, the stiffness enhances while retaining the important attributes of large strain resilient behavior and large strain-to break. Fillers improve the processability, increase the toughness, fracture resistance and stress transfer in elastomers. Filler reinforcement provides fabrication of stronger, lighter or less expensive composites than their traditional neat counterparts. Due to very small size and large surface area and hence surface properties, nanoparticles play an important role as fillers. In nanocomposites, a stronger filler/matrix interaction at the interface exists which leads to a more immobilized rubber shell compared with filler particles of micro dimensions. In compounds containing filler with identical surface area and chemical nature but different shape the storage modulus increases with increase in anisometry. Additive effects of the physical and chemical crosslinks of the chains play an important role at the beginning of the deformation and give higher modulus than pure elastomer [5, 6]. Though rubbers are thermal and electrical insulators, incorporation of conductive fillers could produce conducting composite materials as well. Thus the study of viscoelasticity in case of rubber composites is of much importance and this is indeed the aim of this book.

2 Viscoelasticity

2.1 Non-linear Viscoelasticity

Material behavior can be time dependent or independent and the time dependent behavior is often referred to as linear viscoelasticity. This can be explained based on some equations. Suppose σ1 is the constant load applied to a viscoelastic specimen, then ε1 gives the time dependent strain. After a particular time when the load is removed the specimen tries to recover back and then ε2 becomes the time dependence of the strain upon a larger stress σ2. If t1 and t2 represent the time after loading, ε1 and ε2 are linear strains corresponding to the stresses, σ1 and σ2. Here the stress strain relationship can be given by Eq. (1).

$$\frac{\varepsilon_1(t_1)}{\sigma_1(t_1)} = \frac{\varepsilon_2(t_1)}{\sigma_2(t_1)}, \quad \frac{\varepsilon_1(t_2)}{\sigma_1(t_2)} = \frac{\varepsilon_2(t_2)}{\sigma_2(t_2)} \tag{1}$$

Also at an arbitrary time t, the strains at the two stresses can be expressed as

$$\frac{\varepsilon_1(t)}{\sigma_1(t)} = \frac{\varepsilon_2(t)}{\sigma_2(t)} \tag{2}$$

In a general way the ratio of strain to stress at a certain time is expressed as creep compliance D(t) as shown in Eq. (3).

$$D(t) = \varepsilon(t) \,/\sigma(\mathrm{t}) \tag{3}$$

When this condition is satisfied it is mentioned as linear viscoelasticity. The linear range is marked by the independency of compliance upon stress which is well illustrated in Fig. 1. The transition from linear to nonlinear viscoelasticity is also shown in the figure.

Over time rubber products undergo wear and tear. Technologically this occurrence is mentioned as softening or loss in stiffness and is due to the viscoelasticity and viscoplasticity of the polymer matrix and time-dependent damage growth. The latter covers all microstructural changes such as matrix cracking, fiber/matrix debonding and shear yielding as well as the large scale damages such as transverse cracking, fiber breakage, delamination and catastrophic failure. Since these facts affect the durability of the rubber products a good survey of the reasons behind the softening behavior as well as the ways to eliminate it is very necessary. The material behavior like viscoelasticity, plays a crucial role in the products design and durability as the microstructural changes or damages affect both elastic [4, 5] and viscoelastic [5–8] components of the polymer/rubber. The cracking or damage is time or rate-dependent and thus nonlinear in nature [6–8]. In order to have a thorough understanding about the fabrication, characteristics and durability of rubber products the study of non linear viscoelasticity is very significant. The

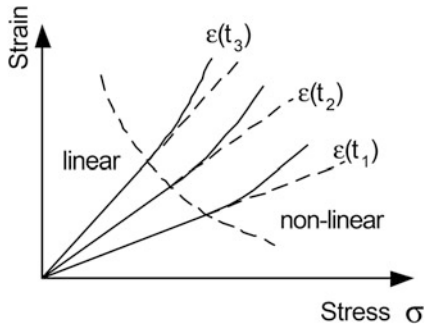

Fig. 1 Linear–nonlinear transition of stress strain relationship with respect to different time levels [16]

study of this effect—both experimental measurements and theoretical studies based on mathematical modeling—would greatly simplify the characterization process [9].

It was Green and Adkins who first derived the general non-linear theory for membrane deformation [10]. Following this many authors addressed the viscoelastic effect and the deformation behavior in rubbers. In the 1960s, Hart-Smith and Crisp [11] and Klingbeil and Shield [12] examined the axisymmetrical hyperelastic membranes for investigating the large deformations in rubber. They have used different hyperelastic non-linear constitutive equations to propose analytical solutions for the circular plane membrane deformation. The results obtained are compared with experimental data for rubber and found good agreement. In another work, Oden and Sato [13] used the Galerkin finite element method (considering the three-nodes triangular elements and corresponding nonlinear equations) to solve the non-linear elastic membrane problems. Wineman and Feng [14, 15] used semi-analytical time-discretization schemes to solve the time-dependent function of non-linear viscoelastic rubber. Rubber-like materials obey non-linear integral viscoelastic constitutive equations such as Christensen's model which describe the material large strain time-dependent behaviour. It was Shrivastava and Tang [17] who developed a three-dimensional method for such model based on the geometric non-linearities and solved the non-linear equations of equilibrium. A review by Jenkins and Leonard explains the dynamic deformation by considering the effect of membrane inertia [18–20]. All the studies are done by applying internal pressure to the membranes under large strains to create deformation and then checking the dynamic responses. The results are then compared with the theoretical solutions of hyperelastic and non-linear viscoelastic constitutive equations. The main advantage of the numerical approach is that the fast processes such as thermoforming or blow-moulding can be better simulated.

2.2 Non-linear Viscoelasticity in Rubber Nanocomposites

The non linear viscoelasticity of various particles filled rubber is addressed in range of studies. It is found that the carbon black filled-elastomer exhibit quasi-static and dynamic response of nonlinearity. Hartmann reported a state of stress which is the superposition of a time independent, long-term, response (hyperelastic) and a time dependent, short-term, response in carbon black filled-rubber when loaded with time-dependent external forces. The short term stresses were larger than the long term hyperelastic ones. The authors had done a comparative study for the non linear viscoelastic models undergoing relaxation, creep and hysteresis tests [20–22]. For reproducible and accurate viscoelastic parameters an experimental procedure is developed using an ad hoc nonlinear optimization algorithm.

The time dependence of the matrix properties greatly enhances when the material undergoes adverse environmental conditions. The stresses cause matrix cracking, softening and fiber-matrix debonding leading to premature structural failure of the fibers, and thus shortening the life of the structure. A theoretical study of these effects was done in the work of Schapery [23, 24], and good experimental techniques and testing methodologies are later developed by some other groups. The initial constant stress and constant stress-rate tensile response of the rubber-glass composite are derived at various temperatures to see the temperature dependence of the damage growth rate. A nonlinear rate-dependent behavior is observed during the first loading of the material due to damage and thus the intrinsic viscoelasticity of the polymer matrix is obtained [25, 26]. The authors found that the study of stress and time dependence depend on the fiber angles and layups and also proposed a quasi-elastic constitutive equation for constant stress and strain rate conditions. Different fiber properties are taken into account using the semi-empirical Halpin-Tsai equations and the importance of this study lies in the tremendous applications of a glass reinforced rubber composite.

2.3 Modeling

The dynamic properties of filled rubbers are widely studied by many researchers in this field of which the contribution made by Payne is the most significant. The dependence of strain amplitude on the storage modulus in filled rubbers is known as the “Payne effect” [27]. At a strain more than 0.1 %, the storage modulus of filled rubber collapses from a plateau value of $G'0$ to a minimum value $G\infty'$ and this decrease is accompanied by a maximum of the loss modulus, G''. The variation in this storage modulus value with respect to the minimum value is called amplitude of the Payne effect, and this increases with the filler content, specific surface and properties of the filler and its dispersion within the matrix. The amplitude inversely changes with temperature. A lot of investigations were performed in order to explain the Payne effect and reasons behind it. Payne neglected the contribution

of the pure polymer matrix towards the effect in his explanations. He assumed the formation of a three-dimensional network structure by the filler particles (carbon black) within the rubber matrix which significantly influences the dynamic viscoelastic properties.

Both filler structure based and debonding theories depend on specific filler characteristics such as surface treatment and thus difficult to distinguish experimentally. The dynamic storage and loss moduli are dependent on the dynamic strains only and independent of a simultaneous static strain [28]. The stress strain curves are also independent of a fully equilibrated static strain. The initial modulus in the constant strain rate test is highly rate dependent whereas the terminal modulus is constant with strain rate. Thus the Payne effect would vanish at lower frequencies 10^{-6}–10^{-5} Hz. The imposition or removal of a static strain/large amplitude dynamic strain causes a subsequent reduction of the storage modulus at low strain that is fully recoverable independent of the nature of disturbance. Both cross-linked elastomers and un-cross-linked polymer melts display similar filler effects on dynamic mechanical properties. For polymer melts the strain amplitude corresponding to the onset of nonlinear behavior is also reduced by the addition of filler, similar to the Payne effect. Micro sized filler particles enhance the dynamic moduli as they could form crosslinks within the polymer. The presence of filler also improves damping. The surface modification of the fillers, volume fraction and the nature of strain amplitude can also affect the moduli. For instance fillers can form weak structures or agglomerations when their sizes are too small, and it is sometimes difficult to distinguish this from filler networks. The network formation by the filler particles can be related to the percolation phenomenon observed in composite systems. i.e. the crosslinks are formed among the particles when the filler concentration is higher than a particular percolation concentration. Below the critical value of loading the contribution of filler networking to low strain mechanical behavior becomes minor. The lowest filler concentration used in Payne's work was 28 vol% for the carbon black whereas for nanocomposites sometimes this value drop as low as 0.05 %. But in short neither filler agglomeration nor network formation is a prerequisite for nonlinear behavior. In addition, the influence of the interface on far-field matrix behavior may be a significant factor in high molecular weight polymers.

Three main mathematical models were derived subsequently in order to explain the Payne effect, of which the one proposed by Kraus stands first [28]. The Kraus model assumes the formation of agglomeration of filler aggregates due to the existing Van der waal's interaction between the particles. The increase in strain amplitude causes deagglomeration kinetics thereby decreasing the storage modulus. This model was further developed by Huber and Vilgis [29] who suggested the dependence of storage modulus on fractal dimensions and the connectivity of the network, and by Kluppel, who introduced the cluster formation [30, 31]. However these concepts do not take in to account the temperature and the frequency dependence of the amplitude of Payne effect. Another criticism was made by Funt [32] who argued the non existence of continuous filler networks within the material with the help of electrical conductivity measurements. Moreover most of

the studies on filler-structure effects were carried out at high volume fractions of fillers and thus the nonlinear viscoelastic behavior at low filler contents should be explored.

In their work, Maier and Goritz proposed the dynamics of adsorption/desorption of the polymer chains at the particle surface [33] and the Payne effect is due to the stress-induced debonding of polymer chains from the filler surface. They derived simple set of equations as well to account for the decrease of storage and loss moduli with strain; however they failed to explain certain other rheological features of the composites. Zhu and Sternstein suggested the polymer-filler interactions including trapped topological entanglements are responsible for the reduction in storage modulus with strain [34, 35]. The polymer filler interfacial interactions vary according to the nature of the polymer-filler interface [36–39]. Maier and Goritz considered the filler particles as multifunctional cross-links which can loosely or strongly anchor to the rubber surface [33, 40]. Thus the amplitude of Payne effect depends on the crosslink density as the loosely tied chains desorb with increase in strain. The mechanism of Payne effect also involves the existence of cooperation between the breakdown and reformation of the filler network and the molecular disentanglement of the bound and free rubber [32, 40, 41].

The bonding and debonding between polymer chains and filler surfaces and its effects on viscoelasticity have been studied and modeled [42, 43]. The studies on the rheology of unfilled polymers could address adhesion and adhesive failure, friction, and flow instabilities such as melt fracture, which can also be explored for filled systems as well. Leger and co-workers [44] showed polymers slip on a flat surface when sheared, regardless of the shear rate. There is a chance of a complex disentanglement process between the tethered chains and the bulk polymer and this develops with respect to shear rate. At sufficiently high strain rates, dynamic decoupling occurs. According to Graham [45], the slip at polymer/filler interface includes the effects of drag on polymer chains, disentanglement, and detachment and reattachment of chains at the solid surface. In composites the entanglements are more and this affect the particle diffusivity in a polymer matrix. The geometrical confinements enhance entanglement interactions between polymer chains even in the case of weak adsorption [46, 47]. In a general way we can say that the filled (cross-linked) elastomers and filled (un-cross-linked) polymer melts show similar nonlinear viscoelastic behavior with respect to both strain and filler characteristics. In both cases, the entanglements are due to topological restraints (e.g. chemical cross-links) or hydrogen bonding interactions. Thus both unfilled and filled elastomers have a common mechanism regarding the origin of the nonlinear viscoelasticity.

Yatsuyanagi et al. [48] considered the existence of a percolation network through a rigid amorphous layer formed around the particles and desorption and adsorption of this layer happens during the Payne effect. It is also proposed that a glass transition gradient exist near the surface of the filled polymer and that the dynamics could be either enhanced or slowed down according to the interaction of the chains with the surface [49, 50]. Montes et al. observed a maximum of reinforcement when a continuous path is formed through the filler aggregates

[51]. In their work, Merabia et al. [52] modeled the Payne effect by considering that the stress is supported mainly by the glassy bridges in a direction normal to the stress. The effect is explained as the local lowering of the glass transition when stress is applied near the aggregates. Here a plasticizing effect is observed which induces the formation of glassy bridges and collapses the storage modulus. Bokobza checked the rheological behavior of elastomers by adding conventional fillers such as carbon black and silica and found an increase in the modulus. She has explained this effect as due to the inclusion of rigid filler particles and increase in polymer–filler interactions and cross-link density [53]. In short the Payne effect can be related to the destruction of filler network [54], filler deagglomeration [55], polymer desorption from filler surface [34], and strain softening of polymer shell surrounding fillers [56].

Cadambi et al. [57] studied the viscoelastic behavior of nanotubes filled hydrogenated nitrilebutadiene rubber by dynamic mechanical thermal analysis and found that the incorporation of nanotubes enhanced the storage modulus while reducing the glass transition temperature. Das et al. [58] achieved a good dispersion of multiwalled carbon nanotubes in a 50:50 blend of styrene–butadiene and butadiene rubber and observed decrease in intensity of tan δ peak as well as enhanced storage modulus above the glass transition. Similar results were also found for single-walled carbon nanotubes filled natural rubber composites [59].

Another dynamic effect common in filled rubber systems is the stress softening effect or "Mullins effect". This is observed at high extensions and characterized by a pronounced decrease in the stress when the filled vulcanizate is stretched for a second time [56]. This effect is related to the rubber network and filler network as well, which can be considered as a hysteretic mechanism related to energy dissipation by the material during deformation [55]. Stress softening is observed for CNTs filled natural rubber [60] and Bhattacharya et al. [61] studied this behavior by loading–unloading cycles. A strong stress-softening effect is noticed especially at 8.3 wt% of oxidized nanotube loading. Carboxylated multiwalled carbon nanotubes filled natural rubber also showed significant stress-softening effect [62]. Chen et al. studied both viscoelastic [63] and stress-softening behavior [64] of EPDM/zinc dimethacrylate composites. Subramaniam et al. [65] prepared conducting chloroprene rubber/imidazolium-based ionic liquid modified multi walled carbon nanotube composites and observed similar trends in viscoelasticity and stress-softening. Since chloroprene rubber shows relatively high polarity, and therefore, better affinity to polar fillers, the nonpolar carbon nanotubes are modified. They have found that ionic liquid modification on nanotubes greatly enhances the viscoelastic properties of the composites.

3 Conclusion

As the first chapter of the book, the aim of this chapter is to give a brief introduction about the non linear viscoelastic behavior of rubber and its composites. The term viscoelasticity and stress softening usually observed in all elastomer systems are

introduced by giving importance to the modeling. The most significant parameter called Payne effect (decrease in storage modulus with strain) in rubber is explained well. A detailed survey of all kinds of nanocomposites and their viscoelastic responses can be seen in the following chapters of this book.

References

1. Ponnamma D, Chirayil CJ, Sadasivuni KK, Somasekharan L, Yaragalla S, Abraham J, Thomas S (2013) Special purpose elastomers: synthesis, structure-property relationship, compounding, processing and applications. Advances in elastomers I. Adv Struct Mater 11:47–82
2. Berins ML (1991) Plastics engineering. Handbook of the Society of Plastics Industry Inc. Chapman & Hall, New York
3. Hishfeld P (1937) Trans Am Soc Mech Eng 59:471
4. Schapery R (1987) Deformation and fracture characterization of inelastic composite materials using potentials. Polymer Eng Sci 27:63–76
5. Schapery R (1990) On some path independent integrals and their use in fracture of nonlinear viscoelastic media. Int J Fract 42:189–207
6. Park S, Schapery R (1997) A viscoelastic constitutive model for particulate composites with growing damage. Int J Solids Struct 34:931–947
7. Ha K, Schapery R (1997) A three-dimensional viscoelastic constitutive model for particulate composites with growing damage and its experimental validation. Int J Solids Struct 35:3497–3517
8. Abdel-Tawab K, Weitsman Y (1998) A coupled viscoelasticity/damage model with application to swirl-mat composites. Int J Damage Mech 7:351–380
9. Bocchieri R (2001) Time-dependent deformation of a nonlinear viscoelastic rubber-toughened fiber composite with growing damage. Ph.D. thesis, The University of Texas at Austin
10. Green AE, Adkins JE (1960) Large elastic deformations. Clarendon, Oxford
11. Hart-Smith LJ, Crisp JDC (1967) Large elastic deformations of thin rubber membranes. Int J Eng Sci 5:1–24
12. Klingbeil WW, Shield RT (1964) Some numerical investigations on empirical strain energy functions in the large axisymmetric extensions of rubber membranes. Zeitschrift ur Angewandte Mathemathik und Physik 15:608–629
13. Oden JT, Sato T (1967) Finite strains and displacements of elastic membranes by the finite element method. Int J Solids Struct 3:471–488
14. Wineman A (1978) On axisymmetric deformations of nonlinear viscoelastic membranes. J Non-Newtonian Fluid Mech 4:249–260
15. Feng WW (1992) Viscoelastic behavior of elastomeric membranes. J Appl Mech 59:S29–S34
16. Long term performance of polymers. http://www.me.umn.edu/labs/composites/Projects/Polymer%20Heat%20Exchanger/Creep%20description.pdf
17. Shrivastava S, Tang J (1993) Large deformation finite element analysis of non-linear viscoelastic membranes with reference to thermoforming. J Strain Anal 28(1):31–51
18. Jenkins CH, Leonard JW (1991) Nonlinear dynamic response of membranes: state of the art. Appl Mech Rev 44(7):319–328
19. Jenkins CH (1996) Nonlinear dynamic response of membranes: state of the art update. Appl Mech Rev 49(10):S41–S48
20. Hartmann S (2001) Numerical studies on the identification of the material parameters of Rivlin's hyperelasticity using tension-torsion tests. Acta Mech 148(1–4):129–155
21. Hahn HT, Tsai SW (1973) Nonlinear elastic behavior of unidirectional composite laminae. J Comp Mater 7:102–118

22. Schapery RA, Sicking DL (1995) On nonlinear constitutive equations for elastic and viscoelastic composites with growing damage. In: Baer A (ed) Mechanical behavior of materials. Delft University Press, Delft, pp 45–76
23. Schapery RA (1997) Nonlinear viscoelastic and viscoplastic constitutive equations based on thermodynamics. Mech Time Depend Mater 1:209–240
24. Schapery RA (1999) Nonlinear viscoelastic and viscoplastic constitutive equations with growing damage. Int J Fract 97:33–66
25. Mienerv LA, Schaoerv RA (1991) Viscoelastic and nonlinear adherend effects in bonded composite joints. J Adhes 34:17–40
26. Schapery RA (1989) Mechanical characterization and analysis of inelastic composite laminates with growing damage. Mech Comp Mater Struct 100:1–9
27. Payne AR (1965) Reinforcement of elastomers. J Appl Polym Sci 8:2661–2680
28. Kraus G (1984) Mechanical losses in carbon black filled rubbers. J Appl Polym Sci Appl Polym Symp 39:75–92
29. Huber G, Vilgis TA (2002) On the mechanism of hydrodynamic reinforcement in elastic composites. Macromolecules 35:9204–9210
30. Heinrich G, Kluppel M, Vilgis T (2002) Reinforcement of elastomers. Curr Opin Solid State Mater Sci 6:195–203
31. Kluppel M, Schuster R, Heinrich G (1997) Structure and properties of reinforcing fractal filler networks in elastomers. Rubber Chem Technol 70:243–255
32. Funt JM (1980) Rubber mixing. Rubber Chem Technol 53:772–779
33. Maier PG, Göritz D (1996) Molecular interpretation on the Payne effect. Kautsch Gummi Kunstst 49:18–21
34. Sternstein SS, Zhu AJ (2002) Reinforcement mechanism of nanofilled polymer melts as elucidated by nonlinear viscoelastic behavior. Macromolecules 35:7262–7273
35. Zhu AJ, Sternstein SS (2003) Nonlinear viscoelasticity of nanofilled polymers: interfaces, chain statistics and properties recovery kinetics. Compos Sci Technol 63:1113–1126
36. Marrone M, Montanari T, Busca G, Conzatti L, Costa G, Castellano M, Turturro A (2004) A Fourier Transform Infrared (FTIR) study of the reaction of Triethoxysilane (TES) and Bis [3-triethoxysilylpropyl]tetrasulfane (TESPT) with the surface of amorphous silica. J Phys Chem B 108:3563–3572
37. Castellano M, Conzatti L, Turturro A, Costa G, Busca G (2007) Influence of the silane modifiers on the surface thermodynamic characteristics and dispersion of the silica into elastomer compounds. J Phys Chem B 111:4495–4502
38. Clement F, Bokobza L, Monnerie L (2005) Investigation of the Payne effect and its temperature dependence on silica-filled polydimethylsiloxane networks. Part I: Experimental results. Rubber Chem Technol 78:211–231
39. Ramier J, Gauthier C, Chazeau L, Stelandre L, Guy L (2007) Payne effect in silica-filled styrene–butadiene rubber: influence of surface treatment. J Polym Sci B Polym Phys 45:286–298
40. Cassagnau P (2003) Payne effect and shear elasticity of silica-filled polymers in concentrated solutions and in molten state. Polymer 44:2455–2462
41. Sun J, Song Y, Zheng Q, Tan H, Yu J, Li H (2007) Nonlinear rheological behavior of silica filled solution-polymerized styrene butadiene rubber. J Polym Sci B Polym Phys 45:2594–2602
42. Wang SQ, Inn YW (1994) Stress-induced interfacial failure in filled polymer melts. Rheol Acta 33:108–116
43. Simhambhatla M, Leonov AI (1995) On the rheological modeling of filled polymers with particle-matrix interactions. Rheol Acta 34:329–338
44. Leger L, Raphael E, Henet H (1999) Surface-anchored polymer chains: their role in adhesion and friction. Adv Polym Sci 138:185–225
45. Yarin AL, Graham MD (1998) A model for slip at polymer/solid interfaces. J Rheol 42:1491

46. Granick S, Hu H (1994) Nanorheology of confined polymer melts. 1. Linear shear response at strongly adsorbing surfaces. Langmuir 10:3857–3866
47. Peanasky J, Cai LL, Granick S (1994) Nanorheology of confined polymer melts. 3. Weakly adsorbing surfaces. Langmuir 10:3874–3879
48. Yatsuyanagi F, Kaidou H, Ito M (1999) Relationship between viscoelastic properties and characteristics of filler-gel in filled rubber system. Rubber Chem Technol 4:657–672
49. Berriot J, Lequeux F, Montes H, Monnerie L, Long D, Sotta P (2002) Filler–elastomer interaction in model filled rubbers, a ^{1}H NMR study. J Non Cryst Solids 307:719–724
50. Berriot J, Montes H, Lequeux F, Long D, Sotta P (2003) Gradient of glass transition temperature in filled elastomers. Europhys Lett 64:50–60
51. Montes H, Lequeux F, Berriot J (2003) Influence of the glass transition temperature gradient on the nonlinear viscoelastic behavior in reinforced elastomers. Macromolecules 36:8107–8118
52. Merabia S, Sotta P, Long DR (2008) A microscopic model for the reinforcement and the nonlinear behavior of filled elastomers and thermoplastic elastomers (Payne and Mullins Effects). Macromolecules 41:8252–8266
53. Bokobza L (2007) Multiwall carbon nanotube elastomeric composites: a review. Polymer 48:4907–4920
54. Zhu ZY, Thompson T, Wang SQ, von Meerwall ED, Halasa A (2005) Investigating linear and nonlinear viscoelastic behavior using model silica-particle-filled polybutadiene. Macromolecules 38:8816–8824
55. Malchev PG, Picken SJ (2007) The strain dependence of the dynamic moduli of short fiber reinforced thermoplastic blends. J Rheol 51:235–260
56. Mullins L (1969) Softening of rubber by deformation. Rubber Chem Technol 42:339–362
57. Cadambi RM, Ghassemieh E (2012) Optimized process for the inclusion of carbon nanotubes in elastomers with improved thermal and mechanical properties. J Appl Polym Sci 124:4993–5001
58. Das A, Stockelhuber KW, Jurk R, Saphiannikova M, Fritzsche J, Lorenz H, Kluppel M, Heinrich G (2008) Modified and unmodified multiwalled carbon nanotubes in high performance solution-styrene–butadiene and butadiene rubber blends. Polymer 49:5276–5283
59. Lopez-Manchado MA, Biagiotti J, Valentini L, Kenny JM (2004) Dynamic mechanical and Raman spectroscopy studies on interaction between single-walled carbon nanotubes and natural rubber. J Appl Polym Sci 92:3394–3400
60. Nah C, Lim JY, Cho BH, Hong CK, Gent AN (2010) Reinforcing rubber with carbon nanotubes. J Appl Polym Sci 118:1574–1581
61. Bhattacharyya S, Sinturel C, Bahloul O, Saboungi ML, Thomas S, Salvetat JP (2008) Improving reinforcement of natural rubber by networking of activated carbon nanotubes. Carbon 46:1037–1045
62. Datta S, Naskar K, Bhardwaj YK, Sabharwal S (2011) A study on dynamic rheological characterisation of electron beam crosslinked high vinyl styrene butadiene styrene block copolymer. Polym Bull 66:637–647
63. Chen YK, Wang YP, Xu CH (2012) Effects of thermal history on isotactic polypropylene. J Macromol Sci B Phys 51:1921
64. Chen YK, Xu CH (2011) Specific nonlinear viscoelasticity behaviors of natural rubber and zinc dimethacrylate composites due to multi-crosslinking bond interaction by using rubber process analyzer 2000. Polym Compos 32:1593–1600
65. Subramaniam K, Das A, Heinrich G (2011) Development of conducting polychloroprene rubber using imidazolium based ionic liquid modified multi-walled carbon nanotubes. Compos Sci Technol 71:1441–1449

Nonlinear Viscoelasticity of One Dimensional Filler Reinforced Elastomer Composites

Karun Kumar Jana, Mrinal Patel, Dipak Rana, and Pralay Maiti

Abstract In this chapter, we review the elastomeric composites with different types of one dimensional nanofillers e.g. nanotubes, nanorods and nanofibers. Various elastomers and nanofillers have been considered along with the preparation methods of the composites. The dispersion level and surface morphologies have been reported having various fillers and how do they vary with the chemical modifications on the filler along with the effect of dispersing agent. The improvement in thermal and mechanical properties including dynamic mechanical properties of elastomers has been discussed in presence of one-dimensional nanofillers. Viscoelasticity has been reviewed for elastomeric systems and, especially, how the non-linearity appears in presence of one-dimensional filler. Rheological properties including curing kinetics, storage and loss modulus, and complex viscosities as a function of frequency of the nanocomposites have been discussed in detail. Dynamic mechanical studies related to various elastomer nanocomposites with various one dimensional fillers have been reported with possible explanations. The influence of the nature of fillers with their chemical modifications of one-dimensional filler on the viscoelasticity has also been assessed.

Keywords Elastomer • One-dimensional nanofiller • Viscoelasticity

1 Introduction

The unique properties of elastomers particularly their durability and reversible high deformation are of enormous industrial importance [1, 2]. To improve the resilience and strength of rubber material further, extensive use of different types of filler materials have been considered for last few decades. Nanometer dimension fillers having large surface areas have added advantages with greater interactions at the

K.K. Jana • M. Patel • P. Maiti (✉)
School of Materials Science and Technology, Indian Institute of Technology (BHU), Varanasi 221 005, India
e-mail: pmaiti.mst@itbhu.ac.in

D. Rana
Industrial Membrane Research Institute, Department of Chemical and Biological Engineering, University of Ottawa, 161 Louis Pasteur St., Ottawa, ON KIN 6N5, Canada

D. Ponnamma, S. Thomas (eds.), *Non-Linear Viscoelasticity of Rubber Composites and Nanocomposites*, Advances in Polymer Science 264, DOI 10.1007/978-3-319-08702-3_2

interfaces [3–12]. Reinforcement with one dimensional fillers like nanotubes, nanorods and nanofibers have the largest surface area per unit volume and plays the crucial role to increase the strength, abrasion resistance, cracking resistance, thermal, gas barrier, structural properties, conductivity and viscoelasticity by increasing the interfacial area [13–17]. This outstanding advantage of properties improvement is due to the filler network and interactions between elastomer and filler. Most of the one dimensional filler based composites of modern era have been focused on the percolation thresholds, minimum loading of the filler to achieve significant improvement of the properties of the matrix phase [18]. However, several thermoplastic elastomers behave differently because of their nonlinear responses induced by various factors such as high deformation and stress softening effect, but, it is important from the application point of view that it combines the characteristics of both rubber and plastic for typical engineering material [19]. Rubber composites reinforced with different fibers are extensively used in many industrial products in automobiles, seal components, screen nets and tyre treads [20, 21]. Carbon based nanofillers like carbon nanotube (CNT), carbon nanofiber (CNF) and carbon nanorods are important class of reinforcing material amongst one dimensional fillers to make a composite with rubber/elastomers due to the high aspect ratio and other outstanding physical properties [22, 23]. The properties of the filled composites mainly depend on the shape, size and concentration of the filler along with its chemical functionalization [24, 25]. However, nanotechnology has been implemented using nanofillers to make composites of elastomers for last two decades [26–28]. For elastomeric composites, the curing reactions play a multifaceted role due to occurrence of many reactive processes simultaneously [29]. Viscoelasticity is an important property of polymeric materials that demonstrates both viscous and elastic character when undergoes deformation. Viscous materials favours shear flow and strain linearly with time when a stress is applied. Elastic materials strain under stress and quickly return to its original state once the stress is removed. Viscoelastic materials combine both elastic and viscous component together making this class of materials unique. Further, when fillers are added to elastomers, is properties alter dramatically especially in presence of nanometer dimension fillers.

2 Different Elastomers

An elastomer is a viscoelastic polymer having low Young's modulus and high elongation at break. Elastomers are amorphous in nature and exist above their glass transition temperature, so that considerable segmental motion is possible. Generally, two types of rubbers have been classified based on their origin; natural and synthetic rubbers and the synthetic rubbers are derived mostly from petroleum byproducts. Elastomers are also categorized structurally into two types (1) unsaturated rubber e.g. cis-1,4-polyisoprene; natural rubber (NR) and trans-1,4-polyisoprene gutta-percha, synthetic polyisoprene, polybutadiene (BR), chloroprene

rubber (CR), butyl rubber (copolymer of isobutylene and isoprene, IIR), halogenated butyl rubbers (chloro butyl rubber: CIIR; bromo butyl rubber: BIIR), styrene-butadiene rubber (copolymer of styrene and butadiene, SBR), nitrile rubber (copolymer of butadiene and acrylonitrile, NBR), etc. which can be cured by sulfur vulcanization and, (2) saturated rubbers e.g. EPM (ethylene propylene rubber), EPDM rubber (ethylene propylene diene rubber, a terpolymer of ethylene, propylene and a diene-component), epichlorohydrin rubber (ECO), polyacrylic rubber (ACM), silicone rubber (SR), fluorosilicone rubber, ethylene-vinyl acetate (EVA) etc.

3 One-Dimensional Fillers

Fillers are classified depending on their shapes and sizes which dramatically alter the properties when mixed with the elastomeric matrix to prepare a composite. When the size of the filler is reduced to nanometer dimension (at least one dimension in the range of 1–100 nm) it is called nano-filler and depending on the confinement of the filler's coordinates it is classified into (1) zero dimensional, all three coordinates are confined, (2) one-dimensional, confinement of any two coordinates, (3) two-dimensional, one coordinate is confined and, (4) three-dimensional, no confinement of any dimension. Therefore, the one-dimensional filler is having only one dimension (length) and other two dimensions are confined to few nanometers making these fillers with highest aspect ratio. Generally, three types of fillers are well known for one-dimensional fillers e.g. nanotube, nanorod and nanofiber.

3.1 Nanotube

Amongst the nanotubes, CNT is widely used and is available with different dimensions. Depending on the number of layers in the side wall it is categorized as single-walled carbon nanotube (SWCNT) and multi-walled carbon nanotube (MWCNT) and can have very large length up to few microns [30, 31]. There are currently at least five methods for producing CNTs: (1) arc discharge [32], (2) chemical vapor deposition (CVD) [33], (3) laser ablation [34], (4) high pressure carbon monoxide (HIPCO) [35], and (5) surface mediated growth of vertically-aligned tubes by plasma enhanced chemical vapor deposition (PECVD) [36]. CNTs have nanoscale dimension ranging from 1 to 100 nm in diameter and having a cylindrical shape containing outstanding optical, thermal conductivity, mechanical and electrical properties with high aspect ratio, suitable for extensive nanodevices. It has conjugated skeleton, appropriate for chemical reaction, making it unique for functionalization through the covalent attachment of chemical groups, and thereby alter the CNTs suitable for easy dispersion and/or soluble in liquids/polymer matrices [37]. CNT derivatives result in 'doping' of a nanotube that changes its

electronic properties. In other words, derivatization can alter the properties of pristine CNT in a tailor made manner. Similarly, gallium nitride (GaN) nanotubes are used for nanoscale electronics, biochemical sensing and in general optoelectronics applications [38].

3.2 Nanorod/Nanowire

Nanorod/nanowire is basically a solid cylinder with the morphology of nanoscale object each of their dimension ranging from 1 to 100 nm. They are synthesized from metals or semiconducting materials with the aspect ratios of 3 to 5. Nanorods/nanowires are produced by chemical synthesis or a combination of ligands acting as shape control agents and bond to different facets of the nanorods with different strengths. This allows the different faces of the nanorod to grow at different rates, producing an elongated nanostructural object like long sticks with a nanoscale dimension having a large length. Zinc oxide (ZnO) nanorods have been used to fabricate nano-scale electronic devices, including field effect transistor, ultraviolet photo-detector, Schottky diode and light-emitting diode. Nanorods of gold, copper, alumina, silicon, platinum and nickel are also produced by direct chemical synthesis or electrochemical methods from porous alumina or polycarbonate membrane templates in presence of a surfactant [39–43].

3.3 Nanofibers

Nanofibers are defined as fibers with diameters less than 100 nm. They can be produced by using interfacial polymerization, electrospinning, and force spinning methods. CNFs are graphitized fibers produced by catalytic syntheses. CNF are formed mainly in gas phase during the process of decaying ethane, methane and other hydrocarbon in presence of a catalyst and then purified to remove aromatic hydrocarbons [44]. Inorganic nanofibers can also be prepared from various kinds of inorganic substances through electrospinning technique. Often used ceramic materials with nanofiber morphology are titanium dioxide (TiO_2) [45], silicon dioxide (SiO_2) [46], zirconium dioxide (ZrO_2) [47], aluminum oxide (Al_2O_3) [48], lithium titanate ($Li_4Ti_5O_{12}$) [49], titanium nitride (TiN) [50] or platinum (Pt) [51]. The synthesis of these nanofibers usually consists of two main steps. In the first step, the polymer (organic) nanofibers are created by conventional electrospinning technique and subsequently they are transformed into ceramics by heat treatment. Other production methods include direct drawing from a solution or melt. Potential uses of nanofibers are in the biomedical arena such as artificial organ components, tissue engineering, implant material, drug delivery, and energy applications like Li-ion batteries [52], photovoltaic cells [53], membrane fuel cells [54] and dye-sensitized solar cells [55] etc. (Scheme 1).

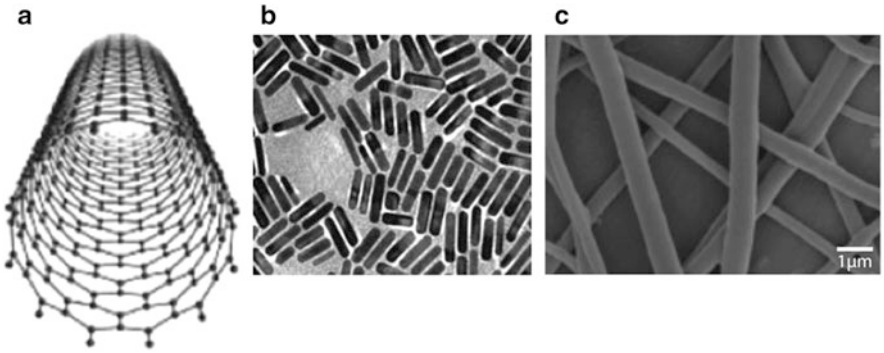

Scheme 1 Schematic representation of an individual (**a**) SWCNT [56], (**b**) transmission electron microscopy images of MTAB functionalized gold nanorods, (**c**) SEM images of PU nanofiber composite. Scale bars: 1 μm [57]

4 Nanocomposites

The general class of rubber nanocomposites has attracted many researchers due to their unique properties. Composites are two phase materials; matrix component holding the other constituent, which in turn is responsible for the reinforcement of the matrix often called filler. When the size of the filler used is of the order of nm dimension, it is called as 'nanocomposite'. Nanocomposites differ from conventional composites by exhibiting better properties than expected from the additive/mixture rule; so called synergistic effect, appears due to exceptionally high surface to volume ratio of the reinforcing phase and/or its exceptionally high aspect ratio [58–61]. Large quantity of filler in conventional composites, required to create a sufficient interface, is now replaced with a few percentages of nanofiller which are able to generate in nanocomposites and, thereby improve the efficacy of the system. It is well known that many rubber nanocomposites with their improved properties are being used nowadays in various products.

4.1 Preparation of Nanocomposites

Several methods have been reported to prepare elastomer nanocomposites. The preparation techniques are divided into three types based on the elastomer and processing conditions.

4.1.1 Solution Casting Method

The nanocomposites of elastomers were prepared through solution route by dissolving elastomer in the dispersion of 1D filler. Shankar et al. has prepared

rubber MWCNT composite using solution casting [62]. Purified Halloysite (aluminosilicate nanotube) is mixed with NR (ISNR-20) in the proportion 1:10 using toluene as a solvent at an elevated temperature. Lima et al. fabricated thermoplastic polyurethane (TPU)/MWCNT composites by spray coating [63] after taking exact amounts of the constituents suspended in DMF. The solution was sprayed on to a stainless steel substrate and a solvent evaporation was carried out at 60 °C. Guo et al. have prepared isophoronediisocyanate (IPDI) and poly(diethylene adipate) (PDA) based polyurethane (PU)/MWCNT composites in methyl ethyl ketone (MEK) at 75 °C for 3 h to synthesize NCO-terminated pre-polymer [64]. Chain extender was slowly charged into the system followed by the addition of MWCNTs dispersed in DMF and the reaction condition was maintained at 50 °C for 2.5 h. Sui et al. fabricated NR/CNT nanocomposites prepared through the solution route followed by processing in two-roll mill in presence of ingredients including vulcanizing agent [65]. Thomas et al. made a blend of epoxy resin and acrylonitrile-butadiene-styrene (ABS) containing 3.6 wt% ABS and mixed with dispersed MWCNTs. Subsequently, the mixture was cured at 180 °C using 4,4′-diaminodiphenylsulfone (DDS) [66].

4.1.2 Melt Mixing Method

Melt mixing is an economic and industrially viable method for composite preparation. However, good dispersion in the composite is essential for satisfactory and uniform properties and homogeneous dispersion is usually obtained at a high shear condition [67, 68], usually true for other thermoplastics or using compatibilizers [69]. CNFs and CNTs have enough functional groups which can act as grafting sites and thereafter suitable for their dispersion considerably [70]. Kong et al. explained extrusion as a high volume manufacturing process for fabricating parts with thermoplastic elastomers [71]. Pedroni et al. prepared nanocomposites of styrene-butadiene-styrene (SBS) and MWCNT through melt mixing using a mini-extruder processed at 150 °C and 90 rpm [72]. Nanocomposites of elastomers can also be prepared using open two-roll mill at room temperature [73]. Siengchin et al. reported the water-assisted melt compounding method [74] where nanofillers have been used in the form of water slurry for better dispersion.

4.2 Dispersion in Nanocomposites

The properties of the nanocomposites depend on the level of dispersion of nanoparticle in the elastomer matrices. The dispersion of the nanoparticle can be checked through electron microscope (transmission electron microscope (TEM), scanning electron microscope (SEM)) or atomic force microscopy). Figure 1A shows the TEM bright field images of NR nanocomposites with different concentration (5–16 wt%) of MWCNTs of mean diameter ~13 nm and length of ~20 μm

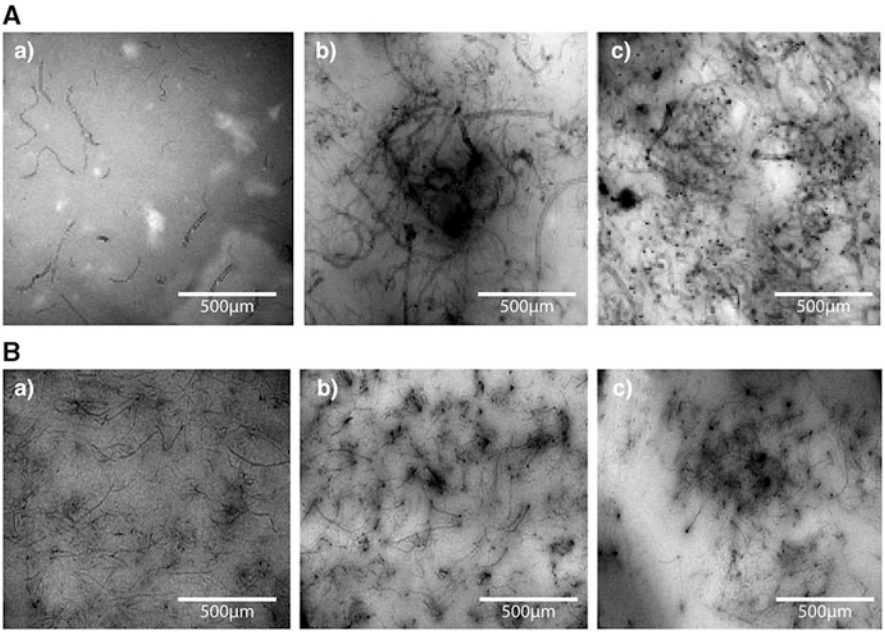

Fig. 1 (**A**) TEM images of the MWCNT/rubber composites containing 5, 9 and 16 wt% of MWNT, respectively [75]. (**B**) 4-phr MWCNTs composites: a′ = MWCNTs/NR, b′ = MWCNTs/SBR, c′ = MWCNTs/EPDM. All the scale bars represent 200 nm [76]

[75]. Three dimensional network is obvious at higher concentration of MWCNTs in the rubber matrix but the overall dispersion is good even at higher percentage of CNT as filler. Good dispersion of different weight percentage of CNT into the various elastomers has been studied in the literature [77, 78]. Cadambi et al. has revealed how to achieve a good level of dispersion of CNTs in the rubber matrix [79]. Figure 1B (a′–c′) compares the dispersion of CNT (similar quantity ~ 4phr) in three different rubber matrices (NR, SBR and EPDM) indicating the best dispersion in NR followed by SBR and EPDM [76]. EPDM being stiffer than the other two rubbers, its dispersion is comparatively inferior as observed from the nanotube bundles in TEM image [80, 81]. However, the level of dispersion depends on the extent of interaction between elastomers and CNTs.

5 Structure and Morphology

5.1 XRD

Most elastomers are amorphous at room temperature unless stretched. Nanofillers being crystalline in nature often exhibit XRD peaks. The presence of nanofillers in

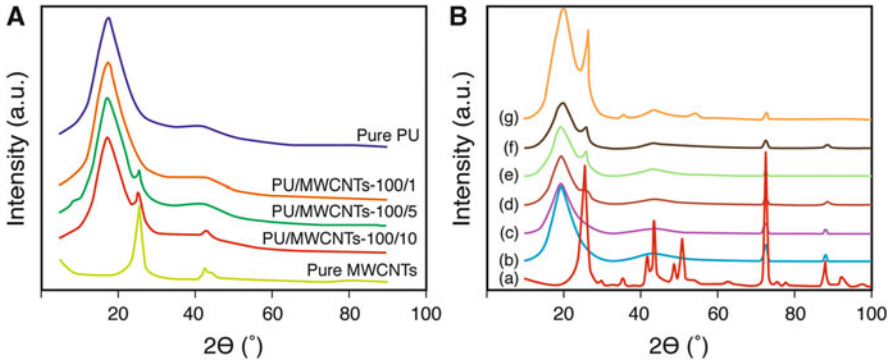

Fig. 2 (**A**) X-ray diffraction patterns of PU, MWCNT and PU/MWCNT composites with different MWCNT loadings [82]. (**B**) X-ray patterns of CNF composites, (a) neat CNF, (b) pure TPU, and (c) 1 wt%, (d) 4 wt%, (e) 7 wt%, (f) 10 wt% and (g) 15 wt% CNF loading TPU/CNF nanocomposites [83]

composite can be confirmed from the prominent peaks corresponding to the nanofiller. The XRD patterns of pure thermoplastic elastomer PU, neat MWCNTs and PU/MWCNT composites are shown in Fig. 2A [82]. Pure PU shows a strong diffraction peak at $2\theta = 17.5^\circ$ presumably due to amorphous halo while the MWCNT has two diffraction peaks at $2\theta = 25.6^\circ$ and 42.8°, corresponding to crystalline graphite. All three peaks are present in the composites indicating the incorporation of small amount of fillers which do not change any structure of matrix or vice-versa. Figure 2B displays the wide angle X-ray diffraction patterns of pure TPU, CNF and their composites with different concentration of CNF. Diffraction peak at $2\theta = 19.75^\circ$ ($d_{110} \sim 4.495$ Å) is consequent to the mixture of both short range ordered usual structure of hard phase and chaotic irregular structure of amorphous phase of TPU matrix [83], while CNF shows an important sharp (002) Bragg's diffraction peak at $2\theta = 25.90^\circ$ ($d_{002} \sim 3.44$ Å) corresponds to the ordered arrangement of different crystal surface of the concentric cylinders of crystalline graphitic carbons [84]. However, for both the cases a minimum amount of filler (5 wt% CNT and 4 wt% CNF) is required to appear for its peak in XRD patterns.

5.2 Surface Morphology

Surface morphology confirms the change in morphology in presence of filler in the composite as evident from the Fig. 3A of SEM images of the poly(styrene-b-ethylene-co-butylene-b-styrene) (SEBS)/MWCNT composites, prepared through melt extrusion technique. MWCNTs are homogeneously dispersed in the SEBS matrix [85] even for higher percentage of fillers. The shear stress overpowers the electrostatic and van der Waals interaction in stacking pattern of the fillers. Torkelson et al. established that an external mechanical force can execute the

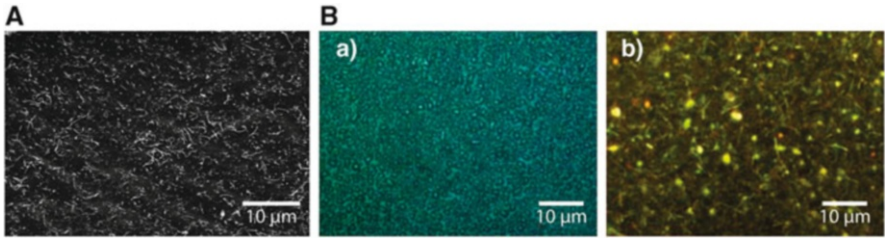

Fig. 3 (**A**) SEM images of poly(styrene-b-ethylene-co-butylene-b-styrene)/MWCNT nanocomposites with nanotube loading of 2.5 wt% [85]. (**B**) Polarizing optical micrographs of (a) neat TPU and, (b) its nanocomposite of 4 wt% CNF [83]

regular dispersion of CNTs in a polymer matrix [86]. However, the entanglement of MWCNTs can be observed forming a suitable nanotube network having at least 2.5 wt% of MWCNTs in the matrix. The biphasic structure and distribution of CNTs in the composites have also been observed by many groups [87].

Polarizing optical microscopy presents the bulk morphology of the materials. Figure 3B displays the neat TPU and its nanocomposites containing 4 wt% CNF. Pure TPU exhibits nice crystallites where globular hard segments are uniformly dispersed within the soft segment of the TPU matrix [83]. However, this type of morphology is hindered in the presence of CNFs. Moreover, a very high aspect ratio of CNF and interaction between TPU and CNF leads to strong interfacial affinity especially towards soft segments zone that compels substantial restriction to the movement of TPU chains causing disruption of crystallite patterns.

6 Thermal Properties

Thermal stability of elastomer can be assessed from the weight loss as a function of temperature. TGA thermograms of pure NR and its composites have been shown in Fig. 4 [65]. Conventional carbon black (CB) dispersed in NR cannot increase the thermal stability of NR while CNT dispersed in NR increase the degradation temperature significantly mainly due to thermal barrier of the nanoparticles. Another reason for this improvement might be due to restriction on the mobilization of rubber macromolecules in presence of CNT and carry out heat homogeneously and avoid heat concentration [88]. On the other hand, Falco et al. has shown similar thermal stability of composites to that of pure SBR with the addition of MWCNT [29].

DSC scans of the elastomer and its composites exhibit glass transition temperature (T_g), melting point and crystallinity. Melting temperature and T_g have not been affected either in presence of conventional filler or nanofillers while heat of fusion or crystallinity considerably decrease in CNT reinforced NR nanocomposite due to interaction between CNTs and rubber matrix [89]. On the other hand, poly

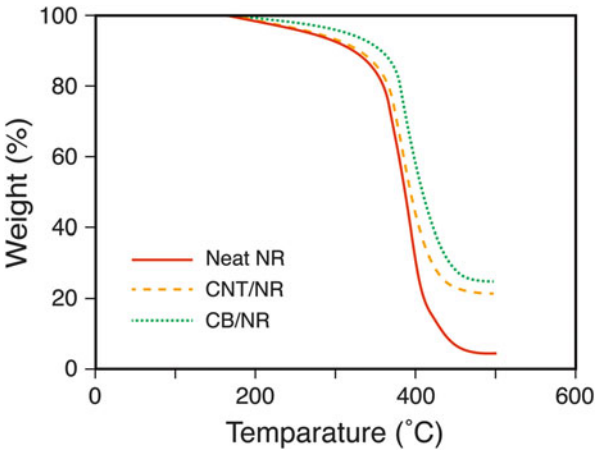

Fig. 4 TGA thermograms of pristine NR and NR composites with carbon black and CNT [65]

(trimethylene terephthalate-b-tetramethylene oxide) elastomer/SWCNT composites exhibit slightly higher melting temperature and crystallinity as compared to pure elastomer [90]. With different weight percentages of CNF, DSC thermograms of neat vistamaxx 6102FL elastomer (VM1) and its nanocomposites exhibit no considerable changes in T_m and heat of fusion [91] where there is no interaction against strong effect observed in thermoplastic systems where specific interactions exist [92, 93].

7 Mechanical Properties

7.1 Tensile Testing

Tensile testing through uniaxial stretching compares the strength of composite against pure elastomer. Figure 5a shows the stress-strain curve of NR composites with different concentration of MWCNT [75]. The modulus increases while elongations at break decrease consistently with increasing filler concentration for all the composites as compared to neat NR indicating CNT as a good reinforcing agent while poor interactions with elastomer lead to the failure at early stage for higher concentration of filler. On the other hand, the improvement in modulus using nanofiller like CNT is significantly higher in comparison to conventional filler like CB of similar concentrations (Fig. 5b) confirming the efficacy of the nanofiller with greater surface area than that of larger particle as filler with relatively lower surface area per unit volume [94]. The high aspect ratio and highly anisotropic nature of nanofiller as compared to macro-filler (CB) helps nanocomposite of elastomer improving the mechanical properties [95, 96]. Substantial improvement in stiffness of the nanocomposites using high-modulus fillers having high aspect ratio have been reported by Paul et al. [97]. Moreover, the tensile strength increased

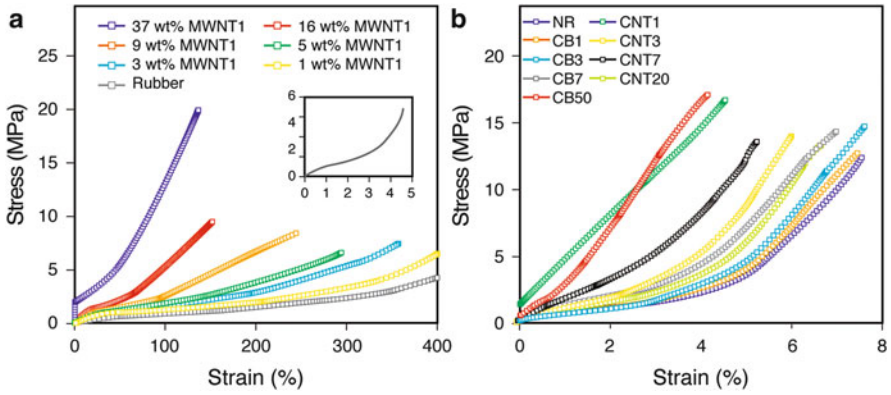

Fig. 5 Stress-strain response of the MWCNT/NR composites under uniaxial tension (**a**) MWNT1/NR composite. The *inset figure* shows a magnified view of NR stress-strain curve [75], and (**b**) comparison of stress-strain curves of NR, NR/CNT and NR/CB composites [94]

considerably with the content of CNT with a corresponding decrease in the elongation at break. Quijano et al. has shown through stress-strain behavior of segmented PU composites that there is a minimum filler concentration required to effectively reinforce the matrix [98].

7.2 *Dynamic Mechanical Analysis*

Dynamic mechanical measurements provide the modulus at a wide temperature range in addition to the loss factor associated with the dynamic strain. The variation of storage modulus and the loss factor (tan δ) measured at 10 Hz in the temperature range of 170–290 K are presented in the Fig. 6a, b for NR composites reinforced with ~8 wt% CNT [99]. The NR exhibits modulus of ~0.6 GPa in the glassy state at low temperature and the elastic modulus rapidly drops by three orders of magnitude with increasing temperature due to an energy dissipation mechanism involving cooperative movement of long chain sequences. The drop in modulus has significantly been reduced in nanocomposites presumably due to restriction imposed by the network of nanoparticles especially in the rubbery region. The loss factor (tan δ) passes through a maximum approximately at 205 K showing the relaxation/glass transition temperature of the samples. Considerable reduction of loss component (tan δ) has been observed with increasing filler concentration in the composite indicating the rigid structure in association with nanofillers. A similar effect is observed in composite of cellulosic whiskers with NR [100]. The reverse trend is usually observed in reinforced composites especially with polymer-2D filler system and was interpreted as a decrease of chain mobility due to interaction with

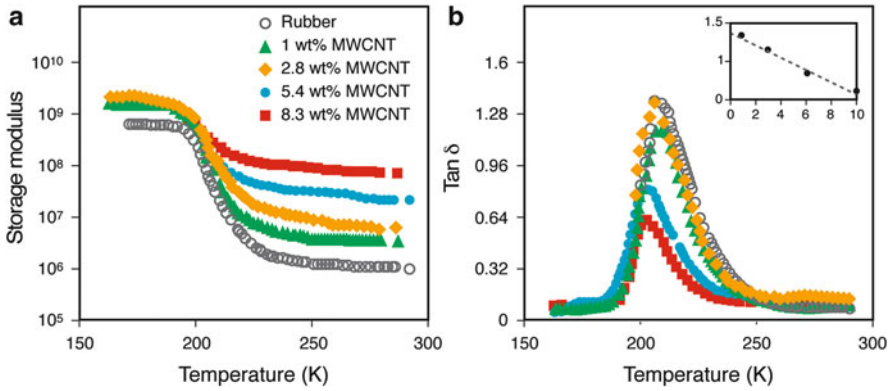

Fig. 6 (**a**) Storage modulus and (**b**) tan δ vs. temperature for NR (*open circle*) and composites with 1 (*filled triangle*), 2.8 (*filled diamond*), 5.4 (*filled circle*) and 8.3 (*open square*) wt% MWCNT. *Inset of Figure b* shows the maximum of tan δ with filler concentration exhibiting linearly decreasing order [99]

nanofillers [101]. For the composite, there is a significant increase in the storage modulus (~1.82 GPa) for 1 wt% of filler in the glassy regime while the increment levels off with further increase in the filler concentration. The composites exhibit a huge increase in the storage modulus with filler (CNT) concentration above T_g (the modulus at $T_g + 70$ K is 75 times higher than that of the pure matrix). Moreover, the tensile modulus, as determined from tensile tests in linear region, is lower than the storage modulus for CNT-NR composites whereas they are equal for pure NR in both static and dynamic measurement due to so called 'Payne effect' at higher dynamic strain amplitude. The difference between tensile modulus E(static) and $E^{/}$(dynamic) increases with filler concentration [99].

Figure 7 illustrates the DMA analysis of storage modulus and tan δ (loss tangent) for NR-cellulose nanofiber composites at 1 Hz as a function of temperature [102]. At low temperatures, the modulus is of nearly constant around 3×10^9 Pa due to the fact that molecular motions are largely restricted to vibration and short-range rotational motions in the glassy state. Though the glassy modulus did not improve with the addition of 5 wt% CNFs (2.1 GPa), but an improvement was observed for 10 wt% CNF. Additionally, it can be seen that the relaxation of polymer chains gets delayed in nanocomposites as compared to NR (tan δ curves). The storage modulus for NR decreases to 1 MPa above the transition temperature while there is substantial increase in modulus for composites in the similar temperature range as compared to NR. Moreover, there was a marked decrease in the tan δ peak intensity along with broadening for composite with 10 wt% CNF primarily due to restriction of chain mobility at the interface of matrix and filler [102].

The variation in $E^{/}$, $E^{//}$ (loss modulus) and tan δ for coir fiber reinforced NR has been shown in Fig. 8 [103]. The maxima in tan δ and $E^{//}$ curves do not coincide in the case of composites as observed for gum compound mainly due to the

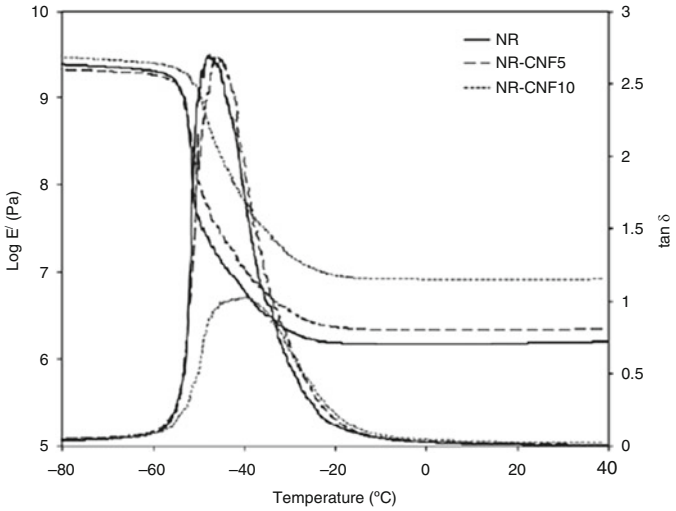

Fig. 7 Dynamic mechanical analysis of pure NR and cellulose nanofiber-based nanocomposites showing the logarithm of the storage modulus ($E^{/}$) and loss angle tangent (tan δ) as a function of temperature [102]

complexity of dynamic mechanical behavior of these composites arising from the restricted movement of NR molecules in the presence of coir fibers.

7.3 Curing Behaviour

To make an appropriate vulcanization processing operation, it is necessary to obtain a complete kinetic characterization of neat polymer and how it is modified in presence of fillers. Figure 9 displays the vulcanization curves of neat NR and purified CNT/NR nanocomposites at various temperatures [104]. The vulcanizing reaction rate of neat NR and CNT/NR nanocomposites was very much related to the temperature. The vulcanization time decreases with increasing temperature both for NR and composites while vulcanization time increases in composite in presence of purified CNT in similar temperature as compared to pure NR. The vulcanization kinetic parameters of specimens were obtained according to the related studies using data on torque versus time in the vulcanizing curves including percentage curing [105]. The degree of conversion (α) in curing reaction is defined as follows (Eq. 1):

$$\alpha = \frac{M_t - M_0}{M_\infty - M_0} \tag{1}$$

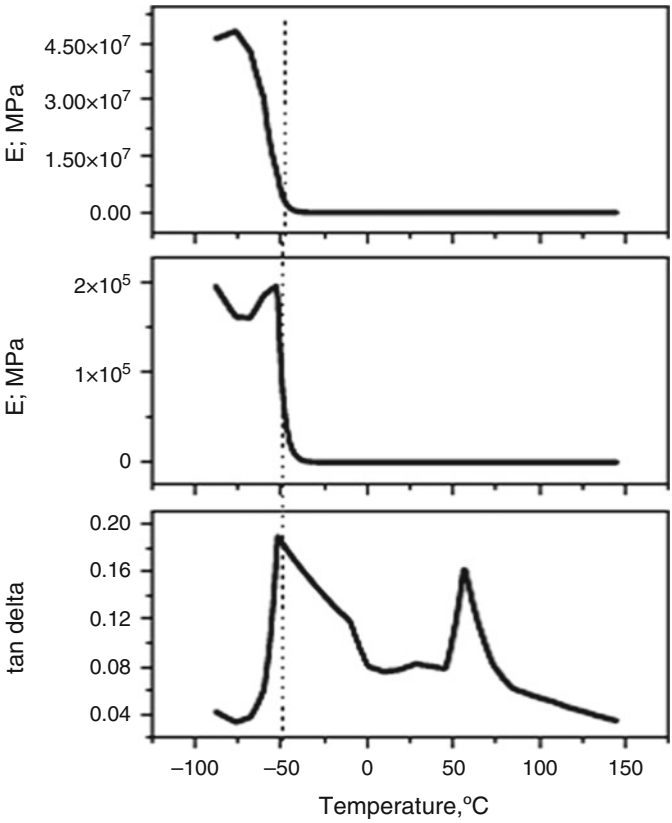

Fig. 8 Dynamic mechanical properties of NR composite at 10 Hz [103]

where, M_0 is the torque value at the initial curing, M_t the torque value corresponding to the time t and M_∞ is the torque value at infinite time (at the end of the curing reaction). It is noteworthy to mention that the above mathematical expression is based on the fact that the crosslinking density is proportional to the stiffness of the rubber materials.

Guo et al. has shown the interfacial interaction in the nanocomposites between carboxylated SBR and halloysite nanotube (HNT) [106]. Lower content of HNT tends to impediment the vulcanization of SBR/HNT compounds, while higher HNT loading promotes the vulcanization presumably due to polar interactions. It is noteworthy to mention that HNT are dispersed uniformly in the matrix with strong interfacial bonding between SBR and HNT.

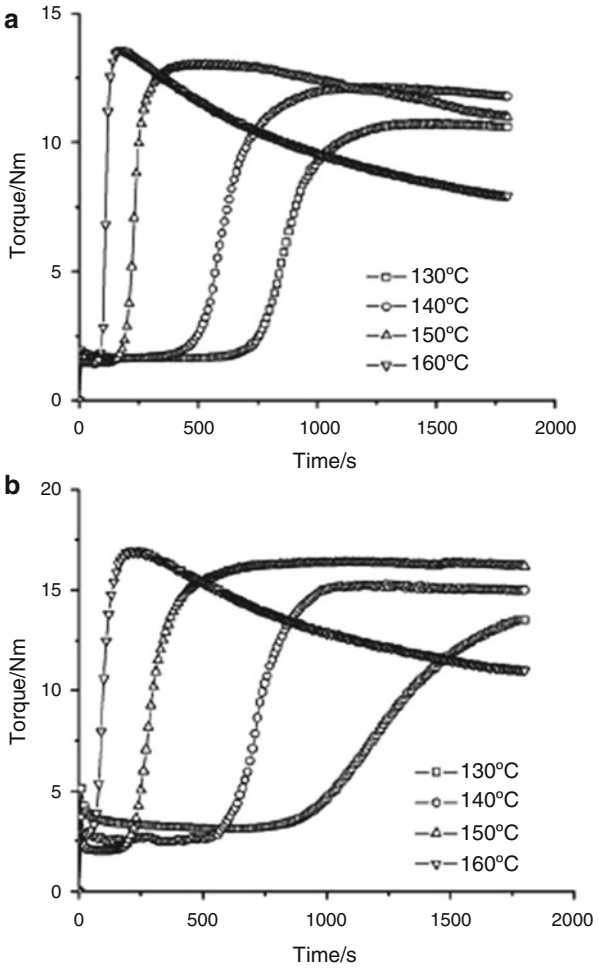

Fig. 9 Vulcanizing curves of neat NR and CNT/NR nanocomposites: (**a**) neat NR, (**b**) CNT/NR nanocomposites [104]

8 Viscoelasticity

Elastomers are typically viscoelastic and exhibit both viscous as well as elastic characteristics when undergoing deformations. The viscous component ($\sigma = \eta \frac{d\varepsilon}{dt}$, where, σ is the stress, η is the coefficient of viscosity and $\frac{d\varepsilon}{dt}$ is the change of strain as a function of time) takes care of the energy dissipated as heat after a strain/stress is applied and followed by its removal while the elastic component ($\sigma = E\varepsilon$) brings back the material towards original dimension, or, in other words, strain depends on stress applied to the materials and time. The overall strain is then governed by the equation where the two terms are separable, as in Eq. (2) is called as linear viscoelasticity and usually it is applicable only for small deformations, where, t is

time, σ(t) is stress, ε(t) is strain, $E_{inst,\ creep}$ is instantaneous elastic moduli for creep and k(t) is the creep function.

$$\varepsilon(t) = \frac{\sigma(t)}{E_{\text{inst,creep}}} + \int_0^t k\left(t - t^{'}\right)\dot{\sigma}\left(t^{'}\right)\mathrm{d}t^{'} \tag{2}$$

On the other hand, when the function is nonseparable it is called as nonlinear viscoelasticity and usually occurs when the deformation is large. Viscoelastic response has elastic and viscous components modeled as linear combinations of springs and dashpots, respectively, and various models such as Maxwell model, Voigt model, and the Standard Linear Solid Model. These models are used to predict the elastomer's response under different loading conditions. Elastomers also exhibit viscoelasticity of both storing and dissipating energy with the relative proportions depending on the frequency applied. The elastic component is quantized by the complex shear modulus G^*, which determines the stress induced in elastomer under oscillatory shear strain at a frequency. The elastic component of the stress is in phase with the applied strain and the ratio of this stress to the strain is considered to be as the storage modulus $G^{/}$ and the real part of G^* while the viscous component of the stress is out of phase with the strain and the ratio of this stress to strain is known as loss modulus $G^{//}$, the imaginary part of G^*.

The linear viscoelastic properties of molten nanocomposites can provide essential insights into the processability of these materials. The effect of CNT dispersion in rubber matrix has been explored through rheology, measuring storage modulus ($G^{/}$) as a function of frequency (Fig. 10a) [107]. The storage moduli gradually increase with CNT content in the composite over the entire frequency range studied (10^{-3} to 200 $rads^{-1}$). The influence of CNT is more prominent in the low frequency region and the slope systematically decrease towards zero at higher concentration of CNT (20 wt%) indicating pseudo-solid like behavior through a percolated network which appears to start at 1 wt% of CNT content in the composite. However, a deviation from linearity is evident in one dimensional filler composite as obvious from the very lower value of the initial slope against the standard value of 2 ($G^{/}\alpha\ \omega^2$) usually obtained for pure homopolymer melt [108]. Figure 10b shows the development of the complex shear viscosity (η^*) of the same specimens indicating large increase of η^* for the composites especially in the low frequency range against the Newtonian plateau observed for pure rubber matrix. Here also, the plateau gradually disappears on and above 1 wt% of CNT in the rubber composite. The composites containing more than 5 wt% of CNT exhibit a linear decrease with frequency known as shear thinning effect. Several authors proposed to fit the flow behaviors in the low-frequency region to determine the change of the rheological behavior of composite vis-à-vis pure elastomers [109, 110].

The chemical modification on CNT surface is an important aspect which eventually alters the properties of the composite as compared to the unmodified CNT composite mentioned earlier. So, it is expected that chemical modification on filler will change the rheological behavior as well. Figure 11 shows the frequency

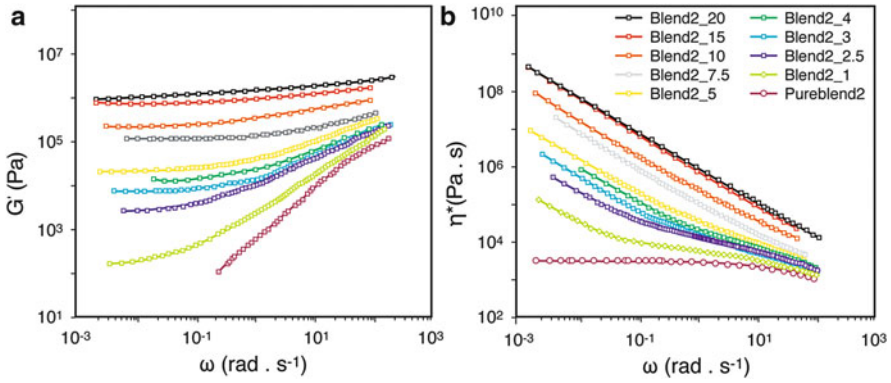

Fig. 10 (**a**) Storage modulus ($G^{/}$) as a function of frequency at T = 120 °C for different CNT contents in rubber matrix. (**b**) Modulus of complex shear viscosity [η*] as a function of frequency for different CNT contents in rubber [107]

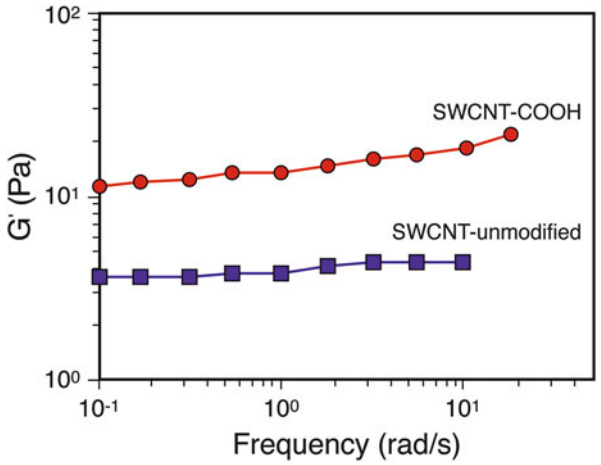

Fig. 11 Frequency response of the storage modulus for dispersions containing 1 wt% SWCNT unmodified or SWCNT-COOH in epoxy precursors [111]

dependence of storage modulus for dispersions containing 1 wt% SWCNT (modified and unmodified) in epoxy precursors. Solid-like behavior is observed for both the dispersions in the low frequency region and importantly, much higher storage modulus was observed for acid functionalized SWCNT in the similar filler loading and frequency as compared to nonfunctionalized SWCNT composite. This phenomenon is explained on the basis of better dispersion of functionalized SWCNT in epoxy precursors due to better interaction with the matrix [111]. The storage modulus increase with filler concentration and a power law relation is used to determine the threshold of rheological percolation [109, 112] $G^{/} \sim (wt\% - wt$

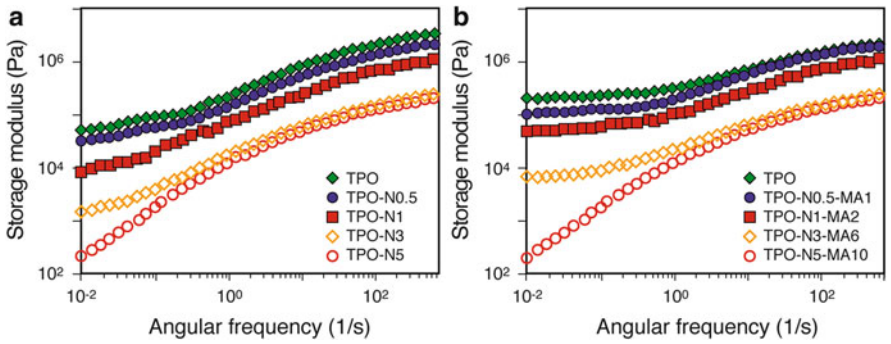

Fig. 12 Storage modulus vs. angular frequency of TPO/SWCNT nanocomposites, showing the effect of functionalization in initial slope: (**a**) uncompatibilized; (**b**) compatibilized nanocomposites [115]

$\%_{crit})^{\beta}$, where $wt\%_{crit}$ is the rheological percolation threshold and β is the critical percolation exponent and the study indicates a percolation threshold of 0.41 % for this system [109]. Viscoelastic measurements are highly susceptible to the nanoscale and mesoscale structure of the nanocomposites and are an influential method to investigate the state of dispersion in such materials [113, 114].

Dispersion can also be controlled by using a third component called compatibilizer for a set of elastomer and nanofillers. Figure 12 reveals the linear viscoelastic behavior of a thermoplastic elastomer polyolefin (TPO) and TPO/SWCNT nanocomposites with polypropylene-grafted-maleic anhydride (PP-g-MA) as a compatibilizer, and the results have been compared without using any compatibilizer for preparing composites with similar filler loading. The storage modulus of the TPO blend shows the terminal behavior at low frequencies and a Newtonian behavior was found at low frequencies for its complex viscosity. With the addition of SWCNTs to the TPO/SWCNTs nanocomposites, the terminal behavior decreased at low frequencies and the complex viscosity increased at low frequencies as compared to pure TPO. Similar results have been observed for other polymers/CNT systems [116], but, interestingly the slope drastically decreases in the presence of compatibilizer as compared to the nanocomposites without any compatibilizer, indicating better dispersion using compatibilizers arising from good interactions. This non-terminal behavior of the storage modulus at low frequencies and the prominent viscosity improvement was related to percolated networks caused by physical interaction of the SWCNT with the matrix. These interactions can be accredited to a better distribution of SWCNTs in matrix which leads to greater hindrance of chain segmental motions.

Dynamic frequency tests are used to explore the microstructure and network formation of the nanocomposites in presence of multiple fillers and their chemical modifications. The storage modulus (G') of neat PU, PU/MWCNT, PU/functionalized MWCNT/CB nanocomposites measured at 150 °C is logarithmically plotted as a function of angular frequency (ω) in Fig. 13 [117]. Incorporation of unmodified MWCNT causes dramatic changes in viscoelasticity of polymer

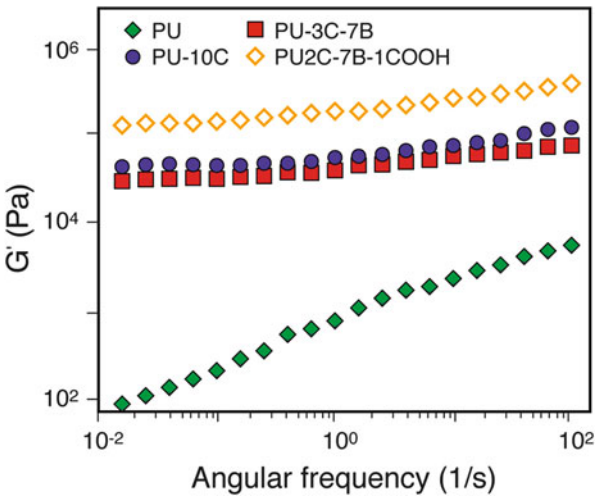

Fig. 13 Logarithmical plots of storage modulus vs. angular frequency; at 150 °C at 0.628 rad/s showing the effect of addition of third component (CB) and acid modification in CNT [117]

melts by increasing the modulus and shifts the initial slope value of 0.461 to 0.27 for PU and 10 wt% MWCNT composite, respectively. Addition of CB also increase the modulus and decreases the initial slope while carboxylic acid functionalization increases further the modulus and lowers the slope value mainly because of a greater interaction and network structure through a) direct bridging, b) bridging through entanglement of adsorbed chains, and c) bridging through entanglement of non-adsorbed chains [118]. Besides, the magnitude of complex viscosity (η*) of nanocomposites substantially increases with increasing filler loading because of the developed interaction in PU-MWCNT, which noticeably opposes the segmental chain mobility of PU matrix. Further, the addition of acid modified MWCNTs (A-MWCNTs) into the PS/SEBS-MA 80/20 blend causes distinct improvements in rheological property with increasing the CNT content and the effect of CNT content is more pronounced at low frequencies than that of higher frequencies [87].

Dynamic frequency sweep tests were also used to explore the cross linked network formation and microstructure of the TPU/CNF composites in the linear viscoelastic region as well as to understand the processability of the nanocomposites. The storage modulus ($G^{/}$) and complex viscosity (η*) obtained from the dynamic frequency measurements at 145 °C for neat TPU and its nanocomposite containing various amounts of CNFs has been reported [83]. The magnitude of $G^{/}$ significantly increases monotonically with increasing applied oscillatory frequency and CNF loading. The higher surface area and aspect ratio of CNF causes the formation of a percolated structure, which enhances the storage modulus of the nanocomposites. The scaling law or power law relation of approximately $G^{/} \propto \omega^2$ (from the slope of the plot) follows for unfilled polymer melts [115]. Therefore, at low frequency region, the virgin TPU exhibits homopolymer-like typical terminal behavior with the scaling properties of $G^{/} \sim \omega^x$ indicating a pseudo-solid-like network in TPU composites. The transition from the liquid-like to

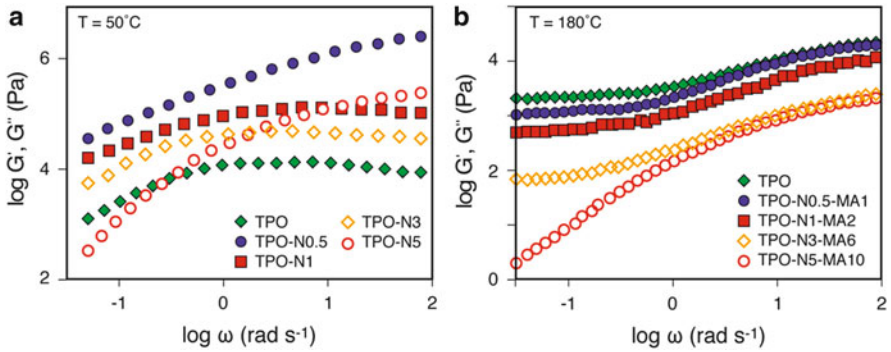

Fig. 14 Frequency dependence of storage and loss moduli for unfilled elastomeric EP random copolymer (*triangles*), 10 wt% (*squares*) and 20 wt% MCNFs nanocomposites (*circles*). The *filled symbols* denote $G^{/}$ and the *unfilled symbols* denote $G^{//}$. The data presented were collected at (**a**) T = 50 °C, and, (**b**) T = 180 °C [120]

solid-like viscoelastic behavior at low frequency region is due to strong filler-filler and filler-polymer interactions, which demonstrate that the dynamics of long-range polymer backbone chains is hindered prominently by the formation of the interconnected or network-like structures of CNFs [119]. The influence of nanofibers on the dynamic viscoelastic response of TPU/CNF nanocomposites is relatively weaker at high frequencies as compared to lower frequencies. The magnitude of viscosity decreases gradually with the increase in applied frequency that is termed as shear thinning characteristic or pseudoplasticity of the polymeric materials at molten state while it increases with the increase in nanofiber loading. In Fig. 14a, b, the dynamic moduli of the elastomeric ethylene-propylene (EP) random copolymer and 10 and 20 wt% well dispersed modified carbon nanofibers (MCNFs) nanocomposites obtained at 50° and 180 °C, respectively. It is apparent that at 50 °C the crossover frequency at the terminal zone shifts to lower values with increasing filler concentration (Fig. 14a) [120]. Moreover, the storage moduli of the filled systems tend to have a higher plateau value (G°_{N}) in comparison to the unfilled polymer. This observation implies that the strong nanofiller-matrix interactions significantly affect the local dynamics of the polymer chains. At 180 °C, G°_{N} cannot be seen within the accessible rheological window (Fig. 14b). However, strong polymer-MCNF interactions are manifested itself in the gelation phenomenon in presence of sufficient nanofibers and thereby pronounced deviations is observed especially in the low frequency region in case of filled polymers.

Figure 15a illustrates the frequency dependence of tan δ for the 1 wt% elastomeric EP random copolymer and well dispersed MCNFs nanocomposites at varying temperatures [120]. For clarity, these curves have been shifted along the x-axis. At high temperatures (i.e. in the range of 130–200 °C), the nanocomposite exhibited a pseudo-solid-like behavior; as determined from the positive slopes in the low frequency regime. At 129 °C, the nanocomposite reached the critical gel state; i.e. the tan δ(ω) curve exhibited a zero-slope plateau in the low frequency regime.

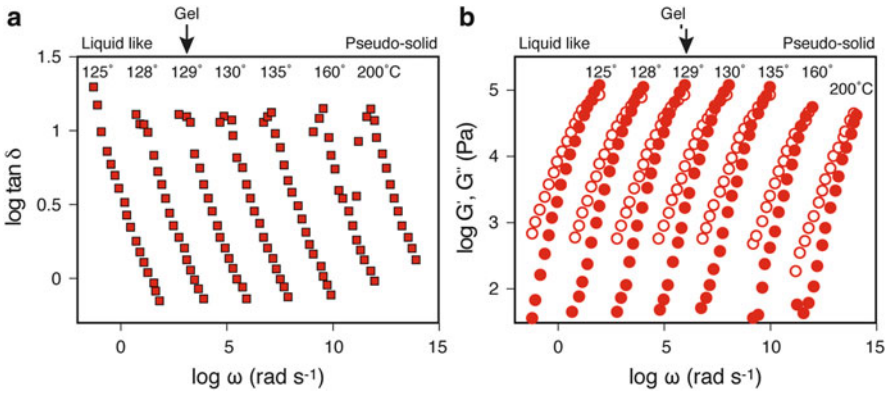

Fig. 15 (**a**) Frequency dependence of tan δ for the 1 wt% elastomeric EP random copolymer and well dispersed MCNFs nanocomposite at varying temperatures. The gel point is indicated by the *arrow*, (**b**) Frequency dependence of storage ($G^{/}$, *filled symbols*) and loss modulus ($G^{//}$, *unfilled symbols*) for the 1 wt% nanocomposite at varying temperatures during cooling. The *curves* have been shifted along the x-axis for clarity [120]

This behavior was further confirmed by observations at 128° and 125 °C, where the nanocomposite showed a liquid-like behavior, i.e. tan δ(ω) curves exhibited negative slopes in the entire region of the rheological spectrum. The values of storage and loss moduli for the 1 wt% nanocomposite at varying temperatures are illustrated in Fig. 15b. It has reported that despite the nanocomposite being within the pseudo-solid-like region at 200 °C, $G^{/}$ was consistently lower than the corresponding $G^{//}$ in the entire frequency range considered. On the other hand, at lower temperatures, the crossover point of $G^{/}(\omega)$ and $G^{//}(\omega)$ curves falls within the accessible frequency range and their slopes approached the values as expected for a typical melt (2 and 1, respectively). The frequency dependencies of tan δ, $G^{/}$ and $G^{//}$ for higher filler loading at 20 wt% MCNF nanocomposite also exhibit similar behavior at varying temperatures and exhibited a pseudo-solid-like behavior at high temperatures (65, 80 and 100 °C) and liquid-like behavior at temperatures below 60 °C. The temperature for the occurrence of the critical gel state was about 60 °C in the 20 wt% nanocomposite, significantly lower than that of 1 wt% nanocomposite (129 °C). For higher filler content composites (20 wt%), $G^{/}$ was found to be larger than $G^{//}$ at the gel point in the entire frequency range studied.

9 Conclusions

Elastomer nanocomposites with one-dimensional nanofillers have been presented in this chapter. The nature of nanofiller has been altered from nanotube to nanorod, and nanofiber with their suitable chemical modifications required for the improvement of various properties. The dispersion and morphology have been explored for

different types of nanofillers and their modifications along with the improvement in thermal and mechanical properties. The structure property relationship has been demonstrated and unique non-linear viscoelasticity arising from network structure in presence of nanofiller has been critically reviewed.

Acknowledgements The author (Karun Kumar Jana) gratefully acknowledges the award of Senior Research Fellowship of CSIR, India.

References

1. Kumar KD, Tsou AH, Bhowmick AK (2010) Unique tackification behavior of needle-like sepiolite nanoclay in brominated isobutylene-co-p-methylstyrene (BIMS) rubber. Macromolecules 43:4184–4193
2. Dannenberg EM (1975) Bound rubber carbon black reinforcement. Rubber Chem Technol 48:410–444
3. Maiti P, Batt CA, Giannelis EP (2007) New biodegradable polyhydroxybutyrate/layered silicate nanocomposites. Biomacromolecules 8:3393–3400
4. Okamoto M, Nam PH, Maiti P, Kotaka T, Nakayama T, Takada M, Ohshima M, Usuki A, Hasegawa N, Okamoto H (2001) Biaxial flow-induced alignment of silicate layers in polypropylene/clay nanocomposite foam. Nano Lett 1(9):503–505
5. Maiti P (2003) Influence of miscibility on viscoelasticity, structure and intercalation of oligo-poly(caprolactone)/layered silicate nanocomposites. Langmuir 19:5502–5510
6. Ray SS, Maiti P, Okamoto M, Yamada K, Ueda K (2002) New polylactide/layered silicate nanocomposites. 1. Preparation, characterization and properties. Macromolecules 35:3104–3110
7. Mishra A, Purkayastha BPD, Roy JK, Aswal VK, Maiti P (2010) Tunable properties of self-assembled polyurethane using two-dimensional nanoparticles: potential nano-biohybrid. Macromolecules 43:9928–9936
8. Tiwari VK, Shripathi T, Lalla NP, Maiti P (2012) Nanoparticle induced piezoelectric, super toughened, radiation resistant, multi-functional nanohybrids. Nanoscale 4:167–175
9. Jana KK, Ray B, Avasthi DK, Maiti P (2012) Conducting nano-channels in an induced piezoelectric polymeric matrix using swift heavy ions and subsequent functionalization. J Mater Chem 22:3955–3964
10. Jana KK, Vishwakarma NK, Ray B, Khan SA, Avasthi DK, Misra M, Maiti P (2013) Nanochannel conduction in piezoelectric polymeric membrane using swift heavy ions and nanoclay. RSC Adv 3:6147–6159
11. Maiti P, Yadav PJP (2008) Biodegradable nanocomposites of poly(hydroxybutyrate-co-hydroxyvalerate): the effect of nanoparticles. J Nanosci Nanotechnol 8:1858–1866
12. Singh NK, Purkayastha BPD, Roy JK, Banik RM, Yashpal M, Singh G, Malik S, Maiti P (2010) Nanoparticle-induced controlled biodegradation and its mechanism in poly(*å*-caprolactone). ACS Appl Mater Interfaces 2(1):69–81
13. Beatty JR (1969) A mechanical method for estimating both tackiness and stickiness of rubber compounds. Rubber Chem Technol 42:1040–1053
14. Beckwith RK, Welch LM, Nelson JF (1950) Tack of butyl and natural rubbers. Rubber Chem Technol 23:933–944
15. Fritzsche J, Lorenz H, Kluppel M (2009) CNT based elastomer-hybrid nanocomposites with promising mechanical and electrical properties. Macromol Mater Eng 294:551–560
16. Bokobza L, Rahmani M, Belin C (2008) Blends of carbon blacks and multiwall carbon nanotubes as reinforcing fillers for hydrocarbon rubbers. J Polym Sci B Polym Phys 46:1939–1951

17. Moniruzzaman M, Winey KI (2006) Polymer nanocomposites containing carbon nanotubes. Macromolecules 39:5194–5205
18. Zhu J, Wei S, Ryu J, Budhathoki M, Liang G, Guo Z (2010) In situ stabilized carbon nanofiber (CNF) reinforced epoxy nanocomposites. J Mater Chem 20:4937–4948
19. Laraba-Abbes F, Ienny P, Piques R (2003) A new 'Tailor-made' methodology for the mechanical behaviour analysis of rubber-like materials: II. Application to the hyperelastic behaviour characterization of a carbon-black filled natural rubber vulcanizate. Polymer 44:821–840
20. Tian M, Su LL, Cai WT, Win S, Chen Q, Fong H, Zhang LQ (2011) Mechanical properties and reinforcement mechanisms of hydrogenated acrylonitrile butadiene rubber composites containing fibrillar silicate nanofibers and short aramid microfibers. J Appl Polym Sci 120:1439–1447
21. Murty VM, De SK (1984) Short-fiber-reinforced styrene-butadiene rubber composites. J Appl Polym Sci 29:1355–1368
22. Wong EW, Sheehan PE, Lieber CM (1997) Nanobeam mechanics: elasticity strength and toughness of nanorods and nanotubes. Science 277:1971–1975
23. Gogotsi Y (2010) High-temperature rubber made from carbon nanotubes. Science 330:1332–1333
24. Shrivastava NK, Suin S, Maiti S, Khatua BB (2013) Ultralow electrical percolation threshold in poly(styrene-co-acrylonitrile)/carbon nanotube nanocomposites. Ind Eng Chem Res 52:2858–2868
25. Dyke CA, Tour JM (2003) Solvent-free functionalization of carbon nanotubes. J Am Chem Soc 125:1156–1157
26. Saengsuwan S, Saikrasun S (2012) Thermal stability of styrene-(ethylene butylene)-styrene-based elastomer composites modified by liquid crystalline polymer, clay and carbon nanotube. J Therm Anal Calorim 110:1395–1406
27. Zha JW, Shehzad K, Li WK, Dang ZM (2013) The effect of aspect ratio on the piezoresistive behavior of the multiwalled carbon nanotubes/thermoplastic elastomer nanocomposites. J Appl Phys 113:014102
28. Heinrich G, Kluppel M, Vilgis TA (2002) Reinforcement of elastomers. Curr Opin Solid State Mater Sci 6:195–203
29. Falco AD, Marzocca AJ, Corcuera MA, Eceiza A, Mondragon I, Rubiolo H, Goyanes S (2009) Accelerator adsorption onto carbon nanotubes surface affects the vulcanization process of styrene-butadiene rubber composites. J Appl Polym Sci 113:2851–2857
30. Singh NK, Singh SK, Dash D, Gonugunta P, Misra M, Maiti P (2013) CNT Induced β-phase in polylactide: unique crystallization, biodegradation, and biocompatibility. J Phys Chem C 117:10163–10174
31. Iijima S (1991) Helical microtubules of graphitic carbon. Nature 354:56–58
32. Kim HH, Kim HJ (2006) Preparation of carbon nanotubes by DC are discharge process under reduced pressure in an air atmosphere. Mater Sci Eng B 133:241–244
33. Che G, Lakshmi BB, Martin CR, Fisher ER (1998) Chemical vapor deposition based synthesis of carbon nanotubes and nanofibers using a template method. Chem Mater 10:260–267
34. Hornbostel B, Haluska M, Cech J, Dettlaff U, Roth S (2006) Arc discharge and laser ablation synthesis of single-walled carbon nanotubes. NATO Science Series II: Mathematics. Phys Chem 222:1–18
35. Dateo CE, Gokcen T, Meyyappan M (2002) Modeling of the HiPco process for carbon nanotube production. 1. Chemical kinetics. J Nanosci Nanotechnol 2:523–34
36. Zajickova L, Jasek O, Elias M, Synek P, Lazar L, Schneeweiss O, Hanzlikova R (2010) Synthesis of carbon nanotubes by plasma-enhanced chemical vapor deposition in an atmospheric-pressure microwave torch. Pure Appl Chem 82:1259–1272
37. Tasis D, Tagmetarchis N, Bianco A, Prato M (2006) Chemistry of carbon nanotubes. Chem Rev 106:1105–1136

38. Wang Z, Zu X, Gao F, Weber WJ (2006) Atomistic simulation of brittle to ductile transition in GaN nanotubes. Appl Phys Lett 89:243123
39. Lohse SE, Purphy CJ (2013) The quest for shape control: a history of gold nanorod synthesis. Chem Mater 25:1250–1261
40. Eustis S, EI-Sayed MA (2006) Why gold nanoparticles are more precious than pretty gold: noble metal surface plasmon resonance and its enhancement of the radiative and nonradiative properties of nanocrystals of different shapes. Chem Soc Rev 35:209–217
41. Burda C, Chen X, Narayanan R, El-Sayed A (2005) Chemistry and properties of nanocrystals of different shapes. Chem Rev 105:1025–1102
42. Koerner H, Kelley J, George J, Drummy L, Mirau P, Bell NS, Hsu JWP, Vaia RA (2009) ZnO nanorod–thermoplastic polyurethane nanocomposites: morphology and shape memory performance. Macromolecules 42:8933–8942
43. Alexander KD, Skinner K, Zhang S, Wei H, Lopez R (2010) Tunable SERS in gold nanorod dimers through strain control on an elastomeric substrate. Nano Lett 10:4488–4493
44. Rybinski P, Janowska G (2012) Thermal properties and flammability of nanocomposites based on nitrile rubbers and activated halloysite nanotubes and carbon nanofibers. Thermochim Acta 549:6–12
45. Wu N, Chen L, Li J et al (2012) Preparation and characterization of Fe^{3+}, La^{3+} Co-doped Tio_2 nanofibers and its photocatalytic activity. J Eng Fibers Fabrics 7:16–20
46. Lu W, Steiqerwalt ES, Moore JT, Sullivan LM, Collins WE, Lukehart CM (2004) Carbothermal transformation of a graphitic carbon nanofiber/silica aerogel composite to a SiC/silica nanocomposite. J Nanosci Nanotechnol 4(7):803–8
47. Borrell A, Rocha VG, Torrecillas R, Fernandez A (2011) Improvement of carbon nanofibers/ZrO_2 composites properties with a zirconia nanocoating on carbon nanofibers by sol–gel method. J Am Ceram Soc 94:2048–2052
48. Azad AM, Noibi M, Ramachandran M (2007) Fabrication and characterization of 1-D alumina (Al_2O_3) nanofibers in an electric field. Bull Pol Acad Tech 55:195–201
49. Zhang B, Liu Y, Huang Z, Oh S, Yu Y, Mai YW, Kim JK (2012) Urchin-like Li4 Ti5O12–carbon nanofiber composites for high rate performance anodes in Li-ion batteries. J Mater Chem 22:12133–12140
50. Tishchenko NI, Kolesnichenko VG, Dubovitskaya NV, Silenko PM, Danilenko NI, Zgalat-Lozinskii OB, Bulanov VN, Ragulya AV (2009) Surface modification of silicon nitride nanofibers with titanium nitride particle. Powder Metallurgy Met Ceram 48:627–633
51. Poudel P, Zhang L, Joshi P, Venkatesan S, Fong H, Qiao Q (2012) Enhanced performance in dye-sensitized solar cells via carbon nanofibers-platinum composite counter electrodes. Nanoscale 4:4726–4730
52. Camean I, Garcia AB, Suelves I (2012) Graphitized carbon nanofibers for use as anodes in lithium-ion batteries: importance of textural and structural properties. J Power Source 198:303–307
53. Monroe N (2011) Increasing the efficiency of a hybrid polymer photovoltaic cell with polymer nanofiber complexes of varied thickness. Young Sci J 8:26–32
54. Ballengee JB, Haugen GM, Hamrock SJ, Pintauro PN (2013) Properties and fuel cell performance of a nanofiber composite membrane with 660 equivalent weight perfluorosulfonic acid. J Electrochem Soc 160(4):F429–F435
55. Jin EM, Zhao XG, Park JY, Gu HB (2012) Enhancement of the photoelectric performance of dye-sensitized solar cells using Ag-doped TiO_2 nanofibers in a TiO_2 film as electrode. Nanoscale Res Lett 7(97):1–5
56. Luo Z, Charlie Johnson AT. Growth of carbon nanotubes via chemical vapor deposition, NSF Award no. EEC-0754741
57. Gao J, Hu M, Dong Y, Li RKY (2013) Graphite-nanoplatelet-decorated polymer nanofiber with improved thermal, electrical, and mechanical properties. ACS Appl Mater Interfaces 5 (16):7758–7764
58. Maiti P, Yamada K, Okamoto M, Ueda K, Okamoto K (2002) New polylactide/layered silicate nanocomposites: role of organoclays. Chem Mater 14:4654–4661

59. Maiti P, Nam PH, Okamoto M, Hasegawa N, Usuki A (2002) Influence of crystallization on intercalation, morphology, and mechanical properties of polypropylene/clay nanocomposites. Macromolecules 35(6):2042–2049
60. Okamoto M, Nam PH, Maiti P, Kotaka T, Hasegawa N, Usuki A (2001) A house of cards structure in polypropylene/clay nanocomposites under elongational flow. Nano Lett 1 (6):295–298
61. Tiwari VK, Prasad AK, Singh V, Jana KK, Misra M, Prasad CD, Maiti P (2013) Nanoparticle and process induced super toughened piezoelectric hybrid materials: the effect of stretching on filled system. Macromolecules 46:5595–5603
62. Shankar SSV, Dinesh R, Thomas T (2010) Experimental study on manufacture and analysis of rubber nanoclay MWCNT composite. Int J Environ Sci Dev 1(2):181–183
63. Lima AMF, de Castro VG, Borges RS, Silva GG (2012) Electrical conductivity and thermal properties of functionalized carbon nanotubes/polyurethane composites. Polímeros Ciencia e Tecnologia 22(2):117–124
64. Guo S, Zhang C, Wang W et al (2008) Preparation and characterization of polyurethane/ multiwalled carbon nanotube composites. Polym Polym Compos 16:471–478
65. Sui G, Zhong WH, Yang XP, Yu YH, Zhao SH (2008) Preparation and properties of natural rubber composites reinforced with pretreated carbon nanotubes. Polym Adv Technol 19:1543–1549
66. Jyotishkumar P, Abraham E, George SM, Elias E, Pionteck J, Moldenaers P, Thomas S (2013) Preparation and properties MWCNTs/poly(acrylonitrilestyrene- butadiene)/epoxy hybrid composites. J Appl Polym Sci 127:3093–3103
67. Tibbetts GG, Lake ML, Strong KL (2007) A review of the fabrication and properties of vapor-grown carbon nanofiber/polymer composites. Compos Sci Technol 67:1709–18
68. Andrews R, Jacques D, Minot M, Rantell T (2002) Fabrication of carbon multiwall nanotube/ polymer composites by shear mixing. Macromol Mater Eng 287:395–403
69. Xie XL, Mai YW, Zhou XP (2005) Dispersion and alignment of carbon nanotubes in polymer matrix: a review. Mater Sci Eng R Rep 49:89–112
70. Tsubokawa N (2005) Preparation and properties of polymer grafted carbon nanotubes and nanofibers. Polym J 37(9):637–655
71. Shanks R, Kong I (2012) Thermoplastic elastomers. InTech. ISBN 978-953-51-0346-2
72. Pedroni LG, Araujo JR, Felisberti MI, Nogueira AF (2012) Nanocomposites based on MWCNT and styrene–butadiene–styrene block copolymers: effect of the preparation method on dispersion and polymer–filler interactions. Compos Sci Technol 72:1787–1492
73. Alipour A (2012) Fabrication and characterization of nanostructured polymer composites prepared by melt compounding. Int J Biosci Biochem Bioinform 2:79–84
74. Siengchin S (2011) Nano-scale reinforcing and toughening thermoplastics: processing, structure and mechanical properties. InTech. ISBN 978-953-307-420-7
75. Deng F, Ito M, Noguchi T, Wang L, Ueki H, Niihara K, Kim YA, Endo M, Zheng QS (2011) Elucidation of the reinforcing mechanism in carbon nanotube/rubber nanocomposites. ACS Nano 5:3858–3866
76. Bokobza L (2012) Enhanced electrical and mechanical properties of multiwall carbon nanotube rubber composites. Polym Adv Technol 23:1543–1549
77. Endo M (1988) Grow carbon-fibers in the vapor-phase. Chem-Tech 18:568–576
78. Endo M, Kim YA, Hayashi T, Nishimura K, Matusita K, Dresselhaus MS (2001) Vapor-grown carbon fibers (VGCFs): basic properties and their battery applications. Carbon 39:1287–1297
79. Cadambi RM, Ghassemieh E (2011) Optimized process for the inclusion of carbon nanotubes in elastomers with improved thermal and mechanical properties. J Appl Polym Sci 124:4993–5001
80. Hu Y, Shenderova OA, Hu Z, Padgett CW, Brenner DW (2006) Carbon nanostructures for advanced composites. Rep Prog Phys 69:1847–1895
81. Coleman JN, Khan U, Blau WJ, Gunko YK (2006) Small but strong: a review of the mechanical properties of carbon nanotube-polymer composites. Carbon 44(9):1624–1652

82. Wang W, Jiang F, Jiang Y, Lu Y, Zhang L (2012) Preparation and properties of polyurethane/multiwalled carbon nanotube nanocomposites by a spray drying process. J Appl Polym Sci 126:789–795
83. Barick AK, Tripathy DK (2012) Preparation and characterization of carbon nanofiber reinforced thermoplastic polyurethane nanocomposites. J Appl Polym Sci 124:765–780
84. Sui G, Zhong WH, Ren X (2009) Structure, mechanical properties and friction behavior of UHMWPE/HDPE/carbon nanofibers. Mater Chem Phys 115(1):404–412
85. Li Y, Shimizu H (2009) Toward a stretchable, elastic, and electrically conductive nanocomposite: morphology and properties of poly[styrene-*b*-(ethylene-*co*-butylene)-*b*-styrene]/multiwalled carbon nanotube composites fabricated by high-shear processing. Macromolecules 42:2587–2593
86. Potschke P, Abdel-Goad M, Alig I, Dudkin S, Lellinger D (2004) Rheological and dielectrical characterization of melt mixed polycarbonate-multiwalled carbon nanotube composites. Polymer 45:8863–8870
87. Fan X, Wang Z, Wang K, Deng H, Chen F, Fu Q (2012) Acid-modified carbon nanotubes distribution and mechanical enhancement in polystyrene/elastomer blends. Polym Eng Sci 52:964–971
88. Puglia D, Valentini I, Kenny JM (2003) Analysis of the cure reaction of carbon nanotubes/epoxy resin composites through thermal analysis and Raman spectroscopy. J Appl Polym Sci 88:452–458
89. Sui G, Zhong W, Yang X, Zhao S (2007) Processing and material characteristics of a carbon-nanotube-reinforced natural rubber. Macromol Mater Eng 292:1020–1026
90. Szymczyk A (2012) Poly(trimethylene terephthalate-block-tetramethylene oxide) elastomer/single-walled carbon nanotubes nanocomposites: synthesis, structure, and properties. J Appl Polym Sci 126:796–807
91. Zhu J, Wei S, Ryu J, Guo Z (2011) Strain-sensing elastomer/carbon nanofiber "Metacomposites". J Phys Chem C 115:13215–13222
92. Maiti P, Nandi AK (1995) Influence of chain structure on the miscibility of poly(viny1idene fluoride) with poly(methyl acrylate). Macromolecules 28:8511–8516
93. Maiti P, Chatterjee J, Nandi AK (1993) Melting and crystallization behaviour of poly (vinylidene fluoride) in its blends with polyacrylates, polyacrylates, poly(vinyl esters) and poly(aryl ether ether ketone). Polymer 34:4273–4279
94. Nah C, Lim JY, Cho BH, Hong CK, Gent AN (2010) Reinforcing rubber with carbon nanotubes. J Appl Polym Sci 118:1574–1581
95. Shanmugharaj AM, Bae JH, Lee KY, Noh WH, Lee SH, Ryu SH (2007) Physical and chemical characteristics of multiwalled carbon nanotubes functionalized with aminosilane and its influence on the properties of natural rubber composites. Compos Sci Technol 67:1813–1822
96. Koerner H, Liu W, Alexander M (2005) Deformation-morphology correlations in electrically conductive carbon nanotube-thermoplastic polyurethane nanocomposites. Polymer 46:4405–4420
97. Fornes TD, Paul DR (2003) Modeling properties of nylon6/clay nanocomposites using composite theories. Polymer 44:4993–5013
98. Quijano JRB, Aviles F, Cauich-Rodriguez JV (2013) Sensing of large strain using multiwall carbon nanotube/segmented polyurethane composites. J Appl Polym Sci. doi:10.1002/APP.1-8
99. Bhattacharyya S, Sinturel C, Bahloul O, Saboungi ML, Thomas S, Salvetat JP (2008) Improving reinforcement of natural rubber by networking of activated carbon nanotubes. Carbon 46:1037–1045
100. Samir MASA, Alloin F, Dufresne A (2005) Review of recent research into cellulosic whiskers, their properties and their application in nanocomposite field. Biomacromolecules 6(2):612–26
101. Tiwari VK, Kulriya PK, Avasthi DK, Maiti P (2009) Poly(Vinylidene fluoride-co-hexafluro propylene)/layered silicate nanocomposites: the effect of swift heavy ion. J Phys Chem B 113:11632–11641

102. Visakh PM, Thomas S, Oksman K, Mathew AP (2012) Effect of cellulose nanofibers isolated from pulp residue on vulcanized natural rubber. BioResources 7(2):2156–2168
103. Geethamma VG, Kalaprasad G, Groeninckx G, Thomas S (2005) Dynamic mechanical behavior of short coir fiber reinforced natural rubber composites. Compos Part A Appl Sci Manuf 36:1499–1506
104. Sui G, Zhong WH, Yang XP, Yu YH (2008) Curing kinetics and mechanical behavior of natural rubber reinforced with pretreated carbon nanotubes. Mater Sci Eng A 485:524–531
105. Kueseng K, Jacob KI (2006) Natural rubber nanocomposites with SiC nanoparticles and carbon nanotubes. Eur Polym J 42:220–227
106. Du M, Guo B, Lei Y, Liu M, Jia D (2008) Carboxylated butadiene-styrene rubber/halloysite nanotube nanocomposites: interfacial interaction and performance. Polymer 49:4871–4876
107. Charman M, Leonardi F, Dominguez S, Bissuel C, Derail C (2011) Dispersion of multiwalled carbon nanotubes in a rubber matrix using an internal mixer: effects on rheological and electrical properties. J Polym Sci B: Polym Phys 49:1597–1604
108. Zhang Q, Rastogi S, Chen D, Lippits D, Lemstra PJ (2006) Low percolation threshold in single-walled carbon nanotube/high density polyethylene composites prepared by melt processing technique. Carbon 44:778–785
109. Du F, Scogna RC, Zhou W, Brand S, Fischer JE, Winey KI (2004) Nanotube networks in polymer nanocomposites: rheology and electrical conductivity. Macromolecules 37:9048–9055
110. Costa FR, Wagenknecht U, Jehnichen D, Goad MA, Heinrich G (2006) Nanocomposites based on polyethylene and Mg-Al layered double hydroxide. Part II. Rheological characterization more. Polymer 47:1649–1660
111. Auad ML, Mosiewicki MA, Uzunpinar C, Williams RJJ (2009) Single-wall carbon nanotubes/epoxy elastomers exhibiting high damping capacity in an extended temperature range. Compos Sci Technol 69:1088–1092
112. Fan Z, Advani SG (2007) Rheology of multiwall carbon nanotube suspension. J Rheol 51 (4):585–604
113. Galgali G, Ramesh C, Lele A (2001) A rheological study on the kinetics of hybrid formation in polypropylene nanocomposites. Macromolecules 34:852–858
114. Schmidt G, Nakatani AI, Butler PD (2000) Shear orientation of viscoelastic polymer-clay solutions probed by flow birefringence and SANS. Macromolecules 33:7219–7222
115. Krishnamoorti R, Vaia RA, Giannelis EP (1996) Structure and dynamics of polymer-layered silicate nanocomposites. Chem Mater 8:1728–1734
116. Hemmati M, Narimani A, Shariatpanahi H (2011) Study on morphology, rheology and mechanical properties of thermoplastic elastomer polyolefin (TPO)/carbon nanotube nanocomposites with reference to the effect of polypropylene-grafted-maleic anhydride (PP-g-MA) as a compatibilizer. Int J Polym Mater 60:384–397
117. Lin L, Liu S, Zhang Q, Li X, Ji M, Deng H, Fu Q (2013) Towards tunable sensitivity of electrical property to strain for conductive polymer composites based on thermoplastic elastomer. ACS Appl Mater Interfaces 5:5815–5824
118. Aranguren MI, Mora E, DeGroot JV, Macosko CW (1992) Rheology and microstructure of filled polymer melts. J Rheol 36:1165–1182
119. Krishnamoorti R, Giannelis EP (1997) Rheology of end-tethered polymer layered silicate nanocomposites. Macromolecules 30:4097–4102
120. Kelarakis A, Yoon K, Chu B et al (2005) Rheological study of carbon nanofiber induced physical gelation in polyolefin nanocomposite melt. Polymer 46:11591–11599

Nonlinear Viscoelasticity of Two Dimensional Filler Reinforced Rubber Nanocomposites

Kishor Kumar Sadasivuni and Yves Grohens

Abstract This chapter describes the effect of two dimensional filler particles on the non-linear viscoelastic properties of elastomer nanocomposites. The distribution of nanosized fillers and the existing interactions—nanofiller-nanofiller and nanofiller-matrix—in the nanocomposite systems are crucial for understanding their behavior under dynamic-mechanical conditions. The non-linear stress response of rubbers and its composites to an applied strain is very significant in formulating the material applications. The reported nonlinear viscoelastic properties for composites of two dimentional fillers such as clay and graphene in different elastomer matrices are critically reviewed. Rheological and dynamic mechanical properties of elastomer nanocomposites are mainly dealt with. The addition of 2D filler particles alters the nonlinear behavior of the loss factor with strain mostly by increasing the level of viscometric properties. Moreover the addition of high-aspect-ratio, sheet-like fillers increase the elasticity as well as the viscosity.

Keywords Clay • Composites • Graphene • Nanocomposites • Rubbers • Two-dimensional fillers

1 Introduction

Viscoelasticity is a phenomenon observed in most of the polymers since they possess elastic and viscous characteristics when deformed. The properties such as creep, stress relaxation, mechanical damping, vibration absorption and hysteresis are included in viscoelasticity. If a material shows linear variation of strain upon the application of stress on it, its behavior is said to be linear viscoelastic. Elastomers and soft biological tissues undergo large deformations and exhibit time dependent stress strain behavior and are nonlinear viscoelastic materials. The non-linear viscoelastic properties of solid polymers are often based on creep and stress-

K.K. Sadasivuni (✉)
School of Chemical Sciences, Mahatma Gandhi University, Priyadarshini Hills P.O., Kottayam 686 560, Kerala, India
e-mail: kishor_kumars@yahoo.com

Y. Grohens
LIMATB Laboratory, Université de Bretagne Sud, rue St Maudé, 56100 Lorient, France

D. Ponnamma, S. Thomas (eds.), *Non-Linear Viscoelasticity of Rubber Composites and Nanocomposites*, Advances in Polymer Science 264, DOI 10.1007/978-3-319-08702-3_3

relaxation measurements, however these techniques are rather time consuming. The dynamic mechanical measurements provide a complementary approach where stress or strain parameters and its dependence on viscoelasticity of polymers can be appropriately checked.

Fillers of various dimensions are added to polymers to alter its processability, properties and uses. Such micro and nano composites obtained may have tremendous possibilities in industries and information on their viscoelasticity is very necessary as far as their processing and applicability are concerned. The dynamic properties of filled elastomers have been a subject of active research since they affect the performance of tyres such as skid, traction, and rolling resistance. Elastomer nanocomposites are most important materials characterized by excellent elasticity and flexibility, and are widely used in various applications such as cables, tyres, tubing, dielectric materials and sensors [1–5]. The non linear features observed in filled elastomers upon a simple shear are as follows. The dynamic storage and loss moduli of the composites are only dependent on the dynamic strains and not on the static strain. In the same way the stress strain curves also do not depend on static strain. Moreover the initial modulus under constant strain rate is highly rate dependent whereas the terminal modulus is independent of strain rate. This initial to terminal modulus ratio in the stress-strain curves is the same as the ratio of the dynamic storage moduli obtained at low and high strains.

The major mechanism behind the reinforcement in elastomer composites and their nonlinear behavior is based on the filler-matrix interactions and not on the filler cluster formation/agglomeration or percolation. The interfacial interactions cause in temporary (labile) bond formation between the polymer chains and the filler surface and this results in trapped entanglements. Such molecular entanglements affect the matrix polymer chain motions both near and far fields and greatly enhance the non-Gaussian (Langevin) chain behavior influencing the storage and loss moduli in various extents. When a strain (stress) is applied on the composite, these trapped entanglements get released and this leads to the reduction in the dynamic moduli. The reinforcement of elastomers by nanofillers and the nonlinear viscoelastic properties of the nanocomposites are very much similar to the phenomenon of Payne effect observed in filled elastomers. This suggests a common mechanism of network formation and breakage arising from the trapped entanglements of macromolecular chains of the elastomer matrices in presence of fillers.

The investigation of the nonlinear dynamic mechanical properties of filled elastomers has long background since A. R. Payne explored this behavior in carbon black filled elastomers [6]. He observed a decrease in dynamic storage modulus in filled elastomers with increasing strain amplitude. However the mechanisms for reinforcement and nonlinearity remain controversial. As already mentioned filler agglomeration and network formation cause high levels of reinforcement in the nanocomposite systems and the deagglomeration and network breakdown result in the nonlinearity with strain [7, 8]. All these mechanisms depend highly on the nature of filler and the mixing method used for composite preparation. The concentration of filler also influences the composite viscoelasticity as many reports concentrate on the non linear viscoelastic properties at high filler volume fractions.

At lower filler loadings, particularly below the percolation threshold this property is little explored. The nonlinear behavior called Payne effect was absent in the neat elastomers at the same strain levels. Kraus, Maier and Goritz [9] and Huber Vilgis proposed various mechanisms in order to explain this effect of which the Maier Goritz mechanism considers various interactions existing within the composite systems. They proposed stress-induced debonding of polymer chains from the filler surface as the reason behind the Payne effect due to filler-structure breakdown. Though the decrease of storage and loss moduli with strain in filled systems were explained mathematically the theory failed to account for many other rheological features. Filler-structure based theories and the debonding theory are difficult to distinguish experimentally since filler-filler and filler-matrix interactions are both dependent on specific filler characteristics such as surface treatment.

Very recently our group has explored the non linear viscoelastic effects in filled elastomers as Ponnamma et al. [10, 11] and Sadasivuni et al. [12] report Payne effect in 2D filler reinforced elastomers. This chapter aims in investigating the effect of layered silicates and graphene nanolayers on various elastomer matrices based on various filler concentrations and filler-matrix interactions.

2 Two-Dimensional Nanoparticles

Graphitic fillers and layered silicates are the main two dimensional fillers used to reinforce elastomer matrices. Here the significance of the most important nanoplatelets—nanoclay and graphene—on the nonlinear viscoelasticity of rubbers is discussed. Figure 1 gives the structural representation of these nanoparticles.

Graphene The structure of graphene consists of two-dimensional (2D) layers of carbon atoms ordered into a honeycomb lattice as shown in Fig. 1a. This planar monolayer of carbon atoms with carbon–carbon bond length of 0.142 nm is one of the allotropes (carbon nanotube, fullerene, diamond) of elemental carbon [13]. The free electrons in graphene behave like massless relativistic particles, which

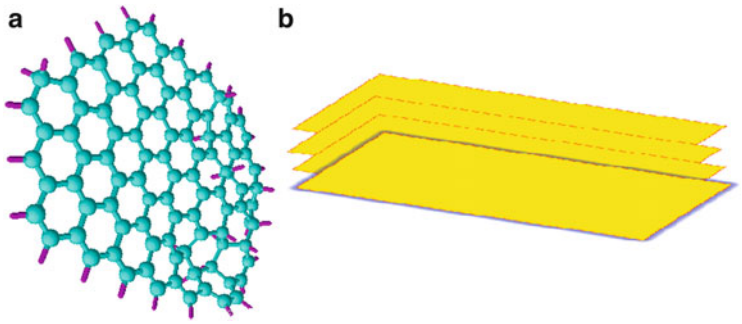

Fig. 1 Two dimensional nanofillers (**a**) Graphene (**b**) nano Clay

contribute to very peculiar properties [14–22] such as Dirac spectrum of low-lying quasiparticles [14], large mean-free-path [15], and high electron mobility [23, 24]. Graphene can be synthesized by various means such as exfoliation and cleavage [15, 25, 26], chemical vapor deposition (CVD) [27–31] and chemical method [32–35]. The nature of graphene is reported to be a gapless semiconductor evident from the Dirac energy dispersion and its density vanishes linearly while approaching the Fermi energy. In fact it acts as a bridging material between semiconductors and metals with a finite density of electronic states at the Fermi energy level. The gap between the adjacent graphene layers can be opened by chemical modifications [36, 37] or lateral confinement [38–40] and this results in pushing the layers apart. During composite fabrication elastomer chains get entrapped in these gaps and bonding occurs thus reinforcing the matrix.

Nanoclay Figure 1b illustrates the structure of nanoclay with individual platelet thickness 1 nm and surface dimensions 300–600 nm. These dimensions enhance its aspect ratio. Examples of nanoclays used in rubber reinforcement include montmorillonite, bentonite, kaolinite, illite, chlorite, smectite etc. Naturally occurring montmorillonite is hydrophilic and so it is of great difficulty to fill organophilic polymers with such clays. In this situation modification of nanoclays with organophilic groups has importance as this process maintains enough rubber-filler compatibility. The surface compatibilization is also known as intercalation and it is possible for the macromolecular chains to get in between the intercalated clay platelets. Sometimes complete delamination of the layers can happen and it is referred to as exfoliation. This is the ideal situation for maximum rubber reinforcement. The clay composites have many applications such as fabrication of impermeable membranes, tyre inner tubes, textile materials etc. The properties such as good hardness, scratch resistance and flexibility make montmorillonite (chemically (Na, Ca) (Al, Mg) $6(SiO_{10})_3(OH)$ 6-nH_2O or hydrated sodium calcium aluminum magnesium silicate hydroxide) the most used clay in textile coating [41].

3 Characterization of 2D Fillers and its Nanocomposites

There are a lot of characterization techniques for the two dimensional filler particles as well as for its composites. Since this is not the subject of this chapter, the two main methods used to investigate such fillers and nanocomposites formation are mentioned in this section. These are the transmission electron microscopy (TEM) and X-ray diffraction (XRD) spectroscopy. A typical TEM image obtained for pristine graphene and nanoclay is shown in Fig. 2. The flake structures of both fillers are very clear from this figure and this technique offers the most useful one to confirm the filler synthesis. The graphene film shown in Fig. 2a has a high contrast and low contamination level. Such image was obtained by dipping the TEM copper grids into the solution processed by ultrasound assisted exfoliation during graphene synthesis and by collecting the graphene flakes on the grids. Thereafter a broad

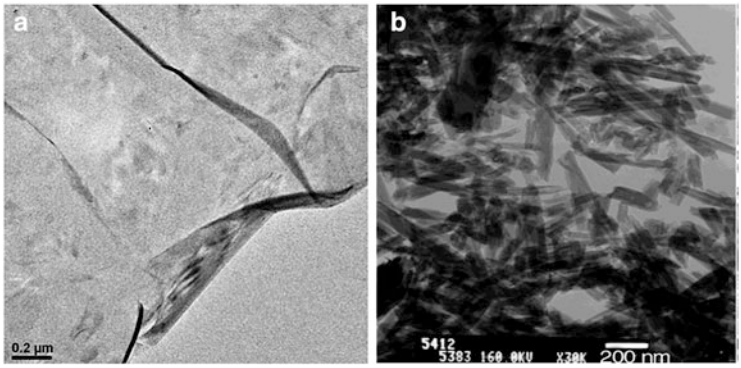

Fig. 2 TEM micrographs of pristine (**a**) graphene [42] (**b**) nanoclay [43]

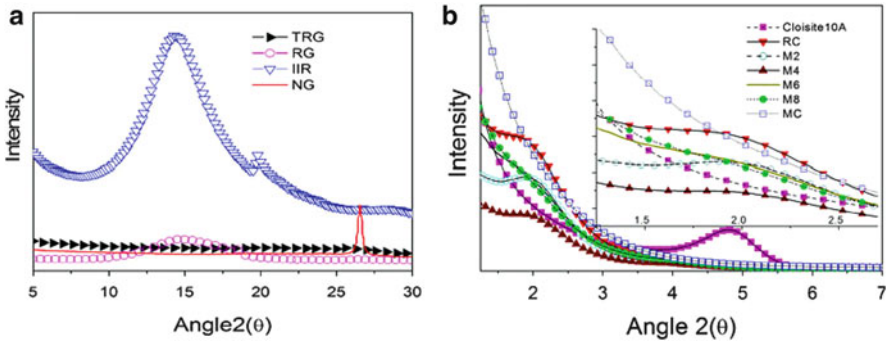

Fig. 3 (**a**) WAXD patterns of a thermally reduced graphene (TRG) and (**b**) Cloisite10A [12]

electron beam is passed through the thin sample to obtain the TEM image due to diffraction or mass-thickness contrast.

The dark lines in Fig. 2b correspond to the silicate layers of nanoclay. The image reveals a regular stacking arrangement of parallel layers present in the clay. The interlayer clay distances vary from 1.01 to 1.74 nm. The variation in this distance and the extent of exfoliation and composite formation are further analysed using X-Ray spectroscopy.

The typical XRD patterns for natural graphite (NG) and thermally reduced graphene (TRG) are presented in Fig. 3a. NG shows a diffraction peak at $2\theta = 26.5°$ corresponding to the stacked arrangement in graphite structure. Whereas in the case of TRG no characteristic peak is obtained, which indicate the complete exfoliation happening during thermal reduction. The XRD profiles for a typical clay cloisite 10A and its rubber nanocomposites are represented in Fig. 3b. The (001) diffraction of cloisite10A at $2\theta = 4.8°$, corresponds to an inter-layer spacing of 1.83 nm [12]. Depending on the composite nature the peak shifts in the spectrum and sometimes it is no longer present. The shifting of the peak to lower angle side

corresponds to the increased interplanar distance and this explains the incorporation of rubber chains inside the clay structure.

4 Theory of Non-linear Viscoelasticity

Rubber nanocomposites possess good nonlinearity in their viscoelastic properties and knowledge on this characteristic is very important in order to regulate various composite applications. The Payne effect is the most important dynamic mechanical measurement used to derive the interactions between the filler and polymer molecules. This effect is observed as the decrease in storage modulus (G′) with strain amplitude due to the breakdown of filler aggregates in rubber composites [44–46]. At higher strain rates, the rate of destruction of filler networks is higher than their rate of reconstruction which causes the dissipation energy associated with the network breaking to decrease [7, 47]. The maximum amount of energy dissipated comes from the consecutive breaking and reformation of all kinds of networks in the composites (filler–filler, filler–polymer, entanglement, glassy bridges, etc.). This phenomenon is assumed to be arising from two factors, one related to the hydrodynamic reinforcement and the other from the filler–filler and filler–elastomer interactions. In the case of a neat matrix, molecular disentanglement does not occur at low strain amplitudes and thus G′ is constant. The mechanism behind the Payne effect is explained as an adsorption–desorption process between the elastomer chains and the filler particles [7, 45–47]. The different interpretations proposed to explain the Payne effect based on mathematical models are shown in Fig. 4.

Of the several mechanisms investigated, the most commonly adopted is based on the filler network breakage [48, 49]. Kraus [7, 50] proposed a phenomenological model of the Payne effect based on this interpretation. In this model, under dynamic deformation, filler-filler contacts are continuously broken and reformed. The Kraus model considers filler–filler interactions but the loss modulus and effect of temperature were not taken into account. In the model of Huber and Vilgis [9, 50, 51] the existence of dynamic processes of breakage and reformation of the filler network is explained. In this model, the Payne effect is related to the fractal nature of the filler surface. At sufficiently high volume fractions of filler, percolation occurs and a continuous filler network is formed, characterized by its fractal dimension and its

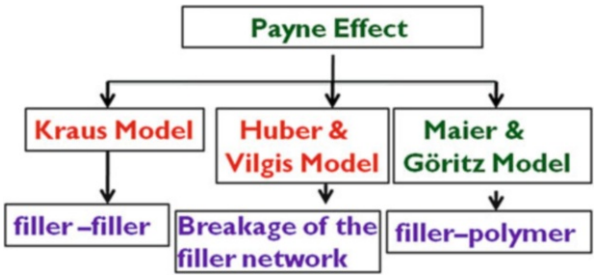

Fig. 4 Schematic representation of Payne effect and important models

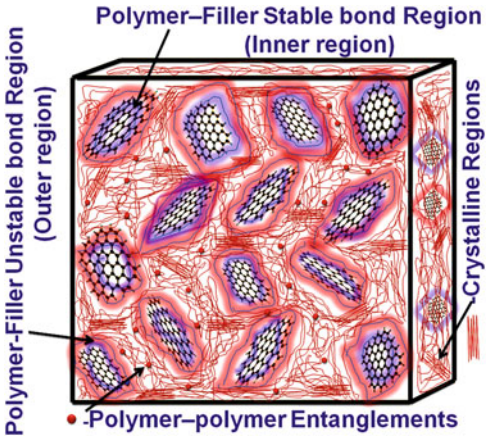

Fig. 5 Schematic representation of the Maier and Goritz model

connectivity. When the strain amplitude increases, the percolation network breaks into smaller and smaller entities. Maier and Göritz proposed yet another explanation to the Payne effect based on filler-rubber interactions contrary to the Kraus model (based on filler network). According to this model, each filler-rubber bond increases the network density, and this network density is supposed to vary with the deformation of the material. It is proposed that the elastic modulus of the filled elastomer has two contributions, the pure elastomer contribution and the filler contribution arising from the filler/elastomer interface instead of the filler network. There are two types of filler-rubber bonds: stable (strong) and unstable (weak) as shown in Fig. 5. The unstable bonds are likely to break when a mechanical stress is applied to the material or when the temperature is raised. Since the Maier and Goritz model considers all interactions within the composites, this model has given more emphasis here in this section.

Maier and Goritz model considers the contributions of both pure rubber and the filler (arising from the filler–rubber interface) to the elastic modulus of the composite. According to this model, the storage modulus (G′) of the composite is explained by Eq. (1).

$$G^{'} = Nk_BT \tag{1}$$

where k_B is the Boltzmann constant, T is the temperature and N is the crosslink density of the filled network. The cross link density itself is a combination of a few components as indicated by Eq. (2)

$$N_{total} = N_c + N_{st} + N_i \tag{2}$$

where N_c is number of chemical bonds from entanglement and N_{st} and N_i are the number of rubber-filler stable and unstable bonds per unit volume of the material. Since N_c denotes the contributions from both the chemical crosslinks and the

trapped entanglements within the composite it can also be defined as the number of elastically active rubber chains per volume unit of the material. The variation in the storage modulus with strain (γ) is represented by Eq. (3).

$$G^{'}(\gamma) = G^{'}_{st} + G^{'}_{i}\left(\frac{1}{1 + c\gamma}\right) \tag{3}$$

with $G^{'}_{st} = (N_g + N_{st})\, k_B T$ and $G^{'}_{i} = N_i k_B T$. $G^{'}_{st}$ is the value of G′ arising from the stable filler-rubber bonds and G'_i that from the unstable bonds, C is the experimental parameter.

Payne effect studies in filled silicone elastomers were carried out by Aranguren et al. [52, 53]. They found that direct filler-filler contacts are very few in the composite especially at the lower filler concentrations since the filler surface is completely wetted by the polymer. This was further confirmed using bound rubber measurements as well. Thus the contacts between filler aggregates exist via the polymer and the Payne effect result from agglomeration/deagglomeration of the filler-rubber-filler network. Recently, Wang et al. [54] also described non linear viscoelasticity of composites based on filler networks formed directly between filler particles and also through the elastomer domains. In the second type of interaction, the elastomer layers, glassy near the filler surface, have a modulus gradually decreasing with the distance from the filler surface. In addition, filler-rubber clusters entrap occluded rubber and this also behaves as filler mechanically. The Payne effect would thus originate from the breakage and reformation of such filler networks and clusters.

Filler modification affects the viscoelasticity since the variation in storage modulus with strain changes with rate of dispersion. This is illustrated in Fig. 6. The unmodified fillers in rubber cause agglomeration and thus result in high Payne effect due to strong inter-aggregate interaction of filler. With modification, the Payne effect of the filled compounds changes as the filler-filler networks is

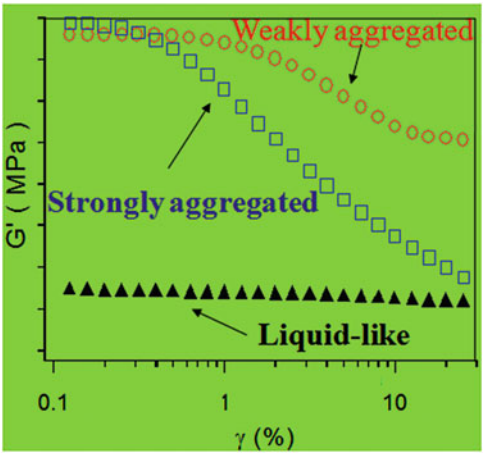

Fig. 6 Effect of filler aggregate (dispersion) on Payne effect

disrupted in this case. Thus Payne effect is closely related to nature of fillers and rate of dispersion.

5 Rubber Nanocomposites

5.1 Graphene/Rubber Nanocomposites

The comparative nonlinear dynamic viscoelastic response of neat natural rubber (NR) and its nanocomposites with reduced graphene oxide are shown in Fig. 7. We have reduced the synthesized graphene oxide thermally at two different temperatures 600 and 200 °C and dispersed in NR matrix along with carbon nanotube (CNT), each filler at 2.5 phr concentration. The variation in storage modulus with strain for such nanocomposites NR–CG600 and NR–CG200 are compared with NR–CNT at 5 phr filler concentration. Figure 7 shows the viscoelasticity at 0.5 Hz [10] frequency and at 25 °C temperature. The decrease in storage modulus with shear amplitude is highly significant for NR–CNT indicating the order of filler–rubber interaction as NR–CNT > NR–CG600 > NR–CG200. It is clear from the results that both the filler surface area and their interactions with the rubber strongly influence the network strength. The behavior is also fitted with Maier and Goritz mathematical modeling and established the good filler rubber compatibility and stable interactions.

The viscoelastic responses of polyurethane (PU)/GO composites at constant frequency of 0.5 Hz with strain sweep at 298 K, 323 K and 348 K temperatures are addressed by monitoring the Payne effect and the results obtained are illustrated

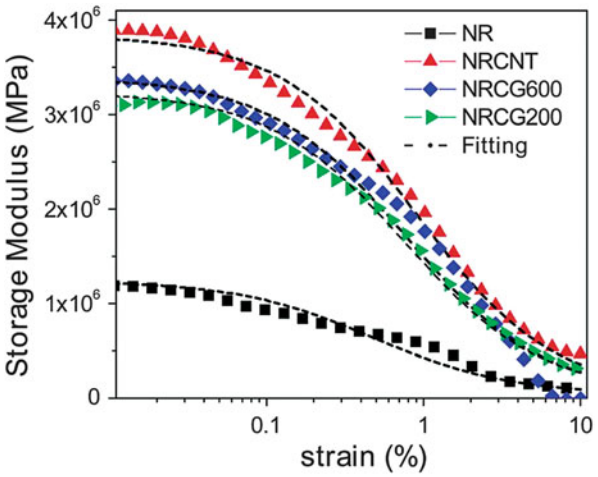

Fig. 7 Strain dependence of the storage modulus (fitted with Maier and Goritz model) for neat NR, NR–CNT, NR–CG600 and NR–CG200 [10]

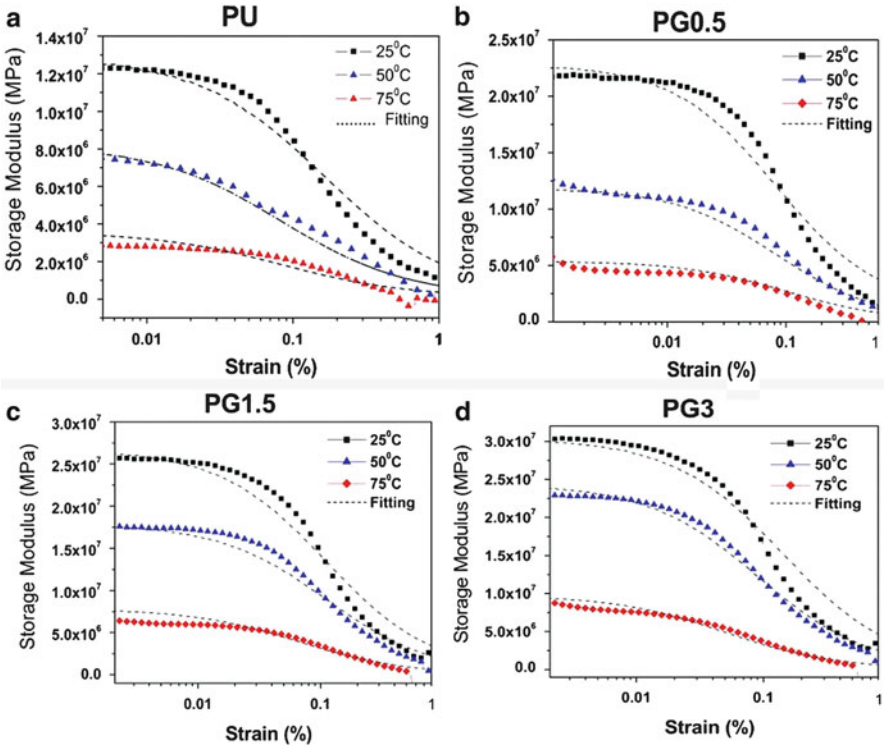

Fig. 8 Strain dependence of the storage modulus (fitted with the Maier and Goritz model) for (**a**) neat PU, (**b**) PG0.5, (**c**) PG1.5 and (**d**) PG3 at different temperatures of 298 K, 323 K and 348 K [11]

in Fig. 8. During this phenomenon, the deformation ratio increases through breakdown processes occurring in the agglomerates in elastomer composites due to the applied strain.

The different volume fractions of GO are marked in the sample names (neat PU, PG0.5 (0.5 phr loading), PG1.5 (1.5 phr loading) and PG3 (3 phr loading)). With increasing weight percentage the storage moduli increase and in all cases the experimental values are fitted well with Maier Goritz modeling indicating good filler matrix interaction. The dotted lines in Fig. 8 represent the model curve fits. The various parameters characterizing the network strength were calculated and the modulus variation is observed to be strongly influenced by the amount of the filler-filler (particles in contact with other particle surfaces form aggregates) and filler–polymer (surface of a particle associated with the adsorbed polymer chains) interactions. Indeed, the adsorption of polymer chains on the filler particles creates a core–shell structure in which the core is a packed particle cluster and the shell is made of immobilized polymer chains that have a different mobility compared to the chains in the bulk. The bonding process between these structures occurs by bridging with the other polymer chains or overlapping at high filler loadings.

Temperature decreases the storage modulus and Payne effect as more and more filler aggregates and clusters present within the nanocomposite break at enhanced temperatures. The decrease in the initial storage modulus of neat PU with increase in temperature is attributed to the loss of entanglements or improvement of soft regions in the matrix at higher temperature. PU/GO nanocomposites also show a similar kind of evolution but they have some additional crosslinks than PU.

5.2 *Clay/Rubber Nanocomposites*

The non linear viscoelastic properties of nanoclay filled rubber systems are widely reported. Figure 9 shows the Payne effect observed for butyl rubber nanocomposites at 25 °C. The filled composites show obviously higher storage modulus (G′) than neat rubber [55]. Here the rubber was grafted with polar group in order to enhance the interfacial compatibility and the properties were compared with that of unmodified clay and graphene filled rubber composites. It is found that the rate of maleic anydride grafting has a strong positive influence on the Payne effect due to the significant reinforcement. The number of rubber–filler stable bonds per unit volume for the neat IIR and various IIR nanocomposites can be calculated using Maier Goritz mathematical equations. The number of rubber–filler stable bonds per unit volume for neat IIR ($N_{st} = 0.12 \times 10^{26}/cm^3$) is observed to be lower than all its nanocomposites due to the lack of additional cross links from the filler side. IIR/graphene (RG, 5phr) shows the highest number of stable bonds ($N_{st} = 3.65 \times 10^{26}/cm^3$) among all nanocomposites because of the strong interactions between rubber and graphene compared to nanoclay.

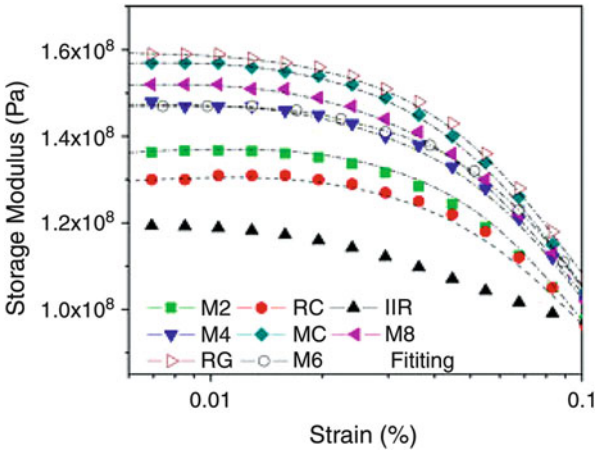

Fig. 9 Strain dependence of storage modulus at 25 °C temperature of neat IIR, IIR/graphene, IIR/cloisite10A, MA-g-IIR/cloisite10A and IIR/cloisite10A nanocomposites containing various loading of MA-g-IIR (*dotted lines* represent the curve fits) [12]

Among the clay nanocomposites, MC (fully maleic anhydride grafted IIR mixed with clay at 5 phr) had the highest number of stable bonds. Figure 9 also shows the increase in the number of stable bonds (increased Payne effect) with the rate of grafting and amount of MA-g-IIR (maleic anhydride grafted IIR). This is attributed to the increased specific surface area with the increase in MA-g-IIR content, which can improve the number of bonds and thus the filler–rubber bond formation. The same conclusion was drawn from the analysis of the unstable bonds as well.

In order to distinguish the importance of nonlinear viscoelastic properties of rubber nanocomposites on nature of filler used, the influence of linear property should also be mentioned. For this the effect observed in the thermoplastic polypropylene (PP) is discussed as last part of this chapter. Figure 10 shows the variation in storage modulus of PP/montmorillonite with strain amplitude. Here the linear viscoelastic domain of the composite is found to decrease with increasing exfoliation degree of organoclay tactoids. The linear region of the modulus depends on the processing conditions of the material and the maximum strain to which the linear viscoelastic domain extends decreases while increasing the clay concentration [56–59]. Thus the decrease in linear viscoelasticity of the composite can be attributed to the degree of dispersion as well as exfoliation. In short the linear viscoelastic properties also has significance in investigating the particle-particle interaction of the filler tactoid physical network but in the case of nanocomposites other than elastomers.

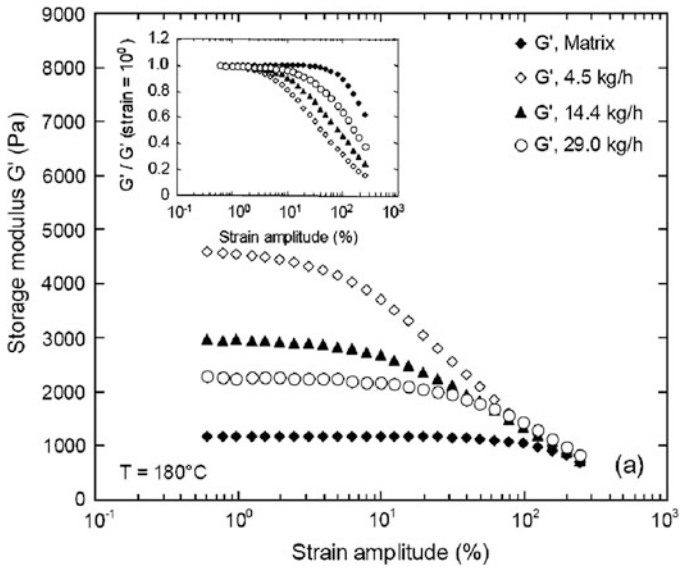

Fig. 10 Strain-dependence of PP/montmorillonite nanocomposite on the exfoliation quality. From a processing point of view, the exfoliation degree is expected to decrease with the increase of the flow rate in the extruder (Reprinted with permission)

6 Summary

Mechanisms governing the nonlinear viscoelasticity of 2D nanoplatelets filled elastomers are explored in the present chapter. Filler size, concentration and the entanglement characteristics of the elastomer matrix appear to be the primary factors determining both reinforcement and nonlinear viscoelasticity of the nanocomposites. The nanofillers provide large interfacial area for enough elastomer-filler interactions and both their particle spacing and size are of comparable dimensions to the macromolecular coil. The effects of filler surface treatment, filler networking, and matrix modification indicate the entanglement structure in the matrix as the dominant factor in determining the viscoelastic behavior of the composite. Trapping elastomer chains at the filler surface results in higher entanglement density and this density varies with distance from the filler surface based on filler surface treatment and its interactions with the matrix polymer. Different models proposed to explain the nonlinear viscoelasticity and to find out crosslink density are discussed. The loss of trapped entanglements resulting from the stress (or strain)-induced debonding of chain segments from the filler surface facilitates the relaxation of the matrix entanglement structure, resulting in the observed viscoelastic nonlinearity. Nanoclay and graphene filled elastomers have much significance in engineering applications and their nonlinear behavior should be considered based on filler agglomeration phenomena and is studied here.

References

1. Sadasivuni KK, Ponnamma D, Thomas S, Grohens Y (2014) Evolution from graphite to graphene elastomer composites. Prog Polym Sci 39:749–780
2. Sadasivuni KK, Castro M, Saiter A, Delbreilh L, Feller JF, Thomas S, Grohens Y (2013) Development of poly(isobutylene-co-isoprene)/reduced graphene oxide nanocomposites for barrier, dielectric and sensing applications. Mater Lett 96:109–112
3. Kawahara S, Kawazura T, Sawada T, Isono Y (2003) Preparation and characterization of natural rubber dispersed in nano-matrix. Polymer 44:4527–4531
4. Paiphansiri U, Tangboriboonrat P (2005) Prevulcanisation of skim latex: morphology and its use in natural rubber based composite material. Colloid Polym Sci 284:251–257
5. Peng Z, Kong LX, Li SD, Chen Y, Huang MF (2007) Self-assembled natural rubber/silica nanocomposites: its preparation and characterization. Compos Sci Technol 67:3130–3139
6. Payne AR (1962) The dynamic properties of carbon black-loaded natural rubber vulcanizates. Part I. J Appl Polym Sci 6:57–63
7. Kraus GJ (1984) Mechanical losses in carbon black filled rubbers. Appl Polym Sci Appl Polym Symp 39:75–92
8. Heinrich G, Kluppel M (2002) Recent advances in the theory of filler networking in elastomers. Adv Polym Sci 160:1–44
9. Maier PG, Göritz D (1996) Molecular interpretation on the Payne effect. Kautsch Gummi Kunstst 49:18–21
10. Ponnamma D, Sadasivuni KK, Strankowski M, Guo Q, Thomas S (2013) Synergistic effect of multi walled carbon nanotubes and reduced graphene oxides in natural rubber for sensing application. Soft Matter 9:10343–10353

11. Ponnamma D, Sadasivuni KK, Strankowski M, Moldenaers P, Thomas S, Grohens Y (2013) Interrelated shape memory and Payne effect in polyurethane/graphene oxide nanocomposites. RSC Adv 3:16068–16079
12. Sadasivuni KK, Saiter A, Gautier N, Thomas S, Grohens Y (2013) Effect of molecular interactions on the performance of poly (isobutylene-co-isoprene)/graphene and clay nanocomposites. Colloid Polym Sci 291:1729–1740
13. Slonczewski JC, Weiss PR (1958) Band structure of graphite. Phys Rev 109:272
14. Castro Neto AH, Guinea F, Peres NMR, Novoselov KS, Geim AK (2009) The electronic properties of grapheme. Rev Mod Phys 81:109
15. Novoselov K, Geim A, Morozov S, Jiang D, Zhang Y, Dubonos S, Grigorieva I, Firsov A (2004) Electric field effect in atomically thin carbon films. Science 306:666
16. Abergel DSL, Apalkov V, Berashevich J, Ziegler K, Chakraborty T (2010) Properties of graphene: a theoretical perspective. Adv Phys 59:261
17. Allen MJ, Tung VC, Kaner RB (2009) Honeycomb carbon: a review of graphene. Chem Rev 110:132–145
18. Yazyev OV (2010) Emergence of magnetism in graphene materials and nanostructures. Rep Prog Phys 73:056501
19. Cresti A, Nemec N, Biel B, Niebler G, Triozon F, Cuniberti G, Roche S (2008) Charge transport in disordered graphene-based low dimensional materials. Nano Res 1:361
20. Beenakker CWJ (2008) Colloquium: Andreev reflection and Klein tunneling in graphene. Rev Mod Phys 80:1337
21. Sarma SD, Adam S, Hwang EH, Rossi E (2010) Electronic transport in two dimensional graphene. Rev Mod Phys 83:407
22. Mucciolo ER, Lewenkopf CH (2010) Disorder and electronic transport in graphene. J Phys Condens Matter 22:273201
23. Bolotin KI, Sikes KJ, Hone J, Stormer HL, Kim P (2008) Temperature-dependent transport in suspended graphene. Phys Rev Lett 101:096802
24. Du X, Skachko I, Barker A, Andrei EY (2008) Approaching ballistic transport in suspended graphene. Nat Nano 3:491
25. Blake P, Brimicombe PD, Nair RR, Booth TJ, Jiang D, Schedin F, Ponomarenko LA, Morozov SV, Gleeson HF, Hill EW, Geim AK, Novoselov KS (2008) Graphene-based liquid crystal device. Nano Lett 8:1704
26. Hernandez Y, Nicolosi V, Lotya M, Blighe FM, Sun Z, De S (2008) High-yield production of graphene by liquid-phase exfoliation of graphite. Nat Nanotechnol 3:563
27. Stankovich S, Dikin DA, Piner RD, Kohlhaas KA, Kleinhammes A, Jia Y, Wu Y, Nguyen SBT, Ruoff RS (2007) Synthesis of graphene-based nanosheets via chemical reduction of exfoliated graphite oxide. Carbon 45:1558
28. May JW (1969) Platinum surface LEED rings. Surf Sci 17:267
29. Shelton JC, Patil HR, Blakely JM (1974) Equilibrium segregation of carbon to a nickel (111) surface: a surface phase transition. Surf Sci 43:493
30. Eizenberg M, Blakely JM (1979) Carbon monolayer phase condensation on Ni (111). Surf Sci 82:228
31. Somani PR, Somani SP, Umeno M (2006) Planer nano-graphenes from camphor by CVD. Chem Phys Lett 430:56
32. Hummers WOR (1958) Preparation of graphite oxide. J Am Chem Soc 80:1339
33. Li D, Muller MB, Gilje S, Kaner RB, Wallace GG (2008) Processable aqueous dispersions of graphene nanosheets. Nat Nanotechnol 3:101
34. Cai WW, Piner RD, Stademann FJ, Park S, Shaibat MA, Ishii Y (2008) Synthesis and solid-state NMR structural characterization of ^{13}C labeled graphite oxide. Science 321:1815
35. Gao W, Alemany LB, Ci L, Ajayan PM (2009) New insights into the structure and reduction of graphite oxide. Nat Chem 1:403
36. Sluiter MHF, Kawazoe Y (2003) Cluster expansion method for adsorption: application to hydrogen chemisorption on graphene. Phys Rev B 68:085410

37. Sofo JO, Chaudhari AS, Barber GD (2007) Graphene: a two-dimensional hydrocarbon. Phys Rev B 75:153401
38. Fujita M, Igami M, Nakada K (1997) Lattice distortion in nanographite ribbons. J Phys Soc Jpn 66:1864
39. Han MY, Özyilmaz B, Zhang Y, Kim P (2007) Energy band-gap engineering of graphene nanoribbons. Phys Rev Lett 98:206805
40. Chen Z, Lin YM, Rooks MJ, Avouris P (2007) Graphene nano-ribbon electronics. Phys E 40:228
41. Utracki LA (2004) Clay containing polymeric nanocomposites. Rapra Technology, Shropshire
42. Wang Y, Liu J, Wang K, Chen T, Tan X, Li CM (2011) Hydrogen storage in NieB nanoalloy-doped 2D graphene. Int J Hydrogen Energy 36:12950–12954
43. Khunova V, Kristóf J, Kelnar I, Dybal J (2013) The effect of halloysite modification combined with in situ matrix modifications on the structure and properties of polypropylene/halloysite nanocomposites. eXPRESS Polym Lett 7(5):471–479
44. Payne AR, Whittaker RE (1971) Low strain dynamic properties of filled rubbers. Rubber Chem Technol 44:440–478
45. Heinrich G, Kluppel M, Vilgis T (2002) Reinforcement of elastomers. Curr Opin Solid State Mater Sci 6:195–203
46. Kluppel M (2003) The role of disorder in filler reinforcement of elastomers on various length scales. Adv Polym Sci 164:1–86
47. Sternstein SS, Zhu AJ (2002) Reinforcement mechanism of nanofilled polymer melts as elucidated by nonlinear viscoelastic behavior. Macromolecules 35:7262–7273
48. Payne AR (1965) In: Kraus G (ed) Reinforcement of elastomers, Chap 3. Wiley Interscience, New York
49. Kraus G, Childers CW, Rollmann KW (1966) Stress softening in carbon black-reinforced vulcanizates. Strain rate and temperature effects. J Appl Polym Sci 10:229–244
50. Kraus G (1963) Swelling of filler-reinforced vulcanizates. J Appl Polym Sci 7:861–871
51. Huber G, Vilgis TA, Heinrich G (1996) Universal properties in the dynamical deformation of filled rubbers. J Phys Condens Matter 8:L409–L412
52. Aranguren MI, Mora E, Macosko CW, Saam J (1994) Rheological and mechanical properties of filled rubber: silica-silicone. Rubber Chem Technol 67:820
53. Aranguren MI, Mora E, DeGroot JV, Macosko CW (1992) Effect of reinforcing fillers on the rheology of polymer melts. J Rheol 36(6):1165
54. Wang MJ (1998) Effect of polymer-filler and filler-filler interactions on dynamic properties of filled vulcanizates. Rubber Chem Technol 71:520
55. Meera AP, Said S, Grohens Y, Thomas S (2009) Nonlinear viscoelastic behavior of silica-filled natural rubber nanocomposites. J Phys Chem C 113:17997
56. Wan T, Clifford MJ, Gao F, Bailey AS, Gregory DH, Somsunan R (2005) Strain amplitude response and the microstructure of PA/clay nanocomposites. Polymer 46:6429–6436
57. Aubry T, Razafinimaro T, Médéric P (2005) Rheological investigation of the melt state elastic and yield properties of a polyamide-12 layered silicate nanocomposite. J Rheol 49:425–440
58. Devendra R, Hatzkiriakos SG, Vogel R (2006) Rheology of metallocene polyethylene-based nanocomposites: influence of graft modification. J Rheol 50:415–434
59. Lertwimolnun W, Vergnes B, Ausias G, Carreau PJ (2007) Stress overshoots of organoclay nanocomposites in transient shear flow. J Nonnewton Fluid Mech 141:167–169

Nonlinear Viscoelasticity in Three Dimensional Filler Reinforced Rubber Composites and Nanocomposites

Michał Strankowski

Abstract This chapter describes the influence of three-dimensional nanofillers used in elastomers on the nonlinear viscoelastic properties. In particular, this part focuses and investigates the most important three-dimensional nanoparticles, which are used to produce rubber nanocomposites. The rheological and the dynamic mechanical properties of elastomeric polymers, reinforced with spherical nanoparticles, like POSS, titanium dioxide and nanosilica, were described. These (3D) nanofillers in are used polymeric matrices, to create new, improved rubber nanocomposites, and these affect many of the system's parameters (mechanical, chemical, physical) in comparison with conventional composites. The distribution of the nanosized fillers and interaction between nanofiller-nanofiller and nanofiller-matrix, in nanocomposite systems, is crucial for understanding their behavior under dynamic-mechanical conditions.

Keywords Three-dimensional fillers • Nanofillers • Composites • Nanocomposites • Rubbers

Abbreviations

0D	Zero-dimensional nanoparticle
3D	Three-dimensional nanofiller
AC	Coupling agent
ACM	Acrylic rubber
APMDS	Aminopropylmethyldiethoxysilane
APTS	3-Aminopropyltrimethoxysilane
AR	Covering agent
ENR	Epoxidized natural rubber
HDTMS	Hexsadecyltrimethoxysilane
MPTS	Methacryloxypropyltriethoxysilane
MWCNT	Multiwall carbon nanotubes

M. Strankowski (✉)
Chemical Faculty, Polymer Technology Department, Gdansk University of Technology, 11/12 Narutowicza Street, 80233 Gdansk, Poland
e-mail: micstran@pg.gda.pl

D. Ponnamma, S. Thomas (eds.), *Non-Linear Viscoelasticity of Rubber Composites and Nanocomposites*, Advances in Polymer Science 264, DOI 10.1007/978-3-319-08702-3_4

POSS	Polyhedral oligomeric silsesquioxane
RNC	Rubber nanocomposites
RTV	Room Temperature Vulcanizing silicone
TDSS	Tetrakis(dimethylsiloxy)silane
TEOS	Tetraethoxysilane
TESPD	Bis-(triethoxysilylpropyl)-disulfane
T_g	Glass transition temperature

1 Introduction

Rubber nanocomposites play a very important role among organic–inorganic hybrid materials. Nanomaterials very often are classified into three categories: nanoparticles, nanotubes and nanolayers, depending on how many dimensions of the dispersed particles are in the nanometer scale [1]. Different types of nanoparticles can be incorporated into the polymer matrix to obtain polymer nanocomposites, especially rubber nanocomposites. Nanocomposites are materials whose components (matrix + nanofiller) are mixed at a nanometer scale. The nature of the nanofillers allows nanocomposites to exhibit different properties in comparison to conventional microcomposites. Rubber nanocomposites, in comparison with classic rubber composites, are capable of improving the mechanical, chemical and physical properties, e.g. flame retardance, impact and heat resistance or barrier properties. These properties can be achieved at very low level loadings of nanofiller (practically, less than 5 wt%). Therefore, an important characteristic of nanocomposites is that they require much lower concentrations of filler than that required conventional microcomposites for similar rheological effects, because of the nanoparticle's larger available surface area and the development of a mesostructural polymer-nanoparticle network. These materials possess significantly increased interfacial interactions between nanoparticles and the polymeric matrix. It is well known that most polymers exhibit linear viscoelastic behavior under relatively large strains. For polymeric nanocomposites the linear viscoelastic properties generally increase with the addition of nanofiller. Recently, many researchers have reported work on nonlinear viscoelastic behavior, including high strain–stress hysteresis, stress softening, and strain-dependent dynamic modulus. Rubber nanocomposites exhibit nonlinear viscoelastic behavior in response to dynamic strain. This nonlinear behavior includes strong shear thinning at relatively low shear rates or strain-dependent viscoelastic moduli at low strain amplitudes and is called the Payne effect [2]. This effect is characteristic for filled and nanofilled polymers in the amorphous state above the glass transition temperature. It was A.R. Payne who investigated this strain-dependent modulus upon dynamic straining for rubber containing fillers over 50 years ago [3, 4]. The general interpretation of the nonlinearity in viscoelastic behavior in elastomeric matrix vs filler systems is connected with filler agglomeration and its network formation, which are responsible for the higher degree of reinforcement, and the nonlinearity varies with

the deagglomeration and the network breakdown of fillers. Understanding and control of the issues related to the Payne effect, especially during the preparation of new polymeric nanocomposites based on nanofillers is very important for materials application. A major role in determining nanofiller effects on nonlinear behavior of nanocomposites is played by the dispersion of the nanofillers in the rubber matrix and the interaction between these components.

The focus of this chapter is to present three-dimensional nanofillers and the influence of these kinds of nanoparticles on the nonlinear viscoelastic behavior of rubber nanocomposite systems.

2 Three Dimensional Fillers: Synthesis, Morphology and Characterization

2.1 Introduction to Three-Dimensional Nanoparticles

There are several methods of classification of polymeric nanocomposites. One of these classifications is based on the dimensionality of the nanoparticles that are dispersed into the polymer matrix.

Figure 1 presents the typical geometries of the nanodimensional fillers which are commonly used to modify the elastomeric matrix [5]. Nanoparticles possess many shapes and sizes (Fig. 1), but primarily they have three simple geometric forms: sphere, cylinder and plate type. Three-dimensional nanofillers (3D) are relatively equiaxed particles, smaller than 100 nm (often below 50 nm [6]), e.g. nano SiO_2, TiO_2. These nanoparticles are described in the Sects. 2.2–2.4. Sometimes in the literature, the term 3D nanofillers (spherical) is described as a zero-dimensional (0D) system, but actually 0D nanofillers are represented by POSS molecules, fullerenes, crystals or quantum dots [6]. What's more, very often the term "physical form" of these nanoparticles is referred to as "agglomerates". The dispersion of particles from agglomerates to nanoparticles seems to be a big challenge to all

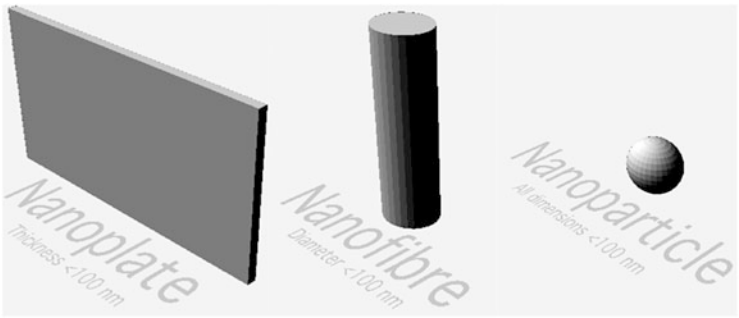

Fig. 1 Different types of nanofillers as defined in ISO/TS27687 (2008)

material-engineering scientists. However, by selection of the proper method of rubber nanocomposite preparation (selection of nanofiller and rubber matrix), it is possible to obtain systems with designed properties.

2.2 Polyhedral Oligomeric Silsesquioxane

Polyhedral oligomeric silsesquioxane (POSS) is one of the innovative inorganic–organic nanofillers, which—depending on the application—can be synthesized and modified in many ways. The POSS exist in a variety of structures and possess unique cage-like structures. These hybrid inorganic–organic composition $R_n(Si_{1.5})_n$, where R represents a range of organic functional groups (e.g. alkyl, alkylene, acrylate, hydroxyl), n is an even integer ≥ 4, has nano sized cage structures (Fig. 2) [7]. In the early 1990s, a scientific team led by Dr. Joseph Lichtenhan at Edwards Air Force Base in California, USA invented the new class of POSS. Since 1990s many research studies have reported work on a large number of POSS monomers and polymers.

When the organic groups of the POSS are non-reactive, they are similar to molecular silica. POSS is described as monofunctional POSS when one of the groups is reactive, or multifunctional POSS—if more than one group is reactive. Silsesquioxane structures can be random, ladder, cage or partial cage [9]. The most common process for obtaining POSS compounds is the hydrolytic condensation of functional silane trialkoxymonomers $XSiY_3$, where X is a chemically stable organic substituent ($-CH_3$, phenyl, vinyl), and Y is a highly reactive substituent ($-$Cl, $-$OH or –OR) [10, 11] (Fig. 3).

Typical structures of POSS are presented in Fig. 4 [12].

POSS molecules have been easily incorporated into polymers via blending, grafting or copolymerization. Incorporation of POSS particles into polymer matrices leads to chemical cross-linking, where the nanofiller particles are covalently bonded with polymer. In a second approach, where the POSS nanoparticles are physically blended with polymer using melt mixing or solvent casting methods, the

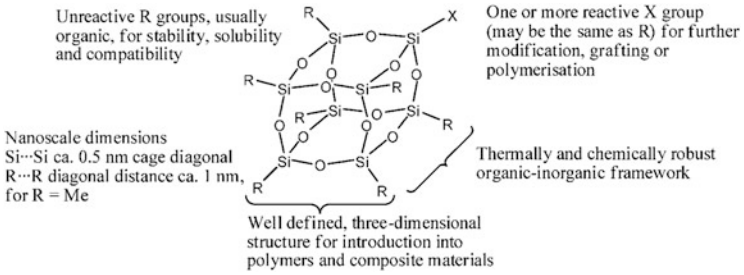

Fig. 2 The molecular structure of a POSS, where R represents unreactive organic groups for solubilization of the molecule and compatibility with other organic compounds. X represents reactive groups for grafting and copolymerization (Reprinted from [8])

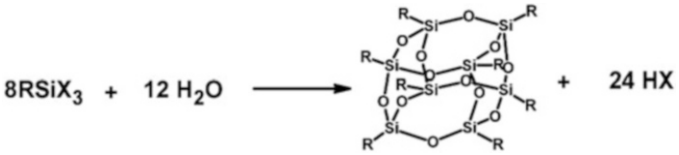

Fig. 3 Synthesis scheme of POSS by hydrolytic condensation (Reprinted from [10])

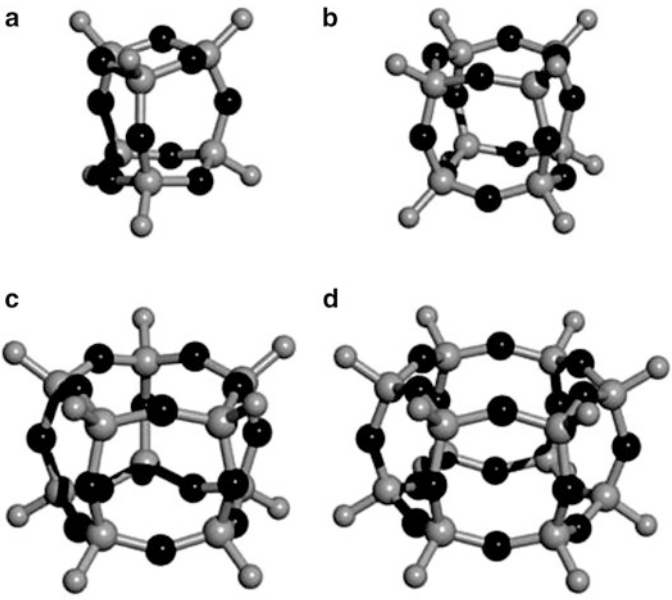

Fig. 4 Typical structures of POSS cages: (**a**) trigonal prismatic (Si_6O_9), (**b**) cubane (Si_8O_{12}) cage, (**c**) double five-ring ($Si_{10}O_{15}$) cage, (**d**) double six-ring ($Si_{12}O_{18}$) cage (Reprinted from [12])

compatibility of the nanofiller particles with the polymer matrix plays a key role [9]. A variety of polymers can be reinforced with POSS by attaching single or multiple polymerizable groups to a POSS cage [11].

Many of the characteristic properties of polymers can be enhanced using nanofillers. Incorporation of POSS into a polymer matrix can result in significant improvements of physical and mechanical properties. Different morphologies of the polymer nanocomposite systems affect these properties. In particular, the addition of POSS into a polymer matrix can increase the glass transition temperature of the nanocomposite and increase the thermal decomposition temperature of the reinforced POSS polymer system. What's more, property enhancements of polymers via POSS result: reduced flammability, extended temperature range, increased oxygen permeability, enhanced blend miscibility and reduced viscosity [13]. A recent nanocomposite review classified POSS as having zero-dimensionality or a sphere-like structure. What's more, these systems have the

ability to create higher dimensionality, through aggregation of crystals of the POSS particles in the polymer matrix [14].

POSS have been used to develop modern reinforced thermoplastic and thermosetting polymers. These materials are commercially manufactured by Hybrid Plastic, Inc. [15]. The company offers POSS-based nanofillers and polymers, which are nano reinforced (e.g. PPE, PEEK, PEI, PP, PA6). Nanostructured POSS chemicals can be used not only in plastics industry applications, but also in the whole technological area. These nanostructures have shown significant promising usage as catalyst supports and in biomedical applications [7].

2.3 *Silicon Dioxide (SiO_2)*

Sol–gel processing is one of the methods that has been widely implemented for manufacturing three-dimensional nanoparticles, which can be used for polymer modification. In the 1950s the Degussa process (Eq. 1) became the method for preparation of nanoparticles based on SiO_2, TiO_2 or Al_2O_3 [13].

$$Si(OC_2H_5)_4 + 2H_2O \rightarrow SiO_2 + 4C_2H_5OH \quad (1)$$

Using this process it is easy to control the particle size and morphology of the nanofiller (Fig. 5).

The sol–gel technique to generate nanosilica particles within a polymer matrix has been a useful process which gives specific interphase impact between the organic matrix and inorganic component. The incorporation of the filler particles into polymers using this process avoids the aggregation of the nanofiller within the polymer matrix [17]. The polymer-silica interaction depends on the size and shape of the nanofiller particles, their volume fraction, and the interparticle interaction [18]. What's more, these parameters also strongly influence the properties of the nanocomposites.

For several years many investigations were focused on the interaction between the nanofiller particles and the polymer chains. Especially, silica is very attractive tool to modify these interactions. The chemical modification of the silica surface

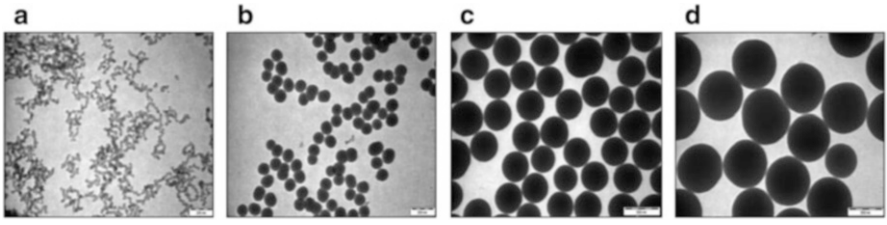

Fig. 5 TEM micrographs of different size of silica, obtained by controlling reaction parameters: (**a**) ~21 nm, (**b**) ~131 nm, (**c**) ~369 nm, (**d**) ~565 nm (Reprinted from [16])

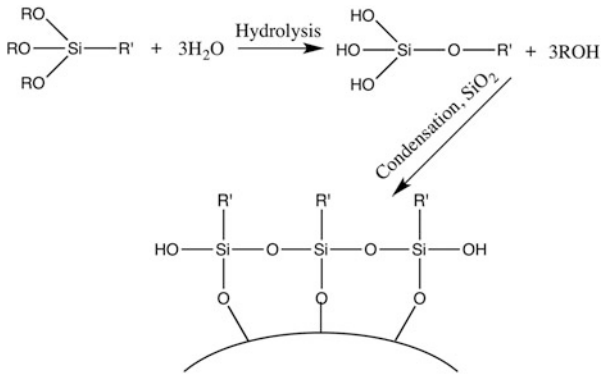

Fig. 6 Chemical modification of silica surface (Based on [16])

with organic functional groups makes it possible to obtain silica-polymer nanocomposites based on many matrices [16, 19, 20]. One of the most useful techniques is modification of a silica surface with silane coupling agents (Fig. 6). These molecules are able to create bonding between inorganic nanoparticles and organic polymer chains. $Si(OR)_3$ group can react with the inorganic reinforcement, while the (R′) group can interact with the polymer [16].

Silica surface modification using silane coupling agents (e.g. 3-aminopropyltrimethoxysilane (APTS), aminopropylmethyldiethoxysilane (APMDS) or methacryloxypropyltriethoxysilane (MPTS) can be carried out in aqueous or non-aqueous solution systems, but for large scale production, an aqueous system is preferred [21, 22].

Silica-polymer nanocomposites can be prepared, using commonly known techniques, from solution, or by in situ polymerization, or from melt mixing processes. The first two techniques (solution mixing and in situ polymerization) lead to a good dispersion of nanoparticles in composite's matrix. Obviously, it is possible to prepare homogenous dispersion of nanofillers, using the melt mixing process, but sometimes achieving acceptable distribution of silica is a big challenge.

Recently, rapid development of silica based nanocomposite materials has been reported. These materials can be used in many industries (e.g. automotive, electronic). Applications of silica nanoparticle reinforced polymer matrices highly depends on many parameters, for e.g. improved thermal [23], mechanical [24], chemical and physical properties. Generally, the addition of silica nanoparticles into the polymer rubbery matrix causes an increase in the glass transition temperature (T_g) and storage modulus, and also an increase in the thermal stability of the system [24–26].

Nanosilica is commercially available under the trademark of AEROSIL® (product of Evonik Industries) [27]. Nanosilica powder is industrially produced by both the fuming method and the precipitation method. In the fuming method it is manufactured by a high temperature vapor process in which $SiCl_4$ is hydrolyzed in a flame of oxygen-hydrogen. Precipitated silica, in turn, is manufactured by a wet

procedure by treating silicates with mineral acids to obtain fine hydrated silica particles in the course of precipitation [28].

These products (fumed silica) are highly dispersed, amorphous, white in color and spherically shaped. The average diameters of the primary particles are in the range of 7–40 nm, according to the AEROSIL® grade [13]. The company offers many products made from silica, e.g. hydrophilic fumed silica, hydrophobic fumed silica or fumed mixed oxides (mixtures of SiO_2 and Al_2O_3) [27].

2.4 Titanium Dioxide

Among the many nanofillers, Titanium dioxide (TiO_2) is very often investigated, in polymeric applications, since it is non-toxic, chemically inert, possess high hardness and has UV filter properties.

Several methods have been developed for generating colloidal titania particles [29]. One of the popular methods to obtain TiO_2 is the sol–gel method, as with SiO_2 nanoparticles. Using this relatively simple method it is possible to control the properties of the product, such as size of the particles or phase composition. The preparation of TiO_2 nanoparticles can be effectively carried out through the hydrolysis and condensation of titanium alkoxides in aqueous media (sol–gel method) [30, 31]. The reactions are presented in Eqs. (2) and (3) below: where R is ethyl, i-propyl, n-butyl group.

$$\mathrm{Ti(OR)_4 + 4H_2O \rightarrow 2Ti(OH)_4 + 4ROH \ \ (hydrolysis)} \tag{2}$$

$$\mathrm{Ti(OH)_4 \rightarrow TiO_2 \, xH_2O + (2 - x)H_2O \ \ (condensation)} \tag{3}$$

Different size and morphology of the TiO_2 strongly depend on the water/titanium molar ratio and the pH of the solution during the reaction. At high ratios of H_2O/Ti, small-sized particles are formed [31]. The second method of producing TiO_2 nanoparticles, is a hydrothermal process which proceeds in aqueous or nonaqueous systems. The particles prepared using hydrothermal synthesis, are expected to have larger surface area, smaller crystalline size, and higher stability than those obtained by other methods [32].

TiO_2 generally occurs in three crystalline phases: rutile, anatase and brookite [33]. The possible transformation is accelerated by heat treatment at temperatures between 450 and 1,200 °C and is dependent on several parameters such as particle size, initial phase, dopant concentration, reaction atmosphere and annealing temperature [34]. Crystalline structure of the TiO_2, amorphous phase content, morphology and size of the particles significantly affect the activity of the nanofiller and matrix improvement [29].

TiO_2 has been extensively explored for many years, due to its effect on the polymer matrix and relatively easy availability. The nano-titanium dioxide used for modification of the polymer can improve optical [35], UV radiation [36], thermal

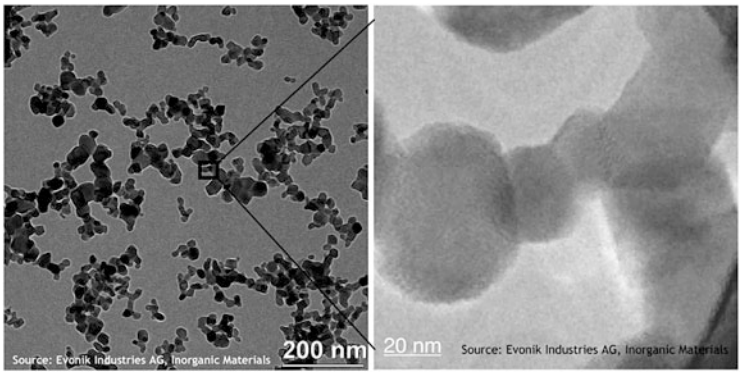

Fig. 7 TEM micrographs of AEROXIDE TiO_2P25, primary crystals (*right*), their aggregates and agglomerates (*left*) (Reprinted from [39])

[37] and mechanical properties [36]. However, in some applications the addition of the TiO_2 nanoparticles into the polymer can catalyze rubber-nanocomposite photodegradation [38]. TiO_2 is strongly photoactive when exposed to sunlight or UV, especially in presence of moisture. Also, TiO_2 nanoparticles have a tendency to agglomerate caused by very high surface energy, which hinders dispersion into the polymer matrix.

The form of TiO_2 most commonly used as a nanofiller is titanium dioxide P25 from Evonik Industries [27] (Fig. 7). TiO_2 is an excellent additive to improve the heat stability of room temperature vulcanized (RTV) silicone adhesive/sealant [13]. Hydrophilic fumed TiO_2 (AEROXIDE® TiO_2 P25) from Evonik Industries can be applied also as a catalyst carrier or active component for photocatalyst reactions, where the crystalline structure and phase (anatase and rutile) content are important. They offer three grades of TiO_2 with different surface areas (50–90 m^2/g) and particle morphologies: AEROXIDE® TiO_2 P25, P90 and P25/20 [39].

3 Rubber Nanocomposites

Rubber nanocomposites have attracted great interest for the past few years due to their unique physical and chemical properties [17]. The properties of rubber nanocomposites can be modified with various nanoparticles. There are a lot of types and shapes of the nanofillers like: silica, TiO_2, POSS, nanocrystals, other oxides (three-dimensional); carbon nanotubes, metallic fibers (two-dimensional); and clays, modified clays or graphene (one-dimensional).

Polymeric nanocomposites can be obtained using one of the following methods: solution casting, in situ polymerization or melt blending. Preparing nanocomposites by solution mixing gives nicely dispersed nanofiller in the polymer; however the use of a solvent is sometimes limited. The second method (in situ) is based on

dispersion of nanofiller in a monomer, which can polymerize. This method gives many possibilities for synthesis and modification (matrix or filler). In the third method (melt blending/mixing), the polymer is processed using extruders, very often a twin-screw extruder. This method, based on polymer processing (in a bulk state) is widely available, but good dispersion of the nanofiller in the polymer matrix is sometimes difficult to achieve [40].

Rubber nanocomposites can be based on many rubber matrices, for example (clay reinforcement): natural rubber [41] or synthetic rubber materials such as styrene-butadiene rubber [42], nitrile-rubber [43], EPDM [44] or polyurethane [45, 46].

Nanoparticles, compared with traditional fillers, provide more reinforcement due to the higher interfacial area. Introduction of these particles into the rubber matrix improves many of its properties, in particular tensile strength, thermal stability, elasticity, processability or barrier improvement. The final properties of nanocomposites are determined by the filler-filler and polymer-filler interactions. Therefore, it is very important to have knowledge of the characteristics of nonlinear viscoelastic behavior for rubber reinforced systems, especially an analysis of the low strain dynamic mechanical properties (Payne effect).

The next sections present the influence of 3D nanofillers in rubber nanocomposites on the nonlinear viscoelastic behavior of these systems.

3.1 Polyhedral Oligomeric Silsesquioxane Rubber Nanocomposites

Poly(dimethylsiloxane) (PDMS) is one of the most popular inorganic elastomers and can be modified with many nanofillers. Pan et al. used silanol-terminated PDMS and modified this matrix with mono-POSS and tetra-POSS cages which were physically blended into the matrix. The authors prepared another type of PDMS which had vinyl terminal groups that are also able to react with the central siloxane core by hydrosilylation. The idea was to obtain larger POSS-based fillers than silica particles typically used to reinforce elastomers (Fig. 8).

Figure 9 gives the dynamic mechanical analysis results showing that the POSS containing composites possess higher storage modulus with increasing POSS content in the low strain modulus amplitude. This behavior is characteristic for the Payne effect. Percolation of the filler particles is part of the filler network interpretation of the Payne effect. The authors expected a dramatic increase in the described effect at loadings of about 15 % wt of the nanofiller. Figure 9a suggests that the percolation threshold is at 10 % wt or more with the addition of POSS. This level of percolation threshold may result from a larger effective filler volume fraction in these systems. Useful information about the filler-networking behavior comes from the loss tangent vs. strain amplitude observed in the Fig. 9b. The maximum of the loss tangent is visible in the 10 % wt POSS-containing

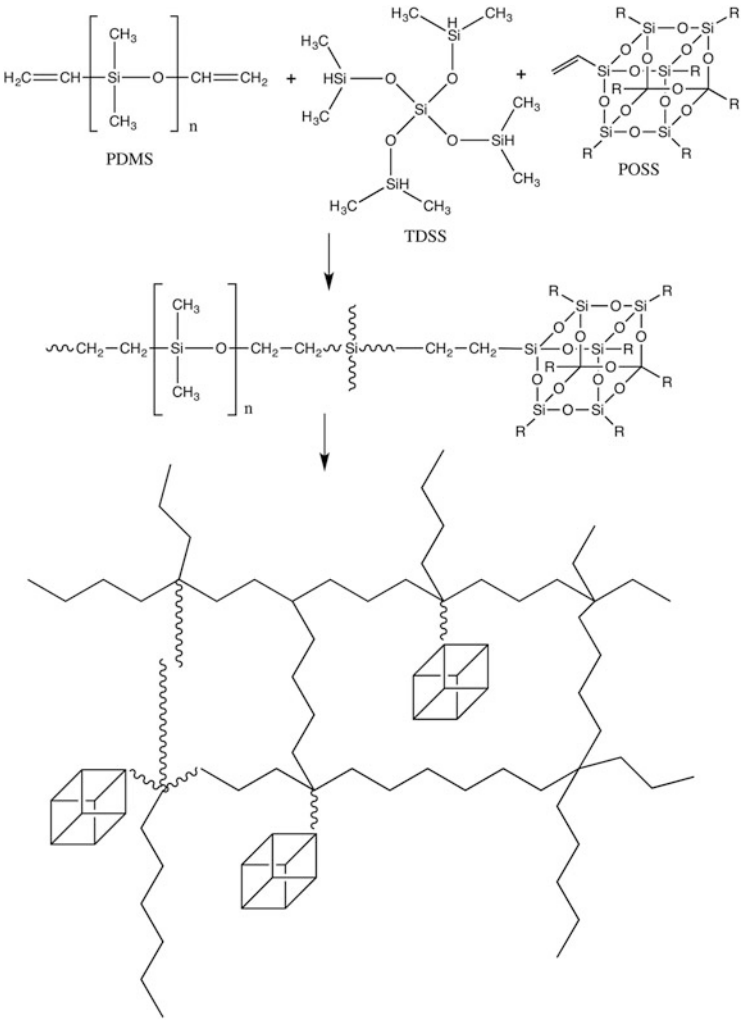

Fig. 8 Chemical incorporation of POSS cages to PDMS networks (Based on [47])

nanocomposite. The authors conclude that peaks occur according to the filler-networking concept presented by Kraus [48]. The maximum loss tangent is correlated with the strain amplitude of the network.

These studies have shown that POSS can reinforce PDMS especially when it is partially bonded to the polymer network. What's more, when POSS fillers blended with a PDMS silanol-terminated matrix (without bonding), the mechanical properties remained on the same level. Chemical bonds between the filler and the matrix are not directly correlated with the reinforcement of the system, but improve the dispersion of the filler in the polymer network. Bonded composites possess a dynamic mechanical response very similar to rubbers filled with colloidal silica.

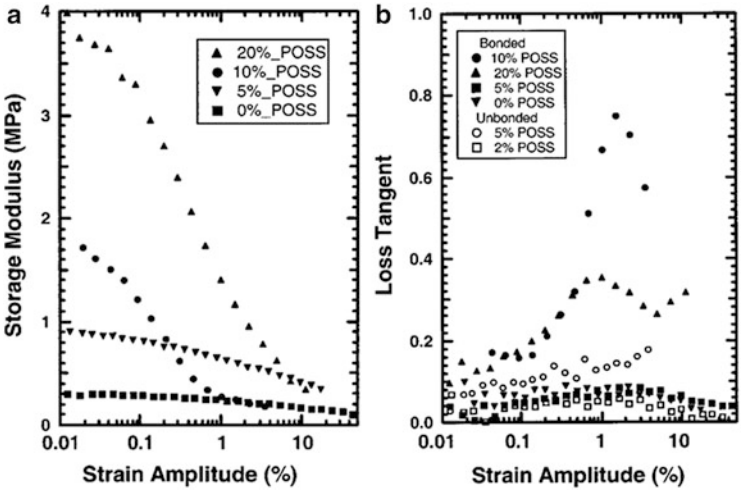

Fig. 9 (**a**) Storage modulus vs. strain amplitude of vinyl-PDMS with various amounts of chemically linked POSS; (**b**) Loss tangent vs. strain amplitude of POSS-filled samples (Reprinted from [47])

Table 1 Summary of nanofiller effects (Reprinted from [49])

Filler	P1000 viscosity	Payne effect	PU T_g	PU modulus	PU toughness
MWCNT	Increased	Yes	~7 K increase	Higher	Negligible change
Nanoclay	Increased	Yes	No change	Higher	Negligible change
POSS	Negligible change	No	~10 K increase	Higher	20 % improvement

Reinforcement in a polyurea matrix by three different nanofillers (multiwall carbon nanotubes (MWCNT), nanolayered silicate (nanoclay) and trisilanolphenyl-functionalized POSS was investigated by Casalini et al. [49]. The effects of the nanofiller are summarized in the Table 1 (Reprinted from [49]).

Many of the characteristic parameters, in obtained nanocomposites, were increased in their values by the addition of nanofiller. The viscosity and the storage modulus of PU/MWCNT and PU/Nanoclay systems increased in comparison to the unmodified polymer. In turn, for PU/POSS nanocomposites a strong influence of this type of nanofiller was observed, on glass transition temperature and PU toughness. Only for PU nanocomposites containing MWCNT and nanoclay, nonlinear viscoelastic behavior was observed. Generally, small filler particles maximize the interfacial area and provide great reinforcement. However, for the POSS nanofiller, the authors didn't observe such improvement, because this nanoparticles, in a polyurea matrix, doesn't behave like a conventional nanofiller, but rather like a chemically reactive additive [49].

3.2 Silicon Dioxide Rubber Nanocomposites

The nonlinear viscoelastic behavior of the nanocomposites based on natural rubber and modified nanosilica have been studied by Meera et al. [50]. In the Fig. 10 the authors present the effect of the strain amplitude on the storage modulus at increasing silica concentrations. The storage modulus is highest at small amplitude and decreases to lower values with increasing strain. This characteristic effect (Payne effect) increases with the silica content as reported by the authors. At high silica content the nanofiller possesses a tendency to agglomerate, which (dispersion and aggregation) has a strong influence on the Payne effect.

A schematic model of the structural breakdown (the decrease of the storage modulus) of the silica agglomerates is presented in Fig. 11. When strain is applied to the nanocomposite containing nanosilica, network damage appears, which causes a decrease in the agglomerate size and desorption of the polymer chains from the nanofiller surface. In a first step bigger silica agglomerates are linked with the polymer chains at several points. However, with increasing strain the bigger agglomerates become smaller, with multiple linked point reduction (Fig. 11b).

The authors also describe the effect of temperature on the Payne effect. With increasing temperature the amplitude of the Payne effect decreases significantly (Fig. 12). Very surprisingly, enhanced Payne-like behavior was observed for rubber vulcanizates at room temperature where filler-filler and filler-polymer interaction are not observed in comparison to the typically filled vulcanizates. The authors concluded that in addition to the contribution from the filler-filler network, there are many other factors that affect the nonlinear viscoelastic behavior. Nevertheless, the Payne effect is assumed to arise from the elementary mechanism consisting of adsorption-desorption of polymer chains from the surface of the particles [50]. Besides the experimental investigation, the authors have applied the Maier

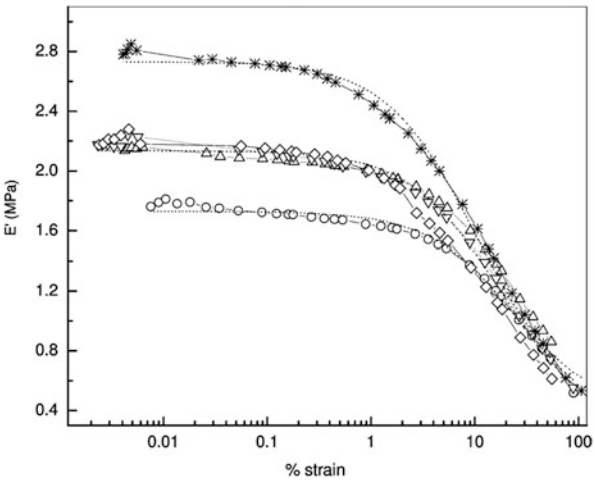

Fig. 10 Storage modulus vs. strain for natural rubber filled with nanosilica: (*open circle*) 0 phr, (*open triangle*) 5 phr, (*inverted open triangle*) 10 phr, (*open diamond*) 15 phr, (*asterisk*) 20 phr (Reprinted from [50])

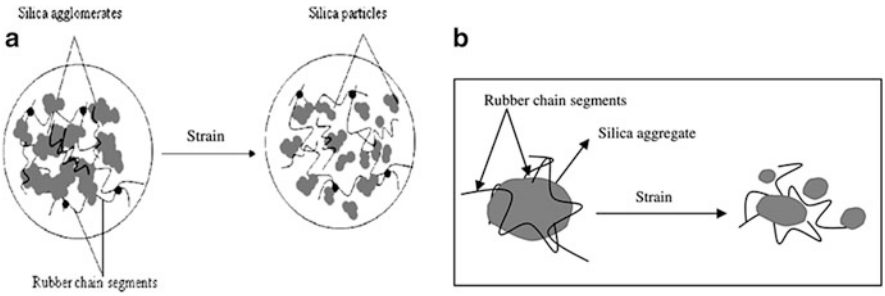

Fig. 11 Schematic representation of (**a**) the breakdown of aggregates and desorption of rubber chain segments from the filler surface in silica-filled NR system (**b**) the multiple points of attachments of rubber chains at the silica surface converting to the single points of attachments on straining (Reprinted from [50])

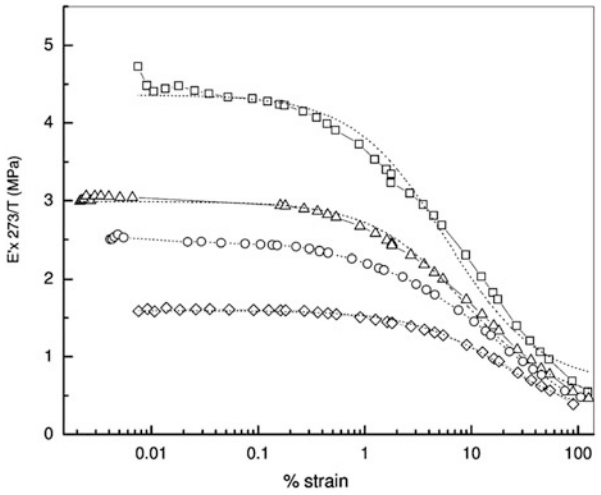

Fig. 12 Effect of temperature on the Payne effect for NR filled with 20 phr silica: (*open square*) 248 K, (*open triangle*) 263 K, (*open circle*) 303 K, (*open diamond*) 273 K (Reprinted from [50])

and Goritz model [51] to explain the nonlinear behavior of the nanocomposite systems.

"Smart" silica-rubber nanocomposites and the influence on filler-rubber interaction through introduction of hydrogen bonding between silica and the modified rubber have been reported by Peng et al. [52]. The authors investigated the influence of hydrogen bonding (HB) interactions on the dynamic mechanical properties of nanocomposites containing surface unmodified and modified silica nanoparticles (obtained from Stöber synthesis) and a thermoreversible crosslinking rubber with controlled functionality (Fig. 13).

This approach allows the incorporation of hydrogen bonds interacting not only between silica particles but between silica and polymer chains as well. Interesting

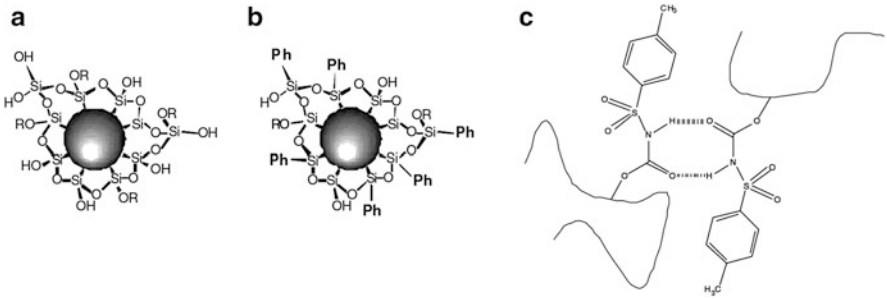

Fig. 13 Components for the "smart" silica-rubber nanocomposites, (**a**) surface unmodified silica (Si-OH), (**b**) surface-modified silica (Si-Ph), (**c**) thermoreversible crosslinking rubber (Reprinted from [52])

schematic comparisons from dynamic strain sweep studies on silica rubber nanocomposites have been presented by the authors (Fig. 14). The authors reported that silica agglomerates formed at lower loadings and the number of filler-filler hydrogen bonding interactions increased significantly with filler loadings. At the same filler loading there was higher filler-rubber hydrogen bonding interaction in Si-OH particles filled PB (polybutadiene) than in Si-Ph particles in the same matrix (Fig. 14). What's more, the filler-rubber hydrogen bonding interaction was more sensitive to temperature than the filler-filler HB interaction. Also, Si-Ph nanoparticles formed more agglomerates than Si-OH fillers.

The degree of polybutadiene (PB) modification, the filler loading and silica surface polarity affect the filler-filler, filler-rubber, and rubber-rubber hydrogen bonding interactions. These studies prove that filler-filler, filler-rubber and rubber-rubber interactions are controlled by the presence of hydrogen bonding. Using this methodology it is possible to reduce the Payne effect and modify the mechanical properties of silica nanocomposites.

Very interesting investigations were performed by Bandyopadhyay et al. [18]. The authors studied the effect of polymer-filler interactions in three different polymer matrices [acrylic rubber (ACM), epoxidized natural rubber (ENR) and poly(vinyl alcohol) (PVA)] which were modified using nano-sized silica (generating by the sol–gel technique), where tetraethoxysilane (TEOS) at different concentrations was used as the precursor for silica generation. The elastic modulus of the unfilled rubbers does not change upon increasing strain amplitude. However, for the nanocomposites it is observed (characteristic behavior) that the elastic modulus decreases upon increasing the strain amplitude. The interaction of silica with the matrix and the self-aggregation of the nanoparticles affect the development of the nanofiller network within the polymer matrix. The authors presented a silica-matrix model (Fig. 15) in which, with the less interactive polymer matrix (ACM) more polymer chains would remain at the periphery of the small nanofiller aggregates and be easily de-agglomerated from the surface aggregated silica particles

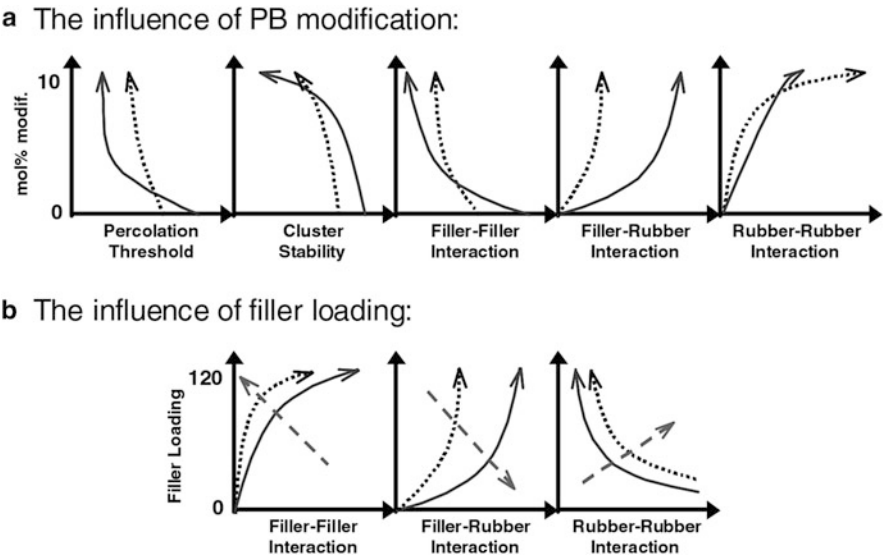

Fig. 14 Schematic comparison, how silica surface polarity and the silica loading impact the hydrogen bonding interactions and the other composites' properties (*continuous line* Si-OH, *broken line* Si-Ph, *dotted line* degree of PB (polybutadiene) modification (Reprinted from [52])

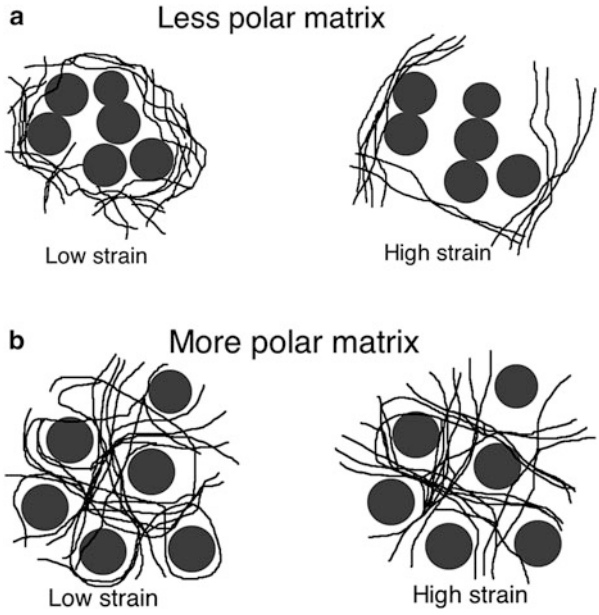

Fig. 15 Polymer silica morphology under low and high strain in (**a**) less polar matrices and (**b**) more polar matrices (Based on [18])

with applied strain. For inter separated nanofiller particles, the polymer chains are placed between smaller silica particles and these are more difficult to disengage under load strain. What is more, when larger silica particles are present some polymer chains may be trapped inside the siloxane networks and behave as filler in polymer matrix [18].

The authors concluded that the drop in storage modulus with applied strain is found to be higher for ACM/silica nanocomposites and lower for PVA/silica systems. For all measured nanocomposites, this effect is higher with increasing temperature. The reported observations are consistent with relatively weaker polymer-filler bonding in ACM/silica and stronger interactions (matrix vs filler) for ENR/silica and PVA/silica nanocomposites [18].

Ramier et al. [53] presented silica-filled vulcanizates based on SBR. The authors studied the interface between the matrix and the silica, which has been tailored by grafting either a covering or a coupling using triethoxy silane. The covering agent (AR) was a monofunctional molecule able to react with the surface silanol groups while the coupling agent (AC) was bis-(triethoxysilylpropyl)-disulfane (TESPD). Based on scanning electron microscopy, nanoparticles had an average size from 9 nm (primary particles) to 70 nm (spherical aggregates).

They have proved that unfilled elastomer (SBR) displays linear viscoelastic behavior, with no change in dynamic storage or loss modulus with strain amplitude. For the AR samples the authors observed a decrease of the magnitude of the nonlinear effect with increased presence of covering agent. The untreated silica shows the highest decrease of modulus vs. strain (the higher Payne effect). For the AC samples a decrease of the initial modulus G_0' at low surface treatment ratio was observed. The Payne effect amplitude is higher in the case of covering agent samples. Surface treatment of silica with coupling agents—that promote covalent bonds between matrix and fillers—reduces the magnitude of the nonlinear behavior. At the same filler loading, the use of coupling agent causes a reduction in Payne effect in comparison to covering agent based materials. It should be noted that it is not possible to distinguish both model (filler-filler and filler-polymer) interactions when they are modified in the same way by grafting the covering agent [53]. The authors also have fitted experimental data to the model of debonding of the polymeric chains from the filler surface proposed by Maier and Goritz [51], and have gotten good correlation.

Interesting investigations concerning the impact of filler surface modification of SBR/silica rubber nanocomposites were performed by Stöckelhuber et al. [54]. The authors have prepared nanocomposites based on solution-polymerized SBR and nanofillers: fumed silicas with surface modification by (dimethyldichlorosilane or bifunctional silane bis(3-triethoxysilylpropyl)-tetrasulfide, precipitated silica (pretreated with the coupling agent) and carbon black. In their dynamic mechanical measurements the influence of filler-filler and the filler-rubber interactions was studied in cured SBR samples. Generally for the filled nanocomposites, the amplitude of the Payne effect decreases. This behavior is visible for the SBR/SiO_2 (unmodified surface) sample (Fig. 16). According to the experimental results

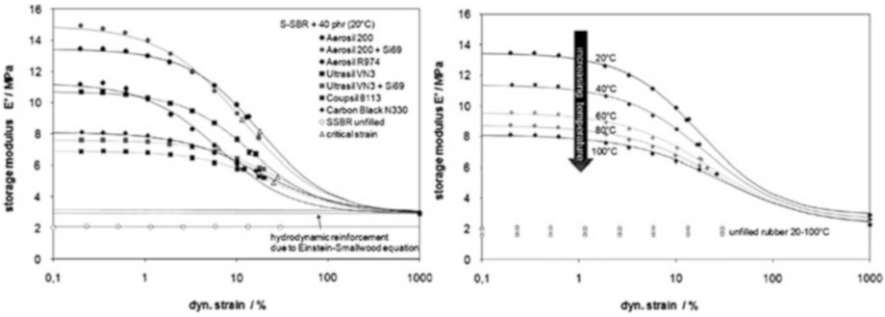

Fig. 16 Strain sweep measurements of the 40 phr filled nanocomposites at 20 °C (*Left*), the lines are fits according the Kraus model; Payne effect measure at different temperatures (*Right*) for SBS filled with 40 phr Aerosil 200 (Reprinted from [54])

chemical linkage of fillers to the polymer (due to bifunctional silanes) is reducing the amplitudes of the Payne effect (Fig. 16).

The authors presented the fundamental impact of surface energetic properties of filled elastomers. Fillers with low filler-polymer interaction possess also low activation energy in nonlinear amplitude behavior. In turn, coupling of the filler surface to the polymer chains (using bifunctional silane) enhances formation of a stable interphase around the filler particles. Based on these experimental investigations, the authors proposed a "layered fiber model". This model is based on the hypothesis that during deformation of the composites the polymer chains slipped from the polymer interface around the filler particles into the gaps between aggregates, to form high strength polymer fibers [54].

Other comparisons of the nanofiller and nanocomposites structure analysis were performed by Li et al. [55]. Hydrogenated nitrile rubber (HNBR) matrix was filled with carbon black, zinc dimethacrylate and SiO_2. What is interesting is that the effects of these nanofillers were investigated independently, and, in addition, two or three kinds of fillers were introduced together in the nitrile rubber matrix. The dispersion of fillers was characterized by the resulting dynamic mechanical properties. During these experiments the Payne effect was the tool used to predict dispersion of the filler into the rubber. What's more, these results are similar to those observed by TEM [55]. The authors reported that with increasing amount of SiO_2 in HNBR some particles have a tendency to agglomerate during the vulcanization process, and then a higher Payne effect was observed.

A new method for producing reinforced PDMS with superhydrophobic nanosilica, (modified by hexadecyltrimethoxysilane (HDTMS) as the treatment agent) has been introduced by Huang et al. [56].

For superhydrophobic silica, the long alkyl chains tethered outside the nanoparticle have good compatibility with the matrix, and the dispersion in PDMS is better than for the unmodified filler. The proposed reinforcement mechanism is presented in Fig. 17. For unmodified silica in the PDMS matrix the silanol groups

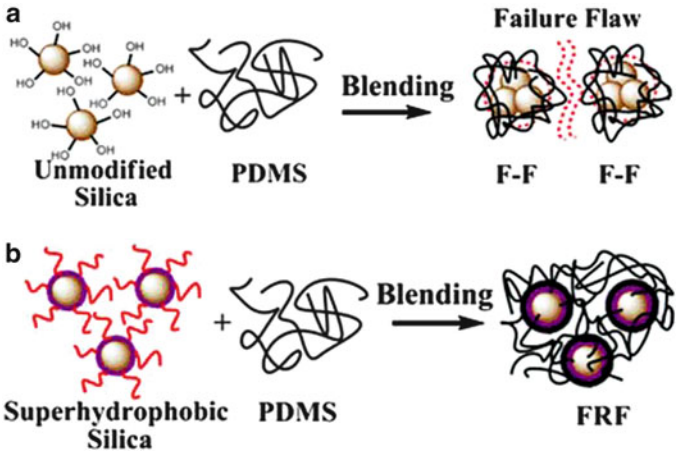

Fig. 17 Reinforcement mechanism for (**a**) untreated and (**b**) superhydrophobic nanosilica filled PDMS system (Reprinted from [56])

cause higher, rigid filler-filler contact and formation of silica aggregations. This filler-filler interaction may lead to the reduction of filler-rubber-filler interaction. In turn, for surface-modified nanosilica the dispersion and miscibility in PDMS can be improved. According to the rheological characteristic, storage modulus vs. strain amplitude, for the same filler loading, the strongest Payne effect was observed for unmodified silica/PDMS composites compared with the effect for modified silica/PDMS [56].

Similar investigations of nonlinear viscoelastic behavior of model polymer nanocomposites (silica filled hybrid hydrogel) were presented by Yang et al. [57]. The authors used silica nanoparticles (SNP) to modify a polyacrylamide matrix (PAM) and describe the nature of the filler associations and their influence on the Payne effect. The greater reinforcement for nanocomposites systems indicates the presence of filler association through chain immobilization on bridging. The authors have presented the concept of layer "glassy bridge", which can be defined as interparticle connections. It is speculated that a "bridging effect" is responsible for the nonlinear viscoelasticity of the silica/polymer systems. The molecular interpretation of the Payne effect involves the existence of equilibrium between the breakdown and rearrangement of the filler network and the polymer chains around the nanoparticles [57]. The proposed concept of the reinforcement of polymeric materials using nanoparticles suggests that a polymer layer near the surface of the nanofiller shows different properties in comparison with the polymer (matrix).

3.3 TiO_2 Rubber Nanocomposites

One of the popular nanofillers, which is commercially available and can reinforce polymeric matrices, is titanium dioxide. In the Sect. 2.4, synthesis and properties of

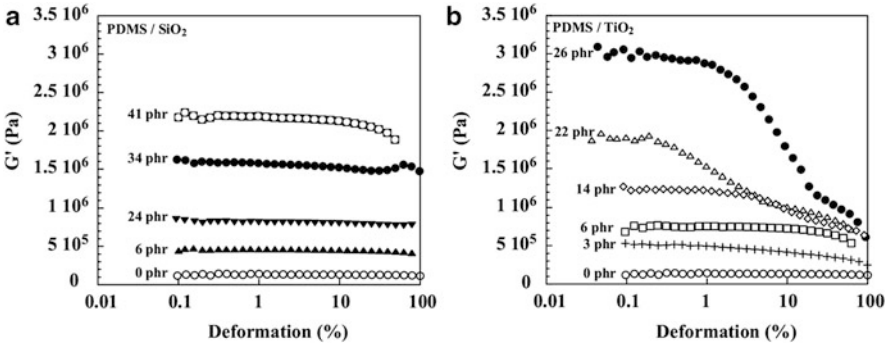

Fig. 18 Strain dependence of the storage modulus of PDMS filled with various amounts of in situ generated particles: (**a**) silica dioxide and (**b**) titanium dioxide [17]

TiO_2 nanoparticles were described. The addition of the nanofiller into a polymer matrix usually leads to an increase in modulus and positive enhancement of abrasion and tear resistance of rubber nanocomposites.

The most available method to produce TiO_2 nanoparticles is the sol–gel method (described in Sect. 2.4), and an in situ process can be performed in inorganic-elastomeric matrix, like PDMS, to obtain nanocomposites reinforced using titanium dioxide. The dispersion of the nanofiller strongly influences the storage modulus behavior in the dynamic mode, and therefore the Payne effect, which is based on agglomeration/disagglomeration of the filler, cannot be observed, because in a well dispersed nanofiller system, no aggregates or agglomerates are formed [17].

A good comparison of nanocomposites based on TiO_2 and SiO_2 nanofillers and (the same) PDMS matrix is presented in the Fig. 18. For PDMS filled with in-situ generated nanosilica, no Payne effect is observed in the whole range of deformation investigated (Fig. 18a). In turn, for the PDMS/TiO_2 composites (Fig. 18b) this effect was strongly visible also for relatively lower amount of TiO_2 nanoparticles, in comparison to the SiO_2 content, in the PDMS matrix [17].

Comparisons of these fillers (TiO_2 and SiO_2), in the natural rubber matrix, have been reported by Meera et al. [58]. The authors state that the rate of stress relaxation increases with increased amounts of filler, and this results from the breakdown of the filler-filler weak matrix-filler network during the relaxation process. For silica rubber composites, higher stress relaxation has been observed in comparison with the TiO_2 rubber composites. This was connected with a high degree of agglomeration in silica vs. TiO_2 (Fig. 19), since silica particles have hydroxyl groups on the surface, which leads to hydrogen bonding and consequently to formation of aggregates.

The studies of nonlinear viscoelastic behavior have been performed not only for rubber matrices, but also reported for polyolefin matrices, for example polypropylene-reinforced TiO_2 nanoparticles. Work by Bahloul et al.—concerning preparation of PP/TiO_2 nanocomposites based on the sol–gel method—reported strain dependence of the viscoelastic properties. The authors observed a change in the storage modulus (G') versus the strain amplitude and a characteristic decrease.

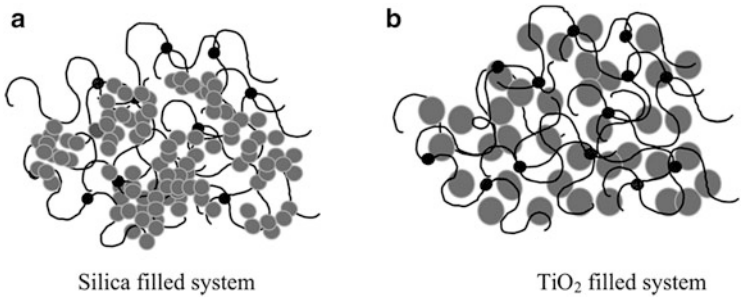

Fig. 19 Schematic structures of silica and TiO_2-filled rubber (Reprinted from [58])

In the analysis of loss modulus (G″) versus strain, all PP/TiO_2 nanocomposites show a well defined maximum in G″; also, the amplitudes of the loss modulus maxima increase with increasing in situ generated TiO_2 and are related to the energy dissipation produced by the breakdown of filler aggregates. Moreover, the observed second plateau modulus at low frequency is correlated to the formation of an aggregate-particle network. The study of the nonlinear viscoelastic behavior (the Payne affect) agrees with this reinforcement mechanism [59].

3.4 Other 3D Nanofillers in Rubber Nanocomposites

There are many commonly used nanoparticles classified as iso-dimensional nanofillers. Most studies have been focused on organic polymers and inorganic nanoparticles, having dimensions smaller than 50 nm. The most popular nanoparticles possess many features, but also some limitations that cause their limited use. Searching for a rubber matrix is still a major challenge. The ideal nanofiller should possess features such as: nanoscale size, spherical shape, good dispersion in the rubber matrix, possible chemical activity on the surface, lower density, and of course lower price [60]. An attempt to find such a nanofiller has been described by Lu et al. [60]. The authors synthesized latex-formed core-shell nanoparticles from cross-linked polystyrene (core) and polyisoprene (shell) and filled the SBR matrix using these core-shell particles. The PS hard core gave stiffness, while the PI shell was designed for setting up filler-matrix interactions. TEM analysis shows a 50–70 nm size for the spherically shaped nanoparticles. In the PS-PI nanoparticle-filled SBR composites, the authors studied the strain dependence of the shear storage modulus to describe the nonlinear viscoelastic behavior in PS-PI/SBR composites. They proved that the Payne effect was weakened as the PI (shell) thickness increased; therefore the PI shell domain plays a very important role in the filler-rubber interactions [60].

The differences between the MgO particle size and their influence on butadiene rubber (BR) nanocomposites have been reported by Naixiu et al. The authors

investigated the effects of the particle size on dynamic mechanical and physical properties. They have proved that nanofiller-MgO (size: 20–50 nm) in rubbery composites causes a significant increase in G′ and G″ modulus, and also, at higher values of tangent δ a clear Payne effect was observed [61].

Very interesting studies of natural rubber reinforcement with ZnO nanoparticles were performed by scientists from India, under the direction of Sabu Thomas [62]. The goal of these studies was to characterize the viscoelastic behavior and reinforcement mechanism of ZnO nanoparticles introduced into the rubber matrix. They have presented a constrained polymer model based on a rubbery region and a ZnO nanoparticle. Very interestingly, the authors presented a core-shell morphology model and constrained polymer model to explain the constrained polymer chains in NR/ZnO nanocomposites [62]. Thanks to this research and the proposed models, it is possible to understand the behavior of nanofillers in the polymer matrix and maybe in the future to develop an ideal nanofiller for use in the rubber matrix.

4 Summary, Conclusions and Future Outlook

In this chapter, the rheology and the dynamic-mechanical behavior of iso-dimensional rubber nanocomposites in the non-linear zone have been reviewed. Briefly described were the effect of nanofiller on the nonlinear viscoelastic properties of rubbers and the mechanism of nonlinearity in these polymeric systems.

The addition of iso-dimensional nanofillers into elastomers causes many changes in mechanical and physical properties, but especially, the effect of nanoparticles on the nonlinear viscoelasticity properties of rubbers has been investigated. In rubber matrices containing nanofillers, exhibition of the Payne effect is strongly connected with the dispersion of the nanofiller and the tendency to create aggregates among the nanoparticles. Filler dispersion plays an important role in determining the nonlinear viscoelastic behavior of these systems—in particular, both the properties of the filler particles and filler-polymer compatibility.

One of the most studied iso-dimensional nanofillers, described in this chapter, is silica, which is a commonly available nanofiller that is susceptible to various chemical modifications. Therefore, the simultaneous formation of the particles and the rubber matrix, usually using the sol–gel process, seems to be interesting and have much potential. Also, creation of new, complex iso-dimensional nanofillers provides the ability to create systems having better physico-mechanical properties and better nanofiller compatibility in the rubber matrix.

The rheological properties, especially the dynamic-mechanical properties, can be very useful in predicting the dispersion of the nanofiller. In rubber nanocomposites, the observed Payne effect can be correlated with microscopic investigation, and often both these characteristics are consistent.

Rubber nanocomposites represent a very attractive field of materials science, bringing new challenges for scientists working in experimental as well as simulation areas. At present the most popular models for predicting the Payne effect are:

the Kraus model (filler-filler interaction) [48] and the Maier and Göritz model (matrix-filler interactions) [51], but still needed is development of new models which will provide enhanced simulation of real polymer nanofilled systems.

Surface modification of the nanofiller will be a challenge in the preparation of new types of rubber nanocomposites. Furthermore, the modification of various nanofillers using other nanofiller systems will be a key to obtaining materials with designed properties. The interactions at the interface between the nanofillers and the matrix are one of the most important factors connected with the production of the new improved polymeric nanocomposites. Understanding the modification of the nanofiller in the polymer matrix, as well as the mechanical behavior in dynamic mode, leads to the possibility of producing new rubber nanocomposites, for example, for tire applications, where enhanced rolling resistance would improve traction [17].

References

1. Bikiaris D (2011) Can nanoparticles really enhance thermal stability of polymers? Part II: An overview on thermal decomposition of polycondensation polymers. Thermochim Acta 523(1–2):25–45
2. Sarvestani AS (2010) Nonlinear rheology of unentangled polymer melts reinforced with high concentration of rigid nanoparticles. Nanoscale Res Lett 5(4):791–794
3. Payne AR (1962) The dymanic properties of carbon black-loaded natural rubber vulcanizates. Part I. J Appl Polym Sci 6:57
4. Payne AR (1965) Reinforcement of elastomers, Chap. 3. Interscience, New York, pp 69–123
5. Ajayan PM, Schadler LS, Braun PV (2003) Nanocomposite science and technology. Wiley, Weinheim
6. Mukhopadhyay AM (2012) Nanoscale multifunctional materials, science and applications. Wiley, Mississauga, ON
7. Li G, Wang L, Ni H Jr, CUP (2002) Polyhedral oligomeric silsesquioxane (POSS) polymers and copolymers: a review. J Inorg Org Polym 11(3):123–154
8. Cordes DB, Lickiss PD, Rataboul F (2010) Recent developments in the chemistry of cubic polyhedral oligosilsesquioxanes. Chem Rev 110(4):2081–2173
9. Ayandele E, Sarkar B, Alexandridis P (2012) Polyhedral oligomeric silsesquioxane (POSS)-containing polymer nanocomposites. Nanomaterials 2(4):445–475
10. Markovic E, ConstantopolousK, Matisons JG (2011) In: Hartmann-Thompson C (ed) Applications of polyhedral oligomeric silsesquioxanes, vol 3. Springer, Dordrecht, pp 1–46
11. Gnanasekaran D, Madhavan K, Reddy BSR (2009) Developments of polyhedral oligomeric silsesquioxanes (POSS), POSS nanocomposites and their applications: a review. J Sci Ind Res 68:437–464
12. Pielichowski K, Janowski JNB (2006) Polyhedral oligomeric silsesquioxanes (POSS) -containing nanohybrid polymers. Adv Polym Sci 201:225–296
13. Koo JH (2009) Polymer nanocomposites, processing, characterization and applications, Chap. 2. An overview of nanoparticles. McGraw-Hill, New York
14. Phillips SH, Haddad TS, Tomczak SJ (2004) Developments in nanoscience. Polyhedral oligomeric silsesquioxane (POSS)-polymers. Curr Opin Sold State Mater Sci 8:21–29
15. http://www.hybridplastics.com
16. Rahman IA, Padavettan V (2012) Synthesis of silica nanoparticles by sol–gel: size-dependent properties, surface modification, and applications in silica-polymer nanocomposites—a review. J Nanomater 1–15

17. Sabu T, Ranimol S (2010) Rubber nanocomposites, preparation, properties and application. Wiley, Singapore
18. Bandyopadhyay A, de Sarkar M, Bhowmick AK (2005) Polymer-filler interactions in sol–gel derived polymer/silica hybrid nanocomposites. J Polym Sci B Polym Phys 43(17):2399–2412
19. Kickelbick G (2003) Concepts for the incorporation of inorganic building blocks into organic polymers on a nanoscale. Prog Polym Sci 28(1):83–114
20. Shu H, Li X, Zhang Z (2008) Surface modified nano-silica and its action on polymer. Prog Chem 20(10):1509–1514
21. Kang S, Hong SI, Choe CR, Park M, Rim S, Kim J (2001) Preparation and characterization of epoxy composites filled with functionalized nanosilica particles obtained via sol–gel process. Polymer 42(3):879–887
22. Yu YY, Chen CY, Chen WC (2002) Synthesis and characterization of organic–inorganic hybrid thin films from poly(acrylic) and monodispersed colloidal silica. Polymer 44(3):593–601
23. Yu YY, Chen WC (2003) Transparent organic–inorganic hybrid thin films prepared from acrylic polymer and aqueous monodispersed colloidal silica. Mater Chem Phys 82(2):388–395
24. Vega-Baudrit J, Navarro-Banon V, Vazquez P, Martin-Martinez JM (2006) Addition of nanosilicas with different silanol content to thermoplastic polyurethane adhesives. Int J Adhes Adhes 26(5):378–387
25. Rodriguez JGI, Carreira P, Diez A, Hui G, Artiaga DR, Marzan LML (2007) Nanofiller effect on the glass transition of a polyurethane. J Therm Anal Calorim 87(1):45–47
26. Chen Y, Zhou S, Yang H, Gu G, Wu L (2004) Preparation and characterization of nanocomposite polyurethane. J Colloid Interface Sci 279(2):370–378
27. https://www.aerosil.com
28. Zou H, Wu S, Shen J (2008) Polymer/silica nanocomposites: preparation, characterization, properties, and applications. Chem Rev 108(9):3893–3957
29. Pal M, Garcı J (2007) Size-controlled synthesis of spherical TiO_2 nanoparticles: morphology, crystallization, and phase transition. J Phys Chem C 111:96–102
30. Campet G, Han SD, Duguet E, Portier J (1994) TiO_2-polymer nano-composites by sol–gel. J Sol-gel Sci Technol 2:121–125
31. Mahshid S, Ghamsari MS, Askari M, Afshar N, Lahuti S (2006) Synthesis of TiO_2 nanoparticles by hydrolysis and peptization of titanium isopropoxide solution. J Mater Process Technol 9:65–68
32. Funda S, Meltem A, Şadiye Ş, Sema E, Murat E, Hikmet S (2007) Hydrothermal synthesis, characterization and photocatalytic activity of nanosized TiO_2, based catalysts for rhodamine B degradation. Turk J Chem 31:211–221
33. Kim TK, Lee MN, Lee SH, Park YC, Jung CK, Boo JH (2005) Development of surface coating technology of TiO_2 powder and improvement of photocatalytic activity by surface modification. Thin Solid Films 475:71–177
34. Ahmad A, Awan GH, Aziz S (2007) Synthesis and application of TiO_2 nanoparticles. In: Pakistan engineering congress, 70th annual session proceedings, vol 676, pp 404–412
35. Nussbaumer J, Caseri WR, Smith P, Tervoort T (2003) Polymer-TiO_2 nanocomposites: a route towards visually transparent broadband UV filters and high refractive index materials. Macromol Mater Eng 288(1):44–49
36. Pandey JK, Reddy KR, Kumar AP, Singh RP (2005) An overview on the degradability of polymer nanocomposites. Polym Degrad Stab 898:234–250
37. Chaudhari S, Shaikh T, Pandey P (2013) A review on polymer TiO_2 nanocomposites. Int J Eng Res Appl 3(5):1386–1391
38. Arantes TM, Leão KV, Tavares MIB, Ferreira AG, Longo E, Camargo ER (2009) NMR study of styrene-butadiene rubber (SBR) and TiO_2 nanocomposites. Polym Test 28(5):490–494
39. Evonik Industries (2011) Inorganic materials for catalyst innovation. Industry Information 2242
40. Cuppoletti J (2011) Nanocomposites and polymers with analytical methods. INTECH Open Access, Rijeka

41. Varghese S, Karger-Kocsis J (2004) Melt-compounded natural rubber nanocomposites with pristine and organophilic layered silicates of natural and synthetic origin. J Appl Polym Sci 91:813
42. Zhang H, Wang Y, Wu Y (2005) Study on flammability of montmorillonite/styrene-butadiene rubber (SBR) nanocomposites. J Appl Polym Sci 97:844
43. Kim JT, OhTS LDH (2003) Preparation and characteristics of nitrile rubber (NBR) nanocomposites based on organophilic layered clay. Polym Int 52:1058
44. Gatos KG, Thomann R, Karger-kocsis J (2004) Characteristics of ethylene propylene diene monomer rubber/organoclay nanocomposites resulting from different processing conditions and formulations. Polym Int 53:1191
45. Tien Y, Wei K (2001) Hydrogen bonding and mechanical properties in segmented montmorillonite/polyurethane nanocomposites of different hard segment ratios. Polymer 42(7):3213–3221
46. Strankowski M, Strankowska J, Gazda M, Piszczyk Ł, Nowaczyk G, Jurga S (2012) Thermoplastic polyurethane/(organically modified montmorillonite) nanocomposites produced by in situ polymerization. Exp Polym Lett 6(8):610–619
47. Pan G, Mark JE, Schaefer DW (2003) Synthesis and characterization of fillers of controlled structure based on polyhedral oligomeric silsesquioxane cages and their use in reinforcing siloxane elastomers. J Polym Sci B Polym Phys 41(24):3314–3323
48. Kraus GJ (1984) Mechanical losses in carbon black filled rubbers. J Appl Polym Sci Appl Polym Symp 39:75–92
49. Casalini R, Bogoslovov R, Qadri SB, Roland CM (2012) Nanofiller reinforcement of elastomeric polyurea. Polymer 53(6):1282–1287
50. Meera AP, Said S, Grohens Y, Thomas S (2009) Nonlinear viscoelastic behavior of silica-filled natural rubber nanocomposites. J Phys Chem C 113(42):17997–18002
51. Maier PG, Göritz D (1996) Molecular interpretation on the Payne effect. Kautsch Gummi Kunstst 49:18–22
52. Peng CC, Göpfert A, Drechsler M, Abetz V (2005) "Smart" silica-rubber nanocomposites in virtue of hydrogen bonding interaction. Polym Adv Technol 16(11–12):770–782
53. Ramier J, Gauthier C, Chazeau L, Stelandre L, Guy L (2007) Payne effect in silica-filled styrene – butadiene rubber: influence of surface treatment. J Polym Sci B Polym Phys 45 (3):286–298
54. Stöckelhuber KW, Svistkov S, Pelevin G, Heinrich G (2011) Impact of filler surface modification on large scale mechanics of styrene butadiene/silica rubber composites. Macromolecules 44(11):4366–4381
55. Li Q, Zhao S, Pan Y (2010) Structure, morphology and properties of HNBR filled with N550, SiO_2, ZDMA, and two of three kinds of fillers. J Appl Polym Sci 117(1):421–427
56. Huang X, Fang X, Lu Z, Chen S (2009) Reinforcement of polysiloxane with superhydrophobic nanosilica. J Mater Sci 44(17):4522–4530
57. Yang J, Han CR (2013) Dynamics of silica-nanoparticle-filled hybrid hydrogels: nonlinear viscoelastic behavior and chain entanglement network. J Phys Chem C 117(39):20236–20243
58. Meera AP, Grohens Y, Luyt AS, Thomas S, Sud B, Maude R, Saint (2009) Tensile stress relaxation studies of TiO_2 and nanosilica filled natural rubber composites. Ind Eng Chem Res 48(7):3410–3416
59. Bahloul W, Lyon D, Umr C (2010) Morphology and viscoelasticity of PP/TiO_2 nanocomposites prepared by in situ sol–gel method. J Polym Sci B Polym Phys 48:1213–1222
60. Lu M, He B, Wang L, Ge W, Lu Q, Liu Y, Zhang L (2012) Preparation of polystyrene–polyisoprene core–shell nanoparticles for reinforcement of elastomers. Compos B Eng 43 (1):50–56
61. Ding N, Hao F, Li L, Sun W, Liu L (2012) Study on physical and dynamic properties of BR based composites filled with different particle size magnesia. Appl Mech Mater 217–219:165–173
62. Bindu P, Thomas S (2013) Viscoelastic behavior and reinforcement mechanism in rubber nanocomposites in the vicinity of spherical nanoparticles. J Phys Chem B 117(41):12632–12648

Non-linear Viscoelastic Behaviour of Rubber-Rubber Blend Composites and Nanocomposites: Effect of Spherical, Layered and Tubular Fillers

Ajalesh B. Nair, Neena George, and Rani Joseph

Abstract This chapter deals with the non-linear viscoelastic behaviour of rubber-rubber blend composites and nanocomposites with fillers of different particle size. The dynamic viscoelastic behaviour of the composites has been discussed with reference to the filler geometry, distribution, size and loading. The filler characteristics such as particle size, geometry, specific surface area and the surface structural features are found to be the key parameters influencing the Payne effect. Non-linear decrease of storage modulus with increasing strain has been observed for the unfilled vulcanizates. The addition of spherical or near-spherical filler particles always increase the level of both the linear and the non-linear viscoelastic properties. However, the addition of high-aspect-ratio, fiber-like fillers increase the elasticity as well as the viscosity.

Keywords Nanocomposites • Rubber blends • Viscoelasticity

Abbreviations

0D	Zero dimensional
1D	One dimensional
AFM	Atomic force microscopy
APS	Aminopropyltrimethoxysilane
APTMS	3-Aminopropyltrimethoxysilane

A.B. Nair
Department of Polymer Science and Rubber Technology, Cochin University of Science & Technology, Kochi 682 022, India

Intelligent Polymer Nanomaterials Lab, Polymer-Nano Science and Technology, Chonbuk National University, 664-14 Duckjin-dong, Duckjin-gu, Jeonju 561-756, Republic of Korea

N. George • R. Joseph (✉)
Department of Polymer Science and Rubber Technology, Cochin University of Science & Technology, Kochi 682 022, India
e-mail: rani@cusat.ac.in

D. Ponnamma, S. Thomas (eds.), *Non-Linear Viscoelasticity of Rubber Composites and Nanocomposites*, Advances in Polymer Science 264, DOI 10.1007/978-3-319-08702-3_5

BMI	1-Butyl 3-methyl imidazoliumbis (trifluoromethylsulphonyl) imide
C15A	Dimethyl dehydrogenated tallow alkyl ammonium cation as modifier
C30B	Bis(2-hydroxyethyl)-methyl tallow alkyl ammonium cation as modifier
CB	Carbon black
CBs	Carbon blacks
CCVD	Catalytic chemical vapour deposition
CNF	Carbon nanofiber
CNTs	Carbon nanotubes
CO	Carbon dioxide
CR	Chloroprene rubber
DMA	Dynamic mechanical analysis
DMS	Diethoxydimethylsilane
DMTA	Dynamic mechanical thermal analysis
DPD	Dissipative particle dynamics model
DTAB	Dodecyltrimethylammonium bromide
E'	Storage modulus
E''	Loss modulus
EVA	Ethylene vinyl acetate copolymer
GCB	Grafted carbon black
GNPs	Graphene nanoparticles
GO	Graphite oxide
HNBR	Hydrogenated nitrile rubbers
HNTs	Halloysite nanotubes
HT	Hydrotalcite
IPTMS	3-Isocyanatopropyltrimethoxysilane
LCM	Liquid compounding method
LDHs	Layered double hydroxides
LTG-HNBR	Low-temperature-grade hydrogenated acrylonitrile butadiene rubber
MMT	Montmorillonite
MWCNT	Multi walled carbon nanotubes
NBR	Nitrile-butadiene rubber
NO	Nitrous oxide
NR	Natural rubber
NR	Natural rubber
OMMT	Organically modified montmorillonite
PLA	Polylactic acid
PNCs	Polymer nanocomposites
RPA	Rubber-Process-Analyzer
SBR	Styrene butadiene rubber
SBR–clay NC	SBR–clay nanocomposite

SDBS	Sodium dodecyl benzene sulfonate
SDS	Sodium dodecyl sulfate
SEN-T	Single edge notched tensile loaded
SH	Sodium humate
SSBR	Solution styrene butadiene rubber
SWCNT	Single walled carbon nanotubes
TEM	Transmission electron microscopy
Tg	Glass transition temperature
TiO_2	Titanium dioxide
TRG	Thermally reduced graphene oxide
XNBR	Carboxylated nitrile rubber

1 Introduction

The addition of active fillers (carbon black, modified silica) to a rubber matrix leads to significant reinforcement of composites. This reinforcement is manifested by an increase in the toughness, durability of elastomers and, consequently a longer service life, whereas their elasticity and ability to multiple reversible deformations caused by stretching remain unchanged. This is mainly due to strong interphase physico-chemical interactions proceeding in the composite. Filled elastomers are heterogeneous materials and have a micro structure consisting of spatially connected clusters. Carbon black and silica are the main fillers used in the compounding recipes.

Recently Polymer composites based on nano-sized fillers (polymer nanocomposites) have become one of the most active research fields in polymer science. The driving force of research in this area is the versatile shape and size of nano-fillers. The obvious perceptive of the reinforcing effect of nanocomposites is important in the design of nanomaterials with desirable properties. The reinforcement of spherical fillers is primarily due to hydrodynamic interactions between the rubber and filler surfaces [1]. Sternstein et al. [2] have found experimentally that the mechanism for reinforcement in nanocomposites can be attributed to filler matrix interactions, rather than filler agglomeration or percolation. It was reported that, in natural rubber (NR)/spherical filler nanocomposites [3] and NR/layered filler nanocomposites [4], there exists a strong interfacial interaction between the rubber matrix and the nanofiller. In NR/tubular filler nanocomposites [5], the strong interfacial bonding between the fillers and the rubber molecules were observed, and therefore, the tubular fillers can transfer stress effectively throughout the rubber matrix and play an important role in the reinforcement in NR nanocomposites. Lopez-Manchado et al. [6] have reports that, in NR-nanoclay vulcanized composites, the presence of nanoclay introduces a dual crystallization mechanism due to the alignment of layered nanoparticles during stretching of the rubber. The

improved properties of NR/layered filler nanocomposites can are attributed to microstructural and morphological changes induced by filler in the NR matrix during crystallization. All of these factors during deformation contribute to the formation of a network structure containing cross-linked chemical chains, nanofiller, and crystallizable networks in the NR/filler nanocomposite. Dishovsky et al. [7] have reported that carbon black filled NR-containing graphene nanoparticles (GNPs) were found to improve the dielectric properties and microwave properties, viz., coefficient of absorption and reflection of the electromagnetic waves and electromagnetic interference shielding effectiveness. Stiffness improvement by thermally reduced graphene oxide (TRG) was found to be more pronounced for elastomers [8], such as NR and styrene butadiene rubber (SBR), due to the higher stiffness between the matrix and the filler.

Introduction of fillers can affect the morphology and change the viscoelastic behaviour of the polymers by introducing filler-matrix interactive forces or restriction of polymer chain mobility by the presence of filler particles. It is thus of much interest to study the viscoelastic behaviour of polymers filled with nanosized fillers, where the nanoparticle size allows interactions with polymer at the molecular level.

Dynamic mechanical thermal analysis (DMTA) or Dynamic mechanical analysis (DMA) measures the response of a given material to an oscillatory deformation as a function of temperature. DMA results are composed of three parameters: (a) the storage modulus (E'), corresponding to the elastic response to the deformation, (b) the loss modulus (E''), the plastic response to the deformation and (c) tan δ; the ratio (E''/E'), a measure of the damping behaviour which is useful for determining the occurrence of molecular mobility transitions, such as the glass transition temperature (Tg). DMA can provide reliable information over the relaxation behaviour of the materials.

1.1 Rubber Blends

By blending different polymers, it is possible to bring the properties of the individual components to a single material. The phenomenon of blending can be implemented more rapidly and economically. This technique has helped to develop many new materials, which are of good quality and are cheaper in market. The fundamental justification for blending two or more elastomers is acquisition of different features exhibited by vulcanizates of the component elastomers in a single composite. Unfortunately, it has been found that co-vulcanization leads to reduction in the mechanical strength of the vulcanizate compared with its expected values. Homogeneity of mixing and retention of the compatibility during the vulcanization are the most relevant issues although micro-heterogeneity is usually desirable to retain the individual properties of the respective elastomer components remaining in a blend.

Mixtures and blends occur at different hierarchical scales in the material range employed in the rubber industry. Composite products such as tires, hoses, belts, and

air springs are composed of metal wire, textile cord, and elastomeric compounds, which form a rubber matrix. The rubber matrix itself is a mixture of elastomer, filler, and plasticizer etc. The elastomer phase is often a blend of different elastomers. However, there are technological problems arising from some types of mutual incompatibility that exist between dissimilar elastomers. Three main types of incompatibility have generally been noted: the thermodynamic incompatibility, incompatibility due to viscosity mismatch, and incompatibility due to the cure rate mismatch [9].

Kim and Hamed [10] prepared a vulcanizate based on a 50/50 natural rubber/*cis*-butadiene rubber (NR/*cis*-BR).This blend has been found to retain the rupture resistance property of NR vulcanizate and resistance to slow fatigue crack growth property of *cis*-BR vulcanizate. Botros et al. [11] studied the properties of acrylonitrile butadiene rubber/polychloroprene rubber blend (NBR/CR). The blend was found to possess the thermal resistance of CR and the oil resistance of NBR.

Natural rubber was blended with synthetic nonpolar rubbers like styrene butadiene rubber (SBR), butadiene rubber (BR) and EPDM and polar rubbers like NBR and CR [12]. NR/SBR and NR/BR blends were compatible, while NR/EPDM, NR/NBR and NR/CR blends were incompatible.

Blends have been developed to meet several industrial requirements such as the need of easier processing and broadening of the properties range, either by varying the type, or by relative amounts or morphology of each component [13, 14].

1.2 Rubber Blend Composites

Addition of fillers to rubber blend has been found to cause severe changes in the properties of the blend. It has been known that the distribution of filler in rubber blends is one of the most important factors affecting the physical properties of rubber final products. It has generally been believed that the main factors controlling the filler distributed in each phase of the blends are the nature of rubber, mixing sequence, and filler–rubber interaction.

Sircar et al. [15] studied the effect of heterogeneous carbon black distribution on the properties of a BR/SBR blend and a BR/NR blend. Varying the sequence of carbon black addition caused the distribution of the carbon black to change. They found that superior hysteresis properties of the blend were obtained when most of the carbon black was in the BR phase. Massie et al. [16] studied the distribution of carbon black in NR/BR blends and found that N550 black has no preference for either the NR or the BR. However, if the blend was prepared by carrying out a phase mixing technique, the majority of the black remained in the polymer to which it was initially added. It was also found that the cut-growth resistance of the rubber blends in which carbon black is mainly in the BR phase is poorer than that of the blend with evenly distributed black.

Besides the mixing sequence, the distributions of carbon black in elastomer blends are affected by viscosity, degree of unsaturation, and polarity of rubbers. For

example, Kluppel et al. [17] studied the distribution of carbon black in BR/ethylene–propylene–diene rubber blend and found that N550 carbon black preferred to migrate into the BR phase. This is due to the higher degree of unsaturation and lower viscosity of BR. Similarly, Hess et al. [18] studied carbon black distribution in many natural rubber//synthetic rubber blends including NR/CR, NR/NBR, and NR/SBR and found that carbon black preferentially resided in the synthetic rubber phases having lower viscosity compared to natural rubber. Recently, Jeon et al. [19] studied distribution of fillers in NR/BR blends by using atomic force microscopy and found that carbon black resides predominantly in the BR phase whereas silica mainly exists in the NR phase. Maiti et al. [20] studied the distribution of carbon black and silica in NR/epoxidized NR (ENR) blends by using DMTA technique. They found that silica migrated preferentially to the ENR phase. It was believed that the reasons for the preferential migration of silica to the ENR phase included the low viscosity of the ENR and a physical interaction between the epoxide group of the ENR and the silanol group of the silica. In addition, they found that the magnitude of the distribution depends on filler loading. When the silica content was increased from 10 to 40 phr, the weight fraction of silica in the ENR phase decreased. The viscosity of the ENR also plays an important role. By increasing the epoxidation level of the ENR from 25 to 50 %, the viscosity of the ENR phase was increased. This increase in viscosity of the ENR-50 inhibited the migration of silica into the ENR phase.

1.3 Rubber-Rubber Blend Nanocomposites

In rubber-rubber blend nanocomposites, nanoparticles are incorporated into a blend which can significantly affect the properties of the matrix. The properties of these composites depend on the type of nanoparticles that are incorporated, their size and shape, their concentration and their interactions with the polymer matrix. It is difficult to produce monodispersed nanoparticles in a rubber blend because of the agglomeration of nanoparticles. This problem can be overcome by modification of the surface of the nanoparticles. Surface modification improves the interfacial interactions between the nanoparticles and the polymer matrix. Nanofillers when added to blend systems are known to cause a considerable change in dynamic properties.

2 Nanofillers Used in Rubber Blend Reinforcement

The properties of rubber blend composites are determined by the particle size, surface structure, and surface activity of filler. If the size of filler particles greatly exceeds the polymer inter-chain distance, it introduces an area of localized stress. This can contribute to elastomer chain rupture on flexing or stretching. Filler with

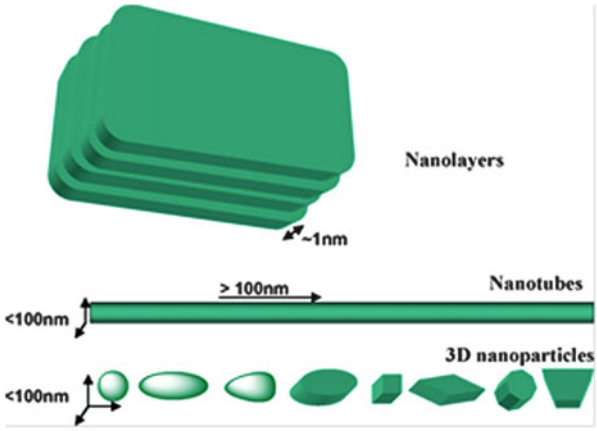

Fig. 1 Dimensional morphology of nanofillers [21]

particles size greater than 10,000 nm are therefore generally avoided because they can reduce performance rather than reinforce or extend. Fillers with particles size between 1,000 and 10,000 nm are used primarily as diluents and usually have no significant effect, positive or negative, on rubber properties. Semi-reinforcing filler, which range from 100 to 1,000 nm, improve strength and modulus properties, the truly reinforcing fillers, which range 10–100 nm significantly, improve rubber properties.

Based on the dimensional morphology nanofillers can have iso-dimensional, elongated or layered structures as shown in Fig. 1.

- *Nanoparticles*: When all the three dimensions of the particulates are in the nanometer range, they are isodimensional nano particles or nano granules or nano crystals.

  e.g. silica, carbon black, zinc oxide, aluminum oxide, titanium dioxide etc.

- *Nanotubes*: When only two dimensions are in the nanometer range and the third is larger, elongated structures as in nanotubes, whiskers or nanofibres are formed.

  e.g. carbon nanotubes, gold or silver nanotubes, carbon nanofibres, cellulose whiskers, boron nitride tubes, boron carbon nitride tubes etc.

- *Nanolayers*: When only one dimension is in the nanometer range, then layered structures having thickness of a few nanometers and length, several hundreds of nanometers are formed.

  e.g. clay (layered silicates), layered double hydroxides (LDHs) and layered graphite flakes.

2.1 Spherical (Zero Dimensional, 0D) Nanofillers

2.1.1 Carbon Black

Carbon Black (CB) is a colloidal form of elemental carbon, which usually consists of spherical particles. Size of these molecules is less than few dozen nanometers. Particles create agglomerations with different spatial configuration. Structure and configurations of particles influence properties of carbon black. The genesis of obtaining carbon black is mainly based on incomplete combustion of carbonaceous materials. The main precursors include: wood, coal, natural gas and hydrocarbons. The basic production methods for this material include: furnace method, lamp method, and now more widely used plasma method. Commercially available carbon black fillers have varying level of structure, particle size, chemical reactivity and pH that lead to different levels of reinforcement.

2.1.2 Silicon Dioxide

Silicon dioxide (SiO_2) is commonly called silica. Silica is a crystalline compound occurring abundantly as quartz, sand and many other minerals. Silica particles are composed of small aggregated particles due to intra-molecular hydrogen bonding. Surface treatment to improve filler-polymer interaction has become very common in rubber industry [22–27]. There are many coupling agents that can be used to enhance polymer filler interaction, which include organosilanes, phosphorous esters, titanate coupling agents and chromium acid complexes. Silane coupling agents have dual reactivity since they are capable of reacting with both polymer and filler.

2.1.3 Titanium Dioxide

Titanium dioxide (TiO_2) nanoparticles have been used as white colour pigment due to its high refractive index, chemical stability and nontoxicity. One of the most interesting properties of TiO_2 based cosmetics is UV-ray absorption and UV-ray scattering [28]. The surface modification of TiO_2 particles has been reported using different silane coupling agents, such as 3-amino propyl triethoxysilane, n-propyl triethoxysilane and 3-methacryloxy propyl trimethoxysilane [29]. Recently Sabzi et al. [30] carried out surface modification of TiO_2 nanoparticles with amino propyl trimethoxy silane (APS) and investigated its effect on the properties of a polyurethane composite coating, demonstrating improved mechanical and UV-protective properties of the urethane clear coating. In a more recent study, the dispersion stability of TiO_2 nanoparticles in organic solvents was improved by treating the particle surface with a silane coupling agent [31].

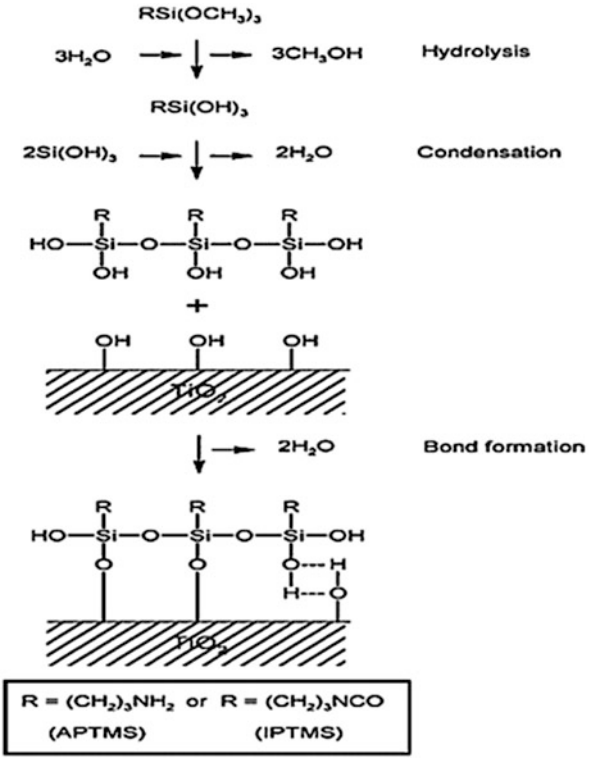

Fig. 2 Chemical grafting of organosilanes onto TiO_2 nanoparticles surface [32]

Zhao et al. [32] carried out a surface modification of TiO_2 nanoparticles with the silane coupling agents; 3-aminopropyl trimethoxysilane (APTMS) and 3-Isocyanato propyl trimethoxysilane (IPTMS). The process of nanoparticle surface modification by silane coupling agents is shown in Fig. 2. Various anionic surfactants have been used to disperse nano TiO_2 [33].

2.2 Tubular (One Dimensional, 1D) Nanofillers

2.2.1 Carbon Nanotubes

There are two basic types of carbon nanotubes (CNT) viz. single walled carbon nanotubes (SWCNT) and multi walled carbon nanotubes (MWCNT) [34]. A special case of MWCNT called double walled carbon nanotubes (DWCNT) contains two concentric graphene cylinders. Figure 3 represents the rolling of graphene sheets to form SWCNT, DWCNT and MWCNT. CNT can be synthesised by arc-discharge [35], laser ablation [36], or catalytic chemical vapour deposition (CCVD) [37] methods. CNTs have a planar hexagonal arrangement of sp^2 bonded carbon atoms, with each carbon atom joined to three neighbours, as in graphite [38].

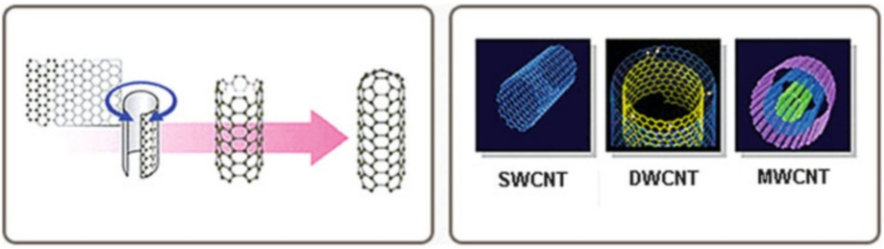

Fig. 3 Rolling of graphene sheets to form different types of nanotubes [34]

Use of surfactants is an effective way for dispersing CNTs [39]. Reports show that the outer most nanotubes in a bundle are treated more than the innermost tubes and the nanotube remains predominantly bundled even after surfactant treatment. But mechanical methods like ultrasonication can debundle the nanotubes by steric or electrostatic repulsions [40]. On sonication the high local shear will unravel the outer carbon nanotubes in a bundle and expose other sites for additional surfactant adsorption, thus the surfactant molecules gradually exfoliate the bundle in an "unzippering" mechanism [41]. Some of the common surfactants used for the dispersion of carbon nanotubes are sodium dodecyl benzene sulfonate (SDBS) [42], dodecyl trimethyl ammonium bromide (DTAB) [43], hexadecyl trimethyl ammonium bromide (CTAB) [44], octylphenol ethoxylate (Triton X-100) [45] and sodium dodecyl sulfate (SDS) [46]. Covalent modification is another way to solubilize the CNTs in different solvents and to improve the interaction with the matrix in composites [47].

2.2.2 Carbon Nanofiber

After the discovery of carbon nanofiber (CNF), most of the works are focused on the use of CNF as thermal, electrical and mechanical reinforcing filler to improve the polymer characteristics [48, 49]. A significant amount of work has been conducted by using the one dimensional carbon fillers like CNT and CNF. The one dimensional filler may connect more polymer chains and afford more effective load transfer, leading to an improvement of mechanical properties [50]. One dimensional fillers can easily transfer the loads or reduce it than spherical fillers. Well dispersed polymer composites filled with CNT or CNF can be achieved by using the fine twin-screw extrusion, surfactant, oxidation of fillers and incorporation of functional groups on the surface of the fillers. The transmission electron microscopy (TEM) images of the fillers are shown in Fig. 4.

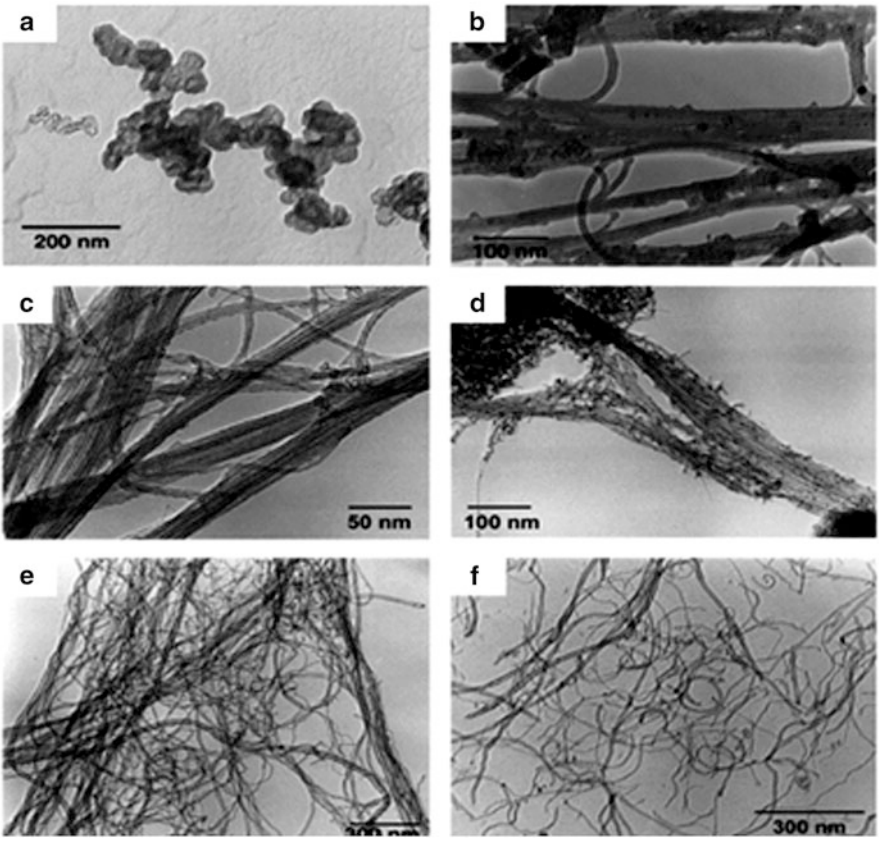

Fig. 4 TEM images of the nanofillers: (**a**) carbon black, (**b**) SWCNT (**c**) DWCNT (**d**) amino-functionalized doublewall CNT (**e**) MWCNT and (**f**) amino-functionalized MWCNT [51]

2.2.3 Halloysite Nanotubes

Halloysite nanotubes (HNT) are unique and versatile nanomaterials that are composed of double layer of aluminium, silicon, hydrogen and oxygen. Recently Ithas reported that HNTs have typical dimensions of 10–50 nm in outer diameter, 5–20 nm in inner diameter with 2–40 mm in length [52]. Figure 5 shows the model, SEM and TEM images of HNTs. Two types of HNT models are developed for effective studies in field of nanotechnology: Single walled halloylsite nanotube model and multi walled halloylsite nanotube model.

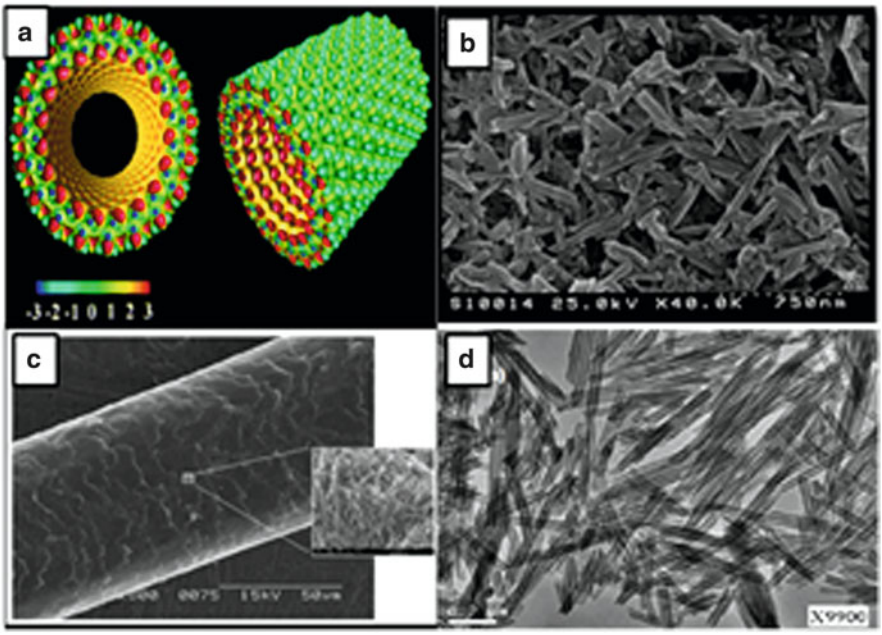

Fig. 5 (**a**) Model of HNT, (**b**) SEM image of HNT, (**c**) a bundle of HNTs compared to the width of human hair and (**d**) TEM image of HNT [53]

2.3 Layered (Two Dimensional, 2D) Nanofillers

2.3.1 Nanoclay

Clays are chemically hydrous silicates of Al, Mg, Fe and other less abundant elements [54]. The most important structural feature of clay mineral is that it is layered. An enhancement in the properties of the composite is achieved only when there is a good dispersion of particles in the matrix and there is adequate interaction between the nanoparticle and the matrix. Montmorillonite and other layered silicates are hydrophilic. To make the hydrophilic layered silicates compatible with the hydrophobic polymer matrices, they have to be modified. A popular and easy method of modifying the clay surface is by ion-exchange. Most popular organic cation used for ion exchanging includes quaternary ammonium salts, alkyl imidazoles and phosphorous ionic compounds. Figure 6 is a schematic representation showing the hydrolysis of functional silanes and its reaction with OH groups on the clay surface.

Based on the interaction between the polymer matrix and layered silicate polymer layered silicate nanocomposites are classified into intercalated and exfoliated nanocomposites [56–58]. Figure 7 represents the intercalated and exfoliated nanocomposites along with the conventionally filled microcomposite.

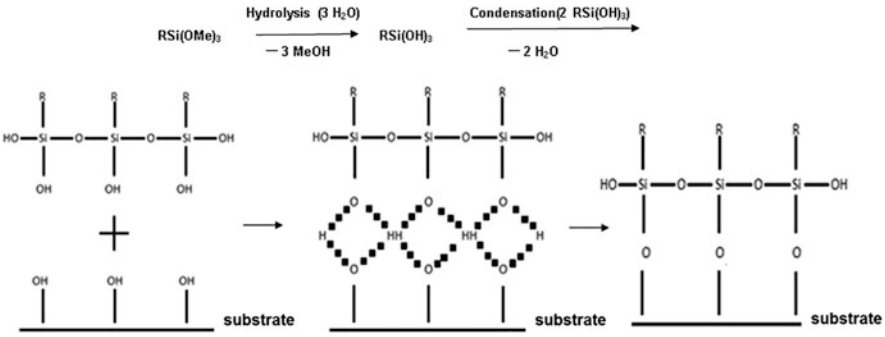

Fig. 6 Schematic representation showing the hydrolysis of functional silanes and its reaction with -OH groups on the clay surface [55]

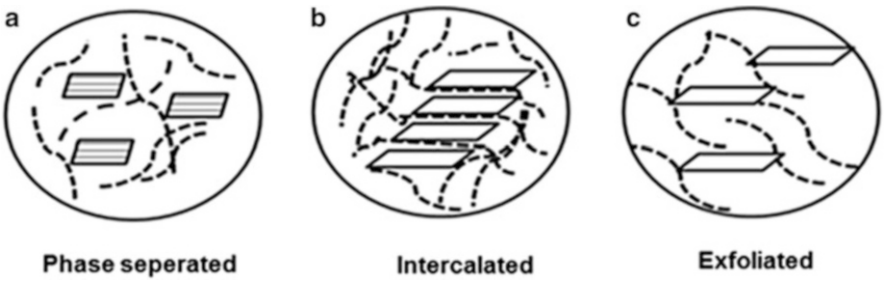

Fig. 7 (**a**) Conventionally filled polymer or microcomposite, (**b**) polymer chains intercalated into the clay layers, (**c**) exfoliation of the layered silicate

2.3.2 Layered Double Hydroxides

Layered double hydroxides (LDHs) have a layered crystalline structure and contain several intercalating anionic moieties. Their capability to interchange these interlayer anions with relatively larger anionic organic moieties makes LDHs very useful candidates as nanofillers for the synthesis of polymer nanocomposites. The second characteristic is very significant because pure and unmodified LDHs are not suitable for the intercalation of large polymer chains or segments of the chain into their gallery space until the original interlayer distance is enhanced through a prior organic modification. LDHs are being considered a very promising material for industrial applications because they combine the traits of classical metal hydroxide-type fillers, such as magnesium hydroxide, with those of unconventional layered silicate-type nanofillers, such as montmorillonite. Another major area of demand in this context is the contribution of LDH materials as potential non-halogenated, non-toxic flame-retardants for polymer matrices. For many years, scientists have been exploring the potential of using nanotechnology to improve the flame retardancy of polymer nanocomposites. The state of fine and

homogeneous dispersion of the inorganic fillers inside the polymer matrix plays a very important role in this area of research. For this purpose, layered silicates and various other nanoparticles, including magnesium oxide, magnesium hydroxide, etc., have generally been attempted following the necessary pre-treatment. LDHs have evolved as a multifunctional material. LDHs possess a high anion exchange capacity and a large surface area because of their structural configuration, qualifying their use as anionic exchangers. These properties are why these materials are very useful as adsorbents for ecologically alarming anions that evolve from dilute aqueous waste streams. Therefore, with the help of LDHs, significant progress has been made toward removing organic, inorganic and nuclear wastes from contaminated water [59].

2.3.3 Graphene

Graphene, considered as the thinnest material in the Universe, is the mother of all graphitic materials like graphite, carbon nanotubes and fullerenes. Graphene as nanofiller has tremendous potential applications owing to its high surface area, aspect ratio, tensile strength, EMI shielding, thermal and electrical conductivity [60]. Graphene sheets when stacked in a honey comb like structure gives graphite. The sheets are separated by 0.334 nm. The sheets can slide past one another giving its lubricating nature. Graphite on controlled oxidation gives graphite oxide and each single sheet of graphite oxide is called graphene oxide [61]. The structure of grapheme, graphite and grapheme oxide is shown in Fig. 8. Graphite oxides contain hydroxyl and epoxide groups on the top and bottom of the sheets and carboxyl and carbonyl groups at the sheet edges. These groups make graphene oxide hydrophilic and readily swell and disperse in water.

Multiple stacked graphene sheets constitute graphene nano platelets and the thickness of graphene platelets is significantly larger than an individual graphene sheet. Graphene can be prepared by chemical vapour deposition of monolayer of graphite on transitional metal surfaces [62], micro-mechanical exfoliation of graphite also called the “scotch tape” or “peel off ” method [63], epitaxial growth on electrically insulating surfaces such as SiC and solution based reduction of graphene oxide. Pristine graphene is not compatible with organic polymers and is

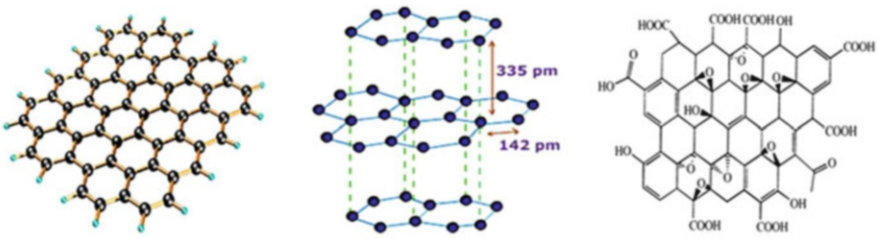

Fig. 8 Structure of graphene, graphite and graphene oxide [61]

unsuitable for intercalation by polymer chains. This is because bulk graphene has a pronounced tendency to agglomerate in the polymer matrix [64].

Graphene dispersions can be prepared in organic or aqueous media using either covalent or noncovalent methods of functionalisation. Noncovalent functionalisation involves wrapping of graphene sheets with surfactants like poly ethylene glycol, CTAB, SDS or through π-π interaction with certain organic molecules [65].

3 Reinforcing Effects of Fillers in Rubber Blends

Elastomers in general are not used in their pure form, but are reinforced by fillers. The reinforcement of rubber by active fillers is a well-recognized phenomenon but the term 'reinforcement' is not well defined. Reinforcement means the marked increase in tensile strength, tear resistance, abrasion resistance and modulus far beyond the values expected on the basis of the Einstein-Guth and Goldtheory [66], taking into account the effects caused by colloidal spherical particles (hydrodynamic effect) and occlusion of rubber. The reinforcement of elastomers by fillers has been studied in depth in numerous investigations [67] and it is generally accepted that this phenomenon is dependent, to a large extent, on polymer properties, filler properties and processing.

The addition of fillers fundamentally changes the properties of rubber: For unfilled rubbers there is increase in modulus with increasing temperature, as predicted by the kinetic theory of rubber elasticity. The addition of fillers significantly changes the temperature coefficient of the modulus; it can even alter the sign of the coefficient resulting in a decrease of the modulus with increasing temperature. Another effect of blending fillers with rubber is the transition to non-linear behavior. The use of reinforcing fillers gives the material unique properties: a combination of high elasticity with high strength. Figure 9 illustrates the influence of the addition of increasing amounts of reinforcing fillers on various properties of an elastomer.

A condition for filler reinforcement is the interaction between the filler particles and the polymer. These interactions can be strong, for example in the case of covalent bonds between functional groups on the filler surface and the polymer, or weak as in the case of physical attractive forces. When carbon black is blended with a polymer, the level of physical interaction is high. In contrast to this, the interaction between silica particles and the polymer is very weak, and only by the use of a coupling agent a bond is formed between the filler and the polymer.

Besides the interaction between the polymer and the filler, an interaction between filler particles occurs, predominantly above a critical concentration threshold, the percolation threshold. The properties of the material change drastically, because a filler-filler network is established. For example; an over proportional increase of electrical conductivity of a carbon black filled compound. But even at

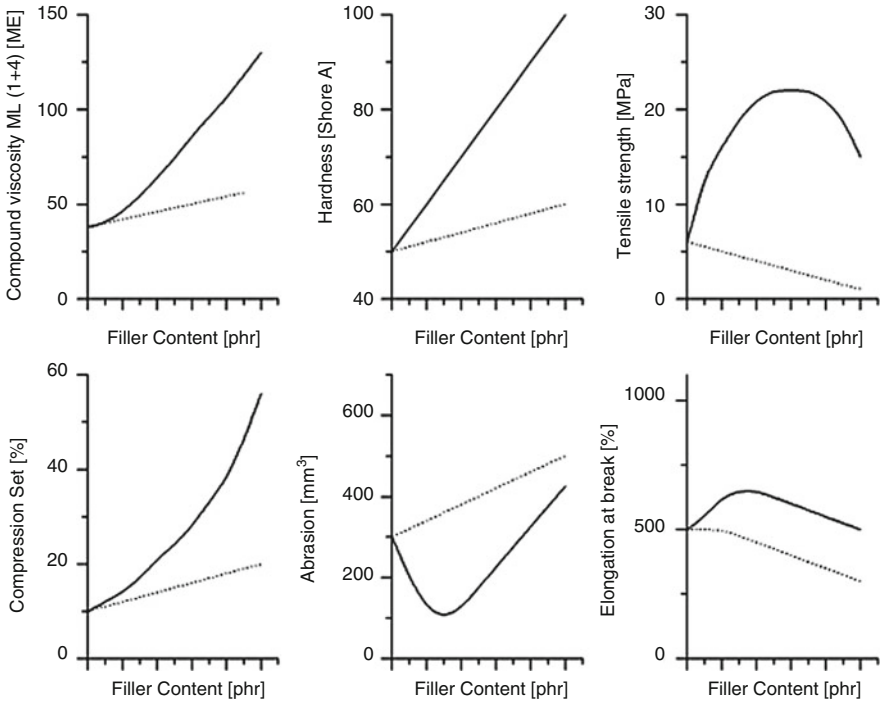

Fig. 9 The influence of reinforcing fillers on the properties of an elastomer (*Continuous line* active fillers, *dotted line* non-active fillers)

lower concentrations, the filler-filler interactions influence the material characteristics, as expressed by the Payne effect. Figure 10 illustrates the strain dependence of the Payne effect and the strain-independent contributions to the shear modulus for carbon black filled compounds and silica filled compounds.

The main contributions to the complex shear modulus are the hydrodynamic effect, the polymer network, the filler-polymer and the filler-filler interaction.

The strain-dependent contribution to the modulus is caused by filler-filler interactions. This effect was first brought into focus by Payne, and he interpreted the sigmoidal decrease of the storage modulus versus the double strain amplitude in logarithmic scale from a limiting zero-amplitude value to a high amplitude plateau as the result of the breakage of physical bonds between filler particles, for example van der Waals or London forces. This effect is largely reversible once the strain is released and is independent of the type of polymer, but is dependent on the type of filler. Figure 10 shows the key difference between carbon black and silica. The Payne-effect is stronger for silica, as a consequence of the strong interparticle forces between the filler particles.

A most important problem is the dispersibility of the filler particles in the rubber matrix. An often ignored issue in rubber technology is the surface energy of the filler particle surface, which is determining the wetting of the filler by the rubber

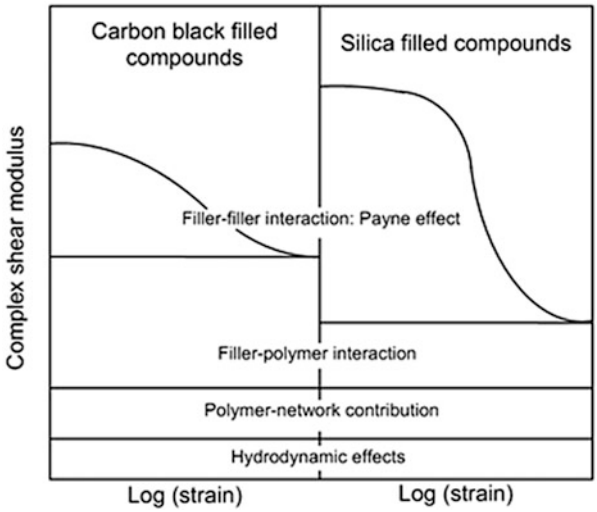

Fig. 10 Effects contributing to the complex shear modulus

polymers. Knowing the surface energy of the filler and the surface tension of the used rubber polymer, it should be possible to predict the dispersibility of the filler particles in this elastomer; or, to say it more precisely, the thermodynamic contribution of the wetting step on the dispersion process. In the case of nanofiller, a surface modification by the use of modifier is state of the art; this processing step leads to a better dispersibility and, additionally, to the formation of chemical linkages between filler and polymer during the vulcanization. Interfacial forces between filler and elastomeric matrix, which are a result of the surface energies of filler particles and polymers, are also important for the mechanical properties of the resulting composites. Hereby, the calculation of a work of adhesion value between filler and elastomer is a useful indicator to estimate the internal adhesion between filler particle surface and rubber polymer.

4 Nonlinear Viscoelastic Behaviour of Rubber Blends

Viscoelasticity is the material property exhibiting both viscous and elastic characteristics when a material is exposed to deformation and exists in many aspects of our daily life, such as human tissue, tires, seismic isolators etc. Viscoelasticity is quantified by three important properties: storage modulus (E'), loss modulus (E''), and damping ratio ($\tan \delta$). Storage modulus measures the elastic nature (stiffness) of a material and describes the ability to instantaneously strain (i.e., deform) and recover when stressed and released, respectively. In contrast the loss modulus measures the viscous nature of the material and expresses the resistance to strain

through energy dissipation. Finally, the damping ratio is the ratio of loss modulus to storage modulus and describes the relative level of viscosity to elasticity, where an ideal elastic material is zero and an ideal viscous fluid would be infinite.

The addition of fillers to rubber compounds has a strong impact on the static and dynamic behavior of rubber samples. Generally, the polymer network contribution depends on the crosslink density of the matrix and the nature of the polymer. The hydrodynamic effect in this model is nothing else than the effect of strain amplification, resulting from the fact that the filler is the rigid phase, which cannot be deformed. As a consequence, the intrinsic strain of the polymer matrix is higher than the external strain yielding a strain-independent contribution to the modulus. The effect of the structure is attributed to the 'in-rubber structure', which can be understood as a combination of the structure of the filler in the in-rubber state and the extent of filler–polymer interaction. The in-rubber structure is the measure for the occluded rubber, which is shielded from deformation and therefore increases the effective filler content leading also to a strain-independent contribution to the modulus. The filler–polymer interaction can be attributed to physical (van der Waals) as well as to chemical linkages or a mixture of both. In the case of the silica–silane system this interaction is formed by chemical linkages. The stress softening at small amplitudes is attributed to the breakdown of the inter-aggregate association respectively to the breakdown of the filler network. This stress softening at small deformations, called Payne-effect [68, 69], plays an important role in the understanding of reinforcement mechanism of filled rubber samples [70].

Most of the rubbers are deformed dynamically and specified dynamic properties are required. Therefore the effect of strain amplitude on the dynamic modulus was observed very intensively. The modulus of filled rubbers decreases with increasing applied dynamic strain up to intermediate amplitudes. A detailed study of the low frequency dynamic properties of filled natural rubber was carried out by Fletcher and Gent [71] and was later extended by Payne [72, 73]. In cyclic strain tests the shear modulus can be simply expressed as a complex modulus, $G^* = G' + iG''$ where G' is the in-phase modulus and G'' the out-of-phase modulus. The phase angle δ is given by, $\tan \delta = G''/G'$.

Elastomers filled with nanoparticles show a solid-like behavior response which includes a non-terminal zone of relaxation, apparent yield stress and a shear-thinning dependence of viscosity on particle concentration and/or dispersion. This particular rheological behavior arises from the presence of a network structure. Actually, the controversial discussion, or at least the main debate in the open literature, is about the origin of this network structure: polymer-particle or/and particle-particle interactions. The strain dependence of the dynamic viscoelastic properties, often referred to as the Payne effect, is well known in elastomers for 40 years. There are experimental data [74, 75] suggesting that the mechanical reinforcement of crosslinked rubbers is mainly related to the secondary structure of filler particles and others [76, 77] suggesting chain stiffening due to the rubber filler interactions is the primary reinforcing mechanism. Intensive discussions have been held on the nature of this effect, but the exact causes of this non-linear behavior are still a matter of investigations and controversial discussions.

In one approach [74], the level of filler dispersion is expected to play a major role in determining the filler effects on non-linear responses of nanocomposites while the other considers the chain stiffening due to reversible trapping of entanglements to be the primary cause of the observed behavior [78]. For example, it is well known that rubber-like materials exhibit an appreciable change in their mechanical properties (stress softening) resulting from the first tensile experiment. This phenomenon is well recognized to be caused by the following mechanisms: (1) physical disentanglement of rubber chains, (2) decrease in the interactions between polymer molecules and filler surfaces, (3) filler network breakdown and (4) chain scission of rubber molecules. A number of research papers and reviews have been dedicated to this behavior termed Payne and Mullins effects [79]. Although different theories have been proposed, it is essential to understand the filler super structure at different length scales.

Maier and Goritz [80–82] take into consideration the adsorption/desorption mechanism by considering the filler particles as multifunctional crosslink with chains which are either loosely or strongly anchor to the surface. The molecular interpretation of the Payne effect is then based on a variable network density when the loosely tied chains are desorbed with the increase of the strain. A compromise is also suggested, considering that the primary mechanism for the Payne effect certainly involves the existence of cooperation between the breakdown and reformation of the filler network and the molecular disentanglement of the bound and free rubber. Another explanation first proposed by Yatsuyanagi et al. [83] considers the existence of a percolation network through the rigid amorphous layer formed around the particles. Their interpretation of the Payne effect equally relies on the competition between desorption and adsorption of this rigid amorphous layer. The amplitude of the Payne effect for ethylene vinyl acetate copolymer (EVA) at different silica fraction at 140 °C is increased with increase in silica concentration [84].

The importance of glassy layers in filled polymer has received considerable attention recently, when it was recognised that a glass transition gradient exists near the surface and that the dynamics could be either enhanced or slowed down according to the interaction of the chains with the surface. In a body of work, Berriot et al. [85–87], Montes and others [88] have clearly shown that, in filled elastomers, a maximum of reinforcement is obtained when this rigid or slow dynamics layer forms a continuous path through the filler aggregates. In their work, Merabia et al. [89] model the Payne effect by considering that the stress is supported mainly by the cross section of glassy bridges in a direction normal to the stress. They explain the strain dependence of the elastic modulus by the local lowering of the glass transition due to the amplification of the stress in the vicinity of the aggregates. This plasticizing effect induces the yielding of the glassy bridges and the collapse of the storage modulus.

Darestani Farahani et al. used RPA to study viscoelastic parameters of natural rubber/reclaimed rubber blends. Viscoelastic behavior of compounds was studied in strain sweep mode at 100 °C, strain range 1–1,200 % and frequency 10 cpm (cycle per minute). They found that torque (S) increases in higher shear strains,

because bigger deformations need more torque but polymer chains flow more easily thus shear modulus (G) decreases in higher strains. S of NR/reclaimed rubber blends is lower than two polymers (i.e. natural rubber and reclaimed rubber), while authors predicted that the torque of blends is between the torque of two polymers. This behavior can be attributed to nonhomogeneity of phases in blends. It seems that friction of polymer chains in a completely homogenized and compatible blend is more than non homogenized one.

They studied the elastic modulus (G′) and loss modulus (G″) of compounds. They observed that the G′ changes with strain can be divided to three different zones: linear viscoelastic in low strains, non-linear viscoelastic in medium strains and linear viscoelastic in high strains. In low strains, G′ of reclaimed rubber is higher than natural rubber due to the fillers left in reclaimed rubber. But non-linear viscoelastic behavior of reclaimed rubber begins in lower strains than NR. This can be attributed to the beginning of the filler-filler and rubber-filler networks breakdown in these strains. In medium strains, elastic modulus (G′) decreases due to rubber-filler and filler-filler networks breakdown and disentanglement of polymer chains. The rate of G′ drop in this non-linear viscoelastic zone in reclaimed rubber is less than NR due to filler presence in reclaimed rubber and its elastic nature. In high strains, G′ of compounds is the same but linear viscoelastic behavior (i.e. the plateau) of reclaimed rubber begins in higher strains than NR. In other words, non-linear viscoelastic zone in reclaimed rubber is longer than NR, begins in lower strains and finishes in higher strains.

The elastic modulus of NR/reclaimed rubber blends is lower than NR and reclaimed rubber which is due to non-homogeneity and non-uniform dispersion of filler in these blends. The G′ of blends has similar trend to their major phase (i.e. NR or reclaimed rubber).

Three zones indicated in G′, can also be detected in the graph of loss modulus (G″) versus strain. In low strain, the first linear viscoelastic zone, G″ of reclaimed is lower than NR due to its filler content. In higher strains, G″ of NR compounds decreases due to disentanglement of polymer chains whereas, reclaimed rubber has different behavior. In medium strains, loss modulus of reclaimed rubber increases due to energy dissipation for rubber-filler and filler-filler networks breakdown and then decreases due to rubber chains disentanglement.

In high strains, moving of polymer chains is completely laminar and all compounds have linear viscoelastic behavior, thus G″ has no significant change. Final G″ of reclaimed rubber is lower than NR which is due the fillers left in reclaimed rubber. Loss modulus G″ of NR/reclaimed rubber blends has similar trend to the major phase of blend (i.e. NR or reclaimed rubber). It is indicated that the increase of loss modulus in non-linear viscoelastic zone can be detected in NR/reclaimed rubber 25/150 blend while this behavior cannot be observed in NR/reclaimed rubber 75/50 blend. In high strains linear viscoelastic zone, nonhomogeneity of phases and non-uniform dispersion of filler cause lower loss modulus of NR/reclaimed rubber blends than NR and reclaimed rubber. In addition, in the first low strain linear viscoelastic zone, G″ of NR/reclaimed rubber blends has no significant difference with reclaimed rubber. It seems filler amount, homogeneity of

phases and filler dispersion have no significant effect on the loss modulus in low strains and effect of these parameters can be detected in medium and high strains.

Study of strain dependence of tanδ shows that, for all compounds tanδ increases with increasing in strain. The trend of tanδ can be divided in two zones i.e. elastic zone ($\tan\delta < 1$) and viscose zone ($\tan\delta > 1$). It is indicated that the elastic zone of reclaimed is longer than NR, and in NR/reclaimed rubber blends with increasing reclaimed rubber content elastic zone becomes longer. This is due to the fillers left in reclaimed rubber. Non-homogeneity of phases and non-uniformed dispersion of fillers in NR/reclaimed rubber 50/100 and 75/50 cause shorter elastic zones in these blends than virgin natural rubber [90].

4.1 Effect of Spherical Fillers in Non-linear Viscoelasticity of Blends

The average particle sizes of carbon blacks commonly available for industrial use; range from 10 nm to 500 nm. Carbon black exists in three dimensional branched structures called aggregates. High structure blacks exhibit a strong aggregation whereas low structure blacks show only a weak aggregation. In the case of the graphitized black a well organized arrangement of the upper graphite layers can be observed as shown in Fig. 11.

The polymer-carbon black filler reinforcement depends widely on the polymer type, carbon black type and structure. Another factor affecting this reinforcement is the filler-filler interaction which leads to the formation of three dimensional aggregation structures within the bulk of the rubber matrix. Figure 12 shows the aggregation and agglomeration of carbon black in the rubber. These aggregations takes various shapes which may be spherical or ellipsoidal with different major and minor

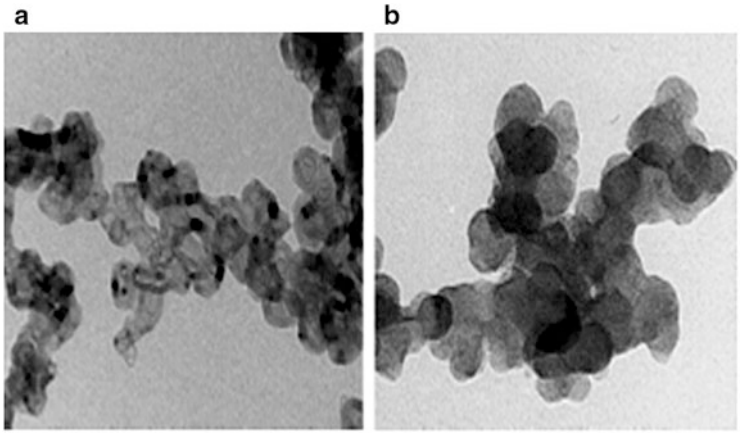

Fig. 11 TEM images of N330 (**a**) graphitized (**b**) nongraphitized

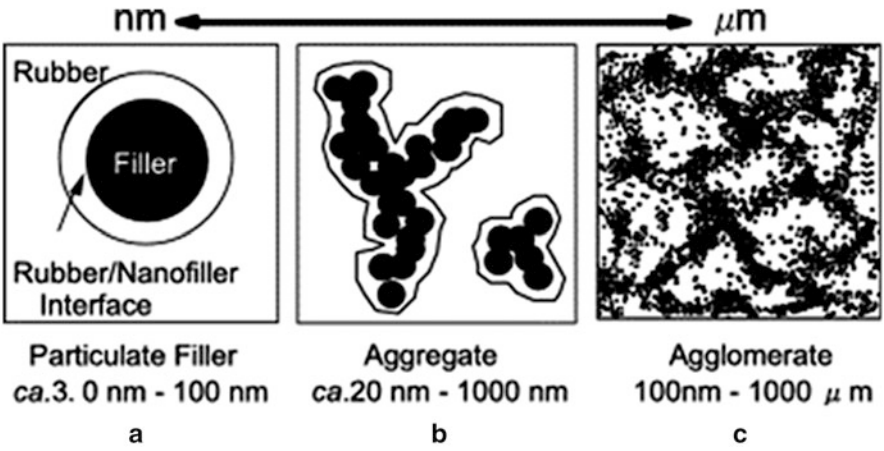

Fig. 12 The aggregation and agglomeration of carbon black in rubber [93]

axes. Several aggregates connect through Van der Waals forces to give weak, giant assembled called agglomerates. Several authors investigated and discussed the structure of these aggregates by using several techniques such as relating the modulus of unfilled rubber to that of filled rubber [91, 92].

The effect of carbon black on hysteresis depends primarily on the particle size of the filler and is related to breakdown and reformation of the agglomerations and the network, to slippage of polymer chains around the periphery of the filler clusters and the presence of occluded rubber. Figure 13 shows the difference of the temperature profiles of carbon black and silica filled rubber compounds.

In the rubber industry the distribution of particle size is considered to be important as it affects the mechanical properties and performance. Aggregate size also varies with particle size. Aggregates can have any shape or morphology. The fundamental property of the filler used in a filled elastomer is the particle size. This affects the reinforcement of elastomer most strongly. One of the sources of reinforcement between the carbon black surface and the rubber matrix is the van der Waals force attraction. Also, rubber chains are grafted onto the carbon black surface by covalent bonds. The interaction is caused by a reaction between the functional group at the carbon black particle surface and free radicals on polymer chains. Hence, filler-rubber interface is made up of complex physical-chemical interaction. The adhesion at the rubber-filler interface also affects the reinforcement of rubber. When the polymer composites are filled with spherical filler (aspect ratio of the particle is equal to unity), the modulus of the composite depends on the modulus, density, size, shape, volume ratio, and number of the incorporated particles.

Wootthikanokkhan et al. studied distributions of carbon black in 30/70 % (w/w) NR/acrylic rubber (ACM) blends as a function of the carbon black content and type using DMTA technique. Two different types of carbon black (N220 and N330) were used, and 10–50 phr carbon black was compounded to the rubber blends. From the DMTA thermograms of various blends, the weight fractions of carbon black in

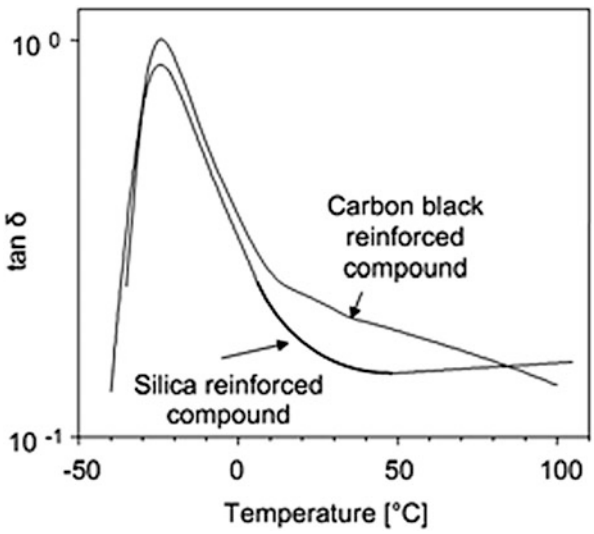

Fig. 13 Temperature profiles of the phase angle for a carbon black filled and a silica filled compound

the NR and ACM phases were calculated. Carbon black was unevenly distributed in the rubber blend. It preferred to migrate into the NR phase, regardless of the amount of carbon black that was used. By increasing the carbon black content, the weight fraction of carbon black in the NR phase decreased whereas that in the ACM phase increased. A change in the type of carbon black from N220 to N330 significantly decreased the weight fraction of carbon black in the NR phase, but it was not sufficiently strong to affect the tensile properties and hardness of the rubber blend [94].

Sirisinha et al. studied the effects of filler and rubber polarity on the distribution of filler in BR/NBR blends, using the DMTA technique. As 30-phr filler is added, the reduction in heights of tan δ is attributed to the dilution effect. It has also been also found that small and large particle sized carbon black prefer to reside in BR phase compared NBR phase in the blends because of the lower viscosity and lower polarity of the BR phase. The addition of silica instead of carbon black leads to an increase in filler migration to the NBR in the 20/80 BR/NBR blend, which is attributed to the strong silica–NBR interaction. In addition, an increase in NBR polarity promotes carbon black migration to the BR phase.

The DMTA results also show that the morphology of BR/NBR blend is the two-phase structure with two relaxation peaks at about −72 and 0 °C, corresponding to the BR and NBR phases, respectively. The addition of filler results in a reduction in tan δ_{max}, which is attributed to the dilution effect. The rigid filler possesses no viscous response and therefore can dilute the viscous response of the elastomeric phase. The use of damping peak tan δ, which decreases with filler loading, will enable one to calculate the distribution of carbon black in each phase of the blends. BR is more preferential than NBR for all three particle sizes of carbon black to reside. As the BR/NBR ratio decreased, the BR phase became saturated with carbon black, which then transferred to the NBR phase. Generally, the main

reasons for the imbalance in carbon black transfer to the BR phase are attributed to the relatively low viscosity of the BR phase and the relatively strong interaction between carbon black and the BR phase. An addition of fillers leads to a decrease in tan δ as a result of the dilution effect, that is, the viscous response of the elastomeric phase is diluted by the nonviscous response of fillers. Carbon blacks with small and large particle sizes, N220, N330, and N660, tend to reside preferentially in the BR phase rather than the NBR phase because of the lower viscosity and non polarity of BR. For the BR/NBR blend ratio of 20/80, the precipitated silica appears to reside increasingly in the polar phase (NBR), compared to carbon black, indicating the strong silica–NBR interaction. However, the filler polarity effect is not observed in the 50/50 BR/NBR blend. Carbon black distribution in BR/NBR blends is affected significantly by the difference in polarity between the BR and NBR. The higher the polarity of the NBR, the smaller the amount of carbon black residing in the NBR phase [95].

Kader et al. studied the dynamic-mechanical properties of gum and filled acrylic rubber (ACM), fluorocarbon rubber (FKM), and their blends of varying compositions. DMTA showed a single tan δ peak corresponding to a single phase transition for both cured and filled blends. The storage modulus of the blend increased from the gum blend to the filled blend, indicating the presence of polymer–filler interaction. The loss tangent peaks, corresponding to glass-transition temperature of unfilled blends and of both cured and uncured gum blends were observed at −1.0 °C and 0 °C, respectively. However, the corresponding peak for the filled system was observed at 5 °C, with reduction in the loss tangent value, indicating the influence of filler on the Tg of the blend. The effect of curing and the addition of filler were also seen with increasing storage modulus values at all measured temperatures because of the restricted mobility of the polymer chain through crosslinking and polymer–filler networking, respectively [96].

Chuayjuljit et al., studied the E′ and tan δ thermograms for the 70/30 XSBR/NR blend vulcanizate, and those with and without the addition of 3 phr of either $nSiO_2$ XSBR and NR rubber blends filled with $nSiO_2$ or PS-$nSiO_2$. These are shown in Fig. 14. The E′ of the nanocomposite containing $nSiO_2$ or PS-$nSiO_2$ in the temperature range from 100 °C up to 20 °C is the lowest, suggesting insufficient crosslinking. This is presumably caused by the acidic OH groups on the silica surface adversely affecting the sulfur-mediated curing of the NR. Therefore, the Tg of NR in this nanocomposite is slightly shifted towards a lower temperature. At a temperature above 20 °C, the E′ of the nanocomposite increases due to the interaction between the $nSiO_2$ and XSBR that induces a restricted mobility of XSBR. However, the $nSiO_2$ may provide two possible effects: firstly a decrease in the cross-link density and secondly the restriction of molecular chain mobility. As the PS-$nSiO_2$ was introduced into the rubber blend matrix, the PS shell improved the compatibility of the nanofiller and the rubber matrix, resulting in a slightly increased E′ value. Nevertheless, the strong interaction between the nanofillers and the XSBR may cause microphase separation in the rubber matrix, resulting in an indirect decrease in the Tg of the soft segment in XSBR. Thus, both the Tg values of XSBR in the nanocomposites are slightly decreased [97].

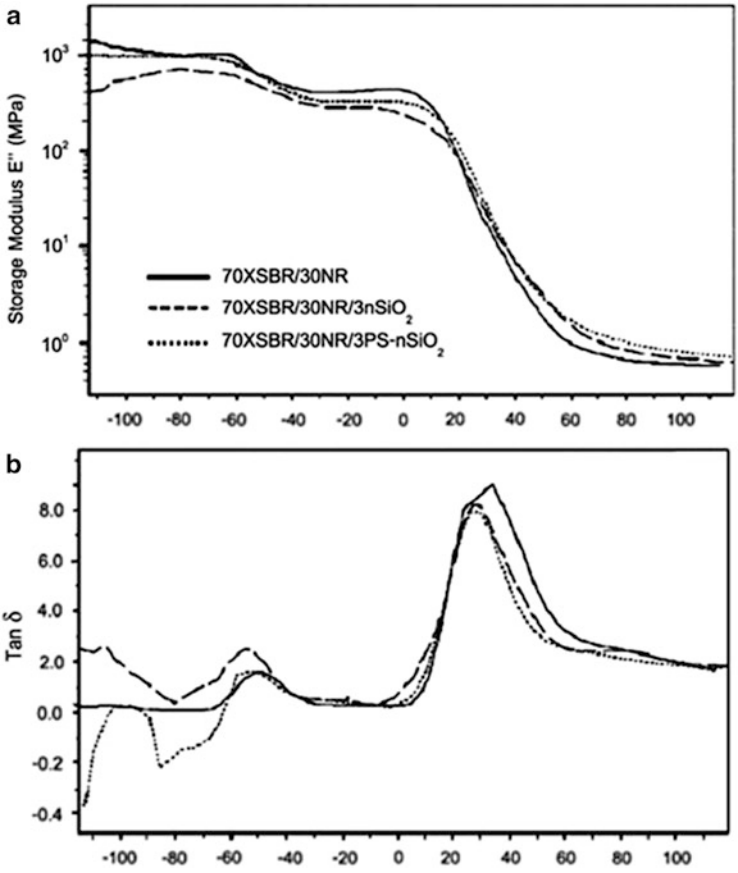

Fig. 14 Temperature dependence of (**a**) Storage modulus (E′) and (**b**) the loss tangent (tan δ) for 70/30 XSBR/NR blend with and without 3 phr of either $nSiO_2$ or PS-$nSiO_2$ [97]

The temperature dependence of E′ and tan δ in the 50/50 XSBR/NR blend, and in their 3 phr $nSiO_2$ and PS-$nSiO_2$ containing nanocomposites are shown in Fig. 15. The addition of $nSiO_2$ increased the E′ of the nanocomposite compared to the neat rubber blend, indicating that as the XSBR loading is lower, the interaction between $nSiO_2$ and XSBR is also decreased, resulting in the aggregation of the $nSiO_2$. These aggregates constrain the movement of the polymer chains. Moreover, the well-dispersed of the PS-$nSiO_2$ in the rubber matrix may cause a slight increase in the E′ at the temperature above 10 °C. However, there is no significant change for either of the Tg values for the NR and XSBR in the rubber blend and their nanocomposites [97].

Finally, the variation in E′ and tan δ of the 30/70 XSBR/NR blend and their 3 phr $nSiO_2$ and PS-nSiO2 containing nanocomposites as a function of temperature are shown in Fig. 16. The addition of the nSiO2 to the NR-rich rubber blend slightly increased the E′ of the system, because the $nSiO_2$ aggregates prevents the free

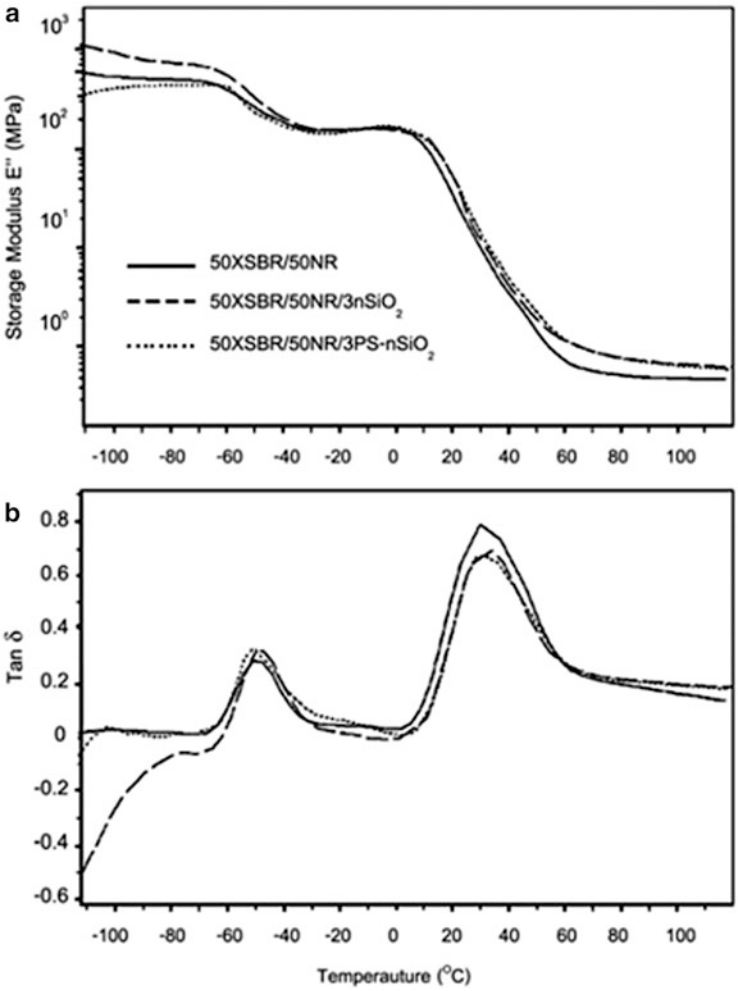

Fig. 15 Temperature dependence of (**a**) Storage modulus (E′) and (**b**) the loss tangent (tan δ) for 50/50 XSBR/NR blend with and without 3 phr of either $nSiO_2$ or PS-$nSiO_2$ [97]

molecular motions to a smaller extent. The effect can be noticed at temperatures above the Tg of NR but the drop in the E′ of the PS-$nSiO_2$ or PS-$nSiO_2$ nanocomposite below 10 °C is clearly observed. This may be attributed to the PS molecules on the surface of the $nSiO_2$ that shield the matrix from the silica nanoparticles leading to an increase in the free volume and the mobility of the rubber molecules. Moreover, the Tg of the NR and XSBR in the rubber blend and nanocomposites, as determined from the tan δ peaks were found to be very close [97].

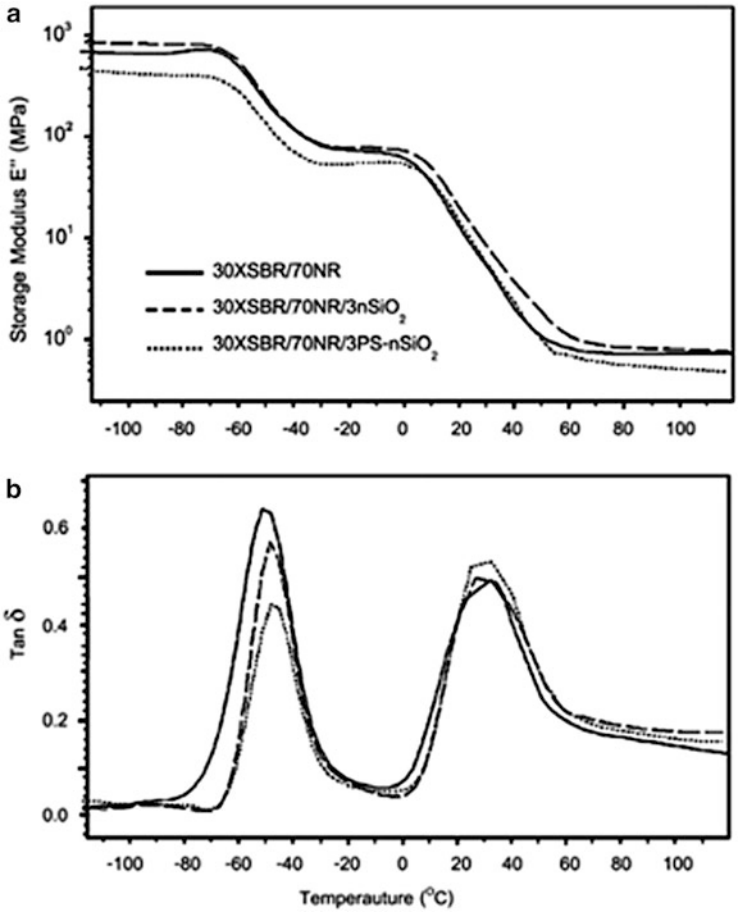

Fig. 16 Temperature dependence of (**a**) Storage modulus (E′) and (**b**) the loss tangent (tan δ) for 30/70 XSBR/NR blend with and without 3 phr of either $nSiO_2$ or PS-$nSiO_2$ [97]

4.2 Effect of Tubular Fillers in Non-linear Viscoelasticity of Blends

The length of a CNT is from a few microns up to millimetres, with a diameter of the order of nanometers. A single nanotube is hundred times stronger and six times lighter than steel and exhibits good electrical and thermal conductivities. Hence, the future of CNT application can be easily envisaged from electrical sensors to reinforcing fillers, especially in the vast world of high performance materials. While clay nanocomposites have started to appear in large quantities in consumer products, carbon-based nanofillers are a promising alternative. SWNTs have become a key player in the field because they lead to improvements in mechanical properties, along with exceptional electrical conductivity, thermal conductivity,

thermal stability, and low flammability. However, their high price poses strong limitations on their large-scale use, and other restrictions are set by the difficult control of the agglomeration of the individual nanotubes into low-modulus bundles that control the mechanical stability and strength of the SWNT polymer nanocomposites. Elastomeric applications generally require and make use of the large deformation extensibility and resilience of the elastomer. Upon incorporation of stiff fillers into elastomers, it is generally desired to enhance the stiffness (i.e., enhance the initial stiffness and retain this stiffness enhancement for overall large strain deformation behavior) while also retaining the important attributes of large strain resilient behavior and large strain-to break.

The outstanding properties of carbon nanotubes have generated scientific and technical interests in the development of nanotube-reinforced polymer composites. Das et al., investigated a novel mixing approach for achieving a good dispersion of MWCNTs in a rubber blend. In this approach the CNTs were incorporated into a 50:50 blend of solution-styrene–butadiene rubber and butadiene rubber. First, the CNTs were predispersed in ethanol and then this CNT–alcohol suspension was mixed with the rubber blend at elevated temperature. The rubber nanocomposites prepared by such method exhibit significantly enhanced physical properties already at very low nanotube concentrations. Dynamic mechanical analysis indicates that the incorporation of CNTs affects the glass transition behaviour by reducing the height of the tan δ peak considerably. Above the glass transition temperature the storage modulus has been increased after incorporation of a small amount of CNTs. Finally, the 'Payne effect', an indication of filler–filler interactions, was observed at very low concentrations of CNT in the rubber matrix [98].

The storage modulus of unfilled rubbers, E′, depends on frequency and temperature and is independent of the deformation amplitude. In contrast, E′ for the filled rubber shows a significant dependency on the dynamic deformation, here the value considerably decreases with an increasing strain amplitude. This non-linear behaviour of filled rubbers is known as 'Payne effect' [74, 99] and has been explained by the existence of a filler network in the rubber matrix above the percolation threshold. With increasing strain amplitude the filler network is breaking down which results in lowering of the E′ value. Figure 17 supplies an evidence of the existence of a carbon nanotube filler network in an S-SBR–BR blend prepared by the wet mixing method. For a pure rubber (not shown here) and at small CNT loading (up to 2 phr) no 'Payne effect' is observed. However, with the increase of the MWCNT content a gradual decrease in E′ is observed in strain sweeps. So, even with 3 phr of MWCNT the tubes obviously form a continuous filler network in the rubber matrix. The OH-functionalised sample with 5 phr of CNT shows a significant lower E′ value compared to the unfunctionalised one, with additional silane modification the value increases. This shows the opposite behaviour as known for silica filled samples, where silanisation reduces the Payne Effect to a certain amount. The concentration of hydroxyl groups, present on the surface of the nanotubes, is obviously not comparable to silica and does not allow the formation of hydrogen bonds between two adjacent modified tubes, hence the silanisation is not reducing the filler–filler interaction.

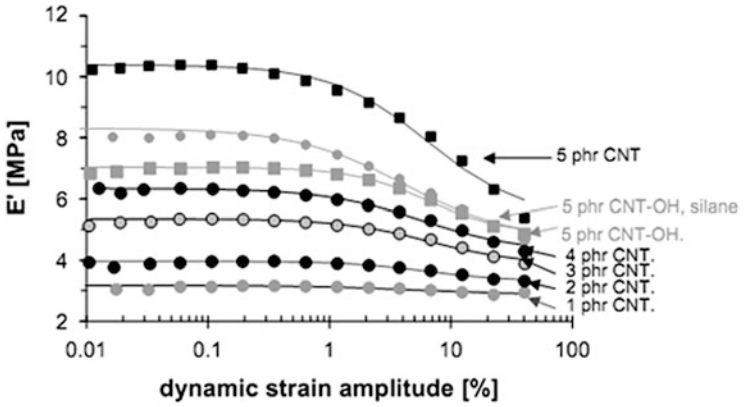

Fig. 17 Strain dependencies of dynamic properties for CNT filled S-SBR–BR blends [98]

The filler–filler network can be reformed again after a certain time interval. Payne revealed that the value of E′ is largely recoverable upon return to smaller amplitudes in the linear regime. So, flexible rubber chains allow the filler particles to rearrange again to form a three-dimensional filler network in the rubber matrix [99]. In order to investigate the ability to recover the strain sweep experiments were also carried out in the reverse direction from higher to lower strain amplitudes for the samples with unmodified CNT dispersed by ethanolic suspension.

It is observed that the values do not reach its initial position within the relaxation time of the experiment, but a recovery of the E′ values have been attained (Fig. 18). This behaviour of a rubber can be explained by the stress softening effect during the dynamic strain. Nevertheless, a high extent of recovery in the reverse amplitude sweep indicates that a good filler–filler network has been re-established at a low loading of tubes in the S-SBR–BR matrix. So, at least it can be said that rather than damage or permanent break of the tubes, the amplitude sweep disrupted the filler–filler network in the rubber matrix. It is noted that the absolute values of E′ at small amplitudes are somewhat differed from each other as compared with the value obtained from the phr CNT-filled compound. The difference may be developed from ageing of the samples.

Figures 19 and 20 show the temperature dependencies of the storage moduli, the loss moduli and the loss factor tan δ of the CNT–rubber nanocomposites. Figure 19 illustrates that with an increase in temperature the storage modulus of all samples decreases which is associated with the glass transition phenomenon of the elastomer chains. Above room temperature the value of E′ increases as well with increasing filler loading. As seen in Fig. 20, the glass transition temperature at the maxima of the tan δ plot does not change with the tube content in the rubber matrix. However, the peak height reduces considerably with higher CNT content. This behaviour also indicates the strong reinforcement efficiency with only low content of CNT.

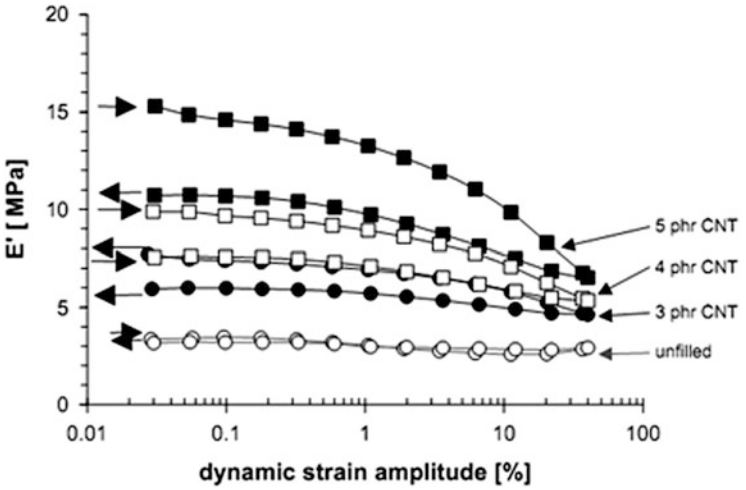

Fig. 18 Strain dependencies of dynamic properties for CNT filled S-SBR–BR blends [98]

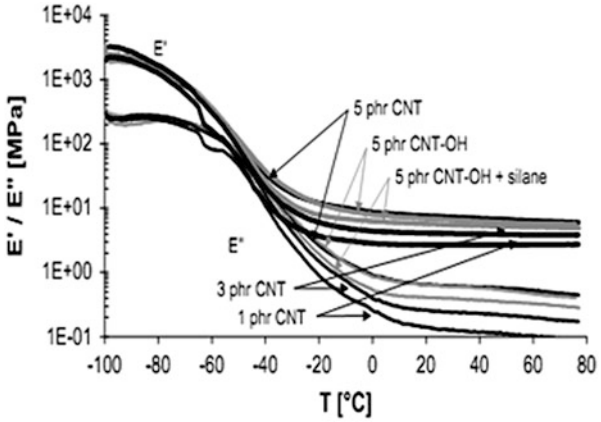

Fig. 19 Storage modulus E′ and loss modulus E″ as a function of the temperature for a CNT filled SBR–BR blend [98]

Boonmahitthisud et al., prepared natural rubber/carboxylated styrene butadiene rubber (NR/XSBR) (80/20) nanocomposites containing different loadings of carbon nanotube (CNT) (0.1–0.4 phr) by a latex stage compounding method. The dynamic mechanical properties, in terms of tan δ and E′, of the neat 80/20 NR/XSBR blend and its nanocomposites were evaluated from −80 to 100 °C. Figure 21 shows the influence CNT loadings, on the tan δ and E′ as a function of temperature for the nanocomposites [100].

The variation in tan δ with temperature of the neat rubber blend and its nanocomposites filled with CNT revealed two tan δ peaks at −60 to −43.4 °C and 30 to 50 °C, that were assigned to the Tgs of NR and XSBR, respectively

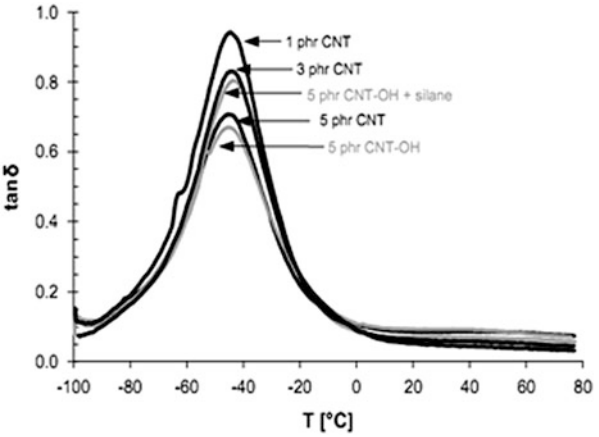

Fig. 20 Loss tangent (tan δ) as a function of the temperature for CNT filled SBR–BR blend [98]

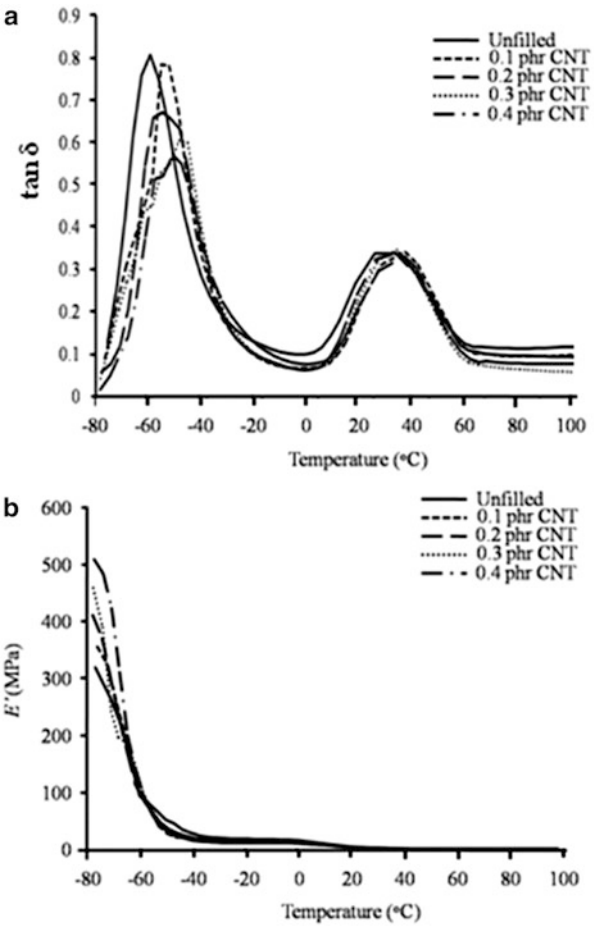

Fig. 21 Representative DMA thermograms of NR/XSBR based nanocomposites filled with different CNT loadings: (**a**) tan δ and (**b**) E′ [100]

(Fig. 21). This indicates that the blends are not compatible and so form a two phase structure in the blend and nanocomposites. The Tg for both NR and XSBR of each rubber nanocomposite tended to increase with increasing CNT loading levels, and so the thermal motion of the rubber chain segments was constrained by the CNT particles.

With respect to the variations in the E′ with temperature, the E′ of each composition decreased with increasing temperatures due to the decrease in stiffness of the samples (Fig. 21). A significant influence of the CNT content on the E′ occurs at a temperature below the Tg of NR. At −80 °C, a temperature selected below the Tg of NR, the E′ of the nanocomposites tends to increase considerably with increasing CNT loadings in comparison with that of the neat rubber blend, most likely due to the stiffening of the rubber matrix, as described previously. Thus, the data for the changes in E′ with increasing CNT loading levels are in agreement with that for the tensile modulus [100].

Kueseng et al. prepared 50/50 NR/NBR blends with various MWCNT loadings by mixing with MWCNT/NR master batches on a two-roll mill and sheeted off at the smallest nip gap. Then, the effect of milling direction, machine direction (MD) and transverse direction (TD), on the mechanical and electrical properties of the blends was elucidated. Results from dynamic mechanical tests also showed that the maximum tan δ in the MD sample was lower than that in the corresponding TD sample. In addition, the storage modulus at 30 °C for the MD sample containing 4 phr MWCNT was 1.15 higher than that of the corresponding TD sample. This stronger reinforcement efficiency resulted from the combination of the greater alignment and dispersion of most MWCNTs in the MD sample [101].

The plots of tan δ of the blends versus temperature are displayed in Fig. 22. It is evident that there are two Tg; around −56 °C and −14 °C corresponding to NR and NBR phases, respectively. It is found that MWCNT loading and alignment direction slightly influence the Tgs of both phases. However, the tan δ max of both phases tends to reduce with increasing MWCNT loading, regardless of the alignment direction. The dilution effect could be used to explain this finding. It is also observed that tan δ in the MD of both phases is lower than that in the TD. Figure 23 shows the average storage modulus values at 30 °C for the blends. It appears that the storage modulus of all blends in MD is higher than that of the corresponding TD samples. This result may be explained by the higher reinforcement efficiency for MWCNT aligned in the longitudinal direction. These results correspond well with the moduli and tear strength of the blends.

Le et al., developed ternary blends based on SBR, NBR and NR. And also studied the characterization of the kinetics of CNT dispersion and distribution in ternary blends [102].

The similarity in morphology of four blends can be proved by the DMA investigation. In Fig. 24 elastic modulus and tan δ of four blends are presented. The dynamic-mechanical behavior of the investigated blends does not differ from each other. It was found that CNTs mainly reside in the polar NBR and non-polar NR but not in weak polar SBR. Such unusual localization of CNTs in ternary SBR/NBR/NR can be explained by taking into consideration the presence of

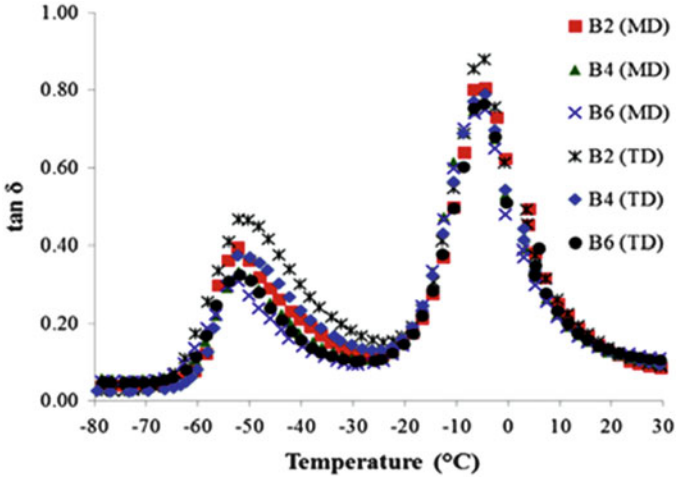

Fig. 22 Loss tangent (tan δ) of various blends in MD and TD as a function of temperature (B2, B4 and B6 represents MWCNT/NR master batches having 4, 8 and 12 phr of MWCNT, respectively) [101]

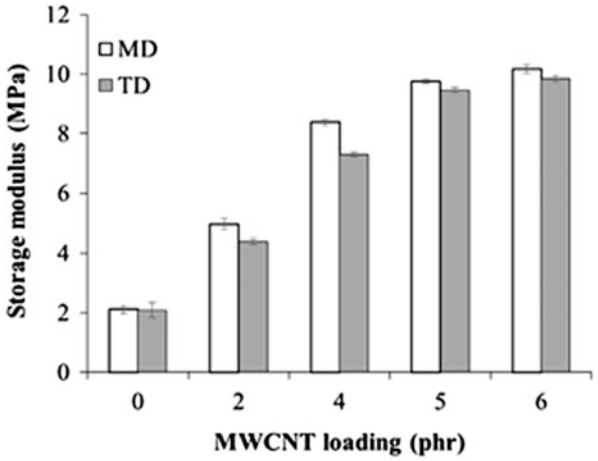

Fig. 23 Storage modulus at 30 °C of the blends in MD and TD at various MWCNT loadings; *MD* machine direction, *TD* transverse direction [101]

phospholipids in NR. Phospholipid can act as coupling agent bonding the α-terminal of NR with the CNT surface through cation-π interactions, which make NR be competitive with NBR with respect to CNT hosting. Setting the equilibrium CNT loadings experimentally determined by the wetting concept into the *Z*-model recently developed in our previous work by keeping unchanged the surface tension values of SBR and NBR a corrected value of surface tension of NR was determined, which involves the effect of phospholipids [102].

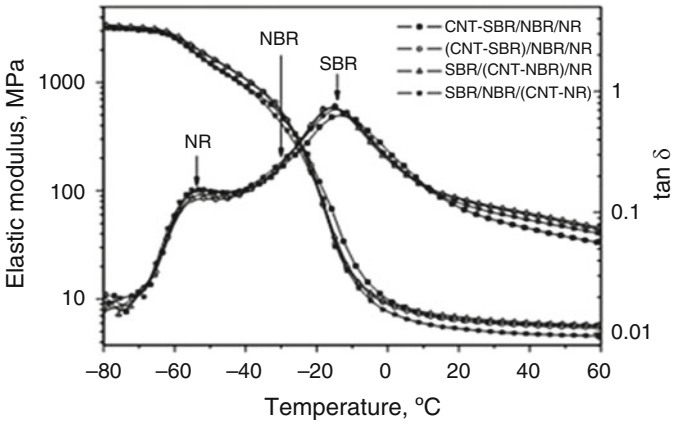

Fig. 24 Dynamic-mechanical properties of (CNT–SBR)/NBR/NR blend four investigated blends [102]

Yan et al., studied Bis-(triethoxysilylpropyl)-tetrasulfane functionalised carbon nanotubes (t-CNTs) were used as compatibiliser along with liquid isoprene rubber (LIR) in the NR/BR blend. SEM and TEM images showed enhanced interfacial adhesion between the binary rubber phases and improved dispersion of the minor phase in the rubber blend respectively with the co-existence of LIR and carbon nanotubes. The co-compatibilisation behaviour of t-CNTs and LIR suggests that t-CNTs have a better effect than CB with the assistance of LIR, which is an effective plasticiser in the NR/BR blend [103].

The tan δ curves for 80NR/20BR/22CB/3t-CNTs with different loadings of LIR are shown in Fig. 25. The tan δ curve of the NR rich phase shows a peak at −46 °C due to the transition arising from the segmental motion, this corresponds to the glass transition temperature Tg of NR in the blend. The Tg of BR rich phase is at −92 °C, as shown by a tan δ peak in the curve. There are two relaxation peaks corresponding to two phases, which suggest the immiscibility of the binary components. However, there is no relaxation peak corresponding to LIR, indicating good miscibility of LIR with both NR and BR phases. It is noteworthy that the tan δ peak value for the NR rich phase increases with increasing LIR content, whereas it decreases for the BR rich phase. The area under the loss modulus curve was calculated by integrating the loss modulus versus temperature curve in the temperature range of −110 to −70 °C, corresponding to the glass transition process of the BR rich phase. It shows that the loss modulus peak area shifts to the lower value with an increase in the LIR content in the 80NR/20BR/22CB/3tCNTs blends. The intensity of the tan δ peak and the loss modulus peak area at the glass transition temperature are considered to reflect the mobility of the molecular chain segments [104, 105]. The decrease in the intensity of the tan δ peak and loss modulus peak area of the BR phase with increasing LIR content indicates the decrease in mobility of the BR molecular chain segments, which suggests the high interfacial interaction between matrix NR and minor BR phase with the assistance of LIR and t-CNTs, which act as a bridge

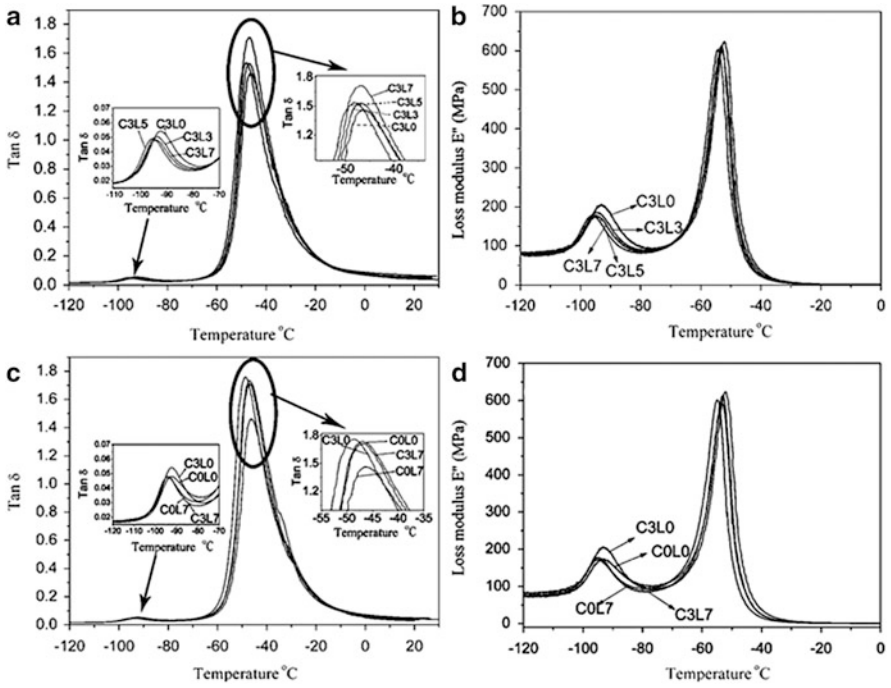

Fig. 25 Dynamic mechanical analysis curves of C0L0, C3L0, C3L3, C3L5, C0L7 and C3L7 blends [103] (C0L0 = 80/20 NR/BR + 0t-CNT + 0 phr LIR, C3L0 = 80/20 NR/BR + 3 phr t-CNT + 0phr LIR, C3L3 = 80/20 NR/BR + 3 phr t-CNT + 3 phr LIR, C3L5 = 80/20 NR/BR + 3 phr t-CNT + 5 phr LIR, C0L7 = 80/20 NR/BR + 0 phr t-CNT + 7 phr LIR, C3L7 = 80/20 NR/BR + 3 phr t-CNT + 7 phr LIR) (**a**) and (**c**) shows variation of tan δ with temperature and (**b**) and (**d**) variation of loss modulus with temperature

connecting the interface of the binary phases. The interfacial interaction can drive the miscibility of the BR with the NR matrix [102].

4.3 Effect of Layered Fillers in Non-linear Viscoelasticity of Blends

Das et al., demonstrates, an approach of compatibilization between polychloroprene (CR) and ethylene propylene diene monomer rubber (EPDM) by using nanoclay (NC) as a compatibilizer and, simultaneously, as a very strong reinforcing nano-filler. With the incorporation of less than 9 wt.% nanoclay, the dynamic storage modulus above the glass transition region of such a blend increases from ~2 MPa to ~54 MPa. This tremendous reinforcing as well as the compatibilization effect of the nanoclay was understood by thermodynamically driven preferential framework-like accumulation of exfoliated nanoclay platelets in the phase

border of CR and EPDM, as observed i.e. from transmission electron microscopy. The extra-ordinary improvement of dynamic modulus can also be understood by a very strong filler–filler networking that we observed in strain sweep experiments. Moreover, we found that the compatibilized blends exhibit an extra dynamic-mechanical relaxation process at higher temperatures (~T + 130 K). The suggested method for compatibilization of incompatible rubber blends offers routes to the design of new rubber based technical products for diversified applications [106].

Figure 26 shows TEM images of CR/EPDM blend at the ratio of 75/25, 50/50 and 25/75, respectively, with 10 phr clay. Every blend is prepared by incorporating all the clay in the EPDM rubber and, subsequently, the resulting composites were mixed with CR. It is obvious from Fig. 26a, b that two phases of CR and EPDM co-exist with a large number of exfoliated and intercalated clay platelets at the interfaces. The dark phase is the CR phase with higher electron density due to the presence of chlorine atoms in the rubber chains. Remarkably, it is found that there are almost no clay layers in the bright phase rather than in the dark phase. CR, being a polar rubber, forces to migrate the clay particles into it, rendering the EPDM phase poor, despite the fact that all the clay was premixed with EPDM. Migration of inorganic clay layers is taken place from non-polar EPDM to polar CR and, as far as viscosity mismatch (Mooney viscosity) is concerned, the migration is also driven by viscosity difference since the Mooney viscosity of EPDM is higher than the viscosity of CR. The migration of clay from EPDM to CR phase can also be well explained as a wetting/dewetting process between polymers and filler. Hereby, the driving force is the difference of the interfacial tensions between the rubbers and clay [106].

The dependence of storage elastic modulus (E′) on the strain amplitude at very low strain values delivers an understanding about the impact of the filler networking within the rubber matrix. Generally, E′ remains unaltered with increasing strain for an unfilled rubber system. However, for a filled system, the storage modulus decreases with increasing strain. This nonlinear behaviour of a filled rubber system is called ‘Payne effect’ and yields information about filler–filler networking in the rubber matrix. In the present investigations, the plots of E′ versus double strain amplitude of the CR/EPDM blends are shown in Fig. 27a. It is evident from this figure that the gum-blend without any filler does not undergo any change in E′ with increasing strain. However, a strong dependency can be observed for all filled samples. Here, all rubber blends are filled with only 10 phr of clay and, obviously, these clay particles, being either exfoliated and/or intercalated, build a strong filler–filler network in the rubber matrix. The preferential localization of the clay at the interface fulfils the demand to remain in contact with hydrogen bonding by the virtue of hydroxyl group of clay (end-to-end coupling). Moreover, it is quite interesting to discuss the very high value of E′ at the low strain region. These findings can be only explained if a large amount of delaminated silicate particles are coming out from the nanoclay stacks by exfoliation process. Here, it can be observed that with the increase of the EPDM content the filler–filler networking decreases which can be attributed to relatively smaller space availability (CR phase) for the clay particles at a fixed volume and, consequently, the clay particles are forced to remain in nonintercalated–exfoliated form. TEM in

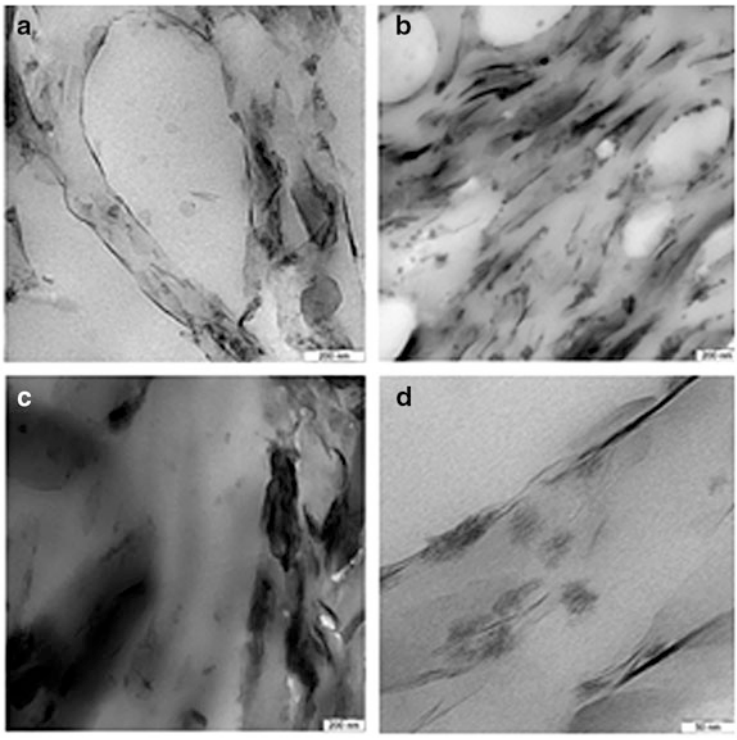

Fig. 26 Transmission electron micrographs of the blends of: (**a**) 25 EPDM: 75 CR, (**b**) 50 EPDM: 50 CR, (**c**) 75 EPDM: 25 CR and (**d**) 25 EPDM: 75 CR filled with 10 phr nanoclay [106]

Fig. 26c also delivers the same explanation behind these facts. It is observed from this TEM image of 75/25 blend of EPDM/CR that clay particles are remaining in the agglomerated form and this finding directly corroborates the above discussions. Nevertheless, the single exfoliated particles can be seen from the Fig. 26d where several single clay platelets are embedded in the 25/75 blend of EPDM/CR matrix. But, in the stress–strain experiment at the low strain regime all blends are exhibiting same nature (Fig. 27b). From this stress–strain experiment it was found that the Young's modulus increases from 1.93 MPa to 27.24 MPa with the addition of 10 phr clay along with 10 phr stearic acid. The tensile properties are also observed to be improved imminently in all three blends by incorporation of 10 phr organoclay [106].

Dynamic mechanical analysis (DMA) has been done to understand the dynamic response of the blend after the addition of clay. The dependency of storage modulus obtained from oscillatory tension deformation as a function of temperature is given in Fig. 28. All samples show a steep decrease of E' value at the temperature range between $T = \sim 50$ and $\sim 20\ ^{\circ}C$ followed by a rubbery plateau (Fig. 28a). The most exciting information, observed in this figure, is the increase of modulus values at room temperature by the addition of the clay. The storage modulus increases from

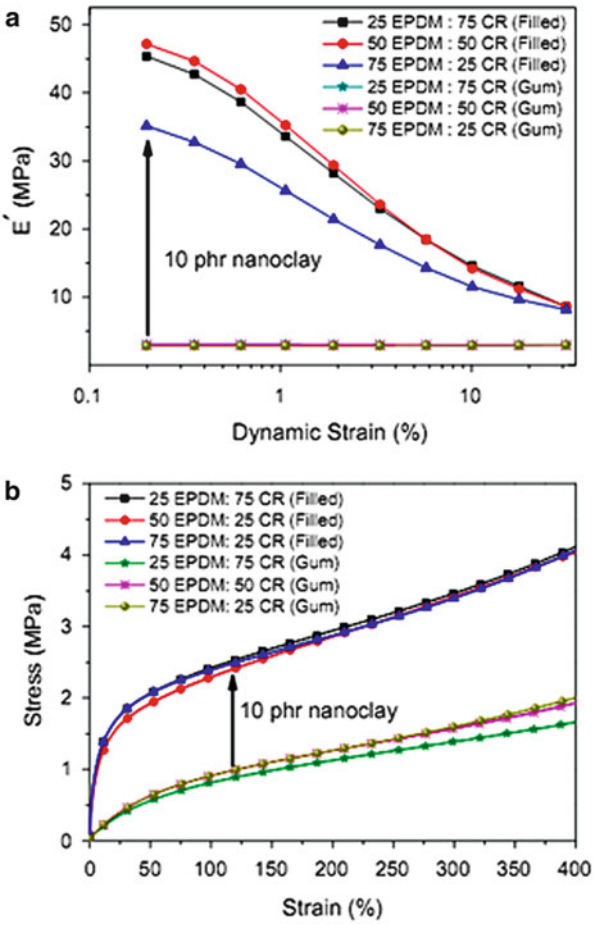

Fig. 27 (**a**) Effect of dynamic strain amplitude on storage modulus, (**b**) stress–strain behaviour of CR/EPDM blend in absence and in presence of nanoclay. For strain sweep experiment, tension mode was selected for the variation of the dynamic strain from 0.01 % to 40 % at 10 Hz frequency [106]

2 MPa to 54 MPa with the addition of only 10 phr clay in the EPDM/CR matrix at a ratio of 25/75. A good state of exfoliation of the clay in the CR matrix reinforced the rubber blend very strongly. A sufficiently strong filler–filler interactions as well as the compatibility between CR and EPDM are playing a major role to give rise to a very highly reinforced rubber matrix.

The glass transition temperature (Tg) of a rubber or polymer depends on the structure and co-operative mobility of the chain segments. In the case of partially compatible blends, the Tgs of the blend components are expected to be shifted towards each other as compared with the pure components. The Tgs remain largely unaltered for a completely incompatible blend. Figure 28b shows the tan δ dependencies on the temperature for the CR/EPDM blend systems. The two pure vulcanized rubbers show a Tg at ~37 and ~24 °C, and even after incorporation of the clay the values remain unaltered [106].

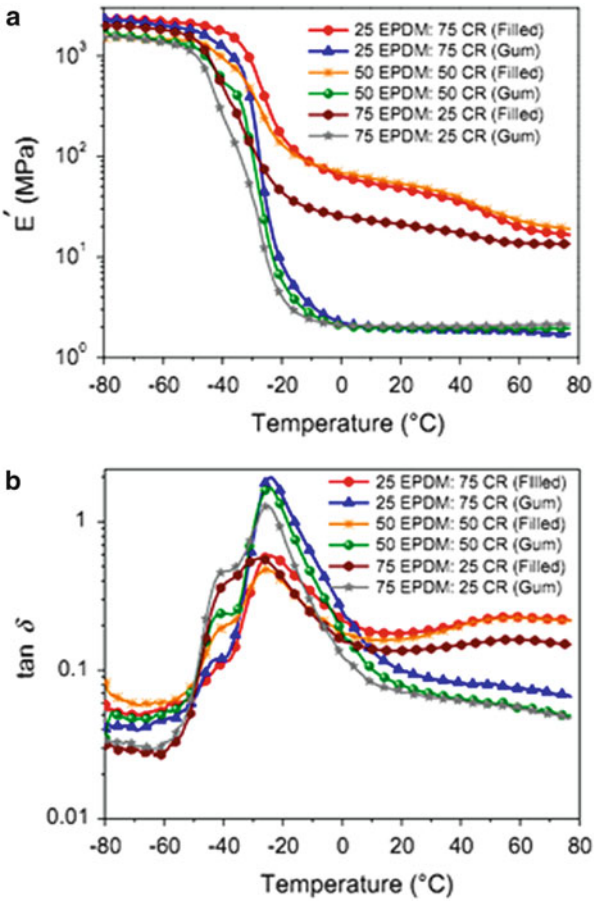

Fig. 28 (**a**) storage modulus (E′) versus temperature and (**b**) tan δ versus temperature plots of CR/EPDM blends in absence and in presence of nanoclay [106]

Stephen et al., studied the viscoelastic properties of nano structured layered silicates reinforced NR, XSBR and their blends [107]. The dynamic mechanical properties of nanocomposites were analyzed as a function of the concentration of filler. It was observed that upon the addition of nano filler the storage modulus increased due to the enhanced contact surface area between polymer and filler. However, at higher concentration the modulus was found to be decreased owing to the agglomeration of filler. As the concentration of nano filler increased the loss modulus also increased. This was explained in terms of the friction between the filler particles and the matrix molecules when the filler particles are uniformly dispersed in the rubber matrix. The damping values were decreased with the amount of filler due to the restricted mobility of the polymer chain segments owing to the intercalation of polymer chain into the layers of silicates. The distribution of fillers in the two phases of 70/30 NR/XSBR blend system was evaluated from the damping values and was observed that the filler migrated

preferentially towards the XSBR phase than NR due to the polarity of XSBR latex [107].

Das et al., used QUAT compound (di-steryldimethyl ammonium) to modify the clay. It is also interesting to look into the chemical interactions of organoclay (QUATmodified MMT) with functionally polar rubbers like XNBR, CR, and their mutual blend. The role of layered silicate on the curing process of CR/XNBR blends was investigated through the study of curing kinetics, mechanical properties, WAXS, and DMA [108].

Figure 29 shows the tan δ dependencies on temperature for the pure CR and XNBR, crosslinked with sulfur and containing 10 phr organoclay. The results are compared with the corresponding gum rubber matrix without any filler. Gum as well as filled CR rubber matrices show a Tg at −25 °C, whereas XNBR shows the transition at −1 °C. In both cases, the incorporation of 10 phr organoclay

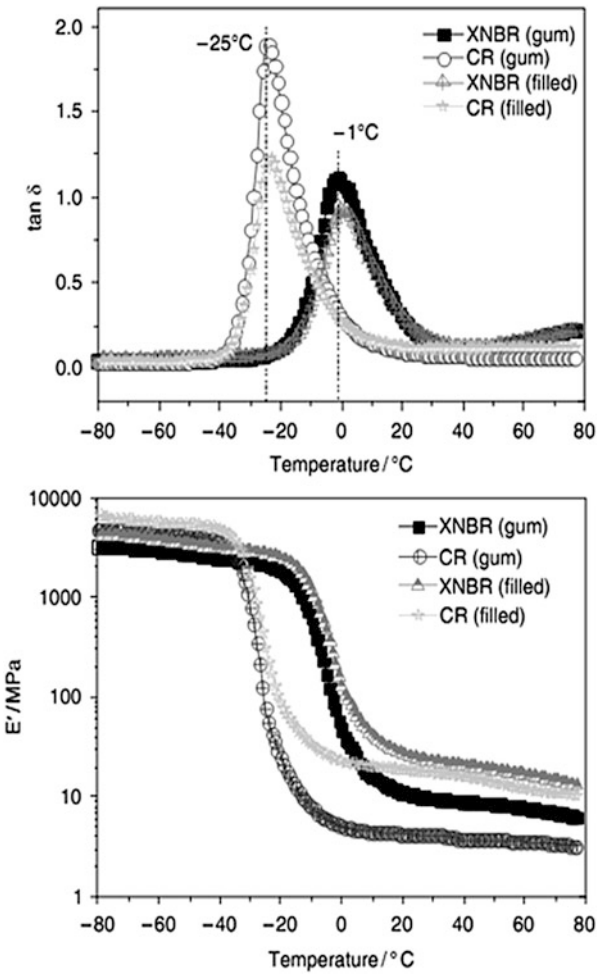

Fig. 29 DMTA plots of tan δ versus temperature (*top*) and storage modulus versus temperature (*bottom*) for XNBR and CR compounds vulcanized by sulfur [109]

remarkably reduces the peak heights, which indicates strong reinforcement by the organoclay. The presence of intercalated organoclays restricts the mobility of the rubber chains due to their confinement between the layers. More precisely, it can be stated that the polar nature of CR and XNBR intercalates or exfoliates the silicate layers very efficiently and a strong rubber–filler interaction is established. The plots of storage modulus with temperature also indicate a strong reinforcement offered by the organoclay, since a considerable increase in storage modulus of moderate temperatures is observed (Fig. 29). It is clear that two widely separated different Tg values primarily indicate the immiscibility of the phase if a blend is prepared with those rubbers. The damping behavior (tan δ) of the blends with increasing temperature delivers some interesting information about the miscibility of the rubber with two different Tg values. The increase of XNBR content the Tg values of CR and XNBR shift to a lower temperature in all composites. This decrease in Tg of the polymers may be explained if one considers the difference in the thermal expansion coefficient of the respective polymers in a blend, resulting in thermal stress across the boundary and development of a negative pressure within the rubber domains. Thus, the free volume of the rubber component increases and, consequently, the motion of the rubber chain becomes easier [109]. It is observed that the separation factor between the two Tg peaks is increased in all blends containing layered silicate, and that the difference between those Tg is maximum for the 50/50 rubber blend. For the clay-containing 50/50 blend, the separation is 26 K, whereas the separation is 20 K for the same blend without organoclay. So, presence of 10 phr organoclay makes the blends more heterogeneous as compared to their virgin composition. This finding also supports the inhibition action of layered silicate to self-crosslinking by blocking the carboxylic group from forming hydrogen bonds with the silanol group of the clay layers, rendering the carboxylic group passive to crosslinking.

As far as the storage modulus of the self-crosslinked blends is concerned, a relaxation at 40 °C is observed in all the blends (Fig. 30). This relaxation arises due to melting of crystalline domains of the CR chains, and the effect is more prominent in blends of higher CR content without any filler. In the presence of organoclay, crystalline nature of the CR phase is reduced. It will be also interesting to discuss the damping behavior of those composites that are crosslinked by sulfur curatives.

Figure 30 shows tan δ versus temperature curves obtained from sulfur-crosslinked CR/XNBR blends in the presence and absence of organoclay. All the curves possess two distinct relaxation peaks at different temperatures.

It can be observed that with the increase of CR content in the blends, the Tg values corresponding to XNBR are shifted to a higher temperature to a remarkable extent; the Tg of XNBR in the 25 XNBR/75 CR blend is shifted from −1 to 17 °C as compared with pure XNBR.

However, the shifting of Tg of the corresponding CR portion is only a few degrees. This may be explained by considering the polarity difference between XNBR and CR. Migration of curatives can take place from the less polar CR part to the more polar XNBR part and, ultimately, the XNBR phase becomes highly crosslinked. Thus, the mobility of the XNBR chains is greatly reduced and the Tg

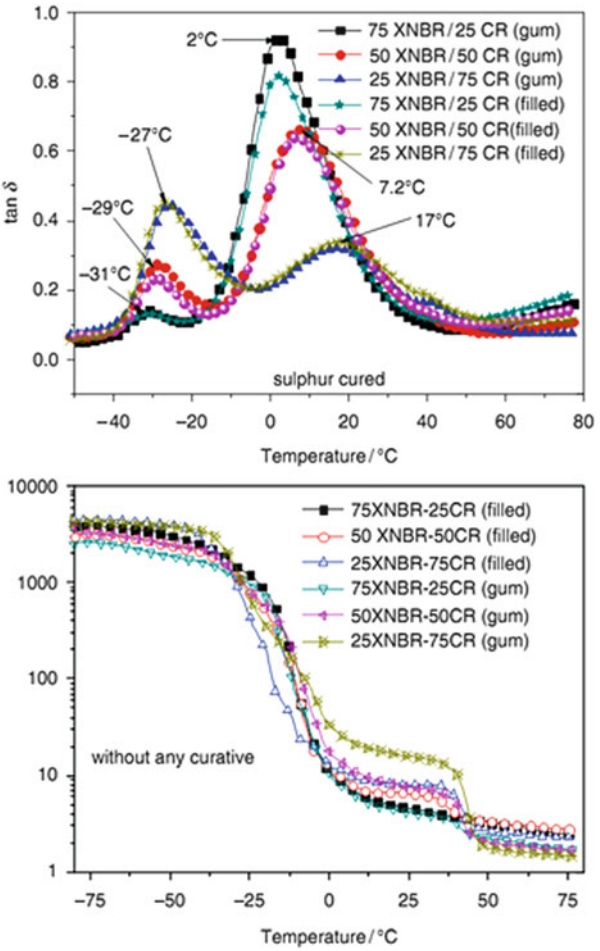

Fig. 30 Tan δ versus temperature plots of CR-XNBR blends vulcanized by sulfur (*top*). Storage modulus versus temperature plots of self-crosslinked CR-XNBR blends (*bottom*) [109]

increases to a considerable extent. Any significant change in the damping behavior is not noticed after incorporation of the organoclay in the rubber blends. It is also evident from Fig. 30 that storage modulus decreases with increasing temperature and that all the blends show a three-step relaxation process. The first two steps arise from the glass transition of the CR and XNBR phase and the third relaxation at 40 °C is supposed to come from the microcrystalline phase of CR chain segments. At this temperature, the crystal structures disappear and an extra slippage within the crystal domain of the rubber chain takes place. The same behavior of storage modulus against temperature can be observed from the sulfur-cured CR/XNBR blends. Figure 31 shows the temperature dependency of the storage modulus of those sulfur-cured samples. From this figure the clear crystalline nature of CR at the blend composition 75 CR/25 XNBR can also be observed. Morphological heterogeneity makes the CR phase more crystalline with the higher content of CR, in spite

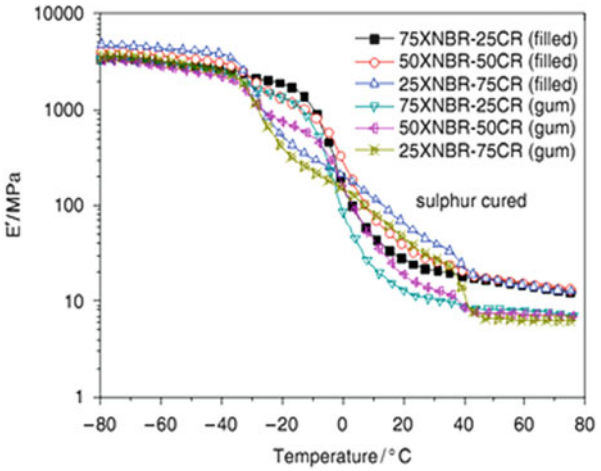

Fig. 31 Storage modulus versus temperature plots of CR-XNBR blends vulcanized by sulfur [109]

of a strong sulfur crosslinking network in the blend matrix. However, above 40 °C the storage modulus of filled blends show a higher E0 value as compared to the corresponding gum blends, demonstrating the apparent reinforcing ability of organoclay in all blends irrespective of their composition.

Gu et al. prepared Octadecyl ammonium montmorillonite/natural rubber/*cis*-1,4-polybutadiene (OMMT/NR/BR) nanocomposites by direct mechanical blending. Two tan δ peaks corresponded to the small glass transition peak of BR at lower and that of NR at higher temperature (Fig. 32). Both of the NR and BR phase of OMMT/NR/BR (4 mass %) showed lower tan δ peak values than the NR/BR hybrids and tan δ of NR phase shifted to higher temperature. These observations can be related to the decreased mobility of the rubber molecules due to the strong interaction between the rubber matrix and OMMT [111–113]. The tan δ value of OMMT/NR/BR (4 mass %) at 0 °C was slightly lower than that of the pure NR/BR, which indicated that the nanocomposite had better wet skid resistance properties [110].

Rajasekar et al. utilized the compatibilizer like epoxidized natural rubber (ENR) safely in exfoliating the nanoclay in the matrix polymer. Epoxidized natural rubber and organically modified nanoclay composites (EC) were prepared by solution mixing. The nanoclay employed in this study was Cloisite 20A. The obtained nanocomposites were incorporated in nitrile butadiene rubber (NBR) with sulphur as a curing agent. The morphological study showed the intercalation of nanoclay in ENR and further incorporation of EC in NBR matrix leads to exfoliation of nanoclay. DMTA results showed drastic improvement in storage modulus and decrease in tan δ value consequently upon increasing EC loading in NBR matrix, this corresponds to the higher reinforcing efficiency of the nanofiller in the matrix [114].

Malas et al. developed expanded graphite (EG) and isocyanate modified graphite nanoplatelets (i-MG) filled SBR/BR blends, which can substitute NR in high performance application. This work also investigated the effect of i-MG on the

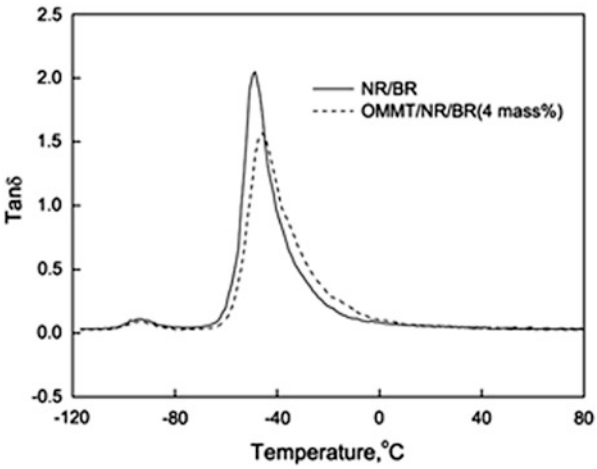

Fig. 32 Tan δ of NR/BR and OMMT/NR/BR (4 mass %) composites [110]

physical, mechanical and thermo-mechanical properties of BR, SBR and SBR/BR blends in the presence of carbon black (CB). Graphite sheets were modified to enhance its dispersion in the rubber matrices, which resulting in an improvement in the overall physical and mechanical properties of the rubber vulcanizates. Compounds based on 50:50 of BR and SBR with ~3 wt% nanofillers with CB were fabricated by melt mixing. The intercalated and delaminated structures of the nanofiller loaded rubber blends were observed. DMTA of the filled rubber compounds shows an increase in the storage modulus compared to the controls. i-MG containing rubber compounds in the presence of CB showed an increase in the mechanical, dynamic mechanical, hardness, abrasion resistance and thermal properties compared to the alone CB filled rubber vulcanizates [115].

The effects of EG and i-MG on the dynamic mechanical properties of BR, SBR and SBR/BR blends were investigated by dynamic mechanical thermal analysis. The temperature dependent E and tan δ of the rubber composites are represented in the Fig. 33a–d. Both the elastic and viscous behaviors of the composite materials affect the resulting strain in the samples due to the application of an oscillating force. The storage modulus can be regarded as the elastic modulus of the rubber composites and loss tangent is interconnected to the energy drenched due to energy dissipation as heat. It can be seen from the Fig. 33a, b that EG and i-MG loaded SBR/BR composites in the presence of CB showed a drastic increase in the storage modulus in a wide range of temperature compared to the BR based nanocomposites. But, in comparison with SBR based nanocomposites, SBR/BR based composites showed an increase in the storage modulus only at very low temperature region and then decrease in the storage modulus from low temperature to a high temperature region, which was due to very low transition temperature of BR. Homogeneous mixing of SBR with BR and as well as good dispersion of nanofillers in the rubber blend increases its stiffness, which resulting in an increase in the storage modulus of the SBR/BR based nanocomposites. Figure 33c, d displayed the temperature

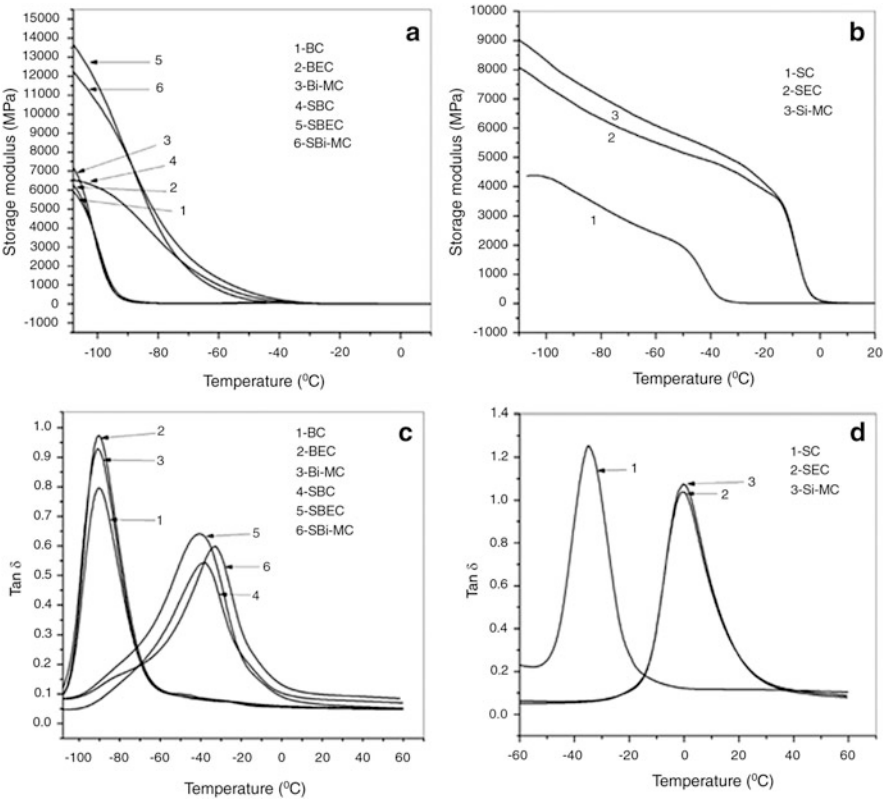

Fig. 33 (**a** and **b**) Storage modulus vs. temperature curves of the rubber composites and (**c** and **d**) tan δ vs temperature curves of the rubber composites (BC = butyl rubber +40 phr carbon black, BEC = butyl rubber +3 phr EG +30 phr carbon black, Bi-MC = butyl rubber +3 phr isocyanate modified EG +30 phr carbon black, SBC = 50:50 butyl rubber-SBR blend and 40 phr black, SBEC = 50:50 butyl rubber-SBR blend + 3 phr EG + 30 phr black, SBi-MC = 50:50 butyl rubber-SBR blend + 3 phr isocyanate modified EG + 30 phr black, SC = SBR + 40 phr black, SEC = SBR + 3 phr EG + 30 phr black and Si-MC = SBR + 3 phr isocyanate modified EG + 30 phr black) [115]

dependent tand curves of the various rubber composites. Conventionally, the greater tan δ value of the rubber composites in the region of −20 to 10 °C can be accounted to figure out the superior anti-skid properties of the rubber composites under wet conditions and lower tan δ value of the rubber materials in the range of 50–60 °C indicates the low rolling resistance of the rubber stuffs. We can see from the respective figures that the tand values of the EG and i-MG filled SBR/BR based composites in the region of −20 to 10 °C were higher than tand values of the only BR based nanocomposites. So, after the homogeneous mixing of SBR with BR in the presence of different nanofillers, the anti-skid property under wet conditions of the BR vulcanizates was significantly improved. At the same time, rolling resistance of the SBR/BR based nanocomposites was lowered (lower tan δ values of the

SBR/BR based composites in the temperature range of 50–60 °C) compared to the rolling resistance of SBR vulcanizates. EG/i-MG containing rubber composites in the presence of CB showed superior storage modulus, antiskid properties and lower rolling resistance compared to the only CB loaded rubber composites, which was due to the better interactions and interfacial adhesion between i-MG sheets and the rubber matrices [115].

5 Conclusions

The properties of rubber-rubber blend composites depend on the size and shape and concentration of nano particles and their interactions with the individual rubber matrix. The interaction between the filler and the matrix are improved by surface modification. In the rubber industry the uniform distribution of nano particles is considered to be important as it affects the mechanical properties and performance of the composite. For rubber-rubber blend composites fillers like carbon black prefer to migrate to less polar, less viscous rubber phase whereas silica and clay particles migrate to more polar rubber phase. CNTs mainly reside in the highly polar and non-polar rubbers but not in weakly polar ones. The Tg remain unaltered for a completely incompatible blend. In the case of partially compatible blends, the Tgs of the blend components are expected to shift towards each other as compared with the pure components. Shifting of Tg of polymers to lower or higher values in a blend depends on the polarity difference and the difference in the thermal expansion coefficient of the respective polymers in the blend.

The storage modulus of unfilled rubbers, E′, depends on frequency and temperature and is independent of the deformation amplitude. In contrast, E′ for the filled rubber shows a significant dependency on the dynamic deformation, here the value considerably decreases with an increasing strain amplitude. This non-linear behaviour of filled rubbers is known as Payne effect and has been explained by the existence of a filler network in the rubber matrix above the percolation threshold. With increasing strain amplitude the filler network gets broken and results in lowering of the E′ value. The amount and morphology of the fillers play a major role in the Payne effect. The Payne effect is assumed to arise from the elementary mechanism consisting of adsorption-desorption of macromolecular chains from the filler surface. It is found that due to the small particle size and high specific surface area, nanofiller forms stronger and more developed filler-filler network and the breakdown of these networks results in larger Payne effect. At low loading, there is not much variation in storage modulus, loss modulus and loss tangent compared to gum vulcanizates. But at higher loading, pronounced effect has been observed for the rubber nanocomposites. There is a gradual increase in E′ of rubber blends with increase in filler content in all temperature regions. In the rubbery region the polymer–filler, filler–filler and filler aggregate interactions have a pronounced effect on storage modulus. With an increase in temperature E′ of rubber blend

nanocomposites decreased which is associated with the glass transition phenomenon of the elastomer chains.

The addition of filler results in a reduction in tan δ_{max}, which is attributed to the dilution effect, that is, the viscous response of the elastomeric phase is diluted by the nonviscous response of fillers. Incorporation of nanoparticles like CNTs are reported to reduce the height of the tan δ peak considerably and even a small amount of CNTs increase the storage modulus above the glass transition temperature. MWCNT-rubber blend composite prepared in the machine direction showed high storage modulus and low tan δ_{max} because of the greater alignment and dispersion of most MWCNTs in the sample.

In the case of rubber blend clay composites good state of exfoliation of the clay, sufficiently strong filler–rubber interactions as well as the compatibility between different rubber phases are playing major role. The presence of intercalated organoclays restricts the mobility of the rubber chains due to their confinement between the layers. As the concentration of nano filler increases the loss modulus increased. This can be explained in terms of the friction between the filler particles and the rubber matrix when the filler particles are uniformly dispersed in the rubber matrix. The damping values are found to decrease with the amount of filler due to the restricted mobility of the polymer chains owing to the intercalation of polymer chains into the layers of silicates.

References

1. Medalia A, Krauss G (1994) Reinforcement of elastomers by particulate fillers. In: Mark JE, Erman B, Erich FR (eds) Science and technology of rubber, 2nd edn. Academic, San Diego, CA, pp 387–418
2. Sternstein SS, Zhu AJ (2002) Macromolecules 35:7262
3. Lin G, Tian M, Lu YL, Zhang XJ, Zhang LQ (2006) Polymer 38:498–502
4. Yahaya LE, Adebowale KO, Menon ARR, Rugmini S, Olu-Owolabi BI, Chameswary J (2010) Afr J Pure Appl Chem 4:198–205
5. Sui G, Zhong WH, Yang XP, Yu YH (2008) Mater Sci Eng 485:524–531
6. Gonzalez JC, Retsos H, Verdejo R, Toki S, Hsiao BS, Giannelis EP, Lopez-Manchado MA (2008) Macromolecules 41:6763–6772
7. Al-Hartomy OA, Al-Ghamdi AA, Al-Salamy F, Dishovsky N, Shtarkova R, Iliev V, El-Tantawy FI (2012) J Mater Chem 2:116–122
8. Kim H, Miura Y, Macosko CW (2010) Chem Mater 22:3441–3450
9. Coran AY (1980) Rubber Chem Technol 53:141
10. Kim HJ, Hamed GR (2000) Rubber Chem Technol 73:743–752
11. Botros SH, Younan AF, Essa MM (2000) Mol Cryst Liq Cryst Sci Technol A 354:409–420
12. Saad Azima LG, El-Sabbagh S, Salwa S (2001) J Appl Polym Sci 79:60–71
13. Perera MCS, Ishiaku US, Ishak ZAM (2000) Polym Degrad Stab 68:393–402
14. Lapa VLC, Visconte LLY, Affonso JES, Nunes RCR (2002) Polym Test 21:443–447
15. Sircar AK, Lamond TG, Pinter PE (1974) Rubber Chem Technol 47:48
16. Massie JM, Hirst RC, Halasa AF (1993) Rubber Chem Technol 66:276
17. Kluppel M, Schuster RH, Schaper (1999) J Rubber Chem Technol 72:91
18. Hess HM, Scott CE, Callan JE (1967) Rubber Chem Technol 40:814
19. Jeon IH, Kim H, Kim SG (2004) Rubber Chem Technol 76:1

20. Maiti S, De SK, Bhowmick AK (1992) Rubber Chem Technol 65:293
21. Kumar AP, Depan D, Singh Tomer N, Singh RP (2009) Prog Polym Sci 34:479–515
22. Li Y, Yu J, Guo ZX (2002) J Appl Polym Sci 84:827–834
23. Dubois C, Rajabian M, Rodrigue D (2006) Polym Eng Sci 46:360–371
24. Yan S, Yin J, Yang Y, Dai Z, Ma J, Chen X (2007) Polymer 48:1688–1694
25. Shu CH, Chiang HC, Tsiang RCC, Liu TJ, Wu JJ (2007) J Appl Polym Sci 103:3985–3993
26. Garrett TM, Gruzins I (1996) Modified polyurethane including silica and method of manufacture thereof. US Patent 5,484,832
27. Chen S, Sui J, Chen L (2004) Colloid Polym Sci 283:66–73
28. Yoichi I, Takashi N, Shigeyoshi M (2006) J Dispers Sci Technol 27:1093
29. Ukaji E, Furusawa TM, Suzuki N (2007) Appl Surf Sci 254:563–569
30. Sabzi M, Mirabedini SM, Zohuriaan-Mehr J, Atai M (2009) Prog Org Coat 65:222–228
31. Wang C, Mao H, Wang C, Fu S (2011) Ind Eng Chem Res 50:11930–11934
32. Zhao J, Milanova M, Warmoeskerken MMCG, Dutschk V (2012) Colloids Surf A 413:273–279
33. Sato K, Kondo S, Tsukada M, Ishigaki T, Kamiya H (2007) J Am Ceram Soc 90:3401–3406
34. Moniruzzaman M, Winey KI (2006) Macromolecules 39:5194
35. Hutchison JL, Kiselev NA, Krinichnaya EP, Krestinin AV, Loufty RO, Morawsky AP et al (2001) Carbon 39:761
36. Zhang Y, Iijima S (1999) Appl Phys Lett 75:3087
37. Endo M, Hayashi T, Kim YA, Muramatsu H (2006) Jpn J Appl Phys 45:4883
38. Bose S, Khare RA, Moldenaers P (2010) Polymer 51:975
39. Rastogi R, Kaushal R, Tripathi S, Sharma AL, Kaur I, Bharadwaj LM (2008) J Colloid Interface Sci 328:421
40. Vaisman L, Wagner HD, Marom G (2006) Adv Colloid Interface Sci 12:37
41. Ciofani G, Raffa V, Pensabene V, Menciassi A, Dario P (2009) Fullerenes Nanotubes Carbon Nanostruct 17:11
42. Matarredona O, Rhoads H, Li Z, Harwell JH, Balzano L, Resasco DE (2003) J Phys Chem B 107:13357–13367
43. Wang Q, Han Y, Wang Y, Qin Y, Guo Z (2008) J Phys Chem B 112:7227
44. Jung R, Kim HS, Jin HJ (2007) Macromol Symp 249:259
45. Islam MF, Rojas E, Bergey DM et al (2003) Nano Lett 3:269
46. Yu J, Grossiord N, Koning CE, Loos J (2007) Carbon 45:618
47. Jeffrey LB, James MT (2002) J Mater Chem 12:1952–1958
48. Choi SUS, Zhang ZG, Yu W, Lockwood FE, Grulke EA (2001) Appl Phys Lett 79:2252
49. Biercuk MJ, Llaguno MC, Radosavljevic M, Hyun JK, Johnson AT, Fischer JE (2002) Appl Phys Lett 80:2767
50. Buxton GA, Balazs AC (2004) Mol Simul 30:249
51. Gojny FH, Wichmann MHG, Fiedler B, Kinloch IA, Bauhofer W, Windle AH, Schulte K (2006) Polymer 47:2036
52. Kirkman JH (1977) Clay Miner 12:199
53. Kamble R, Ghag M, Gaikawad S, Panda BK (2012) J Adv Sci Res 3(2):25–29
54. Thomas S, Stephen R (eds) (1985) Rubber nanocomposites. preparation, properties and application. Wiley, New York, p 209
55. Fukushima Y, Tani M (1996) Bull Chem Soc Jpn 69:3667
56. Giannelis EP, Krishnamoorti R, Manias E (1999) Adv Polym Sci 138:107
57. Alexandre M, Dubois P (2000) Mater Sci Eng 28:1
58. Ray SS, Okamoto M (2003) Progr Polym Sci 28:1539
59. Zümreoglu KB, Ahmet NAV (2012) Chem Pap 66:1–10
60. Kuilla T, Bhadra S, Yao D, Kim NH, Bosed S, Lee JH (2010) Prog Polym Sci 35:1350
61. Li D, Muller MB, Gilje S, Kaner RB, Wallac GG (2007) Nat Nanotechnol 3:101
62. Aizawa T, Souda R, Otani S, Ishizawa Y, Oshima C (1990) Phys Rev Lett 64:768

63. Novoselov KS, Geim AK, Morozov SV, Jiang D, Zhang Y, Dubonos SV, Grigorieva IV, Firsov AA (2004) Science 306:666
64. Stankovich SD, Piner DA, Kohlhaas RD, Kleinhammes KAA et al (2007) Carbon 45:1558
65. Rao CNR, Sood AK, Voggu R, Subrahmanyam KS (2010) J Phys Chem Lett 1:572
66. Wolff S, Donnet JB (1990) Rubber Chem Technol 63:32
67. Brennan JJ, Jermyn TE, Bonnstra BB (1964) J Appl Polym Sci 8:2687
68. Payne AR (1965) Reinforcement of elastomers. Wiley, New York
69. Payne AR, Whittaker RE (1971) Rubber Chem Technol 44:440
70. Medalia AI (1978) Rubber Chem Technol 51:437
71. Fletcher WP, Gent AN (1953) Trans IRI 29:166
72. Payne AR (1962) J Appl Polym Sci 6:57
73. Payne AR (1964) J Appl Polym Sci 8:1661
74. Heinrich G, Klüppel M (2002) Adv Polym Sci 160:1–44
75. Diani J, Fayolle B, Gilormini P (2009) Eur Polym J 45:601
76. Kalfus J, Jancar J (2007) J Polym Sci B Polym Phys 45:1380
77. Cassagnau P (2008) Polymer 49:2183
78. Zhu A, Sternstein SS (2003) Compos Sci Technol 63:1113
79. Mullins L (1969) Rubber Chem Technol 42:339
80. Maier PG, Goritz D (1996) Kautsch Gummi Kunstst 49:18
81. Maier PG, Goritz D (1993) Kautsch Gummi Kunstst 46:11
82. Maier PG, Goritz D (2000) Kautsch Gummi Kunstst 53:12
83. Yatsuyanagi F, Kaidou H, Ito M (1999) Rubber Chem Technol 4:657
84. Cassagnau P (2003) Polymer 44:2455
85. Berriot J, Lequeux F, Montes H, Monnerie L, Long D, Sotta P (2002) J Non-Cryst Solids 307:719
86. Berriot J, Montes H, Lequeux F, Long D, Sotta P (2002) Macromolecules 35:9756
87. Berriot J, Montes H, Lequeux F, Long D, Sotta P (2003) Europhys Lett 64:50
88. Jouault N, Vallat P, Dalmas F, Said S, Jestin J, Boue F (2009) Macromolecules 42:2031
89. Merabia S, Sotta P, Long DR (2008) Macromolecules 41:8252
90. Farahani TD, Bakhshandeh GR, Abtahi M (2006) Polym Bull 56:495–505
91. Donnet JB, Bansal RC, Wang MJ (1993) Carbon black science and technology. Marcel Dekker, New York
92. Vilgis TA (2005) Polymer 46:4223–4229
93. Kohjiya S, Katoh A, Suda T, Shimanuki J, Ikeda Y (2006) Polymer 47:3298–3301
94. Wootthikanokkhan J, Rattanathamwat N (2006) J Appl Polym Sci 102:248–256
95. Sirisinha C, Prayoonchatphan N (2001) J Appl Polym Sci 81:3198–3203
96. Kader MA, Bhowmick AK (2003) J Appl Polym Sci 89:1442–1452
97. Saowaroj C, Wasuthep L (2011) J Elastomers Plast 43:407
98. Das A, Stockelhuber KW, Jurk R, Saphiannikova M, Fritzsche J, Kluppel M, Heinrich G, Lorenz H (2008) Polymer 49:5276–5283
99. Payne AR (1965) In: Kraus G (ed) Reinforcement of elastomers, Chap 3. Inter-science, New York
100. Anyaporn B, Saowaroj C (2012) J Met Mater Miner 22:77–85
101. Pattana K, Pongdhorn S, Chakrit S, Karl IJ, Nittaya R (2013) Polym Test 32:1229–1236
102. Le HH, Sriharish MN, Henning S, Klehm J, Menzel M, Frank W, Wießner S, Stöckelhuber KW, Heinrich G, Radusch HJ, Das A (2014) Compos Sci Technol 90:180–186
103. Yan N, Xia HS, Zhan YH, Fei GX, Chen C (2012) Plast Rubber Compos 4:365
104. Roberts GE (1973) In: Haward RN (ed) The physics of glassy polymers. New York, Wiley
105. Perera MC (2001) Eur Polym J 37:167
106. Das A, Mahaling RN, Stöckelhuber KW, Heinrich G (2011) Compos Sci Technol 71:276–281
107. Ranimol S, Raju KVSN, Siby V, Kuruvilla J, Zachariah O, Sabu T (2007) Rubber Chem Technol 80:672–689

108. Das A, Stockelhuber KW, Heinrich G (2009) Macromol Chem Phys 210:189–199
109. Tomova D, Kressler J, Radusch HJ (2000) Polymer 41:7773
110. Zheng G, Li G, Guojun S, Weisheng L, Peiyao L, Chunpeng S (2010) Appl Clay Sci 50:143–147
111. Gatos KG, Karger KJ (2005) Polymer 46:3069–3076
112. Ahmadi SJ, Huang YD, Li W (2005) Compos Sci Technol 65:1069–1076
113. Tian M, Cheng LJ, Liang WL (2006) J Appl Polym Sci 101:2725–2731
114. Rajasekar R, Pal K, Heinrich G, Das A, Das CK (2009) Mater Des 30:3839–3845
115. Malas A, Pal P, Das CK, Malas A et al (2014) Mater Des 55:664–673

Effect of Hybrid Fillers on the Non-Linear Viscoelasticity of Rubber Composites and Nanocomposites

Suryakanta Nayak and Tapan Kumar Chaki

Abstract The present chapter focuses on the effect of hybrid fillers on the non-linear viscoelastic behaviour of rubber composites and nanocomposites. The viscoelastic behaviour of rubber composites include different properties like cure behavior, rheology, creep, and dynamic mechanical analysis etc. The properties measured under dynamic mechanical analysis are storage and loss moduli and tan δ. The variation of storage and loss moduli of rubber composites filled with different types of filler are discussed in detail. The non-linear viscoelastic behaviour (Payne effect) of rubber composites containing single filler are also discussed. The effect of various hybrid fillers on rubber composites are also discussed in detail and found composites containing hybrid fillers give better mechanical and viscoelastic properties than composites containing single filler. Composites containing hybrid fillers carry the properties of individual fillers. So composites of hybrid fillers are getting importance because they offer a range of properties that cannot be achieved with a single filler. Rubber composites containing hybrid fillers are promising class of materials with emerging applications in different fields like materials science, nanotechnology, and nanobiotechnology etc.

Keywords Hybrid filler • Viscoelastic property • Non-linear • Nanocomposites • Rubber

1 Introduction

Nanocomposites are the composites where at least one of the phases shows dimensions in the nanometer range. These composites are high performance materials which exhibit unusual property combinations and unique designs and are thought of as the materials of the twenty-first century [1]. It has been reported in the earlier literatures that at the nanoscale (below about 100 nm), a material's/composite's property can change dramatically. The reduction in size of the material without

S. Nayak • T.K. Chaki (✉)
Rubber Technology Centre, Indian Institute of Technology, Kharagpur, WB 721302, India
e-mail: tapan@rtc.iitkgp.ernet.in

D. Ponnamma, S. Thomas (eds.), *Non-Linear Viscoelasticity of Rubber Composites and Nanocomposites*, Advances in Polymer Science 264, DOI 10.1007/978-3-319-08702-3_6

changing the material's composition, it can exhibit new properties such as electrical conductivity, insulating behavior, elasticity, greater strength, different color, and greater reactivity characteristics that the very same substances do not exhibit at the micro- or macroscale. Polymer-based nanocomposites have attracted great attention of many researchers for their novel properties [2–5]. These nanocomposites are promising class of hybrid nanostructured materials with emerging applications ranging from packaging to bio-medical [1, 6–8]. Polymer nanocomposites are fabricated by dispersing inorganic/organic fillers, with at least one dimension in the nanometer scale, in both inorganic/organic polymers [9, 10].

Polymer/rubber nanocomposites exhibit enhanced mechanical, thermal stability, toughness, stiffness, and gas-barrier properties compared to those of conventional composites at same filler volume fraction [11–15]. The interaction between the filler and polymer matrix of nanocomposites at the nanometer scale enables the formation of molecular bridges in the polymer matrix. This is the basis for the enhanced mechanical properties of nanocomposite as compared to conventional microcomposites [16, 17]. Nanocomposites containing hybrid fillers add a new dimension to the above enhanced properties. These composites show more advantages to composites containing single filler as the property of the hybrid filler composite depends upon the combined effect of individual filler. The nonlinear viscoelastic behavior of nanocomposites can be influenced differently by hybrid fillers than single filler.

Viscoelasticity is the property of materials that exhibit both viscous and elastic characteristics when undergoing deformation (http://en.wikipedia.org/wiki/Viscoelasticity). Linear viscoelastic behavior is exhibited by a material when it is subjected to a very small or very slow deformation. So when a viscoelastic material is subjected to a deformation that is neither very small nor very slow, its behavior in no longer linear, and there is no universal rheological constitutive equation that can predict the response of the material to such a deformation [18]. Nonlinear viscoelastic behavior is more important than linear properties of rubber/polymer nanocomposites as the industrial processing of viscoelastic materials (rubbers/polymers) always involves large and rapid deformations in which the behavior is nonlinear.

Linear viscoelasticity is when the function is separable in both creep response and load. All linear viscoelastic models can be represented by a Volterra equation connecting stress and strain (http://en.wikipedia.org/wiki/Viscoelasticity):

$$\varepsilon(t) = \frac{\sigma(t)}{E_{\text{inst, creep}}} + \int_0^t K\left(t\text{-}t'\right)\sigma\left(t'\right)dt' \tag{1a}$$

or

$$\sigma(t) = E_{\text{inst, relax}}\varepsilon(t) + \int_0^t F\left(t\text{-}t'\right)\varepsilon\left(t'\right)dt' \tag{1b}$$

where, t is time, σ(t) is stress, ε(t) is strain, $E_{\text{inst, creep}}$ and $E_{\text{inst, relax}}$ are instantaneous elastic moduli for creep and relaxation, K(t) is the creep function, and F(t) is the relaxation function.

Linear viscoelasticity is usually applicable only for small deformations. Nonlinear viscoelasticity is when the function is not separable. It usually happens when the deformations are large or if the material changes its properties under deformations (http://en.wikipedia.org/wiki/Viscoelasticity).

This chapter focuses on the non-linear viscoelastic behavior of rubber composites and nanocomposites. Here, we have discussed about the effect of individual fillers (mineral fillers, nanotubes, carbon nanofillers, fibrous nanofillers, biofillers, special structured fillers viz. nanorods, nanowires, nanoflowers etc.) on the linear/nonlinear viscoelastic behavior of rubber composites. Moreover, as this chapter is more concerned on the non-linear viscoelastic behavior, we have also discussed the effect of hybrid fillers on the nonlinear viscoelastic behavior of rubber composites in more detail.

2 Different Types of Nanofillers and Its Effect on Viscoelasticity Behavior of Rubber Nanocomposites

2.1 Mineral Fillers

Fillers are defined as additives in solid form that differ from the polymer/rubber matrix with respect to their composition and structure. A mineral filler is defined as a finely pulverized inert mineral or rock that is included in a manufactured product (e.g. paper, rubber, and plastics) to impart certain useful properties, such as hardness, smoothness, or strength etc (http://www.mindat.org/glossary/mineral_filler). Mineral particulate fillers are used in rubber/polymer composites to reduce the cost of the final product and to add some mineral property with the host (rubber/polymer) matrix, that is, to improve the properties of the matrix [19–22]. Common mineral fillers include asbestos, kaolin, talc, mica, wollastonite, and calcium carbonate etc (http://www.mindat.org/glossary/mineral_filler) [19].

The characteristics which determine the properties filler that will impart to a composite are particle shape, particle size, surface area, and particle-matrix compatibility (Fig. 1). Particle-matrix compatibility relates to the ability of the polymer to coat and adhere to the filler. The shape of most mineral filler particles can be a sphere, cube, block, plate, needle, or fiber whereas some filler also contain a mixture of shapes. Mineral particles resembling plates, needles, and fibers are further characterized by their aspect ratio (http://www.rtvanderbilt.com/fillersintroweb.pdf). In rubber/polymer composites, applied stress is transferred from the rubber/polymer matrix to the strong and stiff mineral. It seems reasonable that this stress transfer will be better affected if the mineral particles are smaller, because greater surface is thereby exposed for a given mineral concentration. Moreover, if these particles have a high aspect ratio (are needle-like, fibrous or platy in shape), they will better intercept the stress propagation through the matrix (Fig. 2) (http://www.rtvanderbilt.com/fillersintroweb.pdf).

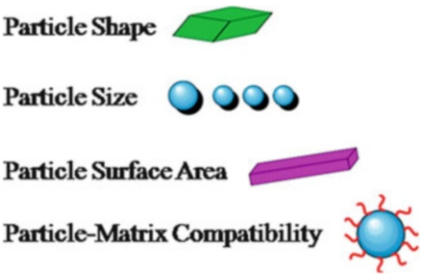

Fig. 1 Effect of different types of mineral filler on the properties of filler-matrix composites (http://www.rtvanderbilt.com/fillersintroweb.pdf)

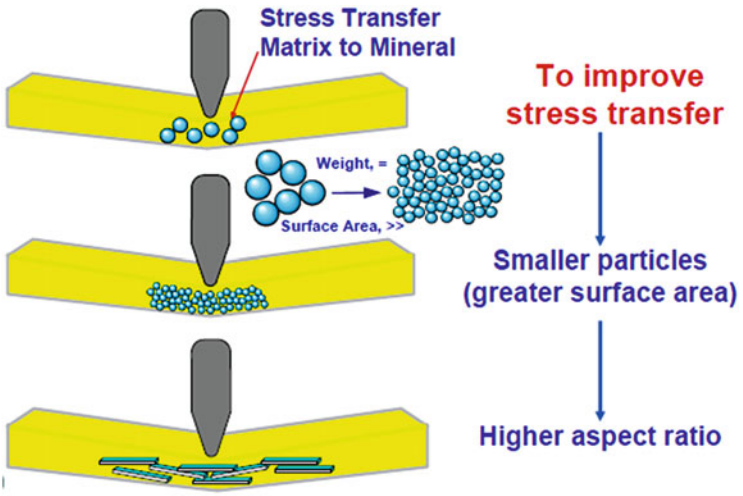

Fig. 2 Effect of size, shape and surface area of filler particles on stress transfer (http://www.rtvanderbilt.com/fillersintroweb.pdf)

The viscoelastic properties of rubber/polymer composites depend on matrix-filler interaction, crystallinity, and the extent of crosslinking. Thomas et al. have reported the dynamic mechanical and rheological properties of nitrile rubber (NBR) nanocomposites based on TiO_2 (TO), $Ca_3(PO_4)_2$ (CP), and layered silicate (LS) [23]. They observed that composites containing layered silicates (LSs) show better matrix-filler interaction as compared to other fillers. The higher interaction in case of layered silicates is due to its higher surface area to volume ratio which resulted in change in glass transition temperature. The storage modulus and complex viscosity of composites are studied with special reference to certain filler loading (10 phr) of different fillers. Figure 3 shows the variation of storage modulus with temperature of composites containing three different fillers having different particle size and chemical nature at a frequency of 1 Hz. It is observed that the

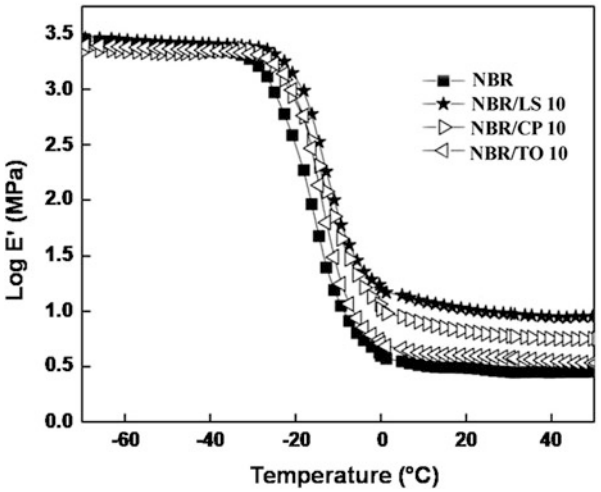

Fig. 3 Storage modulus curves as a function of temperature for NBR and its nanocomposites with different fillers at 10 phr loading (reproduced with permission of PC Thomas et al., Journal of Composite Materials [23])

increase in storage modulus with the incorporation of filler is up to certain limit where the LS filled composite showed maximum storage modulus value indicating the intercalated state of the NBR chains into the galleries of the LS and this will bring strong stress transfer between the matrix and LS. There is more rubber-filler interaction in case of LS filled composites due to its higher surface to volume ratio. The CP/TO filled systems show comparatively less storage modulus which is due to their larger particle size result in the minimum availability of surface area of these fillers, to be intercalated with the NBR matrix. This is the reason why the LS filled composites showed higher storage modulus (E′) than CP/TO filled systems. The frequency dependent complex viscosity (η*) of different filler filled composites is presented in Fig. 4 [23]. It is seen that the complex viscosity of the neat NBR and their composites with different fillers is found to be changed with the increase of frequency representing pseudoplastic nature of the systems. The pseudoplastic nature of polymers arises due to the randomly oriented and entangled polymer chains. The shear rate increases with the increase in frequency and at higher shear rate/frequency, the chains become disentangled and will be oriented in the direction of shear. As a result of the change in orientation and entanglement, the resistance of the chains moving past one another decreases. At lower frequency region, the entanglement is higher and this opposes the flow of the melt thereby the viscosity becomes higher. Moreover, the disentanglement effect is more in presence of fillers and is predominant in presence of LSs. The viscosity of the nanocomposites filled with layered silicates is found to be higher than that of CP/TO filled composites. This may be due to the more interaction between the matrix polymer and the filler [23].

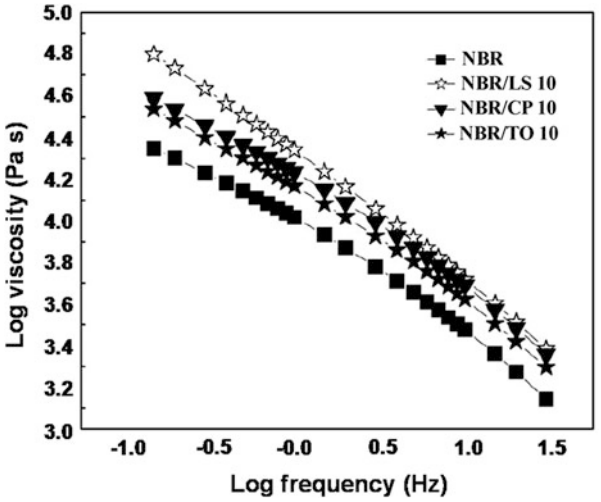

Fig. 4 Variation of complex viscosity with frequency for different fillers at 10 phr loading (reproduced with permission of PC Thomas et al., Journal of Composite Materials [23])

2.2 Nanotubes

A nanotube is a nanometer-scale tube-like structure. It may refer to: (i) carbon nanotube, (ii) silicon nanotube, (iii) boron nitride nanotube, (iv) inorganic nanotube, (v) DNA nanotube, and (vi) membrane nanotube (a tubular membrane connection between cells) (http://en.wikipedia.org/wiki/Nanotube).

Silicon nanotubes are nanoparticles which create a tube-like structure from silicon atoms. There is wide application of silicone nanotubes in electronic materials, as silicon is already a vastly important material in the semiconductor industry. Recently, it has been possible to prepare these nanotubes which are similar to carbon nanotubes (http://en.wikipedia.org/wiki/Silicon_nanotubes). Silicon nanotubes have been considered for use in electronics, because it appears that silicon nano-materials may behave like a metal fuel, since the structure can accommodate molecules of hydrogen so it might resemble coal without the CO_2 (http://www.azonano.com/article.aspx?ArticleID=838#, http://www.australianrdreview.com/ARDR%20documents/opinionsf, %20profiles/Earl_Bardsley_ARDR_04_09.pdf, 06.09.2013). Figure 5 gives an illustration of a carbon nanotube and a silicon nanotube [24]. Though there is no literature report on viscoelastic behavior of polymer nanocomposites filled with silicon nanotubes, some literatures are available on inorganic nanotube (halloysite nanotube, HNT) filled composites. M. Liu et al. have reported the viscoelastic properties of inorganic nanotube (halloysite nanotube, HNT) reinforced epoxy resin nanocomposites [25]. The variation of storage modulus (E′) with temperature for modified halloysite nanotube (m-HNT) filled epoxy composite is given in Fig. 6. The silane modified halloysite nanotubes (m-HNTs) were used for the composite preparation. It is observed that the storage modulus of the filled epoxy is significantly higher than the neat epoxy. About 40 % increase in storage modulus

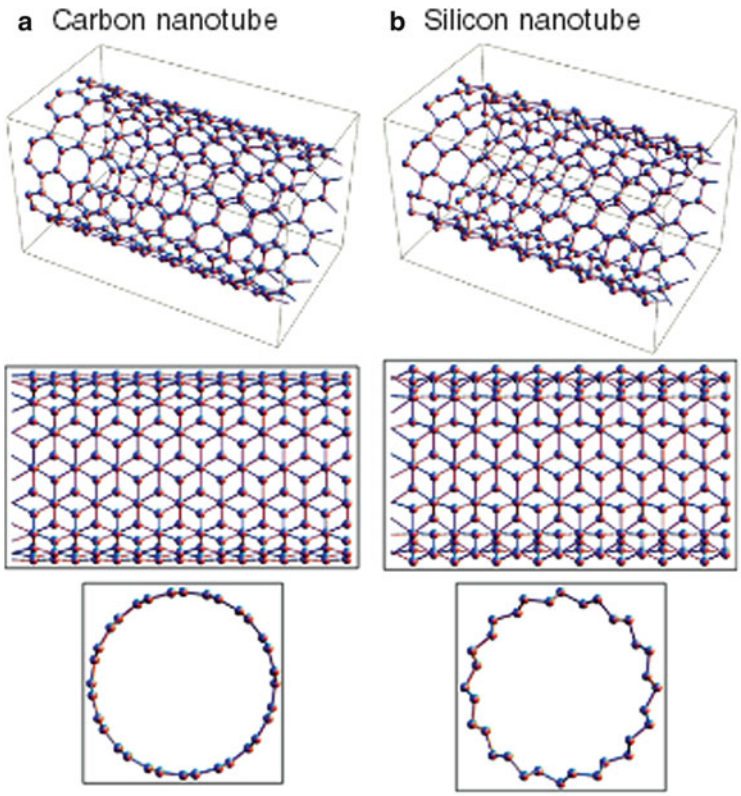

Fig. 5 (**a**) Carbon nanotube and (**b**) silicon nanotube. The lattice is distorted due to a large ionic radius of a silicon atom and forms a buckled structure in the silicon nanotube (reproduced with permission of EPL (Europhysics Letters)—IOP science, M. Ezawa et al., EPL [24])

at 50 °C and 133 % at 210 °C was achieved in the composite incorporating 12 wt % m-HNTs. The significant increased mechanical properties of the nanocomposites were attributed to the unique nanostructure and property of the HNTs since HNTs are rigid silicate nanotubes with high strength and stiffness [25].

In addition, the good compatibility between m-HNTs and the epoxy matrix may also play an important role in the reinforcing effect where the good compatibility is due to the interaction between the silica modified HNT and the epoxy resin. Therefore, the nanocomposites exhibit higher modulus even at the elevated temperatures [25].

Figure 7 shows the tan δ vs. temperature plots of the nanocomposites. It is observed that the tan δ value at glass transition temperature (T_g) of the nanocomposites decrease by the incorporation of m-HNTs, although the trend is not consistent. As the HNTs content increases the height of the loss peak decreases gradually. The decreased tan δ value is due to the restricted mobility of the polymer chains by the uniformly dispersed rigid nanotubes. However, overloading of the m-HNTs (12 wt%) increases the tan δ value at T_g, which may be attributed to the aggregation of m-HNTs at relatively higher content in the epoxy resin [25].

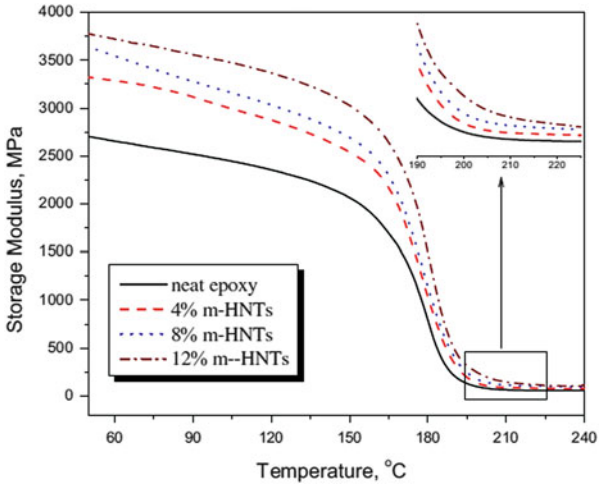

Fig. 6 Storage modulus vs. temperature plots of the epoxy/m-HNTs nanocomposites (reproduced with permission of Springer, M. Liu et al., Journal of Polymer Research [25])

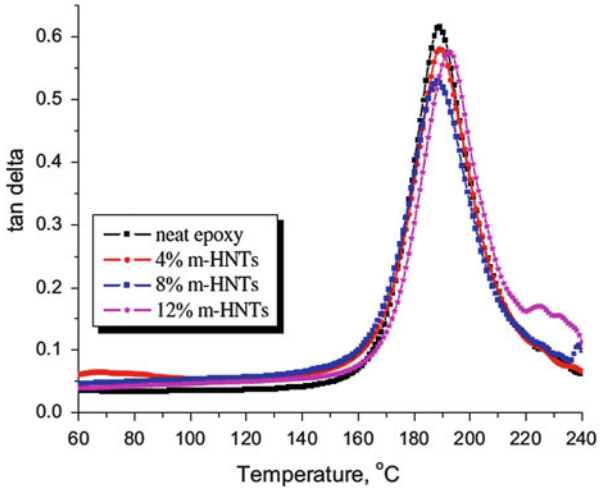

Fig. 7 Tan δ vs. temperature plots of epoxy/m-HNTs nanocomposites (reproduced with permission of Springer, M. Liu et al., Journal of Polymer Research [25])

S.K. Samanta et al. have reported the rheological properties of boron nitride nanotubes (BNNTs) filled gel nanocomposites which indicates that the flow properties of the resulting materials become resistant to applied stress upon incorporation of even a very low wt% of BNNTs. They have prepared gel nanocomposites using a gelator which is made up of all-trans tri-(p-phenylenevinylene) bis (aldoxime) (TPV, 1) which is capable of forming a physical gel in aromatic hydrocarbons such as toluene (Fig. 8a). A transparent solution of 1 (10 mg/mL)

in toluene is obtained upon brief heating (a "sol"), which upon cooling to room temperature over ~20 min develops into an immobilized viscoelastic mass (a "gel") which does not flow under the influence of gravity (Fig. 8b). The above step leading to spontaneous gelation is hastened when repeated in the presence of 0.2 mg (3.2 wt %) of BNNTs [26].

Rheological studies were performed to probe the influence of BNNT incorporation on the viscoelasticity and the flow behavior of gel. Frequency sweep measurements of gel of 1 and the composites containing 0.83 wt% of BNNT (with respect to 1) furnish the storage modulus (G′) and loss modulus (G″) as a function of angular frequency (ω) (Fig. 9a). The G′ and G″ show a plateau region over the entire angular frequency range (0.1–100 rad/s) at 0.01 % strain amplitude. A 20-fold higher G′ value over G″ suggests a substantial elastic response of the gels. The G′ of the composite is ~3 times more than that of the gel, and hence the composite gel is more viscoelastic than that of the gel alone. A gradual increase in G′ value was seen with the increased loading of the BNNTs in the nanocomposite, resulting in progressively more viscoelastic properties of the composites (Fig. 9b).

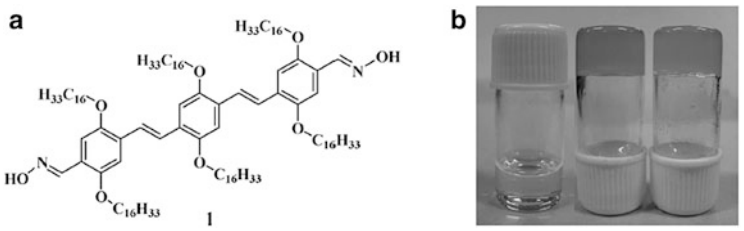

Fig. 8 (**a**) Molecular structure of the gelator 1 used for the nanocomposite preparation with BNNTs. (**b**) Photographs showing (from *left* to *right*): gelator 1 in toluene as "sol", "gel", and BNNT-doped gel (nanocomposite) (reproduced with permission of ACS Publications, S.K. Samanta et al., Langmuir [26])

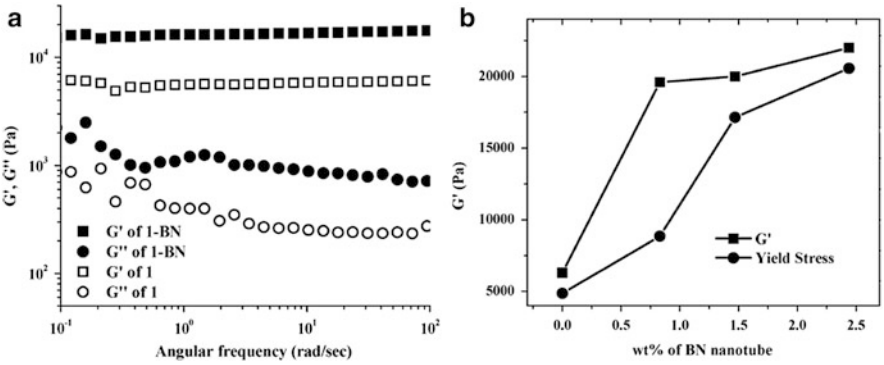

Fig. 9 Plot of (**a**) storage (G′) and loss modulus (G″) of 1 and the nanocomposite gel (0.83 wt% of each BN nanotubes) as a function of angular frequency at 0.01 % strain amplitude; (**b**) typical amplitude sweep experiment showed G′ with concentration variation of BNNTs in nanocomposite gel of 1 (reproduced with permission of ACS Publications, S.K. Samanta et al., Langmuir [26])

2.3 Carbon Nanofillers

There are various types of carbon nanofillers which include carbon black, multi walled carbon nanotubes (MWCNTs), and single walled carbon nanotubes (SWCNTs) [27]. In this section the effect of these nano fillers on viscoelastic behavior is thoroughly discussed. The physicomechanical properties of conductive carbon black (CCB) filled ethylene acrylic elastomer (AEM) vulcanizates have been reported by B.P. Sahoo et al. They have discussed thoroughly about the effect carbon black concentration on the viscoelastic behavior of CCB-AEM nanocomposites with respect to temperature variation. Figure 10a, b represents the variation of storage modulus and loss modulus with temperature. It is observed that the value of storage modulus (E′) increased with increase in filler loading in the

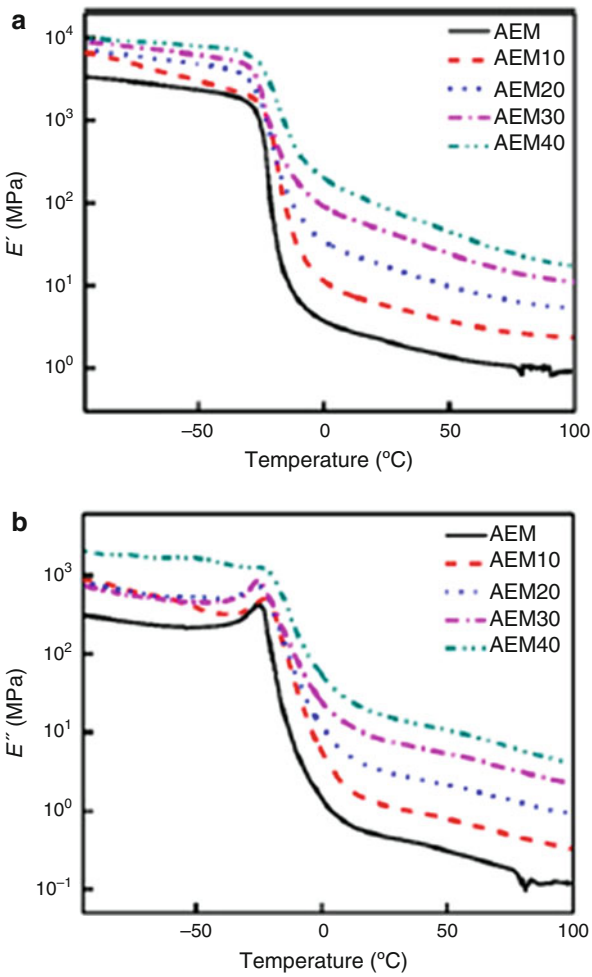

Fig. 10 Variation of (**a**) storage modulus (E′) and (**b**) loss modulus (E″) with temperature and filler loading respectively (reproduced with permission of Springer, B.P. Sahoo et al., Journal of Materials Science [28])

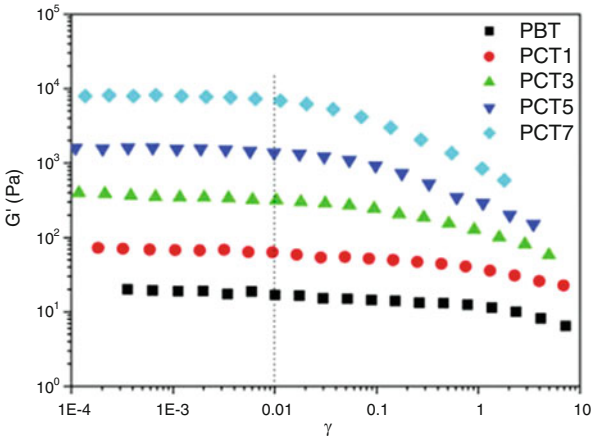

Fig. 11 The storage modulus (G′) for the neat PBT and PCTs samples obtained in dynamic strain sweep (reproduced with permission of John Wiley & Sons, Inc., D. Wu et al., Journal of Polymer Science: Part B: Polymer Physics [29])

whole temperature region whereas the increment is more prominent in the rubbery region [28]. This indicates that carbon black has a strong effect on the elastic properties of pristine AEM due to the restricted movement of AEM molecular chains. The increment in storage modulus throughout the temperature region is due to the enhancement in crosslink density with increase in the CCB loading. The sharp fall in storage modulus after −30 °C confirmed the glass transition (T_g) region as modulus decreased drastically in going from glassy state to rubbery state. The magnitude of the E″ is noticeably less at ambient temperature that signifies low plastic deformation for AEM-CCB vulcanizates than the unfilled AEM vulcanizate.

The linear and nonlinear viscoelastic behavior of poly(butylenes terephthalate)/multi-walled carbon nanotube composites (PCTs) have been studied by D. Wu et al. They have used small amplitude oscillatory shear (SAOS) for the linear viscoelastic measurements whereas large amplitude oscillatory shear (LAOS) for the nonlinear viscoelastic measurements. The dynamic strain sweep measurement was carried out to determine the linear region (Fig. 11). In the figure PCT1/PCT3 indicates percentage (1 % or 3 %) of MWCNT in the poly(butylenes terephthalate) (PBT) matrix. Figure 11 shows the dependence of dynamic storage modulus of the PCTs on the strain (γ_0). It is observed that the storage modulus (G′) increases with the increase in MWCNT loadings, which is attributed to reinforcement effect by MWCNT. If we compare the storage modulus (G′) curve for poly(butylenes terephthalate) [PBT] with that of poly(butylenes terephthalate)/nanotube composites (PCTs) (Fig. 11), it can be observed that the presence of MWCNT reduces the linear viscoelastic region of PBT matrix. So it can be concluded that beyond 1 % strain the composites are showing the nonlinear viscoelastic behavior [29]. So D. Wu et al. have carried out dynamic frequency scan measurement at 1 % strain in case of linear viscoelastic study whereas dynamic frequency scan measurements were carried out at the different strain rates of 10, 20, and 50 % in case of nonlinear viscoelastic behavior of composites for comparison with SAOS (Fig. 12). It is observed from Fig. 12, the G′ value reduces steadily with the increase in amplitude,

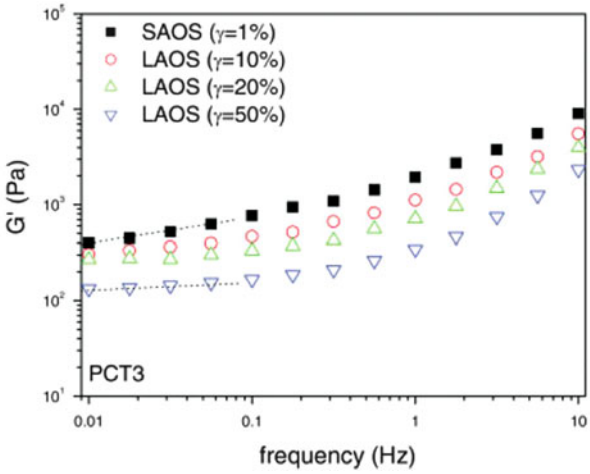

Fig. 12 The dynamic storage modulus (G′) for PCT3 sample obtained at various strain levels (reproduced with permission of John Wiley & Sons, Inc., D. Wu et al., Journal of Polymer Science: Part B: Polymer Physics [29])

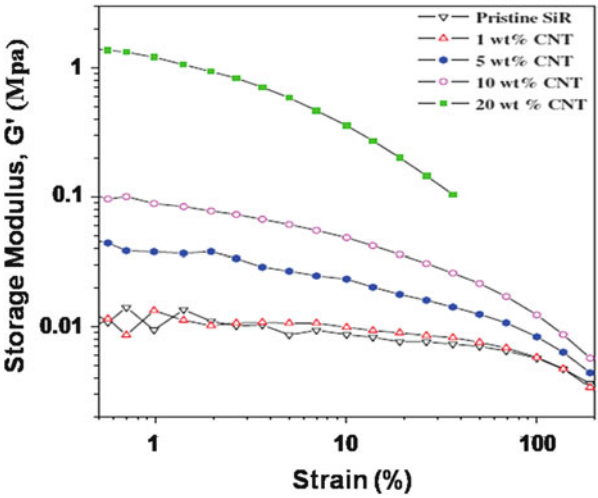

Fig. 13 Dynamical mechanical properties of uncured CNT/SiR used RPA (reproduced with permission of A. Katihabwa et al., Journal of Reinforced Plastics and Composites [30])

indicating the interactions among nanotubes or their transient physical gelation level decreases under the large shear deformation [29]. The viscoelastic properties of rubber nanocomposites also include the dynamic mechanical properties. The dynamic mechanical properties of silicone rubber/carbon nanotube composites have been reported by A. Katihabwa et al. The dynamic mechanical properties of an unfilled rubber depend on temperature and frequency under a given strain. On the other hand, the storage modulus decreases with increasing strain amplitude in filled rubbers which is known as Payne effect. It is observed from Fig. 13 that the Payne effect decreases with decreasing amount of CNTs and is not observable for the nanocomposites containing CNTs less than 5 wt%. It can be concluded that nanocomposites with more than 5 wt% CNTs gives percolating network. Moreover,

significant changes in G′ are observed with increasing strain amplitude, and a pronounced Payne effect is observed for the composite containing 20 wt% or more of CNTs [30].

2.4 Fibrous Nanofillers

Fibrous nanofillers are the materials used to reinforce the polymer/rubber matrix, which are made from fibers, such as jute, polypropylene, cotton, glass, carbon nanofibre, etc. In fact, these nanofillers are used in rubber matrix to improve the properties of the composite material and in order to make them suitable for various applications. B. Lively et al. have described the variation of storage modulus with temperature of polycarbonate/carbon nanofibre (PC/CNF) composites. They have prepared the PC/CNF composites via solution mixing at 1.5 wt% CNF in PC with different preparation procedures and sonication exposures to control dispersion levels as given in Table 1 [31]. During these initial sonication treatments, the solution containing CNF/$CHCl_3$ (ratio of 0.5 g CNF to 10 mL $CHCl_3$) was held in a vial partially submerged in an ice bath to maintain a reasonable temperature. After the treatment, a PC/$CHCl_3$ solution (ratio of 3.0 g PC to 10 mL $CHCl_3$) was added to the CNF solution and spin mixed for about 24 h [31]. After the spin mixing, further treatments were done as per Table 1 before the casting. Casting was performed on a glass substrate and the film thickness was controlled using a casting block with a 0.254-mm (10 mile) gap. The composite films were dried and hot pressed into approximately 1 mm thick panels. The viscoelastic property of the composites was described through dynamic mechanical analysis (DMA). Figure 14a, b demonstrates the effect of temperature on the storage modulus (E′) and loss modulus (E″) respectively for different composites. It can be observed that composite "B" starts with the highest average storage modulus, and the curve slowly becomes very similar to the Composite "A" curve. At 100 °C the storage moduli of composites show the following trend as: A > B > C > D. In general, a better dispersed nanocomposite will yield a higher storage moduli compared to a system with worse dispersion. This is due to more nanofiller available for load transfer compared to a poorly dispersed nanocomposite system. It can be observed from Fig. 14b that all the nanocomposites yield similar peak loss modulus values;

Table 1 Differences in sonication treatments for the different dispersed 1.5 wt% PC/CNF nanocomposite samples analysis (reproduced with permission of John Wiley & Sons, Inc., B. Lively et al., Polymer Composites [31])

Composite	Preparation
A	1 h ultrasonication total; 15 min on, 15 min off
B	1 h ultrasonication, no breaks
C	8 h of bath sonication
D	No treatment

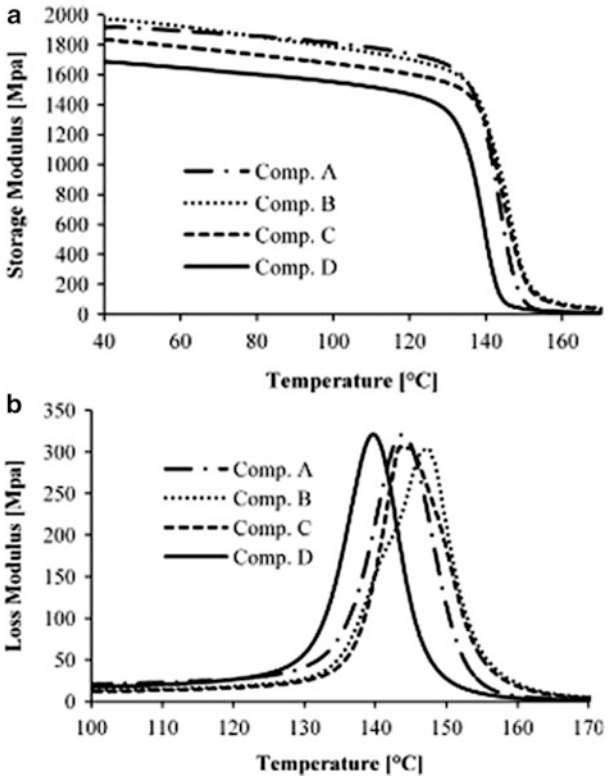

Fig. 14 The effect of temperature on the storage moduli (**a**) and loss modulus (**b**) found via dynamic mechanical analysis (reproduced with permission of John Wiley & Sons, Inc., B. Lively et al., Polymer Composites [31])

however they occur at different temperatures. Composite B's average peak value occurs at the highest temperature, about 147 °C. Next, composites A and C exhibited their peak value at a similar temperature around 144 °C. Finally, Composite D's peak loss modulus occurred at ~140 °C. The differences in loss modulus values can be attributed to different levels of friction between the nanofiller and the polymer matrix. Therefore, according to these curves, composite B would theoretically have the most interaction between the polymer and matrix, followed by composites A and C. Composite D's interaction may be thought of as the worst [31].

2.5 Biofillers

There is plenty of interest in bio-based or bio-friendly fillers, which can be added to rubber/polymer matrices and result in enhanced performance and "greener"

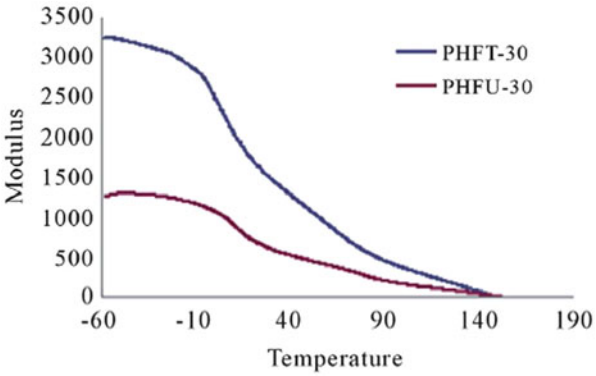

Fig. 15 Storage modulus graph of PP/treated and untreated hybrid fiber composites (reproduced with permission of Scientific Research, P. Upadhyaya et al., Materials Sciences and Applications [32])

content. The major benefit of the polymeric products is that such modified wood fiber/filler is hydrophobic and cheap, but it also lighter than typical mineral fillers. Hydrophobic bio-fiber is expected to be very attractive to the auto/transportation industry, and will certainly be useful in many other thermoplastic and even thermoset polymer applications. Generally, plant based fibers are hydrophilic in nature, which is a problem that gets more complex in the mixing stage and later in the final product. If the fiber fillers do not stay dry, the fiber can take up water, swell, take on fungus, discolor, etc. So for using these types of bio-based fibers one has to treat them and make them hydrophobic (http://www.polymerohio.org/index.php?option=com_content&view=article&id=338:bio-friendly-fillers-for-polymers-&catid=1:latest-news&Itemid=61). P. Upadhyaya et al. have studied the dynamic mechanical properties of polypropylene composite with treated and untreated hybrid filler (wood flour/wheat husk) over a wide temperature range. The storage modulus for composite with treated and untreated hybrid filler at 30 phr loading is shown in Fig. 15. The effect of treatment on storage modulus loss is clearly visible in the figure as the composite filled with treated filler (PHFT-30) shows more storage modulus value than the composite with untreated filler (PHFU-30) [32].

2.6 Special Structured Fillers (Nanorods, Nanowires, Nanoflowers, etc)

In nanotechnology, these entire special structured fillers (nanorods, nanowires, nanocubes, nanoflowers etc.) are having different morphology of nanoscale objects where their dimensions range from 1–100 nm. These materials can be synthesized from metals or semiconducting materials using direct chemical synthesis techniques where the standard aspect ratios are 3–5. Nanorods can be used in display technologies, because the reflectivity of the rods can be changed by changing their orientation with an applied electric field. Nanorods based on semiconducting materials have also been investigated for application as energy harvesting and

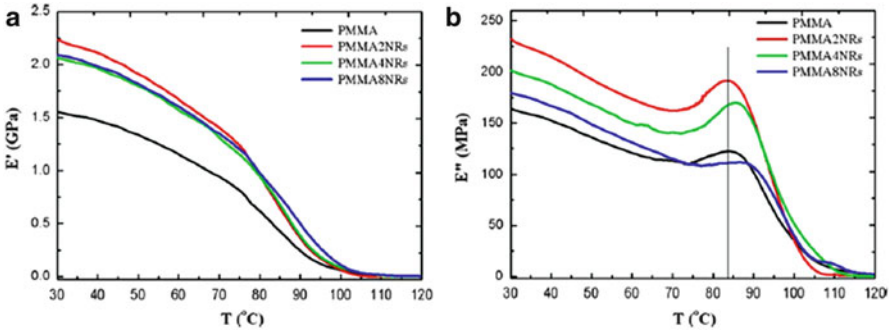

Fig. 16 DMTA curves of (**a**) storage modulus (E′) and (**b**) loss modulus (E″) of PMMA-TiO2 nanocomposites with different concentration as a function of the temperature (reproduced with permission of Elsevier, N. Patra et al., Composites Part B: Engineering [33])

light emitting devices (http://en.wikipedia.org/wiki/Nanorod). Similar to nanorods, nanowire is a nanostructure, with the diameter of the order of a nanometer (10^{-9} m) with average aspect ratios than 20. Typical nanowires exhibit aspect ratios of 1,000 or more and they are often referred to as one-dimensional (1-D) materials. Nanowires have many interesting properties which are not seen in bulk or 3-D materials. This is because electrons in nanowires are quantum confined laterally and thus occupy energy levels that are different from the traditional continuum of energy levels or bands found in bulk materials (http://en.wikipedia.org/wiki/Nanowire). Nanoflower refers to a compound of certain elements that result in formations which in microscopic view resemble flowers (http://en.wikipedia.org/wiki/Nanoflower). Similarly, nanocubes are nanoparticles derived from different origins having cube shape and size ranges from 1–100 nm.

N. Patra et al. have studied the thermal and mechanical characterization of poly (methyl methacrylate) nanocomposites filled with TiO_2 nanorods where they have described the viscoelastic properties PMMA-titania nanorod composites via dynamic mechanical thermal analysis (DMTA). Figure 16 shows the temperature dependence of storage modulus (E′) and loss modulus (E″) of bare PMMA and TiO_2 nanocomposites measured at 1 Hz. It can be observed from Fig. 16 that all the curves of the nanocomposites (colored lines) lie above the curve of the bare PMMA (black line). In both the cases (Fig. 16a, b), the highest values are recorded for the lowest concentration (2 wt%). The significant increase in both storage and loss modulus is due to the PMMA chains becoming stiffer due to the incorporation of TiO_2 nanorods (NRs) in PMMA matrix, restricting the chain movement. Nanocomposite containing 2 wt% NRs shows the highest properties (both storage and loss modulus). This is also due to the fact that with the increase of titania nanorods loading, the aggregates size is also increasing because of the mutual interaction of the nanoparticles trying to hinder themselves inside the polymer matrix. In Fig. 16b, the peaks of loss modulus can be associated to the T_g of the materials. A little change in the peak position as a function of the particles concentration is observed for 4 wt% and 8 wt%, which may be due to the increase

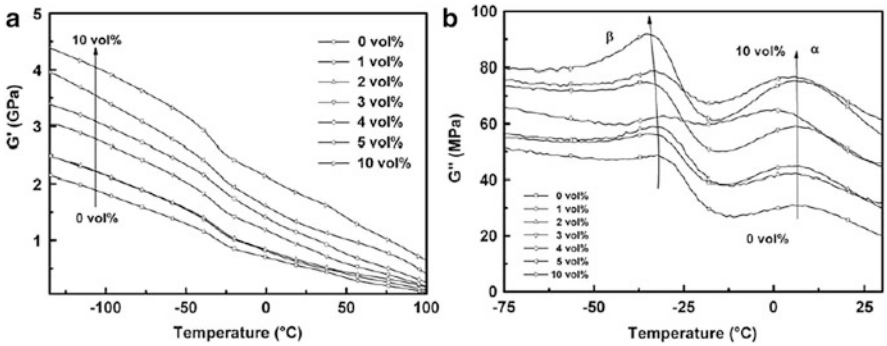

Fig. 17 (**a**) Storage shear modulus (G′) vs. temperature, (**b**) Dissipative shear modulus (G″) of the mechanical β and α relaxations vs. temperature for P(VDF-TrFE)/Ni nanowires from 0 vol.% to 10 vol.% (reproduced with permission of Elsevier, A. Lonjon et al., Journal of Non-Crystalline Solids [34])

in crosslinking density. The interactions between the particles and the PMMA matrix are mainly physical, while the interface does not confer mobility to the chains in the studied concentrations [33]. A. Lonjon et al. have prepared conducting nanocomposites using poly(vinylidene difluoride-trifluoroethylene) [P (VDF-TrFE)] as the base matrix and nickel nanowires (aspect ratio ~250, up to 30 vol.%) as the filler material. They have prepared metallic nanowires based nanocomposites through solvent mixing technique which constitute a new class of multifunctional materials with a high conductivity associated with a ductile polymer matrix characterized by a high rubbery modulus. The variation of both storage shear modulus and dissipative shear modulus with temperature for P (VDF-TrFE)/Ni nanowires from 0 vol.% to 10 vol.% are presented in Fig. 17a, b respectively. It is seen from the figure that storage modulus continuously increases with the increase in Ni nanowire concentration where composites containing 1 vol. % and 2 vol.% show almost same storage modulus in the temperature range of −135 °C to 0 °C and marginal changes in storage modulus is seen above 0 °C. Two relaxation peaks are observed in case of Fig. 17b which corresponds to the α and β relaxation in the polymer matrix [P(VDF-TrFE)]. The β relaxation ($T_\beta = -33$ °C) corresponds to the free amorphous phase whereas α relaxation ($T_\alpha = 7$ °C) is the response of the constrained amorphous phase [34].

2.7 *Hybrid Fillers*

Hybrid fillers for rubber composites/nanocomposites are getting importance because they offer a range of properties that cannot be obtained with a single type of reinforcement. Hybrid composites have attracted the attention of many researchers as a way to enhance the mechanical properties [19, 35]. Hybrid

composites are materials made by combining two or more different types of fillers in a common matrix. The hybridization of two types of mineral fillers having different sizes and shapes offers some advantages over the use of single filler alone in a rubber matrix [19]. Hybrid fillers are also used to enhance the thermal conductivity of polymer composites. Generally, carbon fillers are used to improve the conductivity of polymer composites. However, individual filler [viz graphene nanoplatelets (GNPs) or carbon nanotubes (CNTs)] limit the realization of the desirable thermal conductivity of the composite. But the composites derived from carbon hybrid fillers composed of CNTs directly grown on the GNP support show enhancement in thermal conductivity than the individual fillers [36].

2.8 *Effect of Hybrid Fillers on Non-Linear Viscoelasticity of Rubber Nanocomposites*

In this section, the effect of hybrid fillers on nonlinear viscoelastic properties of rubber composites/nanocomposites is discussed. The viscoelastic properties of rubber nanocomposites include different properties like cure behavior, rheology, creep and dynamic mechanical analysis etc. The properties measured under dynamic mechanical analysis are storage and loss moduli and tan δ. Storage modulus is a measure of the maximum energy stored in the material during one oscillation cycle which represents the elastic nature of the material whereas the loss modulus measures the energy dissipated as heat, representing the viscous portion of the material [37] (http://en.wikipedia.org/wiki/Dynamic_mechanical_analysis). The ratio of loss modulus to storage modulus is referred to as internal damping or loss tangent (tan δ) [37]. The effect of hybrid fillers on these properties is thoroughly discussed under this section. The significant improvement of various properties of rubber/polymer composites derived from different hybrid fillers are studied by many researchers [38–43]. The dynamic mechanical properties of natural rubber (NR) filled with fly ash silica (FASi) and precipitated silica (PSi) is studied by S. Thongsang et al. Different weight fractions of FASi:Psi used in this investigation are 100:0, 75:25, 50:50, 25:75 and 0:100. They measured different mechanical properties with respect to Psi content and observed increase in mechanical properties with increasing Psi content, resulting in a decrease in tan δ_{max} value. The optimum mechanical properties were achieved at 75 % Psi loading. So the dynamic mechanical analysis was done on composites containing 75 % Psi with different fly ash particle sizes and at two different silica loadings (10 phr and 40 phr). The variation of viscoelastic properties (storage modulus, loss modulus, and tan δ) with temperature of NR vulcanizates filled with 75 % Psi fraction in FASi/Psi hybrid filler at total silica contents of 10 and 40 phr is shown in Fig. 18 [37]. It is observed from Fig. 18 that storage modulus of composites containing 40 phr silica is higher than the composite containing 10 phr silica both in glassy and rubbery regions. But this is more pronounced in the rubbery region which is due to the higher stiffness of

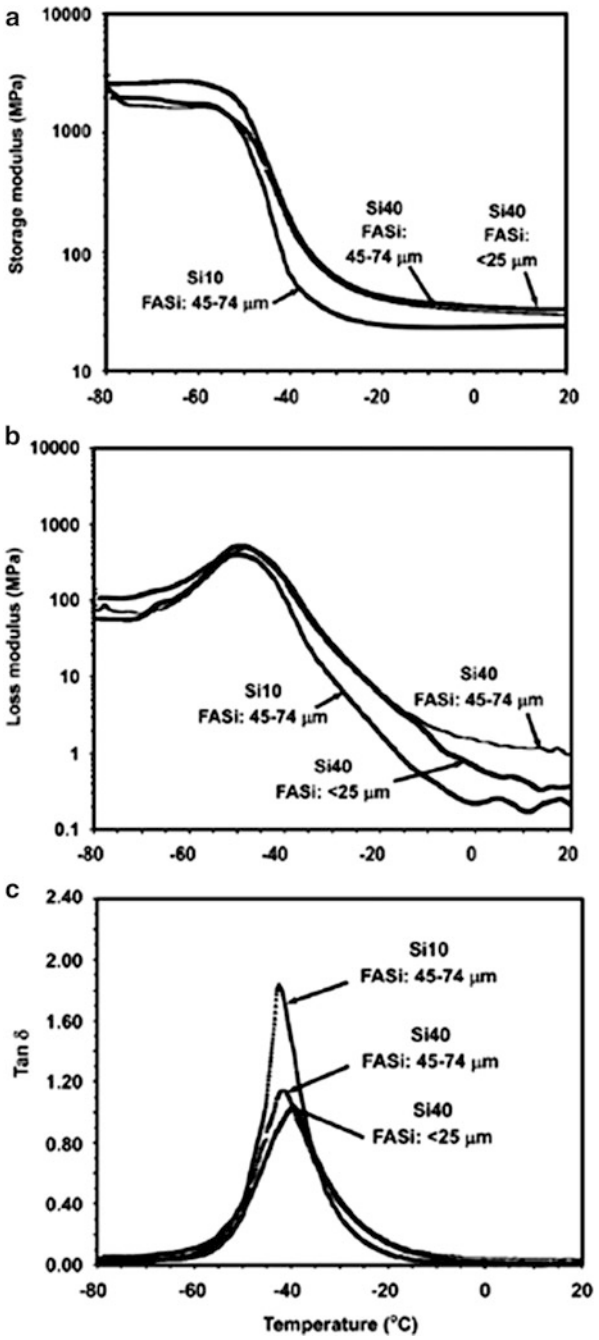

Fig. 18 (**a**) Storage modulus vs. temperature, (**b**) loss modulus vs. temperature; (**c**) tan δ vs. temperature. Traces of NR vulcanizates filled with 75 % Psi weight fraction in FASi/PSi hybrid filler (reproduced with permission of Elsevier, S. Thongsang et al., Tribology International [37])

the composite and the strong interaction between silica and rubber molecules. Composites filled with smaller FASi particles possess higher storage modulus than those with larger particles due to larger surface area, resulting in the formation of more rubber-filler interactions. The loss modulus peaks of composites filled with 40 phr silica became broader than those with 10 phr because of hindrance of the molecular motion. The reduction of the loss modulus for composite with smaller FASi particle sizes is due to the reduction in energy dissipation. From tan δ vs. temperature curve of FASi/PSi-filled composites, it is observed that the incorporation of larger amount of silica into the NR matrix decreased the damping characteristics of the composites, resulting in lower and broader damping peak. This is because the filler acted as a barrier to the mobility of rubber chains, indicating the reinforcing nature of filler with the rubber matrix. Moreover, a reduction in damping peak is observed for FASi/PSi-filled composites filled with small FASi particles [37].

Rheology is the study of flow and deformation of materials under the applied forces (http://www.malvern.com/en/products/measurement-type/rheology-viscosity/). Rheology exhibits the combination of elastic, viscous, and plastic behavior by properly combining the elasticity and (Newtonian) fluid mechanics (http://en.wikipedia.org/wiki/Rheology). Rheological properties of bulk sample deformation can be measured using a mechanical rheometer or microcapillary viscometer or Microrheology (http://www.malvern.com/en/products/measurement-type/rheology-viscosity/). The rheological properties of rubber/polymer composites can be increased by the addition of single/hybrid fillers. The rheological behavior of natural rubber (NR)-carbon black(CB)/nanoclay (OC) hybrid filler composites have been studied by Y.B. Liu et al. To understand the reinforcement effect of the hybrid filler, a series of NR compounds without vulcanising agents were prepared and then dynamic melt rheological behaviour was tested, as shown in Fig. 19. The decrease in modulus with increasing strain amplitude is well known as the Payne effect as discussed earlier in the Sect. 2.3 [30, 44]. From Fig. 19, it is

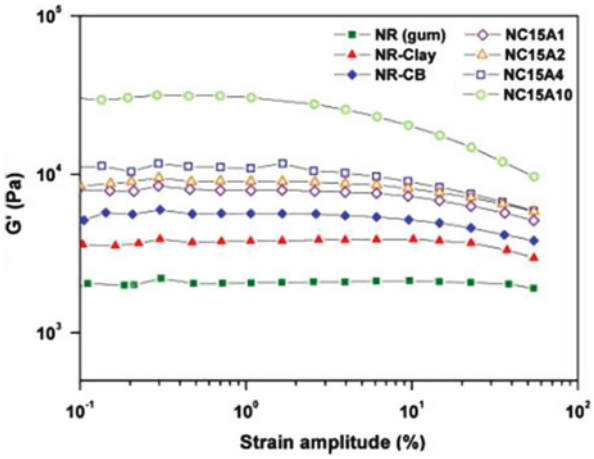

Fig. 19 Plots of G′ vs. strain at 130 °C for NR gum and NR nanocomposites without additives for vulcanisation (measurements were performed at 130 °C) (reproduced with permission of Y.B. Liu et al., Plastics, Rubber and Composites [44])

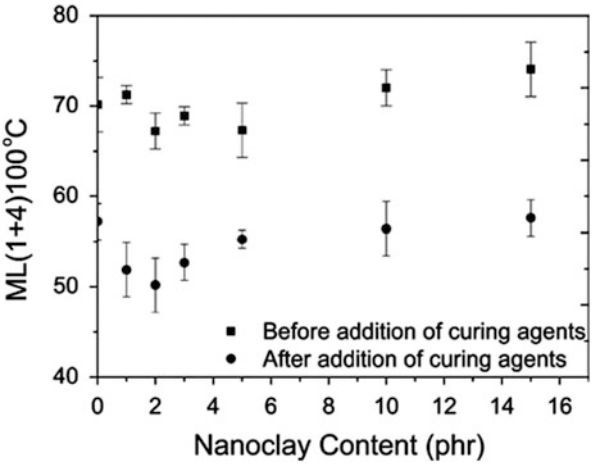

Fig. 20 Mooney viscosity of rubber compounds before and after addition of curing agents (reproduced with permission of Wiley, J. Sapkota et al., Polymer Engineering and Science [45])

observed that the modulus (G′) of compounds derived from hybrid CB/OC dual phase filler is significantly higher than the compounds derived from individual fillers (CB or OC) indicating the hybrid filler system has a significant synergetic reinforcement effect on natural rubber [44].

The viscoelastic behavior of rubber composites can also be understood from its cure characteristics. The influence of organically modified nanoclay-carbon black (CB) hybrid filler on the curing behavior of natural rubber (NR) have been investigated by J. Sapkota et al. [45]. The effect of clay loading on the Mooney viscosity of rubber-clay compounds is given in Fig. 20. A decrease in Mooney viscosity followed by an increase was observed with the increase in filler concentration in the rubber matrix. The initial decrease in viscosity might be caused by the replacement of carbon black (CB) by well dispersed clay. However, at a particular concentration, the nanofiller is no longer well dispersed, leading to an increase in viscosity at higher nanofiller loadings [45]. The cure behavior of composites is studied as a function of clay loading which is presented in Fig. 21. It is apparent from this figure that the curing time decreased with increasing the clay concentration. The decrease in curing time can be explained by the modification of the clay: The modifying agent of the clay contains ammonium compounds which are well known as accelerators for sulfur vulcanization. Therefore, the ammonium group of the modified clay might take part in the amine complexation reaction and thus facilitate the curing of NR. The maximum torque of the compounds was decreased with the increase in nanoclay loading where the maximum torque of the compound containing 15 phr nanoclay is found to be half to that of compound without clay. The modified clay contained a large amount of long chain quaternary ammonium compounds, and at curing temperature, this compound can act as a plasticizer and result in a decrease of the ultimate torque [45].

The viscoelastic properties of natural rubber (NR) nanocomposites filled with silica/multiwall carbon nanotube hybrid fillers have been studied by H. Ismail et al. [46]. The addition of hybrid fillers (MWCNTs + silica) to the NR matrix

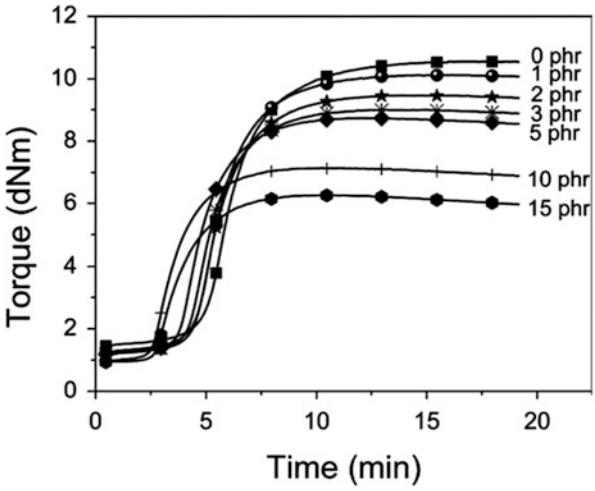

Fig. 21 Curing curves of different NR-CB-clay (QUAT) compounds (reproduced with permission of Wiley, J. Sapkota et al., Polymer Engineering and Science [45])

was varied with the total filler loading fixed at 30 phr. They have achieved the highest tensile strength for composites at a loading ratio of 29 phr silica/1 phr MWCNTs. As the MWCNT loading increased in the silica/MWCNT hybrid, the tensile strength value decreased (Fig. 22) whereas tensile modulus value increased (Fig. 23). The increase in tensile strength was possibly caused by the higher surface area, together with the aspect ratio of MWCNTs compared to silica. Further, as the MWCNT loading ratio increased in the silica/MWCNT hybrid, the MWCNTs tended to agglomerate which weakened the rubber-filler interaction leading to decrease in the tensile strength. The continuous increase in tensile modulus (M_{100}) with the increase in MWCNT is due to the improved stiffness of the nanocomposites (Fig. 23). The high aspect ratio and large surface area of the MWCNTs can give better rubber-filler interaction at low MWCNT loading. Moreover, with the increase in the MWCNT loading the agglomeration also increased which restrict the movement of the NR chain. It caused the composites to become more rigid [46].

The viscoelastic property (storage modulus) of carbon black and mixture of carbon black-phenolic resin filled nitrile rubber was investigated by V. Nigam et al. and also was compared with the storage modulus of pristine elastomer [47]. The influence of phenolic resin could be obtained from the measurement of viscoelastic properties of the vulcanizates as measured in dynamic methods e.g., storage modulus (E′) (Fig. 24). In Fig. 24, E′ was found to be maximum when carbon black and resin used in combination (mix D). Y.B. Liu et al. have reported the reinforcement of natural rubber with carbonblack/nanoclay hybrid filler. They had prepared the nanocomposites by the incorporation of a hybrid filler system, organoclay and carbon black (CB), through melt compounding. It was observed that the hybrid filler exhibited more significant reinforcing effect over the same loading of CB on NR matrix [44].

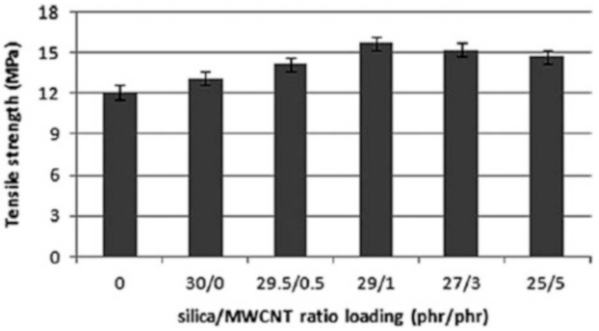

Fig. 22 Effect of the silica/MWCNT hybrid loading ratio on the tensile strength of the NR/silica/MWCNT hybrid nanocomposites (reproduced with permission of John Wiley & Sons, Inc., H. Ismail et al., Journal of Applied Polymer Science [46])

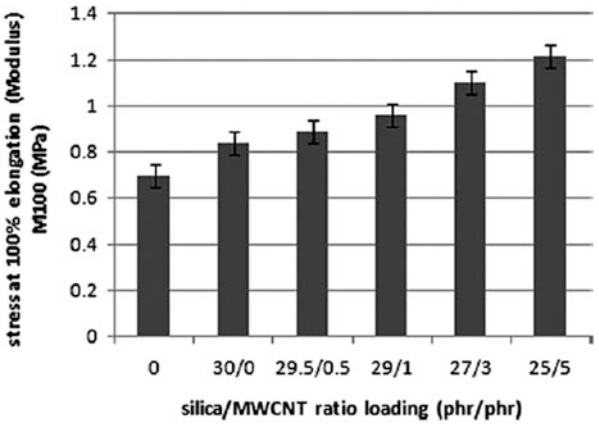

Fig. 23 Effect of the silica/MWCNT hybrid loading ratio on the modulus (M100) of the NR/CB/MWCNT hybrid nanocomposites (reproduced with permission of John Wiley & Sons, Inc., H. Ismail et al., Journal of Applied Polymer Science [46]

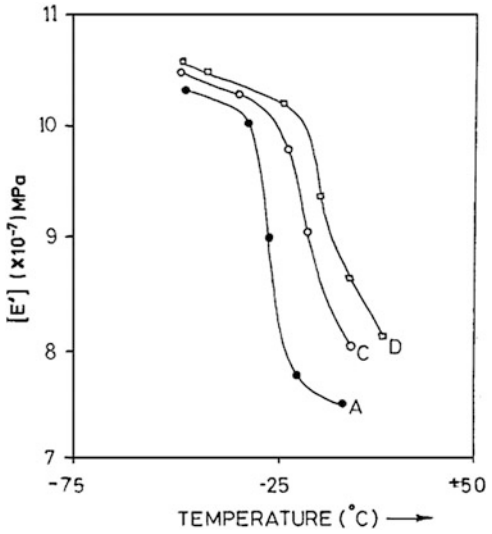

Fig. 24 Storage modulus (E′) vs. temperature plots of (A) unfilled, (C) carbon black and (D) carbon black + phenolic resin filled vulcanizates (reproduced with permission of Springer, V. Nigam et al., Journal of Materials Science [47])

3 Conclusions

Rubber composites/nanocomposites derived from hybrid fillers are promising class of materials with emerging applications in different fields like materials science, nanotechnology, and nanobiotechnology etc. The viscoelastic behavior of rubber composites increases with the increase in filler fraction in the rubber matrix. However, use of hybrid fillers in the cured rubber matrix enhances the viscoelastic properties of the rubber composites to a greater extent than the composites with single filler. Rubber composites derived from hybrid fillers (mixture of fillers) carry the properties of individual fillers. The improvement of viscoelastic properties of rubber composites/nanocomposites depends on different factors (viz. filler concentration in rubber matrix, particle size, curing, rubber-filler interaction, and processing conditions etc.). In addition to the viscoelastic properties, there is enhancement in other properties like thermal stability, mechanical properties, and electrical properties etc by the use of hybrid filler systems. The cure characteristics/behavior of rubber composites are also affected by the use of hybrid fillers.

References

1. Anandhan S, Bandyopadhyay S (2011) Polymer nanocomposites: from synthesis to applications. In: Cuppoletti J (ed) Nanocomposites and polymers with analytical methods. InTech, Croatia. ISBN 978-953-307-352-1
2. Nayak S, Sahoo B, Chaki TK, Khastgir D (2013) Development of polyurethane-titania nanocomposites as dielectric and piezoelectric material. RSC Adv 3:2620
3. Nayak S, Rahaman M, Pandey AK, Setua DK, Chaki TK, Khastgir D (2013) Development of poly(dimethylsiloxane)-titania nanocomposites with controlled dielectric properties: effect of heat treatment of titania on electrical properties. J Appl Polym Sci 127(1):784
4. Liang GD, Tjong SC (2006) Electrical properties of low-density polyethylene/multiwalled carbon nanotube nanocomposites. Mater Chem Phys 100:132
5. Girei SA, Thomas SP, Atieh MA, Mezghani K, De SK, Bandyopadhyay S, Al-Juhani A (2012) Effect of –COOH functionalized carbon nanotubes on mechanical, dynamic mechanical and thermal properties of polypropylene nanocomposites. J Thermoplast Compos Mater 25:333
6. Ramajo LA, Reboredo MM, Castro MS (2007) Characterisation of epoxy/$BaTiO_3$ composites processed by dipping for integral capacitor films (ICF). J Mater Sci 42:3685
7. Ramajo L, Castro MS, Reboredo MM (2010) Dielectric response of Ag/$BaTiO_3$/epoxy nanocomposites. J Mater Sci 45:106
8. Matienzo LJ, Farquhar D (2008) A model system for the optimization of lamination parameters of PTFE-based dielectrics and metal surfaces. J Mater Sci 43:2035
9. Olad A (2011) Polymer/clay nanocomposites. In: Dr. Reddy B (ed) Advances in diverse industrial applications of nanocomposites. InTech, University of Tabriz, Iran. ISBN 978-953-307-202-9
10. Chung T-S, Jiang LY, Li Y, Kulprathipanja S (2007) Mixed matrix membranes (MMMs) comprising organic polymers with dispersed inorganic fillers for gas separation. Prog Polym Sci 32:483
11. Nayak S, Chaki TK, Khastgir D (2013) Development of poly(dimethylsiloxane)/$BaTiO_3$ nanocomposites as dielectric material. Adv Mater Res 622–623:897

12. Sumita M, Tsukumo Y, Miyasaka K, Ishikawa K (1983) Tensile yield stress of polypropylene composites filled with ultrafine particles. J Mater Sci 18:1758
13. Cole DH, Shull KR, Baldo P, Rehn L (1999) Dynamic properties of a model polymer/metal nanocomposite: gold particles in poly(*tert*-butyl acrylate). Macromolecules 32:771
14. Oya A, Kurokawa Y, Yasuda H (2000) Factors controlling mechanical properties of clay mineral/polypropylene nanocomposites. J Mater Sci 35:1045
15. Zeng QH, Yu AB, Lu GQ (2008) Multiscale modeling and simulation of polymer nanocomposites. Prog Polym Sci 33:191
16. Hule RA, Pochan DJ (2007) Polymer nanocomposites for biomedical applications. MRS Bull 32:354
17. Sarvestani AS, Jabbari E (2010) Nonlinear viscoelastic behavior of rubbery bionanocomposites. In: Stephen R, Thomas S (eds) Rubber nanocomposites: preparation, properties, and applications. Wiley Online Library, Singapore, p 331
18. Dealy JM. Nonlinear viscoelasticity. Rheology, vol. 1. Encyclopedia of Life Support Systems (EOLSS)
19. Nurdina A, Mariatti M, Samayamutthirian P (2009) Effect of single-mineral filler and hybrid-mineral filler additives on the properties of polypropylene composites. J Vinyl Addit Technol 15(1):20
20. Leong Y, Bakar A, Ishak Z, Ariffin A, Pukanszky B (2004) Comparison of the mechanical properties and interfacial interactions between talc, kaolin, and calcium carbonate filled polypropylene composites. J Appl Polym Sci 91:3315
21. Sancaktar E, Walker E (2004) Effects of calcium carbonate, talc, mica, and glass-fiber fillers on the ultrasonic weld strength of polypropylene. J Appl Polym Sci 94:1986
22. Hanumantha Rao K, Forssberg K, Forsling W (1998) Interfacial interaction and mechanical properties of mineral filled polymer composites; wollastonite in PMMA polymer matrix. Colloids Surf A Physicochem Eng Asp 133:107
23. Thomas P, Jose ET, George G, Thomas S, Joseph K (2013) Dynamic mechanical and rheological properties of nitrile rubber nanocomposites based on TiO2, Ca3(PO4)2 and layered silicate J Compos Mater: 1
24. Ezawa M (2012) Dirac theory and topological phases of silicon nanotube. EPL (Europhys Lett) 98:67001
25. Liu M, Guo B, Du M, Lei Y, Jia D (2008) Natural inorganic nanotubes reinforced epoxy resin nanocomposites. J Polym Res 15:205
26. Samanta SK, Gomathi A, Bhattacharya S, Rao CNR (2010) Novel nanocomposites made of boron nitride nanotubes and a physical gel. Langmuir 26(14):12230
27. Moskalyuk OA, Aleshin AN, Tsobkallo ES, Krestinin AV, Yudin VE (2012) Electrical conductivity of polypropylene fibers with dispersed carbon fillers. Phys Solid State 54 (10):2122
28. Sahoo BP, Naskar K, Tripathy DK (2012) Conductive carbon black-filled ethylene acrylic elastomer vulcanizates: physico-mechanical, thermal, and electrical properties. J Mater Sci 47:2421
29. Wu D, Wu L, Zhang M (2007) Rheology of multi-walled carbon nanotube/poly(butylene terephthalate) composites. J Polym Sci B Polym Phys 45:2239
30. Katihabwa A, Wang W, Jiang Y, Zhao X, Lu Y, Zhang L (2011) Multi-walled carbon nanotubes/silicone rubber nanocomposites prepared by high shear mechanical mixing. J Reinf Plast Compos 30(12):1007
31. Lively B, Bizga J, Zhong W-H (2013) Analysis tools for nanofiller polymer composites: macro- and nanoscale dispersion assessments correlated with mechanical and electrical composite properties. Polym Compos. doi:10.1002/pc.22628
32. Upadhyaya P, Garg M, Kumar V, Nema AK (2012) The effect of water absorption on mechanical properties of wood flour/wheat husk polypropylene hybrid composites. Mater Sci Appl 3:317

33. Patra N, Salerno M, Cozzoli PD, Barone AC, Ceseracciu L, Pignatelli F, Carzino R, Marini L, Composites AA, Part B (2012) Thermal and mechanical characterization of poly(methyl methacrylate) nanocomposites filled with TiO2 nanorods. Engineering 43:3114
34. Lonjon A, Demont P, Dantras E, Lacabanne C (2011) Mechanical improvement of P(VDF-TrFE)/nickel nanowires conductive nanocomposites: Influence of particles aspect ratio. J Non-Cryst Solids 358:236
35. Ghasemi I, Azizi H, Naeimian N (2008) Rheological behaviour of polypropylene/kenaf fibre/wood flour hybrid composite. Iran Polym J 17(3):191
36. Yu L, Park JS, Lim Y-S, Lee CS, Shin K, Moon HJ, Yang C-M, Lee YS, Han JH (2013) Carbon hybrid fillers composed of carbon nanotubes directly grown on graphene nanoplatelets for effective thermal conductivity in epoxy composites. Nanotechnology 24:155604
37. Thongsang S, Vorakhan W, Wimolmala E, Sombatsompop N (2012) Dynamic mechanical analysis and tribological properties of NR vulcanizates with fly ash/precipitated silica hybrid filler. Tribol Int 53:134
38. Park DH, Lee YK, Park SS, Lee CS, Kim SH, Kim WN (2013) Effects of hybrid fillers on the electrical conductivity and EMI shielding efficiency of polypropylene/conductive filler composites. Macromol Res 21(8):905
39. Yoo TW, Lee YK, Lim SJ, Yoon HG, Kim WN (2014) Effects of hybrid fillers on the electromagnetic interference shielding effectiveness of polyamide 6/conductive filler composites. J Mater Sci 49:1701
40. Imoisili PE, Ukoba KO, Adejugbe T, Adgidzi D, Olusunle SOO (2013) Mechanical properties of rice husk/carbon black hybrid natural rubber composite. Chem Mater Res 3(8):12
41. Zhang Y, Zhang Q, Liu Q, Cheng H, Frost RL (2014) Thermal stability of styrene butadiene rubber (SBR) composites filled with kaolinite/silica hybrid filler. J Therm Anal Calorim 115:1013
42. Nugay N, Erman B (2001) Property optimization in nitrile rubber composites via hybrid filler systems. J Appl Polym Sci 79:366
43. Ismail H, Osman H, Jaafar M (2008) Hybrid-filler filled polypropylene/(natural rubber) composites: effects of natural weathering on mechanical and thermal properties and morphology. J Vinyl Addit Technol 14(3):142
44. Liu YB, Li L, Wang Q (2010) Reinforcement of natural rubber with carbon black/nanoclay hybrid filler. Plast Rub Compos 39(8):370
45. Sapkota J, Poikelispää M, Das A, Dierkes W, Vuorinen J (2013) Influence of nanoclay-carbon black hybrid fillers on cure and properties of natural rubber compounds. Polym Eng Sci 53 (3):615
46. Ismail H, Ramly AF, Othman N (2013) Effects of silica/multiwall carbon nanotube hybrid fillers on the properties of natural rubber nanocomposites. J Appl Polym Sci 2433
47. Nigam V, Setua DK, Mathur GN (2001) Hybrid filler system for nitrile rubber vulcanizates. J Mater Sci 36:43

Effect of Double Networking on Non-Linear Viscoelasticity of Elastomers

Yukun Chen and Chuanhui Xu

Abstract The nonlinear viscoelastic behavior of cured rubber is quite different from that of uncured compound, since the presence of crosslink networks. The factors for the influence of the crosslink networks on the nonlinear viscoelastic behaviors of cured rubbers are very complex and obscure. One of the reasons is that the crosslink networks may be consisted of several different types of networks. However, there are few literatures reporting the nonlinear viscoelastic behaviors of cured rubbers with mutle-networks. We reviewed the literatures dedicated to the topic of the non-linear viscoelasticity of simplest mutle-networks—double-network and summarized the useful information as much as possible in the present paper. Song's transient double-network model, double-network formed by twice curing and the specific crosslink network formed in metal salts of unsaturated carboxylic acids reinforced rubbers are introduced in detail.

Keywords Crosslink rubber • Double-network • Non-linear viscoelasticity

1 Introduction

The nonlinear viscoelastic behavior of elastomers is usually related to their inner structure interaction, namely, the interaction between the matrix molecules, the interaction between the matrix molecules and fillers, and the interaction between the fillers. Of course, the effect of characteristics of the inner structure on the nonlinear viscoelastic behavior of elastomers cannot be ignored, since it is also related to portion of the energy dissipated during dynamic deformation. For instance, the filler parameters are important which influence the dynamic properties of rubber compounds, dynamic hysteresis in particular, as well as their temperature

Y. Chen (✉)
School of Mechanical and Automotive Engineering, South China University of Technology, Guangzhou 510640, China
e-mail: cyk@scut.edu.cn

C. Xu
School of Chemistry and Chemical Engineering, Guangxi University, Nanning 530004, China

School of Materials Science and Engineering, South China University of Technology, Guangzhou 510640, China

D. Ponnamma, S. Thomas (eds.), *Non-Linear Viscoelasticity of Rubber Composites and Nanocomposites*, Advances in Polymer Science 264, DOI 10.1007/978-3-319-08702-3_7

dependence. The effect of filler morphology, namely, its fineness related to surface area and/or particle size and distribution; and its structure related to its aggregate irregularity of shapes and their distribution, has been investigated and reviewed [1]. In addition, the importance of surface characteristics in the dynamic properties of the filled rubbers has also been emphasized in the literature [2].

It is well known that a thin layer of rubber, which is at the surface of nano-fillers, e.g. silica or carbon black, is immobilized by chain adsorption. The estimated thickness of the immobilized layer, the rubber-filler interface, is in the range of two diameters of the monomer unit. Filler aggregates, which are covered by the interface, can be considered as multifunctional physical crosslinks. Traditionally, the physical rubber-filler network is characterized by the content of the apparent "bound" rubber [3], which is determined as the amount of unvulcanized rubber still adhering to the dispersed filler aggregates after extraction. Since the amount of bound rubber is related to the surface area and the surface activity of the fillers, this phenomenon provides indirect proof of a multicontact chain adsorption at the filler surface. The formation and the strength of the physical network influence nonlinear viscoelastic behavior of filled rubbers. Carbon black-filled rubbers show a typical nonlinear viscoelastic behavior [4]. At strains of about 1 %, a significant decrease of storage modulus occurs from the zero-strain value $G_0^{'}$ to a high amplitude plateau value $G_\infty^{'}$ connected with the appearance of a loss modulus G'' maximum [4]. This effect was described by Payne in the 1960s [5, 6], who interpreted this behavior as the result of breakage and reforming of physical bonds between the filler aggregates. These bonds were assumed to build filler agglomerates of different size and, above a certain threshold, an elastic filler-filler network within the rubber matrix. For a typical rubber compound, roughly half of the energy dissipation during cyclic deformation can be ascribed to the agglomerated filler, the rest coming from chain ends and internal friction. Empirical relations have been derived which relate the propensity of carbon black to agglomerate with the heat buildup of the rubber compound. Minimizing this hysteresis can be a major criterion in developing a rubber compound.

The nonlinear viscoelastic behavior of filled vulcanizates is somewhat different from that of filled compounds, since the chemical crosslink network of the rubber matrix is formed and, the physical rubber-filler networks and filler-filler networks are enhanced during curing at a relatively high temperature [7]. Speaking from a broad sense, filled vulcanizates can be viewed as a "double network" structure in which the nanoparticles supplement the inherent viscoelasticity of crosslink rubbers with additional physical network junctions.

In practice, the energy loss in filled vulcanizates during dynamic strain is of great importance, as for example, in vibration mounts and automotive tires where it affects the service performance of these products with regard to heat generation and fatigue life for the former, and rolling resistance, traction and skid resistance for the latter [2]. In fact, with regard to tire applications, it has been well established that repeated straining of the filled vulcanizates due to rotation and braking can be approximated as a process of constant energy input involving different

temperatures and frequencies. Since the discussion of viscoelastic behavior of the elatomers is based on the double network, it could be useful to briefly review some basic conceptions of "double network" in rubbers.

2 Transient Double-Network

2.1 Song's Transient Double-Network Model [8]

Song and coworkers [8] established a double-network model, which consisted of the segments, E and A-constituent chains, the polymeric chains entangled with other ones by multi-entanglement and polymeric chains connected to a great number of destructible particles by multi-adsorption, based on which the E and A-constituent chains could be recreated and released dynamically.

2.1.1 Entangled Network (E-Network) [8]

E-network model is based on that the entangled polymer chain may be decomposed into three and four-body constituent chains by entanglements as shown in Fig. 1a. The constituent chain by entanglement with different sizes is shown in Fig. 2a. They can be divided into the terminal or tail and loop forms which are located at the end and middle of polymer chain, respectively. The entangled segments with different lengths are tail and loop segments which are located at the end and middle of polymer chains, respectively.

2.1.2 Adsorbed Network (A-Network) [8]

A-network model is based on that the adsorbed polymer chain may be decomposed into (f-1) and f-body constituent chains by adsorption on filled particles as shown in Fig. 1b. The constituent chain by adsorption on filled particles with different sizes is shown in Fig. 2b. Similar to the E-network model, they may be divided into the terminal or tail and loop forms which are located at the end and middle of polymer chains, respectively. The adsorbed segments with different lengths have the tail and loop segments which are located at the end and middle of polymer chains, respectively.

The motion of polymer chains in a transient double network is controlled by the change of their conformations and the temporary topological constraints. For quantitatively describing the topological constraint (local entanglements and adsorptions) effect of polymer chains in the loop and terminal entanglement and adsorption spaces per polymer chain (or the average number of trapped and

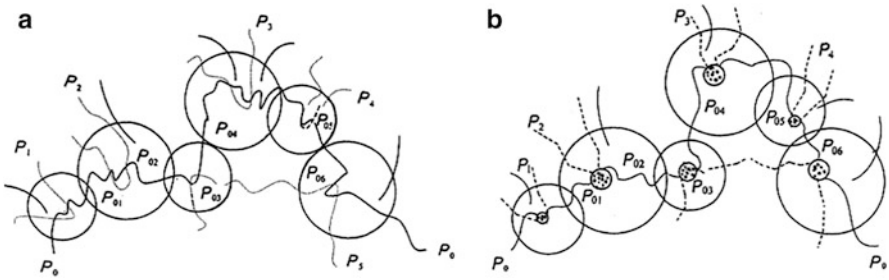

Fig. 1 (**a**) Schematic illustration of polymer chain in multiple entangled state [8] *solid line* is the testing polymer chain, in circle *dotted line* is the polymer segments of entanglements, in circle *broken line* is the tail polymer segments of entanglements (**b**) schematic illustration of polymer chain in multiple adsorptions state *solid line* is the testing polymer chain, in circle *dotted line* is the polymer segments for adsorption, in circle *broken line* is the tail polymer segments of adsorption, in circle æ is filler particle

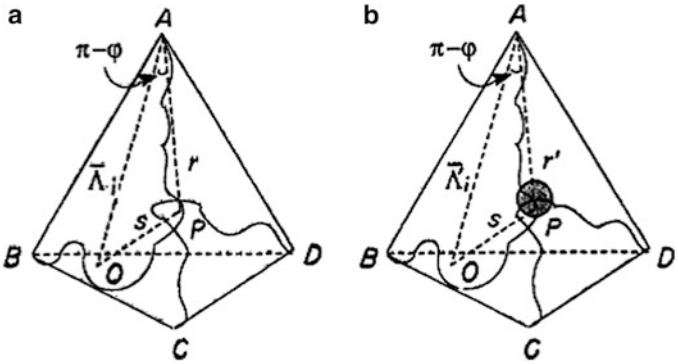

Fig. 2 Model of elementary constituent chain by entanglements (**a**) and adsorptions (**b**) in the double networks [8]

adsorbed segments in every loop and terminal constituent chains per polymer chain), the following structure parameters were introduced by Song [8]:

1. For the E-constituent chains:

$$\sum_{k=1}^{1} \text{N}_{1\text{kE}} = \sum_{m=1} \text{N}_{tmE} = 1 \tag{1}$$

$$a_E = \frac{4}{2}\sum_{k=1} \text{N}_{1\text{kE}} \;\; and \;\; m_E = \frac{3}{2}\sum_{m=1} \text{N}_{tmE} \tag{2}$$

The Eq. (1) is normal condition, the Eq. (2) (a_E and m_E) represents the average constrained dimensional number of loop and terminal E-constituent chains in the long loop and terminal entanglement spaces per polymer chain (or the degree of

freedom for disentanglement per loop and terminal E-constituent chain), where 4 is the number of trapped segments in each loop E-constituent chain, 2 is the number of polymer chains sharing a loop E-constituent chain; 3 is the number of trapped segments in each terminal E-constituent chain, $\text{N}_{1\text{kE}}$ and N_{tmE} are the fractions of the kth loop E-constituent chain in the total loop E-constituent chains and of the mth terminal E-constituent chain in the total terminal E-constituent chains.

2. For the A-constituent chain

$$\sum_{k=1} \text{N}_{1\text{kA}} = 1 = \sum_{m=1} N_{tmA} \tag{3}$$

$$a_A = \frac{f}{2} \sum_{k=1} \text{N}_{1\text{kA}} \quad and \quad m_A = \frac{f-1}{2} \sum_{m=1} N_{tmA} \tag{4}$$

Equations (3) and (4) have the same meanings as declared in Eqs. (1) and (2). f is the functionability of an adsorbed particle.

2.2 *Reputation Mechanism and Properties of Flow Curves [8]*

Song et al. [8] pointed out that there were two different interactions of hydrodynamic and non-hydrodynamic mechanics in polymeric suspensions. When they are continually subjected to a given strain with different deformation rates, the dynamic equilibrium polymeric chains will be made on motion and flow. During the motion the temporary topological constraints can be released and reformed by two kinds of different driving forces: one is the "Brownian motion of tail segments", the other is "the slipping and rupture of loop segments by deformation".

The motion of two kinds of polymer chains in the transient double network can be performed by the following different reputation mechanisms [8].

2.2.1 Reputation Mechanism of the Polymeric Chains and Dynamic Reorganization [8]

With continuous changes of deformation rate, the interactions of hydrodynamics among the entangled and adsorbed chains (point-chain) change continuously. Following five steps are introduced to describe the course that the constituent chains are destroyed and created continuously and dynamically:

1. Brown movement with rate constants μ_{tE} and μ_{ta} for disentanglement and disadsorption of terminal E and A-constituent chains.
2. Deformation with rate constants μ_{lE} and μ_{la} for disentanglement and disadsorption of middle loop E and A -constituent chains.

3. The average rate constants μ_{0E} and μ_{0a} for dynamic disentanglement and disadsorption for polymeric chains.
4. The average recreation rate constants μ_{rE} and μ_{ra} for the two kinds of polymer chains dynamically and reversely reentangled and readsorbed after the disentanglement and disadsorption.
5. With the above multiple dynamic and reversible reorganization (disentanglement and disadsorption, reentanglement and readsorption) of E and A-constituent chains on two kinds of polymer chains, the reputation mechanism leads to the displacement of mass center of polymeric chains and flow of fluids, and demonstrates relaxation spectrum and mechanical behaviors of polymeric suspensions. The corresponding rate constants are expressed as [8]:

$$\mu_{tE} = \left(\frac{G_{NE}^0}{\eta_{0E}}\right)^{1/m_E} \qquad \mu_{ta} = \left(\frac{G_{Na}^0 e^{\tau_\gamma \dot{\gamma}}}{\eta_{0a}}\right)^{1/m_a} \tag{5}$$

$$\mu_{1E} = \left(\frac{G_{NE}^0}{\eta_{0E\dot{\gamma}}}\right)^{a_E} \qquad \mu_{1a} = \left(\frac{G_{Na}^0 e^{\tau_\gamma \dot{\gamma}}}{\eta_{0a}}\right)^{m_a} \tag{6}$$

$$\mu_{0E} = \left(\frac{\eta_{0E}}{G_{NE}^0}\right)^{1/m_E} \left[1 + \left(\frac{\eta_{0E\dot{\gamma}}}{G_{NE}^0}\right)^{a_E}\right] \tag{7}$$

$$\mu_{0a} = \left(\frac{\eta_{0a}}{G_{Na}^0}\right)^{1/m_a} \left[1 + \left(\frac{\eta_{0E} e^{\tau_\gamma \dot{\gamma}} \dot{\gamma}}{G_{Na}^0}\right)^{a_a}\right] \tag{8}$$

where, μ_{0E} and μ_{0a} are average rate constants of the disentanglement and disadsorption, respectively; η_{0E}, η_{0a}, G_{NE}^0 and G_{Na}^0 are viscosity and elastic modulus of entangled and adsorbed chains at zero shear rate, respectively.

2.2.2 Destructibi1ity of Particle in Flowing System [8]

Generally, the hard filler is rigid particle which is hardly deformed. At low deformation rates, the non-hydrodynamic interactions of the particles will dominate the stress of polymeric suspensions. When the stress is larger than the forces of the non-hydrodynamic interactions of the particles, the deformation rates have a strong effect on the non-hydrodynamic interactions of the particles. In this time, the primary particles may be destructed into secondary particles. However, the rate of change in the number of secondary particles $n_{ia}(t)$ is depended both on the number of destructible particles and their coefficient of diffusion. As a result, the number of particles with increasing rate ($\dot{\gamma}$), the corresponding increase in the number of secondary A-constituent chains $n_{ia}(t)$ and modulus $G_{Na}^0(t)$ will be increased while the average constrained dimensional number of A-constituent chains (-ma) with increasing rate ($\dot{\gamma}$) is decreased. When the stress of fluids is equal to the force of non-hydrodynamic interactions of particles,

non-hydrodynamic interactions of particles is not sensitive to the deformation rates. A dynamic equi1ibrium state will be achieved between the stress and the force of non-hydrodynamic interactions of particles, then the number of particles and A-constituent chains have a given dynamic equilibrium value, and display a weak yielding property on the flowing curve. Song [8] also gives the kinetic equation (9) as

$$n_{ia}(t) = n_{ia}(o)e^{(\dot{\gamma}/D\gamma)} = n_{ia}(o)e^{P_e} = n_{ia}(o)e^{\tau_\gamma \dot{\gamma}} \tag{9}$$

where, P_e is Peclet number [9] of the particles, D_r is a coefficient [9] of diffusion rotation, τ_γ is rotation relaxation time, $\dot{\gamma}$ is the rate constant of deformation. Above forces of non-hydrodynamic interactions are also related to physical and chemical properties (shape, size and composition) of particles, interfacial properties between the particle and matrix, etc.

2.2.3 Flow Curve Properties in Steady Shear Flow [8]

There are four characteristic regions in the flow curve as given in Winter's work [10]: (1) low shear rate plateau; (2) apparent yielding; (3) intermediate rate plateau; and (4) shear thinning characteristic regions. The shapes and sizes of the regions change with changing physical and chemical properties of the particles, properties of interface between the particle and matrix, and polymer structure.

2.3 Statistical Conformation of Entangled and Adsorbed Chains [8]

Song et al. [8] also provided the distribution functions which are expressed as follows Eqs. (10) and (11):

$$P_{iNE}(t,R) = \sum_{m=1}^{n_{iE}} \frac{m!}{m(m-1)!} \left[\frac{1}{\Gamma(m_E)} \left(t-t'\right)^{m_E-1} \left(1 - P_{iE}\left(\tau, \overline{\Lambda}_{Ei}\right)\right) e^{-\mu_E\left(t-t'\right)} P_{iE}\left(\tau, \overline{\Lambda}_{Ei}\right) \right]^m$$
$$\left\{ 1 - \left[\frac{1}{\Gamma(m_E)} \left(t-t'\right)^{m_E-1} \left(1 - P_{iE}\left(\tau, \overline{\Lambda}_{Ei}\right)\right) e^{-\mu_E\left(t-t'\right)} P_{iE}\left(\tau, \overline{\Lambda}_{Ei}\right) \right]^m \right\}^{2/2} \left(t > t'\right) \tag{10}$$

$$P_{iNa}(t,R)=\sum_{m=1}^{n_{ia}}\frac{m!}{m(m-1)!}\left[\frac{1}{\Gamma(ma)}\left(t-t^{'}\right)^{m_a-1}\left(1-P_{ia}\left(\tau,\overline{\Lambda}_{ai}\right)\right)e^{-\mu_a\left(t-t^{'}\right)}P_{ia}\left(\tau,\overline{\Lambda}_{ai}\right)\right]^m$$
$$\left\{1-\left[\frac{1}{\Gamma(ma)}\left(t-t^{'}\right)^{m_a-1}\left(1-P_{ia}\left(\tau,\overline{\Lambda}_{ai}\right)\right)e^{-\mu_a\left(t-t^{'}\right)}P_{ia}\left(\tau,\overline{\Lambda}_{ai}\right)\right]^m\right\}^{2/2}\left(t>t^{'}\right) \tag{11}$$

They are fitted for the normalized conditions:

$$\begin{aligned}\int P_{iNE}(t,R)dR&=N_{iE}\\ \int P_{iNa}(t,R)dR&=N_{ia}\end{aligned} \tag{12}$$

$$N_T=\sum_{i=1}N_{ia}+\sum_{i=1}N_{iE}=N_{Ta}+N_{TE} \tag{13}$$

$$\xi_T=\sum_{i=1}\sum_{i=1}\left(\xi_{iE}N_{iNE}+\xi_{ia}N_{iNa}\right) \tag{14}$$

where, N_T is the total number of polymeric chains in the system, ξ_T is the total number of effective elastic chains in the system, N_{TE} and N_{Ta} are the total numbers of entangled and adsorbed chains in the system, respectively; $\Gamma(mE)$ and $\Gamma(ma)$ are Euler Gamma functions of m_E and m_a, respectively; ξ_{iE} and ξ_{ia} are the numbers of effective elastic chains on the i kind of polymeric chains, respectively. In Eqs. (10) and (11), $\left[\frac{1}{\Gamma(m_E)}\left(t-t^{'}\right)^{m_E-1}\left(1-P_{iE}\left(\tau,\overline{\Lambda}_{Ei}\right)\right)e^{-\mu_E\left(t-t^{'}\right)}P_{iE}\left(\tau,\overline{\Lambda}_{Ei}\right)\right]$ and $\left[\frac{1}{\Gamma(ma)}\left(t-t^{'}\right)^{m_a-1}\left(1-P_{ia}\left(\tau,\overline{\Lambda}_{ai}\right)\right)e^{-\mu_a\left(t-t^{'}\right)}P_{ia}\left(\tau,\overline{\Lambda}_{ai}\right)\right]$ represent the probabilities of every single E and A-constituent chain to be reorganized, respectively, therefore, $\left\{1-\left[\frac{1}{\Gamma(m_E)}\left(t-t^{'}\right)^{m_E-1}\left(1-P_{iE}\left(\tau,\overline{\Lambda}_{Ei}\right)\right)e^{-\mu_E\left(t-t^{'}\right)}P_{iE}\left(\tau,\overline{\Lambda}_{Ei}\right)\right]^m\right\}$ and $\left\{1-\left[\frac{1}{\Gamma(ma)}\left(t-t^{'}\right)^{m_a-1}\left(1-P_{ia}\left(\tau,\overline{\Lambda}_{ai}\right)\right)e^{-\mu_a\left(t-t^{'}\right)}P_{ia}\left(\tau,\overline{\Lambda}_{ai}\right)\right]^m\right\}$ represent the probabilities of the tail segments lying on the both ends of testing polymeric chain. When $P_{iNa}<1$, $P_{iNE}<1$, and summation of Eqs. (10) and (11) by geometric series, they can be simplified to be Eqs. (15) and (16):

$$P_{iNE}(t,R)=\frac{1}{\Gamma(m_E)}\left(t-t^{'}\right)^{m_E-1}e^{-\mu_E\left(t-t^{'}\right)}p_{iE}\left(\tau,\overline{\Lambda}_{Ei}\right) \tag{15}$$

$$P_{iNa}(t,R)=\frac{1}{\Gamma(ma)}\left(t-t^{'}\right)^{m_a-1}e^{-\mu a\left(t-t^{'}\right)}pa\left(\tau,\overline{\Lambda}_{ai}\right) \tag{16}$$

For a transient double-network at deformation, the distribution functions of statistical conformation for two kinds of chains are obtained after introducing a condition of affine deformation, which is shown as follow:

$$P^*_{iNE}(t,R,a) = aP_{iNE}(t,R) \tag{17}$$

$$P^*_{iNa}(t,R,a) = aP_{iNa}(t,R) \tag{18}$$

2.4 Viscoelastic Free Energy of Deformation for Polymeric Suspensions [8]

Song described the total free energy of viscoelasticity for polymeric suspensions as Eqs. (19) and (20) [8]:

$$\Delta F_T = kTN_{Ta}\Big[e^{\tau_\gamma\dot{\gamma}}\frac{1}{\Gamma(m_a)}\Big(t-t^{'}\Big)^{ma-1}e^{-\mu_a\left(t-t^{'}\right)}\left(C^a_{100}I_I + C^a_{020}I_{II} + C^a_{200}I_{III}\right)$$

$$+N_{TE}\frac{1}{\Gamma(mE)}\Big(t-t^{'}\Big)^{mE-1}e^{-\mu_E\left(t-t^{'}\right)}\left(C^E_{100}I_I + C^E_{020}I_{II} + C^E_{200}I_{III}\right)\Big] \tag{19}$$

$$I_I = a_x^2 + a_y^2 + a_z^2, \quad I_{II} = \ln\Big[1/3\left(a_x^2 + a_y^2 + a_z^2\right],$$

$$I_{III} = \left(a_x^2 + a_y^2 + a_z^2\right) - 9 \tag{20}$$

where, $C^E_{100} = 1/2kT\xi_E B^E_{100}$, $C^E_{200} = 1/2kT\xi_E C^E_{200}$, $C^E_{020} = 1/2kT\xi_E D^E_{020}$, $C^a_{100} = 1/2kT\xi_a B^a_{100}$, $C^a_{200} = 1/2kT\xi_E C^a_{200}$, $C^a_{020} = 1/2kT\xi_a D^a_{020}$. These parameters are related to the structure of polymers and filled particles. Their meanings and expressions can be found in the literatures [11, 12].

2.5 Relationship Between Stress and Strain [8]

The relationship between stress and strain can be determined by the relation of $\tau = (\partial\Delta F_T/\partial_a)_N$

1. Uni-axial extension $\tau = f/A_0$

$$\tau = N_{TN}\frac{1}{\Gamma(m_E)}\Big(t-t^{'}\Big)^{mE-1}e^{-\mu_E\left(t-t^{'}\right)}$$

$$\cdot\, 2\left(a-a^{-2}\right)\Big[C^E_{100} + C^E_{020}\left(a^2+2/a\right)^{-1} + 2C^E_{200}\left(a^2+2/a\right)\Big]$$

$$+ N_{Ta}e^{\tau_\gamma\dot{\gamma}}\frac{1}{\Gamma(ma)}\Big(t-t^{'}\Big)^{ma-1}e^{-\mu_a\left(t-t^{'}\right)}$$

$$\cdot\, 2\left(a-a^{-2}\right)\Big[C^a_{100} + C^a_{020}\left(a^2+2/a\right)^{-1} + 2C^a_{200}\left(a^2+2/a\right)\Big] \tag{21}$$

2. Equi-biaxial extension ($\tau_x = \tau_y = \tau, \tau_z = 0$)

$$\begin{aligned}\tau = {} & N_{TE}\frac{1}{\Gamma(m_E)}\left(t-t'\right)^{mE-1}e^{-\mu_E\left(t-t'\right)} \\ & \cdot 2\left(a^3+2\right)\left(a-a^{-5}\right)\left[C^E_{100}+C^E_{020}\left(2a^2+a^{-4}\right)^{-1}+2C^E_{200}\left(2a^2+a^{-4}\right)\right] \\ & + N_{Ta}e^{\tau_\gamma\dot{\gamma}}\frac{1}{\Gamma(ma)}\left(t-t'\right)^{ma-1}e^{-\mu_a\left(t-t'\right)} \\ & \cdot 2\left(a^3+2\right)\left(a-a^{-5}\right)\left[C^a_{100}+C^a_{020}\left(2a^2+a^{-4}\right)^{-1}+2C^a_{200}\left(2a^2+a^{-4}\right)\right] \end{aligned} \quad (22)$$

3. Pure shear $\tau_x = \tau, \tau_y = 0, a_z = 1$

$$\begin{aligned}\tau = {} & N_{TE}\frac{1}{\Gamma(m_E)}\left(t-t'\right)^{mE-1}e^{-\mu_E\left(t-t'\right)} \\ & \cdot 2\left(1+a^2\right)\left(a-a^{-3}\right)\left[C^E_{100}+C^E_{020}\left(2a^2+a^{-2}+1\right)^{-1}+2C^E_{200}\left(a^2+a^{-2}+1\right)\right] \\ & + N_{Ta}e^{\tau_\gamma\dot{\gamma}}\frac{1}{\Gamma(ma)}\left(t-t'\right)^{ma-1}e^{-\mu_a\left(t-t'\right)} \\ & \cdot 2\left(1+a^2\right)\left(a-a^{-3}\right)\left[C^a_{100}+C^a_{020}\left(2a^2+a^{-2}+1\right)^{-1}+2C^a_{200}\left(a^2+a^{-2}+1\right)\right] \end{aligned} \quad (23)$$

3 Controlled Double Networks

3.1 Double Networks Formed by Single Chemical Bond: Orientated Crosslinking

In a special sense for rubbers, a double-network means the crosslink networks which are formed by twice curing but constructed by the same chemical bond. This kind of double networks can be viewed as interpenetrating polymer networks in which the same chain segments belong to both networks and, more importantly, the component networks are oriented. After an initial, isotropic crosslinking, the rubber is stretched and maintained at the stretching state, being crosslink once again. Since the second cure results in permanent set, double networks can be obtained by design the crosslink density and stretching ratio. Control of the orientation and crosslink apportionment yields higher modulus, which enable the resultant products obtain the good compromise between elastomer stiffness and strength. Many studies have been carried out on this kind of double networks, including their use to evaluate the contribution of trapped entanglements to rubber elasticity and their wonderful equilibrium in stiffness and strength. Double networks can also arise spontaneously via chain scission, via strain-induced crystallization, or in the presence of reinforcing fillers [13–33].

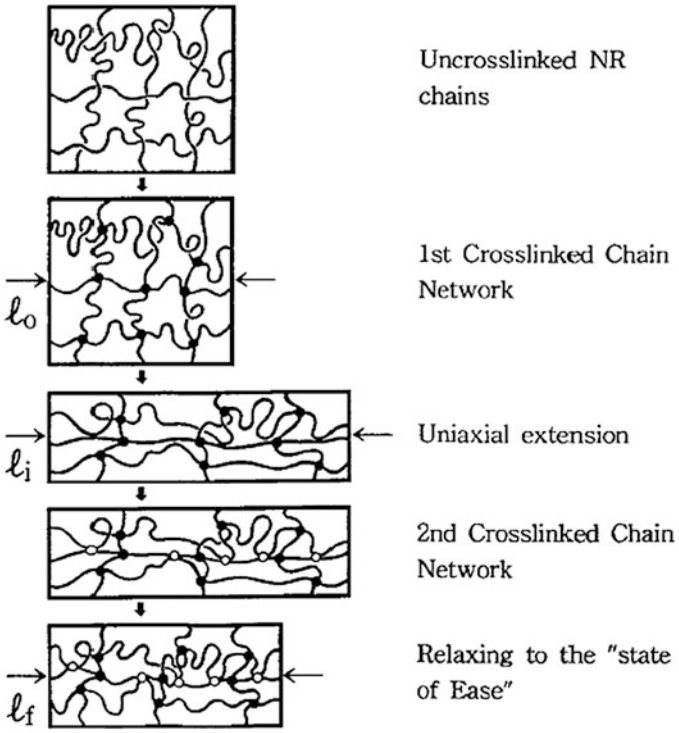

Fig. 3 Sketch of formation of the double-network structure [32]

Obviously, this kind of double networks differ to the former introduced transient double-network. The controlled double networks exhibit anisotropic properties, and are usually characterized in terms of their residual stretch ratio, λR, equal to the ratio of their length along the stretch direction of the second cure to the initial length (prior to the second curing, or equivalently, in the uncured state). However, λR does not uniquely define a double network, as different cure strains and crosslink apportionment between the two networks can yield the same residual strain, but different mechanical properties [32]. Figure 3 shows a schematic diagram of a possible change in the network structure of NR during vulcanization.

3.2 Payne Effect in Double Networks [34]

Generally speaking, the modulus of a double network rubber will higher than the modulus of the corresponding isotropic rubber: the higher residual strains, the higher equilibrium modulus [33]. It is well known that rubber hysteresis is the primary energy loss mechanism of a rolling tire, and thus intensive mixing of rubber and fillers to disperse and distribute the filler aggregates is a common useful method

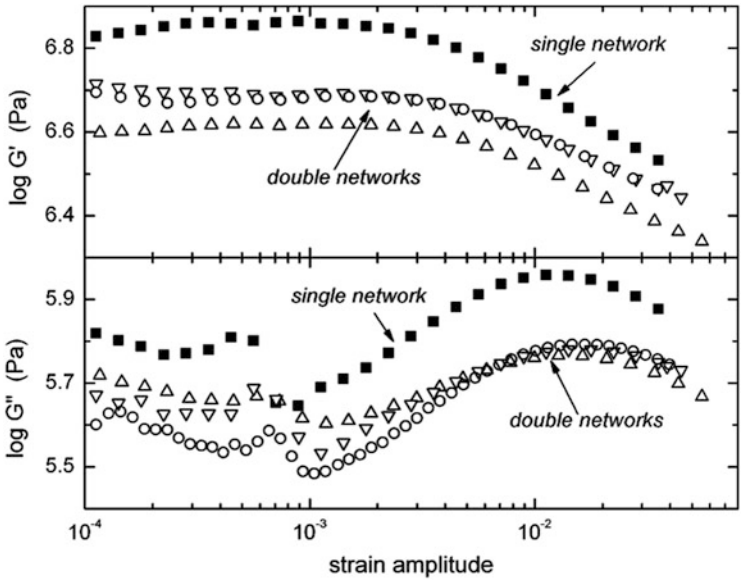

Fig. 4 Dynamic storage (*upper panel*) and loss (*lower panel*) moduli of single network ($\lambda R = 1$, *filled symbols*) and double networks [$\lambda R = 1.34$ (*open triangle*); $\lambda R = 1.67$ (*open circle*); $\lambda R = 2.00$ (*inverted triangle*)], measured using torsional shear of ring samples at 10 Hz and 30 °C. The plateau in G′ is due to flocculated filler, the disruption of which at higher strain gives rise to the maximum in G″. The magnitude of these two characteristic features is smaller, reflecting less carbon black agglomeration, in the double networks. The structure in the loss moduli data below ca. 0.1 % strain is an instrumental artifact [34]

for minimizing the agglomeration and obtaining good mechanical properties. Crosslinking of a double network after straining may stabilize the de-agglomerated filler network, which contributes to lower rubber hysteresis. Wang et al. [34] employed different test mode to investigate the Payne effect of peroxide cured and sulfur-cured double networks of the carbon black filled rubber. They found that the Payne effect is reduced after introducing double networks. This result can be found in different elastomers.

Figure 4 shows the dynamic storage (G′) and loss (G″) moduli of peroxide cured carbon black filled rubber which was measured in shear for two double networks having respective $\lambda R = 1.34$, 1.67 and 2.00, along with data for a single network ($\lambda R = 1$). Payne effect can be observed in both single and double networks, reflecting the carbon black network is formed even in the peroxide cured double networks for a $\lambda R = 2.00$. However, the Payne effect of the double networks is obvious weaker than that of the single network. Wang et al. [34] also pointed out that the plateau in G′ and the maximum in G″ of double networks were one-third lower than that of single network and all these results showed that the carbon black agglomeration was reduced in the double networks. Another finding by Wang is that the magnitude of this reduction does not depend on the residual strain of the double network; any differences in the degree of filler deagglomeration are within

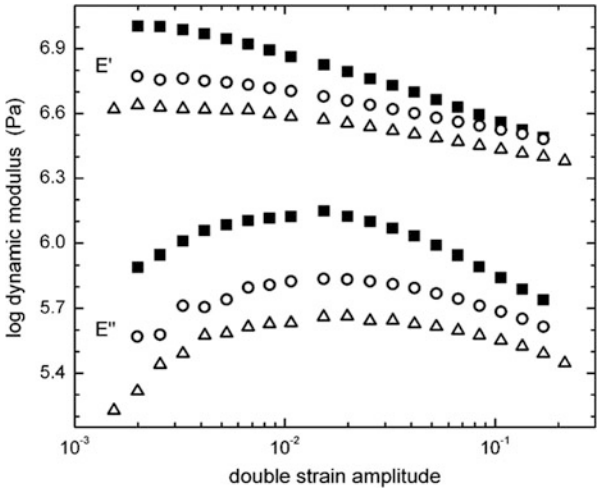

Fig. 5 Dynamic storage (*upper curves*) and loss (*lower curves*) moduli of two double networks [NR-D2 (*open circle*); NR-D4 (*open triangle*)] and the corresponding single network (*filled square*), measured in tension, applied parallel to the orientation of the double network at 0.1 Hz and RT [34]

the experimental scatter. The data in Fig. 4 were obtained on ring samples, sheared in the plane of the double network orientation [34].

Generally, the mechanical properties of double networks exhibit some anisotropy, Roland and Peng [16] investigated the electrical properties of carbon black filled double networks, finding that the electrical conductivity was lower than for single networks. After an initial minimum at low strains, however, the conductivity of the double networks increased more strongly with strain. Hamed and Huang [17] observed highly anisotropic mechanical properties in natural rubber double networks containing carbon black, the tensile and tear strengths being higher for deformations parallel to the orientation. Thus Wang [34] also investigated the Payne effect for other deformation modes. Figure 5 shows the results for biaxial tension, showing a reduction in both the E′ and E″ for the double network. In both twisted mode and tension mode, the dynamic strain associated with breakup of the filler network is not affected by the presence of the double network, but the Payne effect is apparent reduced. This is due to the residual strain which is always much greater than the strain (about 1 %) associated with disruption of the filler network. During the formation of double network, the stretching during the second cure disrupts the filler-filler networks in the rubber matrix. At least a part of the deflocculated filler-filler networks or filler structures can be stabilized by the second crosslinking to a certain extent, resulting in a substantially reduced mechanical hysteresis of rubber. The recovered filler-filler networks or filler structures will be response to the resultant Payne effect.

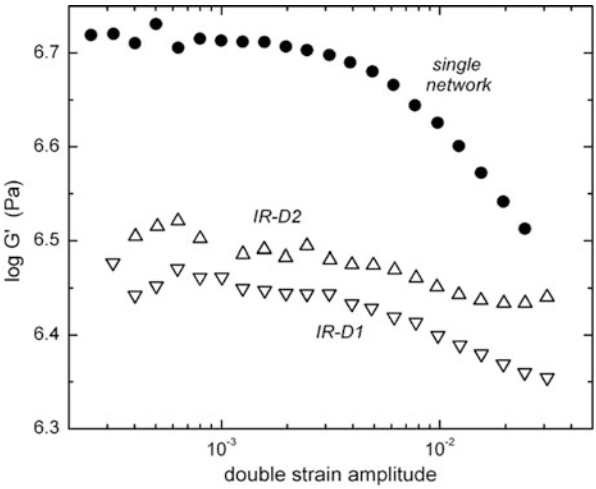

Fig. 6 Dynamic storage modulus of double networks (*hollow symbols*) and the corresponding single network (*filled symbols*), measured using torsional shear of rectangular strips at 1 Hz and RT. The absence of a filler network in the double networks occasions the disappearance of the strain-dependent plateau [34]

The reduction in both the storage and loss moduli for the double network is not only found in the peroxide-cured double networks, the effects described above are also observed in sulfur-cured double networks. Wang et al. [34] produced a sulfur-cured double networks using synthetic cis-1,4-polyisoprene (IR-1, $\lambda R = 1.15$ and IR-2, $\lambda R = 1.30$). The measurements were carried out differently, via torsion of a rectangular strip. This deformation involves bending as well as shear modes perpendicular to the double network principle orientation. The G' for the two double networks and a (control) single network are shown in Fig. 6. In comparison to the isotropic sample, the double networks exhibit a marked reduction in the plateau associated with the filler network. Compared with the peroxide-cured double networks, the sulfur-cured double networks having a larger residual strain appear to have a weaker Payne effect. The trivial variations may be related to the preparation and processing of the materials, but no consistent trend with λR was observed [34].

It is noteworthy that there is orientation along the stretching direction during the second cure. However, the lower dynamic hysteresis observed by Wang [34] is independent of the deformation direction: dynamic measurements using three different geometries—shear (in the plane of the double network principle orientation), uniaxial extension (parallel to the orientation of the double network), and torsion (combining bending and shear deformations). For all cases, the double networks showed lower hysteresis. Thus, the import of a double network structure may be a generally useful approach to more energy efficient elastomers.

4 Three-Network Concept

In a filled rubber, agglomeration of the particles produces a filler network, in addition to the network of covalently-bonded polymer chains. In fact, Reichert et al. [30] modeled the deformation of single network of filled rubber as a double network, adopting an approach similar to that used to analyze unfilled double networks [35–37]. This implies that double-network rubber reinforced with filler can be viewed as a composite of three distinct networks.

5 Double Network in Metal Salts of Unsaturated Carboxylic Acids Reinforced Rubbers [38–59]

Another type of double network is that the constituted networks are formed by different chemical bonds, namely covalent bond and ionic bond. The typical representative of this kind of double network is the metal salts of unsaturated carboxylic acids reinforced rubbers. This kind of metal salts can be polymerized during the vulcanization of rubber matrix in the present of free radicals. The ionic crosslinks are formed by metal salts graft-polymerized onto the rubber chains because of large numbers of ion pairs in polymerized metal salts molecules and the strong electrostatic interaction between ion pairs, while the polymerized metal salts repulse from the rubber matrix, forming nano-size particles. Thus, the crosslink network contains covalent crosslinks and ionic crosslinks [38–52]. Chen and Xu [53–59] have commenced a series of studies on the crosslink network of zinc dimethacrylate (ZDMA) and magnesium dimethacrylate (MDMA) reinforced rubbers. They found that a developed ionic crosslink network can be formed in the ZDMA or MDMA reinforced natural rubber (NR) at high filler contents. The ionic crosslink network exerts a strong influence on the non-linear viscoelasticity of NR.

5.1 Viscoelasticity of Uncured NR/ZDMA Compounds

In the uncured NR/ZDMA compounds, the interaction between ZDMA-ZDMA is very weak since the ZDMA particles are micrometer grade. They may agglomerate and even form a filler-filler network at high loading. This filler-filler network is somewhat similar to the CB network (in fact, the CB rigid network is much stronger than the ZDMA network) but so weak that it can be disrupted at low shear strain amplitudes. Figure 7 shows the G' and G'' versus the strain for the uncured NR/ZDMA compounds. The compounds having higher content of ZDMA exhibit strong dependence of G' on shear strain, showing the severe disruption of filler-filler interaction. More agglomeration or filler-filler network structure are formed at high loading of ZDMA, thus more energy dissipated during the rupture of the filler

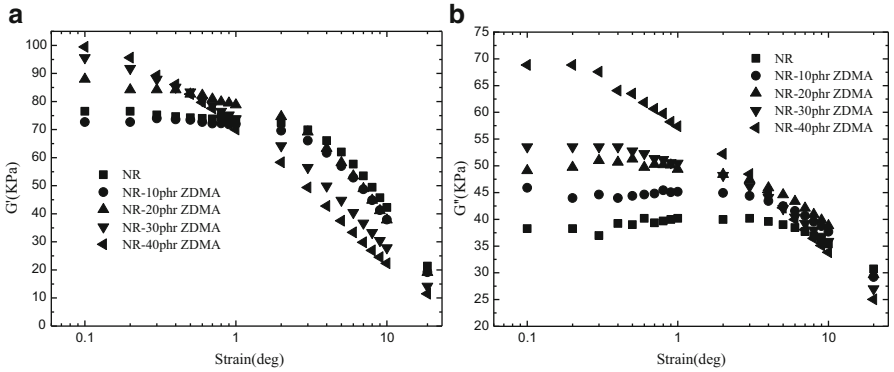

Fig. 7 Strain sweep on NR/ZDMA compounds, test temperature 60 °C and frequency 1 Hz [57]

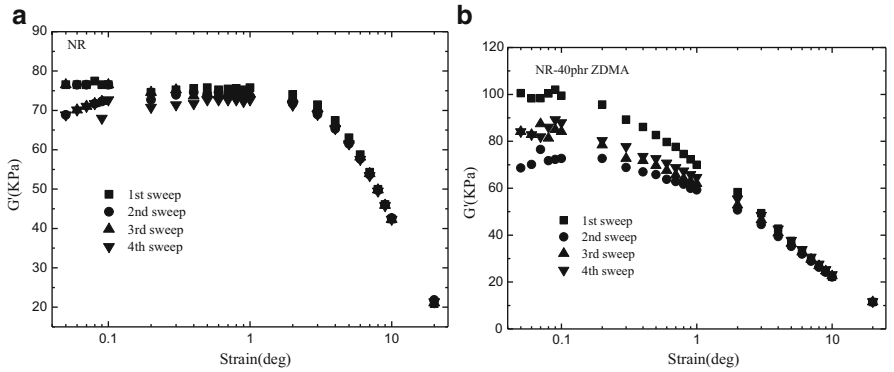

Fig. 8 Stress-softening of G′ of NR/ZDMA compounds, test temperature 60 °C and frequency 1 Hz [58]

structures at low shear strain region, resulting in a higher value of G″. At larger strain region (around 10°), the weak filler structures have been destroyed completely. In this case, the micro-size particles of ZDMA played a dilution effect on rubber chains, resulting in a lower G″ at higher ZDMA loading [57].

Chen and Xu [58] studied the G′ of uncured NR/ZDMA compounds during consecutive strain sweeps (Fig. 8). After the first sweep, the rupture of the weak filler-filler network formed by high load of ZDMA leads to an apparent softening behavior. However, the polarity of ZDMA and the softened rubber molecules by first sweep are beneficial to accelerate the aggregation of ZDMA, resulting in a subsequent interesting behavior that the G′ of third and forth sweep showing an increase [58].

5.2 *Viscoelasticity of NR/ZDMA Vulcanizate*

The non-linear viscoelasticity of NR/ZDMA vulcanizate is quite different from that of uncured compound. During the vulcanization, the polymerization of ZDMA leads to an increase molecular weight of poly-ZDMA. When the molecular weight of poly-ZDMA exceeds the critical value, the poly-ZDMA chains separate from the NR matrix and aggregate to nano-scaled particles, leading to a pronounced Payne effect. At the same time, the ionic crosslinks introduced by poly-ZDMA function as "soft interaction" between particles-rubber molecules, resulting a complex crosslink structure. In the present of ionic crosslinks, the NR/ZDMA vulcanizates shows a different mechanism of the Payne effect.

The crosslink density of the metal salts of unsaturated carboxylic acids reinforced rubbers is usually determined by equilibrium swelling experiments. To distinguish ionic crosslinks from covalent crosslinks, vulcanizate is first swollen in toluene to determine the total crosslink density V_r. Then, the swollen sample is transferred into a mixture of toluene/chloroacetic acid or acetone/hydrochloric acid to cut off the ionic crosslinks. Finally, covalent crosslink density V_{r1} can be calculated. Thus V_{r2}, which is calculated by subtracting V_{r1} from V_r, is used to represent the ionic crosslink density. A classic crosslink density corresponding to the concentration of ZDMA is shown in Fig. 9. The total crosslink density and the ionic crosslink density show a significant increase with increasing ZDMA content, whereas the covalent crosslink density decreases slightly [60].

After vulcanization, the chemical crosslinks network is formed, which largely enhance the mechanical properties of rubber. The poly-ZDMA nano-particles dispersed in NR matrix, yielding a pronounced Payne effect. As shown in Fig. 10, the linear viscoelastic region (LVE) of vulcanizate with high loading of ZDMA corresponded to an elastic modulus independent to deformation, which can be observed at middle strain amplitudes (even to 1°, equal to ≈14 %). This

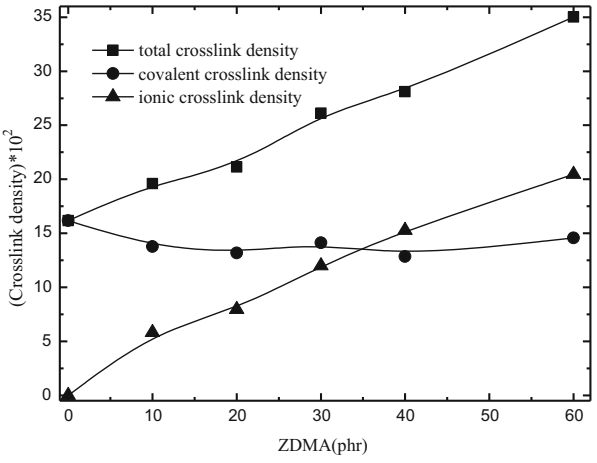

Fig. 9 Typical crosslink density corresponding to the concentration of ZDMA [60]

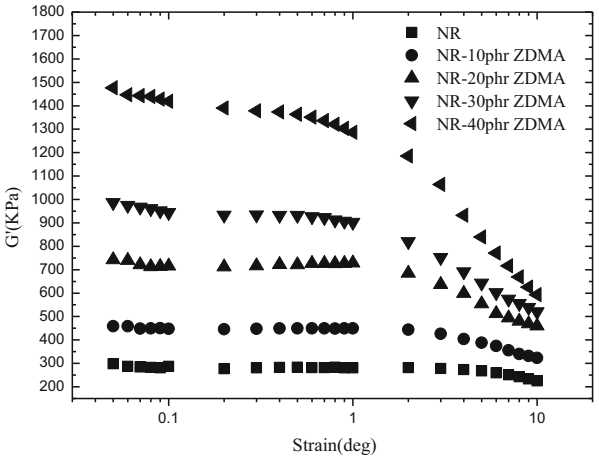

Fig. 10 G′-strain curve of NR/ZDMA vulcanizates, test temperature 60 °C and frequency 1 Hz [58]

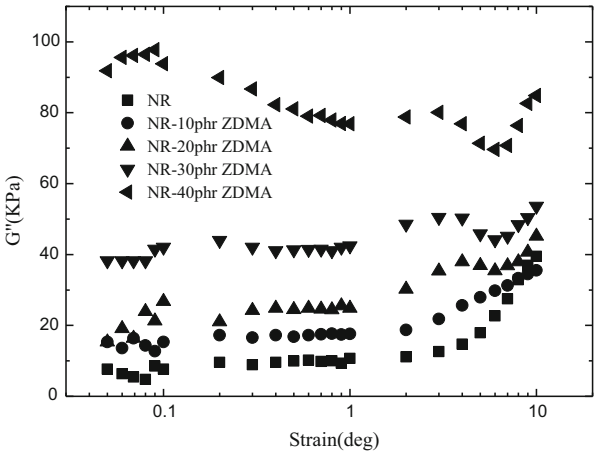

Fig. 11 G″-strain curve of NR/ZDMA vulcanizates, test temperature 60 °C and frequency 1 Hz [58]

experimental result demonstrates that a developed and strong filler network has been formed in the vulcanizate. Generally, the stronger the rebuilt ability of the filler network, the higher the strain amplitudes to break down the filler network. However, this is not applicable to the NR/ZDMA vulcanizate since the LVE region is too long [58]. Strain of 14 % is a large value for the filler-filler interaction, because most of the rigid filler-filler structures have been ruptured at a strain much lower than 14 %.

The ionic crosslinks are easy to slip during the deformation. Energy dissipates in this process, leading to an increase in G″. The ionic crosslink network can be formed at certain ZDMA content, namely more than 20 phr. As shown in Fig. 11, small loss peak, appeared at about 3° strain amplitude, is regarded as the energy dissipated involving ionic crosslinks slippage (deformation of ionic crosslink

network) and rubber covalent crosslinks deformation. For the sample with 10 phr ZDMA, the developed ionic network is not formed, since the sample with 10 phr ZDMA and NR gum do not show such a loss peak. At high strain amplitudes (near 10°, equal to ≈ 140 %), more energy dissipated in deforming of the rubber crosslink network, thus G″ show an apparent increase [58]. Compared to uncured compounds, the vulcanizates yield much higher G′ and G″ because of the chemical crosslinks and nano polymerized ZDMA.

When the strain amplitude increases to a certain degree, both the covalent and ionic crosslink networks will be stretched to be deformed. At this moment, some debondings may occur similar to the situation of carbon black [61, 62], since the presence of nano-particles of poly-ZDMA. Moreover, lots of ionic bonds will be slipped and simultaneously, new ionic crosslinks can be formed rapidly [61]. This instantaneous ionic crosslink network can adapt to the status and cease back to the initial structure. This results in a weak recovery and a high softening behavior of G′ at high ZDMA loading. The weak recovery of G′ is attributed to the reconstruction of poly-ZDMA nano-particle network and the elastic NR crosslink network. However, in the case of conventional reinforcing filler such as CB [61, 63], the reconstruction of the CB filler-filler structures results in a remarkable recovery of G′. The results of consecutive strain sweeps for NR/ZDMA vulcanizates are shown in Fig. 12 [58]. After three consecutive scans at 60 °C, the temperature was firstly raised to 100 °C and kept for 30 min. After that, the sample was kept intact within the confinement of the cavity of RPA 2000 and the temperature was reduced to 60 °C to undergo the forth scan. The sample was kept at 100 °C isothermally for 30 min, in order to accelerate the recovery of stress-softening. Differing to the uncured compounds, the vulcanizates showed an apparent stress-softening behavior. After the first scan, the LVE region of vulcanizates was shorten with increasing ZDMA, the recovery degree of G′ at the forth scan was also reduced with increasing ZDMA. Thus, Chen and Xu [58] attributed it to the disrupture of the developed ionic crosslink network during the stretching or tearing. After the first sweep, the disappearance of the LVE region of 30 phr and 40 phr ZDMA revealed that the rigid filler-filler network became fractured that initiated the sharp decrease of modulus at low strain amplitude. This demonstrated that a more developed ionic crosslink network might handicap the reformation of filler-filler networks.

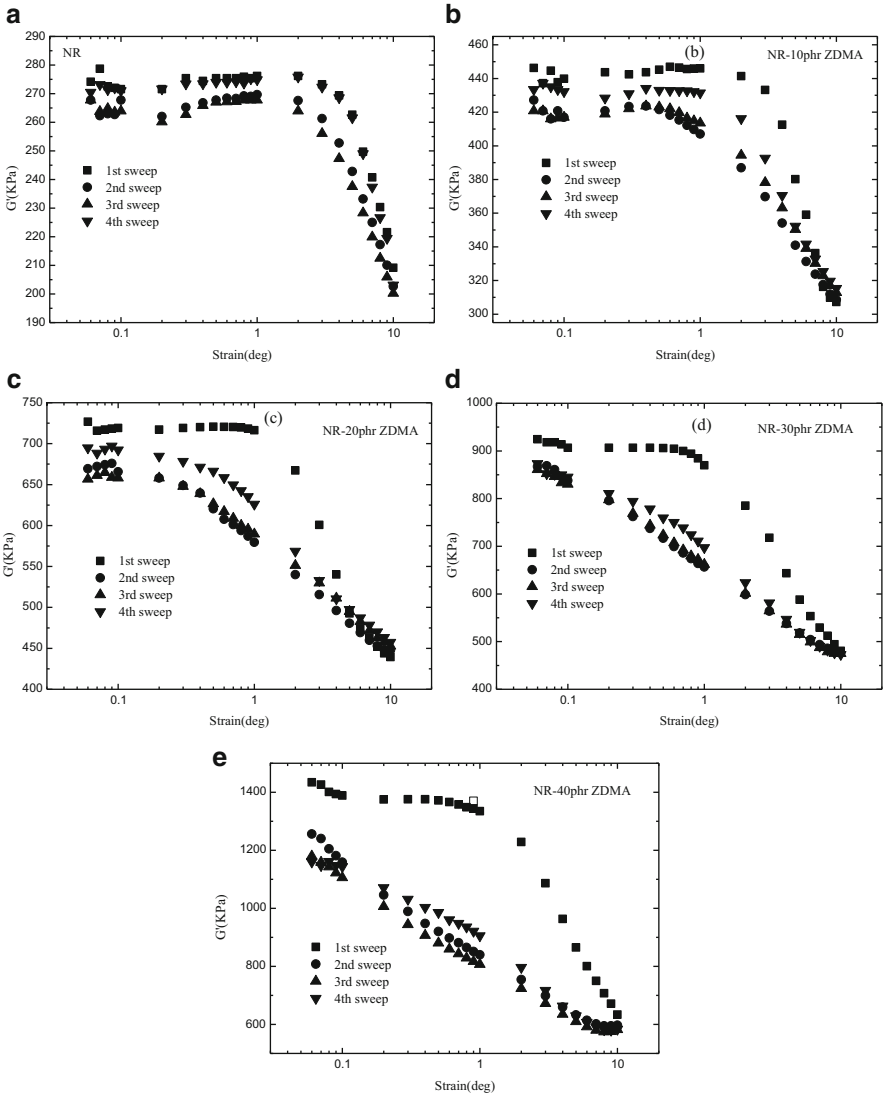

Fig. 12 Stress-softening of G′ of NR/ZDMA vulcanizates, test temperature 60 °C and frequency 1 Hz [58]

5.3 A Simple Discussion on the Possible Networks Deformation in the Dynamical Strain Sweep

Chen and Xu [58] thought that the ionic crosslinks resulted in an obscure mechanism of the Payne effect of the NR/ZDMA vulcanizates. They chose the NR vulcanizate with 30 phr ZDMA as an instance to illustrate a tentative district of

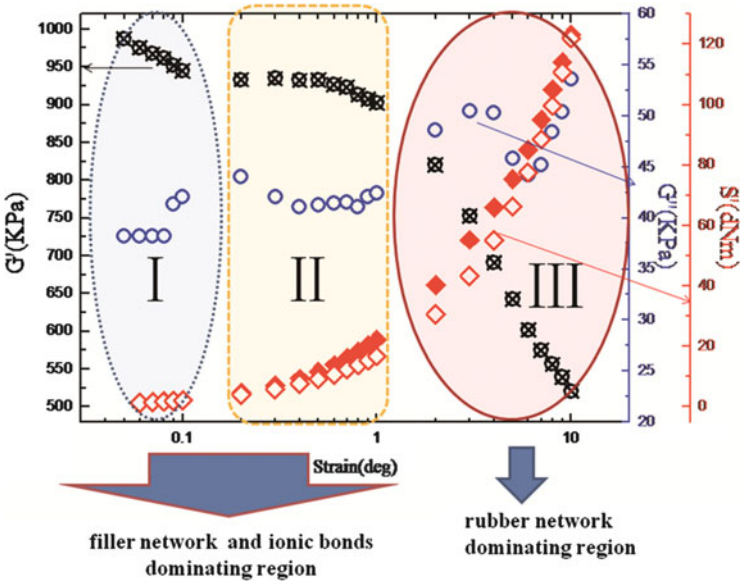

Fig. 13 Illustration of the different mechanism dominating regions on strain [58]

networks deformation during dynamic strain sweep. As shown in Fig. 13, the strain amplitude is divided into two major regions [58]:

1. It was well known that, using black carbon as a reinforcing filler, a rigid three-dimensional network was formed which contributes mainly to the modulus of composites. At a very small strain (below 1 %), the filler network could not be fractured. With the increase of strain amplitude, the rigid filler network became fractured, which initiated the sharp decrease of modulus. Generally speaking, the apparent decrease occurred at about 1 % strain [63] which was equal to about 0.07° in RPA2000. In the region from 0 to about 0.1° in Chen's experiment, the filler structure seemed weak because the drop of G′ was remarkable this strain amplitude region. The drop the G′ was due to the rupture of poly-ZDMA aggregates network. Chen explained that the developed ionic crosslinks maintain the instantaneous structure, which was not favorable to rebuild the poly-ZDMA network. The first loss peak appeared at about 0.1° strain amplitude was a good support of energy dissipating caused by rupture of poly-ZDMA aggregates network, at least to some extent. They proposed that a developed and strong filler-filler network was formed because of a "LVE region" appeared in the region from about 0.1° to 1°. In fact, this "LVE region" was mainly due to the slippage and exchange reaction of ionic bonds under the dynamical stress instead of rebuilt of poly-ZDMA aggregates network. The ionic crosslinks were considered to play an important role in the remarkable mechanical properties of NR/ZDMA composites. See the stress-softening behavior of S′ (elastic torque) starting at the strain amplitudes exceed 0.1°. This demonstrated that the crosslink network was got involved in the deformation of structure at such a strain amplitude. Furthermore,

the G′ of a black carbon filled rubber vulcanizate [63] generally shows a notable drop in the region from about 0.1° to 1° which is equal to about 1.4 % to 14 %. Generally speaking, the rupture of rubber covalent crosslink could not take place at this strain. Therefore, the "LVE region", observed in the region from about 0.1° to 1°, is related to the action of the ionic bonds. However, it is difficult to distinguish the filler network effect and ionic bonds effect, thus they summarized the two types network deformation together.

2. The rubber network deformed when the strain amplitudes exceeded about 1°. G′ decreased to a low level which was mainly contributed by rubber matrix at this time. G″ and elastic torque (S′) showing an abrupt increase at the high strain amplitudes was associate with the rubber network deformation. The second loss peak locating in this region was mainly attributed to the complex results in combination of ionic crosslinks and rubber covalent network.

5.4 *The Non-Linear Viscoelasticity of the NR/ZDMA Composites at the Initial Stage of Curing*

Chen and Xu [60] found that a primary "ionic crosslink network" was formed at the initial stage of curing. At this time, the continuous covalent crosslink network of the NR matrix was not formed; the whole "crosslink network" is dominated by ionic crosslinks. As shown in Chen and Xu's studies [60], the initial curing time is about in the first 1 min. The ionic crosslinks, with some physical crosslinks and primary covalent crosslink points, construct the crosslink backbone in this period. Although there are very small amounts of covalent crosslink points, they can not constitute a fundamental covalent network. Because of the formation of poly-ZDMA nano-particles, some physical adsorption points also exist in this period. The non-linear viscoelasticity of the NR/ZDMA composites is quite different at this time.

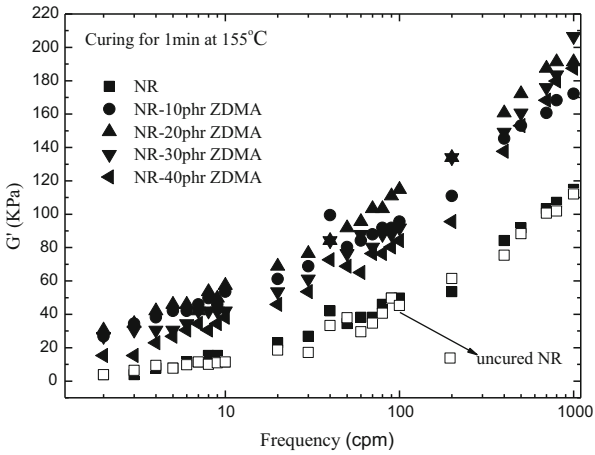

Fig. 14 Frequency sweeps for NR/ZDMA compounds cured for 1 minute, test temperature 100 °C, strain amplitude: 0.1° [57]

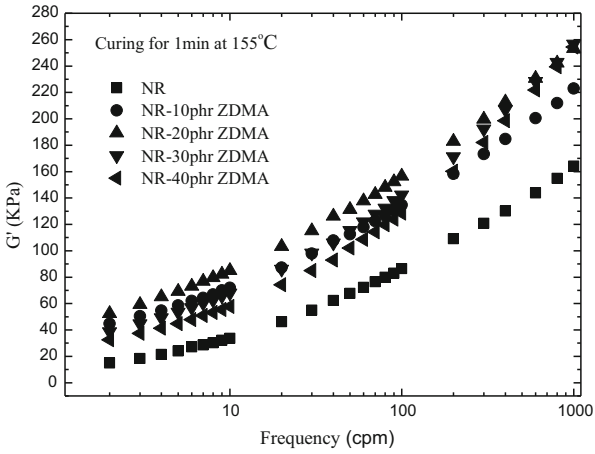

Fig. 15 Frequency sweeps for NR/ZDMA compounds cured for 1 min, test temperature 60 °C, strain amplitude: 1° [57]

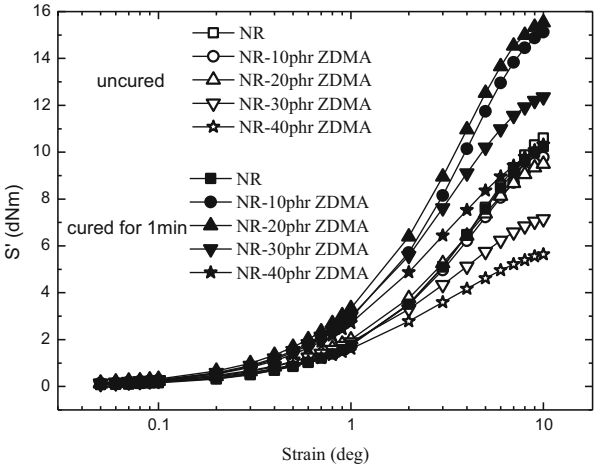

Fig. 16 Strain sweeps for S′ of the NR/ZDMA samples, test temperature 60 °C and frequency 1 Hz [57]

Figures 14 and 15 show the results of frequency sweeps for G′ of the NR/ZDMA compounds cured for 1 minute at a stain amplitude of 0.1° and 1°, respectively. The most interesting finding by Chen and Xu is that [57]: In the low frequency region, values of G′ from the highest to the lowest are in follow sequence: 20 phr, 10 phr, 30 phr, and 40 phr. In normal concept, the G′ should be increased as increasing the filler content. However, the above unusual phenomena araised at this condition also can be found in strain sweeps for S′ (Fig. 16) and strain sweeps for G′ (Fig. 17).

This specific behavior is due to the specific crosslink structure formed at the initial stage of curing. Nie [47] clearly described the reaction process of ZDMA in NR. Peroxide radical abstracted hydrogen from methylene of molecular chains of NR, produced rubber radicals. When two rubber radicals met, a crosslinking bond was formed. Simultaneously, ZDMA underwent polymerization initiated by peroxide radicals. Because of the double bonds in the rubber, polymerized ZDMA

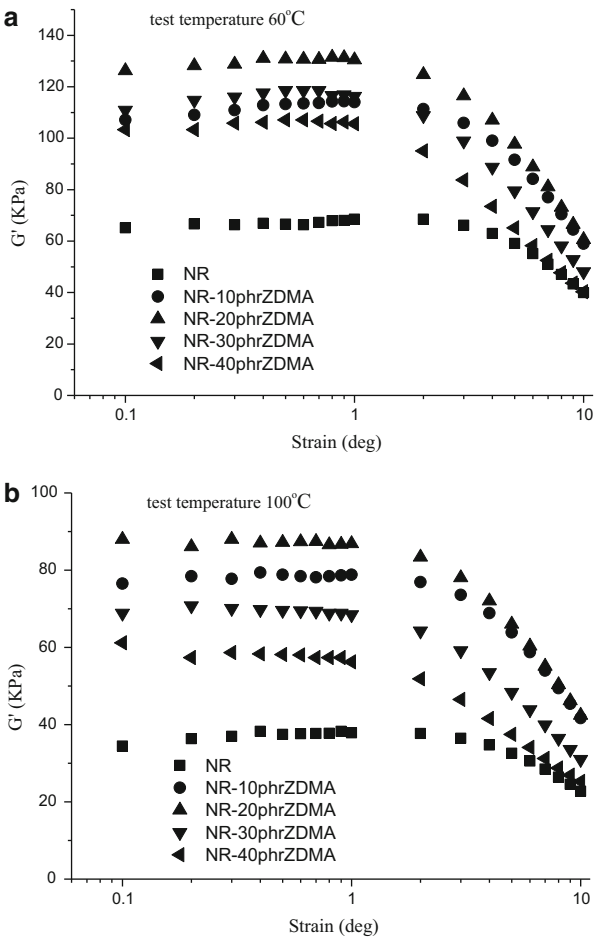

Fig. 17 Strain sweeps for G′ of the NR/ZDMA compounds cured for 1 minute, (**a**) test temperature 60 °C and (**b**) 100 °C, frequency 1 Hz [57]

(PZDMA) radicals also reacted with NR radicals, forming NR-graft-PZDMA [47]. Moreover, when two PZDMA radicals met or one PZDMA radical abstracted hydrogen from a rubber chain, an un-grafted PZDMA molecule appeared [47]. The apparent activation energy (Ea) of polymerization of ZDMA was lower than that of curing the pure NR, thus the ability that ZDMA to capture peroxide radicals was stronger than that of the pure NR in the same condition.

At a high concentration of ZDMA, majority of the limited peroxide radicals are captured by ZDMA to form PZDMA while a small quantity of peroxide radicals is consumed by crosslinking of NR; at a low concentration of ZDMA, the majority of the limited peroxide radicals can be consumed by crosslinking of NR. Thus the more ZDMA in the NR, the less peroxide radicals consumed in NR crosslinking at this time. The NR/ZDMA compound cured for 1minute contains un-crosslink NR macromolecules, primary covalent crosslink points, residual ZDMA, PZDMA and NR-graft-PZDMA. Majority of NR-graft-PZDMA exist in the interface of NR and

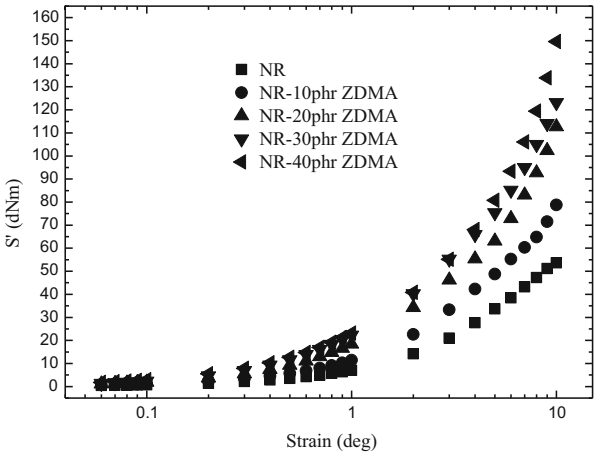

Fig. 18 Strain sweeps for S′ of the NR/ZDMA vulcanizates, test temperature 60 °C and frequency 1 Hz [57]

PZDMA. Because of the large numbers of ion pairs in PZDMA molecules and the strong electrostatic interaction between ion pairs, aggregates consisting of several pairs called "multiplets" could be formed, restricting the mobility of adjacent polymer chains [47]. Moreover, the PZDMA also can form a filler network, which is similar to a black carbon network. Thus, a considerable PZDMA and cross-links of NR form a relatively developed "primary network" (containing covalent crosslink points, ionic cross-links, physical adsorption and filler-filler joints). As a result, the fact that the 1 min-cured sample with 20 phr ZDMA show the highest G′ and S′ is a result of the developed "primary network".

Generally speaking, G′ shows a rapid decrease at a high strain about 100–200 %, which is mainly contributed by the rubber matrix. In this high strain amplitudes region, the filler-filler networks have been destroyed completely and rubber is stretched to deform. In Chen's study, the G′ curves of 10 phr and 20 phr are very close, whereas the 40 phr and pure NR are very close. This reflects that the higher density of cross-links formed in the samples with 10 phr and 20 phr ZDMA than in neat NR and sample with 40 phr ZDMA.

As for the vulcanizates, the continuous covalent crosslink network of the NR matrix and ionic crosslink network results in a normal increasing law that the elastic torque increases as a function of increasing ZDMA concentration at high strain amplitudes. Chen et al. [57] also found that the developed crosslink network of NR/ZDMA vulcanizates gets involved in the deformation of structure when the strain amplitudes exceed 0.1°, which can be deduced from Fig. 18. The S′ overlap each other when the strain amplitudes below 0.1°, but separate when the strain amplitude exceed 0.1° [57].

It was accepted that reinforcement was related to the combinational contribution of the filler-filler and the filler-rubber interactions and breakdown of these interactions were considered to be responsible for strain softening. Chen and Xu found that the 1-min cured NR/ZDMA compounds during continuous strain sweeps also showed softening behavior of G′ (Fig. 19) and S′ (Fig. 20). The higher ZDMA loading, the greater softening of G′ showing. Because of the very low crosslink

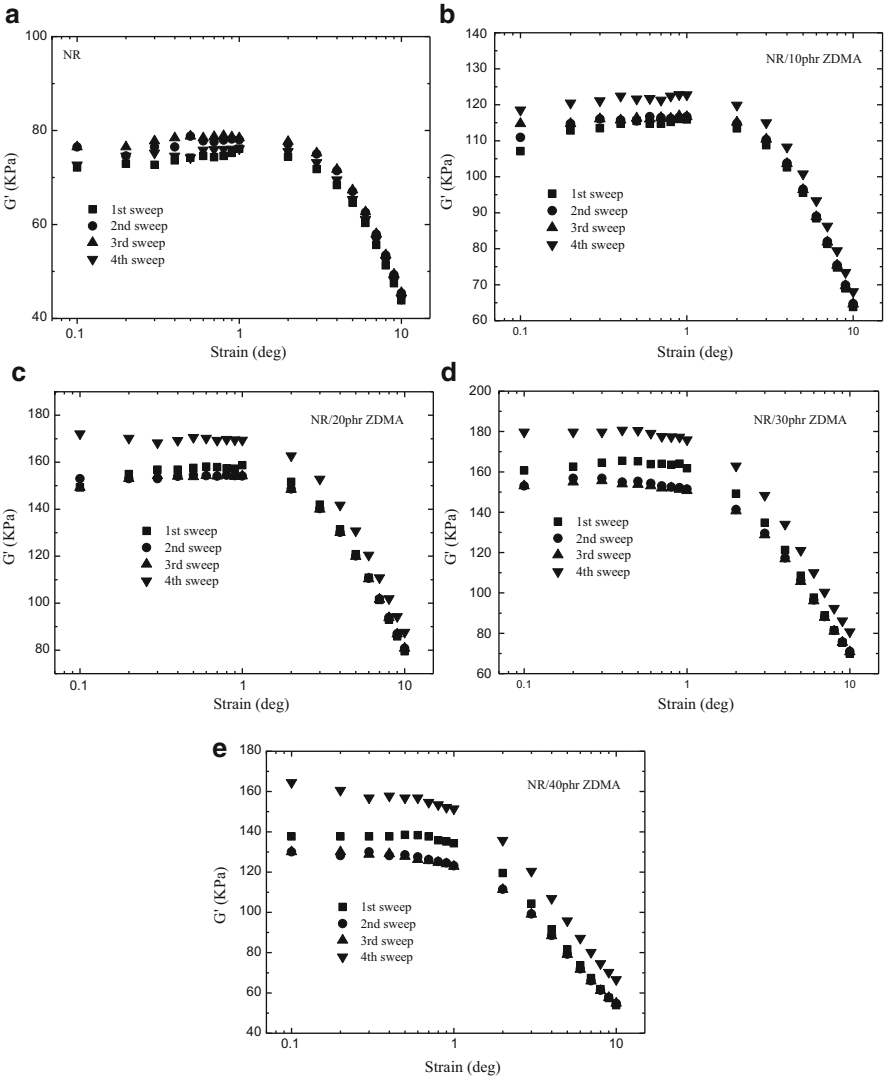

Fig. 19 Stress-softening of G′ of NR/ZDMA samples cured for 1 minute, test temperature 60 °C and frequency 1 Hz [57]

density, the NR matrix retained some fluidity. When the temperature was raised, the PZDMA aggregated together to rebuilt the filler-filler structures which contributed to the recovery of G′ after rest at 100 °C for 30 min. Chen and Xu also pointed out that the residual DCP might decompose to generate radicals to continue the crosslink reaction during rest at 100 °C for 30 min, resulting in a higher G′ and S′ of the forth scan than that of the first scan [57].

As shown in Fig. 20, no signs of the rupture of the rubber network were observed for the 1-min cured NR/ZDMA compounds, since the S′-strain curves of the first

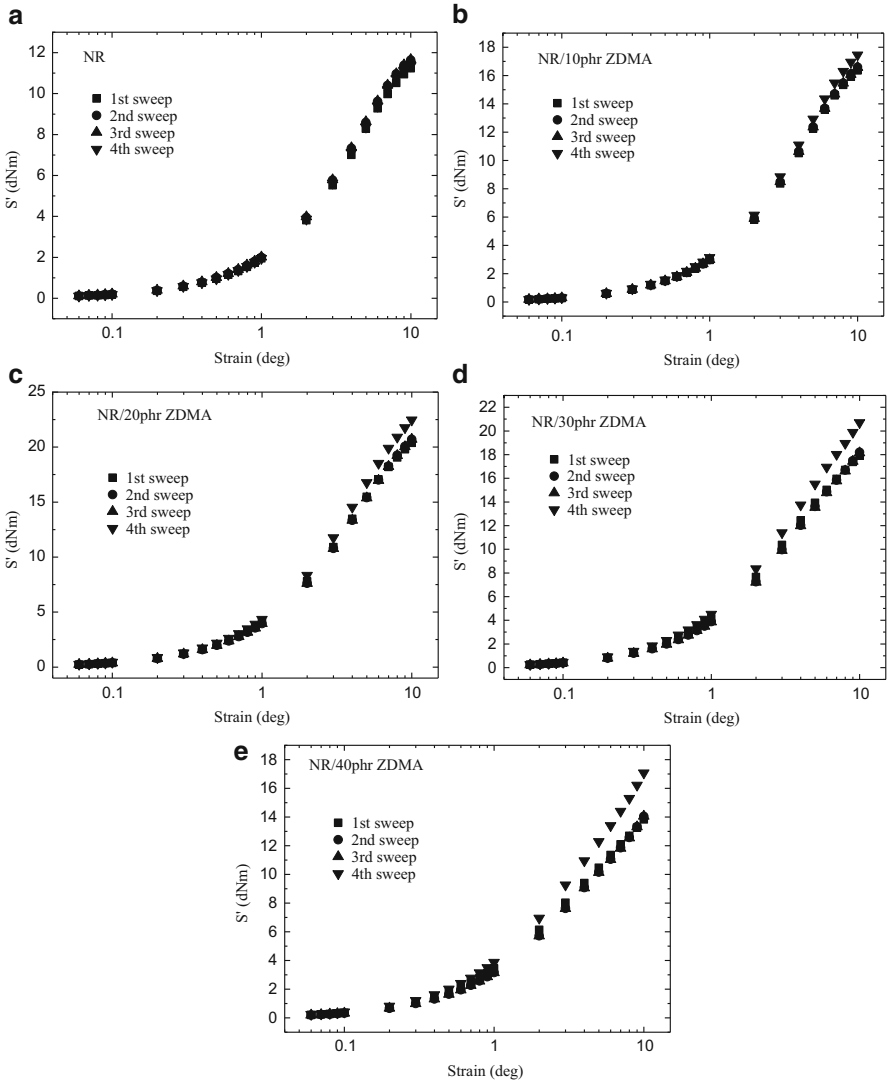

Fig. 20 Stress-softening of S′ of NR/ZDMA samples cured for 1 minute, test temperature 60 °C and frequency 1 Hz [57]

three sweeps overlapped. Generally speaking, rupture of the crosslink network in a cured rubber occurs at about 10° (equal to about 140 %). After rest at 100 °C for 30 min, the forth scan of the neat NR still show no changes, while the ZDMA filled samples exhibited an apparent increase of S′ at high strain amplitudes. This suggested that some cross-links were really formed during the rest at 100 °C. They considered that the increased crosslinks were mainly attributed to the ionic crosslinks, cooperating with a little of primary covalent crosslink points and some physical adsorption [57].

6 Conclusions

This paper mainly summarizes the introduction of Song's transient double-network model, non-linear viscoelasticity of double-network formed by twice curing and non-linear viscoelasticity of the NR/ZDMA composite with ionic and covalent crosslink networks.

In Song's double-network model, the interactions of non-hydrodynamic and hydrodynamic forces and their dependence on the deformation rate were all taken into account, the polymeric chains entangled with other ones by multi-entanglement and polymeric chains connected to a great number of destructible particles by multi-adsorption, which could be recreated and released dynamically. As for the double-network formed by twice curing, the double networks showed lower hysteresis, plateau in G' and the maximum in G'' than single network, because that the carbon black agglomeration was reduced in the double networks. In addition, the dynamic strain associated with breakup of the filler network is not affected by the presence of the double network. The ionic crosslinks are formed by metal salts graft-polymerized onto the rubber chains because of the large numbers of ion pairs in polymerized metal salts molecules and the strong electrostatic interaction between ion pairs, resulting that the cured rubbers contain covalent crosslinks and ionic crosslinks. The slippage and exchange reaction of ionic bonds under the dynamical stress led to a long "LVE region" in NR/ZDMA vulcanizate and a remarkable stress softening. The primary "ionic crosslink network" formed at the initial stage of curing shows specific non-linear viscoelasticity to the NR/ZDMA compounds.

References

1. Medalia AI (1978) Effects of carbon black on dynamic properties of rubber. Rubber Chem Technol 51(3):437–523
2. Wang MJ (1998) Effect of polymer-filler and filler-filler interactions on dynamic properties of filled vulcanizates. Rubber Chem Technol 71(3):520–589
3. Meier JG, Kluppel M (2008) Carbon Black Networking in Elastomers Monitored by Dynamic Mechanical and Dielectric Spectroscopy. Macromol Mater Eng 293(1):12–38
4. Vieweg S, Unger R, Heinrich G, Donth E (1999) Comparison of dynamic shear properties of styrene-butadiene vulcanizates filled with carbon black or polymeric fillers. J Appl Polym Sci 73(4):495–503
5. Payne AR (1965) In Kraus G (ed) Reinforcement of elastomers. Interscience Publisher, New York (Chap 3)
6. Payne AR (1964) The role of hysteresis in polymers. Rubber J 146(1):36–49
7. Zhao F, Shi XY, Chen X, Zhao SG (2010) Interaction of Vulcanization and Reinforcement of CB on Dynamic Property of NR Characterized by RPA2000. J Appl Polym Sci 117(2):1168–1172
8. Song MS, Wen Z, Hu GX (1999) Rheological behavior of polymer melts and concentrated solutions. part V: a new molecular theory of non-linear viscoelasticity for polymeric suspensions. J Mater Sci Technol 15(2):169–177

9. Collier AA, Clegg DW (1988) Rheological measurement. Elsevier Appl Sci, New York, 483
10. Stephen TS, Winter HH, Gottlieb M (1988) The steady shear viscosity of filled polymeric liquids described by a linear superposition of two relaxation mechanisms. Rheol Acta 27 (3):263–272
11. Song MS, He ZR (1990) The molecular theory of viscoelasticity for thermoplastic elastomer SBS(SIS) at large deformations. Rheol Acta 29(1):31–45
12. Song MS (1989) Studies on the relationship between the network structure and the mechanical properties of rubber vulcanizates (1) theory of elasticity for rubber vulcanizates with carbon black fillers in large deformation. Chin J Chem Eng 4(2):162–177
13. Roland CM, Warzel ML (1990) Orientation effects in rubber double networks. Rubber Chem Technol 63(2):285–297
14. Santangelo PG, Roland CM (1994) The mechanical behavior of double network elastomers. Rubber Chem Technol 67(2):359–365
15. Santangelo PG, Roland CM (1995) Failure properties of natural rubber double networks. Rubber Chem Technol 68(1):124–131
16. Roland CM, Peng KL (1991) Electrical conductivity in rubber double networks. Rubber Chem Technol 64(5):790–800
17. Hamed GR, Huang MY (1998) Tensile and tear behavior of anisotropic double networks of a black-filled natural rubber vulcanizate. Rubber Chem Technol 71(5):846–860
18. Kaang S, Nah C (1998) Fatigue crack growth of double-networked natural rubber. Polymer 39 (11):2209–2214
19. Hvidt S, Kramer O, Batsberg W, Ferry JD (1980) Contribution of entanglements to the equilibrium modulus of 1,2-polybutadiene networks at small strains and estimate of the front factor. Macromolecules 13(4):933–939
20. Batsberg W, Kramer O (1981) A direct experimental determination of the elastic contribution of chain entangling in a tightly cross-linked elastomer. J Chem Phys 74(11):6507–6508
21. Granick S, Ferry JD (1983) Entangled chain structure trapped in a styrene-butadiene random copolymer by cross-linking in simple extension. Macromolecules 16(1):39–45
22. Kramer O (1988) Selective quenching of large-scale molecular motions by cross-linking in the strained state. ACS Symp Ser 367:48–58
23. Twardowski TE, Gaylord RJ (1989) The localization model of rubber elasticity and the stress-strain behavior of a network formed by cross-linking a deformed melt. Polym Bull 21(4):393–400
24. Gaylord RJ, Twardowski TE, Douglas JF (1988) The localization model of rubber elasticity and the deformation of a network formed by cross-linking a strained melt. Polym Bull 20 (3):305–310
25. Tobolsky AV, Takahashi Y, Naganuma S (1972) Effect of additional cross-linking of continuous chemical stress relaxation of cis-polybutadiene. Polym J 3(1):60–66
26. Gillen KT (1988) Effect of cross-links which occur during continuous chemical stress-relaxation. Macromolecules 21(2):442–446
27. Flory PJ (1956) Theory of elastic mechanisms in fibrous proteins. J Am Chem Soc 78 (20):5222–5235
28. Mandelkern L, Roberts DE, Diorio AF, Posner AS (1959) Dimensional changes in system of fibrous macromolecules: polyethylene. J Am Chem Soc 81(16):4148–4157
29. Hikmet RAM, Lub J, Vanderbrink PM (1992) Structure and mobility within anisotropic networks obtained by photopolymerization of liquid crystal molecules. Macromolecules 25 (16):4194–4199
30. Reichert WF, Goritz D, Duschl EJ (1993) The double network, a model describing filled elastomers. Polymer 34(6):1216–1221
31. Mott PH, Roland CM (2000) Mechanical and optical behavior of double network rubbers. Macromolecules 33(11):4132–4137
32. Kaang S, Gong D, Nah C (1997) Some physical characteristics of double-networked natural rubber. J Appl Polym Sci 65(5):917–924

33. Aprem AS, Joseph K, Thomas S (2004) Studies on double networks in natural rubber vulcanizates. J Appl Polym Sci 91(2):1068–1076
34. Wang J, Hamed GR, Umetsu K, Roland CM (2005) The Payne effect in double betwork elastomers. Rubber Chem Technol 78(1):76–83
35. Flory PJ (1960) Elasticity of polymer networks cross-linked in state of strain. Trans Faraday Soc 56:722–743
36. Baxandall LG, Edwards SF (1988) Deformation-dependent properties of polymer networks constructed by addition of crosslinks under strain. Macromolecules 21(6):1763–1772
37. Termonia Y (1990) Molecular model for the mechanical properties of elastomers. 3. networks cross-linked in a state of strain. Macromolecules 23(7):1976–1979
38. Dontsov A, Decandia F, Amelino L (1972) Elastic properties and structure of polybutadiene vulcanized with magnesium methaceylate. J Appl Polym Sci 16(2):505–518
39. Saito Y, Nishimura K, Asada M, Toyoda A (1994) Polymerization behavior of zinc methacrylate study of zinc methacrylate/rubber/peroxide compounds; Part 2. J Jpn Rubber Soc 67 (12):867–872
40. Gao GX, Zhang ZC, Zheng YS, Jin ZH (2009) Effect of magnesium methacrylateand zinc methacrylate on bond properties of thermal insulation material based on NBR/EPDM blends. J Appl Polym Sci 113(6):3901–3909
41. Yin DH, Zhang Y, Zhang YX, Peng ZL, Fan Y, Sun K (2002) Reinforcement of peroxide-cured styrene-butadiene rubber vulcanizates by mathacrylic acid and magnesium oxide. J Appl Polym Sci 85(13):2667–2676
42. Yin DH, Zhang Y, Peng ZL, Zhang YX (2003) A comparison between the SBR vulcanizates reinforced by magnesium methacrylate added directly or prepared in situ. Eur Polym J 39 (1):99–105
43. Lu YL, Liu L, Yang C, Tian M, Zhang LQ (2005) The morphology of zinc dimethacrylate reinforced elastomers investigated by SEM and TEM. Eur Polym J 41(3):577–588
44. Peng ZL, Liang X, Zhang YX, Zhang Y (2002) Reinforcement of EPDM by in situ prepared zinc dimethacrylate. J Appl Polym Sci 84(7):1339–1345
45. Yuan XH, Peng ZL, Zhang Y, Zhang YX (1999) The properties and structure of peroxide-cured NBR containing magnesium methacrylate. Polym Polym Comp 7(6):431–436
46. Du AH, Peng ZL, Zhang Y, Zhang YX (2003) Properties of EVM vulcanizates reinforced by in situ prepared sodium methacrylate. J Appl Polym Sci 89(8):2192–2200
47. Nie YJ, Huang GS, Qu LL, Zhang P, Weng GS, Wu JR (2010) Cure kinetics and morphology of natural rubber reinforced by the in situ polymerization of zinc dimethacrylate. J Appl Polym Sci 115(1):99–106
48. Du AH, Peng ZL, Zhang Y, Zhang YX (2002) Effect of magnesium methacrylate on the mechanical properties of EVM vulcanizate. Polym Test 21(8):889–895
49. Lu YL, Liu L, Shen DY, Yang C, Zhang LQ (2004) Infrared study on in situ polymerization of zinc dimethacrylate in poly(α-octylene-*co*-ethylene) elastomer. Polym Int 53(6):802–808
50. Klingender RC, Oyama M, Saito Y (1990) High-strength compound of highly saturated nitrile and its applications. Rubber World 202(3):26–31
51. Lu YL, Liu L, Tian M, Geng HP, Zhang LQ (2005) Study on mechanical properties of elastomers reinforced by zinc dimethacrylate. Eur Polym J 41(3):589–598
52. Du AH, Peng ZL, Zhang Y, Zhang YX (2004) Fracture morphology and mechanical properties of ethylene/vinyl acetate rubber vulcanizates reinforced by in situ prepared sodium methacrylate. J Polym Sci B 42(9):1715–1724
53. Chen YK, Xu CH (2012) Stress-strain behaviors and crosslink networks studies of natural rubber-zinc dimethacrylate composites. J Macro Sci B Phys 51(7):1384–1400
54. Xu CH, Chen YK, Cao LM, Wang YP, Zeng XR (2013) Study of the crosslinking evolution of the styrene-butadiene rubber/zinc dimethacrylate based on dissolution/swelling experiments. J Macro Sci B Phys 52(2):319–333

55. Xu CH, Chen YK, Huang J, Zeng XR, Ding JP (2012) Thermal aging on mechanical properties and crosslink network of natural nubber/zinc dimethacrylate composites. J Appl Polym Sci 124 (3):2240–2249
56. Xu CH, Chen YK, Zeng XR (2012) A Study on the crosslink network evolution of magnesium dimethacrylate/natural rubber composite. J Appl Polym Sci 125(3):2449–2459
57. Chen YK, Xu CH, Wang YP (2012) Viscoelasticity behaviors of lightly cured natural rubber/ zinc dimethacrylate composites. Polym Compos 33(6):967–975
58. Chen YK, Xu CH (2012) Specific nonlinear viscoelasticity behaviors of natural rubber and zinc dimethacrylate composites due to multi-crosslinking bond interaction by using rubber process analyzer 2000. Polym Compos 32(10):1593–1600
59. Xu CH, Chen YK, Cao LM, Zeng XR (2012) Dynamic viscoelasticity behaviors of magnesium dimethacrylate/natural rubber composites with different cure extent. Polym Compos 33 (7):1244–1253
60. Chen YK, Xu CH (2011) Crosslink network evolution of nature rubber/zinc dimethacrylate composite during peroxide vulcanization. Polym Compos 32(10):1505–151
61. Chen YK, Xu CH (2012) Stress softening of NR reinforced by in situ prepared zinc dimethacrylate. J Appl Polym Sci 123(2):833–841
62. Roozbeh D, Mikhail I (2009) A network evolution model for the anisotropic Mullins effect in carbon black filled rubbers. Int J Solids Struct 46(16):2967–2977
63. Jong L (2005) Dynamic mechanical properties of soy protein filled elastomers. J Polym Environ 13(4):329–338

Modeling of Non-Linear Viscoelastic Behavior of Filled Rubbers

Gordana Marković, Milena Marinović-Cincović, Vojislav Jovanović, Suzana Samaržija-Jovanović, and Jaroslava Budinski-Simendić

In memory to my parents Gordana Marković

Abstract The nonlinear viscoelastic behavior of the composites of rubber filled with carbon black, silica, carbon nanotube (CNT), clay and surface-modified nanosilica were studied. The behavior of carbon black-filled rubber is thoroughly analyzed with the intention of developing a constitutive model able to reproduce both static and dynamic material responses. Several nonlinear viscoelastic models have been examined thoroughly and for each of them advantages and disadvantages are highlighted. A series of experiments concerning both static and dynamic tests were performed aimed at measuring all the relevant nonlinear effects. Temperature and strain rate dependencies were investigated and discussed. The standard methodology was applied to perform both tensile and compressive quasi-static tests. Some shortcomings of this procedure, resulting in a unreliable stress-strain constitutive curve around the undeformed configuration, were identified. This lead to the design a non-standard cylindrical specimen able to bear both tensile and compressive loading. Consequently, the influence of the shape factor was removed and the same boundary conditions, in tension and compression, were applied. This allowed the stiffness around the undeformed configuration to be evaluated in detail. The quasi-static experimental results also allowed the influence of the Mullins effect on the quasi-static response to be investigated: during the loading cycles, there is a significant reduction in the stress at a given level of strain, which is a consequence of the internal material rearrangement, i.e., the Mullins effect. This damage phenomenon is sometimes reported to induce transverse isotropy in the material, which

G. Marković (✉)
Tigar, Nikole Pašića 213, 18300 Pirot, Serbia
e-mail: gordana1markovic@gmail.com

M. Marinović-Cincović
University of Belgrade, Institute of Nuclear Science Vinča, Belgrade, Serbia

V. Jovanović • S. Samaržija-Jovanović
Faculty of Natural Science and Mathematics, University of Priština, Kosovska Mitrovica, Serbia

J. Budinski-Simendić
Faculty of Technology, University of Novi Sad, Novi Sad, Serbia

D. Ponnamma, S. Thomas (eds.), *Non-Linear Viscoelasticity of Rubber Composites and Nanocomposites*, Advances in Polymer Science 264, DOI 10.1007/978-3-319-08702-3_8

is usually assumed to be isotropic. The Payne effect becomes more pronounced at higher silica loading. The filler characteristics such as particle size, specific surface area, and the surface structural features were found to be the key parameters influencing the Payne effect. A nonlinear decrease in storage modulus with increasing strain was observed for unfilled compounds also. The results reveal that the mechanism includes the breakdown of different networks namely the filler-filler network, the weak polymer-filler network, the chemical network, and the entanglement network. The model of variable network density proposed by Maier and Goritz has been applied to explain the nonlinear behavior. The model fits well with the experimental results. The interaction between epoxidized elastomeric matrix and silica as filler was extremely improved, even in the presence of very low content of epoxy groups into the polymer chain.

Keywords Rubber reinforcement • Elastomers • Rheology

1 Introduction

The role of active fillers (carbon black, silica, CNT) has been studied in the rubber matrix for a better understanding of the rubber performance and the mechanism of reinforcement. The elastomer reinforcement by using filler needs, generally, strong physical interactions between the segments of the polymer chain and the filler surface [1, 2]. In some cases the reinforcement is supported by chemical bond of the polymer with the filler surface, by using coupling agent [3, 4]. This interaction can strongly affect the physical properties, as well as the dynamic-mechanical properties. The modulus of an unfilled compound practically has no change with the variation in the deformation amplitude, but this modulus decrease significantly to filled rubber compounds [5]. The non-linear dependency of G′ as a function of deformation amplitude (Payne effect) can be explained due to the breakdown of the filler network considering a continuous increase in the periodic deformation [6, 7]. Through the improvement of the polymer-filler interaction and filler dispersion, the dependency of the modulus as a function of variation in deformation amplitude becomes to be less pronounced.

The dynamic properties of filled elastomers have been a subject of active research because they affect the performance of tires such as skid, traction, and rolling resistance to cite but a few [8–11].

The “Payne effect” [9] has been extensively investigated because it directly impacts the fuel consumption. From a phenomenological point of view, beyond a strain higher than a few 0.1 %, the storage modulus of filled rubber departs from a plateau value $G_0^{'}$ and collapse to a minimum value $G_\infty^{'}$. The decrease in the storage modulus is accompanied by a maximum of the loss modulus, G''. The amplitude of the Payne effect, ΔG) $G_0^{'} - G_\infty^{'}$ increases with the filler content, the specific surface of the filler [12] and strongly depends on the surface properties of the fillers and its dispersion [13] within the matrix. On the contrary it decreases with temperature

[14]. A number of different local mechanisms have been proposed so far to explain this phenomenon, but no consensus has emerged yet.

According to Payne, the three-dimensional structure network constructed by the aggregation of carbon black filler significantly influences the dynamic viscoelastic properties of carbon black filled rubbers. Kraus [15] proposed a model based on the agglomeration/ deagglomeration kinetics of filler aggregates by assuming a Van der waal's type interaction between the particles. This model was further developed by Huber and Vilgis [16–18] who relate G' and G'' to the fractal dimension and the connectivity of the network, and by Kluppel [19] who introduces the idea of cluster. The fact that the temperature and the frequency dependence of the amplitude of the Payne effect are not taken into consideration is certainly the most accepted criticism of this approach. However, one of the major drawbacks comes from the evidence brought by Funt [20] who shows from electrical conductivity measurements that the Payne effect might occur although a continuous filler network does not exist through the sample. As an alternative to the destruction and reformation of a filler network, it has also been proposed that the dynamics of adsorption/desorption of the polymer chains at the particle surface may be responsible for various linear and nonlinear effects. Maier [21], Zhu and Sternstein [22, 23] have suggested that the reduction of the storage modulus with the applied strain could be related to polymer-filler interactions including the aspects of trapped topological entanglements.

The interaction between the filler particles and the rubber matrix, which leads to the adsorption of polymer chains on the particle surface, can be controlled by varying the nature of the polymer-filler interface [24–29].

Maier and Goritz [30, 31] take into consideration the adsorption/ desorption mechanism by considering the filler particles as multifunctional cross-link with chains which are either loosely or strongly anchor to the surface. The molecular interpretation of the Payne effect is then based on a variable network density when the loosely tied chains are desorbed with the increase of the strain. A compromise is also suggested, considering that the primary mechanism for the Payne effect certainly involves the existence of cooperation between the breakdown and reformation of the filler network and the molecular disentanglement of the bound and free rubber [20, 32–34]. Another explanation first proposed by Yatsuyanagi et al. [35] considers the existence of a percolation network through the rigid amorphous layer formed around the particles. Their interpretation of the Payne effect equally relies on the competition between desorption and adsorption of this rigid amorphous layer.

The importance of glassy layers in filled polymer has received considerable attention very recently, when it was recognized that a glass transition gradient exist near the surface and that the dynamics could be either enhanced or slowed down according to the interaction of the chains with the surface. In a body of work, [36–38] Montes et al. [38] among others have clearly shown in filled elastomers that a maximum of reinforcement is obtained when this rigid or slow dynamics layer forms a continuous path through the filler aggregates. In their work, [39] model the Payne effect by considering that the stress is supported mainly by the cross section

of glassy bridges in a direction normal to the stress. They explain the strain dependence of the elastic modulus by the local lowering of the glass transition due to the amplification of the stress in the vicinity of the aggregates. This plasticizing effect induces the yielding of the carbon-filled rubber can reasonably be assumed isotropic, only isotropic constitutive relations are considered. Uniaxial stretch histories are investigated by reducing the general three-dimensional model to the one-dimensional case. In this context, the concept of dynamic moduli, introduced in linear viscoelasticity and referred to as storage and loss moduli, is applied, in a consistent manner, to nonlinear constitutive equations: it is proved that for most of the integral models used in the literature, the sensitivity of the storage modulus with respect to the frequency vanishes when assessed at low frequency. The constitutive behavior of filled-elastomers is highly nonlinear for what concerns both the quasi-static and the dynamic response. Fosdick and Yu, Hallquist's, Yang's and Shime's models are able to qualitatively describe the behavior of the rubber-like material under investigation, even if they cannot properly catch the dissipated energy undergoing the deformation process, especially at lower strain rate. Fung's model firstly introduced to describe the behavior of soft biological tissues, has revealed completely unable to describe the dissipation properties both at higher and lower strain rates; Hibbet's model, instead, has produced a fitting model which underestimates the material stiffness at very low strain in all the considered experimental cases. For silica-filled rubber Payne effect becomes more pronounced. Since, in many engineering applications, the material is subjected to a strain lower than 10 %, a relevant stiffness error within this range should be consider a serious drawback for the model applied. This allowed the stiffness around the undeformed configuration to be evaluated in detail. The quasi-static experimental results also allowed the influence of the Mullins effect on the quasi-static response to be investigated: during the loading cycles, there is a significant reduction in the stress at a given level of strain, which is a consequence of the internal material rearrangement, i.e., the Mullins effect. This damage phenomenon is sometimes reported to induce transverse isotropy in the material, which is usually assumed to be isotropic.

2 Rubber Phenomenology

The behavior of carbon black-filled rubber in relation to quasi-static and dynamic responses is examined in detail. In particular, the main features of the micro-structure of the material and their influence on the macro-mechanical response are highlighted. The effects of strain, strain-rate and temperature on the constitutive response are discussed. Mullins and Payne effects, which are peculiar in the behavior of filled elastomers, are reviewed and new results are shown.

Owing to its unique physical properties, rubber plays a key role in countless industrial applications. Tyres, vibration absorbers and shoe soles are only but a few of the myriad uses of rubber in an industry which in 2009 had an estimated market

value of two billion euro. The term rubber is actually misleading: it is used both to indicate the material, technically referred to as natural rubber, and the broad class of synthetic elastomers which share with natural rubber some fundamental chemical properties. Indeed, the majority of rubber used for industrial applications are synthetically produced and derived from petroleum 1. Rubber, or elastomer, has an internal structure which consists of flexible, long chain molecules that intertwine with each other and continually change contour due to thermal agitation. Elastomers are polymers with long chains [40]. The morphology of an elastomer can be described in terms of convolution, curls and kinks. Convolutions represent the long-range contour of an entire molecular chain, which forms entanglements (knots). Curls are shorter range molecular contours that develop between entanglements and crosslinks, and kinks are molecular bonds within a curl. Each molecular bond has rotational freedom that allows the direction of the chain molecule to change at every bond. Thus the entire molecular chain can twist, spiral and tangle itself or with adjacent chains. This basic morphology is shared among all the fifty thousand compounds used in the market today and generically referred to by the term rubber. Despite this intricate internal structure, the random orientation of the molecular chains results in a material which is externally isotropic and homogeneous.

Prior of using, the neat elastomer is subjected to physical/chemical treatments to enhance its mechanical properties. One of these treatments consists of the addition, through heating, of sulfur-based curatives which create crosslinks among the macromolecules chains; this process is commonly called vulcanization [41].

Figure 2 highlights the different behavior of a vulcanized and a non-vulcanized rubber specimen subjected to a tensile loading. Initially, both of the elastomers have a similar intertwined internal structure. When stretched, the macromolecules of the non-vulcanized compound disentangle themselves according to the direction of the applied force. This microstructural change results in a more ordered internal state with a subsequent reduction in entropy. Thereafter, the macro-brownian motions of the macromolecules cause the chains to slide back, one onto each other, to the disordered state. Finally, once the external load is removed (step d in the figure), each macromolecule maintains its state of maximum entropy. Therefore, the initial overall shape is not recovered: all the energy externally supplied to stretch the specimen is dissipated by the viscous friction among the macromolecules. A different microstructural response occurs during the deformation of the vulcanized specimen.

Indeed, when subjected to an external traction, the molecular chains dispose parallel to the macro-displacement and because of the crosslinks introduced by the vulcanisation, they cannot slide back to the initial disordered state. By removing the external loading, the system tends towards the initial state of maximum entropy and the specimen recovers the initial length. In this case, the external supplied energy is totally recovered. The behavior of a real elastomer slightly differs from this simplified description. Indeed, even if the elastomer is vulcanized, the macromolecules can partially slide one onto each other with a dissipation of the mechanical energy.

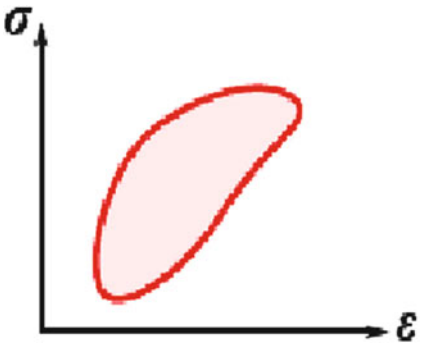

Fig. 1 The energy dissipation is a primary feature to be predicted in many engineering applications such as the estimate of the rolling resistance of tires and hysteretic losses in biological tissues and the design of vibration absorbers

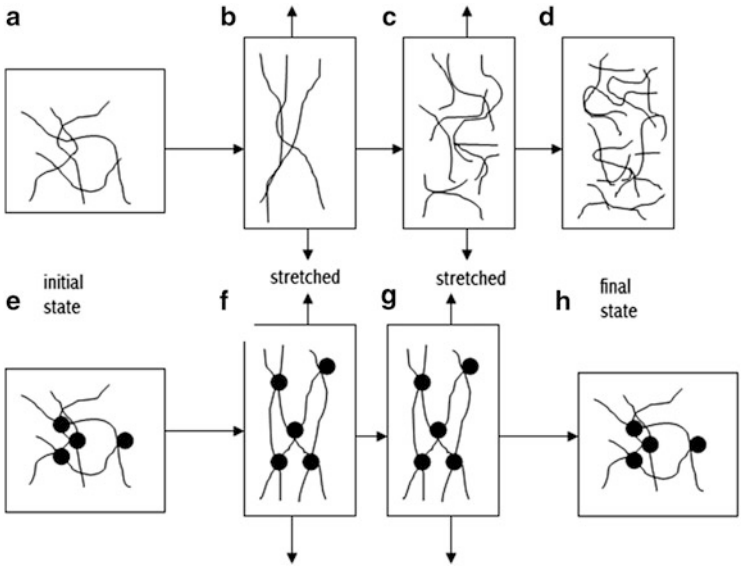

Fig. 2 Effects of stretching on a non-vulcanized (*above*) and a vulcanized (*below*) elastomer

At the end of the vulcanization process for some specific applications, such as in tyres, reinforcing filler, usually carbon black is added to the compound. This carbon based curative lends to the material the black color typical of tires.

The tensile strength of rubber increases with increasing filler content up to a certain level. Beyond this level, the tensile strength decreases with higher filler concentrations. Goldberg et al. [42] suggested that this is because high amounts of carbon black fillers cause the carbon black to agglomerate into large clusters and these clusters impart flaws that can easily create cracks and lead to a catastrophic

failure. The quantity of filler present in the elastomer is measured in phr, parts per hundred by weight of elastomer; the concentration at which maximum tensile strength is obtained, varies with the type of carbon black. For carbon black fillers with smaller particle size, the maximum tensile strength is attained at lower concentrations than those for large particle sized carbon black fillers.

The resulting mechanical characteristics such as strength, tear and abrasion resistance, along with stiffness, considerably increase with respect to the neat elastomer. The addition of filler contributes also to alter greatly the viscous behavior and temperature dependence. For example, unfilled elastomers exhibit a linear viscoelastic behavior for shear strains up to 20 % or more, while a carbon black-filled elastomer shows a pronounced nonlinear behavior at shear strains as low as 0.5 % [43].

The standard phenomenology of carbon black-filled rubber will be presented and the influence on the constitutive response of temperature and filler concentration will be discussed. Although the focus is on traditional vulcanized rubber, other thermoplastic elastomers show similar mechanical properties even if their chemical composition is quite different. Moreover, from a macroscopic point of view, the behavior of such materials is very close to the behavior of some biological soft tissues, such as ligaments and tendons, for what concerns both their static and dynamic responses.

2.1 Background

Although the reinforcement of rubber by active fillers is a well-recognized phenomenon the term ‘reinforcement’ is not well defined. Briefly it can be stated that reinforcement means the pronounced increase in tensile strength, tear resistance, abrasion resistance and modulus far beyond the values expected on the basis of the Einstein-Guth and Gold theory [44], taking into account the effects caused by colloidal spherical particles (hydrodynamic effect) and occlusion of rubber. The reinforcement of elastomers by fillers has been studied in depth in numerous investigations [45] and it is generally accepted that this phenomenon is dependent, to a large extent, on polymer properties, filler properties and processing. Generally speaking, the primary filler factors influencing elastomer reinforcement are: The primary particle size or specific surface area, which, together with loading, determines the effective contact area between the filler and polymer matrix. The structure or the degree of irregularity of the filler unit, which plays an essential role in the restrictive motion of elastomer chains under strain. The surface activity, which is the predominant factor with regard to filler–filler and filler–polymer interaction.

Most of the elastomeric components are deformed dynamically and specified dynamic properties are required. Therefore the effect of strain amplitude on the dynamic modulus was observed very intensively. The modulus of filled rubbers decreases with increasing applied dynamic strain up to intermediate amplitudes.

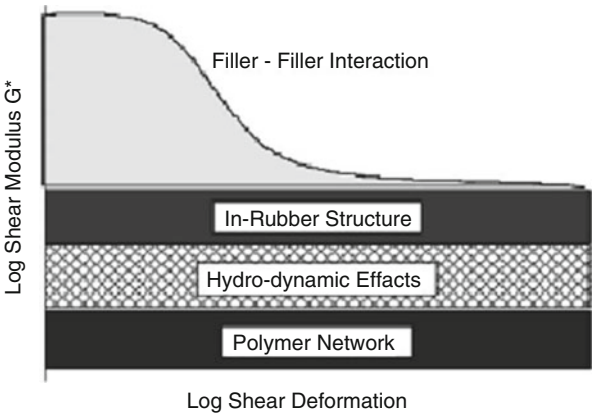

Fig. 3 Idealized form of a typical elastic modulus curve

A detailed study of the low frequency dynamic properties of filled natural rubber was carried out by Fletcher and Gent [46] and was later extended by Payne [47]. In cyclic strain tests the shear modulus can be simply expressed as a complex modulus $G^* = G' + iG''$ where G' is the in-phase modulus and G'' the out-of-phase modulus. The phase angle δ is given by $\tan\delta = G''/G'$.

The addition of fillers to rubber compounds has a strong impact on the static and dynamic behavior of rubber samples. Figure 3 shows the typical behavior of the complex shear modulus of filled rubber samples versus dynamic shear deformation. Similar to the model of Payne, we see the strain-independent part of the modulus as a combination of the polymer network, the contribution from the hydrodynamic effect and the modulus resulting from the in-rubber structure.

(a) The polymer network contribution depends on the crosslink density of the matrix and the nature of the polymer.
(b) The hydrodynamic effect—in this model—is nothing else than the effect of strain amplification, resulting from the fact that the filler is the rigid phase, which cannot be deformed. As a consequence, the intrinsic strain of the polymer matrix is higher than the external strain yielding a strain-independent contribution to the modulus.
(c) The effect of the structure is attributed to the 'in-rubber structure', which can be understood as a combination of the structure of the filler in the in-rubber state ('in-rubber DBP') and the extent of filler–polymer interaction. The in-rubber structure is the measure for the occluded rubber, which is shielded from deformation and therefore increases the effective filler content leading also to a strain-independent contribution to the modulus. The filler–polymer interaction can be attributed to physical (van der Waals) as well as to chemical linkages or a mixture of both. In the case of the silica–silane system this interaction is formed by chemical linkages.
(d) The stress softening at small amplitudes is attributed to the breakdown of the inter-aggregate association respectively to the breakdown of the filler network.

This stress softening at small deformations, called Payne-effect [10, 47], plays an important role in the understanding of reinforcement mechanism of filled rubber samples [48].

Perhaps the most general nonlinear viscoelastic theory using a single convolution integral instead of multiple integrals was introduced by Schapery [49] based on irreversible thermodynamics. These models have the form of the convolution integrals of linear viscoelasticity with the nonlinearities appearing only in the measures of stress and strain and in the reduced time. So far most of these models were established for high-modulus (e.g. glassy) polymers, using the usual stress and strain measures of infinitesimal deformation. However, for rubbery polymers, strong geometrical nonlinearities such as finite strains and finite rotations are present, making different stress and strain measures possible for constitutive modeling. One of the main restrictions in selecting these stress and strain tensors is to make use of conjugate pairs, such as the second Piola–Kirchhoff stress and Green strain or the Piola stress and deformation gradients (see Ogden [50] for the other conjugate pairs). Another restriction is that the constitutive laws should satisfy the principle of objectivity (material frame-indifference) to ensure that the stress-strain response is not altered by any superposed rigid-body motions.

The range of time-dependent, finite strain constitutive models for rubbery materials is quite limited. Perhaps the most simple and effective models are the so called pseudo stress and pseudo strain models introduced by Schapery [49].

Basically, the time dependence of the nonlinear behavior is considered to be in a separable form, where the viscoelasticity is accounted for by a relaxation function that is independent of stress or strain, while the effects of large deformations are incorporated in a reference potential. Simo [51] developed a nonlinear viscoelastic model based on a free energy with uncoupled volumetric and deviatoric parts. The time-dependent effects are contained in the deviatoric stress component, while volumetric stress response is assumed to be elastic.

Govindjee and Simo [52] combined micromechanical and phenomenological approaches to develop a continuum damage model for carbon black filled elastomers, where the softening effect is considered as the detachment of carbon particles from the elastomer matrix.

The nonlinear constitutive models used in this study are the so-called pseudo stress and pseudo strain models of Schapery [49]. They were quite easily implemented and the former yielded a reasonable representation of the rubber used in this work. The time-dependent, finite strain constitutive model from the finite element code, ABAQUS, was also used in this study.

2.2 Standard Phenomenology

2.2.1 Quasi-static

The behavior of filled elastomers can be primarily described as hyperelastic: under static or quasi-static loading dissipative effects are negligible. There have been numerous experimental studies addressing the response of rubber under quasi-static loading conditions, including uniaxial tension/compression, shear, equibiaxial tension [53–56].

In all these experimental conditions, the resulting constitutive curves are strongly nonlinear. However, constitutive nonlinearities coupled with heterogeneous strain field could lead to experimental results which are very difficult to analyze. Thus, displacement fields leading to homogeneous deformation should be opted for. A typical example is the equibiaxial (two-dimensional) extension test which is preferred to the equivalent uniaxial compression, because the difficulties related to the bulging of the specimen under compressive loading are avoided [56]

The typical stress-strain constitutive curves of a carbon black-filled elastomer are shown in Fig. 4 [57].

The material is subjected to uniaxial tension/compression, and pure shear. In the typical working range ($0.8 \leq \lambda \leq 2.0$) the constitutive nonlinearities are evident; indeed, as the breaking point is approached, the material stiffness rapidly increases so that the slope of the experimental curves begins to rise. As a consequence of the intertwining internal structure, during compression, high levels of loading force are suddenly reached, i.e. the material is much stiffer with a non-symmetric behavior between tensile and compressive stresses.

From Fig. 4, it is evident that the shear modulus G around the undeformed configuration, i.e., nominal strain equal to 1, has a lower value compared to the Young modulus E in tensile experiments. The ratio E/G is approximately equal to 3, which corresponds to a Poisson function in the undeformed configuration equal to $\nu = 0.5$, meaning that the material is incompressible.

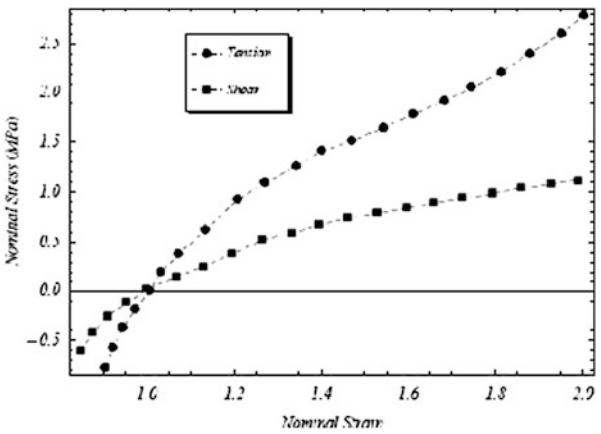

Fig. 4 Experimental data on carbon black-reinforced styrene butadiene rubber for tensile (*circle*) and pure shear (*square*) tests [57]. The ratio of the tangent stiffness around the undeformed configuration, i.e., nominal strain equal to 1, is approximately equal to 3

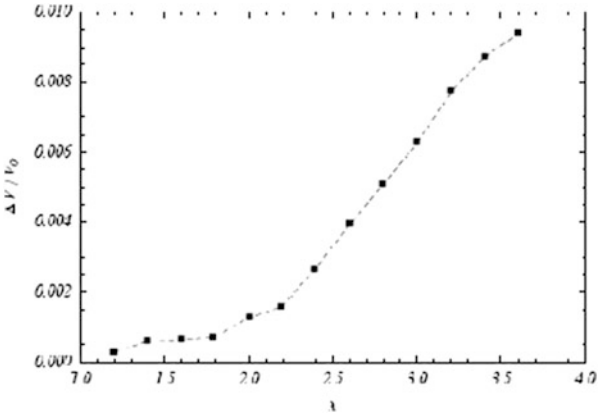

Fig. 5 Volume dilatation for a rubber specimen undergoing a uniaxial tensile experiment [62]. The volume change remainslimited over a wide strain range

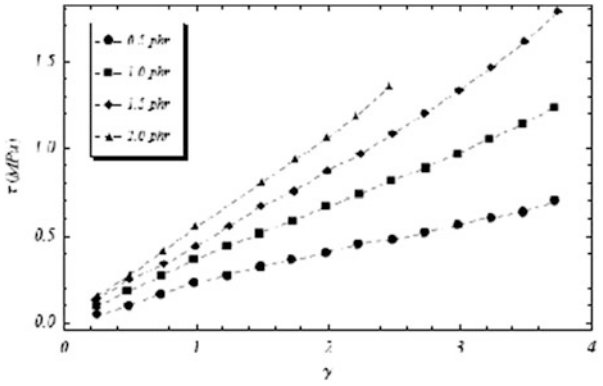

Fig. 6 Results of shear tests on rubber specimens with an increasing filler concentration [66]. The initial material stiffness shows a monotonic growth for higher value of filler content in the range $\phi \in \{\mathbf{0.5}; \mathbf{1.0}; \mathbf{1.5}; \mathbf{2.0}\}$ phr

The incompressibility of carbon black-filled rubber has been confirmed by a number of different researchers over the years [58–62]. Experiments by [62] in Fig. 5 show a limited volume variation ($\Delta V/V0 \cong 0.01$) at large strain ($\lambda \cong 4$) corroborating the incompressibility constraint introduced in many constitutive equations [63–65].

The effects upon the quasi-static response of an increasing quantity of reinforcing filler have been studied and results have been provided in [66] for pure shear tests (see Fig. 6).

The addition of carbon black produces higher value of the initial stiffness (i.e., tangent modulus around the undeformed configuration) with respect to the neat elastomer, while it makes the compound more sensitive to temperature variations. Indeed, the same qualitative behavior has been reported whatever the loading conditions.

The influence of the temperature on the stress-strain curve is shown in Fig. 7. At very low temperatures, the polymer will behave like glass and exhibit a high modulus. As the temperature is increased, the polymer will undergo a transition from a hard "glassy" state to a soft "rubbery" state in which the modulus can be

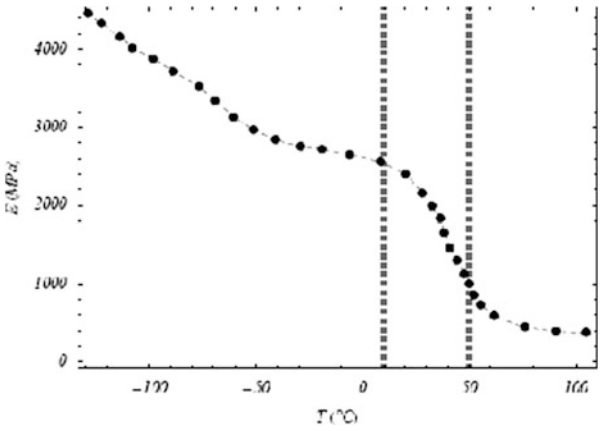

Fig. 7 Young modulus as function of temperature for polyamide-6. The *thick dashed lines* indicate the transition leathery zone [67]

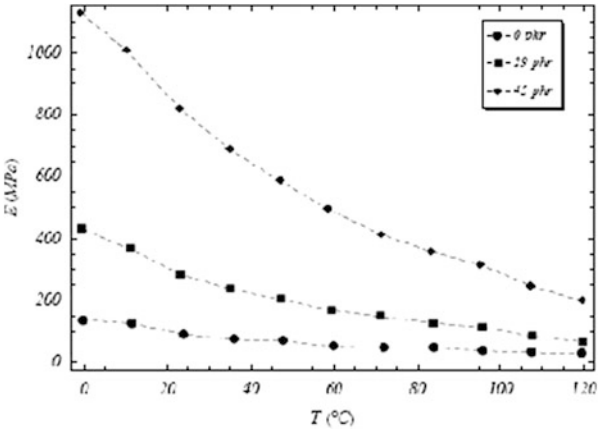

Fig. 8 Young modulus temperature dependence of a rubber-polyethylene blend for a filler content in the range {0, 29, 45} phr [68]

several orders of magnitude lower than it was in the glassy state. The transition from glassy to rubbery behavior is continuous and the transition zone is often referred to as the leathery zone. The onset temperature of the transition zone, moving from glassy to rubbery, is known as the glass transition temperature, or Tg.

The stiffness reduction produced by the temperature is strongly affected by the amount of filler. Results in Fig. 8 by [68] show that a compound with filler content of 45 phr has a percentage variation of the stiffness with the temperature higher than a compound with 0 phr of filler.

On Fig. 9 the nominal stress as function of time for a relaxation experiment on Adiprene-L100 is shown.

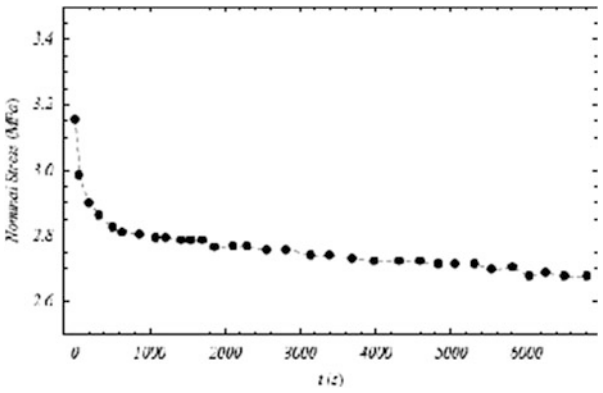

Fig. 9 Nominal stress as function of time for a relaxation experiment on Adiprene-L100 [69]

2.3 Dynamic

The material behavior above-described refers to the quasi-static response. However, elastomers subjected to real world loading conditions possess fluid-like characteristics typical of a viscoelastic material. When loaded by means of a stepwise strain, they stress-relax, i.e., the reaction force resulting from the application of an initial peak falls to an asymptotic value, which is theoretically reached after an infinite time [69]. Moreover, if an external force is suddenly applied, creep is observed and the strain begins to change slowly towards a limiting value.

Both these phenomena are caused by the complex geometrical entanglements between chains, which produce a local enhancement of the residual (Vander Waals) force. Under prolonged loading, such "entanglement-cohesion" will slowly breakdown, giving rise to the phenomena of stress-relaxation and creep described above [56]. For shorter times of stressing, these effects are limited and the elastic contribution is predominant.

This behavior provides evidence of the fading memory property of the material. Therefore, the entire strain (and temperature) history must affect the constitutive behavior of filled rubber elastomers. While the strain-rate sensitivity and the failure time dependency are recognized and well-documented in the case of other materials such metals, the incorporation of history-dependent properties of elastomers requires further clarification.

A frequently employed characterization of elastomers is achieved through sinusoidal strain histories of frequency ω. This type of material characterization is frequently referred to as dynamic meaning that it implicates moving parts, differing from methods leading to quasi-static response. Therefore, in this context, the adjective "dynamic" is not reserved to phenomena involving inertia (e.g., wave propagation) which can be neglected in most of the experimental conditions.

Under the action of dynamic loading, the deformation of rubber, like other viscoelastic solids, occurs with a certain delay owing to viscous friction inside the material. Under harmonic deformation, this delay manifests itself by a phase

shift between the applied displacement and the load [70]. This shift is proportional to the viscous losses.

In order to explain thoroughly elastomers behavior under oscillatory deformation, let be the longitudinal displacement in an uniaxial deformation from which the nonlinear Lagrangian strain follows as:

$$u(t) = u_0 + \Delta u \sin(\varpi t) \tag{1}$$

$$\in(t) = \in_0 + \Delta \in_1 \sin(\omega t) \tag{2}$$

obtained by dividing u by the length l_0 of the undeformed specimen. The imposed strain function (2) implies, in the nonlinear case, the time-dependent nominal stress response σ (t), i.e., force applied to the specimen divided by the initial area, whose steady state response is assumed to have the Fourier series

$$\sigma(t) = \frac{b_0}{2} + \sum_{k=1}^{\infty} [a_k \sin(k\omega t) + b_k \cos(k\omega t)] \tag{3}$$

Here

$$S(\in_0, \omega, \Delta \in_1) := \frac{1}{\Delta \in} a_1(\in_0, \omega, \Delta \in_1) \tag{4}$$

$$L(\in_0, \omega, \in_1) := \frac{1}{\Delta \in_1} b_1(\in_0, \omega, \in_1) \tag{5}$$

are the storage and loss moduli, also generically referred to as complex moduli.

In general, neither S nor L depend on $\Delta \in_1$ if $|\Delta \in_1|$ is small (small strain). On the contrary, the aforementioned moduli for carbon black-reinforced rubber show a rather strong dependence on $\Delta \in_1$ in the case $|\Delta \in_1|$ is large. This nonlinear amplitude dependence is called the Payne effect (see Sect. 1.3).

The storage and loss moduli frequency dependence bears no special name, but it is of fundamental importance to understand the dynamic behavior of elastomers.

Figure 10 outlines the dynamic moduli as function of the frequency ω for different values of static prestrain $\in_0$ [71]. At lower frequencies ($\omega \to 0$) the storage modulus tends to a finite nonzero value with a nonzero derivative. This behavior cannot be described by (linear or nonlinear) standard viscoelastic constitutive equations. The data collated by [71] suggest a non-monotonic dependence of the storage modulus upon the static prestrain $\in_0$: from $\in_0 = 0.65$ to $\in_0 = 0.75$, the storage modulus S considerably decreases, but it increases again at $\in_0 = 0.95$. A similar, but less accentuated, trend is shown by the loss modulus. Experiments collated in [72, 73] and more recently in [74] are in agreement with Lee and Kim's results.

As in the static case, the dynamic behavior of elastomers also exhibits very strong temperature dependence. This effect is much more pronounced than in the comparable types of tests conducted upon metals, where the mechanical properties

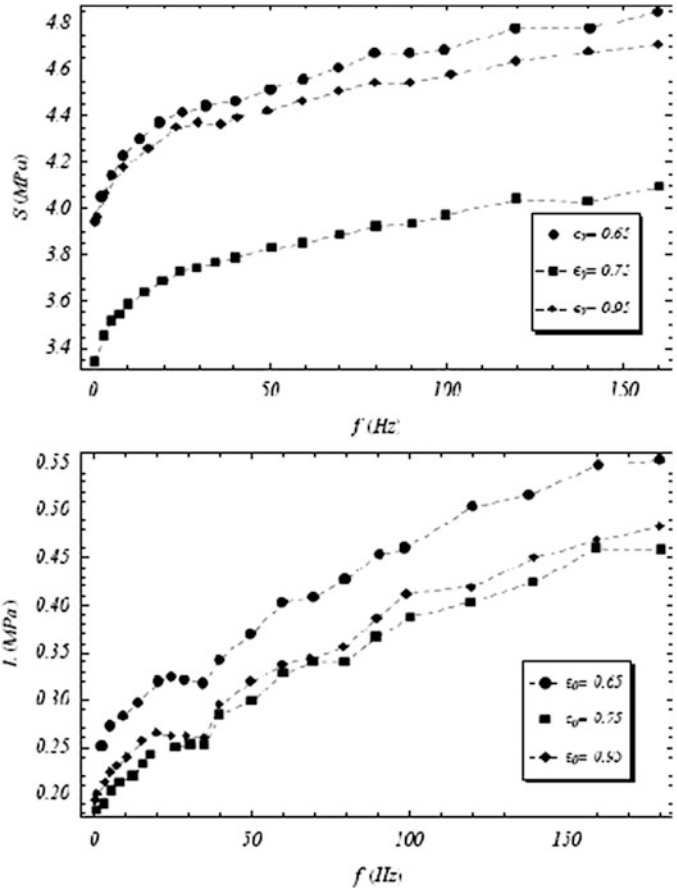

Fig. 10 Storage S and loss L moduli as functions of the frequency ω in the range $\omega \in [0, 1{,}200]$ Hz for different values of static prestrain $e_0 \in \{\mathbf{0.65}; \mathbf{0.75}; \mathbf{0.95}\}$. The amplitude value was $\Delta e_1 = \mathbf{0.63}$ for all the experiments [71]

could reasonably be taken as temperature independent within the common working range.

A standard assumption made in the modeling of filled elastomers, which can be corroborated by experimental data, is the so-called thermorehologically simple behavior. Within this context, the basic postulate is that a viscoelastic mechanical property—relaxation function, creep function or complex moduli—at a series of different temperatures, when plotted against the logarithm of time or frequency can be superimposed to form a single curve [75, 76], shifting the various curves at different temperatures along the time or frequency axis. Such as temperature dependence is schematically shown in Fig. 11 for the storage S and loss L moduli.

Similar temperature dependence is shown for the relaxation function in Figs. 12 and 13 [77]. Materials obeying this empirical principle are called thermorheological

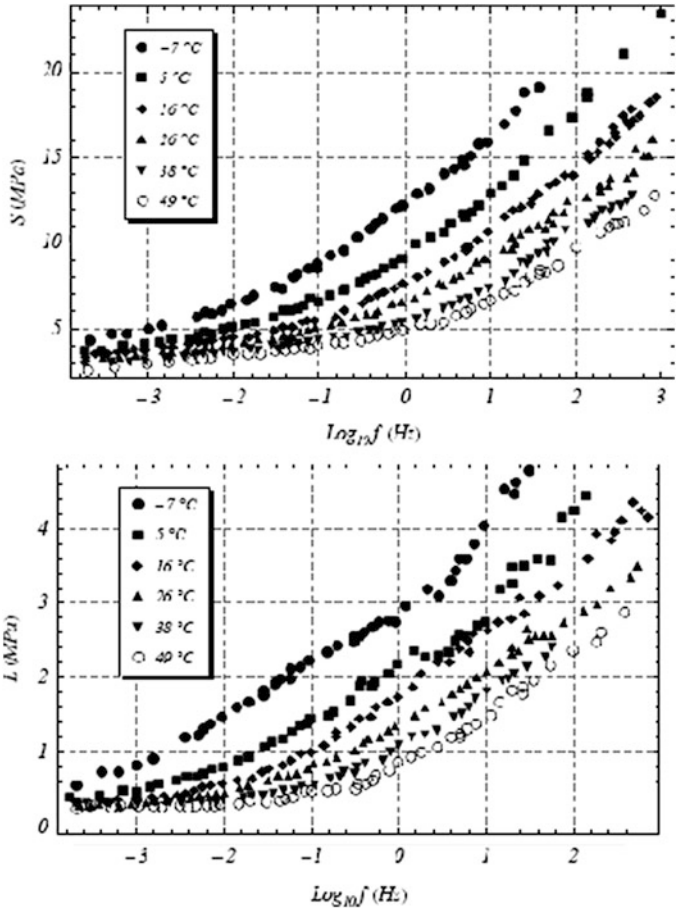

Fig. 11 Storage S and loss L moduli plotted against logarithmic frequency ($\log_{10} f$) for six different temperatures $\mathbf{T} \in \{-\mathbf{7}, \mathbf{5}, \mathbf{16}, \mathbf{26}, \mathbf{38}, \mathbf{49}\}^{\mathbf{o}}\mathbf{C}$ [72]. The same results are shown in a linear frequency scale in Fig. 12

simple. Even for thermorheological simple materials such a procedure can be expected to be valid only over a limited time and temperature range, primarily above the glass transition temperature [78].

The influence of the carbon black loading on the dynamic modulus of the green compound as well as of the vulcanizate can be seen in Fig. 14. The carbon black N 115 was chosen as example, but in principle the behavior is similar for all grades of carbon black. The unfilled rubber shows no indication of non-linearity in the green compound as well as in the vulcanizate. After adding the filler, the low strain modulus G_0 rises more that the high strain modulus G, resulting in a non-linear viscoelastic behavior, known as Payne-effect G_0–G_∞

The viscoelastic behavior vs. strain is investigated for silica filled natural rubber and the results show the qualitative features generally observed for the Payne effect.

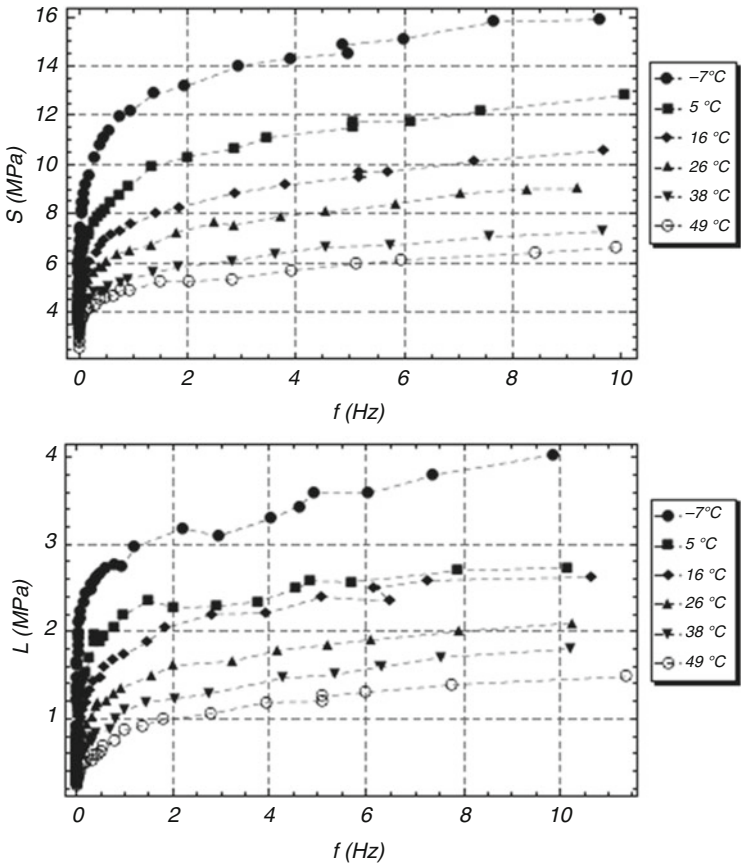

Fig. 12 Storage S and loss L moduli plotted against frequency in the range f $\in$ [0, 15] Hz for six different temperatures T $\in \{-7, 5, 16, 26, 38, 49\}^{o}$C [72]

The effect of the strain amplitude on the storage modulus at various silica concentrations for the composites is shown in Fig. 15.

The storage modulus is the highest at small amplitude (referred to as $E_0^{'}$) and gradually decreases to a low value (referred to as $E_\infty^{'}$). The magnitude of the Payne effect ($E_0{'}$–E'_∞) increases with the silica content. At low silica loading, the observed variation in the amplitude of the Payne effect is weak. But as the silica concentration increases, significant and pronounced variation is observed. This is principally due to the breakdown of the filler networks at high strains. At low filler loading, the chances of forming agglomerates are practically nil. But at higher loading, because of the small particle size (12–13 nm) and high specific surface area [160 (25 m^2/g)], silica particles tend to agglomerate to higher extent. The structure of filler particles within the rubber matrix, i.e., the state of dispersion and aggregation has a strong influence on the Payne effect. In the rubber matrix, the state of

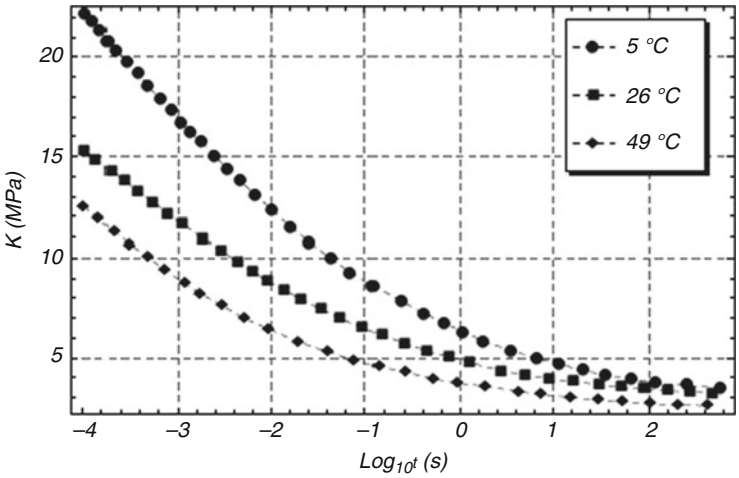

Fig. 13 Relaxation function plotted against logarithmic time ($\log_{10} t$) for three different temperatures $T \in \{5, 26, 49\}^{o}C$ [77]

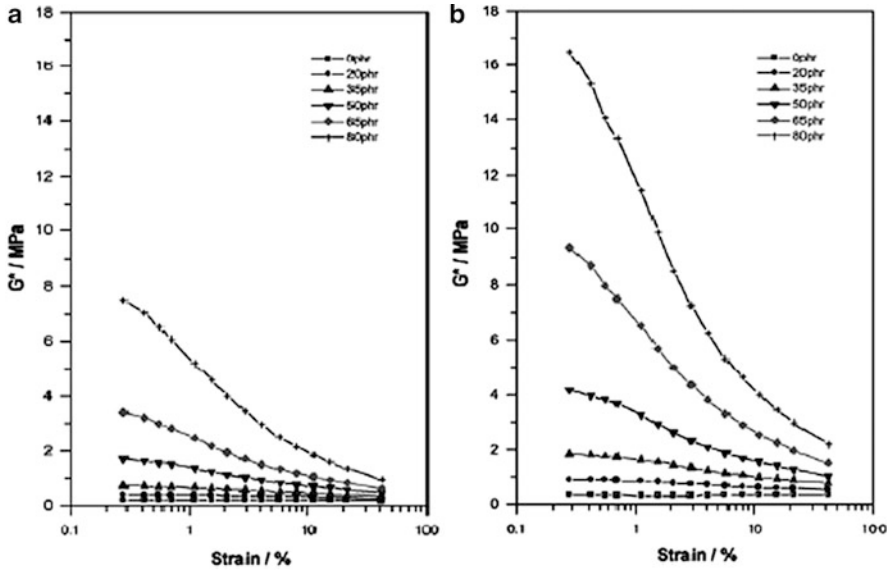

Fig. 14 Strain amplitude dependence of G* of N115 at different loadings (**a**) green compound, (**b**) vulcanizate

dispersion of spherical particles can vary from highly dispersed to totally aggregate depending on the thermodynamics of the system and kinetics of samples preparation. The clustering of filler particles is favored by strong van der Waals forces.

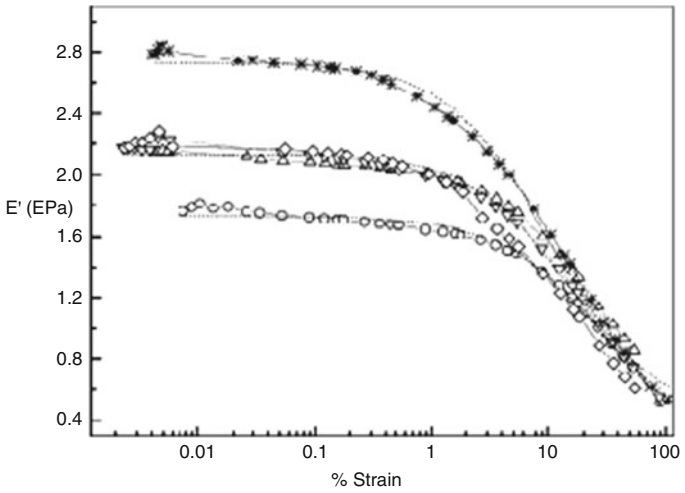

Fig. 15 Strain dependence of the storage modulus for NR filled with nanosilica: (*open circle*) 0 phr, (*open triangle*) 5 phr, (*inverted triangle*) 10 phr, (*open diamond*) 15 phr, (*asterisk*) 20 phr; the *dotted lines* represent the curve firs according to the model

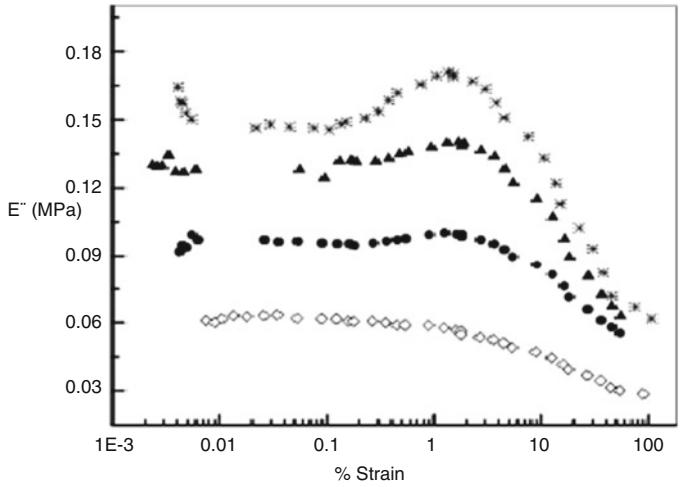

Fig. 16 Strain dependence of loss modulus for silica-filled NR: (*open diamond*) 0 phr, (*filled circle*) 5 phr, (*filled triangle*) 15 phr, (*asterisk*) 20 phr

A maximum in the loss modulus E'' is observed for the composites as shown in Fig. 16.

At filler loading higher than 10 phr, a pronounced maximum is observed. It is thus very appealing to make the hypothesis that different contributions are at stake

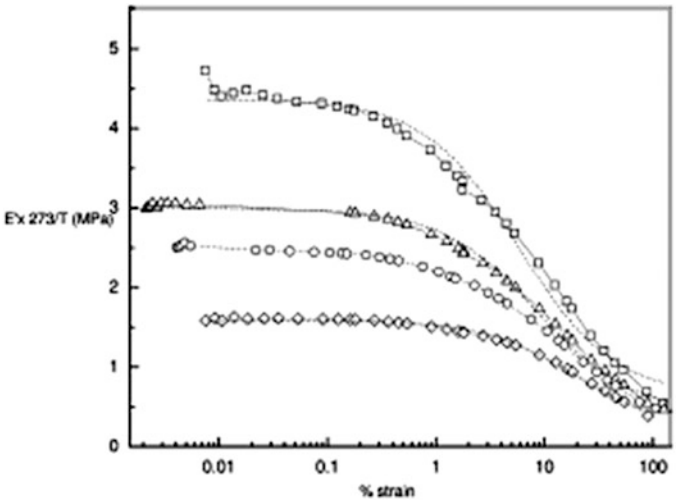

Fig. 17 Effect of temperature on the Payne effect for NR filled with 20 phr silica: (*open square*) 248 K, (*open triangle*) 263 K, (*open circle*) 303 K, (*open diamond*) 373 K. The *dotted lines* represent the curve fits according to the model

in the dissipated energy. One contribution comes from the rubbery matrix and is mainly independent from the filler content. A second one comes from the shearing of the glassy layers around the filler particles. Another contribution may be ascribed to the mechanism responsible for the collapse of the storage modulus. Within the frame of the Kraus model, this extra contribution to the energy dissipation comes from the friction between the filler particles. For models involving bound rubber, it might be related to the friction of the chains, either on the surface of the filler particles or within the glassy layer during its softening under the effect of the applied stress. In those two former mechanisms, the amount of energy dissipated scales the total surface of the particles. The maximum comes from the competition between the breaking and the reformation of the network whatever the nature is (filler-filler, entanglement, glassy bridges, etc.). When the strain increases, the destruction of the network starts and increases the dissipated energy. For higher value of the strain, the rate of destruction is higher than the rate of the reconstruction of the network. As a consequence, the dissipation energy associated with the breaking of the network decreases and the loss modulus goes through a maximum with the strain.

Figure 17 shows the effect of temperature on the Payne effect for natural rubber filled with 20 phr of nano silica

The amplitude of the Payne effect decreases dramatically with temperature. This is contrary to the theory of rubber elasticity, according to which the modulus should increase linearly with the temperature. In agreement with the former explanation given for the Payne effect, the temperature increases the rate of destruction of the network by weakening its cohesion. In the Kraus' model, the temperature affects

the strength of the van der Waals forces between the particles. In the Merabia's vision, the thickness of the glassy layer decreases, diminishing as a consequence the number of glassy bridges forming the network. For Maier and Goritz, the rate of the chains desorption increases with temperature.

Application of the Model of Variable Network Density In the Maier and Goritz model, [21, 30, 31] is assumed that the rubber molecules come in contact with the filler surface and get adsorbed. After forming the first link, the neighboring segments have a high probability to attach to the next interaction position. These chains form stable bonds to the filler surface, whereas the remaining chains coming afterward form unstable bonds having very weak links to the particle. These can be easily removed by a tensile force or by raising the temperature. According to this model, the network density of a filled vulcanised elastomer (N) comes from the overall contribution of the chemical network density, N_c, the chains network density caused by stable bonds at the filler surface, N_{st}, and the density of unstable bonds between chains and filler, N_l

$$N = N_c + N_{st} + N_l \tag{6}$$

Storage modulus $E'(\gamma) = Nk_BT$ where N is the network density, k_B is the Boltzmann constant, and T is the temperature in Kelvin. The strain dependent modulus can be described by means of the theory of entropy and elasticity with

$$E'(\gamma) = (N_c - N_{st} + N_l(\gamma))k_BT \tag{7}$$

By analogy with the Langmuir isotherm formation, it is assumed that the adsorption/desorption process reaches a balance after a certain time. On the assumption that the desorption rate is proportional to the strain amplitude, γ, the dependence of the modulus on γ can be written as

$$E(\gamma) = E'_{st} + E_l/(1 + c\gamma) \tag{8}$$

with

$$E'_{st} = (N_e + N_{st})k_BT \tag{9}$$

and

$$E'_1 = N_k k_B T \tag{10}$$

The experimental curves were fitted to Eq. (8). Figure 16 shows the curve fits for the storage modulus versus the strain amplitude. The fit parameters, E'_{st} and E'_1 and the values of 2/DOF and R_2 to assess the quality of fit are given in Table 1. Both E'_1 and E'_{st} increase with an increase in silica content. The values characterizing the unstable part of the network are strongly influenced by the filler content, as can be

Table 1 Fit parameters of Eq. (6)

Silica content (phr)	E'_{st}(MPa)	E'_{l}(MPa)	c	χ^2/DOF	R^2
0	0.17	1.56	0.03	0.001	0.992
10	0.32	1.82	0.03	0.002	0.993
15	0.43	1.75	0.11	0.002	0.993
20	0.57	2.22	0.15	0.003	0.994

seen from the table. The model equally applies when no filler is added, suggesting that part of the entanglement network has a longer relaxation time than the experimental time defined as the inverse of the frequency.

Both E'_{st} and E'_{l} increase with an increase in silica content. The values characterizing the unstable part of the network are strongly influenced by the filler content, as can be seen from the table. The model equally applies when no filler is add, suggesting that part of the entanglement network has a longer relaxation time than the experimental time defined as the inverse of the frequency.

2.4 Other Nonlinear Effects

Apart from the standard phenomenology described in the previous section, carbon black filled elastomers present some effects peculiar of this class of materials. These effects are the Mullins effect, which concerns the quasistatic behavior, and the Payne effect, dealing with the dynamic response.

2.4.1 Mullins Effect

The Mullins effect [79] is a strain induced softening phenomenon, which is associated mainly with a significant reduction in the stress at a given level of strain during the unloading path as compared with the stress on initial loading in stress-strain cyclic tests [80] (Fig. 18).

In filled rubber this phenomenon is due to the mechanical hysteresis from filler particles debonding from each other or from the polymer chains caused by the stretching. Owing to this, highly reinforced elastomers suffer a more pronounced stiffness reduction than those with low filler content. After the first few loading/unloading cycles the internal microstructure reaches a permanent state and changes in stiffness become no more significant. Figure 18 represents typical loading/unloading curves for a rubber specimen subjected to multiple cycles of uniaxial stretching [80]. Although this an elastic effect is irreversible for a fixed temperature, an increase in the temperature of the specimen could result in a partial recovery of the previously broken bonds and, consequently, on a recovery of the material stiffness.

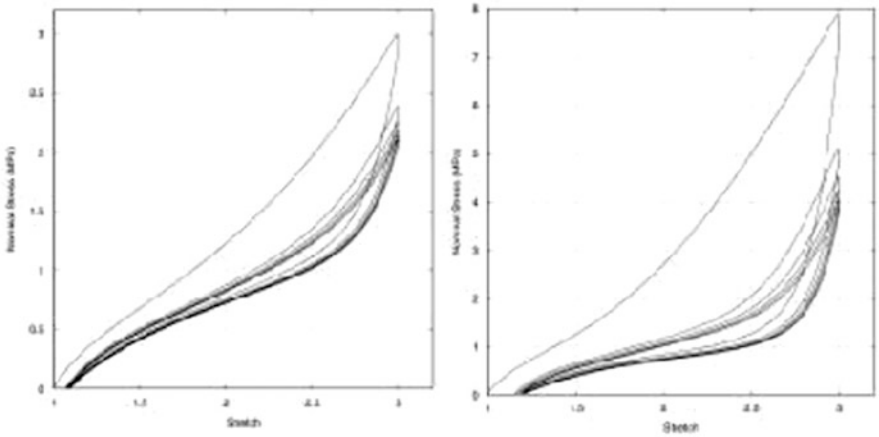

Fig. 18 Pre-conditioning cycles of a particle-reinforced dumbbell specimen with 20 phr (*left*) and 60 phr (*right*) of carbon black with maximum stretch $\lambda := \ell/\ell_0 = 3$ [81]

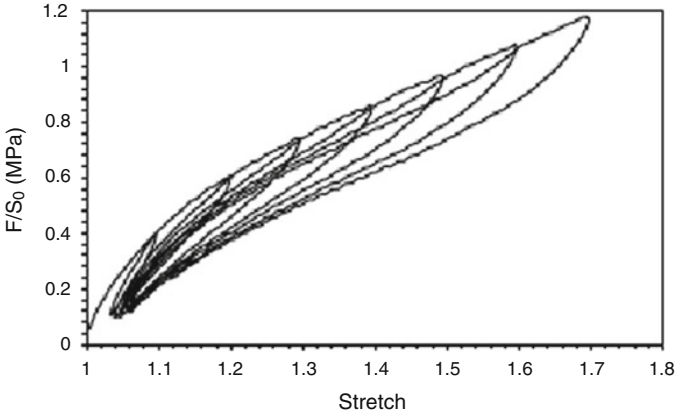

Fig. 19 Mullins effect at small and moderate deformations observed on a 50 phr carbon-black filled SBR submitted to cyclic uniaxial tension

The Mullins effect at small and moderate deformations observed on a 50phr carbon-black filled SBR submitted to cyclic uniaxial tension are represented in Fig. 19.

The literature reports Mullins effect for various materials (see Table 2).

The first attempt to develop a quantitative theory to account for the softening resulting from rubber stretching was developed by [93]. They considered that value of the shear modulus G is a measure of the total number of cross-links within rubber and a reflection of the chemical cross-links produced within vulcanization as well as linkages between rubber and filler. They suggested that the decrease in G was due to

Table 2 Examples of materials showing some Mullins softening

Gum nature	No filler	Carbon black fillers	Silica fillers	Other fillers
NR	[82–84]	[82–84]	[90]	[90]
SBR		[83, 85, 86]	[18]	
NBR	[87]			
EPDM		[85, 86, 88]		
PDMS			[89, 91, 92]	
Neoprene		[86]		

the breakdown of linkages between filler and rubber. Their interpretation has provided a useful starting point for the work of other researchers.

One of the other early investigations was done by Mullins and Tobin [94] who considered the filled rubber as a heterogeneous system comprising hard and soft phases. The hard phase was considered to be inextensible and the soft phase to have the characteristics of gum rubber. During deformation, hard regions are broken down and transformed into soft regions. Then the fraction of the soft region becomes greater with the increasing tension which in turn is responsible for the reduced material stiffness. However, Mullins and Tobin did not provide a direct physical interpretation for their model. More recently, new insights into Mullin's effect have been obtained and many researchers proposed their own constitutive model [52, 81, 95–97].

In [52] a micromechanically based continuum damage model for carbon-black filled elastomers was introduced. The key point of the paper was to incorporate both a damage induced phenomenon such as Mullin's effect and the viscous behavior of a theory of viscoelasticity. Within the framework of damage elasticity, relaxation processes in the material are described via stress-like convected internal variables, governed by dissipative evolution equations they are interpreted as the nonequilibrium interaction stresses between the polymer chains in the network. Ogden and Roxburgh [97] proposed to account for the Mullins effect with a phenomenological model based on the theory of incompressible isotropic elasticity amended by the incorporation of a single continuous damage parameter. The dissipation is measured by a damage function which depends only on the damage parameter and on the point of the primary loading path from which unloading begins. A specific form of this function with two adjustable material constants, coupled with standard forms of the (incompressible, isotropic) strain-energy function, was used to illustrate the qualitative features of the Mullins effect in both simple tension and pure shear. However any effects of residual strain were not incorporated. Dorfmann and Ogden [81] introduced a constitutive model for the Mullins effect with permanent set in particle-reinforced rubber. The theory of pseudoelasticity has been used for this model, the basis of which is the inclusion of two variables in the energy function in order to capture separately the stress softening and residual strain effects. The dissipation of energy i.e. the difference between the energy input during loading and the energy returned on unloading is

also accounted for in the model by the use of a dissipation function, which evolves with deformation history.

A phenomenological model based on the limiting chain extensibility associated with the Gent model of rubber elasticity has been proposed by [96]. The Gent strain energy function [98] was modified to incorporate stress softening characteristics typical of the Mullins effect. Although the Gent model is phenomenological in nature, a microscopically based interpretation was given to all of its constitutive parameters. In this way, it has been possible to develop a model for the Mullins effect based on the alteration of the polymeric network. Indeed they showed that their approach is a particular case of the more general framework of pseudo-elasticity developed in [97].

Simo [51] proposed to penalize the classic elastic strain energy densities, W_0(F), designed to fit the hyperelastic stress-strain responses of rubber-like materials submitted to the deformation gradient F, by a reducing parameter of the Kachanov form [99].

$$W(F) = (1 - d)W_0(F) \tag{11}$$

The parameter d defines a damage, which is a priori unknown and may cover any physical phenomenon like chain and multichain damage, microstructural damage, microvoid formation. . .. During the past three decades, various models have been defined according to equation.

The influence of the epoxidation in the main chain of SBR can be better understanding through the linear viscoelastic behavior of filled compounds. This normally reflects the state of the filler network and the breakdown of this network is induced by the increase in the amplitude of deformation during the dynamic-mechanical experiment.

A vulcanized sample, obtained from a reference mixture, contained mainly SBR-2 non epoxidized and precipitated silica, presents a value of the storage modulus (G′) at low amplitude of deformation, which is 4 times higher than that value showed by a mixture of SBR-2(ep7)/silica. This reduction of G′ shows a slightly network, due to the favorable energetically interaction between epoxy groups of the epoxidized rubber and the silanol groups present onto the silica surface. Because of that, it is possible to have a better dispersion leading to a reduction of the Payne effect (Fig. 20).

The modification of the silica surface activity is obtained via silanization *in situ*, which has been used to reduce the silica polarity. As expected, it was observed a reduction in the G′ and in the Payne effect as the silanization takes place in the precipitated silica. Analyzing the dependency of G′ as function of deformation amplitude to the compound SBR-2/silica/silane, it can be seen that the silanization leads to a decrease of 2.5 ties of the G′ value in comparison to the reference compound. However, it should be noticed that first, the reduction of the Payne effect is remarkably lower than that obtained to the SBR-2(ep7) and non silanized silica compound and, second, the value of G' obtained to SBR-2(ep7) and silanized silica is comparable to the SBR-2/sílica/silano system.

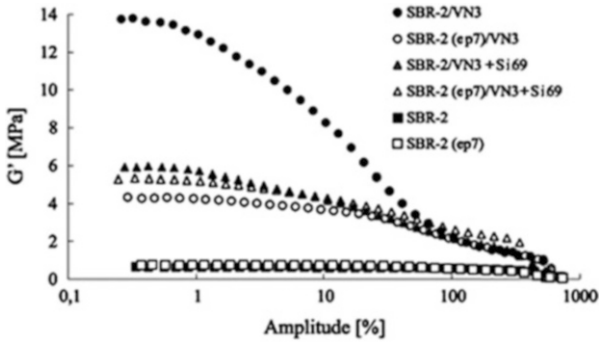

Fig. 20 Influence of silica modification on the interaction on the interaction elastomer-filler of SBR-2 and SBR-2

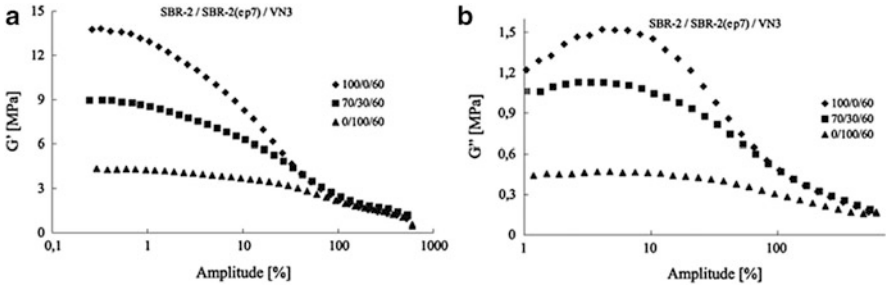

Fig. 21 Influence of the epoxidized rubber content on (**a**) storage modulus and (**b**) loss modulus, considering a rubber compound filled with 60 phr of silica

Taking into account the vulcanized SBR-2(ep7), the *in situ* silanization of the precipitated silica leads to a small increase in the G′ values, indicating that the polymer-filler interaction is masked by the modification of the silica surface activity. As the silica surface becomes partially hydrophobic by the *in situ* silanization, the epoxy groups, which are polar, cannot interact anymore which the same intensity as they do with the non silanized silica. Taking this into account the filler-filler interaction becomes to be stronger and *G′* is higher. Based on that, the idea, that *G′* is very sensitive to changes in the polymer-filler interaction and can be caused either by the functional groups of the polymer or by modification in the filler surface activity, becomes more pronounced. The study of the influence of the epoxidation on the dynamic-mechanical behavior of SBR blends, original and epoxidized, is presented in Fig. 21a, b.

It is important to see, that as the content of SBR-2(ep7) with 7 mol% of epoxy groups) is increased in blends, the G′ value decrease remarkably. Only 30 parts (weight) of SBR-2(ep7) in blends, which is similar to 2 mol% of epoxy groups in the total of the blend, leads to a decrease of 40 % in the G′ value. Considering the broad amplitude region of deformation, it can be seen a very small increase in the G′

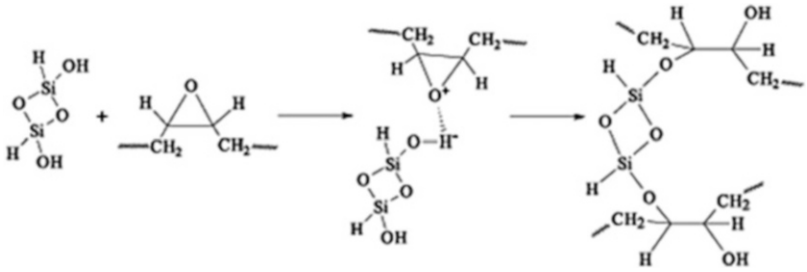

Fig. 22 Schema of a proposed for the epoxidized rubber-silica interaction

value, as the epoxidation content increase. Analysing the loss modulus, G″, it was observed a decrease about 35 % of the maximum value of this modulus, as the content of SBR-2(ep7) increases, confirming the idea of a more efficient rubber-filler interaction.

The relatively strong interaction, which occurs between epoxidized SBR and precipitated silica, can be attributed to formation of hydrogen bonds or even chemical bonds formed after a possible ring opening (epoxy group) and covalent bond. An proposed schema of this mechanism is presented in Fig. 22.

The influence of the silica precipitated presence in blends on the G' and G'' moduli for epoxidized and non epoxidized SBR, considering a sweep temperature experiment at amplitude of deformation and frequency constant. It is already ready known that important information about the rubber-filler interaction can be obtained from the analysis of the loss modulus of a filled compound in the glass transition region as a function of temperature [100]. The area of the maximum peak of the loss modulus indicates the dissipated energy by volume unit of a sample during the transition from the glass region (rigid) to the flexible stage. If the rubber-filler interactions are present a polymer system, a fraction of the polymer chain is immobilized in the interface rubber-filler. Therefore the dissipated energy during the glass transition increase above the level of the sample without filler, due to the contribution of the fixed polymeric chain. For this increase there are two main contribution, the volume fraction of the immobilized polymeric layer and the rubber-filler interaction. Consequently, monitoring the increase of the amplitude (or area) of the maximum in G'' in the glass transition, qualitative information about the rubber-filler interaction can be deduced. The changes in the G'' caused by the incorporation of 60 phr of silica in SBR and SBR-2(ep7), respectively, becomes to be evident when the values are compared with those of the vulcanized without filler (Fig. 23).

Considering the system without filler, even 7 mol% of epoxy groups in the main chain lead to considerable variation in the Tg and maximum value of G''. This result underlines the thermo-analytical variations considering dynamic changes in the chains. The incorporation of precipitated silica in both polymers leads to small changes in the glass transition temperature and, at the same time, causes remarkably increase of the maximum G'' value. A more detailed date evaluation shows that by

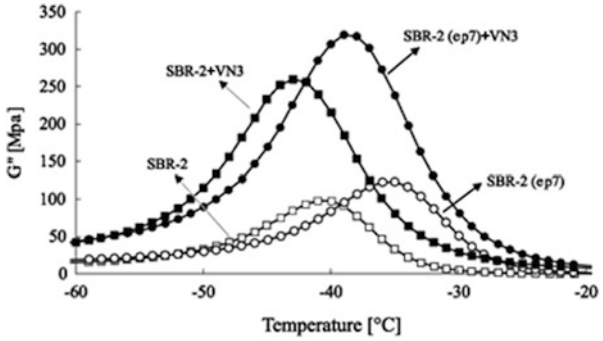

Fig. 23 Interaction analysis between rubber matrix, SBR-2 and SBR-2 (ep7), filled with 60 phr of silica (VN3) considering the loss modulus 60 phr variation in a sweep temperature experiment at constant amplitude deformation (0.1 %)

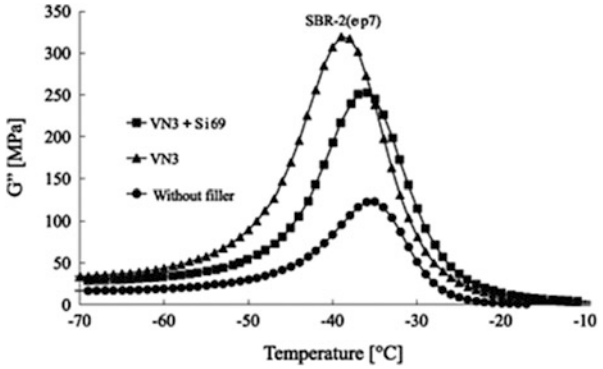

Fig. 24 Influence of the silica polarity on the rubber filler interaction of an elastomer with 7 mol% of epoxy groups-SBR-2 (ep7)

the relative increase of the G'' maximum is more pronounced to SBR-2(ep7)/silica than to SBR/silica, if the unfilled compound is taking as reference. Considering that the effect of hydrodynamic reinforcement act in the same manner in both systems, it is possible to say that this higher maximum G" value for SBR-2/silica occurs due to the specific interaction rubber-filler.

Another point is achieved by comparing the dynamic-mechanical effects caused by the use of silanized and non silanized silica (Fig. 24).

Considering the same filler content , the compound with silanized silica presents a maximum G'' value lower (70 MPa) than that with non silanized silica. This result can be understanding, in the case when the silica surface activity decrease, due to the silanization reaction. As consequence of the silanization, the physical interaction of the less polar filler surface with epoxidized SBR, or the cross section of the chemical bond became reduced. Both mechanisms cause a decrease in the volume

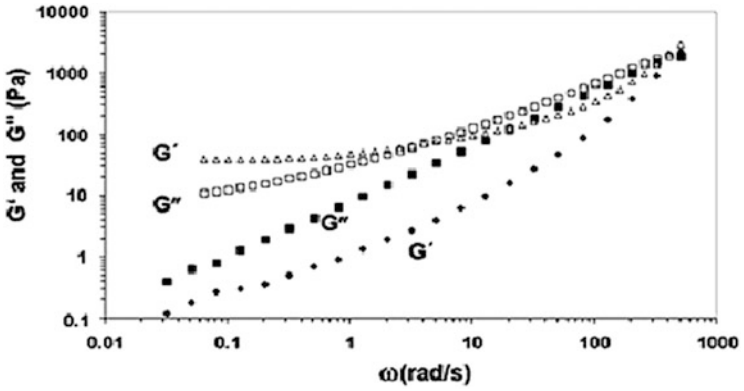

Fig. 25 Variation of the complex shear modulus of the PDMS/CNT suspension. *Filled symbol*: viscoelastic behaviour measured just after the compressive deformation, the CNT's are supposed to be well dispersed in the PDMS matrix. *Open symbols*: viscoelasticity beahaviour measured at the end the aggregation process under $\gamma_0 = 30\,\%$

fraction of the polymeric chain strongly immobilized onto the filler surface. Therefore less mechanical energy is dissipated during the glass transition process for systems containing silanized silica.

Figure 25 shows that the viscoelastic behaviour strongly depends on nanotube dispersion. When the nanotubes are supposed to be well dispersed in an isotropic configuration, the variation of the complex shear modulus (under 5 % strain) shows a rheological behaviour close to the viscoelastic behaviour of the PDMS matrix, i.e. a liquid viscoelastic behaviour. After the aggregation process, the viscoelastic behaviour of the composite shows a solid-like behaviour, at least in the frequency window used in the present study, due to the formation of the CNT network from dynamic CNT aggregation.

2.4.2 Payne Effect

Another softening phenomenon which manifests the dependence of the stress upon the entire history of deformation is the so-called Payne effect. Like the Mullins effect, this is a softening phenomena but it concerns the behavior of carbon black-filled rubber subjected to oscillatory displacement. Strain dependence of the storage and loss moduli (Payne effect) at 70 °C and 10 Hz for a rubber compound with different concentration of carbon black filler [7] (Fig. 26). Indeed, the dynamic part of the stress response presents a rather strong nonlinear amplitude dependence, which is actually the Payne effect [8, 16, 43].

For a dynamic strain arising from a harmonic displacement, the storage and loss moduli depends nonlinearly upon the strain amplitude $\Delta \in_1$ as shown in Fig. 26 for a strain amplitude in the range $\Delta \in \in$ [0:1; 0:6] and a frequency $f = 2\pi/\omega = 10$ Hz

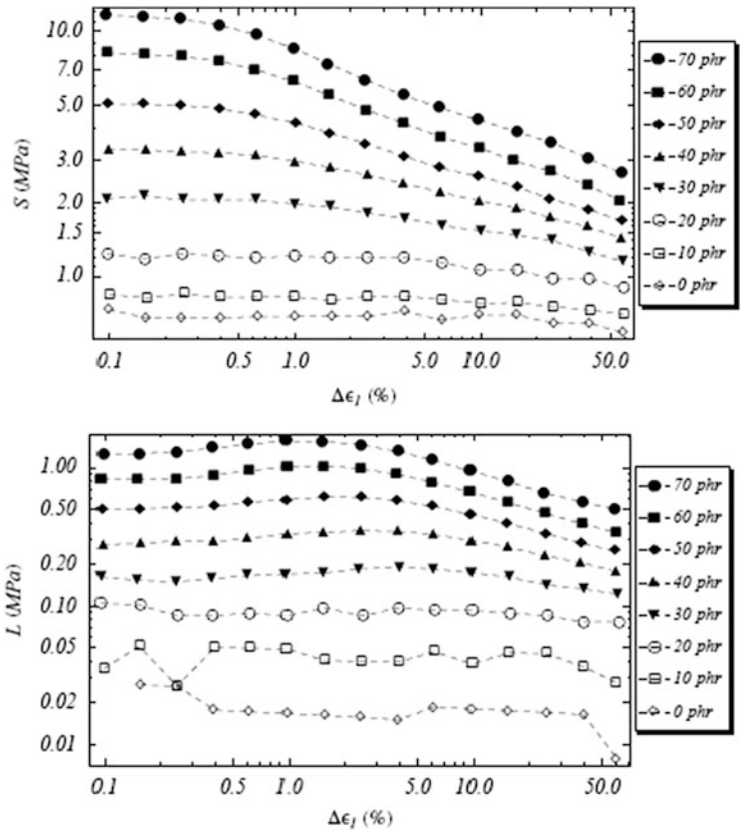

Fig. 26 Strain dependence of the storage and loss moduli (Payne effect) at 70 °C and 10 Hz for a rubber compound with different concentration of carbon black filler [7]. The graphs suggest a monotonic dependence of the dynamic moduli on the filler content in the range $\phi \in [0; 70]$ phr. The Payne effect becomes unnoticeable for low reinforced elastomers ($\phi \in [0; 10]$phr)

There have been several attempts to explain the Payne effect by macroscale mechanism based models. Chazeau et al. [43] classify them as (i) filler-structure models, (ii) matrix filler bonding and debonding models and (iii) phenomenological or nonlinear network models. They also state: "Payne himself suggested qualitatively that the amplitude dependence of the torage and loss moduli were due to a filler network in which the filler contacts depended on the strain amplitude. At lower amplitudes, he argued that the filler contacts are largely intact and contribute to the high value of the modulus [moduli, the author]. Conversely, at higher amplitudes the filler structure has broken down and does not have time to reform". Therefore, Payne's explanation is of class (ii).

Following the work of Payne, [1] proposed an empirical model based on the agglomeration/deagglomeration kinetics of filler aggregates, assuming a Van der Waals type interaction between the particles. In a paper addressing universal

properties in the dynamic deformation of filled rubbers, [146] introduced the rheological model of Zener with a nonlinear and linear spring and a dashpot to corroborate the phenomenologically based formula

$$\frac{G^{'} - G^{'}_{\infty}}{G^{'}_{0} - G^{'}_{\infty}} = \frac{1}{1 + (\Delta \in_1 / a_c)^{2m}} \tag{12}$$

where G' is the storage modulus, $G^{'}_{\infty}$ its value at very large strain and $G^{'}_{0}$ the corresponding value at very small strain. Moreover, a_c is a constant and m 0.6 is nearly universal, i.e. to a large extent independent of temperature, frequency, filler content and type of carbon.

Whilst Huber et al. [146] obtained result is still based on a rheological model. Chazeau et al. [43] stress this effect in their paper, and so it qualifies no or no much, better than the phenomenological approach of continuum mechanicians [101] who postulate nonlinear stress strain behavior. In those approaches the matrix filler bonding and debonding is formulated considering the dependence upon the entire stress history with the debonding modeled by the appropriate irreversibility properties. In 1999 Wang [7] investigated the impact of the filler network, both its strength and architecture on the dynamic modulus and hysteresis during dynamic strain. It was found that the filler network can substantially increase the effective volume of the filler due to rubber trapped in the agglomerates, leading to high elastic modulus. During the cyclic strain, while the stable filler network can reduce the hysteresis of the filled rubber, the breakdown and reformation of the filler network would cause an additional energy dissipation resulting in the higher hysteresis.

Therefore, higher hysteresis at low temperature and low hysteresis at high temperature could be achieved by depressing filler network formation.

Even though the Payne effect has been known for more than 40 years, a model able to describe such a phenomenon in the relevant frequency and amplitude range is still missing.

The storage modulus is less strain-dependent in the low strain region for $\gamma < 1\ \%$; whereas a strain-dependence behaviour occurs over two decades at high strains. For the EVA concentrations below the entangled regime, Payne effect is still observed even at low concentration of silica particles ($\Phi < vol 3.3\ \%$) below to the percolation threshold as calculated later. This observation evidences that the nonlinear behaviour associated with trapped entanglement cannot be considered as relevant here. Indeed, the Payne effect is observed for non-entangled dilution. Moreover, the non-linear behaviour associated with break down of particle network cannot be invoked, as Payne effect is observed at silica concentration far below the percolation threshold.

Actually, the non-linear behaviour can be imagine associated with both mechanisms of chain disentanglements and filler breakdown depending of silica concentration and amplitude deformation. Indeed, the degree of non-linearity increases continually with filler concentration for filled molten EVA (Fig. 27a) whereas, the

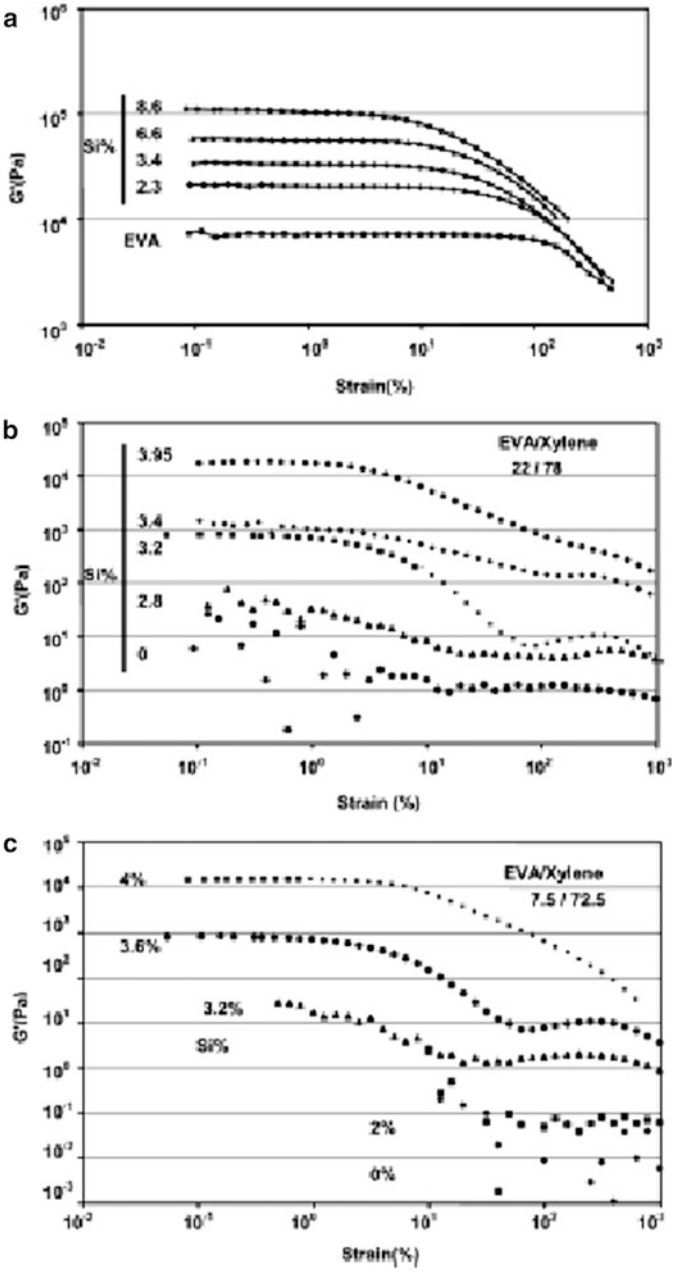

Fig. 27 Payne effect variation of the storage modulus versus deformation at different silica concetration $\omega = 10$ rad/s. (**a**) EVA/xylene, 100/0, melt EVA, T = 140 °C, (**b**) EVA/xylene: 78/22, t = 21 °C (**c**) EVA/xylene 92.5/7.5, T = 21 °C

degree of non-linearity seems to be constant for diluted solutions whatever the concentration in silica (Fig. 27c) and concentrations in polymer below φ_c. Furthermore, a singular behaviour is observed at strains above 10 % for diluted solution of EVA in xylene. Usually, a sigmodal decline is observed leading to a lower plateau at high deformations. Figure 27c shows that for diluted solution the storage modulus slightly increases for deformation higher than 100 % and goes through a maximum around 300 % before decreasing again. However, this behaviour is less pronounced for concentrated solution ($\varphi \geq \varphi_c$) as the amplitude dependence of the storage modulus only exhibits a shoulder around 300 % (Fig. 27b). It can be pointed out that same trends were observed for the variation of the loss modulus. This singular behaviour could be explained by a re-arrangement of the filler particles in the flow direction after the break down of the equilibrium filler network. However, another explanation could be the stress-induced debonding of polymer chains from the filler surface at high deformation.

The dynamic behavior of filled rubbers is of great importance in the performance of rubber engineering components and is essential in tire applications.

The modulus drop ($\Delta G = G_0^{'} - G_\infty^{'}$) with strain amplitude, showing a typical nonlinear behavior, represents the Payne effect. At larger deformations, the difference between unfilled and filled rubber (G¤) contains the contribution arising from the inclusion of rigid particles (accounted for by the Guth and Gold expression) and also the contribution of the polymer–filler cross links to the network structure31 (Fig. 28a). The Payne effect is influenced by filler parameters: concentration, surface area, distribution, surface characteristics, and temperature. As seen in Fig. 28a, the chemical modification of the silica particles by means of the coupling agent reduces the amplitude of the Payne effect (modulus drop with strain amplitude), the loss modulus, and tgδ, which is an important parameter in the rolling resistance of tires.

The main aspects of the nonlinear theory of elasticity are presented. As nonlinear elasticity, and, in particular, hyperelasticity, is such a useful tool in the description of the behavior of carbon black-filled rubber undergoing quasi-static loadings, the main methodologies for describing the behavior of materials subjected to large strains are introduced. Some of the results herein presented will be applied to nonlinear viscoelastic constitutive models and discussed in subsequent review.

3 Nonlinear Elasticity

3.1 Kinematics

In the following section, the basic concepts used to describe the (finite) deformation of a simple material are briefly presented. A comprehensive introduction of finite elasticity can be found, for instance, in [97, 102, 103].

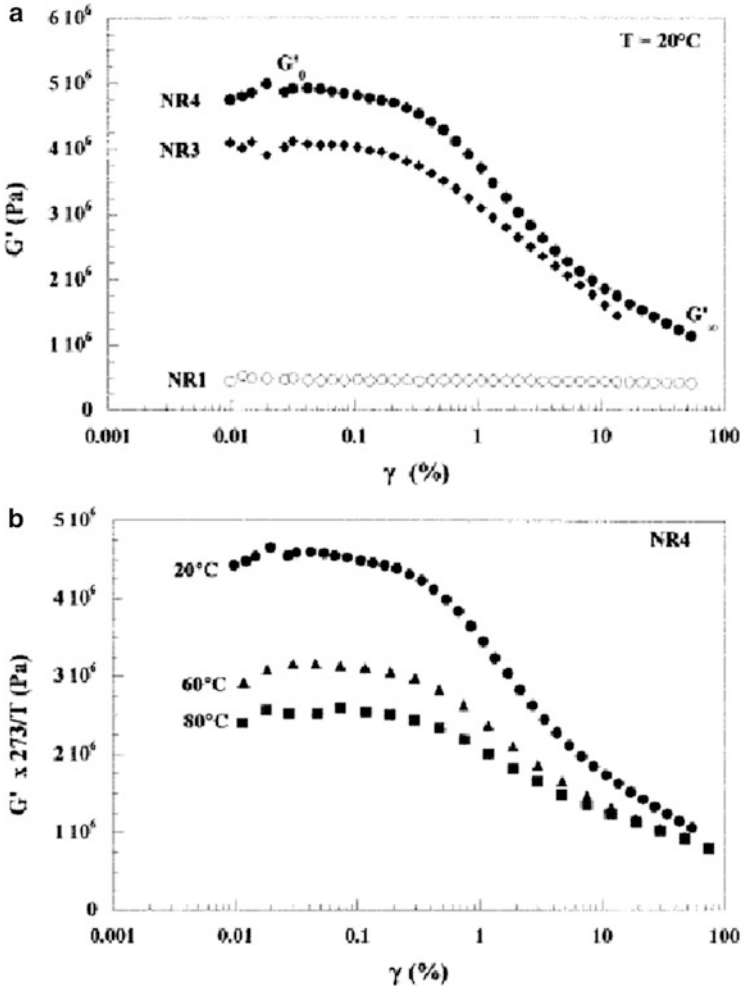

Fig. 28 Effect of the nature of the interface (**a**) and on the temperature (**b**) on the Payne effect

We consider a continuous body which occupies a connected open subset of a three dimensional Euclidean point space, and we refer to such a subset as a configuration of the body. We identify an arbitrary configuration as a reference configuration and denote this by $\mathfrak{R}_r$.

Let points in $\mathfrak{R}_r$ be labelled by their position vectors X relative to an arbitrarily chosen origin and let $\partial\mathfrak{R}_r$ denote the boundary of $\mathfrak{R}_r$. Now suppose that the body is deformed quasi-statically from $\mathfrak{R}_r$ so that it occupies a new configuration, $\mathfrak{R}$ say, with boundary $\partial\mathfrak{R}$. We refer to $\mathfrak{R}$ as the current or deformed configuration of the body. The deformation is represented by the mapping: $\mathfrak{R}_r \rightarrow \mathfrak{R}$ which takes points X in $\mathfrak{R}_r$ to points x in $\mathfrak{R}$. Thus,

$$x = \chi(X), X \in \mathfrak{R}_r \tag{13}$$

where x is the position vector of the point X in $\mathfrak{R}$. The mapping is called the deformation from $\mathfrak{R}_r$ to $\mathfrak{R}$ and is required to be one-to-one. Its inverse χ^{-1} satisfies

$$X = \chi^{-1}(x), x \in \mathfrak{R} \tag{14}$$

Both χ and its inverse are assumed to satisfy proper regularity conditions, e.g., $C^2(\mathfrak{R}_r) \cap C^0(\overline{\mathfrak{R}_r})$. For simplicity we consider only Cartesian coordinate systems and let X and x respectively have coordinates X_α and x_i, where $\alpha, i \in \{1, 2, 3\}$, so that $x_i = \chi(X_\alpha)$. Greek and Roman indices refer, respectively, to $\mathfrak{R}_r$ and $\mathfrak{R}$ and the usual summation convention for repeated indices is used.

The deformation gradient tensor, denoted F, is given by

$$F = Gradx \tag{15}$$

and has Cartesian components $F_{i\alpha} = \partial x_i / \partial X_\alpha$, Grad being the gradient operator in $\mathfrak{R}_r$. Local invertibility of requires that F be non-singular. Similarly, for the inverse deformation gradient

$$F^{-1} = gradX, \left(F^{-1}\right)_{\alpha i} = \frac{\partial_\alpha}{\partial x_i} \tag{16}$$

where grad is the gradient operator in $\mathfrak{R}$. With the use of the notation defined by

$$J = \det F \tag{17}$$

The equation

$$dx = FdX \tag{18}$$

(in components $dx = F_{i\alpha} dX_\alpha$) describes how an infinitesimal line element dX of material at the point X transforms linearly under the deformation into the line element dx at x.

Following [50], we can define a tensor measure of strain:

$$G = \frac{1}{2}\left(F^T F - I\right) \tag{19}$$

where I is the identity tensor, and G is called Green strain tensor.

Other suitable strain measures are:

$$C = F^T F, \quad B = FF^T \tag{20}$$

which are called, respectively, the right and the left Cauchy-Green deformation tensors.

3.2 Strain Energy Function

Materials whose constitutive behavior is only a function of the current state of deformation, measured through C or G, are generally known as elastic or Cauchy elastic materials. In this setting a more useful concept from both theory and applications is hyperelasticity (or Green elasticity), which is a particular case of Cauchy elasticity. In the case of hyperelastic materials the existence of a strain energy function ψ defined on the space of deformation gradient is postulated: the work done by the stresses during a deformation process is only dependent on the initial and final body configurations.

For such materials the following stress measure can be introduced:

$$T = \frac{\partial \Psi(G)}{\partial G} \tag{21}$$

which is called the second Piola-Kirchhoff stress tensor: it represents a contact force density measured in the current configuration per unit area of the reference shape.

According to (21), we can introduce other well-known stress measures, e.g.,

$$\prod = FT = F\frac{\partial \Psi}{\partial G} \tag{22}$$

$$\sigma = J^{-1}\prod F^T = J^{-1}F\frac{\partial \Psi}{\partial G}F^T \tag{23}$$

where J = det F, T is the so called nominal stress tensor and σ is the Cauchy stress tensor. The mechanical interpretation of these stress measures are:

- The second Piola-Kirchhoff stress tensor represents a contact force density measured in the reference configuration per unit of reference area.
- The Cauchy stress tensor represents a contact force density measured in the current configuration per unit of current area.
- Π^T is called first Piola-Kirchhoff; it expresses the contact force density in the reference frame per unit of current area.

We remark that the only assumption used to introduce definitions (21)–(23) is that a strain energy density function can be defined in the reference configuration. Indeed, this is the most general way of describing nonlinear elastic simple

materials. Moreover, since the function depends only on the Cauchy-Green strain tensor G and it is defined in the reference configuration, it is not affected by any change of observer. The previous requirement is mechanically known as Principle of Frame Invariance and for the constitutive relations (21)–(23) is automatically fulfilled [104–108]. In order to clarify this assertion, let us suppose that a rigid-body motion, i.e.,

$$x^* = Qx + c$$

is superimposed on the deformation x $=\chi$(X), where Q and c are constant with respect to the position X (c is the translation vector). Q belongs to the class of the orthogonal tensor, which we will call Orth3. The resulting deformation gradient, say F^*, is given by

$$F^* = QF$$

and

$$G^* := \frac{1}{2}\left(F^{*T}F^* - I\right) = G$$

Therefore, using Eq. (23) the following relation for the Cauchy stress tensor holds for each deformation gradient F and for all Q $\in$ Orth$_3$:

$$\sigma^* = Q\sigma Q^T \tag{24}$$

Relation (24) expresses the fact that the constitutive law (23) is objective. In essence, it means that the material properties are independent on superimposed rigid-body motions.

3.3 Restrictions on the Strain Energy Function

The form of the constitutive law can be simplified if the material is characterized by some symmetry properties. From the physical point of view this means that there exists change in the reference placement such that after this change the material is indistinguishable.

The set of all material symmetry transformations at a material point X depends on the selected reference configuration and for hyperelastic materials can be defined as

$$gR, x = \left\{H \in Lin^+ | \det H = 1 \wedge \Psi\left(H^T G H\right) = \Psi(G)\right\} \tag{25}$$

where Lin$^+$ is the space of the positive definite tensor. The set gR,x is a group [50], for the completed proof) and it is called material symmetry group. Materials which

are indistinguishable after every rotation of the reference frame are called isotropic materials. In such a case, it results

$$Orth_3^+ \subset gR, x \tag{26}$$

i.e., the symmetry group contains the class of all the rotations of the reference frame. Constitutive equations for isotropic materials are, actually, the simplest ones.

According to (25), for isotropic materials the energy function must fulfill the condition:

$$\forall Q \in Orth_3^+, \Psi\left(Q^T G Q\right) = \Psi(G) \tag{27}$$

$Orth_3^+$ being the class of all the rotations.

Every scalar function ψ of a symmetric tensor G which satisfies (27) is called an Isotropic Tensor Function of G. An isotropic scalar-valued function of G is also called a scalar invariant of G. It may easily be checked that the principal invariants of G, defined by

$$\widehat{I}_1(G) = trG \tag{28}$$

$$\widehat{I}_2(G) = \frac{1}{2}\left[I_1^2(G) - trG^2\right] \tag{29}$$

$$\widehat{I}_3(G) = \det G \tag{30}$$

are scalar invariants in accordance with definition (27).

Rivlin and Ericksen [109] showed that a scalar-valued function of a symmetric tensor G is isotropic if and only if it is expressible as a function of I_1(G), I_2(G) and I_3(G).

Hence, for isotropic materials the strain energy density function takes the form:

$$X = \chi(X), X \in \Re_r$$

or, since

$$\Psi(G) = \widehat{\Psi}\left(\widehat{I}_1(G), \widehat{I}_2(G), \widehat{I}_3(G)\right) \tag{31}$$

$$G = \frac{1}{2}(C - I) \tag{32}$$

it is natural to express the strain energy density function in terms of the invariants of the strain tensor C, i.e.,

$$\Psi(C) = \Psi(I_1, I_2, I_3) \tag{33}$$

where

$$I_1 = \widehat{I}_1(C), I_2 = \widehat{I}_2(C), I_3 = \widehat{I}_3(C) \tag{34}$$

According to Eq. (31) and definitions (28)–(30), the most general form of the second Piola-Kirchhoff stress tensor for an isotropic and hyperelastic material is:

$$T = 2\frac{\partial \Psi}{\partial C}$$
$$T = 2\left(\frac{\partial \Psi}{\partial I_1} + I_1 \frac{\partial \Psi}{\partial I_2}\right) I - 2\frac{\partial \Psi}{\partial I_2} C + 2I_3 \frac{\partial \Psi}{\partial I_3} C^{-1} \tag{35}$$

where the following equalities have been used:

$$\frac{\partial I_1}{\partial C} = I, \frac{\partial I_2}{\partial C} = I_1 I - C, \frac{\partial I_3}{\partial C} = I_3 C^{-1} \tag{36}$$

From Eq. (23), the relation between the Cauchy stress and the strain invariants follows:

$$\begin{aligned} \sigma &= 2I_3^{1/2} \frac{\partial \Psi}{\partial I_3} I + 2I_3^{-1/2} \left(\frac{\partial \Psi}{\partial I_1} + I \frac{\partial \Psi}{\partial I_{21}}\right) B - 2I_3^{-1/2} \frac{\partial \Psi}{\partial I_2} B^2 \\ &= \theta_0(I_1, I_2, I_3) I + \theta_1(I_1, I_2, I_3) B + \theta_2(I_1, I_2, I_3) B^2 \end{aligned} \tag{37}$$

By applying the Cayley-Hamilton theorem, the previous equation can rewritten as

$$\sigma = \alpha_0(I_1, I_2, I_3) I + \alpha_1(I_1, I_2, I_3) B + \alpha_{-1}(I_1, I_2, I_3) B^{-1} \tag{38}$$

being

$$\begin{cases} \alpha_0 = \theta_0 - I_2 \theta_2 \\ \alpha_1 = \theta_1 + I_1 \theta_2 \\ \alpha_{-1} = I_3 \theta_3 \end{cases} \tag{39}$$

Assuming that the stress vanishes in the reference configuration (T(I) = 0), one gets the following restriction on the strain energy ψ:

$$\frac{\partial \Psi}{\partial I_1}|_{C=I} + 2\frac{\partial \Psi}{\partial I_2}\Big|_{C=I} + \frac{\partial \Psi}{\partial I_3}|_{C=I} = O \tag{40}$$

A stress-free reference configuration is commonly called a natural state.

3.4 Compressibility

A typical choice to model compressible materials is to decompose the left Cauchy-Green strain tensor into a pure isochoric and a pure volumetric part [110, 111]

$$C = \overline{C}\left(I_3^{1/3} I\right) \tag{41}$$

so that

$$\det\ \overline{C} = 1$$

Furthermore, the first and the second modified invariants are introduced as the invariants of $\overline{C}$ in the same manner of those of C in (28) and (29):

$$\bar{I}_1 = I_1\left(\overline{C}\right) = I_3^{-1/3} I_1, \bar{I}_2 = I_2\left(\overline{C}\right) = I_3^{-2/3} I_1 \tag{42}$$

According to (41), the relation $\bar{I}_3 = 1$ holds for all deformations.

In the field of nonlinear mechanics, an ansatz assumed by several researchers is that the strain energy function ψ is additively decomposed as

$$\psi(I_1, I_2, I_3) = \psi_I\left(\bar{I}_1, \bar{I}_2\right) + \psi_V(I_3) \tag{43}$$

where ψ_I depends only upon the isochoric part of the deformation and ψ_V depends on changes in volume [50, 111, 112]. This choice could eventually leads to a non-physical behavior at large strains [113].

From Eq. (37), the Cauchy stress tensor becomes

$$\sigma = 2I_3^{1/2}\left(\frac{\partial \psi_I}{\partial I_3} + \frac{\partial \psi_V}{\partial I_S}\right) I + 2I_3^{1/2}\left(\frac{\partial \psi_I}{\partial I_1} + I_1 \frac{\partial \psi_I}{\partial I_2}\right) B - 2I_3^{1/2} \frac{\partial \psi_I}{\partial I_2} B^2 \tag{44}$$

and from definitions (42) one gets the following derivatives of the the strain energy function with respect to the modified invariants I_1, I_2 and I_3.

$$\begin{aligned} \frac{\partial \psi_I}{\partial I_1} &= I_3^{-1/3} \frac{\partial \psi_I}{\partial \bar{I}_1} \\ \frac{\partial \psi_I}{\partial I_2} &= I_3^{-2/3} \frac{\partial \psi_I}{\partial \bar{I}_2} \\ \frac{\partial \psi_I}{\partial I_{31}} &= -\frac{1}{3} I_3^{-1}\left[\frac{\partial \psi_I}{\partial \bar{I}_1} \bar{I}_1 + 2 \frac{\partial \psi_I}{\partial \bar{I}_2} \bar{I}_2\right] \end{aligned} \tag{45}$$

By substituting Eqs. (45) into (44), one gets:

$$\sigma_D(\overline{B}_D) = 2I_3^{-1/2}\left(\frac{\partial \psi_I}{\partial \overline{I}_1} + \overline{I}_1 \frac{\partial \psi_I}{\partial \overline{I}_2}\right)\overline{B}_D - 2I_3^{-1/2}\frac{\partial \psi_I}{\partial \overline{I}_2}\left(\overline{B}^2\right)_D \tag{46}$$

$$\sigma_V(I_3 I) = 2I_3^{1/2}\frac{\partial \psi_V}{\partial I_3} I \tag{47}$$

in which the subscripts D and V represent the deviatoric and the volumetric part of the tensor. Equations (46) and (47) state that:

1. A superimposed deviatoric stress doesn't produce any volume changes, but only shape changes ($\mathrm{tr}\,\sigma_D = 0$).
2. A superimposed pressure uniquely produces a volume change.

Points 1 and 2 are the extension to the nonlinear case of the deviatoric/volumetric stress decomposition introduced in the framework of linear elasticity (and are consistent with that).

Equation (47) implies that the reference configuration is stress-free if the following restriction on the function ψ_V is valid:

$$\left.\frac{\partial \psi_V}{\partial I_3}\right|_{I_3=1} = 0 \tag{48}$$

Therefore, assuming a sufficient regularity for the function ψ_V, expression (43) can be expanded by Taylor series around the undeformed configuration ($I_3 = 1$) as:

$$\psi_V(I_3) = \sum_{i=2}^{\infty} \frac{1}{D_i}(I_3 - 1)^i \tag{49}$$

where

$$(D_i)^{-1} = \frac{1}{i!}\left.\frac{\partial^i \psi_V}{\partial I_S^i}\right|_{I_3=1} \tag{50}$$

With similar assumptions, one obtain the following expansion around the reference configuration ($I_1 = 3, I_2 = 3$) for the function ψ_I:

$$\psi_I(\overline{I}_1, \overline{I}_2) = \sum_{i,j}^{\infty} c_{ij}(\overline{I}_1 - 3)^i(\overline{I}_2 - 3)^j \tag{51}$$

where
If $(i, j) = (0, 0)$

$$c_{ij} = \begin{cases} 0 & \\ \frac{1}{i!j!} & \left.\frac{\partial^{i+j}\psi}{\partial^i I_1 \partial^j I_2}\right|_{I_1=3, I_2=3} \end{cases} \quad \text{otherwise} \tag{52}$$

3.5 *Incompressibility*

Experimental evidence has revealed a negligible change in volume occurring during the deformation. This behavior allows the modeling of rubber as an incompressible material. From one hand, this assumption simplifies the determination of equilibrium solutions, but, on the other hand, it makes the constitutive relation hard to implement in a numerical code. Therefore, both near-incompressible and incompressible materials will be considered in the following.

Every deformation allowed in a hyperelastic incompressible material must satisfy:

$$I_3 = \det C = 1 \tag{53}$$

The constraint (53) defines an hypersurface in the space of the deformation gradients. Any stress normal to this surface, i.e., in the direction $\partial \mathrm{detC}/\partial \mathrm{F}$, does not expend work on any (virtual) incremental deformation $\delta \mathrm{x}$ compatible with the constraint. The stress is, hence, determined by the constitutive law unless a vector parallel to $\partial \mathrm{detC}/\partial \mathrm{F}$. From an energetic point of view this is tantamount to assume the strain energy function as

$$\psi(I_1, I_1, I_3) = \psi(I_1, I_1, 1) - p(I_3 - 1) \tag{54}$$

where $\mathrm{p}(I_1, I_2)$ is the Lagrange multiplier associated to the constraint (53) which depends upon boundary conditions.

Once more, assuming a sufficient regularity of the function ψ_I, one obtains the following Taylor expansion around the reference configuration

$$\psi_I(I_1, I_2) = \sum_{i=1}^{N} c_{ij} (I_1 - 3)^i (I_2 - 3)^j \tag{55}$$

Equation (55) was firstly introduced by [114], and for this reason it is sometimes called Rivlin-Saunders's expansion. Some of the most used material models and the respective parameters c_{ij} are reported in Table 3.

The following expression of the Cauchy stress for an incompressible material follows from Eqs. (37) and (54):

Table 3 Material models based on Rivlin's expansion [115]

Author/model								
Mooney Rivlin	C_{10}	C_{01}						
Isihara et al.	C_{10}	C_{01}		C_{20}				
Neo-Hooke	C_{10}							
Yeoh	C_{10}			C_{20}			C_{30}	
James et al.	C_{10}	C_{01}	C_{11}	C_{20}			C_{30}	
Biderman	C_{10}	C_{01}		C_{20}			C_{30}	
Tschoegl	C_{10}	C_{01}	C_{11}					
Tschoegl	C_{10}	C_{01}				C_{22}		
Lion	C_{10}	C_{01}						C_{50}
Haupt/Sedlan	C_{10}	C_{01}	C_{11}		C_{02}		C_{30}	

$$\sigma = -pI + 2\left(\frac{\partial \psi}{\partial I_1} + I_1 \frac{\partial \psi}{\partial I_2}\right)B - 2\frac{\partial \psi}{\partial I_2}B^2 \tag{56}$$

In order to verify the stress-free condition ($\sigma(\mathrm{I}) = 0$) in the reference configuration, the unknown pressure field p must satisfy:

$$p(I_1, I_2)|_{C=I} = p(3,3) = 2\left.\frac{\partial \psi}{\partial I_1}\right|_{C=I} + 4\left.\frac{\partial \psi}{\partial I_2}\right|_{C=I} \tag{57}$$

3.6 Homogeneous Deformations

In the following we analyze some elementary problems in which the deformation is homogeneous, i.e. the deformation gradient F is constant in whole body. Homogeneous deformations are equilibrium solution for all the class of hyperelastic materials; for this reason they are called universal solutions [116].

3.6.1 Simple Tension

In the case of simple tension or simple compression the deformation is given by

$$x_1 = \lambda_1 X_1, x_2 = \lambda_2 X_2, x_3 = \lambda_3 X_3 \tag{58}$$

hence the deformation gradient is a diagonal matrix

$$F = Diag\{\lambda_1, \lambda_2, \lambda_3\} \tag{59}$$

where λ_1, λ_2 are called principal stretches, which are constant because the deformation is homogeneous. Here the λ1-direction is the direction of the external load.

Since in a simple tension test, the lateral surfaces of the specimen are supposed to be unloaded, the principal stresses corresponding to the directions 2 and 3 vanish.

For deformation (59) the strain invariants become:

$$\widetilde{I}_1 = \lambda_1^2 + 2\lambda_2^2, \widetilde{I}_2 = \lambda_1^{-2} + 2\lambda_2^{-2} \tag{60}$$

Incompressible Materials

In the case of incompressibility, the constraint (53) must be satisfied, and the following relation between the stretches must hold:

$$\lambda\lambda_2^2 = 1 \Leftrightarrow \lambda_2 = \lambda_1^{-1/2} \tag{61}$$

hence the strain invariants depend only upon λ_1, e.g.,

$$\widetilde{I}_1 = \lambda_1^2 + 2\lambda_1^{-1}, \widetilde{I}_2 = \lambda_1^{-2} + 2\lambda_1 \tag{62}$$

The unknown pressure field can be determined from the condition that the stresses σ_{22} and σ_{33} vanish

$$p = 2\left[\frac{\partial\psi}{\partial I_1} + I_1\frac{\partial\psi}{\partial I_2}\right]_{I=\widetilde{I}_1, I_2=\widetilde{I}_2}\lambda_1^{-1/2} - 2\left[\frac{\partial\psi}{\partial I_2}\right]_{I_1=\widetilde{I}_1, I_2=\widetilde{I}_2}\lambda_1^{-1} \tag{63}$$

In the following the solution of the simple tension problem will be presented for three of the most used nonlinear elastic models, viz. Neo-Hooke, Mooney-Rivlin and Yeoh model. The strain energy function in the Neo- Hookean model is

$$\psi_1 = c_{10}(I_1 - 3) \tag{64}$$

thus, from Eq. (56):

$$\sigma = -pI + \mu_0 B \tag{65}$$

where $\mu_0 = 2c_{10}$ is the so called initial shear modulus (shear modulus in the reference configuration).

From Eq. (63), the expression of the pressure field follows:

$$p = \mu_0\frac{1}{\lambda} \tag{66}$$

and the stress in the direction 1 becomes:

Table 4 Simple shear test results for some of the most used material models

Model	σ_{12}
Neo-Hooke	$\sigma_{12} = 2c_{10}\gamma$
Mooney-Rivlin	$\sigma_{12} = 2(c_{10} - c_{01})\gamma$
Yeoh ($c_{30} = 0$)	$\sigma_{12} = 2[c_{10} + 2c_{20}(I_1 - 3)]\gamma$

$$\sigma_{11} = \mu_0\left(\lambda^2 - \frac{1}{\lambda}\right) \tag{67}$$

In the same manner by means of Eq. (56) the unidimensional stress-strain relation can be obtained for Mooney-Rivlin and Yeoh model. These results are shown in Table 4.

Compressible Materials

In the compressible case the relation (61) is not anymore valid, thus the orthogonal stretch λ_2 must be derived from the implicit relation:

$$\sigma_{22}(\lambda_1, \lambda_2) = 0 \tag{68}$$

or equivalently $\sigma_{33}(\lambda_1, \lambda_2) = 0$, which follows from the condition that the components of the stress σ_{22} and σ_{33} vanish. Eq. (68) has to be solved numerically for each λ_1.

3.6.2 Simple Shear

Another example of a homogeneous deformation state is a simple shear defined by

$$x_1 = X_1 + \gamma X_2, x_2 = X_2, x_3 = X_3 \tag{69}$$

where γ is the amount of shear strain. Thus,

$$F = \begin{bmatrix} 1 & \gamma & 0 \\ 0 & 1 & 0 \\ 0 & 0 & 1 \end{bmatrix}, B = \begin{bmatrix} 1+\gamma^2 & \gamma & 0 \\ \gamma & 1 & 0 \\ 0 & 0 & 1 \end{bmatrix}, C = \begin{bmatrix} 1 & \gamma & 0 \\ \gamma & 1+\gamma^2 & 0 \\ 0 & 0 & 1 \end{bmatrix} \tag{70}$$

And

$$I_1(C) = 3 + \gamma^2, I_2(C) = 3 + \gamma^2, I_3(C) = 1 \tag{71}$$

that is the strain invariants are even function of the shear strain.

The simple shear is an isochoric deformation that is possible in every compressible, homogeneous, and isotropic hyperelastic material. The constitutive relation (38) shows that the shear stress related to the shear strain γ is given by:

$$\sigma_{12} = \gamma\alpha(I_1, I_2, 1) \tag{72}$$

Where in the generalized shear response function is defined by

$$\alpha(I_1, I_2, 1) = \alpha(I_1, I_2, 1) - \alpha_{-1}(I_1, I_2, 1) \tag{73}$$

From (38) one gets

$$\begin{cases} \alpha_0(I_1, I_2, 1) = 2\dfrac{\partial\psi}{\partial I_3} - 2I_2\dfrac{\partial\psi}{\partial I_2} \\ \alpha_0(I_1, I_2, 1) = 2\dfrac{\partial\psi}{\partial I_1} \\ \alpha_{-1}(I_1, I_2, 1) = -2\dfrac{\partial\psi}{\partial I_2} \end{cases} \tag{74}$$

thus

$$\sigma_{12} = 2\left(\frac{\partial\psi}{\partial I_1} - \frac{\partial\psi}{\partial I_2}\right)\gamma \tag{75}$$

It is seen that the shear stress is an odd function of the amount of shear.

Furthermore notice that the shear stress is in the direction of the shear if and only if $\alpha(I_1, I_2, 1) > 0$. However, the only presence of shear stress cannot produce a simple shear state.

It also follows from (44) that the scalar function $\alpha 1$ and α^{-1} are determined by the normal stress differences; we have:

$$\sigma_{11} - \sigma_{33} = \alpha_1\gamma^2 \tag{76}$$

$$\sigma_{22} - \sigma_{33} = \alpha_{-1}\gamma^2 \tag{77}$$

where

$$\sigma_{33} = \alpha_0 + \alpha_1 + \alpha_{-1} = \tau(\gamma^2)\gamma^2 \tag{78}$$

where since α_i are even function of γ, this dependence has been explicitly shown in the last term. Moreover the last relation allows to determine $\tau(\gamma^2)$, hence α_0. We highlight that the normal stresses are unchanged if the shear is reverted. If these are not furnished, the block will tend to contract or to expand. Such normal stress effects are typical of problems in finite elasticity.

The most striking feature of the simple shear problem is that the results (76)-(78) do not involve the shear stress. On the contrary, the shear stress is determined by the difference of the normal stresses:

$$\gamma\sigma_{12} = \sigma_{11} - \sigma_{22} \tag{79}$$

and it is determined in the same way for every homogeneous, isotropic hyperelastic material, regardless of the form of the response functions. The formula (79) is an example of an universal relation in the finite elasticity theory.

4 Nonlinear Viscoelasticity

4.1 Nonlinear Theory of Viscoelasticity

The theory of viscoelasticity is crucial when describing materials, such as rubber, which exhibit time dependent stress-strain behavior.

Indeed, carbon black-filled rubber, when loaded with time-dependent external forces, suffers a state of stress which is the superposition of two different aspects: a time independent, long-term, behavior (sometimes improperly called "hyperelastic") opposed to a time dependent, short-term, response. Step-strain relaxation tests suggest that short term stresses are larger than the long term or quasi-static ones [117]. Moreover, oscillatory (sinusoidal) tests indicate that dissipative anelastic effects are significant, which leads to the consideration of a constitutive relation which depends not only on the current value of the strain but on the entire strain history. This assumption must be in accordance with some principles which restrict the class of reliable constitutive equations. These restrictions can be classified as "physical" and "constitutive". The former are restrictions to which every rational physical theory must be subjected to, e.g., frame indifference. The latter, on the other hand, depends upon the material under consideration, e.g., internal symmetries.

The principle of determinism [108] belongs to the first class. It states that: the stress at a given material point is determined by the entire past history of the motion in a neighborhood of the considered point.

Another basic assumption in every rational constitutive theory is the principle of frame indifference: the response of the system must be the same for all observers [104–108].

Then one is lead to consider constitutive restrictions. One important assumption, proposed by [118], postulates that the material is simple, which means that the stress at a given material point depends only on the history of the first order spatial gradient of the deformation, in a small neighborhood of the material point. Therefore, the influence of the higher order spatial gradients is ignored. Although this assumption is usually considered non-constitutive, it legitimately belongs to the

class of constitutive restrictions because there exist materials, e.g., porous media and functionally graded, leading to an unacceptable approximation if higher order spatial gradients are ignored.

Other simplifications of the constitutive laws are obtained by assuming that the material is non-aging, which means that the microscopic changes at the time-scale of experimental test can be ignored, which indeed, complies with the experimental observations [119]. An additional assumption, which is also corroborated by the experimental data, is the isotropy of the material, i.e., the material at a given point in one reference configuration is indistinguishable in its response from the same material after it has been statically rotated into another reference configuration. Then, the constitutive equation is simplified accordingly. As expected, the constitutive laws for isotropic materials are, by far, the simplest ones. Finally, the internal material constraints of incompressibility is yet another way to restrict and simplify the constitutive laws.

All the results presented are consistent with these principles.

In the following, we are motivated to develop a general nonlinear theory of viscoelasticity because, in the practical application of tire industry, rubber materials are used under conditions which do not comply with the infinitesimal deformation assumptions of the linear theory. For these materials, the range of deformation beyond which superposition and thereby linearity holds is extremely limited. Anyway, one of the first requirements for a nonlinear constitutive law is that, for a very small deformation, the model reduces to the corresponding linear model [120].

In the following section a review of the constitutive equations used to model nonlinear viscoelastic solids undergoing isothermal deformation is provided.

4.1.1 Pioneering Works

Polymeric materials, such as rubber, exhibit a mechanical response which cannot be properly described neither by means of elastic nor viscous effects only. In particular, elastic effects account for materials which are able to store mechanical energy with no dissipation. On the other hand, a viscous fluid in a hydrostatic stress state dissipates energy, but is unable to store it. As the experimental results reported in Part 1 have shown, filled rubber present both the characteristics of a viscous fluid and of an elastic solid. Viscoelastic constitutive relations have been introduced with the intent of describing the behavior of such materials able to both store and dissipate mechanical energy.

The origin of the theory of viscoelasticity may be traced to various isolated researchers in the last decades of the nineteenth Century. This early stage of development is essentially due to the work of Maxwell, Kelvin and Voigt who independently studied the one dimensional response of such materials. The linear constitutive relationships introduced therein are the base of rheological models which are still used in many applications [121]. Their works led to Boltzmann's [122] first formulation of three dimensional theory for the isotropic medium, which

was generalized later to the anisotropic case by [123]. However, in filled rubber, constitutive nonlinearities turn out to be significant even at small strains because of their internal entangled structure. In addition, when the material is able to bear large strains, geometrical nonlinearities also become relevant. Therefore an approach considering both constitutive and geometrical nonlinearities must be pursued.

The early stage of development, following the works of Maxwell, Kelvin and Voight, has constituted the starting point for many other researchers. In particular in the mid 40s different modeling strategies have actually been used to describe nonlinear viscoelastic solids.

4.1.2 Internal-Variables Formulations

A general approach, introduced by [124], is to formulate the constitutive equation in terms of thermodynamic state-variables: the internal energy is expressed as function of both the current values of strain (stress) and the so-called internal state variables [125–127]. The latter may be identified with local micro-structural quantities, e.g., filler content [49]. Rate effects are introduced through evolution equations, which usually relate time rates-of-change of internal variables to thermodynamic forces, which are the derivatives of the internal energy with respect to each internal variable. Simo [51] proposed a constitutive equation based on an internal variables formulation which has provided a starting point for many successive works [52, 128–130]. In Simo's approach, the internal energy is split according to the multiplicative decomposition of the deformation gradient into dilatational and volume-preserving parts 2.

Even though this choice might lead to non-physical results at finite strains [113], Simo's model is able to reproduce the hysteretic behaviors of carbon-filled rubber, incorporating also the Mullins effect. In this case the internal energy is split as the sum of three different parts: (i) a volumetric term depending upon the volume change $J = \det F$, (ii) a term depending upon the isochoric deformation $\overline{F} = J^{-1}F$ and (iii) a term relying on the internal variable q representing the nonequilibrium part of the stress. The evolution equation of q is postulated assuming the generalized force is proportional to the derivative of the internal energy with respect to the isochoric strain. This approach is found to be computationally very efficient, and thus adopted in many commercial finite element codes. However, Simo's model has not been conclusively proven to satisfy the second law of thermodynamics for all the admissible processes. Hence, it is essentially restricted to viscoelastic response for strain states near the elastic equilibrium.

Govindjee and Simo [52] developed a similar model on the basis of the micromechanical structures of the carbon black particles and rubber matrices: the relaxation processes in the material were described through stress-like internal variables. These variables are governed by dissipative evolution equations, and interpreted as the nonequilibrium stresses due to the interaction between the polymer chains. Holzapfel [128] proposed a model in which the internal energy is

additively partitioned in the standard volumetric term plus an isochoric part. The latter depends both on the isochoric strain and a set of internal variables Γ_α that can be regarded as an internal strain tensor. This approach generalizes the additive decomposition introduced by Simo.

An advantage of the state-variable formulations is that, in contrast to the other approaches, it is not restricted to isotropic responses. Anisotropic effects could be easily taken into account, e.g., by introducing state variables depending upon fiber orientations as in [129]. Moreover physical theories, such as dislocation models, may be introduced directly in the formulation of the evolution equations. However, it has been reported that the viscosity alone is not enough to reproduce the large hysteretic energy behavior of high-damping rubber, used in vibration absorbers. Thus, Yoshida et al. [130] proposed a constitutive model consisting of two parts: an elastoplastic term with a strain-dependent isotropic hardening law, representing the energy dissipation of the material, and a second part consisting of a hyperelastic body with a damage model, which expresses the evolutional direction of the stress tensor.

4.1.3 Additive Decomposition of ψ

A decomposition of the deformation gradient into elastic and inelastic terms leads to alternative formulations of the strain energy function [131]. This decomposition was first proposed by [132] Sidoroff and later by Lubliner [133] who extended the pioneering work of Green and Tobolsky [134]. Although in the framework of elastoplasticity the decomposition of the deformation gradient, into elastic and plastic terms, relies on clear physical assumptions, there is a lack of evidence in the context of viscoelasticity. However, it has been successfully applied in many nonlinear constitutive equations [135–140] and many others.

In this context, it is assumed that the deformation gradient can be decomposed as

$$F = F_e F_i \tag{80}$$

The inelastic term F_i, sometimes called viscous term F_v, introduces an intermediate configuration.

However, the decomposition (80) is a conceptual one, and cannot generally be determined experimentally since neither F_{ie}; F_i are observable quantities [141]. The inelastic term in (80) was also extended to three, four or more deformation parts

$$F = F_i^{(1)} F_i^{(N)} \tag{81}$$

and was adopted and studied, for example, in elastoplasticity and viscoelasticity ([131, 135, 137], and references therein). The decomposition (80) is generally followed by the ansatz on the internal energy for which ψ is split as the sum of an equilibrium part and an overstress term, i.e.,

$$\Psi = \Psi_e(C) + \Psi_0(C_e) \tag{82}$$

Here C is the right-Cauch-Green strain tensor and $C_e = F_e^T F_e$ is the elastic strain in the intermediate configuration. This form of the internal energy has been postulated by several researchers [135–140] proposed a more general equation for ψ, e.g.,

$$\Psi = \Psi_e(C) + \Psi_0(C, C_i) \tag{83}$$

in which the overstress term depends both on the whole strain tensor C and on the inelastic (viscous) strain $C_i = F_i^T F_i$ assuming that the viscous components is proportional to the long term expression, e.g.,

$$\Psi_0(C, C_i) = \alpha \Psi_e(C_e) \tag{84}$$

Equation (83) reduces to (82).

All these constitutive choices for the free energy ψ lead to different expressions of the stress in terms of the deformation gradient. By applying the Coleman and Noll procedure [124], i.e., by restricting the form of the stress tensor in such a way that the Clausius-Plank inequality is verified for every admissible process, the Piola symmetric stress tensor is shown below

$$T = T_e + T_i \tag{85}$$

where Te is the equilibrium stress and Ti the overstress. In particular, for an internal energy of the form (82), the following relations between ψ_e, ψ_0 and T_e, T_i are valid:

$$T_e = \frac{\partial \Psi_e}{\partial C} T_i = \frac{\partial \Psi_0}{\partial C_i} \tag{86}$$

Equation (86) is not sufficient to determine the behavior of the material. In order to complete the description, the evolution equations (or flow rules) of the internal variables Fe and/or Fi, which determine the way viscoelastic processes evolve, must be defined. Often the evolution equations are suitably defined to be efficient with respect to time integration algorithms [129]. A common choice for the flow rule is to apply a generalization of the one-dimensional linear Maxwell-model to the three-dimensional and nonlinear regime. In this case the evolution equations are assumed to be linear, and the overstress term arising from them is the generalization of the extra-stress arising in Maxwell element [103, 140, 146] proposed nonlinear evolution equations based on strain, time and temperature. Bonet [135] also used nonlinear evolution equations of rate type for the internal variables. These are based on a particular linear relaxation form of the Maxwell model which leads to a viscoelastic formulation that can be seen as a particular case of a large strain viscoplastic model. A variational formulation of Bonet's model has been developed in [147]

4.1.4 Integral Formulation

The internal-variables formulation is not the only way to define the internal energy. Following the seminal work of [122, 148] Boltzmann and Green and Rivlin and successively Coleman and Noll [124] proposed constitutive relations for which the stress a time t depends upon the entire history of deformation up to the current time instant. However, the definition of the internal energy was developed accordingly and in agreement with the fading memory properties, i.e., strains which occurred in the distant past have less influence on the present value of ψ than those which occurred in the more recent past.

To mathematically express the fading memory property, Coleman and Noll [124] introduced the following inner product in the space of deformation histories.

$$C_1^t(s) : C_2^t(s) := \int_0^\infty tr\left\{C_1^t(s)C_2^t(s)\right\}h^2(s)ds \tag{87}$$

which induces the norm

$$\left\|C^2(s)\right\|_{\wp^t} := \left(C^t(s) : C^t(s)\right)^{1/2} \tag{88}$$

Here, C^t represents the history of the right-Green strain tensor up to time t, i.e.,

$$C^t(s) = C(t-s), s \in [0, \infty) \tag{89}$$

Moreover $h(t)$ is called obliviator of order r and it satisfies the following conditions (Truesdell and Noll 1965):

1. $h(s)$ is defined for $0 \leq s < \infty$ and has a positive real value: $h(s) > 0$.
2. $h(s)$ is normalized by the condition $h(0) = 1$.
3. $h(s)$ decays to zero monotonically for large s in such a way that

$$\lim_{s \to \infty} s^r h(s) = 0 \tag{90}$$

The norm (88) equipped with a function h satisfying properties 1, 2 and 3 is called fading memory norm; in this topology, two deformation histories are distant if they are distant in the recent past, i.e., deformations which occur in the recent past have more weight than those which occurred in the distant past. It should be noted that the existence of a proper obliviator h, satisfying 1–3, does not guarantee the existence of an equilibrium solution of the elastic problem [149].

The mathematical assumptions behind the theory of fading memory have been recently reviewed by Drapaca et al. [150]. Definition (88) leads to the so-called Strong Principle of Fading Memory [108] (SPFM) 1, which defines the class of admissible internal energy functionals:

There exists an obliviator h(t) of order greater than n + 1/2 such that the constitutive function ψ is defined and n-times Fréchet-differentiable in a neighborhood of the zero strain history.

The SPFM alone is not sufficient to define properly an internal energy, but rather restrictive conditions must be satisfied to assure the existence of a stationary point of ψ [151].

Over the years, many researchers have dealt with a proper definition of internal energy accounting for deformation histories ([152–154] and references therein). It is well known that the internal energy and entropy of a material with memory is generally not uniquely defined [155]. A fundamental result in this area is due to Gurtin and Hrusa [156] who obtained a necessary and sufficient condition for the existence of the internal energy arising from a stress-strain constitutive relation of single integral type. Moreover they were able to develop the following explicit formula for ψ

$$\Psi(C^t) = \Psi_1(C(t)) + \int_0^\infty \psi(\tau, C(t-\tau))d\tau \tag{91}$$

The majority of models obtained from an a priori internal energy fits within this single hereditary framework [101, 144, 157]. The stress arising from the constitutive assumption (91) involves a single hereditary integral of a nonlinear function of the strain2. In this wide sense, single integral constitutive relations encompass a class of viscoelastic models equivalent to differential and fractional differential models [158–160]. The theory of single integral constitutive equations developed by Gurtin and Hrusa was extended to multiple integral functionals by Hanyga and Seredynska [160]. In this context, the internal energy ψ reads as

$$\Psi(C^t) = \Psi_1(C(t)) + \\ + \sum_{n=1}^{N} \int_0^\infty \ldots . \int_0^\infty \psi(\tau, C(\tau), C(t-\tau_1), ..., C(t-\tau_n))d\tau_1 \ldots . d\tau_n \tag{92}$$

where N is a positive integer. The models introduced by Green and Rivlin, Pipkin and Rogers, and Hassani et al. [148, 161, 162] fit into this enlarged framework1. However, in general, their applicability to describe the behavior of real materials is questioned since many parameters are necessary to fit the experimental data (see Chap. 5 of [163]).

4.1.5 Single Integral Formulation

In applied viscoelasticity not all the constitutive equations are formulated by an a-priori defined internal energy ψ, but the constitutive model is expressed directly by the functional relation between the stress and the strain through an hereditary integral. In rheology this class of constitutive models is called Rivlin-Sawyers models; Fung's [164], Fosdick and Yu's [165] and many other models currently used belong to this constitutive class.

Because Rivlin-Sawyers models are not obtained with the Coleman and Noll's procedure, their thermodynamic consistency must be verified a posteriori.

Single hereditary formulation has proven to reproduce all the crucial aspects of rubber behavior (hysteresis, relaxation and creep). In the simplest situation, the current value of the stress is the sum of two different contributions: a purely elastic term depending on the current value of the strain and a hereditary integral depending on the whole strain history. In the linear model of viscoelasticity, introduced by Bernstein et al. [166], the stress dependence on the strain history is assumed to be linear, i.e.,

$$\sigma(t) = 2\mu G(t-s) + \lambda tr\{G(t)\}I \tag{93}$$

$$+\int_0^t \dot{k}(s)[2\mu G(t-s) + \lambda tr\{\{G(t-s)\}I]ds \tag{94}$$

where k(t) is the so-called viscoelastic kernel (or relaxation function), λ and μ the Lamé moduli and E the Green-Lagrangian strain tensor. A common choice for the relaxation function is to assume $k(0) = 1$, thus k is referred to as reduced relaxation function.

A suitable kernel in the integral can account for both the short and long term strain contributions to the current stress value. To be consistent with the second principle of thermodynamics, k(t) must be a completely monotonic function of t [167], i.e., it must be infinitely differentiable and satisfy

$$\forall n \in IN, \forall t > 0, \ (-1)^n \frac{\partial^n k}{\partial t^n} \geq 0 \tag{95}$$

The condition of infinite differentiability can be dropped obtaining a much weaker requirements for k [101]. In order to express the reduced relaxation function k(t), a discrete relaxation spectrum, whose form was derived by various molecular models [161], is generally used. Formally,

$$k(t) \geq 0, \quad k^{'}(t) \leq 0, \quad k^{''}(t) \geq 0$$

$$k(t) = \sum_{i=1}^{N} k_i + \sum_{i=1}^{N} (1-k_i)e^{\frac{t}{t_i}}, \quad \sum_{i=1}^{N} k_i < 1 \tag{96}$$

Equation (95) is commonly referred to as Prony's series.

Recently fractional calculus has started to play an increasing role in polymer rheology [101, 142, 143, 159, 168, 169]. This is due to the fact that the frequency dependence of the dynamic moduli of filler-reinforced rubber is fairly weak and essentially of the power-law type [101]. As shown in the literature such behavior can be represented with a minimum of material constants using the fractional calculus.

In terms of fractional derivatives, the relaxation function can be defined as

$$k(t) = 1 + \frac{1}{\Gamma(1-\alpha)} \int_0^t (t-s)^{-\alpha} \eta(s) ds \tag{97}$$

Where $0 < \alpha < 1$, $\Gamma(x) = \int_0^\infty z^{x-1} e^{-z} dz$ is the Eulerian Gamma function and $\eta(s)$ is a suitable function such that $\lim_{t \to \infty} k(t) < \infty$. The time derivative of k becomes the left-sided Riemann-Liouville fractional derivative, i.e.,

$${}_0D_t^0 \eta(t) = \frac{1}{\Gamma(1-\alpha)} \frac{d}{dt} \int_0^t (t-s)^{-\alpha} \eta(s) ds \tag{98}$$

The behavior of the dynamic moduli arising from a fractional order viscoelastic kernel, like (96), has been studied in Rogers [170].

Another way to introduce fractional derivatives is through rheological models of fractional order. In particular, the fractional Maxwell element corresponds to a spring in series with a fractional damper. The one-dimensional linear stress, σ, versus strain, $\in$, relation of a spring in parallel with the fractional Maxwell element can expressed in terms of fractional derivatives [171], e.g.,

$$\sigma(t) = \int_0^t \left[\mu_{eq} + \mu_{0v} E_\beta \left(-\frac{(t-s)^\beta}{\varsigma^\beta} \right) \right] \in (s) ds \tag{99}$$

Where the kelner

$$E_\beta(t) = \sum_{i=0}^{\infty} \frac{t^i}{\Gamma(1+\beta i)} \tag{100}$$

is the Mittag-Leffler function ([142, 171], and references therein). Since E1 (t) equals the exponential function, the Mittag Leffler function is also known as the fractional exponential function.

Fractional order models present a relevant drawback due to the difficulty in handling numerically constitutive equations of fractional order, in particular of differential type [158]. Moreover, the identification of the constitutive parameters relies on a strongly ill-conditioned minimization problem. For this reason, they are rarely implemented in commercial codes and therefore their use is very limited.

4.1.6 Quasi-Linear Viscoelasticity

Because of the inherent nonlinear behavior exhibited by most of carbon black-filled rubber, the linear formulation is not applicable in general.

In the context of nonlinear viscoelasticity, one of the simplest model is the Quasi-Linear viscoelastic model proposed by Fung [164]. In one dimension, he

suggested the following relationship for the second Piola-Kirchhoff stress T in terms of the stretch $\lambda := l/l_0$.

$$T(t) = \int_{-\infty}^{t} k(t-s) \frac{\partial T^e[\lambda(s)]}{\partial \lambda} \frac{\partial \lambda}{\partial s} ds \tag{101}$$

that is, the tensile stress at time t is the sum of contributions of all the past changes, each governed by the same relaxation function. $T^e(\lambda)$, a function of λ alone, is the nonlinearly elastic response.

Rewriting Eq. (101) in the form

$$T(t) = \int_{-\infty}^{t} k(t-s) \dot{T}^e(s) ds \tag{102}$$

we see that the stress response depends linearly upon the nonlinear function of the strain $T^e(\lambda)$, from which the name "Quasi-Linear" derives. If the material is in the natural state for $t < 0$, Eq. (102) reduces to

$$T(t) = T^e[\lambda(t)] + \int_0^t \frac{\partial k(t-s)}{\partial (t-s)} T^e[\lambda(s)] ds \tag{103}$$

since $k(0) = 1$ and all the functions are smooth in $0 \leq t < \infty$. Equation (103) states that the tensile stress at time t is equal to the instantaneous elastic response Te decreased by an amount depending on the past history, since $\dot{k}(t)$ is negative.

Recently many investigators have proposed their own nonlinear viscoelastic constitutive relationship. Among them, the predictive capabilities of the models introduced in [172–176] will be analyzed with respect to the experimental data.

There are several applications of the viscoelastic theory concerning the behavior of carbon black-filled elastomers at high strain rates ($10^2 - 10^3$ s^{-1}) [145, 174, 176]. In all these models the time derivative of the strain ex plicitly appears in the hereditary term. Hoo Fatt and Ouyang's model is developed from the BKZ constitutive equation [166] and is reported to be able to capture the high modulus due to high strain rates. However, it shows some shortcomings owing to a zero. In particular, for this model, the Cauchy stress σ arising from a constant strain rate test, say $\dot{\in}_0$, such that $\lambda = 1 + \dot{\in}_0 t$, is

$$\sigma = 2\alpha_1 (I_1 - 3)^{\alpha_2} \left(\lambda^2 - \frac{1}{\lambda}\right) - \left(\lambda^2 - \frac{1}{\lambda}\right) \int_1^{\lambda} \left[2\beta_1 k \left(\frac{\lambda - \zeta}{\in_0}\right) \left(\zeta^2 + \frac{2}{\zeta} - 3\right) \left(\zeta - \frac{1}{\zeta^2}\right)\right] d\zeta \tag{104}$$

and, hence, the Young's modulus around the undeformed configuration is zero ($[\partial\sigma/\partial\lambda]_{\lambda=1} = 0$), which contrasts with the experimental evidence.

Advanced finite element codes are often called upon to simulate tires and biological soft tissues because of the complex behavior of these NLV materials. Among

many, two of the most used FEA codes, which includes a finite viscoelasticity model, are the Abauqs FEA and the LS-Dyna code. Both of these numerical tools are used in different branches of engineering (e.g, aeronautical, automotive, structural).

In particular, the LS-Dyna finite viscoelastic relationship [175] takes into account rate effects through linear viscoelasticity by a convolution integral. The model corresponds to a Maxwell fluid consisting of dampers and springs in series. The Abaqus FEA model is reminiscent of, and similar to, a well-established model of finite viscoelasticity, namely the Pipkin–Rogers model [161]. This model, with an appropriate choice of the constitutive parameters, reduces to the Fung (QLV) model [173, 177].

4.2 Differential Viscoelasticity

Finally, it is worth mentioning another approach used to describe nonlinear viscoelastic solids: nonlinear differential viscoelasticity [49, 178, 179]. This theory has been successfully applied to model finite amplitude waves propagation [180–182]. It is the generalization to the three-dimensional nonlinear case of the rheological element composed by a dashpot in series with a spring. Thus in the simplest case, the stress depends upon the current values of strain and strain rate only. In this sense, it can account for the nonlinear short-term response and the creep behavior, but it fails to reproduce the long-term material response (e.g., relaxation tests). The so-called Mooney-Rivlin viscoelastic material [183] and the incompressible version of the model proposed by Landau and Lifshitz [184] belong to this class.

The substantive "grade 1" is generally used referring to such models for remarking the dependence of stress on the strain rate only [108]. Constitutive equations with higher order time derivatives are also used [165].

4.2.1 Quasi-Linear Viscoelasticity

Fung's Model

A quite general integral series representation of the internal energy ψ was proposed by Pipkin and Rogers [161]. Dai [185] used the first term of such an integral series to describe the nonhomogeneous deformation of a nonlinearly viscoelastic slab. The constitutive relation they obtained is

$$T(t) = R[C(t), 0] + \int_0^t \frac{\partial}{\partial (t-s)} (R[C(s), t-s]) ds \tag{105}$$

Here $R[C(\tau),0]$ represents the stress due to an instantaneous deformation occurring at time t = 0, while $R[C(s),\xi]$ is a strain dependent tensorial relaxation function which in the case of isotropy has the form

$$R[C(\tau),\xi] = \varphi_0(\tau, I_i(\xi))I + \varphi_1(\tau, I_i(\xi))C(\tau) + \varphi_{-1}(\tau, I_i(\xi))C^{-1}(\tau) \tag{106}$$

where $\phi_0, \phi_1, \phi_{-1}$ are scalar functions of time ξ and of the principal strain invariants I_1, I_2 and I_3 (28)–(30) at time τ. The expression given be Eq. (103) incorporates the assumption that there has been no deformation prior to time t = 0.

Johnson [186] have shown that, if the relaxation property can be described by a scalar function k(t), the single integral representation (103) is equation Viscoelastic (QLV) model first introduced by Fung [164], i.e.,

$$\begin{aligned} T(t) &= \widehat{\theta}_0(t)I + \widehat{\theta}_1(t)C(t) + \widehat{\theta}_{-1}(t)C^{-1}(t) \\ &+ \int_0^t k(t-s)\Big\{\widehat{\theta}_0(s)I + \widehat{\theta}_1(s)C(s) + \widehat{\theta}_{-1}(s)C^{-1}(s)\Big\}ds \end{aligned} \tag{107}$$

which follows from (105) and (106) with the identification

$$\phi_i(\tau, I_i(\xi)) = k(\xi)\widehat{\theta}_i(I_1(\tau), I_2(\tau), I_2(\tau)), i \in \{1, -1, 0\} \tag{108}$$

where $k(t)$ is the reduced viscoelastic kernel. In the next, the dependence of θ_i upon the strain invariants I_1, I_2 and I_3 will be specified only when necessary.

The Quasi-Linear Viscoelastic (QLV) model has proven to be a successful phenomenological model for describing the nonlinear viscoelastic behavior of solids [186–188].

If the reference configuration is stress free, the coefficients $\theta_0, \theta_1, \theta_{-1}$ cannot be arbitrary assigned, but the following restriction

$$\theta_0(3,3,1) + \theta_1(3,3,1) + \theta_{-1}(3,3,1) = 0 \tag{109}$$

must hold.

In the case of incompressibility Fung's model reads as

$$\begin{aligned} T(t) &= p(t)C^{-1}(t) + \theta_0(t)I + \theta_1(t)C(t) \\ &+ \int_0^t \dot{k}(t-s)\{\theta_0(s)I + \theta_1(s)C(s)\}ds \end{aligned} \tag{110}$$

where $p(t)$ is the Lagrange multiplier associated to the incompressibility constraint, which in the dynamic case reads as

$$\forall t, \det C(t) = 1 \tag{111}$$

As in the static case, $p(t)$ must be determined from equilibrium equations and boundary conditions. Equation (110) states that the stress at time t is equal to the

instantaneous response decreased by an amount depending on the past history, since $\dot{k}(t)$ is generally negative valued.

In other words, the QLV model reflects strain history dependent stress and fading memory. In order to express relaxation properties, Prony's series (97) might be used, i.e.,

$$k(t) = \sum_{i=1}^{N} \frac{\mu_i}{\mu_0} + \sum_{i=1}^{N} \left(1 - \frac{\mu_i}{\mu_o}\right) e^{-\frac{t}{\tau_i}}, \sum_{i=1}^{N} \mu_i = \mu_\infty \tag{112}$$

where μ_0 is a real constant representing the shear modulus in the reference configuration, μ_∞ is the ultimate value to which the shear modulus settles after an infinite time and τ_i are the characteristic time constants. To emphasize some limits of Fung's model, we henceforth focus on an incompressible viscoelastic solid for which the instantaneous response is modeled by a Neo-Hookean stressstrain relationship, i.e.,

$$T_e = pC^{-1} + \mu_0 I \tag{113}$$

Then from (110) we have the identification $\theta_0 = \mu_0$, $\theta_1 = \theta_{-1} = 0$, that yields:

$$T(t) = p(t)C^{-1}(t) + \mu_0 k(t) I \tag{114}$$

since $k(0) = 1$, or for the Cauchy stress tensor:

$$\sigma(t) = p(t)I + \mu_0 k(t) B(t) \tag{115}$$

Let us consider an uniaxial deformation described by

$$x_1 = \lambda(t)X_1, x_2 = \lambda(t)^{-1/2}X_2, x_3 = \lambda(t)^{-1/2}X_3, \tag{116}$$

where $\lambda(t)$ is the stretch ratio in the direction of the extension. The resulting deformation gradient has the diagonal form

$$F(t) = Diag\left[\lambda(t), \lambda(t)^{-1/2}, \lambda(t)^{-1/2},\right] \tag{117}$$

Assuming that the uniaxial deformation arises from a uniaxial tension with $\sigma_{11} \neq 0$, $\sigma_{22} = \sigma_{33} = 0$ enables us to compute the Lagrange multiplier p(t). The resulting non-zero component of the Cauchy stress is

$$\sigma_{11}(t) = \left[\mu_\infty + \sum_{i=1}^{N} (\mu_0 - \mu_i)\exp^{-t/\tau_1}\right]\left[\lambda^2(t) - \lambda^{-1}(t)\right] \tag{118}$$

hence, system response in the steady state $t >> \max\{\tau_1, \ldots ... \tau_N\}$ is

$$\sigma_{11}^{SS}(t) = \mu_\infty\left[\lambda^2(t) - \lambda^{-1}(t)\right] \tag{119}$$

which is the response of a purely elastic non-dissipative material.

Fosdick and Yu's Model

In the framework of nonlinear viscoelasticity, Fosdick and Yu [165] proposed their own constitutive equation. They assumed that the second Piola-Kirchhoff stress tensor is given by

$$\begin{aligned} T(t) &= \theta_0(t)I + \theta_1(t)C(t) + \theta_{-1}(t)C^{-1}(t) \\ &\quad + J(t)F^{-1}(t)\left\{\int_0^\infty k(s)[C_t(t-s) - I]ds\right\}F^{-T}(t) \end{aligned} \tag{120}$$

where $C_\tau(s)$ is the relative right Cauchy-Green strain tensor:

$$C_t(s) = F_t^T(s)F_t(s) = F^{-T}(s)F^T(s)F(s)F^{-1}(t) \tag{121}$$

being $F_t(s) = F(s)F^{-1}(t)$

If a strain C(t) is suddenly applied at time t = 0, e.g.,

$$C(t) = \begin{cases} I & if \quad t \le 0 \\ C^+(t) = I & if \quad t > 0 \end{cases} \tag{122}$$

Equation (120) takes the following form

$$\begin{aligned} T(t) &= T^e(t) \\ &\quad + J(t)F^{-1}(t)F^{-T}(t)\left\{\int_0^t k(t-s)[C(s) - C(t)]ds\right\}F^{-1}(t)F^{-T}(t) \end{aligned} \tag{123}$$

where

$$T^e(t) = \theta_0(t)I + \theta_1(t)C(t) + \theta_{-1}(t)C^{-1}(t) \tag{124}$$

is the instantaneous part of the stress.

For an incompressible material, a Lagrangian multiplier accounting for the constraint det C = 1 must be introduced and, hence, Eq. (120) becomes

$$T(t) = q(t)C^{-1}(t) + \theta_0(t)I + \theta_1(t)C(t) + F^{-1}(t)F^{-T}(t)\left\{\int_0^t \dot{k}(t-s)[C(s)]ds\right\}F^{-1}(t) \tag{125}$$

or in terms of Cauchy stress,

$$\sigma(t) = \widehat{q}\,(t)I + \widehat{\theta}_0(t)B(t) + \widehat{\theta}_1(t)B^2(t) + F^{-T}(t)\left\{\int_0^t \dot{k}(t-s)[C(s)]ds\right\}F^{-1}(t) \tag{126}$$

Fosdick and Yu's model has been successfully applied to describe finite amplitude wave propagation [180, 182, 189].

By comparing (125) with Fung's constitutive Eq. (110), the differences between the two models appear:

- The "instantaneous" part of the stress is the same in the two models;
- The "dissipative" term of Fosdick's model differs from that of the QLV model (110)

since it represents the history of the symmetric Piola-Kirchhoff stress transformed by push-forward and pull-back deformations.

To investigate thoroughly the behavior of Fosdick and Yu's model, let us consider a simple shear deformation of amount γ(t) in the plane 12, e.g.

$$F(t) = \begin{bmatrix} 1 & \gamma(t) & 0 \\ 0 & 1 & 0 \\ 0 & 0 & 1 \end{bmatrix} \tag{127}$$

Hence, the right-Cauchy-Green strain tensor reads as

$$C(t) = \begin{bmatrix} 1 & \gamma(t) & 0 \\ \gamma(t) & 1+\gamma^2(t) & 0 \\ 0 & 0 & 1 \end{bmatrix} \tag{128}$$

If there is no traction acting on the lateral surfaces, it results $\sigma_{33}(t) = 0$, then the Lagrangian multiplier p(t) into (126) can be computed. The Cauchy stress resulting from Eq. (120) has the following components:

$$\sigma_{11}(t) = \gamma^2(t)\left[\widehat{\theta}_0(t) + 3\widehat{\theta}_1(t) + \widehat{\theta}_1(t)\gamma^2(t)\right]$$

$$\sigma_{12}(t) = \gamma(t)\left[\widehat{\theta}\,(t) + 2\widehat{\theta}_1(t) + \widehat{\theta}_1(t)\gamma^2(t)\right] + \int_0^\infty \dot{k}(t-s)[\gamma(s) - \gamma(t)]ds$$

$$\sigma_{12}(t) = \widehat{\theta}_1(t)\gamma^2(t) + \int_0^\infty \dot{k}(t-s)[\gamma(s) - \gamma(t)]^2 ds$$

While the stresses σ_{12} and σ_{22} consist of an elastic term plus a dissipative integral as the standard one-dimensional model of linear viscoelasticity, σ_{11} is a purely elastic force distribution, i.e., there is no stress-relaxation. This behavior seems in contrast to the assumed isotropy of the material.

Abaqus FEA Model

Commercial finite element codes are often called upon to simulate the behaviour of tyres in real-world applications. These numerical codes are mostly used as "black-boxes", and the validity of the results is rarely questioned, even though they might provide a decisive argument in favour of, or against, the viability of a given tyre model.

With this aim we introduce the ABAQUS FEA finite viscoelasticity constitutive relation1 and we investigate the resulting material behavior by means of two prototype experiments. Section 4.8.2 of the ABAQUS Theory Manual [173] gives the constitutive relation for modeling nonlinear viscoelastic effects in the form:

$$\sigma(t) = \sigma_e(t) + SYM\left\{F(t)\left[\int_0^t \frac{J(s)}{J(t)}\dot{k}(t-s)F^{-1}(s)\sigma_e(s)F(s)ds\right]F^{-1}(t)\right\} \quad (129)$$

where σ_e is the instantaneous elastic Cauchy stress response (elastic response at very short times), k is the so-called viscoelastic kernel, which characterizes the stress relaxation and satisfies k(0) = 1.

Also, "SYM" represents the symmetric part of the bracketed term. The constitutive relation (129) is valid for compressible as well as incompressible solids. In the latter case the hydrostatic term $-\widehat{p}\,I$ in σ_e (where $\hat{p}$ is a Lagrange multiplier) is a workless constraint stress in both the instantaneous response and in the history term, as expected. Indeed, for an incompressible solid, it results J(t) = 1, for each t, and σ_e has the general form:

$$\sigma_e = -\hat{p}\,I + \psi_1 B + \psi_2 B^2 \quad (130)$$

Where ψ_1, ψ_2 are scalar functions of time and of the first and second principal invariants, I_1, I_2 of C. Then (129) reduces to

$$\sigma(t) = -p(t)I + \psi_1(t)B(t) + \psi_2(t)B(t)^2 + \sum_{i=1}^{2} SYM\left\{F(t)\left[\int_0^t k(t-s)\psi_i(s)C(s)^i ds\right]F^{-1}(t)\right\} \tag{131}$$

where $p(t) = \dot{p}(t) + \int_0^7 \dot{k}(t-s)\dot{p}(s)ds$ is arbitrary and remains to be determined from initial/ boundary conditions.

On inspection of Eqs. (110) and (131), it can be seen that there are two main differences between the models. First, the integral term in Eq. (129) is generally nonsymmetric, in contrast to the integral term in Eq. (110). This is taken care of in an ad hoc manner by using the "SYM" operator. Also, the history (time integral) term in the ABAQUS model terminates with $F(t)^{-1}$ in contrast to the history term in the the QLV model, which terminates with $F(t)^T$. The latter fits more naturally with the usual expression for the traction σ nda via Nanson's formula F^T nda = JNdA connecting reference and deformed area elements (J = 1 here). In fact, the 'push-forward' to the configuration at time t from that at time s of the (symmetric) Cauchy stress e(s) should involve $F(t)F^{-1}(s)\sigma_e(s)F^{-T}(s)F^T(t)$ rather than the $F(t)F^{-1}(s)\sigma_e(s)F(s)F^{-1}(t)$ that appears in (131). This change would remove the need to apply the SYM operation. However, for an incompressible material use of (130) then leads to a term in p that doesn't give a workless constraint stress. This can be corrected by, for example, dropping this term from (130) in the integral, in which case (131) would be replaced by

$$\sigma(t) = -p(t)I + \psi_1(t)B(t) + \psi_2(t)B(t)^2 + F(t)\left[\int_0^t \dot{k}(t-s)\psi_i(s)C(s)^i ds\right]F^T(t) \tag{132}$$

with p(t) the arbitrary pressure. This is then a special case within the model (110).

A numerical comparison between the QLV and the Abaqus FEA model for the simple shear and uniaxial extension case has been performed to further highlight the differences between the two models.

4.3 Dynamic Moduli of Nonlinear Viscoelastic Models

In this section, the dependence of the storage and loss moduli on the frequency is computed for the classes of differential and integral viscoelastic models considered. Consequently, it is proved that the vanishing sensitivity of the storage modulus at low frequencies does not depend on the nonlinear relationship between stress and strain history, but rather on the material memory's rate of decay.

4.4 Differential Viscoelasticity

A constitutive equation in the form

$$\sigma(t) = g\left[E(t), \dot{E}(t)\right] \tag{133}$$

is generally referred to as differential viscoelastic model [49, 178, 179]. Hereafter superimposed dots will represent the time derivatives. The substantive "grade 1" is also used to refer to (131) in order to emphasize only the dependence of σ on the strain rate only2.

Any constitutive relation in the form (133) clearly satisfies (149). Hence, in the case of imposed deformation (148), we can let $t_0 \to -\infty$ and study the response to a simple harmonic deformation $E_s(t) = E_0 + E_1 \sin(\omega t)$ without further reference to the time instant t_0 at which the test began. The resulting steady-state stress response is periodic of period $T = 2\pi/\omega$, since:

$$\sigma_s(t+T) = g[E_0 + E_1 \sin(\omega t + \omega T), E_1 \omega \cos(\omega t + \omega T)] = \hat{\sigma}_s(t) \tag{134}$$

Through the change of coordinates $s = \omega\tau/\pi$ the definitions (151)-(152) become

$$S = \frac{1}{E_1}\int_{-1}^{1} g[E_0 + E_1 \sin(\pi s), \omega E_1 \cos(\pi s)] \sin(\pi s) ds \tag{135}$$

$$L = \frac{1}{E_1}\int_{-1}^{1} g[E_0 + E_1 \sin(\pi s), \omega E_1 \cos(\pi s)] \cos(\pi s) ds \tag{136}$$

If the material is elastic, i.e., $g\left[E, \dot{E}\right] = g[E]$ both the moduli are independent of the frequency. Moreover, if the function $g[E_0 + E_1 \sin(\pi s), \omega E_1 \cos(\pi s)]$ is analytic with respect to E_1, its Taylor's expansion around the prestrained configuration ($E_1 = 0$) is

$$g[E_0 + E_1 \sin(\pi s), E_1 \omega \cos(\pi s)] = \sum_{i=0}^{\infty} \sum_{n=0}^{i} \frac{\omega^{i-n} E_1^i}{n!(i-n)!} g^{i,i-n}(E_0) \sin(\pi s)^n \cos(\pi s)^{i-n} \tag{137}$$

where

$$g^{(i,i-n)}(E_0) = \left[\left(\partial^n g / \partial E^n\right)\left(\partial^{i-n} g / \partial \dot{E}^{i-n}\right)\right]_{E_1=0} \tag{138}$$

By substituting Eq. (137) into Eqs. (135) and (136), the storage and loss modulus of a differential viscoelastic model can be expressed as

$$S = \sum_{i=0}^{\infty} \sum_{n=0}^{i} \frac{\omega^{i-nE_1^i}}{n!(i-n)!} g^{i,i-n}(E_0) \int_{-1}^{1} \sin(\pi s)^{n+1} \cos(\pi s)^{i-n} ds \tag{139}$$

$$L = \sum_{i=0}^{\infty} \sum_{n=0}^{i} \frac{\omega^{i-nE_1^i}}{n!(i-n)!} g^{i,i-n}(E_0) \int_{-1}^{1} \sin(\pi s)^{n} \cos(\pi s)^{i-n+1} ds \tag{140}$$

provided that the infinite summation has been taken out of the integral sign since the series (139) uniformly converges. Equations (137) and (138) allow the sensitivities $\partial S/\partial\omega$ and $\partial L/\partial\omega$ to be evaluated at $\omega = 0$. In this case, the non-vanishing terms in the series (135) are those with indices $n = i - 1$, thus

$$\left.\frac{\partial S}{\partial \omega}\right|_{\omega=0} = \sum_{i=1}^{\infty} \frac{E_1^i}{(i-1)!} g^{(i-1,1)}(E_0) \int_{-1}^{1} \sin(\pi s)^{i} \cos(\pi s) ds = 0 \tag{141}$$

Equation (141) proves that for every constitutive equation in the form (133), the sensitivity of the storage modulus vanishes when assessed at low frequency.

A constitutive equation in the form:

$$\sigma(t) = f\left[E(t), \dot{E}(t)\right] + l\left[E(t), \dot{E}(t)\right] \int_{-\infty}^{t} \dot{k}(t-s) h\left[E(s)\dot{E}(s)\right] ds \tag{142}$$

The linear viscoelastic model (129) is recovered by choosing

$$f\left[E, \dot{E}\right] = k_0 E, l\left[E, \dot{E}\right] = 1, h\left[E, \dot{E}\right] = E \tag{143}$$

For the case (143), to guarantee that the work associated with a process starting at equilibrium is non-negative, the viscoelastic kernel k(t) must be a smooth function of time and satisfy the conditions [167]

$$k(t) \geq 0, \dot{k}(t) \leq 0, \ddot{k}(t) \geq 0 \tag{144}$$

together with

$$\lim_{t\to\infty} k(t) = k_\infty < \infty, \lim_{t\to\infty} \dot{k}(t) = 0, k_0 = k(0) < \infty \tag{145}$$

moreover, from the positivity of the derivative, $k_\infty < k_0$

Again, any constitutive relation in the form (142), whose kernel satisfies (144)-(145), also satisfies (128); hence, for the case of imposed deformation (131), we can let $t_0 \to -\infty$ and study the steady-state response to the harmonic deformation $E_s(t) = E_0 + E_1 \sin(\omega t)$. Again this stationary stress response is periodic with period $T = 2\pi/\omega$ viz.

$$\sigma_s(t+T) = f\left[E_s(t+T), \dot{E}_s(t+T)\right] + l\left[E_s(t+T), \dot{E}_s(t+T)\right]$$
$$\int_0^{+\infty} k(\tau) h\left[E_s(t+T-\tau), \dot{E}_s(t+T-\tau)\right] dr = f\left[E_s(t), \dot{E}_s(t)\right] + l\left[E_s(t), \dot{E}_s(t)\right]$$
$$\int_0^{+\infty} k(\tau) h\left[E_s(t-\tau), \dot{E}_s(t-\tau)\right] dr = \sigma_s(t) \tag{146}$$

Setting the lower limit of the integral in (142) to $-\infty$, i.e., letting $t_0 \to -\infty$ allowed the transient response to be filtered out. In order to evaluate explicitly the dependence of the stationary stress on deformation parameters ω, E0 and E1, stronger regularity requirements, with respect to the previous case, must be considered. In particular, it is assumed that the Fourier series of the functions f, g and l are absolutely convergent1; then, by means of the Cauchy formula for the product between two series [190], the constitutive equation (142) can be expressed as

$$\sigma_s(t) = \frac{\sigma_0}{2} + \sum_{i=1}^{\infty} \left[\sigma_i^S \sin(i\omega t) + \widetilde{\sigma}_i^C \cos(i\omega t)\right] \tag{147}$$

with

$$\sigma_0 = \sigma_0(f_0, l_0, H_0) \tag{148}$$
$$\sigma_i^S = \sigma_i^S\left(f_i^S, f_i^C, l_i^S, l_i^C, H_i^S, H_i^C; \omega\right) \tag{149}$$
$$\sigma_i^C = \sigma_i^C\left(f_i^S, f_i^C, l_i^S, l_i^C, H_i^S, H_i^C; \omega\right) \tag{150}$$

and

$$H_0 = h_0(k_\infty - k_0) \tag{151}$$
$$H_i^S = h_i^S \int_0^{+\infty} \dot{k}(s) \cos(i\omega s) ds - h_i^C \int_0^{+\infty} \dot{k}(s) \sin(i\omega s) ds \tag{152}$$
$$H_i^C = -h_i^S \int_0^{+\infty} \dot{k}(s) \sin(i\omega s) ds - h_i^C \int_0^{+\infty} \dot{k}(s) \cos(i\omega s) ds \tag{153}$$

Here, $f_i^S, f_i^C, l_i^S, l_i^C, h_i^S$ and h_i^C are the Fourier coefficients of the functions f, l and h respectively (the explicit relationship between σs and these coefficients is reported in Appendix). All the coefficients depend on all deformation parameters, but this dependence has been omitted in (148)-(153) for the sake of conciseness. The existence of the integrals in (154)-(118) is assured by the smoothness of k(t) and the asymptotic properties (3.87).

The dynamic moduli are obtained by a standard projection of (147) over sin(ωt) and cos(ωt) (see Appendix); the result is

$$S = \frac{1}{E_1}\left[f_1^S + \frac{l_0}{2}H_1^S + \frac{l_1^S}{2}H_0\right] + \frac{1}{2E_1}\sum_{i=1}^{+\infty}\left[-l_i^S H_{i+1}^C + l_{i+1}^S H_i^C + l_i^C H_{i+1}^S - l_{i+1}^C H_i^S\right] \tag{154}$$

$$L = \frac{1}{E_1}\left[f_1^C + \frac{l_0}{2}H_1^C + \frac{l_1^C}{2}H_0\right] + \frac{1}{2E_1}\sum_{i=1}^{+\infty}\left[-l_i^S H_{i+1}^S + l_{i+1}^S H_i^S + l_i^C H_{i+1}^C - l_{i+1}^C H_i^C\right] \tag{155}$$

In order to evaluate the sensitivities of the dynamic moduli at low frequency, the derivatives $\partial H_i^S/\partial\omega$ and $\partial H_i^C/\partial\omega$ must be computed and assessed at $\omega \to 0$. With this intent, it has been assumed that the kernel satisfies the following integrability condition:

$$\int_0^{+\infty} s\left|\dot{k}(s)\right| ds < +\infty \tag{156}$$

Incidentally, the previous condition is satisfied by most viscoelastic kernels commonly employed in the literature, as it is shown in the next section. Because $\dot{k}(s) < 0$ for each s, if holds true, then the integrals:

$$\int_0^{+\infty} \dot{k}(s)s\sin(\omega s)ds \tag{157}$$

$$\int_0^{+\infty} \dot{k}(s)ds \tag{158}$$

$$\int_0^{+\infty} \dot{k}(s)s\cos(\omega s)ds \tag{159}$$

have finite values. The following derivative can, therefore, be computed,

$$\frac{\partial}{\partial\omega}\int_0^{+\infty} \dot{k}(s)s\cos(\omega s)ds = -\int_0^{+\infty} \dot{k}(s)s\sin(\omega s)ds \tag{160}$$

similar derivatives occur when evaluating the sensitivities of H_i^S and H_i^C with respect to frequency. The actual expressions of both $\partial H_i^S/\partial\omega$ and $\partial H_i^S/\partial H_i^C$, under assumption (156), are given in Appendix.

Furthermore, if f, l and h are analytic functions with respect to E1, Eq. (154) allow the sensitivity of the storage modulus to be evaluated at $\omega = 0$, that is

$$\left.\frac{\partial S}{\partial \omega}\right|_{\omega=0} = \left.\frac{l_0}{2E_1}\frac{\partial H_1^S}{\partial \omega}\right|_{\omega=0} + \frac{1}{2E_1}\sum_{i=1}^{\infty}\left[-\frac{\partial l_i^S}{\partial \omega}H_{i+1}^C - l_i^S\frac{\partial H_{i+1}^C}{\partial \omega} + \frac{\partial l_{i+1}^C}{\partial \omega}H_i^C + l_{i+1}^S\frac{\partial H_i^C}{\partial \omega}\right]_{\omega=0} + \frac{1}{2E_1}\sum_{i=1}^{\infty}\left[\frac{\partial l_i^C}{\partial \omega}H_{i+1}^S + l_i^C\frac{\partial H_{i+1}^S}{\partial \omega} - \frac{\partial l_{i+1}^C}{\partial \omega}H_i^S - l_{i+1}^C\frac{\partial H_i^S}{\partial \omega}\right]_{\omega=0} = 0 \quad (161)$$

Indeed, in Appendix, it is shown that for $\omega \to 0$, H_i^S and l_i^S (H_i^C and l_i^C) vanish if i is even (odd); furthermore, the derivatives $\partial H_i^S/\partial\omega$ and $\partial l_i^S/\partial\omega$ ($\partial H_i^C/\partial\omega$ and $\partial l_i^C/\partial\omega$) vanish if i is odd (even). Therefore, for each i the square bracketed terms in (161) are zero.

Equation (159) proves that, for every constitutive equation in the form (142), whose kernel satisfies (144)-(145) and (156), the sensitivity of the storage modulus vanishes when assessed at low frequencies. Remarkably, there is no nonlinear functional dependence of stress on the current and past strain values, which can overcome the effect of a kernel which decays sufficiently fast to satisfy the condition (156).

A general misbehavior of differential and integral viscoelastic models has been highlighted (Table 5).

The nonlinear viscoelastic behavior of the composites of natural rubber filled with surface-modified nanosilica was studied with reference to silica loading [191]. The effect of temperature on the nonlinear viscoelastic behavior has been investigated. It was observed that Payne effect becomes more pronounced at higher silica loading. The filler characteristics such as particle size, specific surface area, and the surface structural features were found to be the key parameters influencing the Payne effect. A nonlinear decrease in storage modulus with increasing strain was observed for unfilled compounds also. The results reveal that the mechanism includes the breakdown of different networks namely the filler – filler network, the

Table 5 Material models based on the proposed generalized formulation

Model name		$\Pi_{ES}^{(e)}$		Λ	Ψ
		ϕ_1	ϕ_2		
1.	Fung	$2[\alpha_1+\alpha_2 I_1(t)]$	$-2\alpha_2$	I	$\mathrm{F}^{-1}(s)\Pi_{ES}^{(e)}(s)$
2.	Fosdick and Yu	$2[\alpha_1+\alpha_2 I_1(t)]$	$-2\alpha_2$	$C^{-1}(t)$	$\beta[C(s)C^{-1}(t)-I]$
3.	Hallquist	$2[\alpha_1+\alpha_2 I_1(t)]$	$-2\alpha_2$	I	$-\beta\dot{C}(s)$
4	Yang et al.	α_1	α_2	I	$-[\beta_1+\beta_2 I(s)]\dot{C}(s)$
5	Shimet et al.	α_1	α_2	$[1+\gamma_1 I_2(t)]I$	$-\left[\beta_1\frac{\dot{I}_1(s)}{I_1(s)}C(s)+2\beta_2 C\right]$
6	Hibbet et al.	$2[\alpha_1+\alpha_2 I_1(t)]$	$-2\alpha_2$	I	$\mathrm{F}^{-1}(s)\Pi^{(e)}(s)C(s)C^{-1}(t)$

weak polymer – filler network, the chemical network, and the entanglement network. The model of variable network density proposed by Maier and Goritz has been applied to explain the nonlinear behavior. The activation energy of desorption was calculated and found to be within the range of Van der Waal's interaction energy. The model fits well with the experimental results large deformation continuum theory (Pseudo Stress Models and ABAQUS model) should be used instead of geometrically linear theory [192].

5 Conclusions and Perspectives

If the viscoelastic kernel, i.e., the material memory, decreases too fast in time, the sensitivity of the resulting storage modulus vanishes at low frequency, in contrast to the experimental evidence collated. An integrability condition has been introduced to discriminate, among the kernels, those with a sufficiently slow rate of decay. Luckily, this is not in contrast with the Principle of Fading Memory which, instead, imposes a sufficiently fast decay of the material's memory. Indeed, we have shown two examples of kernels satisfying both requests: the well-known fractional kernel, derived from fractional rheological models, and the hypergeometric kernel, an original proposal. The standard linear viscoelastic model endowed with such kernels is able to match accurately the experimental data. With respect to the fractional kernel, the hypergeometric one requires a lower computational effort and could encompass a finite sensitivity of the storage modulus when $\omega \to 0$. Moreover, while the fractional kernel is obtained from the solution of a fractional differential equation, which necessarily involves time integrals, the possibility of representing the hypergeometric kernel as the solution of evolution equations of selected internal variables should be carefully investigated. This possibility could be a crucial ingredient to implement the hypergeometric model into finite element codes: implementations of kernels in terms of evolution equations are drammatically less time-consuming and memory-expensive.

The dynamic viscoelastic properties of nanosilica-filled natural rubber composites was investigated. The objective of the present study was to look at the nonlinear viscoelastic behavior of natural rubber filled with commercially used nanosilica. The Payne effect is assumed to arise from the elementary mechanism consisting of adsorption-desorption of macromolecular chains from the filler surface. It was found that because of the small particle size and high specific surface area, nanosilica forms stronger and more developed filler-filler network and the breakdown of these networks results in larger Payne effect. Also, the amount and morphology of the fillers played a major role on the Payne effect.

At low loading, there is not much variation in storage modulus, loss modulus, and loss tangent compared to gum vulcanizates. But at higher loading, a pronounced effect has been observed. This is due to the breakage of weak polymer-filler linkages and filler-filler networks at higher strain amplitude. But surprisingly, enhanced Payne-like behavior has been observed for gum vulcanizates at room temperature where there are no filler-filler and no filler-polymer interactions, which

are typically associated with filled vulcanizates. This is explained by the effect of chain disentanglements on straining. The model of variable network density has been applied and the calculated activation energy for NR filled with 20 phr silica is found to be within the range of Van der Waal's interaction energy. Hence it is concluded that the number of unstable fixed chains adsorbed on the filler surface is also responsible for the reduction in modulus with increase in temperature. Finally, it is concluded that in addition to the contribution from filler-filler network, there are a lot of factors that affect the nonlinear viscoelastic behavior including the breakdown of different networks, namely, filler-filler networks, weak polymer-filler networks, chemical networks, and entanglement networks.

Dynamic Moduli of Nonlinear Viscoelastic Models

In Eq. (161) f, l and h are nonlinear functions of the strain and the strain rate. Under weak

$$\begin{aligned} f(t) &= f[E_0 + E_1 \sin(\omega t), E_1 \omega \cos(\omega t)] \\ &= \frac{f_0}{2} + \sum_{i=1}^{\infty} \left[f_i^S \sin(i\omega t) + f_i^C \cos(i\omega t) \right] \end{aligned} \tag{162}$$

Where

$$f_0 = f_0(E_0, E_1), \quad f_i^S = f_i^S(E_0, E_1, \omega), \quad f_i^C = f_i^C(E_0, E_1, \omega)$$

regularity assumption, their Fourier series are uniformly convergent, e.g.,

The Fourier coefficients of l and h will be denoted as l_i^S, l_i^C and h_i^S, h_i^C, respectively.If the series (162) are also absolutely convergent, by means of the Cauchy formula, the following expression of the stationary stress is recovered

$$\begin{aligned} \sigma_s(t) = &\frac{f_0}{2} + \frac{H_0 l_0}{4} \\ &+ \sum_{i=1}^{\infty} \left[\left(f_i^S + \frac{l_0}{2} H_i^S + \frac{l_i^S}{2} H_0 \right) \sin(i\omega t) + \left(f_i^C + \frac{l_0}{2} H_i^C + \frac{l_i^C}{2} H_0 \right) \cos(i\omega t) \right] + \\ &+ \sum_{i=1}^{+\infty} \sum_{n=1}^{i} l_n^S \left[H_{i-n+1}^S \sin[(i-n+1)\omega t] + H_{i-n+1}^C \cos[(i-n+1)\omega t] \right] \sin(n\omega t) + \\ &+ \sum_{i=1}^{+\infty} \sum_{n=1}^{i} l_n^C \left[H_{i-n+1}^S \sin[(i-n+1)\omega t] + H_{i-j+1}^C \cos[(i-n+1)\omega t] \right] \cos(n\omega t). \end{aligned} \tag{163}$$

By projecting $\sigma_s(t)$ over $\sin(\omega t)$ and $\cos(\omega t)$, Eqs. (3.94)-(3.95) of the storage and loss moduli are recovered.In order to evaluate the derivatives $\partial S/\partial\omega$ and $\partial L/\partial\omega$, $\partial H_i^S/\partial\omega$ and $\partial H_i^C/\partial\omega$ can be derived from Eqs. (3.91)-(3.93), i.e.,

$$\frac{\partial H_i^S}{\partial\omega} = \frac{\partial h_i^S}{\partial\omega}\int_0^{+\infty}\dot{k}(s)\cos(i\omega s)ds - h_i^S\int_0^{+\infty} is\dot{k}(s)\sin(i\omega s)ds$$
$$-\frac{\partial h_i^C}{\partial\omega}\int_0^{+\infty}\dot{k}(s)\sin(i\omega s)ds - h_i^C\int_0^{+\infty} is\dot{k}(s)\cos(i\omega s)ds \tag{164}$$

$$\frac{\partial H_i^S}{\partial\omega} = \frac{\partial h_i^S}{\partial\omega}\int_0^{+\infty}\dot{k}(s)\sin(i\omega s)ds - h_i^S\int_0^{+\infty} is\dot{k}(s)\cos(i\omega s)ds$$
$$-\frac{\partial h_i^C}{\partial\omega}\int_0^{+\infty}\dot{k}(s)\cos(i\omega s)ds - h_i^C\int_0^{+\infty} is\dot{k}(s)\sin(i\omega s)ds \tag{165}$$

provided that the integrability condition (3.96) holds. As a consequence, when assessed at low frequencies, the result is

$$\frac{\partial H_i^S}{\partial\omega}|_{\omega=0} = (k_\infty - k_0)\frac{\partial h_i^S}{\partial\omega}|_{\omega=0} - h_i^C|_{\omega=0} i\int_0^{+\infty} s\dot{k}(s)ds \tag{166}$$

$$\frac{\partial H_i^C}{\partial\omega}|_{\omega=0} = (k_\infty - k_0)\frac{\partial h_i^C}{\partial\omega}|_{\omega=0} - h_i^S|_{\omega=0} i\int_0^{+\infty} s\dot{k}(s)ds \tag{167}$$

and, therefore, these sensitivities depend upon the sensitivities of the constitutive functions h_i^S and h_i^C, respectively. To evaluate these quantities, let us assume that the functions f, l and h are analytic with respect to E_1. By expanding h in Taylor series, as in Eq. (156), and by projecting over $\sin(i\omega t)$ and $\cos(i\omega t)$, the Fourier coefficients h_i^C and h_i^S are obtained, e.g.,

$$h_i^S = \sum_{p=0}^{\infty}\sum_{q=0}^{p}\frac{\omega^{p-q}E_1^p}{q!(p-q)!}h^{(q,p-q)}(E_0)\int_{-1}^{1}\sin(\pi s)^q\cos(\pi s)^{p-q}\sin(i\pi s)ds \tag{168}$$

$$h_i^C = \sum_{p=0}^{\infty}\sum_{q=0}^{p}\frac{\omega^{p-q}E_1^p}{q!(p-q)!}h^{(q,p-q)}(E_0)\int_{-1}^{1}\sin(\pi s)^q\cos(\pi s)^{p-q}\cos(i\pi s)ds \tag{169}$$

When assessing h_i^C and h_i^S at $\omega\to 0$, the only term not vanishing in the infinite summations (168) and (169) are those corresponding to $n = m$, that is

$$h_i^S|_{\omega=0} = \sum_{p=0}^{\infty}\frac{E_1^p}{p!}h^{(p,0)}(E_0)\int_{-1}^{1}\sin(\pi s)^p\sin(i\pi s)ds\begin{cases} = 0, & iEven \\ \neq 0, & iOdd \end{cases} \tag{170}$$

$$h_i^C|_{\omega=0} = \sum_{p=0}^{\infty} \frac{E_1^p}{p!} h^{(p,0)}(E_0) \int_{-1}^{1} \sin(\pi s)^p \cos(i\pi s) ds \begin{cases} = 0, & iOdd \\ \neq 0, & iEven \end{cases} \tag{171}$$

with the corresponding derivatives given by

$$\frac{\partial h_i^S}{\partial \omega}|_{\omega=0} = \sum_{p=0}^{\infty} \frac{E_1^p}{(p-1)!} h^{(p-1,1)}(E_0) \int_{-1}^{1} \sin(\pi s)^{p-1} \cos(\pi s) \sin(i\pi s) ds \begin{cases} = 0, & iOdd \\ \neq 0, & iEven \end{cases} \tag{172}$$

$$\frac{\partial h_i^C}{\partial \omega}|_{\omega=0} = \sum_{p=0}^{\infty} \frac{E_1^p}{(p-1)!} h^{(p-1,1)}(E_0) \int_{-1}^{1} \sin(\pi s)^{p-1} \cos(\pi s) \sin(i\pi s) ds \begin{cases} = 0, & iEven \\ \neq 0, & iOdd \end{cases} \tag{173}$$

As a result, the sensitivities $\partial H_i^S/\partial\omega$ and $\partial H_i^S/\partial\omega$ can be assessed at $\omega = 0$, i.e.

$$\frac{\partial H_i^S}{\partial \omega}|_{\omega=0} = \begin{cases} = 0, & iOdd \\ \neq 0, & iEven \end{cases} \tag{174}$$

$$\frac{\partial H_i^C}{\partial \omega}|_{\omega=0} = \begin{cases} = 0, & iEven \\ \neq 0, & iOdd \end{cases} \tag{175}$$

Equations (168)–(173) allow the sensitivities of f_i^S, f_i^C, l_i^S and l_i^C to be estimated and, consequently, Eq. (161) to be recovered.

Acknowledgment The financial support for this study was granted by the Ministry of Science and Technological Development of the Republic of Serbia (Projects nos. 45022 and 45020).

References

1. Kraus G (1965) Reinforcement of elastomers. Wiley-Interscience, New York
2. Donnet J-B (1993) In some cases the reinforcement is supported by chemical bond of the polymer with the filler surface, by using coupling agent. In: Bansal RC, Wang MJ (eds) Carbon black science and technology. Marcel, New York
3. Görl U, Hunsche A, Müller A, Koban HG (1997) Rubber Chem Technol 70:608–623
4. Fröhlich J, Lugisland HD (2001) Rubber World 28:244–248
5. Payne AR (1962) The dynamic properties of carbon black loaded natural rubber vulcanizates. Part II. J Appl Polym Sci 6:368–372
6. Medalia AI (1986) Rubber Chem Technol 59:432–454
7. Wang MJ (1999) The role of filler networking in dynamic properties of filled rubber. Rubber Chem Technol 72:430–448
8. Payne AR (1962) The dynamic properties of carbon black-loaded natural rubber vulcanizates. Part I. J Appl Polym Sci VI:57–63
9. Payne AR (1965) Reinforcement of elastomers. Interscience: New York, p 69 (Chap. 3)
10. Payne AR, Whitaker RE (1971) Rubber Chem Technol 44:440–478

11. Robertson CG, Lin CJ, Rackaitis M, Roland CM (2008) Macromolecules 41:2727–2731
12. Kraus G (1984) J Appl Polym Sci 39:75–92
13. Medalia AI (1973) Rubber World 168:49
14. Wang M (1998) Rubber Chem Technol 71:520–589
15. Kraus G (1984) Mechanical losses in carbon-black-filled rubbers. In: Applied polymer symposia, 75–92, Phillips Petroleum Co, Bartlesville, OK, USA, Phillips Petroleum Co, Bartlesville, OK, USA
16. Huber G, Vilgis TA (2002) On the mechanism of hydrodynamic reinforcement in elastic composites. Macromolecules 35:9204–9210
17. Witten TA, Rubinstein M, Colby RH (1993) Reinforcement of rubber by fractal aggregates. J Phys II 3:367–383
18. Heinrich G, Klüppel M, Vilgis TA (2002) Reinforcement of elastomers. Curr Opin Sol Stat Mater Sci 6:195–203
19. Kluppel M, Schuster R, Heinrich G (1997) Rubber Chem Technol 70:243–255
20. Funt JM (1999) Rubber Chem Technol 4:657–675
21. Maier PG, Goritz D (1996) Kautsch. Gummi Kunstst 49, Jahrgang.Nr. 1/96
22. Zhu AJ, Sternstein SS (2003) Nonlinear viscoelasticity of nanofilled polymers: interfaces, chain statistics and properties recovery kinetics. Compos Sci Technol 63:1113–1126
23. Sternstein SS, Zhu AJ (2002) Reinforcement mechanism of nanofilled polymer melts as elucidated by nonlinear viscoelastic behavior. Macromolecules 35:7262–7273
24. Marrone M, Montanari T, Busca G, Conzatti L, Costa G, Castellano M, Turturro A (2004) J Phys Chem B 108:3563–3572
25. Bokobza L (2004) The reinforcement of elastomeric networks by fillers. Macromol Mater Eng 289:607–621
26. Castellano M, Conzatti L, Turturro A, Costa G, Busca G (2007) J Phys Chem B 111:4495–502
27. Clement F, Bokobza L, Monnerie L (2005) Investigation of the Payne effect and its temperature dependence on silica-filled polydimethylsiloxane networks. Part I: Experimental results. Rubber Chem Technol 78:211
28. Paquien JN, Galy J, Gerard JF, Pouchelon A (2005) Rheological studies of fumed silica–polydimethylsiloxane suspensions. Colloids Surf A 260:165–172
29. Ramier J, Gauthier C, Chazeau L, Stelandre L, Guy L (2007) J Polym Sci B Polym Phys 45:286–298
30. Maier PG, Goritz D (1993) Kautsch Gummi Kunstst 46, Jahrgang. Nr. 11/93
31. Maier PG, Goritz D (2000) Kautsch Gummi Kunstst 53, Jahrgang. Nr. 12/2000
32. Cassagnau P (2003) Payne effect and shear elasticity of silica-filled polymers in concentrated solutions and in molten state. Polymer 44:2455–2462
33. Cassagnau P (2008) Melt rheology of organoclay and fumed silica nanocomposites. Polymer 49:2183–2196
34. Sun J, Song Y, Zheng Q, Tan H, Yu J, Li H (2007) J Polym Sci B Polym Phys 45:2594–2602
35. Yatsuyanagi F, Kaidou H, Ito M (1999) Rubber Chem Technol 4:657–672
36. Berriot J, Montes H, Lequeux F, Long D, Sotta P (2003) Europhys Lett 64:50–56
37. Berriot J, Lequeux F, Montes H, Monnerie L, Long D, Sotta PJ (2002) Non-Cryst Solids 719:307–310
38. Montes H, Lequeux F, Berriot J (2003) Influence of the glass transition temperature gradient on the nonlinear viscoelastic behavior in reinforced elastomers. Macromolecules 36:8107–8118
39. Merabia S, Sotta P, Long DR (2008) A microscopic model for the reinforcement and the nonlinear behavior of filled elastomers and thermoplastic elastomers (Payne and Mullins Effects). Macromolecules 41:8252–8266
40. Ferry JD (1980) Viscoelasticity properties of polymer, 3rd edn. Wiley, New York
41. Callister W (2007) Materials science and engineering. Wiley, City

42. Goldberg A, Lesuer DR, Patt J (1989) Fracture morphologies of carbon-blackloaded SBR subjected to low-cycle, high-stress fatigue. Rubber Chem Technol 62:272–287
43. Chazeau L, Brown JD, Yanyo LC, Sternstein SS (2000) Modulus recovery kinetics and other insights into the Payne effect for filled elastomers. Polym Compos 21:202–222
44. Wolff S, Donnet J-B (1990) Rubber Chem Technol 63:32–61
45. Brennan JJ, Jermyn TE, Bonnstra BB (1964) J Appl Polym Sci 8:2687–2706
46. Fletcher WP, Gent AN (1953) Trans IRI 29:266–80
47. Payne AR (1964) J Appl Polym Sci 8:1661–1667
48. Medalia AI (1978) Rubber Chem Technol 51:437–523
49. Schapery R (1997) Nonlinear viscoelastic and viscoplastic constitutive equations based on thermodynamics. Mech Time-Depend Mater 1:209–240
50. Ogden RW (1997) Non-linear elastic deformations. Dover Publications, New York
51. Simo JC (1987) On a fully three-dimensional finite-strain viscoelastic damage model: Formulation and computational aspects. Comput Meth Appl Mech Eng 60:153–173
52. Govindjee S, Simo JC (1992) Mullins effect and the strain amplitude dependence of the storage modulus. Int J Solids Struct 29:1737–1751
53. Drozdov AD, Dorfmann A (2003) Finite viscoelasticity of filled rubber: experiments and numerical simulation. Arch Appl Mech 72:651–672
54. Laraba-Abbes F, Ienny P, Piques R (2003) A new 'Tailor-made' methodology for the mechanical behaviour analysis of rubber-like materials: II. Application to the hyperelastic behaviour characterization of a carbon-black filled natural rubber vulcanizate. Polymer 44:821–840
55. Przybylo P, Arruda E (1998) Experimental investigations and numerical modeling of incompressible elastomers during non-homogeneous deformations. Rubber Chem Technol 71:730–749
56. Treloar L (2005) The physics of rubber elasticity. Clarendon Press, Oxford
57. Drozdov AD (2007) Constitutive equations in finite elasticity of rubbers. Int J Solids Struct 44:272–297
58. Bischoff J, Arruda E, Grosh K (2001) A new constitutive model for the compressibility of elastomers at finite deformations. Rubber Chem Technol 74:541–559
59. MacKnight W (1966) Volume changes accompanying the extension of rubber-like materials. J Appl Phys 37:4587
60. Ogden RW (1976) Volume changes associated with the deformation of rubber-like solids. J Mech Phys Solids 24:323–338
61. Penn RW (1970) Volume changes accompanying the extension of rubber. J Rheol 14:509–517
62. Reichert WF, Hopfenmueller MK, Goritz D (1987) Volume change and gas transport at uniaxial deformation of filled natural rubber. J Mater Sci 22:3470–3476
63. Mott P, Roland C (2010) Response to "Comment on paper " The bulk modulus and Poisson's ratio of "incompressible" materials". J Sound Vib 329:368–369
64. Mott P, Dorgan J, Roland C (2008) The bulk modulus and Poisson's ratio of "incompressible" materials. J Sound Vib 312:572–575
65. Voinovich P (2010) Comment on paper "the bulk modulus and Poisson's ratio of "incompressible" materials" by P.H. Mott, J.R. Dorgan, C.M. Roland. J Sound Vib 329:366–367
66. Yeoh O, Fleming P (1997) A new attempt to reconcile the statistical and phenomenological theories of rubber elasticity. J Polym Sci Pt B Polym Phys 35:1919–1931
67. Shan GF, Yang W, Yang M, Xie B, Feng J, Fu Q (2007) Effect of temperature and strain rate on the tensile deformation of polyamide 6. Polymer 48:2958–2968
68. Chanliau-Blanot MT, Nardiim M, Donnet JB, Papirer E, Roche G, Lau-renson P, Rossignol G (1989) Temperature dependence of the mechanical properties of EPDM rubber-polyethylene blends filled with aluminium hydrate particles. J Mater Sci 24:641–648

69. Khan AS, Lopez-Pamies O, Kazmi R (2006) Thermo-mechanical large deformation response and constitutive modeling of viscoelastic polymers over a wide range of strain rates and temperatures. Int J Plast 22:581–601
70. Boiko AV, Kulik VM, Seoudi BM, Chun H, Lee I (2010) Measurement method of complex viscoelastic material properties. Int J Solids Struct 47:374–382
71. Lee JH, Kim KJ (2001) Characterization of complex modulus of viscoelastic materials subject to static compression. Mech Time-Depend Mater 5:255–271
72. Gottenberg W, Christensen R (1972) Prediction of the transient response of a linear viscoelastic solid. J Appl Mech 6:448–450
73. Osanaiye GJ (1996) Effects of temperature and strain amplitude on dynamic mechanical properties of EPDM gum and its carbon black compounds. J Appl Polym Sci 59:567–575
74. Luo W, Hu X, Wang C, Li Q (2010) Frequency- and strain-amplitude-dependent dynamical mechanical properties and hysteresis loss of CB-filled vulcanized natural rubber. Int J Mech Sci 52:168–174
75. Pipkin A (1986) Lectures on viscoelasticity theory. Springer, Berlin
76. Williams M, Landel R, Ferry J (1955) The temperature dependence of relaxation mechanisms in amorphous polymers and other glass-forming liquids. J Am Chem Soc 77:3701–3707
77. Christensen R (2003) Theory of viscoelasticity, 2nd edn. Dover Publications, New York
78. Singh A, Lakes R, Gunasekaran S (2006) Viscoelastic characterization of selected foods over an extended frequency range. Rheol Acta 46:131–142
79. Mullins L (1947) Effect of stretching on the properties of rubber. J Rubber Res 16:275–289
80. Dorfmann A, Ogden RW (2003) A pseudo-elastic model for loading, partial unloading and reloading of particle-reinforced rubber. Int J Solids Struct 40:2699–2714
81. Dorfmann A, Ogden RW (2004) A constitutive model for the Mullins effect with permanent set in particle-reinforced rubber. Int J Solids Struct 41:1855–78
82. Harwood JAC, Mullins L, Payne AR (1966) Stress softening in natural rubber vulcanizates. Part II. Stress softening effects in pure gum and filler loaded rubbers. Rubber Chem Technol 39:814–22
83. Harwood JAC, Payne AR (1966) Stress softening in natural rubber vulcanizates III. Carbon black filled vulcanizates. J Appl Polym Sci 10:315–23
84. Mullins L, Tobin NR (1957) Theoretical model for the elastic behavior of filler reinforced vulcanized rubbers. Rubber Chem Technol 30:555–71
85. Klüppel M, Schramm M (2000) A generalized tube model of rubber elasticity and stress softening of filler reinforced elastomer systems. Macromol Theory Simul 9:742–54
86. Diani J, Brieu M, Vacherand JM (2006) A damage directional constitutive model for Mullins effect with permanent set and induced anisotropy. Eur J Mech Solids/A 25:483–96
87. Kakavas PA (1996) Mechanical properties of bonded elastomer discs subjected to triaxial stress. J Appl Polym Sci 59:251–61
88. Flamm M, Steinweger T, Spreckels J, Brüger T (2008) In mechanical properties of EPDM. In: Boukamel A, Laiarinandrasana L, Méo S, Verron E (eds) In constitutive models for rubber. V. Balkema, Netherlands, pp 233–242
89. Clément F, Bokobza L, Monnerie L (2001) On the Mullins effect in silica filled polydimethylsiloxane networks. Rubber Chem Technol 74:846–70
90. Mullins L (1948) Effect of stretching on the properties of rubber. J Rubber Res 16:275–82
91. Stevenson I, David L, Gauthier C, Arambourg L, Davenas J, Vigier G (2001) Influence of SiO2 fillers on the radiation ageing of silicone rubbers. Polymer 42:9287–92
92. Hanson DE, Hawley M, Houlton R, Chitanvis K, Rae P, Orler EB et al (2005) Stress softening experiments in silica-filled polydimethylsiloxane provide insight into a mechanism for the Mullins effect. Polymer 46:10989–95
93. Blanchard AF, Parkinson D (1952) Breakage of carbon-rubber networks by applied stress. J Ind Eng Chem 44:799–812
94. Mullins L, Tobin N (1957) Theoretical model for the elastic behavior of fillerreinforced vulcanized rubbers. Rubber Chem Technol 30:551–571

95. Qi HJ, Boyce MC (2004) Constitutive model for stretch-induced softening of the stress-stretch behavior of elastomeric materials. J Mech Phys Solids 52:2187–2205
96. Horgan CO, Ogden RW, Saccomandi G (2004) A theory of stress softening of elastomers based on finite chain extensibility. Proc R Soc A 460:1737–1754
97. Ogden RW, Roxburgh DG (1999) A pseudo-elastic model for the Mullins effect in filled rubber. Proc R Soc A 455:2861–2877
98. Gent A (1996) A new constitutive relation for rubber. Rubber Chem Technol 69:59–61
99. Kachanov LM (1958) Time of the rupture process under creep conditions. Izvestiya Akad Nauk SSR Otd Tekh Nauk 58:26–31
100. Ziegler J, Schuster RH (2003) Kautsch Gummi Kunstst 56(4):159–163
101. Lion A, Kardelky C (2004) The Payne effect in finite viscoelasticity: constitutive modelling based on fractional derivatives and intrinsic time scales. Int J Plast 20:1313–1345
102. Beatty M (1996) Nonlinear effects in fluids and solids, chap. 2, Introduction to Nonlinear Elasticity, 13–112. Plenum Press, New York
103. Holzapfel G (2000) Nonlinear solid mechanics: a continuum approach for engineering. Wiley, New York
104. Liu IS (2004) On Euclidean objectivity and the principle of material frame-indifference. Continuum Mech Thermodyn 16:177–183
105. Murdoch AI (2005) On criticism of the nature of objectivity in classical continuum physics. Continuum Mech Thermodyn 17:135–148
106. Rivlin R (2002) Frame indifference and relative frame indifference. Math Mech Solids 10:145–154
107. Rivlin RS (2005) Some thoughts on frame indifference. Math Mech Solids 11:113–122
108. Truesdell CA, Noll W (1965) The non-linear field theories of mechanics, 3rd edn. Springer, New York
109. Rivlin R, Ericksen J (1955) Stress-deformation relations for isotropic materials. J Rat Mech Anal 4:323–425
110. Flory P (1961) Thermodynamic relations for high elastic materials. Trans Faraday Soc 57:829–838
111. Sansour C (2008) On the physical assumptions underlying the volumetric-isochoric split and the case of anisotropy. Eur J Mech A Solids 27:28–39
112. Simo J, Taylor R, Pister K (1985) Variational and projection methods for the volume constraint in finite deformation elasto-plasticity. Comput Meth Appl Mech Eng 51:177–208
113. Eihlers W, Eppers G (1998) The simple tension problem at large volumetric strains computed from finite hyperelastic material laws. Acta Mech 137:12–27
114. Rivlin R, Saunders D (1952) The free energy of deformation for vulcanized rubber. Trans Faraday Soc 48:200–206
115. Hartmann S (2001) Numerical studies on the identification of the material parameters of Rivlin's hyperelasticity using tension-torsion tests. Acta Mech 148:129–155
116. Pucci E, Saccomandi G (1997) On universal relations in continuum mechanics. Continuum Mech Thermodyn 9:61–72
117. Johnson AR, Quigley CJ, Freese CE (1995) A viscohyperelastic finite-element model for rubber. Comput Meth Appl Mech Eng 127:163–180
118. Noll W (1958) A mathematical theory of the mechanical behavior of continuous media. Arch Rational Mech Anal 2:197–226
119. Wineman A (2009) Nonlinear viscoelastic solids–a review. Math Mech Solids 14:300–366
120. Quintanilla R, Saccomandi G (2007) The importance of the compatibility of nonlinear constitutive theories with their linear counterparts. J Appl Mech 74:455–460
121. Malkin A (1995) Rheology fundamentals. ChemTec Publishing, Toronto-Scarborough
122. Boltzmann L (1874). Zur Theorie der elastischen Nachwirkung. Sitzungsber Math Naturwiss Kl Kaiserl Akad Wiss 70:275–306
123. Volterra V (1912) Sur les equations integro-differentielles et leurs applications. Acta Math 35:295–356

124. Coleman BD, Noll W (1961) Foundations of linear viscoelasticity. Rev Mod Phys 33:239–249
125. Coleman BD (1964) Thermodynamics of materials with memory. Arch Rational Mech Anal 17:1–46
126. Coleman BD, Gurtin ME (1967) Thermodynamics with Internal State Variables. J Chem Phys 47:597–613
127. Coleman BD, Noll W (1963) The thermodynamics of elastic materials with heat conduction and viscosity. Arch Rational Mech Anal 13:167–178
128. Holzapfel GA (1996) On large strain viscoelasticity: Continuum formulation and finite element applications to elastomeric structures. Int J Num Methods Eng 39:3903–3926
129. Holzapfel GA, Gasser TC (2001) A viscoelastic model for fiber-reinforced composites at finite strains: continuum basis, computational aspects and applications. Comput Meth Appl Mech Eng 190:4379–4403
130. Yoshida J, Abe M, Fujino Y (2004) Constitutive model of high-damping rubber materials. J Eng Mech 130:129–141
131. Meggyes A (2001) Multiple decomposition in finite deformation theory. Acta Mech 146:169–182
132. Sidoroff F (1974) Nonlinear viscoelastic model with an intermediate configuration. J Mécaniques 13:679–713
133. Lubliner J (1985) A model of rubber viscoelasticity. Mech Res Commun 12:93–99
134. Green M, Tobolsky A (1946) A new approach to the theory of relaxing polymeric media. J Chem Phys 14:80–92
135. Bonet J (2001) Large strain viscoelastic constitutive models. Int J Solids Struct 38:2953–2968
136. Hasanpour K, Ziaei-Rad S, Mahzoon M (2009) A large deformation framework for compressible viscoelastic materials: constitutive equations and finite element implementation. Int J Plast 25:1154–1176
137. Haupt P, Sedlan K (2001) Viscoplasticity of elastomeric materials: experimental facts and constitutive modelling. Arch Appl Mech 71:89–109
138. Hoo Fatt M, Al-Quraishi A (2008) High strain rate constitutive modeling for natural rubber. In: Proceedings of the 5th European Conference on Constitutive Models for Rubber, ECCMR 2007. University of Akron, Akron, OH, United States, pp 53–60
139. Huber N, Tsakmakis C (2000) Finite deformation viscoelasticity laws. Mech Mater 32:1–18
140. Lion A (1997) A physically based method to represent the thermo-mechanical behaviour of elastomers. Acta Mech 123:1–25
141. Vidoli S, Sciarra G (2002) A model for crystal plasticity based on micro-slip descriptors. Continuum Mech Thermodyn 14:425–435
142. Haupt P, Lion A, Backhaus E (2000) On the dynamic behaviour of polymers under finite strains: constitutive modelling and identification of parameters. Int J Solids Struct 37:3633–3646
143. Haupt P (1985) On the concept of an intermediate configuration and its application to a representation of viscoelastic-plastic material behavior. Int J Plast 1:303–316
144. Haupt P, Lion A (2002) On finite linear viscoelasticity of incompressible isotropic materials. Acta Mech 159:87–124
145. Hoo Fatt MS, Ouyang X (2007) Integral-based constitutive equation for rubber at high strain rates. Int J Solids Struct 44:6491–6506
146. Huber G, Vilgis TA, Heinrich G (1996) Universal properties in the dynamical deformation of filled rubbers. J Phys Cond Matter 8:L409–L412
147. Fancello E, Ponthot J, Stainier L (2008) A variational framework for nonlinear viscoelastic models in finite deformation regime. J Comput Appl Math 215:400–408
148. Green AE, Rivlin RS (1957) The mechanics of non-linear materials with memory. Arch Rational Mech Anal 1:1–21
149. Fichera G (1979) Avere una memoria tenace crea gravi problemi. Arch Rational Mech Anal 70:101–112

150. Drapaca CS, Sivaloganathan S, Tenti G (2007) Nonlinear constitutive laws in viscoelasticity. Math Mech Solids 12:475–501
151. Fabrizio M, Giorgi C, Morro A (1995) Internal dissipation, relaxation property and free-energy in materials with fading memory. J Elast 40:107–122
152. Del Piero G, Deseri L (1997) On the concepts of state and free energy in linear viscoelasticity. Arch Rational Mech Anal 138:1–35
153. Fabrizio M, Morro A (1992) Mathematical problems in linear viscoelasticity. Society for Industrial and Applied Mathematics, Philadelphia
154. Golden JM (2005) A proposal concerning the physical rate of dissipation in materials with memory. Q Appl Math 63:117–155
155. Golden JM (2001) Consequences of non-uniqueness in the free energy of materials with memory. Int J Eng Sci 39:53–70
156. Gurtin ME, Hrusa WJ (1988) On energies for nonlinear viscoelastic materials of single-integral type. Q Appl Math 46:381–392
157. Höfer P, Lion A (2009) Modelling of frequency- and amplitude-dependent material properties of filler-reinforced rubber. J Mech Phys Solids 57:500–520
158. Adolfsson K, Enelund M, Olsson P (2005) On the fractional order model of viscoelasticity. Mech Time-Depend Mater 9:15–34
159. Hanyga A (2007) Fractional-order relaxation laws in non-linear viscoelasticity. Continuum Mech Thermodyn 19:25–36
160. Hanyga A, Seredynska M (2007) Multiple-integral viscoelastic constitutive equations. Int J Non Linear Mech 42:722–732
161. Pipkin AC, Rogers TG (1968) A non-linear integral representation for viscoelastic behaviour. J Mech Phys Solids 16:59–72
162. Hassani S, Alaoui Soulimani A, Ehrlacher A (1998) A nonlinear viscoelastic model: the pseudo-linear model. Eur J Mech A Solids 17:567–598
163. Lockett F (1972) Nonlinear viscoelastic solids. Academic, Boston
164. Fung YC (1972) Stress-strain-history relations of soft tissues in simple elongation. In: Fung NPYC, Anliker M (eds) Biomechanics: its foundations and objectives. Prentice Hall, Englewood Cliffs, pp 181–208
165. Fosdick RL, Yu JH (1998) Thermodynamics, stability and non-linear oscillations of viscoelastic solids. 2. History type solids. Int J Non-Linear Mech 33:165–188
166. Bernstein B, Kearsley EA, Zapas LJ (1963) A study of stress relaxation with finite strain. J Rheol 7:391–410
167. Hanyga A (2005) Viscous dissipation and completely monotonic relaxation moduli. Rheol Acta 44:614–621
168. Adolfsson K, Enelund M (2003) Fractional derivative viscoelasticity at large deformations. Nonlinear Dyn 33:301–321
169. Gil-Negrete N, Vinolas J, Kari L (2009) A nonlinear rubber material model combining fractional order viscoelasticity and amplitude dependent effects. J Appl Mech 76:011009
170. Rogers L (1983) Operators and fractional derivatives for viscoelastic constitutive equations. J Rheol 27:351–372
171. Metzler R, Nonnenmacher T (2003) Fractional relaxation processes and fractional rheological models for the description of a class of viscoelastic materials. Int J Plast 19:941–959
172. Fosdick RL, Yu JH (1996) Thermodynamics, stability and non-linear oscillations of viscoelastic solids.1. Differential type solids of second grade. Int J Non-Linear Mech 31:495–516
173. Hibbit D, Karlsson B, Sorensen P (2007) ABAQUS/theory manual, 6th edn. Hibbitt, Karlsson & Sorensen, Inc., Rhode Island
174. Shim VPW, Yang LM, Lim CT, Law PH (2004) A visco-hyperelastic constitutive model to characterize both tensile and compressive behavior of rubber. J Appl Polym Sci 92:523–531
175. Hallquist J (1998) LS-DYNA theoretical manual. Livermore Software Technology Corporation

176. Yang LM, Shim VPW, Lim CT (2000) A visco-hyperelastic approach to modelling the constitutive behaviour of rubber. Int J Impact Eng 24:545–560
177. Ciambella J, Destrade M, Ogden RW (2009) On the ABAQUS FEA model of finite viscoelasticity. Rubber Chem Technol 82:184–193
178. Biot MA (1954) Theory of Stress-Strain Relations in Anisotropic Viscoelasticity and Relaxation Phenomena. J Appl Phys 25:1385–1391
179. Tvedt B (2008) Quasilinear equations for viscoelasticity of strain-rate type. Arch Rational Mech Anal 189:237–281
180. Destrade M, Saccomandi G (2004) Finite-amplitude inhomogeneous waves in Mooney-Rivlin viscoelastic solids. Wave Motion 40:251–262
181. Destrade M, Ogden R, Saccomandi G (2009) Small amplitude waves and stability for a pre-stressed viscoelastic solid. Z Angew Math Phys 60:511–528
182. Hayes MA, Saccomandi G (2000) Finite amplitude transverse waves in special incompressible viscoelastic solids. J Elast 59:213–225
183. Beatty MF, Zhou Z (1991) Universal motions for a class of viscoelastic materials of differential type. Continuum Mech Thermodyn 3:169–191
184. Landau L, Lifshitz E (1986) Theory of elasticity: volume 7. Butterworth-Heinemann, Oxford
185. Dai F, Rajagopal K, Wineman A (1992) Non-uniform extension of a non-linear viscoelastic slab. Int J Solids Struct 29:911–930
186. Johnson G, Livesay G, Woo SY, Rajagopal K (1996) A single integral finite strain viscoelastic model of ligaments and tendons. J Biomech Eng 118:221–226
187. Rajagopal K, Wineman A (2008) A quasi-correspondence principle for Quasi-Linear viscoelastic solids. Mech Time-Depend Mater 12:1–14
188. Destrade M, Saccomandi G (2006) Solitary and compactlike shear waves in the bulk of solids. Phys Rev E 73:065604
189. Salvatori MC, Sanchini G (2005) Finite amplitude transverse waves in materials with memory. Int J Eng Sci 43:290–303
190. Rudin W (1976) Principles of mathematical analysis. McGraw-Hill, New York
191. Meera AP, Said S, Grohens Y, Thomas S (2009) Nonlinear viscoelastic behavior of silica-filled natural rubber nanocomposites. J Phys Chem C 113(42):17997–18002
192. Wu JD, Liechti KM (2000) Multiaxial and time dependent behavior of a filled rubber. Mech Time-Depend Mater 4:293–331

A Multiparametric Approach of the Nonlinear Viscoelasticity of Rubber Materials

Jean L. Leblanc

Abstract Rubber materials are viscoelastic systems whose properties, broadly speaking, are complex functions of time, strain, strain rate, temperature (and composition if they are inhomogeneous). Material functions are mathematical relationships that intend to describe the behavior of a material, either a solid or a liquid, when submitted to a range of strains or strain rates, with obviously temperature effects. For viscoelastic materials, such as rubber gum and compounds, these functions obviously encompass both the linear and the nonlinear domains. Providing material functions are considered in their full complexity, in other terms with respect to a multiparametric approach, they provide information about the processing behavior and the mechanical properties of rubber systems.

For pure, unfilled, homogeneous polymers and within the asymptotic limit of linear viscoelasticity, there are theoretical interconnections between the various material functions. In a few cases, relationships between linear viscoelastic material functions and fundamental polymer characteristics have also been established. For complex polymer systems, such as filled rubber compounds, heterogeneity and nonlinear viscoelastic behavior are the rule, all the more if strain amplitude and/or strain rate correspond to the processing range. Unfortunately, a comprehensive theory for nonlinear viscoelasticity is not yet available, and of course heterogeneity and interactions between phases add to complexity so that, in what rubber science and technology are concerned, the experimental approach of material functions and their pragmatical connection with processing aspects remain mandatory. How some material functions may be evaluated and analyzed with respect to processing behavior is discussed in this chapter.

Keywords Material functions • Mechanical properties • Model • Nonlinear viscoelasticity • Processing

J.L. Leblanc (✉)
UPMC – Paris Sorbonne Universités, Polymer Rheology and Processing, 60, rue Auber, Vitry-sur-Seine, France
e-mail: jleb.bsi@gmail.com

D. Ponnamma, S. Thomas (eds.), *Non-Linear Viscoelasticity of Rubber Composites and Nanocomposites*, Advances in Polymer Science 264, DOI 10.1007/978-3-319-08702-3_9

Abbreviations

aPP	Atactic polypropylene
DMA	Dynamic mechanical analyzers
EPDM	Ethylene-Propylene-Diene rubber
FS	Frequency sweep
IPPD	N-isopropyl-N′-phenyl-p-phenylene diamine
MWD	Molecular Weight Distribution
RPA	Rubber Process Analyzer
SBR	Styrene-butadiene rubber
SS	Strain sweep
TMQ	Trimethylquinoline, polymerized
VBA	Visual basic for applications
WLF	William-Landel-Ferry

1 Introduction

As sketched out in Fig. 1, material functions are mathematical relationships between stress, strain or rate of strain tensors that intend to describe the behavior of a solid or a liquid when submitted to a range of strains or strain rates. With polymer materials, temperature effects must also be taken into consideration. Polymer systems, whose behavior is far to correspond to either the ideal elastic solid or the ideal viscous fluid, fall in the category of so-called viscoelastic materials whose properties, broadly speaking, are complex functions of time, strain, strain rate, temperature (and composition if they are inhomogeneous). By definition, a modulus is the ratio of the stress tensor over the strain tensor, whatever is the mode of deformation, for instance shear, extensional or compressive. The mode of deformation defines the non-zero components of both the stress and strain tensors and because, with polymers, modulus varies with time and temperature, the concept of modulus functions was appropriately introduced. Conversely a viscosity is the ratio of the stress tensor over the rate of strain tensor, and again non-zero components of the tensors define the type of flow, either shear or extensional. Modulus and viscosity functions play a key role in polymer science and technology. The time, temperature and composition dependencies of modulus and viscosity functions are particularly important for polymer systems because, in the former case they allow understanding how a given polymer behaves over a large time span, and in the latter case, they position the material with respect to both its usage and processing windows.

Within the asymptotic limit of infinitesimally small strain (and/or strain rate), modulus and viscosity functions of polymers are nowadays understood with respect to the theory of linear viscoelasticity [1] and, in principle, conversion between the various functions is possible, whatever is the mode of deformation [2]. The current practice of linear viscoelastic concepts reveals however that such conversions are

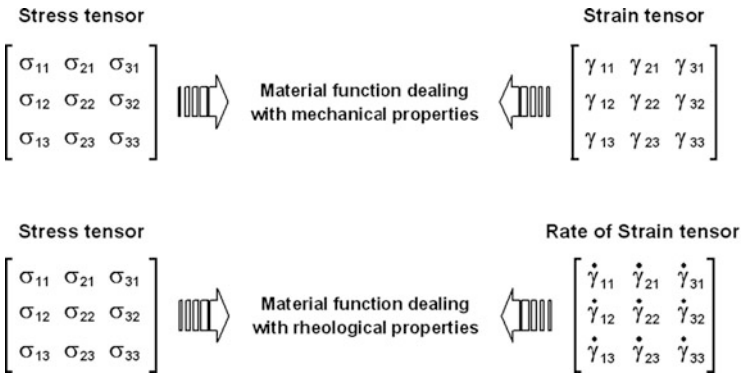

Fig. 1 Material functions for mechanical and rheological properties (isothermal conditions)

readily possible only in the case of simple macromolecular systems with relatively narrow molecular weight distribution (MWD), for instance linear homopolymers as well as certain polymers having simple, well defined architecture, for instance H-type or pom-pom polymers, at the expense however of sometimes quite complex calculations. Reasons are well known: on one side "real" polymers such as those used worldwide by millions tons/year in the industry are rarely conform to ideal macromolecular models and, on the other side, relatively large MWD polymers are preferred by engineers because of their easier processing. Despite undeniable progresses achieved over the last decades in controlling (certain) polymerization processes, synthetic materials still exhibit a number of architectural "accidents" that make the application of the linear viscoelastic theory somewhat limited, not to mention the side effects of residues from the synthesis (e.g. catalyst residues, soaps and other emulsifying agents) as well as the sometimes significant role of purposely added ingredients (e.g. oils, waxes, antidegradant,. . .) that, even in small quantities, are known to modify the viscoelastic behavior. The situation is of course worst with polymers of natural origin, with the notable example of Natural Rubber (with worldwide consumption of around 10 millions tons/year) whose true structure is still subject to investigation despite key findings in recent years [3], namely the role of the so-called non-rubber ingredients, i.e. protein residues, phospholipids, etc. In addition, a growing number of macromolecular-based materials nowadays used in the polymer industry are in fact complex polymer systems (with the typical case of filled rubber compounds) that exhibit a strong nonlinear viscoelastic character of internal (or morphological) origin, even at the lowest possible strain in available experimental techniques. Indeed, when submitted to sufficiently large strains, any simple (pure) polymer eventually exhibits non-linear viscoelastic properties; in such case the observed behavior is called **extrinsic** non-linear viscoelasticity, since owing to external factors (i.e. the applied strain). With complex polymer systems, an **intrinsic** nonlinear character superimposes to the non-linearity associated with large strain. This additional response to applied strain has an internal origin, i.e. their morphology. As demonstrated elsewhere [4, 5], harmonic testing

allows to easily distinguish between **extra** (i.e. strain-induced) and **intra** (i.e. morphology-induced) **nonlinear viscoelasticity**.

Despite their invaluable merits, the tools and concepts of the theory of linear viscoelastic must be used with care when addressing complex polymer systems such as rubber compounds. Careful and reproducible measurements of the various material functions remain thus an essential step in the science and industry of "real" polymers. The objectives of this chapter are (1) to review a few material functions for rubber systems, (2) to describe how they can be experimentally assessed and (3) to demonstrate a few mathematically simple but multiparametric models that can successfully account for the measured quantities.

2 A General Approach of Material Functions

Whatever test is performed to investigate the mechanical or the rheological properties of a (polymer) material, one has to measure simultaneously elementary mechanical or physical quantities that can be sorted out in three categories: force, strain (or rate of strain) and temperature. Appropriate combinations of such elementary quantities allow defining mechanical or rheological quantities, for instance the stress (unit: N/m or Pa) and the strain (unit: none or %) in the case of a "mechanical" test, and the stress and the strain rate (unit: s^{-1}) in the case of a "rheometrical" test. Combinations of mechanical or rheological quantities give access to so-called material functions whose variables are any of the mechanical or rheological quantities. Such a concept is easily illustrated in the case of simple shear flow with the shear viscosity function $\eta(\dot{\gamma}, T)$, where $\dot{\gamma}$ is the shear rate and T the temperature and η the ratio of the shear stress over the shear rate.

Material functions must however be considered with respect to the mode of deformation and whether the applied strain is constant or not in time. Two simple modes of deformation can be considered: simple shear and uniaxial extension. When the applied strain (or strain rate) is constant, then one considers steady material functions, e.g. $\eta(\dot{\gamma}, T)$ or $\eta_E(\dot{\varepsilon}, T)$, respectively the shear and extensional viscosity functions. When the strain (purposely) varies with time, the only material functions that can realistically be considered from an experimental point of view are the so-called dynamic functions, e.g. $G^*(\omega, \gamma, T)$ and $\eta^*(\omega, \gamma, T)$ or $E^*(\omega, \gamma, T)$ and $\eta_E^*(\omega, \gamma, T)$ where the complex modulus G* (and its associated complex viscosity η^*) specifically refers to shear deformation, whilst E* and η_E^* stand for tensile deformation. It is worth noting here that shear and tensile dynamic deformations can be applied to "solid" systems with currently available instruments, whilst in the case of "molten" or "fluid" systems, only shear dynamic deformation can practically be experimented. There are indeed experimental and instrumental contingencies that severely limit the study of polymer materials in the conditions of nonlinear viscoelasticity, relevant to processing.

The set of material functions introduced above, i.e.:

$\eta(\dot{\gamma}, T)$;
$\eta_E(\dot{\varepsilon}, T)$;
$G^*(\omega, \gamma, T)$ and $\eta^*(\omega, \gamma, T)$;
$E^*(\omega, \gamma, T)$ and $\eta_E^*(\omega, \gamma, T)$

are obviously complex, exist in multidimensional spaces and, as such, concern only homogeneous systems.

If heterogeneous polymer systems e.g. filled rubber compounds, are considered, then the volume fractions of ingredients further complicate the material functions, which must now be written as (restricted to the case of shear deformation):

$\eta(\dot{\gamma}, T, \Phi)$
$G^*(\omega, \gamma, T, \Phi)$
$\eta^*(\omega, \gamma, T, \Phi)$

where Φ is a parameter describing the system in term of volume fraction. As we will see later, the volume fraction is however not always sufficient in describing heterogeneous materials that exhibit interactions between phases, as it is typically the case with carbon black filled rubber compounds.

With respect to the number of variables, it is fairly obvious that material functions are necessarily nonlinear but, of course, in well-selected asymptotic conditions of one of the parameters, with all the others constant, one may recover a linear behavior. For instance, at constant temperature, the shear viscosity function at vanishing shear rate of a pure, unfilled polymer is the so-called pseudo-Newtonian viscosity, i.e.: $\eta_0 = \lim_{\dot{\gamma}\to 0}\eta(\dot{\gamma})$, and for (infinitesimally) low strain amplitude, the complex modulus function reduces to:

$$G^*(\omega, T) = G'(\omega, T) + i \cdot G''(\omega, T) \tag{1}$$

where G' and G'' are the so-called elastic and viscous moduli.

3 Practically Assessing Material Functions of Rubber Materials

3.1 Shear Viscosity Function

Following Newton (1640), the viscosity is defined as the ratio of the stress over the deformation rate. Whether a shear or a simple extensional flow is considered, one has then the shear or the extensional viscosity, and if such quantities are rate dependent, one deals with shear or extensional viscosity functions. Experimentally,

steady state shear conditions are relatively easy to establish with appropriate instruments in laboratory conditions but steady state extensional conditions require that an initial reference length (of the material) is growing exponentially with time. There are thus inherent complexities in assessing extensional viscosity, whose detailed discussion is outside the scope of this chapter but is found in many textbooks [6, 7]. Practically extensional rheometry is limited to very delicate and tedious laboratory practices, on a limited number of polymer systems.

In order to observe the full shear viscosity function of a pure, homogeneous polymer, several decades of shear rate must be investigated. It follows that several instruments are needed, with commercial devices available only for the low-to-medium shear rate range (i.e. rotational rheometers, cone-plate or parallel disks; 10^{-2} to 10^{1} s^{-1}) and the medium-to-high range (i.e. extrusion rheometers, capillary or slit die; 10^{1} to 10^{3} s^{-1}). The very low shear range, where the so-called pseudo-Newtonian plateau can expectedly be observed, requires laboratory prototype instruments such as the so-called "sandwich" rheometer [8–10] or the sliding cylinder rheometer [11, 12], operated either in creep (i.e. under the action of a dead-weight) or in constant rate mode (through the action of a rate-controlled ram). Figure 2 shows the shear viscosity function of an unfilled SBR1500 compound as measured over 8 decades of shear rate, using several instruments in the author's laboratory. Quite typical for rubber materials, the pseudo-Newtonian plateau or even its occurrence is not yet seen down to 10^{-4} s^{-1}. Similar observations were reported by Toki and White [13] for gum rubbers; with gum SBR1500 namely, no plateau was detected at 10^{-7} s^{-1}. At best a downward curvature was observed that suggests that a zero-shear viscosity might be extrapolated, to be around 8×10^{8} Pa s.

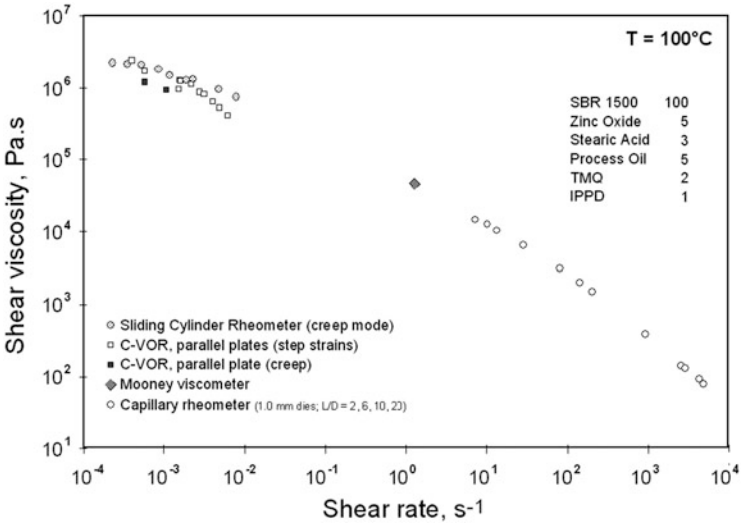

Fig. 2 Shear viscosity function of an unfilled SBR1500 compound as measured at 100 °C with various instruments in the author's laboratory

It thus appears that, in sharp contrast with (some) molten thermoplastic polymers, there is nearly no experimental evidence of a linear viscoelastic region for rubber materials, whatever low is the shear rate range investigated.

3.2 Dynamic Functions

When a pure, homogeneous viscoelastic material is submitted to a harmonic (i.e. cyclic) strain $\gamma(t)$ a stress response $\sigma(t)$ is obtained, which is also harmonic. In the limit of (infinitesimally) small strain, stress and strain are generally simply proportional. In such a case, one experimentally addresses the linear viscoelastic response of the test material. The material must be maintained in an appropriate "testing gap" where a homogeneous strain field is expected to develop (see Fig. 3). If the material is in the *solid state*, a sample of appropriate geometry, e.g. a right parallelepiped or a cylinder, is the testing gap and test instruments are called dynamic mechanical analyzers (DMA). DMA's are commercially available from various manufacturers and, through the use of the appropriate sample holder, various deformation modes are possible, e.g. tensile, three points bending, simple shear, etc. When the material is in the *liquid state*, it must be maintained within a truly speaking testing gap. Whilst simple shear in "sandwich" type fixtures is available with certain DMA's, the most common method is torsional shear between appropriate dies, in which case instruments are called dynamic rheometers. There are essentially two types of torsional dynamic rheometers: open gap instruments (cone-plan and parallel disks) and closed-cavity testers. Like molten

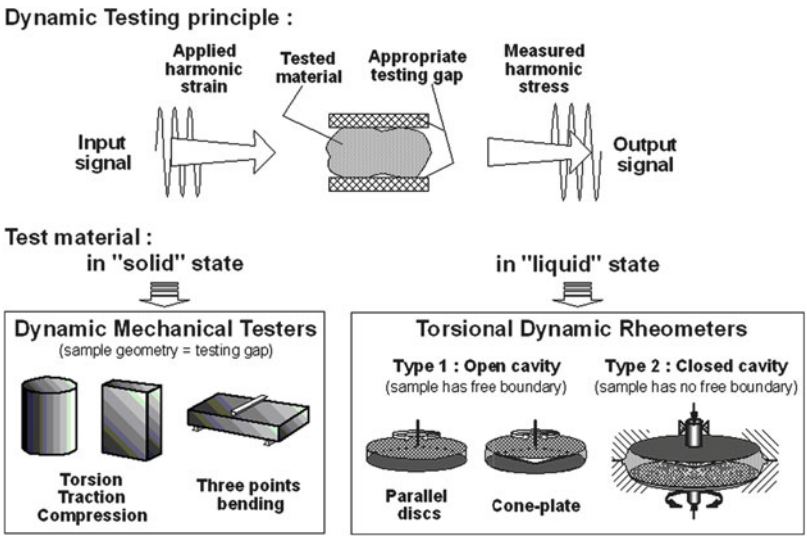

Fig. 3 Principle of dynamic testing of polymer materials

thermoplastics, rubber materials can in principle be tested with both types of instruments, but experience reveals that closed-cavity torsional rheometers are easier to handle and provide more accurate and reproducible results with rubber systems, even simple gum rubbers [14], as will be shown in Sect. 2.2 below.

Whatever are the test techniques, cyclic strains applied to materials correspond to easy and simple mathematical definition, e.g. $\gamma(t) = \gamma_0 \sin(\omega t)$ where γ_0 is the maximum strain amplitude, ω the frequency (rad/s) and t the time (s). In all generality, one expects the stress response to be described through a summation of terms, i.e. $\sigma(t) = \sum_i \sigma_i \sin(\omega t - \delta_i)$ where the δ_i terms allow accounting for an out-of-phase retard of the stress with respect to the applied strain. In the limit of very small strains, such a series is expected to reduce to only the first term when the material is exhibiting a so-called linear viscoelastic response [15]. When higher terms are necessary to (mathematically) describe the actual stress response of the material, the latter is said to be in its nonlinear viscoelastic domain. It has been established either through numerical simulation [16] or through experiments [17], that only odd terms of the summation do contain material's information. Even terms are due either to imperfect boundary conditions or secondary flows in the testing gap, or more simply imperfections in the (mechanically) applied strain.

There are essentially two types of test protocols with dynamic rheometers, depending one want to probe the material in the linear viscoelastic or in the nonlinear viscoelastic domain. Providing the strain amplitude is small enough for no strain-dependency of the (complex) modulus to be observed, then *frequency sweep* (FS) tests document the linear viscoelastic character of the material (at the test temperature). When performing FS tests at several temperatures, results can be treated to build a mastercurve at a reference temperature by making use of the time-temperature superposition principle. *Strain sweep* (SS) tests allow investigating material responses in the whole viscoelastic domain, from the linear to the nonlinear range, depending on the capabilities of the instrument. For instance, with commercially available closed-cavity rheometers operated at frequencies below 0.5 Hz, one can routinely probe materials in the 0.1–1,000 % strain range. Modern rheometers are computer controlled so that, with most commercial instruments, quite complex test protocols can be designed by the user, by combining test sequences in many ways to investigate frequency, strain and temperature ranges. Correctly treating experimental data is consequently the key aspect in obtaining meaningful results, as will be shown below.

4 Experimental Material Functions in Rubber Science

4.1 Material Functions in the Linear Viscoelastic Range

4.1.1 Shear Viscosity

In principle, the shear viscosity function in the linear viscoelastic range reduces to the so-called pseudo-Newtonian shear viscosity, defined as: $\eta_0 = \lim_{\dot{\gamma}\to 0}\eta(\dot{\gamma})$. This quantity is not a function per se but a material property that is directly related to macromolecular characteristics, for instance the molecular weight and its distribution. The only relevant shear viscosity function in the linear domain is thus the temperature dependent $\eta_0(T)$, for which the so-called Arrhenius approach is found generally valid, so that one can write:

$$\eta_0(T) = \eta_0(T_0) \times \exp\left[\frac{Ea}{R}\left(\frac{1}{T} - \frac{1}{T_0}\right)\right] \tag{2}$$

where Ea (J/mol) is the activation energy (of the shear flow process), R the gas constant (8.3145 J/K mol), and T_0 a reference temperature. T and T_0 must conveniently be expressed in Kelvin.

As mentioned above, the Newtonian plateau is (or has been) rarely observed with gum rubbers so that $\eta_0(T)$ must be obtained by extrapolating experimental data towards zero shear rate, by making use of an appropriate model for the shear viscosity function. In the author's experience, a most flexible model is the so-called Carreau-Yasuda equation, i.e. (at a given temperature T):

$$\eta(\dot{\gamma})|_T = \eta_0|_T[1 + |\lambda\dot{\gamma}|^a]^{\frac{n-1}{a}} \tag{3}$$

where $\eta_0|_T$ is the pseudo-Newtonian viscosity (at T), λ a characteristic time of the material, n and a are parameters of the model. It is clear that, in the asymptotic limit $\dot{\gamma} \to 0$ (i.e. the linear viscoelastic domain), the equation yields η_0 (at T) and in the asymptotic limit $\dot{\gamma} \to \infty$ (i.e. the far nonlinear domain), one gets the power law. The reverse of λ corresponds to a shear rate value that can be considered as the "frontier" between the linear and the nonlinear viscoelastic behavior; a loose frontier however if the parameter a is different from 2. Combining Eqs. (2) and (3) yields quite a general model for the $\eta(\dot{\gamma}, T)$ function.

Figure 4 illustrates how the Carreau-Yasuda model meets the shear viscosity data of Fig. 2. A non-linear fitting algorithm (i.e. Marquardt-Levenberg) was used to obtain the parameters given in the inset. As can be seen the fit curve provides a shear viscosity function that corresponds reasonably well with experimental data so that the high shear behavior is asymptotic to a power law and the very low shear behavior corresponds to the pseudo-Newtonian viscosity η_0. The characteristic time λ (56.55 s) can be considered as the reverse of a critical shear rate (i.e. $\frac{1}{\lambda} = \dot{\gamma}_c = 0.0177\ s^{-1}$) that corresponds to the intersection between the high shear power

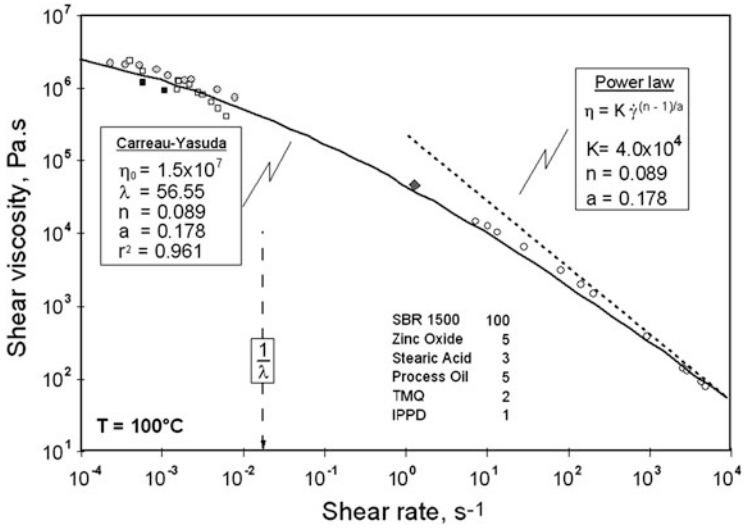

Fig. 4 Shear viscosity function of an unfilled SBR1500 compound at 100 °C as fitted with the Carreau-Yasuda model; see Fig. 1 for symbols' meaning

law behavior and a horizontal line drawn at $\eta_0 = 1.5 \times 10^7$ Pa s. With respect to the curvature of the shear viscosity in the 10^{-3} to 10^{-1} s^{-1} region, it is clear that considering that $\dot{\gamma}_c$ marks the linear-to-nonlinear transition is rather a matter of convention, as for rubber systems there is no sharp change in the shear rate dependency of $\eta(\dot{\gamma})$, in contrast with many observations on molten thermoplastics (see for instance Fig. 6.5.5 in [6]). The only linear viscoelastic data that is so extracted from steady shear experiments data is the pseudo-Newtonian shear viscosity, clearly an extrapolated value, far from the experimental window.

Data in Fig. 4 have been obtained at the expense of several weeks of experimental effort with various instruments, essentially because (1) any rheometer can cover only a limited shear rate range, (2) low shear data requires long periods for steady conditions to be achieved, (3) high shear data can only be obtained with the capillary rheometer whose operation is tedious and time consuming. To repeat the exercise at several temperatures in order to document $\eta_0(T)$ is quite tedious and in practice never or rarely made. A useful approach consists in performing single rate experiments, for instance the Mooney test, at several temperatures so that the (apparent) activation energy at around 1.5 s^{-1} is obtained through Eq. (2). This activation energy value is then assumed to be the same in the linear viscoelastic region.

Figure 5 shows steady shear viscosity data for a carbon black filled high cis-1.4 polybutadiene compound, as obtained using various rheometers. The Carreau-Yasuda equation was used to yield fit parameters given in the lower right inset: the shear viscosity function $\eta = f(\dot{\gamma})$ is drawn in the left graph. As can be seen, a

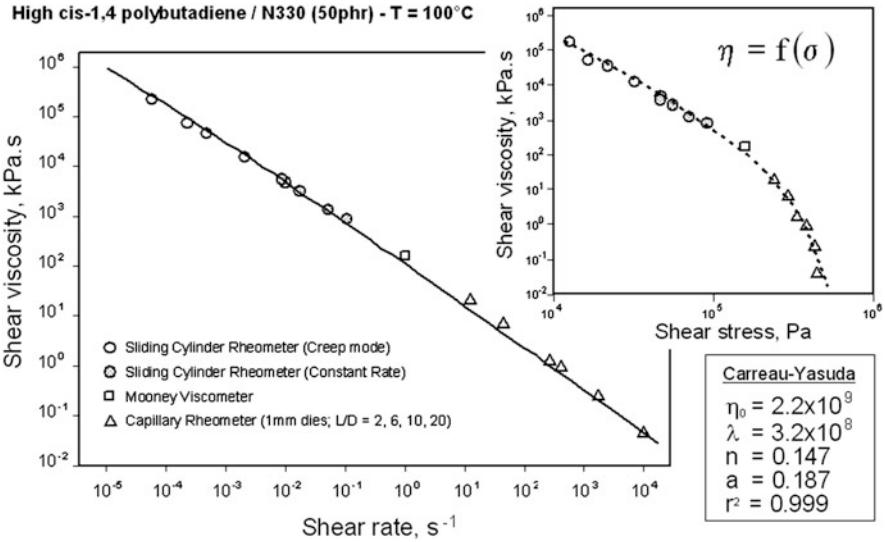

Fig. 5 Experimental data and fitted shear viscosity function of a carbon black filled polybutadiene compound at 100 °C, as obtained in the author's laboratory

nonlinear behavior is observed in the overall experimental shear rate window and consequently the values obtained for both η_0 and λ appear quite unrealistic.

It has long been reported in literature [18, 19] that (carbon black) filled compounds are yield stress materials, i.e., when plotted versus the shear stress, the shear viscosity appears bounded by a critical shear stress σ_c so that below it, no flow occurs (in other words, the viscosity goes to infinity as the shear stress decreases towards σ_c). The right graph in Fig. 4 shows indeed that the shear viscosity $\eta(\sigma)$ increases, as the shear stress decreases, but one would hardly derive a bounding critical shear stress from such data. In other terms, that filled rubber compounds are essentially nonlinear viscoelastic materials is experimentally well demonstrated but that they are yield stress materials might be considered as a controversial subject.

4.1.2 Dynamic Functions

Providing tests are performed at low strain amplitude, small enough for the complex modulus to exhibit no strain dependency, then dynamic testing yields in principle linear viscoelastic functions. This implies that, with an unknown material, a preliminary strain sweep test is performed in order to experimentally detect the maximum strain amplitude for a linear response to be observed [i.e. $G^*|_\omega \neq f(\gamma)$]. As illustrated in Fig. 6 with data from Dick and Pawlowsky [20], such a requirement is practically never met within the available experimental window with filled rubber materials, whose linear region tends to move back to a lower and lower strain range as the filler content increases.

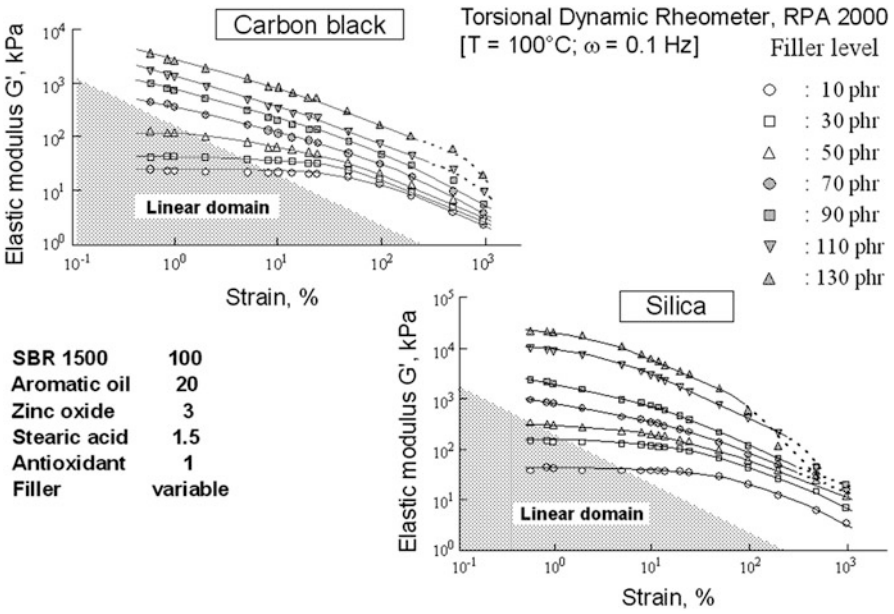

Fig. 6 Strain sweep experiments on carbon-black and silica filled SBR compounds with a closed-cavity torsional dynamic tester; drawn using data from Dick and Pawlowsky [20]

With either pure, unfilled elastomers or slightly filled rubber compounds (typically filler volume fraction lower than 10 %) however, a linear viscoelastic region is observable within the experimental window of most dynamic rheometers providing the strain amplitude does not exceed 10−20 %.

Once the strain amplitude for safe linear testing is known, a technique of choice with modern, automatic rheometers consists in performing frequency sweep tests at several temperatures in order to build a mastercurve at a reference temperature. With closed-cavity rheometers, the same sample can be used for all the procedure because the pressurized sealing of the material in the test cavity minimizes exposure to air, so that thermo-oxidative degradation is practically negligible (for reasonable test duration however; practically up to four hours with well protected rubber materials, in the author's experience). Open gap rheometers are more delicate to use in this respect, not only because thermo-oxidative degradation is frequently observed at the periphery of the testing gap (at least with unfilled gum or when white fillers are used, because discoloration can be seen), but also because when temperature increases material softens and tends to flow out of the testing gap. In such cases, tests at different temperatures must be repeated on several samples (of the same material), a practice that obviously makes the experiments tedious and time consuming. All the results that will be presented below have therefore been obtained with closed-cavity rheometers.

Figure 7 shows G′ and G″ data as measured at constant strain amplitude (1.0 deg; 13.96 %) on a gum Ethylene-Propylene-Diene rubber EPDM 2504 using a closed-

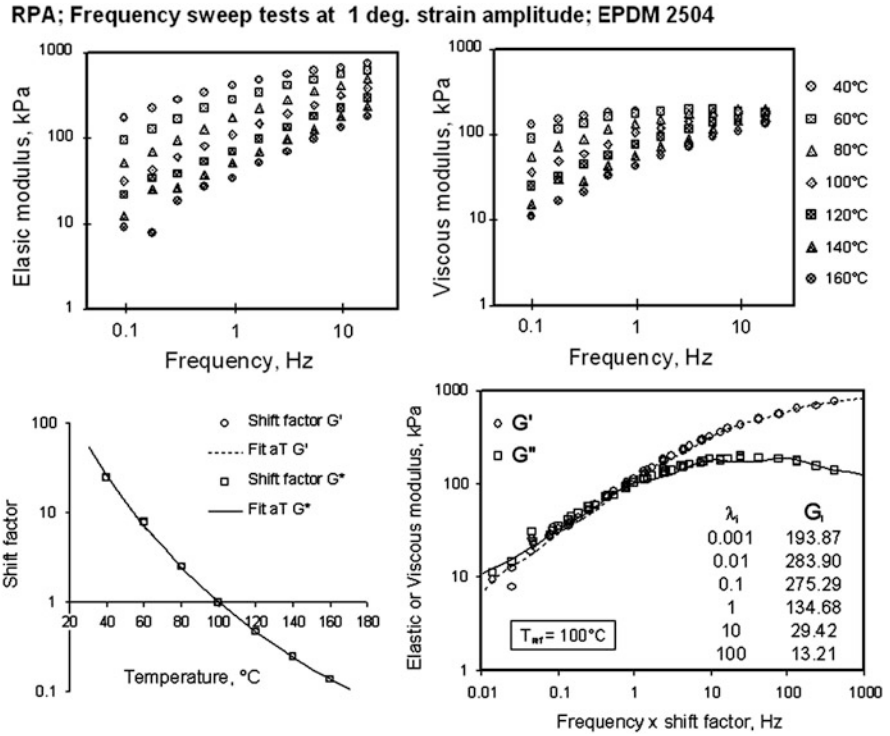

Fig. 7 Frequency sweep experiments on a gum EPDM; G′ and G″ measured data, WLF plots and mastercurves at 100 °C

cavity torsional rheometer. According to a well-established test protocol, two samples were tested along frequency steps (0.1−17 Hz) repeated at several temperatures in the 60−160 °C range. Each sample was tested using five frequency steps, entangled so that by combining the results of both tests 10 applied frequencies in the 0.1−17 Hz were probed. Such a procedure lasts around 2×30 min. Using a VBA macroinstruction program both tests results, as recorded by the built-in system of the RPA, are loaded in an Excel worksheet. A data handling program, written in MathCad®8.0 (MathSoft Inc., now PTC, Needham, MA, USA) then extracts the shift factors for G′, G″ and G* experimental data, calculates the mastercurves at the selected reference temperature and returns all results to the Excel worksheet. The whole data treatment lasts less than 10 seconds per sample.

Shift factors are given in the bottom left graphs with respect to a reference temperature of 100 °C. The curves were drawn using a Williams-Landel-Ferry (i.e. WLF) type equation with the following (fitting) constants: $C_1 = 4.47$ and $C_2 = 250.7$ for G′; $C_1 = 4.27$ and $C_2 = 242.9$ for G″. Differences are marginal and consequently the drawn curves cannot be distinguished from each other. Mastercurves at 100 °C are given in the bottom right graph. It is worth noting that, with respect to the experimental frequency window (i.e. 0.1–17 Hz), the

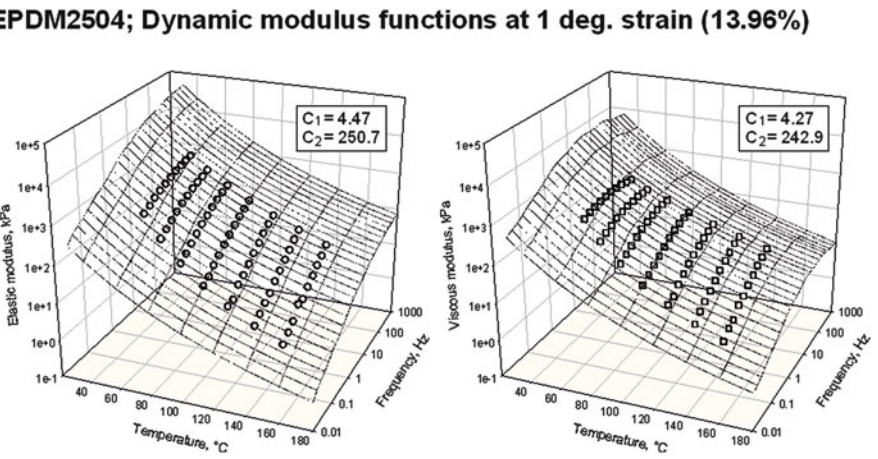

Fig. 8 Linear elastic and viscous modulus functions $G'(\omega, T)$ and $G''(\omega, T)$ of gum EPDM2504, drawn using the λ_i, G_i of a six elements generalized Maxwell model and the respective C1, C2 parameters of a WLF type equation with 100 °C as reference temperature; experimental data from a frequency-temperature sweep protocol at 1 deg. strain amplitude with a closed-cavity torsional harmonic rheometer are displayed for comparison with the calculated maps

time-temperature superposition principle allows the dynamic properties of the materials to be obtained over about five decades of frequency, encompassing thus the terminal zone and a part of the rubbery plateau.

G′ and G″ mastercurves were fitted with a six elements generalized Maxwell model whose characteristic relaxation times were arbitrarily selected in order to correspond with logarithmic decades. As can be seen, fits are excellent within the experimental frequency range. In summary, the overall linear viscoelastic behavior of the material in the 0.01–1,000 Hz frequency range and the 40–160 °C temperature range is known, using only 6 λ_i, G_i couples, 2 WLF coefficients (C_1 and C_2) and standard equations from linear viscoelasticity. Figure 8 illustrates this aspect; using the λ_i, G_i set given in Fig. 6 and the C_1, C_2 parameters respective to G′ and G″, maps of the linear $G'(\omega, T)$ and $G''(\omega, T)$ functions were calculated using the following equations:

$$a_T(T_{ref}) = 10^{\left[\frac{-C_1(T-T_{ref})}{C_2+T-T_{ref}}\right]} \tag{4a}$$

$$G'(\omega, T) = a_T(T_{ref}) * \sum_1^6 \frac{G_i \cdot (\omega \cdot \lambda_i)^2}{1 + (\omega \cdot \lambda_i)^2} \tag{4b}$$

$$G''(\omega, T) = a_T(T_{ref}) * \sum_1^6 \frac{G_i \cdot (\omega \cdot \lambda_i)}{1 + (\omega \cdot \lambda_i)^2} \tag{4c}$$

As seen in Fig. 8, experimental G′ and G″ data well superimpose with the calculated maps (as expected) and further demonstrate that, through only two

times 30 min experiments and the appropriate data handling, a mere exploitation of well established principles of linear viscoelasticity yields a precise characterization of a gum elastomer in the room-to-processing temperature range, and in a wide frequency range. It is worth underlining here that, because of the arbitrary choice of λ_i values (in fact logarithmic frequency decades within the experimental window), the number of parameters needed to drawn a linear dynamic function is remarkably small: 6 G_i and 2 WLF parameters.

Furthermore using data given in Fig. 7 and basic relationships from linear viscoelasticity, additional information can be obtained through easy calculation. Indeed, by definition, the dynamic viscosity is: $\eta'(\omega)\big|_T = \left.\frac{G''(\omega)}{\omega}\right|_T$, so that data points in Fig. 9 are easily obtained and plotted with respect to the product $\omega \times a_T(T_{ref})$. Such data points correspond to the experimental dynamic viscosity function at the reference temperature T_{ref}.

An attractive mathematical model for such a dynamic viscosity function is again the Carreau-Yasuda model, i.e.:

$$\eta'(\omega)\big|_T = \eta_0'\big|_T \times \left[1 + |\lambda\omega|^a\right]^{\frac{n-1}{a}} \tag{5}$$

where $\eta_0'|_T$ is the pseudo-Newtonian dynamic viscosity (at T), λ a characteristic time of the material, n and a are parameters of the model. However, using a nonlinear fitting algorithm to boldly apply this model to experimental data such as given in Fig. 8 does not generally yield satisfactory results in the author's experience, essentially because the pseudo-Newtonian plateau is clearly out of reach of experimental capabilities. Consequently the fitting algorithm yields η_0' values with a very poor degree of confidence. Considering the following relationships from the theory of linear viscoelasticity can solve the problem:

$$\eta_0 = \lim_{\dot{\gamma}\to 0}\eta(\dot{\gamma}) = \lim_{\omega\to 0}\eta'(\omega) \tag{6a}$$

and

$$\eta_0 = \sum_{i=1}^{n} G_i\lambda_i \tag{6b}$$

Indeed η_0' in Eq. (5) can be calculated using Eq. (6b) and the λ_i, G_i set obtained through the frequency-temperature sweep experiments and the use of the generalized Maxwell model. Moreover, a fair estimate of the flow index n can be obtained by fitting a power law to high frequency data. The non-linear fitting problem reduces thus in estimating only two parameters, i.e. λ and a, that are in fact within the experimental window. The dynamic viscosity function drawn in Fig. 8 illustrates the validity of this approach. The function so obtained yields information about the likely behavior of the material when submitted to shear flow, providing

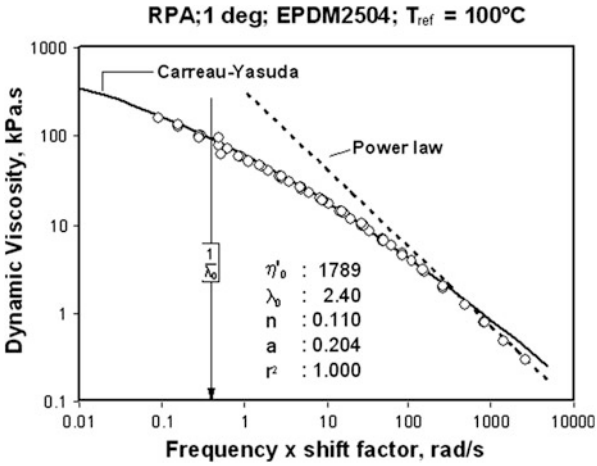

Fig. 9 Dynamic Viscosity function of gum EPDM2504 at 100 °C; authors's experimental data and fitted Carreau-Yasuda model

however that the following Cox-Merz equality [21] applies to the material tested, i.e.:

$$\frac{d\sigma(\dot{\gamma})}{d\dot{\gamma}} = \eta'(\omega) \quad \dot{\gamma} = \omega \tag{7}$$

Let us consider the same approach on a typical filled rubber compound. Figure 9 shows G′ and G″ data as measured at constant strain amplitude (1.0°; 13.96 %) on a carbon black filled SBR1500 compound using a closed-cavity torsional rheometer and a frequency-temperature sweep test protocol. It is worth underlining here that such data could hardly be obtained with an open-gap rheometer because of the stiffness of the material. The shift factors and the corresponding WLF curves are given in the bottom left graphs with respect to the reference temperature of 100 °C. The (fitting) constants are: $C_1 = 2.78$ and $C_2 = 151.7$ for G′; $C_1 = 2.71$ and $C_2 = 147.7$ for G″. Mastercurves at 100 °C are given in the bottom right graph, as well as the λ_i, G_i set corresponding to a 6 elements generalized Maxwell model.

In principle, the time-temperature superposition principle applies only to materials that are said "thermo-rheologically simple" and therefore its use with filled rubber compounds should give poor results. As seen in Fig. 10, this is not the case and, in the author's experience, it is common observation that good mastercurves are obtained with many complex polymer materials through time-temperature superposition, providing experimental data are of quality. In this respect, closed-cavity rheometers offer obvious advantages over open-gap instruments.

The summarizing capabilities of the generalized Maxwell model combined with the WLF approach are illustrated in Fig. 11 in the case of the filled compound. Again well-established principles of linear viscoelasticity yield a precise characterization of filled rubber compounds in the room-to-processing temperature range, and in a wide frequency range, likely encompassing the overall processing. Maps were calculated with Eqs. (4a–c), using the λ_i, G_i set and the C_1, C_2 given in the

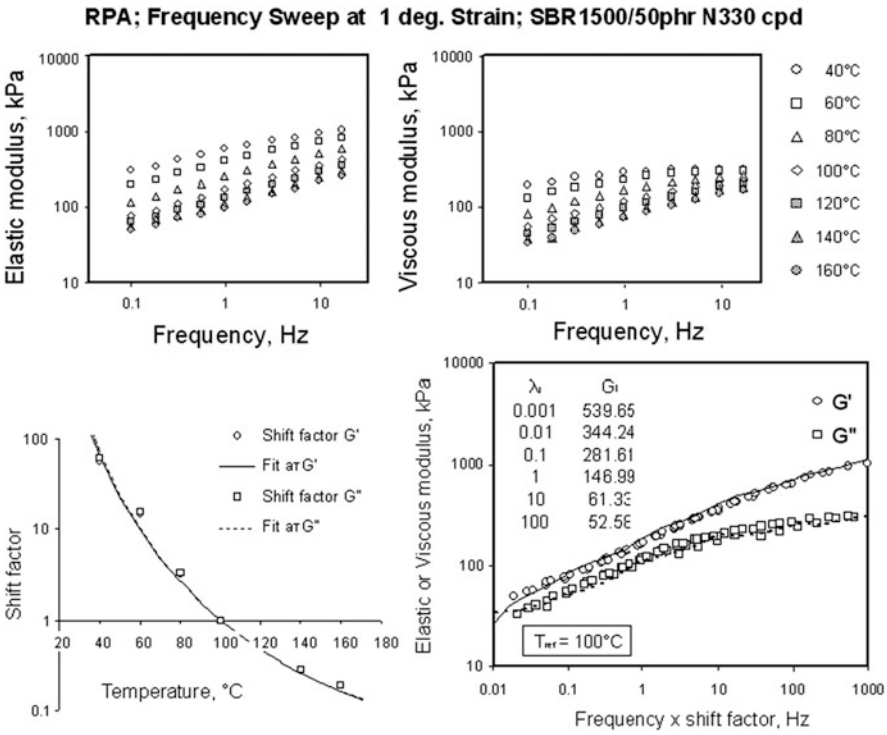

Fig. 10 Frequency sweep experiments on a carbon black filled SBR1500 compound; G′ and G″ measured data, WLF plots and mastercurves at 100 °C; compound formulation (phr) : SBR1500: 100; N330 Carbon Black: 50; Naphtenic oil: 5; ZnO: 5; Stearic acid: 3; TMQ (trimethylquinoline, polymerized): 2; IPPD (N-isopropyl-N′-phenyl-p-phenylene diamine): 1

figure. As already seen in Fig. 10 (right lower graph), $G'(\omega, T)$ and $G''(\omega, T)$ maps illustrate a typical feature of filled rubber compounds: the elastic character dominates all the rheological behavior in the terminal zone, i.e. $G' > G''$, at least in what the linear viscoelasticity is concerned. This observation is in sharp contrast with experiments on thermoplastic melts, whose flow behavior is controlled by the viscous character, i.e. $G'' > G'$.

The dynamic viscosity function at 100 °C is shown in Fig. 12. The Carreau-Yasuda was fitted to experimental data by first calculating the pseudo-Newtonian dynamic viscosity with Eq. (6b) and the set of λ_i, G_i values obtained by averaging the respective sets given in Fig. 11 for G′ and G″. The flow index was derived from high frequency data, so that the nonlinear fitting algorithm concerned only λ and a. As mentioned above, this procedure ensures robust nonlinear fitting with a high degree of confidence in the obtained parameters. Whilst it may be argued that applying a generalized Maxwell model to such a heterogeneous system as a (highly) filled system is not really conform to any theoretical consideration, Figs. 11 and 12 clearly show the practical interest of this approach.

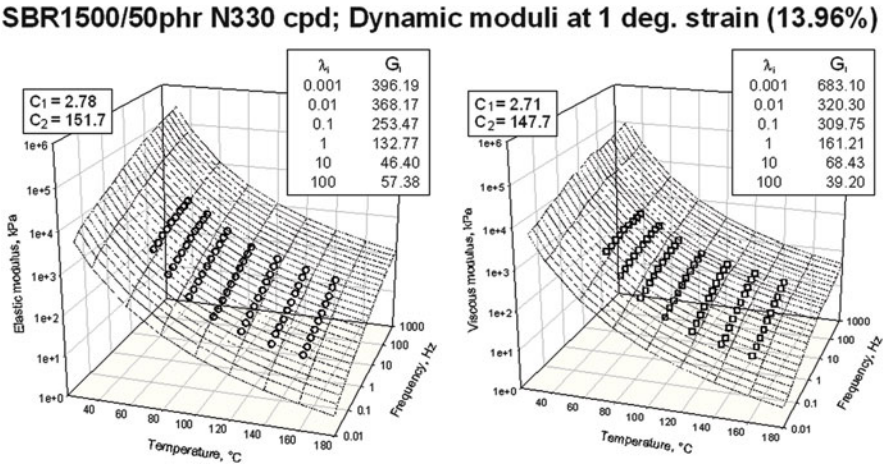

Fig. 11 Linear elastic and viscous modulus functions $G'(\omega, T)$ and $G''(\omega, T)$ of a SBR1500/50phr N330 carbon black compound, drawn using the λ_i, G_i of a six elements generalized Maxwell model and the respective C1, C2 parameters of a WLF-type equation with 100 °C as reference temperature; experimental data from a frequency-temperature sweep protocol at 1 deg. strain amplitude with a closed-cavity torsional harmonic rheometer are plotted in comparison with calculated maps

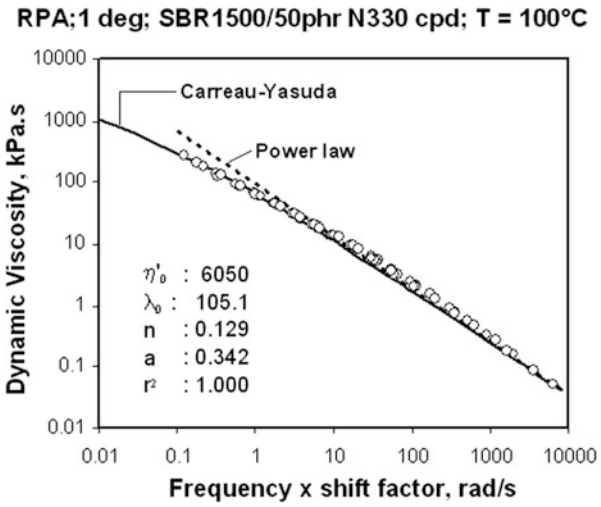

Fig. 12 Dynamic Viscosity function of gum EPDM2504 at 100 °C; author's experimental data and fitted Carreau-Yasuda model

4.2 Material Functions in the Nonlinear Viscoelastic Range

4.2.1 Shear Viscosity Function

The shear thinning behavior, as generally observed with polymer systems, is a typical nonlinear viscoelastic effect, so that by combining the Carreau-Yasuda and the Arrhenius equations a general model for the shear viscosity function can be written as follows:

$$\eta(\dot{\gamma}, T) = \eta_0(T) \times \exp\left[\frac{Ea}{R}\left(\frac{1}{T} - \frac{1}{T_0}\right)\right] \times \left[1 + (\lambda\dot{\gamma})^a\right]^{(n-1)/a} \quad (8)$$

Such an equation implies that it is essentially the pseudo-Newtonian viscosity, which depends on temperature. The validity of this approach is illustrated in Fig. 13 with capillary rheometry data on a gum ethylene-propylene rubber, by using the "reduced viscosity" approach proposed by Vinogradov and Malkin [22]. The left graph in the figure shows the shear viscosity data as obtained at three temperatures with a capillary rheometer (note that a series of 1 mm dies, L/D = 2, 5, 10 were used in order to apply the correction for entrance pressure effects; the Rabinowitch correction for the non-Newtonian character was also applied). Data were fitted with a Carreau-Yasuda model, whose parameters are given in the inset. The viscosity measured at the three temperatures was divided by the pseudo-Newtonian viscosity and plotted versus the reduced shear rate, i.e. the shear rate multiplied by $\eta_0(T)$. As can be seen all the data merge on a single curve that plateaus out as the reduced shear rate goes to zero.

Capillary rheometer experiments are tedious and time consuming. For instance, in the author's experience, a skilled operator has to work half-a-day to generate the shear viscosity function at one temperature, within the typical 10–10,000 s^{-1} shear rate range. The interest of Eq. (8) is immediately obvious since, from the measured

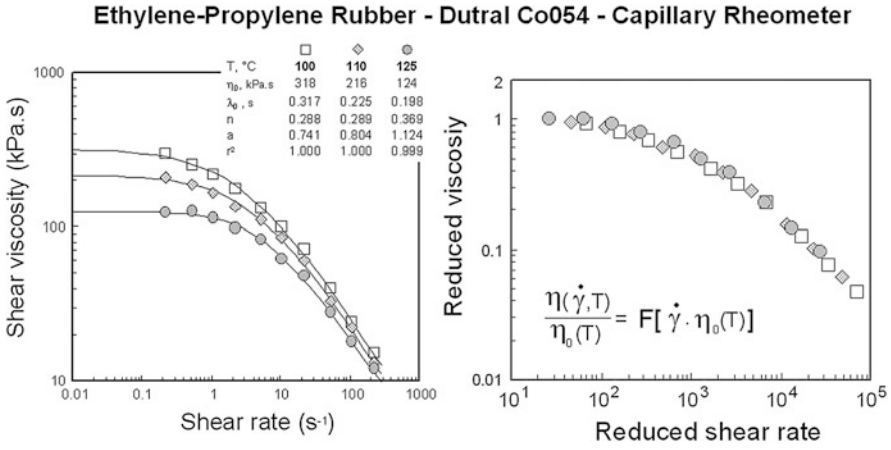

Fig. 13 Shear viscosity function of a gum Ethylene-Propylene rubber as measured at three temperatures with a capillary rheometer (author's unpublished data)

shear viscosity curve at a reference temperature and the knowledge of the activation energy Ea, the shear viscosity function at other temperatures can easily be calculated. As mentioned above, apparent activation energy data can be obtained by repeating a single rate viscosity test at several temperatures and by treating the results with the Arrhenius equation.

4.2.2 Dynamic Functions

Strain sweep tests with torsional dynamic rheometers are quite convenient to assess the nonlinear viscoelastic behavior of polymer materials, providing however that a sufficiently large strain range is investigated, without significance changes in boundary conditions. Such a requirement severely limits the interest of open-gap rheometers when compared with closed-cavity instruments. Indeed practical experience shows that, even with relatively simple material, for instance gum elastomers, the maximum strain range that can be tested with the former rarely exceeds 50 % strain. Figure 14 compare measurements made with an open-gap

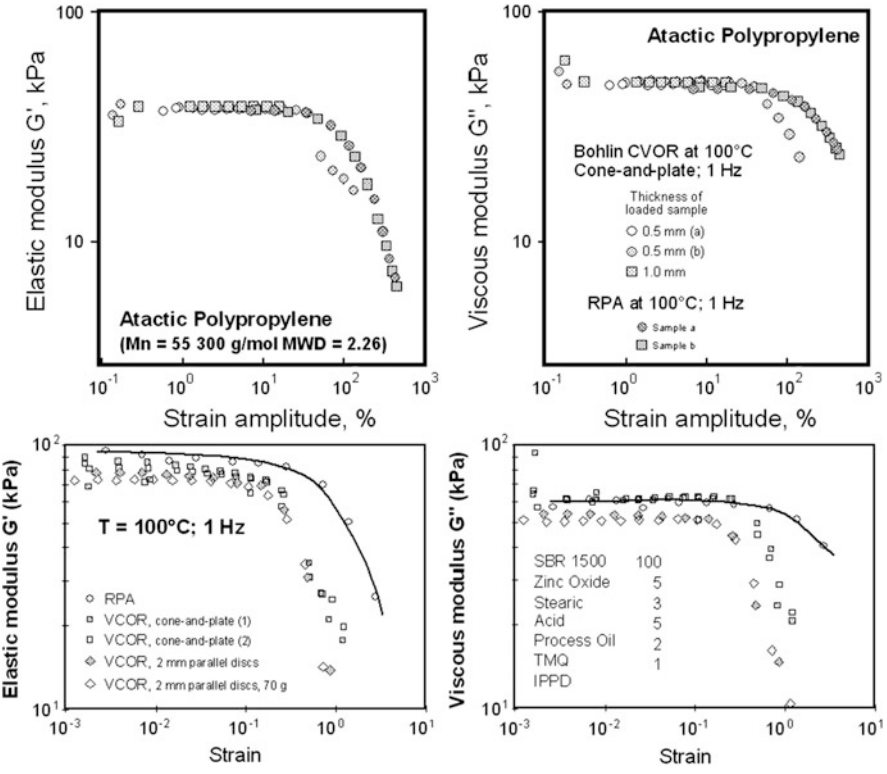

Fig. 14 Strain sweep tests on a pure atactic polypropylene and an unfilled styrene-butadiene rubber compound using either an open-gap (VCOR) or a closed-cavity (RPA) torsional dynamic rheometer (author's experimental data)

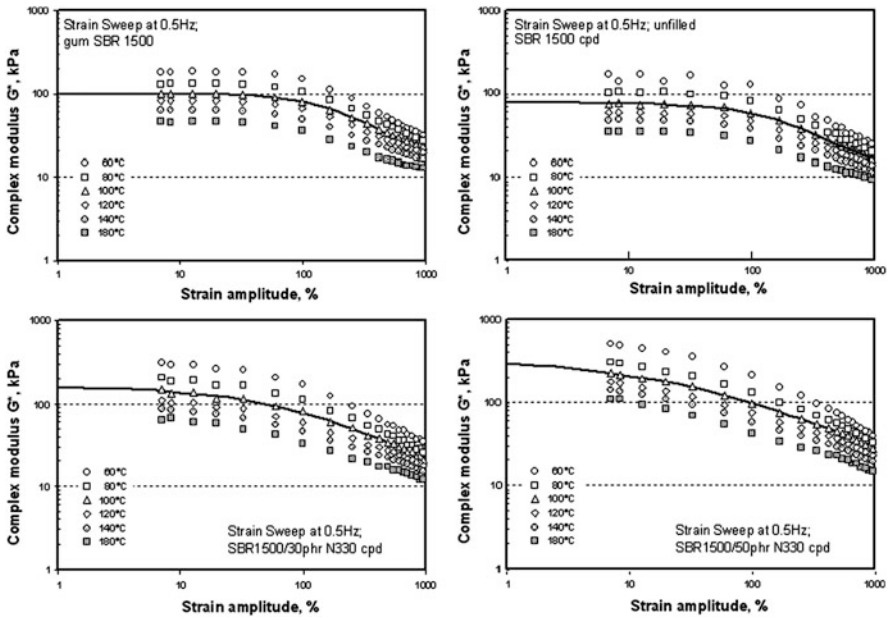

Fig. 15 Strain sweep tests on various SBR1500 based materials; gum SBR is a sample cut from the bale; compounds were prepared in a Haake mixer with Banbury rotors according to the following formulation (phr): SBR1500: 100; N330 Carbon Black: 0, 30 or 50; Naphtenic Oil: 5; Zinc oxide: 5; Stearic acid: 3; TMQ (trimethylquinoline, polymerized): 2; IPPD (N-isopropyl-N′-phenyl-p-phenylene diamine): 1

(VCOR-Bohlin) and a closed-cavity (RPA-Alpha Technology) rheometers. The upper graphs show elastic and viscous moduli as measured during strain sweep experiments on a pure atactic polypropylene (aPP) sample, whilst the lower graphs display results obtained on an unfilled rubber compound. As can be seen, with aPP both rheometers yield comparable G′ and G″ results in the linear viscoelastic region but, whilst the closed-cavity instrument gives quite reproducible results in the nonlinear region, results with the open-gap tester are doubtful above around 30 % strain, likely due to poor boundary conditions. When a (unfilled) compound is tested, results with the open-gap rheometer appear to suffer from an excessive experimental scatter when either different test geometries are used (i.e., cone-plate and parallel discs) or when tests are repeated with the same geometry. In contrast, a smooth variation from the linear to the nonlinear region is observed with the closed-cavity tester. Similar observations were reported on a series of gum Natural Rubber grades [14] and, in the author's experience with open-gap rheometers, it is practically impossible to test highly filled rubber compounds in the nonlinear range, because their high stiffness makes hardly possible a reproducible loading of the material in the testing gap.

With a closed-cavity dynamic torsional rheometer, typical nonlinear viscoelastic experiments are Strain Sweep (SS) tests in the widest strain range at fixed frequency and temperature. Figure 15 shows complex modulus vs. strain curves as measured

in the room-to-curing temperature range (i.e. 60 to 180 °C) on several SBR 1500 based materials using a RPA®2000 (Alpha Technologies). As can be seen the gum rubber and the no black compound (upper graphs) exhibit a linear viscoelastic behavior (i.e., flat G* plateau) up to about 20–30 % strain, then a typical strain thinning behavior that marks the nonlinear response. The filled compounds (lower graphs) do not show any linear behavior within the experimental window and the higher the carbon black loading the severer the nonlinearity.

For a number of rubber systems (gums and compounds) it has been shown [14, 23, 24] that, at constant frequency and temperature, the (complex) modulus variation with strain amplitude is well modeled with the following relationship:

$$G^*(\gamma) = G_f^* + \left[\frac{G_0^* - G_f^*}{1 + \left(\frac{\gamma}{\gamma_{md}}\right)^B}\right] \quad \text{or} \quad G*(\gamma) = \frac{G_0^* + G_f^* \times \left(\frac{\gamma}{\gamma_{md}}\right)^B}{1 + \left(\frac{\gamma}{\gamma_{md}}\right)^B} \tag{9}$$

where γ is the set strain amplitude (%), G_0^* the modulus in the linear region, G_f^* the final modulus, γ_{md} the strain for reaching the mid-modulus value, i.e. $(G_0^* + G_f^*)/2$, and B a parameter related to the strain sensitivity of the material.

Equation (9) has an empirical origin but a theoretical foundation can be proposed as follows. Indeed, quite a common assumption in many approaches of nonlinear viscoelasticity consists in considering time-strain separability (or factorability). Such an assumption readily means that the nonlinear relaxation modulus function $G(t, \gamma)$ can be separated into a time-dependent and a strain-dependent contributions, so that:

$$G(t, \gamma) = G(t) \times h(\gamma) \tag{10}$$

where $h(\gamma)$ is the so-called "damping function". Various mathematical forms (see [25] for a recent review on damping functions) have been proposed for $h(\gamma)$, e.g., in shear flow $h(\gamma) = A \cdot \gamma^{-2}$ (Doi-Edward prediction [26]; see also [27]), $h(\gamma) = B \cdot \exp(-C \cdot \gamma), h(\gamma) = \frac{1}{1+D\cdot\gamma^2}$, etc., to mention a few of the simples ones, where A, B, C and D are parameters. All these mathematical forms correspond to decaying curves and the last one is particularly interesting because if D = A, the damping function at sufficiently high strain corresponds exactly to the Doi-Edwards prediction. Let us now rewrite this equation in the following form:

$$h(\gamma) = \frac{1}{1 + \left(\frac{\gamma}{\sqrt{\gamma_c}}\right)^2} \tag{11}$$

so that the adjustable parameter appears as a critical strain that obviously corresponds to the intersection between a horizontal line $\log h(\gamma) = 1$ and the high strain asymptote, i.e., $\lim_{\gamma\to\infty}(\gamma_c \cdot \gamma^{-2})$. A simpler but similar form of this equation can be written as:

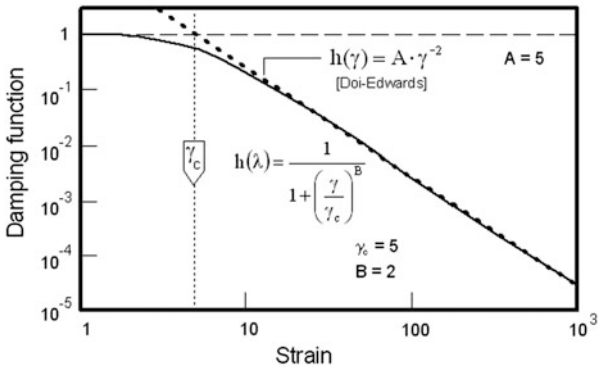

Fig. 16 Damping function according to Eq. (12), compared with Doi-Edwards' proposal

$$h(\gamma) = \frac{1}{1 + \left(\frac{\gamma}{\gamma_c}\right)^B} \tag{12}$$

with an adjustable parameter B, would one want to be unlinked to the Doi-Edwards prediction (see Fig. 16). Consequently, when applying the time-strain separability concept to (complex) dynamic modulus, i.e., $G^*(\gamma)|_{\omega,T} = G^*{}_0|_{\omega,T} \cdot h(\gamma)$, and expressing the damping function with the equation above, one obtains immediately Eq. (9) above if one considers that there is a residual modulus at infinite strain.

The curves drawn in Fig. 15 correspond to Eq. (9), as fitted to experimental data at 100 °C. Similar curves are drawn for test data at other temperatures using fit parameters given in Table 1.

In Eq. (9), G_0^* is the modulus in the linear region; a readily observed quantity with the gum and the no-black compound, and an extrapolated one with filled compounds. A close examination of G_0^* values in Table 1 reveals a temperature dependency that seems to correspond to the Arrhenius equation. As shown in Fig. 17, compounding effects are however obvious: a simple downward shift versus the gum rubber in the case of the unfilled compound (likely due to mixing effects); an upward shift and a change of slope with filled compounds. In the 60–180 °C range, the carbon black is of course not affected by temperature, which means that essentially the rubber matrix is temperature sensitive. In Fig. 17, the slope reflects the activation energy, so that the change of slope clearly demonstrates that high carbon black loadings do modify the viscoelastic response of compounds, likely through specific rubber–filler interactions as thoroughly discussed by the author in a recent paper [28].

In the simple cases of the gum and the unfilled compounds, the overall complex modulus function at constant frequency, i.e. $G^*(\gamma, T)|_\omega$ is easily obtained by considering only the strain sensitivity at a reference temperature (let's say 60 °C) through parameters G_0^*, G_f^*, γ_{md} and B at that temperature and the activation energy. Figure 18 compares experimental results and modeled $G^*(\gamma, T)|_\omega$ in the cases of the gum SBR 1500 and the unfilled compound using parameters given in Table 2. Note that activation energy values were optimized in order to have the best correlation

Table 1 Strain sweep tests experiments on SBR based materials

SBR1500 gum						
Temp., °C	60	80	100	120	140	180
G_0^*, kPa	185.0	131.6	100.4	82.2	64.0	46.4
G_f^*, kPa	21.6	19.3	16.8	15.2	13.5	11.6
γ_{md}, %	199.4	208.9	201.9	193.3	180.0	163.3
B	1.692	1.644	1.585	1.587	1.597	1.732
r^2	0.9999	0.9998	0.9999	0.9998	0.9999	0.9998
SBR1500 No Black cpd						
Temp., °C :	60	80	100	120	140	180
G_0^*, kPa	191.60	108.80	79.82	62.92	50.30	36.84
G_f^*, kPa	17.0	12.2	12.1	11.2	9.6	9.0
γ_{md}, %	154.3	201.5	193.9	185.4	180.7	155.8
B	1.507	1.514	1.484	1.509	1.481	1.602
r^2	0.9988	0.9993	0.9993	0.9997	0.9995	0.9996
SBR1500/30phr N330 cpd						
Temp., °C :	60	80	100	120	140	180
G_0^*, kPa	323.4	217.5	159.3	122.0	99.1	75.5
G_f^*, kPa	6.7	−1.5	1.3	3.9	5.0	6.6
γ_{md}, %	99.9	101.1	91.3	81.7	72.9	59.5
B	1.041	0.865	0.808	0.799	0.800	0.852
r^2	0.9992	0.9973	0.9974	0.9989	0.9999	0.9981
SBR1500/50phr N330 cpd						
Temp., °C :	60	80	100	120	140	180
G_0^*, kPa	608.4	408.8	331.7	258.4	232.8	186.8
G_f^*, kPa	−16.2	−13.3	−6.6	0.2	1.0	4.1
γ_{md}, %	47.1	35.3	25.1	23.1	15.2	12.4
B	0.769	0.630	0.588	0.611	0.579	0.617
r^2	0.9999	0.9999	0.9998	0.9998	0.9998	0.9995

coefficients between the modeled maps and the data; correlation coefficients are higher than 0.99 in both cases.

As shown by Figs. 15 and 16 (carbon black) filled compounds exhibit a more complex dependency on strain and temperature essentially because strong interactions develop between the filler and a part of the rubber matrix. An approach of the complex modulus function $G^*(\gamma, T, \Phi)|_\omega$ [where Φ stands for filler volume fraction] of carbon black filled rubber compounds was recently proposed by the author [28] but its detailed discussion is outside the scope of the present chapter. It will only be noted here that an appropriate equation for $G^*(\gamma, T, \Phi)|_\omega$ combines a member that represents the response of the polymer matrix to increasing strain (the so-called polymer component) and a member that describes the response of a rubber-filler network embedded in the matrix (the so-called filler component).

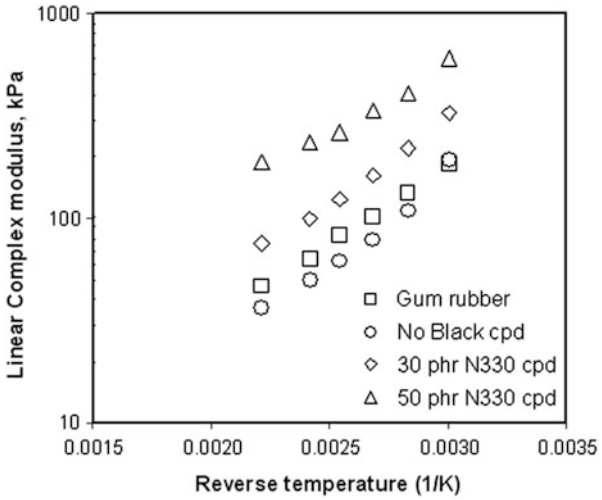

Fig. 17 Arrhenius plots of linear complex modulus G_0^* of SBR1500 based materials (author's experimental data)

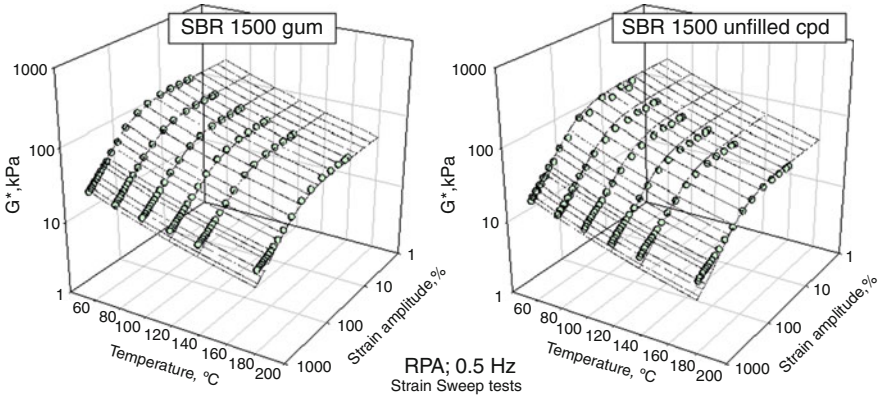

Fig. 18 Comparing modeled (maps) and measured complex modulus (*gray circles*) at 0.5 Hz in the 60–180 °C temperature range and the 1–1,000 % strain amplitude range in the cases of gum SBR1500 and SBR1500 No Black compound; model parameters are given in Table 2

Table 2 Model parameters for 3D maps in Fig. 18

Test material :	SBR1500 gum	SBR 1500 No Black cpd
G*(γ) modeling at 60 °C [Eq. (9)]		
G_0^*, kPa	185.0	191.60
G_f^*, kPa	21.6	17.0
γ_{md}, %	199.4	154.3
B	1.692	1.507
r^2	0.9999	0.9988
Activation energy		
Ea, kJ/mol	15.5	16.8

5 Conclusions

So-called material functions, for instance the shear viscosity and the dynamic (complex, elastic and viscous) moduli functions, play a key role in polymer science and technology. By describing how a material behaves with respect to the strain (or strain rate) and the stress tensors, such complex functions provides information dealing with the processing behavior and the mechanical properties. The mode of deformation defines the non-zero components of both the strain (strain rate) and the stress tensors and, in what polymer systems are concerned the effect of external parameters such as the time and the temperature deserves a special attention. Time effects allow understanding how a system behaves with respect to a large time span; temperature effects concern the usage and processing windows of the material. In the specific case of rubber compounds, the presence of reinforcing fillers further complicates the material functions.

Throughout this chapter it was shown that, correctly assessed, the shear viscosity and the dynamic (complex, elastic and viscous) moduli functions are the necessary material properties that one needs to know with respect to the processing behavior of rubber systems and their mechanical properties after vulcanization. Overall shear viscosity functions, i.e., $\eta(\dot{\gamma}, T)$ and $\eta(\dot{\gamma}, T, \Phi)$ are difficult to obtain through rather tedious and time consuming experiments, with different type of instruments, not all commercially available. By nature however, the shear viscosity function encompasses the linear and the nonlinear viscoelastic behavior. In contrast with many thermoplastic polymers, (filled) rubber systems hardly exhibit a linear behavior within the practical shear rate window of available rheometers. This aspect severely restraints the applicability of considerations based on the theory of linear viscoelasticity, at least in what steady shear is concerned. From a practical point of view however, because most processing operations occur in the nonlinear viscoelastic region, the fact that the asymptotic high shear viscous behavior of rubber material reduces to a simple power law is of course of high interest for engineering purposes.

Multiparametric dynamic functions, i.e. $G^*(\omega, \gamma, T)$ and $\eta^*(\omega, \gamma, T)$; $G^*(\omega, \gamma, T, \Phi)$ and $\eta^*(\omega, \gamma, T, \Phi)$ are relatively easy to obtain with modern dynamic rheometers, providing the correct tests protocols and the appropriate data treatment are used. This was extensively demonstrated in the chapter. It is however worth noting that (filled) rubber materials are generally so stiff that open-gap rheometers do not give reproducible results. Closed-cavity torsional rheometers must be used with such materials and commercially available instruments are so robust that their use can be considered on the factory floor. Depending on the test protocol considered, dynamic rheometers give access either to the linear or to the nonlinear viscoelastic behavior and it was shown in the chapter that tests must be repeated within the room-to-curing temperature range for an overall characterization to be obtained. Frequency–Temperature sweep tests address the linear domain, Strain–Temperature sweep tests concern nonlinear viscoelasticity. In the former case, all the resources of the theory of linear viscoelasticity can be used, namely the possibility to derive the

dynamic viscosity function from dynamic modulus measurement. In the latter case, correctly interpreting results is still an active research subject but relatively simple modeling approaches can be used to offer in a glance an overall view of the viscoelastic properties of interest for processing and applications.

References

1. Tschoegl NW (1989) The phenomenological theory of linear viscoelastic behavior. Springer, Berlin. ISBN 3-540619173-9
2. Ferry JD (1980) Viscoelastic properties of polymers, 3rd ed.. Wiley, New York. ISBN 0-471-04894-1
3. Tanaka Y (2001) Structural characterization of natural polyisoprenes: solve the mystery of Natural Rubber based on structural study. Rubb Chem Technol 74:355–375
4. Leblanc JL (2004) Dynamic testing of intrinsically nonlinear viscoelastic materials – D.I.K., Kautschuk-Herbst-Kolloquium 2004 – Hannover, November 11–13, 2004 – Proceedings, pp 19−29
5. Leblanc JL (2008) Large amplitude oscillatory shear experiments to investigate the nonlinear viscoelastic properties of highly loaded carbon black rubber compounds without curatives. J Appl Polym Sci 109:1271–1293
6. Macosko CW (1994) Rheology: Principles, measurements and applications. VCH Publishers, Inc., New York. ISBN 1-56081-579-5
7. Collyer AA. In Clegg DW (Ed) (1998) Rheological measurement, 2nd ed. Chapman & Hall, London. ISBN 0 412 720302 2
8. Middleman S (1969) Transient response of an elastomer to large shearing and stretching seformations. Trans Soc Rheol 13:123–139
9. Furuta I, Lobe VM, White JL (1976) Experimental study of the rheological properties of butadiene-styrene gum elastomers and compounds. J Non-Newtonian Fluid Mech 1:207–222
10. Goldstein C (1974) Transient and steady shear behavior of SBR polymers. Trans Soc Rheol 18:357–369
11. Barrès C, Leblanc JL (2000) Recent developments in shear rheometry of uncured rubber compounds. I. Design, construction and validation of a sliding cylinder rheometer. Polym Testing 19:177–191
12. Barrès C, Leblanc JL, Guilet S (2001) Recent developments in shear rheometry of uncured rubber compounds. I. Use of the sliding cylinder rheometer to probe sample anisotropy. Polym Testing 20:329–338
13. Toki S, White JL (1982) Rheological and solid wall boundary condition characterization of unvulcanized elastomers and their compounds. J Appl Polym Sci 27:3171–3184
14. Leblanc JL (2007) Non-linear viscoelastic characterization of natural rubber gum through large amplitude harmonic experiments. J Rubb Res 10(2):63–88
15. Giacomin AJ, Dealy JM (1998) Using large-amplitude oscillatory shear, Chapter 11, 327–356 (1998). In: Collyer AA, Clegg DW (eds) Rheological measurements, 2nd edn. Kluwer Academic Publishers, Dordrecht, Netherlands
16. Atalik K, Keunings R (2004) On the occurrence of even harmonics in the shear response of viscoelastic fluids in large amplitude oscillatory shear. J Non-Newtonian Fluid Mech 122:107–116
17. Klein OC, Spiess HW, Calin A, Balan C, Wilhelm M (2007) Separation of the nonlinear oscillatory response into a superposition of linear, strain hardening, strain softening, and wall slip responses. Macromolecules 40:4250–4259
18. Montes S, White JL (1982) A comparative rheological investigation of natural and synthetic cis-1,4 polyisoprenes and their Carbon Black compounds. Rubb Chem Technol 55:1354–1369

19. Montes S, White JL, Nakajima N (1988) Rheological behavior of rubber Carbon Black compounds in various shear flow histories. J. Non-Newtonian Fluid Mech 28:183–212
20. Dick JS, Pawlowski H (1996) Applications of the rubber process analyzer in characterizing the effects of silica on uncured and cured compound properties. ACS, Rubb. Div. Mtg, Montreal, Canada (May 4-8 -paper 34)
21. Cox WP, Merz EH (1958) Correlation of dynamic and steady flow viscosities. J Polym Sci 28 (118):619–622
22. Vinogradov GV, Ya Malkin A (1964) Temperature-independent viscosity characteristics of polymer systems. J Polym Sci A 2(5):2357–2372
23. Leblanc JL (2010) Non-linear viscoelasticity of (unvulcanized) natural rubber, derived materials and compounds through large amplitude oscillatory strain (LAOS) testing. Rubb Chem Technol 83:65–96
24. Leblanc JL, Putman M, Pianhanuruk E (2011) A thorough study on the relationships between dispersion quality and viscoelastic properties in carbon black filled SBR compounds. J Appl Polym Sci 121:1096–1117
25. Rolón-Garrido VH, Wagner MH (2009) The damping function in rheology. Rheol Acta 48:245–284
26. Doi M, Edwards SF (1986) The theory of polymer dynamics. Oxford Univ Press, Oxford, See Sect. 7.5.4. ISBN 019 852033 6
27. Osaki K, Watanabe H, Inoue T (1996) Damping function of the shear relaxation modulus and the chain retraction process of entangled polymers. Macromolecules 26:3611–3614
28. Leblanc JL (2013) What large amplitude oscillating shear characterization and modeling reveal about carbon-black/rubber interactions. Rubb Chem Technol 86:261–285

Index

D. Ponnamma, S. Thomas (eds.), *Non-Linear Viscoelasticity of Rubber Composites and Nanocomposites*, Advances in Polymer Science 264, DOI 10.1007/978-3-319-08702-3